frontiers | Research Topics

Inflammation and lipid signaling in disease pathogenesis

Edited by
Paola Patrignani, Angelo Sala, Bernhard Brüne,
Dieter Steinhilber and Pietro Minuz

Published in
Frontiers in Pharmacology
Frontiers in Immunology

ISSN 1664-8714
ISBN 978-2-8325-6399-1
DOI 10.3389/978-2-8325-6399-1

About Frontiers

Frontiers is more than just an open access publisher of scholarly articles: it is a pioneering approach to the world of academia, radically improving the way scholarly research is managed. The grand vision of Frontiers is a world where all people have an equal opportunity to seek, share and generate knowledge. Frontiers provides immediate and permanent online open access to all its publications, but this alone is not enough to realize our grand goals.

Frontiers journal series

The Frontiers journal series is a multi-tier and interdisciplinary set of open-access, online journals, promising a paradigm shift from the current review, selection and dissemination processes in academic publishing. All Frontiers journals are driven by researchers for researchers; therefore, they constitute a service to the scholarly community. At the same time, the *Frontiers journal series* operates on a revolutionary invention, the tiered publishing system, initially addressing specific communities of scholars, and gradually climbing up to broader public understanding, thus serving the interests of the lay society, too.

Dedication to quality

Each Frontiers article is a landmark of the highest quality, thanks to genuinely collaborative interactions between authors and review editors, who include some of the world's best academicians. Research must be certified by peers before entering a stream of knowledge that may eventually reach the public - and shape society; therefore, Frontiers only applies the most rigorous and unbiased reviews. Frontiers revolutionizes research publishing by freely delivering the most outstanding research, evaluated with no bias from both the academic and social point of view. By applying the most advanced information technologies, Frontiers is catapulting scholarly publishing into a new generation.

What are Frontiers Research Topics?

Frontiers Research Topics are very popular trademarks of the *Frontiers journals series*: they are collections of at least ten articles, all centered on a particular subject. With their unique mix of varied contributions from Original Research to Review Articles, Frontiers Research Topics unify the most influential researchers, the latest key findings and historical advances in a hot research area.

Find out more on how to host your own Frontiers Research Topic or contribute to one as an author by contacting the Frontiers editorial office: frontiersin.org/about/contact

Inflammation and lipid signaling in disease pathogenesis

Topic editors

Paola Patrignani — University of Studies G. d'Annunzio Chieti and Pescara, Italy
Angelo Sala — University of Milan, Italy
Bernhard Brüne — Goethe University Frankfurt, Germany
Dieter Steinhilber — Goethe University Frankfurt, Germany
Pietro Minuz — University of Verona, Italy

Citation

Patrignani, P., Sala, A., Brüne, B., Steinhilber, D., Minuz, P., eds. (2025). *Inflammation and lipid signaling in disease pathogenesis*. Lausanne: Frontiers Media SA.
doi: 10.3389/978-2-8325-6399-1

Table of contents

frontiers | Frontiers in Pharmacology

TYPE Editorial
PUBLISHED 16 May 2025
DOI 10.3389/fphar.2025.1623707

OPEN ACCESS

EDITED AND REVIEWED BY
Wai Po Chong,
Hong Kong Baptist University, China

*CORRESPONDENCE
Paola Patrignani,
ppatrignani@unich.it
Dieter Steinhilber,
steinhilber@em.uni-frankfurt.de

RECEIVED 06 May 2025
ACCEPTED 09 May 2025
PUBLISHED 16 May 2025

CITATION
Patrignani P, Brüne B, Sala A, Minuz P and Steinhilber D (2025) Editorial: Inflammation and lipid signaling in disease pathogenesis. *Front. Pharmacol.* 16:1623707. doi: 10.3389/fphar.2025.1623707

Editorial: Inflammation and lipid signaling in disease pathogenesis

Paola Patrignani[1]*, Bernhard Brüne[2], Angelo Sala[3], Pietro Minuz[4] and Dieter Steinhilber[5]*

[1]Department of Neuroscience Imaging and Clinical Science, and CAST, "G.d'Annunzio" University, School of Medicine, Chieti, Italy, [2]Department of Biochemistry I, Faculty of Medicine, Goethe University Frankfurt, Frankfurt, Germany, [3]Department of Pharmaceutical Sciences, University of Milan, Milan, Italy, [4]Department of Medicine, University of Verona, Verona, Italy, [5]Institute of Pharmaceutical Chemistry, Goethe University Frankfurt, Frankfurt, Germany

KEYWORDS

inflammation, lipid mediators, eicosanoids, cyclooxygenase, leukotrienes, NSAIDs, inflammatory-related diseases

Editorial on the Research Topic
Inflammation and lipid signaling in disease pathogenesis

Introduction

Inflammation is a highly coordinated biological response involving a network of immune and inflammatory cells, platelets, stromal and vascular components, and various molecular mediators (Ricciotti and FitzGerald, 2011; Patrignani and Patrono, 2015; Schebb et al., 2022; Yang et al., 2025). This complex process is essential for eliminating harmful stimuli, clearing damaged cells, and facilitating tissue repair. Although inflammation is crucial for host defense reactions, it can become maladaptive if it persists in chronic form or is excessively triggered, leading to pathophysiological states associated with various diseases, including malignancies, asthma, and cardiovascular conditions such as atherosclerosis and heart failure. Understanding the molecular and cellular pathways regulating inflammation is essential for developing targeted therapeutic strategies. In this Research Topic, studies have investigated novel mechanisms associated with inflammation, offering new insights into the intricate cellular dynamics involved. Furthermore, this Research Topic of studies addresses cutting-edge pharmacological approaches, highlighting promising therapeutic avenues to improve treatment efficacy.

Zhang et al. have investigated the role of interleukin-6 (IL-6) in the JAK2-STAT1/3 pathway during gout inflammation in patients with acute-phase gout (AG), intermittent gout (IG), and healthy controls. It was found that gout patients had lower mRNA levels of IL6, JAK2, and STAT1/3 than controls, indicating a negative feedback mechanism. In the AG group, IL-1β and IL6, JAK2 and STAT1/3 proteins increased significantly, while the IG group had elevated IL-1β but lower phosphorylated proteins. Higher IL-6 levels in AG may enhance JAK2 activation and inflammation. The study highlights the role of the IL-6/JAK2/STAT1/3 pathway in acute gout inflammation.

5-Lipoxygenase (5-LO), encoded by *ALOX5*, is involved in leukotriene biosynthesis, playing a key role in inflammatory diseases and linked to certain tumors. Hyprath et al. have investigated how the leukemogenic fusion protein MLL-AF4 upregulates *ALOX5* gene

expression. It was demonstrated that MLL-AF4 and MLL-AF9 strongly activate the *ALOX5* promoter in B-lymphocytic cells, with MLL-AF4 effects mediated by the tandem GC box. Additionally, it was identified that several AF4 domains bind the super elongation complex and are essential for inducing *ALOX5* promoter activity.

Wickert et al. have discussed how ferroptosis influences inflammatory pathways and the effect of iron metabolism on immune cell ferroptosis during inflammation. Ferroptosis is an iron-dependent form of cell death characterized by lipid peroxidation and membrane damage. Interest in this process has grown significantly over the past decade, highlighting various regulatory components. Pathways such as NF-κB and HIFs influence ferroptosis and iron metabolism, while inflammation alters iron regulatory systems, leading immune cells like macrophages and neutrophils to adopt iron-sequestering phenotypes.

Contursi et al. have reviewed the link between inflammation, platelets, and tumor progression, highlighting the potential to develop cancer prevention strategies. Platelets create an inflammatory microenvironment that supports tumor growth and metastasis. The use of antiplatelet agents, particularly low-dose aspirin, can reduce cancer risk, especially for colorectal cancer. Further research is needed on the anti-cancer effects of other antiplatelet drugs, including ADP $P2Y_{12}$ receptor antagonists and new agents that are in clinical development, to find treatments with minimal effects on hemostasis.

Tao et al. have reviewed the multiple functions of apolipoprotein A-I (ApoA-I), a high-density lipoprotein (HDL) component. ApoA-I has a cholesterol reversal transport function and exerts anti-inflammatory effects mainly by regulating the functions of immune cells such as monocytes/macrophages, dendritic cells, neutrophils, and T lymphocytes. It also modulates the function of vascular endothelial cells and adipocytes. Additionally, ApoA-I directly exerts anti-inflammatory effects against pathogenic microorganisms or their products.

Wu et al. have examined the immunostimulatory effects of flavonoids from Epimedium, particularly icaritin and icariins I and II, both *in vitro* and *in vivo*. Key findings indicate that these flavonoids enhance the expression of co-stimulatory molecules (CD40, CD80, CD86) and MHC-I/II in dendritic cells, increasing the production of chemokines and pro-inflammatory cytokines. *In vivo*, they function as vaccine adjuvants, elevating serum levels of OVA-specific IgG. Icaritin and icariins I and II emerge as promising TLR7/8 immunomodulators with lower toxicity and higher bioavailability, potentially benefiting anticancer applications by inhibiting tumors and improving the tumor microenvironment.

Osteoarthritis (OA) is a common degenerative joint disease, and there are currently no approved treatments for modifying its progression.

Qian et al. have investigated the effects of AFK-PD, a novel pyridone agent, on OA induced by medial meniscus destabilization (DMM) *in vivo* and on chondrocytes treated with IL-1β *in vitro*. Results showed that AFK-PD reduced OA progression by inhibiting cartilage degeneration, inflammation, and osteophyte formation. It also decreased chondrocyte inflammation and macrophage M1 polarization, promoting chondrocyte anabolism and reducing catabolism and apoptosis. Mechanistically, AFK-PD suppressed key signaling molecules in the MAPK and NF-κB pathways. These findings suggest that AFK-PD could be a promising therapeutic candidate for OA treatment.

Stigmasterol, a natural plant sterol found in various herbs and vegetables with anti-inflammatory, antioxidant, and cholesterol-lowering effects, has been explored for its therapeutic potential in Acute Pancreatitis (AP) by Zhao et al. The authors utilized network pharmacology and experimental verification in a sodium taurocholate-induced AP mouse model. Analysis of protein-protein interactions revealed MAPK3 (ERK1) as a crucial target for the effects of stigmasterol in AP. Molecular docking indicated a strong binding affinity of stigmasterol for ERK1. Both *in vivo* and *in vitro* experiments demonstrated that stigmasterol treatment mitigated pancreatic injury, reduced lipase and amylase serum levels, improved inflammatory responses, and lessened acinar cell necrosis. Mechanistically, stigmasterol inhibited the activation of the ERK signaling pathway, facilitating a transition from necrosis to apoptosis in pancreatic acinar cells, thus averting inflammation.

Ammazzalorso et al. using an *in silico* approach, identified a novel chemical scaffold that is highly selective and potent in inhibiting cyclooxygenase(COX)-2 activity in inflammatory and cancer cells. AA520 is a unique molecule with dual inhibitory effects on COX-2 and PPARα at the same concentration range. Considering the synergistic impact between PPARα and COX-2 inhibitors in limiting tumorigenesis, developing molecules with these dual pharmacological targets is of clinical relevance.

Gastric contents aspiration is one of the most common causes of acute lung injury (ALI) and acute respiratory distress syndrome (ARDS), conditions associated with significant morbidity and mortality. In an HCl-induced ALI/ARDS mouse model, Dong et al. have evaluated polyvinylalcohol-carbazate (PVAC), a polymer that binds aldehydes, reducing oxidative stress and inflammation. PVAC treatment improved airway hyperresponsiveness, reduced pulmonary edema, and decreased lung damage while lowering neutrophil recruitment and inhibiting IL-6, TNF-α, and leukotriene B4 levels. These findings indicate PVAC could serve as a potential treatment for ALI/ARDS due to gastric acid aspiration and help manage asthma-like symptoms in gastroesophageal reflux patients.

Messler et al. have focused on elucidating the potential role of docosahexaenoic acid (DHA), a polyunsaturated fatty acid, in conjunction with acetylsalicylic acid (ASA) in angiogenesis, utilizing both *in vitro* and *in vivo* experimental models. The findings from these studies indicate that ASA may facilitate the formation of specific monohydroxylated metabolites of DHA, which appear to exert a significant influence over angiogenic processes.

Kiprina et al. investigated the effects of exogenous anandamide (AEA) in a mouse AirPouch model of acute inflammation through analysis of immune cell infiltrates. The study found that AEA limits the infiltration of myeloid cells but increases the presence of T cells at the site of inflammation. This action is mediated by the NR4A transcription factor instead of CB receptors. AEA effectively inhibits TH17 responses without hindering TH1 differentiation, indicating its potential for managing chronic inflammation while preserving vital immune functions.

Author contributions

PP: Writing – original draft. BB: Writing – review and editing. AS: Writing – review and editing. PM: Writing – review and editing. DS: Writing – original draft.

Funding

The author(s) declare that no financial support was received for the research and/or publication of this article.

Conflict of interest

The authors declare that the research was conducted in the absence of any commercial or financial relationships that could be construed as a potential conflict of interest.

The author(s) declared that they were an editorial board member of Frontiers, at the time of submission. This had no impact on the peer review process and the final decision.

Generative AI statement

The author(s) declare that no Gen AI was used in the creation of this manuscript.

Publisher's note

References

Patrignani, P., and Patrono, C. (2015). Cyclooxygenase inhibitors: from pharmacology to clinical read-outs. *Biochim. Biophys. Acta* 1851, 422–432. doi:10.1016/j.bbalip.2014.09.016

Ricciotti, E., and FitzGerald, G. A. (2011). Prostaglandins and inflammation. *Arterioscler. Thromb. Vasc. Biol.* 31, 986–1000. doi:10.1161/ATVBAHA.110.207449

Schebb, N. H., Kühn, H., Kahnt, A. S., Rund, K. M., O'Donnell, V. B., Flamand, N., et al. (2022). Formation, signaling and occurrence of specialized pro-resolving lipid mediators-what is the evidence so far? *Front. Pharmacol.* 13, 838782. doi:10.3389/fphar.2022.838782

Yang, J., Yamashita-Kanemaru, Y., Morris, B. I., Contursi, A., Trajkovski, D., Xu, J., et al. (2025). Aspirin prevents metastasis by limiting platelet TXA_2 suppression of T cell immunity. *Nature* 640, 1052–1061. doi:10.1038/s41586-025-08626-7

frontiers | Frontiers in Immunology

TYPE Review
PUBLISHED 08 July 2024
DOI 10.3389/fimmu.2024.1417270

OPEN ACCESS

EDITED BY
Paola Patrignani,
University of Studies G. d'Annunzio Chieti and Pescara, Italy

REVIEWED BY
Stefania Tacconelli,
University of Studies G. d'Annunzio Chieti and Pescara, Italy
Pietro Minuz,
University of Verona, Italy

*CORRESPONDENCE
Kaiyang Wang
kaiyang3937@126.com

†These authors have contributed equally to this work and share first authorship

RECEIVED 14 April 2024
ACCEPTED 19 June 2024
PUBLISHED 08 July 2024

CITATION
Tao X, Tao R, Wang K and Wu L (2024) Anti-inflammatory mechanism of Apolipoprotein A-I. *Front. Immunol.* 15:1417270. doi: 10.3389/fimmu.2024.1417270

Anti-inflammatory mechanism of Apolipoprotein A-I

Xia Tao†, Ran Tao†, Kaiyang Wang* and Lidong Wu

Department of Emergency, The Second Affiliated Hospital, Jiangxi Medical College, Nanchang University, Jiangxi, China

Apolipoprotein A-I(ApoA-I) is a member of blood apolipoproteins, it is the main component of High density lipoprotein(HDL). ApoA-I undergoes a series of complex processes from its generation to its composition as spherical HDL. It not only has a cholesterol reversal transport function, but also has a function in modulating the inflammatory response. ApoA-I exerts its anti-inflammatory effects mainly by regulating the functions of immune cells, such as monocytes/macrophages, dendritic cells, neutrophils, and T lymphocytes. It also modulates the function of vascular endothelial cells and adipocytes. Additionally, ApoA-I directly exerts anti-inflammatory effects against pathogenic microorganisms or their products. Intensive research on ApoA-I will hopefully lead to better diagnosis and treatment of inflammatory diseases.

KEYWORDS

Apolipoprotein A-I, macrophage, dendritic cell, neutrophil, T lymphocyte, anti-inflammatory

1 Introduction

ApoA-I is a member of blood apolipoproteins, which constitutes a major component of HDL (1). In addition to participating in cholesterol reversal, ApoA-I also has powerful anti-inflammatory functions (2). It is considered an anti-inflammatory protein, with levels reduced by at least 25% during acute inflammation (3). ApoA-I attenuates the inflammatory response through inhibit the production of TNF-a and IL-1 in rheumatoid arthritis, Crohn's disease and other immune diseases (4). A negative correlation between ApoA-I levels and the severity of pancreatitis has also been found in pancreatitis (5–7). Furthermore, our previous study revealed a negative correlation between ApoA-I levels and disease severity in hypertriglyceridemic pancreatitis (8). In cases of sepsis, there is a negative correlation between ApoA-I and the severity of the condition (9). Additionally, the administration of ApoA-I mimetic peptide has been shown to improve survival rates in septic rats (10). The anti-inflammatory function of ApoA-I also plays an important role in the inhibition of atherosclerosis and anti-tumor growth (11). A negative correlation between reduced ApoA-I and disease severity was also found in COVID-19 infections (12, 13). However, the exact anti-inflammatory mechanism of ApoA-I is not well understood. In this article, we review the production, assembly and possible anti-inflammatory mechanism of ApoA-I.

2 Production and assembly

The human ApoA-I gene is located in the 11q23 region of human chromosome 11,and is thought to be of the same genetic origin as Apolipoprotein A-II, Apolipoprotein A-IV, Apolipoprotein C-I, Apolipoprotein C-III, and Apolipoprotein E (14). The liver and intestine are the main sites of ApoA-I production in human tissues, but small amounts of ApoA-mRNA expression have been demonstrated in other organs, such as the pancreas and heart (15). The regulation of human ApoA-I gene expression is very complex and is controlled at multiple levels. Hepatocyte Nuclear Factor 4, Liver Receptor Homologue 1 and ApoA-I Regulatory Protein 1 are thought to be the major regulators of ApoA-1 initiation and repression (16). Translated ApoA-I is pruned intracellularly and then secreted as a lipid-poor protein or lipid-free protein (Figure 1). ApoA-I gene mutations have been demonstrated to be associated with the development of numerous diseases, including those observed in diabetic patients. In particular, polymorphisms at the -75 bp locus of the ApoA-I gene have been linked to an increased risk of myocardial infarction in these patients (17). Individuals with the CC genotype of SNP rs5069 are more susceptible to oxidative imbalance and are at a higher risk of developing pancreatitis (18).

The primary structure of ApoA-I consists of 4 Tryptophan (Trp), 21 Lysine (Lys), 5Histidine (His), 16 Arginase (Arg), 16 Aspartic acid (Asp), 10 Threonine (Thr), 15 Serine (Ser), 27 Glutamic acid (Glu), 10 Proline(Pro), 10 Glycine (Gly), 19 Alanine (Ala), 13 Valine (Val), 3 Methionine (Met), 37 Leucine (Leu), 7 Tyrosine (Tyr), and 6 Phenylalanine (Phe), a total of 243 amino acid residues to form a single-chain peptide, which molecular weight is 28 KDa (19). This single-chain polypeptide may contain a plurality of 11 and 22 repeating amino acid residues, and these residues are typically separated by Pro residues. Among them, the 22 repeating amino acid residues can form the α-helix of ApoA-I, and the secondary structure of each ApoA-I contains about 8-9 tandem alpha helices (20). These α-helix play an important role in the biological function of ApoA-I (21–23). ApoA-I binds to the first extracellular domains(ECD1) of ATP-binding Cassette transport A1 (ABCA1), resulting in the transfer of cholesterol and cytosolic phospholipids from the cell membrane to ApoA-I, which then forms an initially lipidated ApoA-I (24). Initially lipidated ApoA-I can continue to form discoidal HDL in the presence of Dimyristoyl Phosphatidylcholine and egg phosphatidylcholine or palmitoyloleyl phosphatidylcholine (25). Studies of discoidal HDL mainly come from vitro models, as it is short-lived and difficult to isolate in plasma (26). Initially, it was believed that the binding of the α-helix to phospholipids in discoidal HDL was in the form of a spiked hedge fence. The α-helix consists of 22 repeating amino acids centered on a repeating proline residue crossing the edges of a bilayer parallel to the acyl chain (27). However, with research progressed, the 'two-band' model of discoidal HDL was considered the best possible model of α-helix binding to phospholipids. In this model, two cyclic ApoA-I molecules wrap a phospholipid bilayer in an antiparallel orientation. Discoidal HDL convers to spherical HDL by lecithin-cholesterol acyltransferase (LCAT) (28) (Figure 1). The globular HDLsubpopulation can be classified according to size and density into five major subpopulations: HDL3c, HDL3b, HDL3a, HDL2a, and HDL2b. Each subpopulation is distinguished by its unique molecular

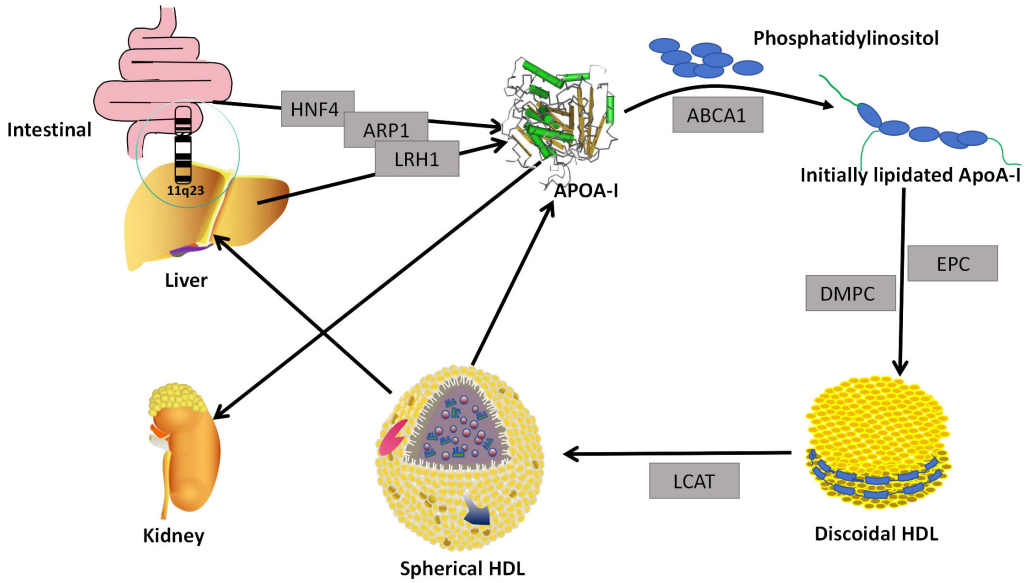

FIGURE 1
Generation and assembly. The ApoA-I gene located in the liver and small intestine secretes lipid-free ApoA-I under the regulation of HNF4, LRH1, and ARP1. Lipid-free ApoA-I binds to phosphatidylinositol to form Initially lipidated ApoA-I. Initially lipidated ApoA- I forms discoidal HDL in the presence of EPC and DMPC, and discoidal HDL forms globular HDL in the presence of LCAT. When globular HDL is reconstituted, lipid-free ApoA-I is formed. Most of the lipidated ApoA-I is metabolized in the liver, and the lipid-free ApoA-I is eliminated by the kidneys. HNF4, Hepatocyte Nuclear Factor4; ARP1, ApoA-I Regulatory Protein 1; LRH1, Liver Receptor Homologue 1; ABCA1, ATP-binding Cassette transport A1; DMPc, Dimyristoyl Phosphatidylcholine; EPC, egg phosphatidylcholine; LCAT, lecithin-cholesterol acyltransferase.

composition and biological function (29). ApoA-I is floating in the phospholipid molecules and serves to regulate HDL diameter in globular HDL (30).

ApoA-I constitutes the primary constituent of HDL, representing approximately 70%,ApoA-II accounts for 15-20%, while the remaining proteins are amphiphilic (1). ApoA-I not only determines the size and shape of HDL but is also a functional protein, such as determining the composition of HDL soluble lipids, transporting cholesterol from peripheral cells, activating LCAT activity to convert circulating cholesterol to cholesteryl esters, and delivering cholesteryl esters to the liver or to steroidogenic tissues via cell surface receptors (2). Most of ApoA-I is found in the blood associated with lipoproteins, with only about 5-10% present in a non-lipoprotein-associated state. This non-lipidated ApoA-I can be obtained from HDL remodeling or triglyceride-rich lipoproteins, or secreted directly by the liver or intestines (31). ApoA-I in plasma is about 100-150 mg/dl,and its half-life is about 4 days (32, 33). Most lipidated ApoA-I is metabolized in the liver (34), Non-lipidated ApoA-I can pass through glomerular filtration and be degraded, excreted in urine, or partially reabsorbed (35) (Figure 1).

3 Possible anti-inflammatory mechanism of ApoA-I

3.1 Regulation of immune cells

The inflammatory response is primarily determined on the function and activity of immune cells (36). Monocytes are an important component of the defense system of body, which play a crucial role in the immune system, and can induce a specific immune response in lymphocytes through antigen presentation (37). Macrophages are terminally differentiated monocyte, which have a variety of biological functions in the inflammatory response, including phagocytosis of microorganisms, mediation and promotion of the inflammatory response, antigen processing and presentation, modulation of the immune response, direct killing of target cells, adjuvant or inhibitory production of antibodies by B-lymphocytes, and production of cytokines (38). Immature dendritic cells have a strong migratory ability, and mature dendritic cells can effectively activate the initial T-cells to initiate the immune response (39). In the inflammatory response, neutrophils have multiple biological functions, such as chemotaxis, phagocytosis, apoptosis, degranulation, activation, production of reactive oxygen species and extra-neutral trapping networks (40). T cells play a key role in regulating the immune response, and which have responsible for mediating of the immune effector mechanisms (41).

ApoA-I exerts a modulatory effect on the immune functions of monocytes, macrophages, dendritic cells, neutrophils, and T lymphocytes. It also suppresses inflammatory responses through multiple pathways (42, 43). First, ApoA-I can exert anti-inflammatory effects by regulating the production of immune cells. In a mouse model of acute myocardial infarction, ApoA-I has been observed to inhibit the expansion of monocytes and macrophages in the blood, spleen, and myocardium of mice (44). Upon leaving the bloodstream and entering tissues, monocytes can differentiate into Dendritic Cells(DCs),ApoA-I upregulates Prostaglandin E2 (PGE2) and Interleukin-10 (IL-10) in monocytes, and inhibits their differentiation to dendritic cells (45). In neutrophil generation, ApoA-I can reduce neutrophil production by decreasing the production of granulocyte colony stimulating factor (G-CSF) (46). Furthermore, ApoA-I has been demonstrated to reduce neutrophil counts in patients with acute myocardial infarction, resulting in less myocardial inflammatory injury (47). ApoA-I also has an effect on lymphocyte production, it deficiency leads to increase of CD45RA+, CD16+, and CD56+ lymphocytes in the blood (48). Transplantation of bone marrow from ApoA-I knockout mice into LDL receptor knockout mice resulted in a significant increase in lymphocytes (49). Second, ApoA-I can exert anti-inflammatory effects by regulating the expression and production of related factors of immune cells. The expression and production of related factors of immune cells are closely related to anti-inflammatory functions, such as spreading, recognition and chemotaxis. ApoA-I can directly inhibit the spreading and antigen-presenting ability of monocytes by down-regulating the expression of monocyte CDC42, CD11c, CD86, CD14, and HLA-DR (50, 51). Expression of vascular cell adhesion molecule-1 (VCAM-1), monocyte chemotactic protein 1 (MCP-1), and macrophage inflammatory protein 1 (MIP-1) was also inhibited by ApoA-I, which also significantly reduced the release of sL-selectin and soluble Inter-cellular Adhesion molecule 1(sICAM-1), and decreased monocyte chemotaxis, adhesion and activation function (52, 53). ApoA-I inhibits the synthesis of IL-8 by activated neutrophils, limiting their chemotaxis to local sites of inflammation (53). It was also found that ApoA-I reduces the expression of CD11b in neutrophils, leading to the decreased of adhesion, migration and spreading capacity of neutrophils (54). In polymorphonuclear leukocytes, ApoA-I was also found to have the ability to inhibit the expression of CD11/CD18, resulting in the decreased of adhesion of polymorphonuclear leukocyte(PMN) (55). Third, ApoA-I can exert anti-inflammatory effects by regulating the interaction of immune cells. In the inflammatory response, immune cells can coordinate and influence each other. As previously discussed, ApoA-I can affect the differentiation between monocytes and dendritic cells. ApoA-I also inhibits T-cell proliferation via DCs, and inhibits the reciprocal response between DCs and NK cells, resulting in decreased of IFN-γ and IL-12p70 (56). Fourth, It can exert anti-inflammatory effects by altering the expression of ApoA-I in immune cells. It has been found that ApoA-I is also expressed in macrophages, and the effect of its expression also affects macrophage function (57, 58). In monocytes, the expression of CD11b, CD11c, and CD29 was negatively correlated with ApoA-I levels in all monocyte subpopulations, and ApoA-I levels directly affected the anti-inflammatory activity of monocytes (59) (Figure 2).

Based on the available research, the regulation of the anti-inflammatory function of immune cells by ApoA-I may be achieved through the following molecular mechanisms: First, ApoA-I causes cholesterol efflux from immune cells to affect the expression of

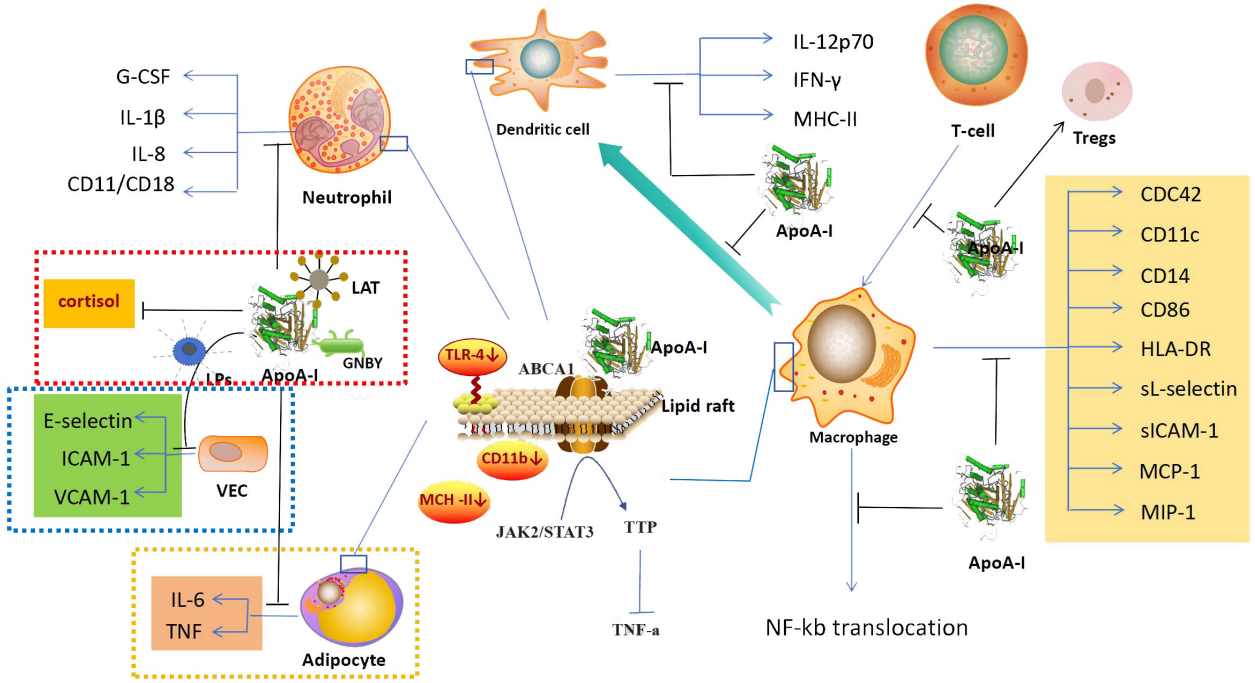

FIGURE 2
anti-inflammatory mechanism. In addition to its anti-inflammatory effects mainly through the regulation of immune cells,ApoA-I also exerts anti-inflammatory effects through the regulation of vascular endothelial cells (blue dashed area), the action on microorganisms and their products (red dashed area), and the regulation of adipocytes (yellow dashed area). In the regulation of immune cells, ApoA-I can inhibit the generation of immune cells, affect the expression of related factors, and inhibit the synergistic effect of immune cells. Its molecular mechanism is mainly to increase the efflux of cholesterol, regurate lipid raft-mediated signaling pathways and inhibit NF-kB nuclear translocation. ApoA-I, Apolipoprotein A-I; G-CSF, Granulocyte Colonystimulating Factor; IL-1β, interleukin 1β; IL-8, interleukin 8; LAT, Lipophosphatidic acid; LPs, lipopolysaccharide; GNBY, Gram-negative bacterium Yersinia; ICAM-1, Inter-cellular Adhesion molecule 1; VCAM-1, Vascular Cell Adhesion Molecule 1; VEC, Vascular endothelial cell; IL-6, interleukin 6; TNF, tumor necrosis factor; IL-12p70, interleukin 12p70; IFN-γ, Interferon γ; MHC-II, Major Histocompatibility Complex II; ABCA1, ATP-binding cassette transporter protein A1; TLR-4, Toll-like receptor; JAK2/STAT3, Janus kinase 2/Signal Transducer and Activator of Transcription 3; TTP, tristetraprolin; CDC42, Cell Division Cycle 42; HLA-DR, Human Leukoyte Antigen DR; sICAM-1, soluble Inter-cellular Adhesion molecule 1; MCP-1, Monocyte Chemotactic Protein 1; MIP-1, Macrophage Inflammatory Protein 1.

related factors. ApoA-I has a powerful cholesterol transporter function, it can modulate cellular biological functions by altering the cholesterol in cells, as previously demonstrated, the regulation of cholesterol in arterial vascular endothelial cells (60), and the recently discovered of regulation in pancreatic islet cells (61). ApoA-I has the same cholesterol-transporting effect in immune cells (62). Studies have shown that the decrease of CD11b and TLR-4 expression in monocytes by ApoA-I is due to the exocytosis of cholesterol from monocyte lipid rafts as a result of ApoA-I binding to ABCA1 in monocyte lipid rafts (52, 63), and the inhibition of macrophage antigen presentation and activation of T cells is also due to ApoA-I causing a decrease in the cholesterol content in macrophage lipid rafts (64). Second, ApoA-I affects the expression of related factors through lipid raft-mediated signaling pathways. After treating macrophages with ApoA-I, Yin Kai et al. found that the binding of ApoA-I to ABCA1 activated the Janus kinase 2/Signal Transducer and Activator of Transcription 3 (JAK2/STAT3), and upregulated the expression the tristetraprolin(TTP),which in turn promoted the degradation of TNF-a mRNA through AU-rich elements (AREs) in the 3-untranslated regions (3-UTR), leading to a reduction in the production of TNF-a and a decrease of inflammatory response (65). Third, suppression of gene activation in immune cells by inhibiting NF-kB nuclear translocation. NF-kB translocation plays a crucial role in intracellular signaling pathways and regulates various biological processes (66). In immune cells, stimulation by various factors can cause the transfer of the NF-kB subunit to the nucleus, activating numerous NF-kB-specific target genes, this activation leads to the initiation or enhancement of the immune response (67). ApoA-I inhibits NF-kB nuclear translocation in THP-1 differentiated monocytes, and the expression of VCAM-1 was inhibited and the release of sL-selectin and sICAM-1 were decreased. This reduced the chemotaxis, adhesion and activation functions of monocytes and inhibited the anti-inflammatory effects of monocytes (52, 68) (Figure 2). However, whether the initiating link of ApoA-I for NF-kB translocation inhibition is also due to ApoA-I affecting monocyte cholesterol is not known, and more studies are expected to further explore this.

3.2 Regulation of vascular endothelial cells

Vascular endothelial cells are a single layer of flat epithelium that covers the inner surface of blood vessels. During inflammation,

vascular endothelial cells express adhesion molecules and interact with leukocyte surface adhesion molecules in the bloodstream. They also regulate leukocyte crossing of the vessel wall through signaling (69). In a study of a mouse model of type 2 diabetes revascularization, ApoA-I was found to reduce the inflammatory response of endothelial cells in the reconstructed blood vessels and promote vascular repair (70). ApoA-I can directly bind to LPs and influence its stimulatory effect on vascular endothelial cells. This results in the inhibition of E-selectin and intercellular adhesion molecule 1 (ICAM-1) expression in vascular endothelial cells, which leads to reduced adhesion of neutrophils to endothelial cells (56). *In vivo* experiments were conducted on New Zealand white rabbits infused intravenously with lipid-free ApoA-I, the results showed a reduction in the expression of VCAM-1 and ICAM-1, as well as a decrease in endothelial neutrophil infiltration (71) (Figure 2). However, the specific molecular mechanisms by which ApoA-I regulates vascular endothelial cell function are not well understood.

3.3 Action on microorganisms and their products

ApoA-I binds to a wide range of Gram-positive and Gram-negative bacteria, as well as to lipopolysaccharides and lipophosphatidic acids. In addition, ApoA-I has *in vitro* antimicrobial activity against Gram-negative bacteria (72). The C-terminal structural domain of ApoA-I serves as an effector site that provides bactericidal activity and contributes to complement mediated killing of the Gram-negative bacterium Yersinia enterocolitica in the small intestine (73) (Figure 2). In addition, ApoA-I was also found to possess *in vitro* antimicrobial properties against Gram-positive and Gram-negative bacteria in studies with tilapia, and ApoA-I inhibited inflammation and apoptosis and increased the likelihood of survival to bacterial infection (74), and its antimicrobial effect is not affected by temperature, even when the a-helix of ApoA-I is damaged by high temperature, ApoA-I still has the activity of killing bacteria directly (75). Therefore, the structure of ApoA-I may not be closely related to its antimicrobial activity.

Lipoteichoic acid (LTA) is an amphiphilic cationic glycolipid and a major cell wall component of Gram-positive bacteria. It has a structure similar to that of LPs from Gram-negative bacteria. LTA has been implicated as one of the major immunostimulatory components that may trigger systemic inflammatory response syndromes (76). ApoA-I significantly reduces L-929 cell mortality induced by LTA activated macrophages in a dose-dependent manner (77). LPs is one of the most potent stimulators of innate immune activation, and have important effects on human monocyte and macrophage (78). ApoA-I can neutralize the inflammatory effects of LPs through direct binding to LPs and can also regulate cortisol hormone production to play an anti-inflammatory role. In the sepsis model with ApoA-I knockout mice, it was found that ApoA-I knockout mice had a decreased ability to neutralize LPs compared to wild-type mice, and their serum cortisol hormone production was impaired, and the sepsis protection of the mice was reduced (79) (Figure 2).

3.4 Others

In adipocytes, ApoA-I inhibits the expression of IL-6 and TNF induced by palmitate, and it translocate TLR-4 to lipid rafts, thereby inhibiting inflammatory responses in adipocytes (80) (Figure 2).

4 The anti-inflammatory of 4F and CSL

Based on the robustness of ApoA-I and findings in the clinic, ApoA-I supplementation is considered a viable approach to treatment disease. Therefore, ApoA-I which can be used as a medicine has become the focus of attention. Such as ApoA-I mimetic peptides and ApoA-I based infusions.

Anantharamaiah et al. synthesized the first apoA-I mimetic peptide 18A in, 1985,which comprises 18 amino acids (81). Subsequently, the amino acid and α-helix structures of ApoA-I mimetic peptides have been modified to enhance their functionality (82, 83). To date, ApoA-I mimetic peptides in the pilot study phase are 4F,6F,FX-5A,ATI-5261 and ETC-642 (84). Among the many mimetic peptides, 4F has the most prominent anti-inflammatory effects. *In vitro*,4 F reduces IL-6 secretion in SARS-CoV-2 infected Vero-E6 and Calu3 cells (85), and it has an inhibitory effect on IL-4-induced selective activation of macrophages (43), 4F also inhibits Reactive Oxygen Species(ROS) production and ameliorates oxidative damage in endothelial cells (86). It has been shown in animal studies that ApoA-I mimetic peptides have the inflammation inhibition (87). In mice,4F inhibits the expression of interleukin-6(IL-6), interleukin-1β(IL-1β) and tumor necrosis factor-α (TNF-α) (88), it reduce macrophage infiltration in the liver (89). It also upregulates vascular endothelial growth factor protein expression to improve endothelial cell function in animal studies (90). An *in vivo* study in humans also showed that oral administration of apoA-I mimetic peptides 6F and 4F reduced plasma and intestinal tissue cytokines (TNF-a, IL-6) and chemokines (CX3CL1), and reduced systemic and intestinal inflammation in chronic treatment of HIV (91).

ApoA-I based infusions include HDL-VHDL infusion, purified ApoA-I infusion, ApoA-I_{Milano} infusion, CSL-111 and CSL-112 infusion,CER-001 infusion and modified ApoA-I (84). Of these, CSL-112 is considered the most viable infusion. CSL-112 consists of purified human ApoA-I and phosphatidylcholine, because it binds less phosphatidylcholine than CSL-111, it does not have the dose toxicity of CSL-111 (92). In previous studies, CSL-111 has been shown to have the effect of downregulating macrophages to reduce inflammation (93, 94). CSL112 also has shown anti-inflammatory effects ex vivo studies, including markers of monocyte chemotactic factor-1 and proinflammatory cytokines interleukin-1β (95).

5 Discussion

ApoA-I goes through a series of complex processes from generation to assembly (96). Thus, both the expression of the

ApoA-I gene and the changes in its α-helix structure are susceptible to interference by external environmental factors, and these changes may be associated with the development of the disease (23, 97). ApoA-I is the primary component of HDL, and the biological functions of HDL, including cholesterol regulation (98), inflammatory response modulation (99), and tumor growth modulation are believed to be closely related to ApoA-I (100), which is an effective performer of HDL's biological functions (101). As described above, ApoA-I plays a pivotal role in the inhibition of the inflammatory response, and this is achieved through the inhibition of immune cell production and activity, the reduction of the recognition of immune cells by vascular endothelial cells, and the direct destructive effect on microorganisms and their products. Specific molecular regulatory mechanisms have focused on the study of immune cells. According to the literature review, most of the regulatory effects of ApoA-I on immune cell function are related to its regulation of cholesterol, in which the effect on lipid rafts is an important target for ApoA-I to regulate immune cells, but a clearer and more systematic mechanism is still not well described, and more and more in-depth studies are expected to be conducted in the future. The decrease of ApoA-I has been detected in many diseases (102–105), especially in those related to inflammation (4–13). However, the underlying cause of the decrease is not clear. Whether the reduction is due to a decrease in ApoA-I production or an increase in ApoA-I depletions is necessary to explore.

As previously described, several studies have shown that ApoA-I mimetic peptides have some anti-inflammatory effects. However, even with studies showing that ApoA-I mimetic peptide does not play a role in suppressing inflammation. In the aortic constriction rabbit model, ApoA-I mimetic infusions did not significantly improve echocardiographic parameters nor molecular markers of cardiac inflammation, oxidative stress and fibrosis (106). This includes previous trial in patients with coronary artery disease or at high risk for cardiovascular disease that showed conflicting results on the effect of oral and parenteral administration of 4F on HDL inflammation indices (107). The contradictory test results may be attributed to the fact that the functions of the simulated components are distinct (108, 109) and that the final evaluation criteria differ for each test. ApoA-I mimetic peptide is a synthetic substance that is similar to ApoA-I. However, its molecular structure differs from ApoA-I, which means that it cannot exert the same effect when it enters the body. Furthermore, the pharmacokinetics and pharmacokinetics of ApoA-I mimetic peptides *in vivo* require further comprehensive and in-depth investigation. Research on the anti-inflammatory effects of ApoA-I mimetic peptides have been focused on *in vitro* and *in vivo* studies, with few clinical trials in humans. The main factors limiting the development of these may be related to the contradictory results of ApoA-I mimetic peptide tests and concerns about their safety. The development of ApoA-I mimetic peptides that are closer to the molecular structure of ApoA-I and safer may require more difficult work. However, from the theoretical standpoint, the structure of CSL-112 is more closely aligned with ApoA-I mimetic peptide, which should result in a more robust anti-inflammatory effect and enhanced safety profile. But the majority studies of CSL-111/112 on immune cells come from atheromatous plaque formation, lack of extensively studied as the ApoA-I mimetic peptides in inflammation. And concerns have been raised about the efficacy of CSL-112 due to the findings of recent clinical studies, which indicated that patients with acute myocardial infarction treated with CSL-112 did not experience a significant reduction in major adverse cardiovascular events (110). We are looking forward to deeper study and bigger breakthroughs in the anti-inflammatory treatment of CSL-112.

6 Conclusions

The production and assembly of ApoA-I is influenced by multiple factors, and ensuring the structural integrity of ApoA-I is a prerequisite for its anti-inflammatory effects. ApoA-I can exert its anti-inflammatory effects through regulate immune cells, vascular endothelial cells, and direct interaction with microorganisms and their products. Several experiments have demonstrated that ApoA-I mimetic peptides and ApoA-I based infusions inhibit inflammatory responses. It is anticipated that safer and more efficacious ApoA-I drugs will emerge in the near future as research progresses.

Author contributions

XT: Writing – original draft. TR: Writing – original draft. KW: Conceptualization, Writing – review & editing. LW: Writing – review & editing.

Funding

The author(s) declare that no financial support was received for the research, authorship, and/or publication of this article.

Conflict of interest

The authors declare that the research was conducted in the absence of any commercial or financial relationships that could be construed as a potential conflict of interest.

Publisher's note

References

1. Nazir S, Jankowski V, Bender G, Zewinger S, Rye K-A, van der Vorst EPC. Interaction between high-density lipoproteins and inflammation:Function matters more than concentration. *Adv Drug Deliv Rev*. (2020) 159:94–119. doi: 10.1016/j.addr.2020.10.006

2. Pownall HJ, Rosales C, Gillard BK, Gotto AM Jr. High-density lipoproteins, reverse cholesterol transport and atherogenesis. *Nat Rev Cardiol*. (2021) 18:712–. doi: 10.1038/s41569-021-00538-z

3. Gabay C, Kushner I. Acute-phase proteins and other systemicresponses to inflammation. *N Engl J Med*. (1999) 340:448 –54. doi: 10.1056/NEJM199902113400607

4. Georgila K, Vyrla D, Drako E. Apolipoprotein A-I (ApoA-I), immunity, inflammation and cancer. *Cancers*. (2019) 11:1097. doi: 10.3390/cancers11081097

5. Wu J, Wang Y, Li H, Tan W, Chen X, Ye. S. Serum apolipoprotein B-toapolipoprotein A1 ratio is independently associated with disease severity in patients with acute pancreatitis. *Sci Rep*. (2019) 9:7764. doi: 10.1038/s41598-019-44244-w

6. Yu Ge, Jiang W, Cheng Z, Wan R. Predictive value of serum apolipoprotein A-I in the organ failure of acute pancreatitis: a retrospective cohort study. *Scand J Gastroenterol*. (2023) 58:1049–55. doi: 10.1080/00365521.2023.2200500

7. Li Y, Zheng R, Gao F, Wang L, Feng S, Li J, et al. Association between high-density lipoprotein cholesterol and apolipoprotein A-I and severe acute pancreatitis: a case-control study. *Eur J Gastroenterol Hepatol*. (2021) 33:1517–23. doi: 10.1097/MEG.0000000000002095

8. Hu Y-q, Tao X, Wu H-b, Li W-g, Chen D-y, Liu Y-f, et al. Predicting severity in hypertriglyceridemiaInduced acute pancreatitis: the role of neutrophils, calcium, and apolipoproteins. *Med Sci Monit*. (2024) 30:942832. doi: 10.12659/MSM.942832

9. Wendel M, Paul R, Heller AR. Lipoproteins in inflammation and sepsis. II. Clinical aspects. *Intensive Care Med*. (2007) 33:25–35. doi: 10.1007/s00134-006-0433-x

10. Zhang Z, Datta G, Zhang Y, Miller AP, Mochon P, Chen Y-F, et al. Apolipoprotein A-I mimetic peptide treatment inhibits inflammatory responses and improves survival in septic rats. *Am J Physiol Heart Circ Physiol*. (2009) 297:H866–73. doi: 10.1152/ajpheart.01232.2008

11. Busnelli M, Manzini S, Chiara M. Aortic gene expression profiles show how apoA-I levels modulate inflammation, lysosomal activity, and sphingolipid metabolism in murine atherosclerosis. *Arterioscler Thromb Vasc Biol*. (2024) 41:651–67. doi: 10.1161/ATVBAHA.120.315669

12. Feingold KR. The bidirectional interaction of COVID-19 infections and lipoproteins. *Best Pract Res Clin Endocrinol Metab*. (2023) 37:101751. doi: 10.1016/j.beem.2023.101751

13. Hilser JR, Han Y, Biswas S, Gukasyan J, Cai Z, Zhu R, et al. Association of serum HDL-cholesterol and apolipoprotein A1 levels with risk of severe SARS-CoV-2 infection. *J Lipid Res*. (2021) 62:100061. doi: 10.1016/j.jlr.2021.100061

14. Arinami T, Hirano T, Kobayashi K, Yamanouchi Y, Hamaguchi H. Assignment of the apolipoprotein A-I gene to 11q23 based on RFLP in a case with a partial deletion of chromosome 11, del(11)(q23. 3—qter). *Hum Genet*. (1990) 85:39–40. doi: 10.1007/BF00276323

15. Zannis VI, Cole FS, Jackson CL, Kurnit DM, Karathanasis SK. Distribution of apolipoprotein A-I, C-II, C-III, and E mRNA in fetal human tissues. Time-dependent induction of apolipoprotein E mRNA by cultures of human monocyte-macrophages. *Biochemistry*. (1985) 24:4450–5. doi: 10.1021/bi00337a028

16. Kardassis D, Mosialou I, Kanaki M, Tiniakou I, Thymiakou E. Metabolism of HDL and its regulation. *Curr Med Chem*. (2014) 21:2864–80. doi: 10.2174/09298673216614030315343O

17. Casillas FA, Fernández DEM, Valle Y, Ramírez MA, Parra-Reyna B, Pulido SS, et al. APOA1 (-75 G>A and 83 C>T) and APOB (2488 C>T) polymorphisms and their association with myocardial infarction, lipids and apolipoproteins in patients with type 2 diabetes mellitus. *Arch Med Sci*. (2022) 18:1438–45. doi: 10.5114/aoms/108674

18. Sciskalska M, Milnerowicz H. Importance of Polymorphisms in the Gene of Paraoxonase-1 (SNP rs662) and Apolipoprotein A-I (SNP rs670 and rs5069) in Non-Smoking and Smoking Healthy Subjects and Patients with Acute Pancreatitis. *GENES*. (2022) 13:1968. doi: 10.3390/genes13111968

19. Brewer HBJr, Fairwell T, LaRue A, Ronan R, Houser A, Bronzert TJ. The amino acid sequence of human ApoA-I,an apolipoprotein isolated from high density lipoproteins. *Biochem Biophys Res Commun*. (1978) 80:623–30. doi: 10.1016/0006-291X(78)91614-5

20. Segrest JP, Garber DW, Brouillette CG, Harvey SC, Anantharamaiah GM. The amphipathic α helix: A multifunctional structural motif in plasma apolipoproteins. *Adv Protein Chem*. (1994) 45:303–69. doi: 10.1016/S0065-3233(08)60643-9

21. Liu M, Mei X, Herscovitz H, Atkinson D. N-terminal mutation of apoA-I and interaction with ABCA1 reveal mechanisms of nascent HDL biogenesis. *J Lipid Res*. (2019) 60:44–57. doi: 10.1194/jlr.M084376

22. Gorshkova IN, Meyers NL, Herscovitz H, Mei X, Atkinson D. Human apoA-I [Lys107del] mutation affects lipid surface behavior of apoA-I and its ability to form large nascent HDL. *J Lipid Res*. (2023) 64:100319. doi: 10.1016/j.jlr.2022.100319

23. Battle S, Gogonea V, Willard B, Wang Z, Fu X, Huang Y, et al. The pattern of apolipoprotein A-I lysine carbamylation reflects its lipidation state and the chemical environment within human atherosclerotic aorta. *J Biol Chem*. (2022) 298:101832. doi: 10.1016/j.jbc.2022.101832

24. Kawanobe T, Shiranaga N, Kioka N, Kimura Y, Ueda K. Apolipoprotein A-I directly interacts with extracellular domain 1 of human ABCA1. *Biosci Biotechnol Biochem*. (2019) 83:490–7. doi: 10.1080/09168451.2018.1547106

25. Nichols AV, Gong EL, Blanche PJ, Forte TM. Characterization of discoidal complexes of phosphatidylcholine, apolipoprotein A-I and cholesterol by gradient gelelectrophore. *Biochim Biophys Acta*. (1983) 750:353–64. doi: 10.1016/0005-2760(83)90040-1

26. Brouillette CG, Anantharamaiah GM, Engle JA, Borhani DW. Structural models of human apolipoprotein A-I: a critical analysis and review. *Biochim Biophys Acta*. (2001) 1531:4–46. doi: 10.1016/S1388-1981(01)00081-6

27. Klon AE, Segrest JP, Harvey SC. Comparative models for human apolipoprotein A-I bound to lipid in discoidal high-density lipoprotein particles. *Biochemistry*. (2002) 41:10895–905. doi: 10.1021/bi020315m

28. Mishra VK, Palgunachari MN, Segrest JP, Anantharamaiah GMJ. Interactions of synthetic peptide analogs of the class A amphipathic helix with lipids. Evidence for the snorkel hypothesis. *J Biol Chem*. (1994) 269:7185–91. doi: 10.1016/S0021-9258(17)37266-6

29. Malajczuk CJ, Gandhi NS, Mancera RL. Structure and intermolecular interactions in spheroidal high-density lipoprotein subpopulations. *J Struct Biol X*. (2020) 10:5. doi: 10.1016/j.yjsbx.2020.100042

30. Melchior JT, Street SE, Vaisar T, Hart R, Jerome J, Kuklenyik Z, et al. Apolipoprotein A-I modulates HDL particle size in the absence of apolipoprotein A-II. *J Lipid Res*. (2021) 62:100099. doi: 10.1016/j.jlr.2021.100099

31. Frank PG, Marce YL. Apolipoprotein A-I: structure–function relationships. *J Lipid Res*. (2000) 41:853–72. doi: 10.1016/S0022-2275(20)32028-9

32. Gould R,G. Lipid metabolism and atherosclerosis. *Am J Med*. (1951) 11:209–27. doi: 10.1016/0002-9343(51)90107-6

33. Fidge N, Nestel P, Ishikawa T, Reardon M, Billington T. Turnover of apoproteins A-I and A-II of high density lipoprotein and the relationship to other lipoproteins in normal and hyperlipidemic individuals. *Metabolism*. (1980) 29:643–53. doi: 10.1016/0026-0495(80)90109-2

34. Christensen EI, Gburek J. Protein reabsorption in renal proximal tubule-function and dysfunction in kidney pathophysiology. *Pediatr Nephrol*. (2004) 19:714–21. doi: 10.1007/s00467-004-1494-0

35. Yang H, Fogo AB, Kon V. Kidneys: key modulators of high-density lipoprotein levels and function. *Curr Opin Nephrol Hypertens*. (2016) 25:174–9. doi: 10.1097/MNH.0000000000000217

36. Ward AC. Immune factors, immune cells and inflammatory diseases. *Int J Mol Sci*. (2024) 25:2417. doi: 10.3390/ijms25042417

37. Murray PJ. Immune regulation by monocytes. *Semin Immunol*. (2018) 35:12–8. doi: 10.1016/j.smim.2017.12.005

38. Verschoor CP, Puchta A, Bowdish DME. The macrophage. *Methods Mol Biol*. (2012) 844:139–56. doi: 10.1007/978-1-61779-527-5_10

39. Granucci F, Foti M, Ricciardi-Castagnoli P. Dendritic cell biology. *Adv Immunol*. (2005) 88:193–233. doi: 10.1016/S0065-2776(05)88006-X

40. Liew PX, Kubes P. The neutrophil's role during health and disease. *Physiol Rev*. (2019) 99:1223–48. doi: 10.1152/physrev.00012.2018

41. Hickling JK. Measuring human T-lymphocyte function. *Expert Rev Mol Med*. (1998) 13:1–20. doi: 10.1017/S1462399498000313

42. Mu W, Sharma M, Heymans R, Ritou E, Rezek V, Hamid P, et al. Apolipoprotein A-I mimetics attenuate macrophage activation in chronic treated HIV. *AIDS*. (2021) 35:543–. doi: 10.1097/QAD.0000000000002785

43. Song X, Shi Y, You J, Wang Z, Xie L, Zhang C, et al. D-4F, an apolipoprotein A-I mimetic, suppresses IL-4 induced macrophage alternative activation and pro-fibrotic TGF-β1 expression. *Pharm Biol*. (2019) 57:470–6. doi: 10.1080/13880209.2019.1640747

44. Hamid T, Ismahil MA, Bansal SS, Patel B, Goel M, White CR, et al. The apolipoprotein A-I mimetic L-4F attenuates monocyte activation and adverse cardiac remodeling after myocardial infarction. *Int J Mol Sci*. (2020) 21:3519. doi: 10.3390/ijms21103519

45. Kim KD, Lim HY, Lee HG, Yoon D-Y, Choe Y-K, Choi I, et al. Apolipoprotein A-I induces IL-10 and PGE2 production in human monocytes and inhibits dendritic cell differentiation and maturation. *Biochem Biophys Res Commun*. (2005) 338:1126–36. doi: 10.1016/j.bbrc.2005.10.065

46. Dai C, Yao X, Keeran KJ, Zywicke GJ, Qu X, Yu Z-X, et al. Apolipoprotein A-I attenuates ovalbumin-induced neutrophilic airway inflammation via a granulocyte colony-stimulating factor dependent mechanism. *Am J Respir Cell Mol Biol*. (2012) 47:186–95. doi: 10.1165/rcmb.2011-0322OC

47. Kingwell BA, Duffy D, Clementi R, Velkoska E, Feaster J, Gibson CM. CSL112 (Apolipoprotein A-I [Human]) reduces the elevation in neutrophil-to-lymphocyte ratio induced by acute myocardial infarction. *J Am Heart Assoc*. (2024) 13:e033541. doi: 10.1161/JAHA.123.033541

48. Pashinskaya KO, Samodova AV, Dobrodeeva LK. The effect of the content of ApoA-I in peripheral blood on the state of immune homeostasis in people living in extreme climatic conditions of the Arctic. *Klin Lab Diagn*. (2021) 66:539–45. doi: 10.51620/0869-2084-2021-66-9-539-545

49. Ouweneel AB, Reiche ME, Snip OSC, Wever R, van der Wel EJ, Schaftenaar FH, et al. Apolipoprotein A1 deficiency in mice primes bone marrow stem cells for T cell lymphopoiesi. *J Cell Sci*. (2022) 135:jcs258901. doi: 10.1242/jcs.258901

50. Diederich W, Orso E, Drobnik W, Schmitz G. Apolipoprotein AI and HDL(3) inhibit spreading of primary human monocytes through a mechanism that involves cholesterol depletion and regulation of CDC42. *Atherosclerosis*. (2001) 159:313–24. doi: 10.1016/S0021-9150(01)00518-4

51. Richart AL, Reddy M, Khalaji M, Natoli AL, Heywood SE, Siebel AL, et al. ApoA-I nanoparticles delivered post myocardial infarction moderate inflammation. *Circ Res*. (2020) 127:1422–36. doi: 10.1161/CIRCRESAHA.120.316848

52. Wang Li, Chen W-Z, Wu M-P. Apolipoprotein A-I inhibits chemotaxis, adhesion, activation of THP-1 cells and improves the plasma HDL inflammatory index. *Cytokine*. (2010) 49:194–200. doi: 10.1016/j.cyto.2009.08.008

53. Smythies LE, White CR, Maheshwari A, Palgunachari MN, Anantharamaiah GM, Chaddha M, et al. Apolipoprotein A-I mimetic 4F alters the function of human monocyte-derived macrophages. *Am J Physiol Cell Physiol*. (2010) 298:C1538–48. doi: 10.1152/ajpcell.00467.2009

54. Cockerill GW, McDonald MC, Mota-Filipe H, Cuzzocrea S, Miller NE, Thiemermann C. High density lipoproteins reduce organ injury and organ dysfunction in a rat model of hemorrhagic shock. *FASEB J*. (2001) 15:1941–52. doi: 10.1096/fj.01-0075com

55. Murphy AJ, Woollard KJ, Suhartoyo A, Stirzaker RA, Shaw J, Sviridov D, et al. Neutrophil activation is attenuated by high-density lipoprotein and apolipoprotein A-I in *in vitro* and *in vivo* models of inflammation. *Arterioscler Thromb Vasc Biol*. (2011) 31:1333–41. doi: 10.1161/ATVBAHA.111.226258

56. Moundry R, Spycher M, Doran J. Reconstituted high density lipoprotein modulates adherence of polymorphonuclear leukocytes to human endothelial cells. *Shock*. (1997) 7:175–81. doi: 10.1097/00024382-199703000-00004

57. Chen W, Wu Y, Lu Q, Wang S, Xing D. Endogenous ApoA-I expression in macrophages: A potential target for protection against atherosclerosis. *Clin Chim Acta*. (2020) 505:55–9. doi: 10.1016/j.cca.2020.02.025

58. Nekrasova EV, Larionova EE, Danko K, Kuzmina DO, Shavva VS, Kudriavtsev IV, et al. Regulation of Apolipoprotein A-I Gene Expression in Human Macrophages by Oxidized Low-Density Lipoprotein. *Biochemistry (Mosc)*. (2021) 86:1201–13. doi: 10.1134/S0006297921100047

59. Patel VK, Williams H, Li SCH, Fletcher JP, Medbury HJ. Monocyte subset recruitment marker profile is inversely associated with blood apoA1 level. *Front Immunol*. (2021) 12:616305. doi: 10.3389/fimmu.2021.616305

60. Borja MS, Zhao L, Hammerson B, Tang C, Yang R, Carson N, et al. HDL-apoA-I exchange: rapid detection and association with atherosclerosis. *PloS One*. (2013) 8: e71541. doi: 10.1371/journal.pone.0071541

61. Manandhar B, Pandzic E, Deshpande N, Chen S-Y, Wasinger VC, Kockx M, et al. ApoA-I protects pancreatic β-cells from cholesterol-induced mitochondrial damage and restores their ability to secrete insulin. *Arterioscler Thromb Vasc Biol*. (2024) 44:e20–38. doi: 10.1161/ATVBAHA.123.319378

62. Méndez-Lara KA, Farré Núria, Santos D. Human apoA-I overexpression enhances macrophage-specific reverse cholesterol transport but fails to prevent inherited diabesity in mice. *Int J Mol Sci*. (2019) 20:655. doi: 10.3390/ijms20030655

63. Ciesielska A, Matyjek M, Kwiatkowska K. TLR4 and CD14 trafficking and its influence on LPS-induced pro-inflammatory signaling. *Cell Mol Life Sci*. (2021) 78:1233–61. doi: 10.1007/s00018-020-03656-y

64. Wang S-h, Yuan S-g, Peng D-q, Zhao S-p. HDL and ApoA-I inhibit antigen presentation-mediated T cell activation by disrupting lipid rafts in antigen presenting cells. *Atherosclerosis*. (2012) 225:105–14. doi: 10.1016/j.atherosclerosis.2012.07.029

65. Yin K, Deng X, Mo Z-C, Zhao G-J, Jiang J, Cui L-B, et al. Tristetraprolin-dependent post-transcriptional regulation of inflammatory cytokine mRNA expression by apolipoprotein A-I. *J Biol Chem*. (2011) 286:13834 –13845. doi: 10.1074/jbc.M110.202275

66. Zinatizadeh MR, Schock B, Chalbatani GM. The Nuclear Factor Kappa B (NF-kB) signaling in cancer development and immune diseases. *Genes Dis*. (2020) 8:287–97. doi: 10.1016/j.gendis.2020.06.005

67. Mussbacher M, Derler M, Basílio José, Schmid JA. NF-κB in monocytes and macrophages - an inflammatory master regulator in multitalented immune cells. *Front Immunol*. (2023) 14:1134661. doi: 10.3389/fimmu.2023.1134661

68. Yan Y-j, Li Y, Lou B, Wu M-p. Beneficial effects of ApoA-I on LPS-induced acute lung injury and endotoxemia in mice. *Life Sci*. (2006) 79:210–5. doi: 10.1016/j.lfs.2006.02.011

69. Krüger-Genge A, Blocki A, Franke R-P, Jung F. Vascular endothelial cell biology: an update. *Int J Mol Sci*. (2019) 20:4411. doi: 10.3390/ijms20184411

70. Babu M, Devi D, Mäkinen P, Örd T, Aavik E, Kaikkonen M, et al. ApoA-I nanotherapy rescues postischemic vascular maladaptation by modulating endothelial cell and macrophage phenotypes in type 2 diabetic mice. *Arterioscler Thromb Vasc Biol*. (2023) 43:e46–61. doi: 10.1161/ATVBAHA.122.318196

71. Wu BJ, Chen K, Shrestha S, Ong KL, Barter PJ, Rye K-A. High-density lipoproteins inhibit vascular endothelial inflammation by increasing 3β-hydroxysteroid-Δ24 reductase expression and inducing heme oxygenase-1. *Circ Res*. (2013) 112:278–88. doi: 10.1161/CIRCRESAHA.111.300104

72. Wang W, Qu Q, Chen J. Identification,expression analysis, and antibacterial activity of Apolipoprotein A-I from amphioxus (Branchiostoma belcheri). *Comp Biochem Physiol B Biochem Mol Biol*. (2019) 8:110329. doi: 10.1016/j.cbpb.2019.110329

73. Biedzka-Sarek M, Metso J, Kateifides A. Apolipoprotein A-I Exerts Bactericidal Activity against Yersinia enterocolitica Serotype O:3. *J Biol Chem*. (2011) 286:38211–9. doi: 10.1074/jbc.M111.249482

74. Huang Y, Feng J, Li Q, Zhang Z, Jiang B, Amoah K, et al. Apolipoprotein A-I (ApoA-I) protects Nile tilapia (Oreochromis niloticus) against bacterial infection. *Fish Shellfish Immunol*. (2023) 139:108925. doi: 10.1016/j.fsi.2023.108925

75. Karan S, Mohapatra A, Ko P, et al. Structural-functional characterization of recombinant Apolipoprotein A-I fromLabeo rohitademonstrates heat-resistant antimicrobial activity. *Microbiol Biotechnol*. (2020) 104:145–59. doi: 10.1007/s00253-019-10204-

76. Jiao Y-l, Wu M-P. Apolipoprotein A-I diminishes acute lung injury and sepsis in mice induced by lipoteichoic acid. *Cytokine*. (2008) 43:83–7. doi: 10.1016/j.cyto.2008.04.002

77. Ahmad I, Xuan T, Wang Q, Zhang S, Wang L, Gu J, et al. Bacterial lipoteichoic acid induces capsular contracture by activating innate immune response. *Plast Reconstr Surg*. (2023) 8:342–56. doi: 10.1097/PRS.0000000000011054

78. Rossol M, Heine H, Meusch U, et al. LPS-induced cytokine production in human monocytes and macrophages. *Crit Rev Immunol*. (2011) 31:379–446. doi: 10.1615/CritRevImmunol.v31.i5

79. Yamada H, Umemoto T, Kawano M, et al. High-density lipoprotein inhibits human M1 macrophage polarization through redistribution of caveolin-1. *Br J Pharmacol*. (2016) 173:741–51. doi: 10.1111/bph.13319

80. Guo L, Ai J, Zheng Z, Howatt DA, Daugherty A, Huang B, et al. High density lipoprotein protects against polymicrobe-induced sepsis in mice. *J Biol Chem*. (2013) 288:17947–53. doi: 10.1074/jbc.M112.442699

81. Anantharamaiah GM, Jones JL, Brouillette CG, Schmidt CF, Chung BH, Hughes TA, et al. Studies of synthetic peptide analogs of the amphipathic helix. Structure of complexes with dimyristoyl phosphatidylcholine. *J Biol Chem*. (1985) 260:10248–55. doi: 10.1016/S0021-9258(17)39238-4

82. Venkatachalapathi YV, Phillips MC, Epand RM, Epand RF, Tytler EM, Segrest JP, et al. Effect of end group blockage on the properties of a class A amphipathic helical peptide. *Proteins*. (1993) 15:349–59. doi: 10.1002/prot.340150403

83. Wool GD, Reardon CA, Getz GS. Apolipoprotein A-I mimetic peptide helix number and helix linker influence potentially anti-atherogenic properties. *J Lipid Res*. (2008) 49:1268–83. doi: 10.1194/jlr.M700552-JLR200

84. Stoekenbroek RM, Stroes ES, Hovingh GK. ApoA-I mimetics. *Handb Exp Pharmacol*. (2015) 224:631–48. doi: 10.1007/978-3-319-09665-0_21

85. Kelesidis T, Madhav S, Petcherski A, Cristelle H, O'Connor E, Hultgren NW, et al. The ApoA-I mimetic peptide 4F attenuates in *vitro* replication of SARS-CoV-2, associated apoptosis, oxidative stress and inflammation in epithelial cells. *Virulence*. (2021) 12:2214–27. doi: 10.1080/21505594.2021.1964329

86. Guo Y, Li W, Qian M, Jiang T, Guo P, Du Q, et al. D-4F ameliorates contrast media-induced oxidative injuries in endothelial cells via the AMPK/PKC pathway. *Front Pharmacol*. (2021) 15:11. doi: 10.3389/fphar.2020.556074

87. Paul S, Gangwar A, Bharg K, Ahmad Y. D-4F prophylaxis enables redox and energy homeostasis while preventing inflammation during hypoxia exposure. *BioMed Pharmacother*. (2021) 133:111083. doi: 10.1016/j.biopha.2020.111083

88. Lu J, Gao J, Sun J, Wang H, Sun H, Huang Q, et al. Apolipoprotein A-I attenuates peritoneal fibrosis associated with peritoneal dialysis by inhibiting oxidative stress and inflammation. *Front Pharmacol*. (2023) 28:14. doi: 10.3389/fphar.2023.1106339

89. McGrath KC, Li X, Twigg SM, Heather AK. Apolipoprotein-AI mimetic peptides D-4F and L-5F decrease hepatic inflammation and increase insulin sensitivity in C57BL/6 mice. *PloS One*. (2020) 15:e0226931. doi: 10.1371/journal.pone.0226931

90. Moreira RS, Irigoyen MC, Capcha JMC, Sanches TR, Gutierrez PS, Garnica MR, et al. Synthetic apolipoprotein A-I mimetic peptide 4F protects hearts and kidneys after myocardial infarction. *Am J Physiol Regul Integr Comp Physiol*. (2020) 318:R529–44. doi: 10.1152/ajpregu.00185.2019

91. Daskou M, Mu W, Sharma M, Vasilopoulos H, Heymans R, Ritou E, et al. ApoA-I mimetics reduce systemic and gut inflammation in chronic treated HIV. *PloS Pathog*. (2022) 18:e1010160. doi: 10.1371/journal.ppat.1010160

92. Gille A, Easton R, D'Andrea D, Wright SD, Shear CL. CSL-112 enhances biomarkers of reverse cholesterol transport after single and multiple infusions in healthy subjects. *Arterioscler Thromb Vasc Biol*. (2014) 34:2106–14. doi: 10.1161/ATVBAHA.114.303720

93. Nasr H, Torsney E, Poston RN, Hayes L, Gaze DC, Basser R, et al. Investigating the efect of a single infusion of reconstituted highdensity lipoprotein in patients with

symptomatic carotid plaques. *Ann Vasc Surg*. (2015) 29:1380–91. doi: 10.1016/j.avsg.2015.04.084

94. Richart AL, Reddy M, Khalaji M, Natoli AL, Heywood SE, Siebel AL, et al. ApoA-I nanoparticles delivered post myocardial infarction moderate infammation. *Circ Res*. (2020) 127:1422–36. doi: 10.1161/CIRCRESAHA.120.316848

95. Didichenko SA, Adam J, Navdaev AV, Wong M, Alhamdoosh M, Saxenhofer M, et al. Abstract 10491: CSL112 suppresses infammation in human monocyte-derived macrophages. *Circulation*. (2021) 144:A10491. doi: 10.1161/circ.144.suppl_1.10491

96. Mogilenko DA, Shavva VS, Dizhe EB, Orlov SV. Characterization of distal and proximal alternative promoters of the human apoA-I gene. *Mol Biol (Mosk)*. (2019) 53:485–96. doi: 10.1134/S0026898419030121

97. Frankel R, Sparr E, Linse S. On the aggregation of apolipoprotein A-I. *Int J Mol Sci*. (2022) 23:8780. doi: 10.3390/ijms23158780

98. Nilsson O, Lindvall M, Obici L, Ekström S, Lagerstedt JO, Del Giudice R. Structure dynamics of ApoA-I amyloidogenic variants in small HDL increase their ability to mediate cholesterol efflux. *J Lipid Res*. (2021) 62:100004. doi: 10.1194/jlr.RA120000920

99. Su X, Zhang G, Cheng Ye, Wang B. New insights into the emerging effects of inflammatory response on HDL particles structure and function. *Mol Biol Rep*. (2021) 48:5723–33. doi: 10.1007/s11033-021-06553-0

100. Zamanian-Daryoush M, Lindner DJ, Buffa J, Gopalan B, Na J, Hazen SL, et al. Apolipoprotein A-I anti-tumor activity targets cancer cell metabolism. *Oncotarget*. (2020) 11:1777–96. doi: 10.18632/oncotarget.v11i19

101. Chroni A, Kardassis D. HDL dysfunction caused by mutations in apoA-I and other genes that are critical for HDL biogenesis and remodeling. *Curr Med Chem*. (2019) 26:1544–75. doi: 10.2174/0929867325666180313114950

102. King TW, Cochran BJ, Rye K-A. ApoA-I and diabetes. *Arterioscler Thromb Vasc Biol*. (2023) 43:1362–8. doi: 10.1161/ATVBAHA.123.318267

103. Lee M, Lim J-S, Kim Y, Park SH, Lee S-H, Kim C, et al. High apoB/apoA-I ratio predicts post-stroke cognitive impairment in acute ischemic stroke patients with large artery atherosclerosis. *Nutrients*. (2023) 15:4670. doi: 10.3390/nu15214670

104. Zuin M, Cervellati C, Trentini A, Passaro A, Rosta V, Zimetti F, et al. Association between serum concentrations of apolipoprotein A-I (ApoA-I) and alzheimer's disease: systematic review and meta-analysis. *Diagnostics (Basel)*. (2021) 11:984. doi: 10.3390/diagnostics11060984

105. Lin J, Si Z, Wang A. Predictive value of ApoB/ApoA-I for recurrence within 1 year after first incident stroke. *Front Neurol*. (2024) 11:14. doi: 10.3389/fneur.2023.1308442

106. Nachar W, Merlet N, Maafi F, Mihalache-Avram T, Mecteau M, Gélinas D, et al. ApoA-I mimetic does not improve left ventricular diastolic dysfunction in rabbits without aortic valve stenosis. *Int J Cardiol*. (2021) 15:331. doi: 10.1016/j.ijcard.2020.12.089

107. Bloedon LT, Dunbar R, Duffy D, Pinell-Salles P, Norris R, DeGroot BJ, et al. Safety, pharmacokinetics, and pharmacodynamics of oral apoA-I mimetic peptide D-4F in high-risk cardiovascular patients. *J Lipid Res*. (2008) 49:1344–52. doi: 10.1194/jlr.P800003-JLR200

108. Watson CE, Weissbach N, Kjems L, Ayalasomayajula S, Zhang Y, Chang I, et al. Treatment of patients with cardiovascular disease with L-4F, an apo-A1 mimetic, did not improve select biomarkers of HDL function. *J Lipid Res*. (2011) 52:361–73. doi: 10.1194/jlr.M011098

109. D'Souza W, Stonik JA, Murphy A, Demosky SJ, Sethi AA, Moore XL, et al. Structure/function relationships of apolipoprotein a-I mimetic peptides: implications for antiatherogenic activities of high-density lipoprotein. *Circ Res*. (2010) 107:217–27. doi: 10.1161/CIRCRESAHA.110.216507

110. Gibson CM, Duffy D, Korjian S, Bahit MC, Chi G, Alexander JH, et al. Apolipoprotein A1 infusions and cardiovascular outcomes after acute myocardial infarction. *N Engl J Med*. (2024) 390:1560–71. doi: 10.1056/NEJMoa2400969

frontiers | Frontiers in Pharmacology

TYPE Original Research
PUBLISHED 29 August 2024
DOI 10.3389/fphar.2024.1439678

OPEN ACCESS

EDITED BY
Paola Patrignani,
University of Studies G.d'Annunzio Chieti and Pescara, Italy

REVIEWED BY
Stefania Tacconelli,
University of Studies G.d'Annunzio Chieti and Pescara, Italy
Tao Zhang,
Anhui Agricultural University, China

*CORRESPONDENCE
Wenjie Ren,
wjren1966@163.com
Xiaohua Liao,
504034593@qq.com
Lei Wang,
lwang0522@163.com

†These authors have contributed equally to this work

RECEIVED 28 May 2024
ACCEPTED 21 August 2024
PUBLISHED 29 August 2024

CITATION
Qian Z, Xu J, Zhang L, Deng Q, Fan Z, Guo X, Liang Z, Wang W, Wang L, Liao X and Ren W (2024) AFK-PD alleviated osteoarthritis progression by chondroprotective and anti-inflammatory activity .
Front. Pharmacol. 15:1439678.
doi: 10.3389/fphar.2024.1439678

AFK-PD alleviated osteoarthritis progression by chondroprotective and anti-inflammatory activity

Zhuang Qian[1†], Jie Xu[1†], Lei Zhang[1†], Qian Deng[1], Zhenlin Fan[1], Xueqiang Guo[1], Zhuo Liang[1], Weiyun Wang[1], Lei Wang[1*], Xiaohua Liao[2*] and Wenjie Ren[1*]

[1]Clinical Medical Center of Tissue Engineering and Regeneration, Institutes of Health Central Plain, The Third Affiliated Hospital of Xinxiang Medical University, Xinxiang Medical University, Xinxiang, China, [2]Department of Rheumatology and Immunology, Nanjing Drum Tower Hospital, The Affiliated Hospital of Nanjing University Medical School, Nanjing, China

Osteoarthritis (OA) is the most prevalent cartilage degenerative and low-grade inflammatory disease of the whole joint. However, there are currently no FDA-approved drugs or global regulatory agency-approved treatments OA disease modification. Therefore, it's essential to explore novel effective therapeutic strategies for OA. In our study, we investigated the effects of AFK-PD, a novel pyridone agent, on the development of OA induced by destabilization of the medial meniscus (DMM) *in vivo*, and its impact on the function of chondrocytes treated with IL-1β *in vitro*. Our results demonstrated AFK-PD alleviated OA progression through inhibiting cartilage degeneration, articular inflammation and osteophyte formation. Notably, AFK-PD inhibited chondrocyte inflammation and synovial macrophage M1 polarization, leading to the attenuation of articular inflammation. Additionally, AFK-PD promoted chondrocyte anabolism while mitigating catabolism and apoptosis, effectively inhibiting cartilage degeneration. Mechanistically, AFK-PD suppressed the expression of key signaling molecules involved in the MAPK pathway, such as p-ERK1/2 and p-JNK, as well as the NF-κB signaling molecule p-p65, in IL-1β-induced chondrocytes. These findings suggest AFK-PD ameliorates the development of OA by protecting chondrocyte functions and inhibiting articular inflammation in chondrocytes and synovial macrophages. Overall, our study highlights AFK-PD as a promising therapeutic candidate for the treatment of OA.

KEYWORDS

AFK-PD, osteoarthritis, chondrocyte, inflammation, MAPK/ NF-κB pathways

1 Introduction

OA is the most prevalent chronic musculoskeletal disease characterized by pain and disability. It is widely recognized that OA is a whole joint disease characterized by cartilage degeneration, synovial inflammatory (synovitis), osteophyte formation and subchondral bone remodeling. Synovial and articular inflammatory environment within the joint are the key factors for chondrocyte apoptosis and cartilage degeneration. Specifically, degraded cartilage matrix releases damage-associated molecular patterns (DAMPs), which trigger

inflammatory responses of chondrocytes and synovial macrophages by secreting proinflammatory cytokines (including IL-1β, TNF-α and IL6) and matrix-degradative enzymes such as matrix metalloproteinases (MMPs) (Zhang et al., 2020; Hashizume et al., 2024). Nowadays, conventional non-steroidal anti-inflammatory drugs (NSAIDs) are widely used to alleviate joint inflammation. However, they only provide symptomatic relief without improving cartilage degeneration and are associated with inevitable side effects (Zhou et al., 2019). Therefore, it's important to explore novel effective therapeutic strategies for OA.

IL-1β is a major inducer of chondrocytes inflammation and metabolism imbalance. When exposed to IL-1β inflammatory stimuli, catabolic factors (MMP13) are increased whereas anabolic factors (Col2a1, Acan and Sox9) are decreased. This imbalance in chondrocyte metabolism and the subsequent apoptosis ultimately lead to cartilage degradation (Wang et al., 2023). A large number of research have confirmed MAPK and NF-κB signaling pathways were activated in OA cartilage and IL-1β-induced mouse chondrocytes (Saklatvala, 2007). In detail, during OA progression, inflammatory mediators (such as IL-1β) induce phosphorylation of p38, JNK, and ERK1/2, the key factors of in MAPK signaling pathway, and translocation of these phosphorylated factors to the nucleus in chondrocytes. In addition, inflammatory mediators also activate the phosphorylation and nucleus translocation of NF-κB p65, the key factor in NF-κB signaling pathway, in chondrocytes. These phosphorylated factors further lead to the release of pro-inflammatory cytokines, metaloproteinases (MMPs) and aggrecanases, which shift chondrocytes metabolism towards a catabolic state, ultimately leading to chondrocytes apoptosis and cartilage matrix degeneration (Yan et al., 2020; Gratal et al., 2022; Lu et al., 2023). So, targeting inflammation-associated factors and signaling pathways holds promise as alternative and innovative therapies.

AKF-PD (1-(3-fluorophenyl)-5-methyl-2-(1H)-pyridone), referred to as Fluorofenidone, is a novel low-molecular-weight pyridone agent. Increasing evidence has demonstrated AFK-PD possesses various pharmacological properties, including anti-inflammation, anti-apoptosis and anti-oxidative in conditions such as liver fibrosis, liver failure, kidney injury and lung injury (Jiang et al., 2019; Lv et al., 2021; Tu et al., 2021; Gu et al., 2023). Recently, it has been shown that Pirfenidone, an analogue of AFK-PD, attenuated OA progression by inhibiting synovial fibrosis and inflammation (Wei et al., 2021). In addition, Many of studies have uncovered AFK-PD had anti-inflammatory and anti-apoptotic effects by restraining MAPK and NF-κB pathways in many of diseases such as liver fibrosis, kidney injury and lung injury (Peng et al., 2013; Qin et al., 2015; Tang et al., 2015; Jiang et al., 2019; Peng et al., 2019; Lv et al., 2021; Tu et al., 2021; Gu et al., 2023). However, it's unclear whether AFK-PD ameliorates OA progression by regulating chondrocyte inflammation and metabolism, as well as the MAPK and NF-κB signaling pathways involved in such fine-tuned regulation.

In this study, we aimed to investigate the impact of AFK-PD on the progression of OA and elucidate the underlying mechanism by which AFK-PD regulates inflammation and chondrocyte metabolism in IL-1β-induced mouse chondrocytes. Our findings demonstrated that AFK-PD effectively inhibited synovial and chondrocytes inflammation and shifted chondrocytes catabolic to anabolic metabolism via mitigating MAPK/NF-κB signaling. Ultimately, these effects resulted in the amelioration of OA progression.

2 Materials and methods

2.1 Primary chondrocytes extract and treatment

Primary chondrocytes were isolated from the femoral condyles and tibial plateau of 3-day-old mice, following the previously described methods (Salvat et al., 2005; Gosset et al., 2008). Briefly, the mice were euthanized and sterilized with 75% ethanol for 2 min. The articular cartilage was then isolated from the femoral condyles and tibial plateau under a dissecting microscope. Subsequently, the articular cartilage was incubated in 0.2% collagenase (C5138, Sigma-Aldrich, Missouri, United States) for 30 min at 37°C. After three washes with PBS, the articular cartilage was incubated in 0.2% collagenase for an additional 3 h at 37°C. The resulting cell suspension was aspirated repeatedly and filtered through a 100-μm cell strainer. The cells were then rinsed in PBS, counted, and seeded in 6-well plates at a density of 1 million cells per well in DMEM (11965092, Thermo Fisher Scientific, Massachusetts, United States) supplemented with 100 units/mL penicillin, 100 μg/mL streptomycin, 50 μg/mL ascorbic acid, and 10% fetal bovine serum (A5670701, Thermo Fisher Scientific, Massachusetts, United States). The chondrocytes were subsequently treated with recombinant IL-1β (10 ng/mL; P06804, R&D Systems, Minnesota, United States) and AFK-PD (Provided by Professor Lijian Tao from Central South University) for 24 h.

2.2 Cell viability

Cell viability was assessed by Cell Counting Kit-8 (BS350B, Biosharp, Wuhan, China) following the manufacturer's instructions. Primary chondrocyte (8×10^3/well) seeded in 96-well plates were exposed to AFK-PD at various concentrations for 48 h. Subsequently, the absorbance was recorded at 450 nm using a microplate reader (Bio-Rad, Hercules, CA, United States) (Lou et al., 2023).

2.3 Knee osteoarthritis model

The adult C57/BL6 mice were purchased from Beijing Vital River Laboratory Animal Technology Co. Ltd.

Osteoarthritis was established in 8-week-old male mice by destabilizing the medial meniscus (DMM) following previous studies (Glasson et al., 2007). Briefly, mice firstly were anesthetized with isoflurane (1349003, Sigma-Aldrich, Missouri, United States). The right knee was then subjected to the transection of the medial meniscotibial ligament under a dissecting microscope. The sham operation was only subjected with medial capsulotomy in right knee. The mice that underwent the DMM procedure were randomly divided into two groups (n = 8).

One week after the operation, AFK-PD treated group received an intra-articular injection of 8 μL AFK-PD (dissolved in saline at a concentration of 400 μg/mL). The control group was injected with saline. In the sham group, mice were injected with the same volume of saline (n = 8). All group were administered intra-articular injection once a week for 7 weeks.

All animal studies were authorized and conducted in accordance with the Animal Care and Use Committee of Xinxiang Medical University.

2.4 Histological analysis

After 8-week OA surgery, mice were sacrificed and the right knee joints were fixed in 4% paraformaldehyde. Subsequently, decalcification was performed using 10% EDTA for 4 weeks, and the joints were embedded in paraffin. Coronal sections with a thickness of 4 μm were obtained through the knee joints. These sections were stained with Safranin O/Fast Green (G1371, Solarbio, Nanjing, China) according to the recommended protocol. Histologic changes of articular cartilage were scored using recommended Osteoarthritis Research Society International (OARSI) (cartilage OA histopathology scoring system, on a scale of 0–6) (Glasson et al., 2010). Additionally, the sections were stained with hematoxylin and eosin (H&E) (G1120, Solarbio, Nanjing, China) to assay joint synovitis using synovitis scoring system (Gerwin et al., 2010).

All slides were evaluated independently by two investigators who were blinded to the treatment regimen.

2.5 Micro-computed tomography (micro-CT)

Mice knee joints were fixed in 4% PFA, and subsequently, the microstructure of the joints was analyzed using a micro-CT scanner (mCT80; Scanco Medical AG) as described (Li et al., 2022). The three-dimensional (3D) reconstruction images of the joints were obtained using Scanco Medical software.

2.6 Immunohistochemistry

Immunohistochemical staining was performed using the DAB staining method according to the recommended protocol. Briefly, after deparaffinization and rehydration, antigen retrieval was carried out using 2.5 mg/mL trypsin for 40 min. The sections were then treated with 3% H_2O_2 for 10 min to block endogenous peroxidase activity. Subsequently, after blocking with 5% BSA (37,520, Thermo Fisher Scientific, Massachusetts, United States) for 1 h at 37°C, the sections were incubated overnight at 4°C with the primary antibody. On the following day, the sections were incubated with HRP-labeled secondary antibodies for 1 h at 37°C. The protein expression signal was visualized as a brown reaction product using the peroxide substrate 3,3′-diaminobenzidine (DAB) (ZLI-9017, ZSGB-BIO, Beijing, China), and counterstained with hematoxylin. The number of stained cells was counted in five random high-magnification fields within the articular cartilage by three investigators who were blinded to the treatment regimen. The average percentage of positive cells to total cells was calculated.

2.7 Immunofluorescence staining

Immunofluorescence staining was performed on 4 μm paraffin sections. Briefly, after deparaffinization, rehydration, and antigen retrieval, the sections were incubated overnight at 4°C with the indicated primary antibodies. Subsequently, the sections were incubated with fluorochrome-labeled secondary antibodies (Fluor 488 or TRITC) (115-025-003 and 115-545-003, Pennsylvania, United States) at 37°C for 1.5 h. Nuclei were stained with 4,6-diamidino-2-phenylindole (DAPI) (P0131, Beyotime Biotechnology, Shanghai, China) for 15 min at room temperature. Images were captured using a fluorescence microscope (Nikon Eclipse Ti-S, Tokyo, Japan). The number of positive cells was quantified in five random high-magnification fields within the articular cartilage by three investigators who were blinded to the treatment regimen. The average percentage of positive cells to total cells was calculated.

2.8 Chondrocytes micro-mass culture and alcian blue staining

The 20 μL suspension containing primary 2×10^5 chondrocytes in DMEM medium was dropped into each well of 24-well plate. After 2 h, micro-masses were treated with IL-1β and AFK-PD in DMEM with 10% FBS for 7 days. Alcian blue staining was performed with Alcian Blue Stain Kit (G1565, Solarbio, and Beijing, China) according to the recommended protocol. The micro-masses were washed with PBS, fixed with paraformaldehyde for 10 min, rinsed with 0.1 N HCl, and then stained with 1% alcian blue at room temperature for 30 min (Atsuta et al., 2019).

2.9 RAW264.7 cells culture

RAW264.7 cells were obtained from the Cell Bank of Type Culture Collection of Chinese Academy of Science (Shanghai, China) and cultured in DMEM supplemented with 10% fetal bovine serum and 100 units/mL penicillin and 100 μg/mL streptomycin at 37°C and 5% CO_2 condition. 1×10^5 RAW264.7 cells were polarized to M1 macrophage with 50 ng/mL lipopolysaccharide (LPS) (#L2630, Sigma-Aldrich, St. Louis, MO, United States), and subsequently treated with AFK-PD (400 μg/mL for 24 h to detect the mRNA level of M1-related markers).

2.10 TUNEL assay

Apoptotic cells from articular cartilage and primary chondrocytes were detected by *In Situ* Cell Death Detection Kit (No.12156792910, Roche, Mannheim, Germany), according to the manufacturer's instructions. TUNEL-labeled cells visualized as red

fluorescence, while nuclei were counterstained with DAPI. The percentage of TUNEL-positive cells was calculated as the number of labeled cells/total cells per high-magnification field. All determinations were made by the same observer blinded to the treatment category.

2.11 Western blot

The cells were washed with chilled PBS and lysed in a lysis buffer. The lysates were then subjected to 10% sodium dodecyl sulfate-polyacrylamide gel electrophoresis (SDS-PAGE) and transferred to polyvinylidene difluoride (PVDF) membranes. Following transfer, the membranes were incubated overnight at 4°C with the respective primary antibodies as indicated. The next day, the membranes were incubated with secondary antibodies for 60 min. Subsequently, the protein bands were visualized using an enhanced chemiluminescence detection system (WBKLS0100, Millipore, Burlington, United States). The resulting bands were quantified using the ImageJ software through densitometry analysis (Qian et al., 2023).

2.12 RNA extraction and quantitative real-time PCR

Total RNA was extracted from cells using RNA-Quick Purification Kit (RN001, ES Science, Shanghai, China). The isolated RNA was reverse transcribed using HiScript Ill 1st Strand cDNA Synthesis Kit (R312-02, Vazyme, Nanjing, China) to synthesize cDNA. Real-time quantitative PCR was carried out in a MJ Mini Real-Time PCR Detection System using Taq Pro Universal SYBR qPCR Master Mix (Q712-02, Vazyme, Nanjing, China). Gene expression was normalized to GAPDH, and relative expression was calculated using the $2^{-(\Delta\Delta Ct)}$ method. The following primer sequences were described in Supplementary Table S2.

2.13 Statistical analysis

All the data were presented as the mean ± SD. Data analysis was conducted using PASW Statistics 17 (SPSS Inc.). And statistical significance was determined by an unpaired, two-tailed Student t test between the 2 groups or one-way ANOVA for more than 2 groups. Values of $p < 0.05$ were considered statistically significant.

3 Results

3.1 Effect of AFK-PD on metabolism and apoptosis of IL-1β-induced chondrocytes

Firstly, the cytotoxicity of AFK-PD on mouse primary chondrocytes was tested using CCK-8. The results showed that AFK-PD had no cytotoxicity at concentration of 0–400 μg/mL (Supplementary Figure S1). Furthermore, we explored the protein expression of MMP13, a catabolic marker for chondrocytes, in primary IL-1β-induced chondrocytes treated with AFK-PD at concentration of 0–400 μg/ml. As shown in Supplementary Figure S2, AFK-PD at concentrations of 200 and 400 μg/mL significantly inhibited the MMP13 expression in IL-1β-induced chondrocytes. Based on many of evidence confirming the effective concentration of AFK-PD to be 400 μg/mL in different kinds of cells (Jiang et al., 2019; Lv et al., 2021; Tu et al., 2021; Gu et al., 2023), subsequent experiments involving AFK-PD treatment were performed at this concentration.

To clearly study the effect of AFK-PD on chondrocyte's metabolism, we firstly detected the mRNA expression level of catabolic and anabolic makers in AFK-PD-treated primary chondrocytes using RT-qPCR analysis. The results exhibited the increased expression of anabolic makers (Sox9, Acan and Col2a1) but no markedly difference of catabolic marker Mmp13 in AFK-PD-treated chondrocytes compared to control (Figures 1A–D). Additionally, when primary chondrocytes were induced with IL-1β for 24 h, AFK-PD ameliorated the IL-1β-mediated low expression of anabolic makers and high expression of Mmp13 (Figures 1A–D). We further confirmed the effect of AFK-PD at the protein level. Western blot experiments uncovered AFK-PD increased Collagen II expression but had no effect on MMP13 expression in chondrocytes (Figures 1E–G). After IL-1β intervention, Collagen II expression was inhibited, and MMP13 expression was enhanced. Moreover, AFK-PD rescued the decreased Collagen II and increased MMP13 in chondrocytes induced by IL-1β (Figures 1E–G). Similar results are also observed in immunofluorescence (IF) analysis (Figure 2A). Next, chondrocyte micro-mass cultures were used to assess the contribution of AFK-PD to chondrocyte differentiation. After 6 days of AFK-PD treatment, alcian blue staining displayed a more robust stain in AFK-PD-treated chondrocytes compared to the control. Moreover, AFK-PD improved the reduced stain in IL-1β-induced chondrocytes (Figure 2B).

Because of the important role of chondrocytes apoptosis in OA progression (Hosseinzadeh et al., 2016), we further explored the influence of AFK-PD on apoptosis in chondrocytes with or without IL-1β using TUNEL staining. As showed in Figure 2A, there were no chance observed between AFK-PD and control chondrocytes. However, AFK-PD inhibited the high occurrence of TUNEL-positive cells in IL-1β-induced chondrocytes. The above results indicated AFK-PD promoted chondrocyte's anabolism, as well as inhibited chondrocyte's catabolism and apoptosis in IL-1β-induced chondrocytes.

3.2 AFK-PD inhibited inflammation in IL-1β-induced chondrocytes

Considering IL-1β as a major inducer of chondrocytes inflammation (Wang et al., 2023), we studied the involvement of AFK-PD in inflammation in IL-1β-induced chondrocytes. RT-qPCR results revealed no significant difference in the mRNA expression of *Inos, Il6* and *Cxcl5* but a decreased expression of *Cox2*, *Il1b* and *Cxcl3* in chondrocytes after AFK-PD treatment. However, AFK-PD obviously inhibited IL-1β-induced high mRNA expression of *Inos*, *Cox2*, *Il6*, *Il1b*, *Cxcl3* and *Cxcl5* in primary chondrocytes (Supplementary Figure S3). These data suggested AFK-PD suppressed IL-1β-induced inflammation in chondrocytes.

10.3389/fphar.2024.1439678

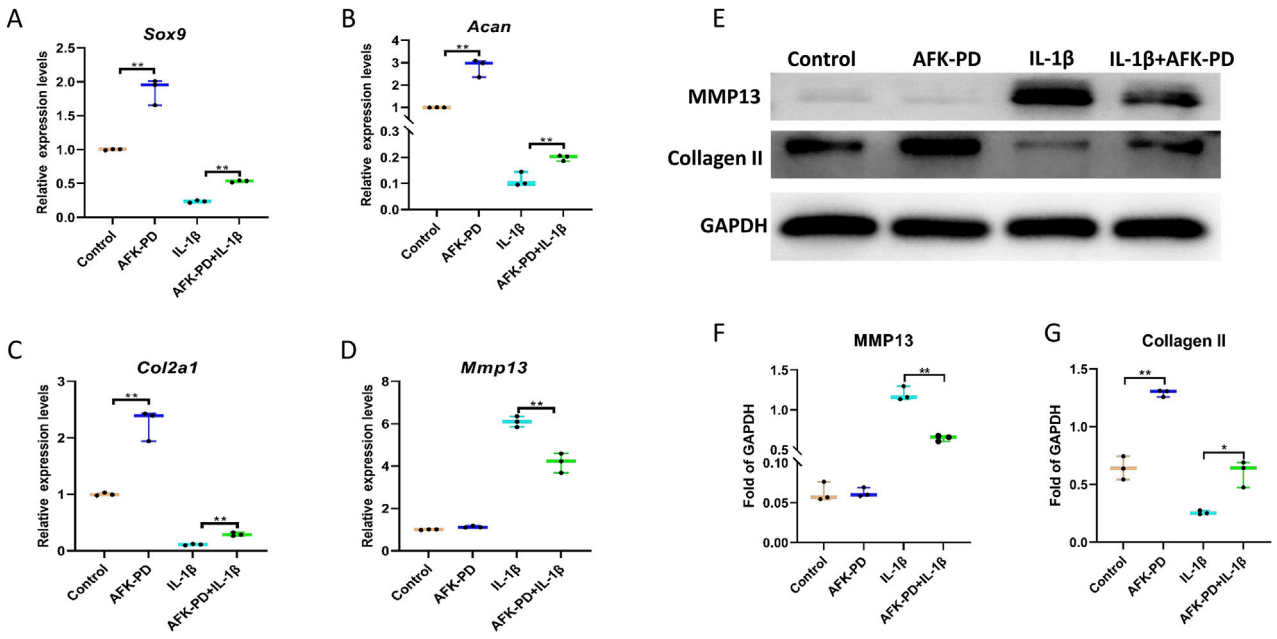

FIGURE 1
The influence of AFK-PD on chondrocyte anabolism and catabolism in IL-1β-induced primary chondrocyte. Primary chondrocytes were isolated from the femoral condyles and tibial plateau of 3-day-old mice. **(A–D)** RT-qPCR for Sox9, Aggrecan, Col2a1 and Mmp13 in IL-1β-induced primary chondrocyte with or without AFK-PD. **(E)** Western blot for Collagen II and MMP13 in IL-1β-induced primary chondrocyte with or without AFK-PD. And quantitative of Collegan II and Mmp13 was shown on the bottom **(F, G)**. Data are presented as mean ± SD. (n = 3/group, Student t test; *$p < 0.05$, **$p < 0.01$).

3.3 AFK-PD restrained MAPK and NF-KB pathways in IL-1β-induced chondrocytes

To further explore the potential molecular mechanisms underlying the effect of AFK-PD on IL-1β-induced chondrocytes function, we performed RNA-sequencing analysis on IL-1β-induced chondrocytes with and without AFK-PD treatment. The volcano plot showed differentially expressed genes (DEGs) between AFK-PD-treated and control chondrocytes in the presence of IL-1β. Among these DEGs, 457 genes were downregulated and 260 genes were upregulated in AFK-PD-treated chondrocytes compared to control chondrocytes (Figure 3A). Furthermore, Kyoto Encyclopedia of Genes and Genomes (KEGG) analysis exhibited the top 20 enrichment signaling pathways (Figure 3B). Notably, the MAPK and NF-κB signaling pathways, which are known to play important roles in chondrocyte differentiation, apoptosis, and inflammation (Lu et al., 2023), were among the identified pathways (Figure 3B).

First, we examined the expression of key factors in the MAPK signaling pathway, namely, p-ERK1/2, p-JNK, and p-p38, in chondrocytes with or without AFK-PD treatment. Western blot revealed AFK-PD inhibited the protein expression of p-ERK1/2 but had no effect on p-JNK and p-p38. And also, AFK-PD decreased IL-1β-induced high expression of p-ERK1/2 and p-JNK (Figures 3C–F) in chondrocytes. Similar results were confirmed by IF analysis (Figures 4A, B). Next, we assessed the expression of p-p65, a key factor in the NF-κB signaling pathway, using western blot analysis. AFK-PD-treated chondrocytes showed decreased expression of p-p65 compared to the control. Moreover, AFK-PD mitigated the increased expression of p-p65 in chondrocytes induced by IL-1β (Figures 3C, G). Similarly, IF analysis revealed that AFK-PD resulted in decreased expression of p-p65 in chondrocytes with or without IL-1β stimulation (Figure 4C). Hence, it was proposed that AFK-PD inhibited MAPK and NF-κB pathways in IL-1β-induced chondrocytes.

3.4 AFK-PD ameliorated the development of DMM-induced OA

The above results demonstrate that AFK-PD inhibits catabolic metabolism, apoptosis, and inflammation while promoting anabolic metabolism in IL-1β-induced chondrocytes *in vitro*. To further dissect the contribution of AFK-PD to the progression of OA, we conducted *in vivo* experiments. Mice underwent destabilized medial meniscus (DMM) surgery or sham surgery on their right knees. One week post-operation, mice were administrated intra-articular injection of AKK-PD once a week. After 7-week treatment, histological changes of articular cartilage were evaluated using Safranin-O staining and scoring of OARSI grade. Sham-operated mice showed no changes in the articular cartilage, while DMM-operated mice exhibited extensive loss of Safranin-O staining and vertical erosion extending to the calcified cartilage, encompassing over 25% of the area. However, AFK-PD-treated OA mice revealed minimal loss of Safranin-O staining and cartilage (Figure 5A). Further, the OARSI scoring system revealed lower scores in AFK-PD-treated OA mice compared to OA mice (Figure 5B).

Micro-CT was subjected to assess osteophyte formation, a major pathological feature of OA. Sham-operated mice showed no signs of osteophyte formation, while OA mice exhibited numerous

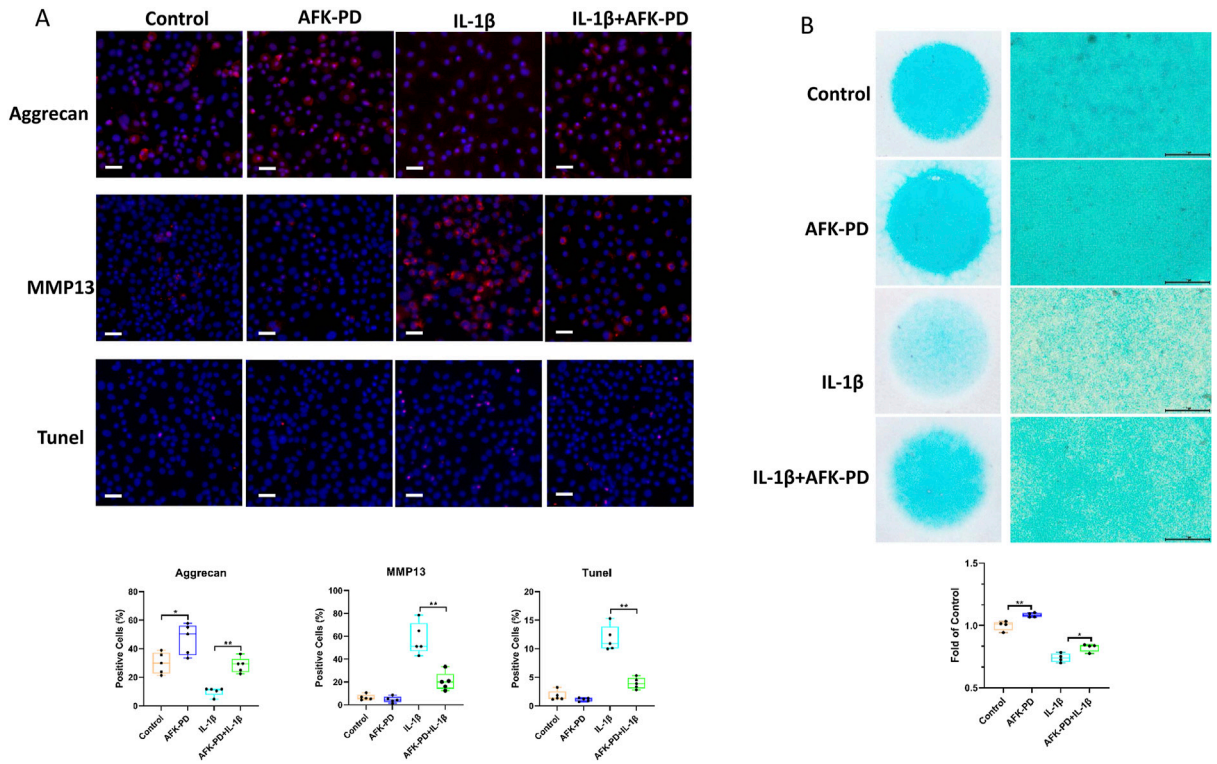

FIGURE 2
The effects of AFK-PD on chondrocyte anabolism, catabolism and apoptosis in IL-1β-induced primary chondrocyte. **(A)** The alcian blue staining of chondrocyte micro-mass in IL-1β-induced primary chondrocyte with or without AFK-PD for 6 /s (scale bars: 500 μm). The alcian blue staining was quantized on the bottom (n = 4). **(B)** The immunofluorescence for Aggrecan, MMP13 and TUNEL expression in primary chondrocyte IL-1β-induced primary chondrocyte with or without AFK-PD (scale bars: 50 μm). And quantitative of the positive cells was shown on the bottom (n = 5). Data are presented as mean ± SD. (Student t test; *$p < 0.05$, **$p < 0.01$).

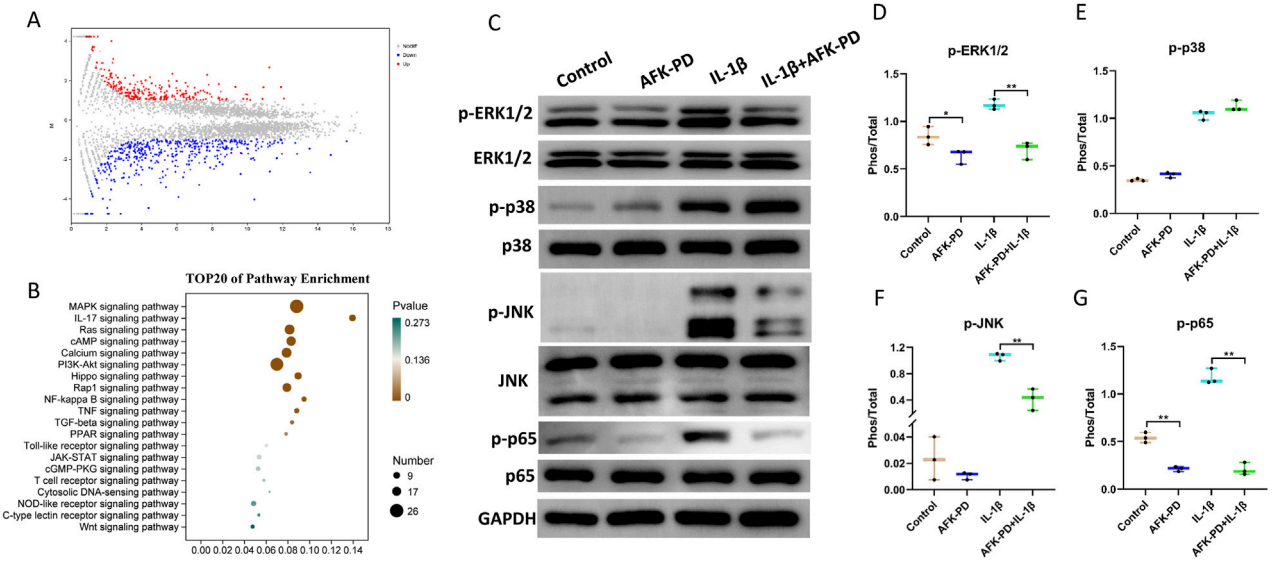

FIGURE 3
AFK-PD inhibited MAPK and NF-κB pathways in IL-1β-induced primary chondrocytes. **(A)** Volcano plot of RNA-seq analysis for differentially expressed genes between IL-1β-induced primary chondrocyte with and without AFK-PD. **(B)** Bar plot showing the top 20 enriched KEGG pathways in the differentially expressed genes between IL-1β-induced primary chondrocyte with and without AFK-PD. **(C)** Western blot for the protein expression of p-ERK1/2, ERK1/2, p-p38, p38, p-JNK, JNK, p-P65 and p65 in L-1β-induced primary chondrocyte with or without AFK-PD. Quantitative of the protein expression is was shown on the right **(D–G)**. Data are presented as mean ± SD. (n = 3/group, Student t test; *$p < 0.05$, **$p < 0.01$).

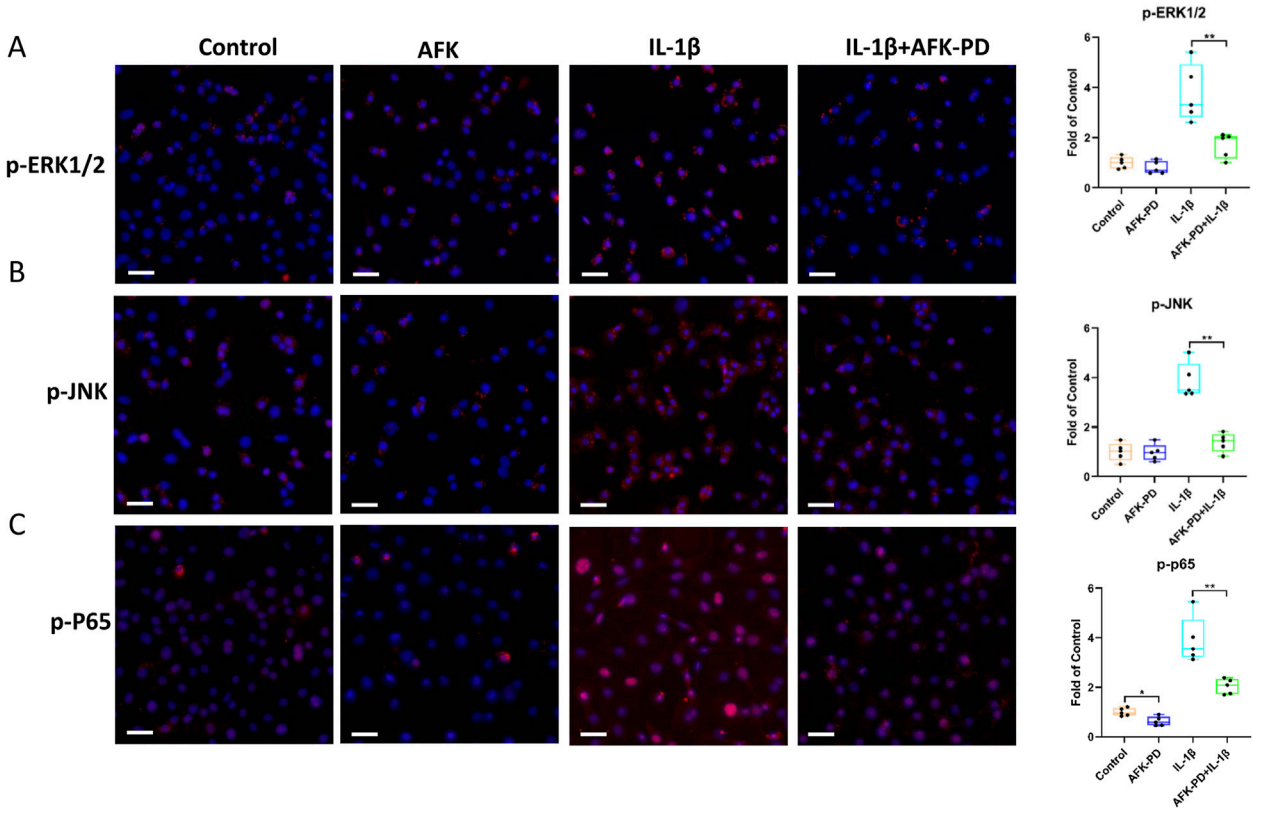

FIGURE 4
AFK-PD restrained MAPK and NF-κB pathways in IL-1β-induced primary chondrocytes. **(A–C)** The immunofluorescence for p-ERK1/2, p-JNK and p-p65 expression in primary chondrocyte IL-1β-induced primary chondrocyte with or without AFK-PD (scale bars: 50 μm). And quantitative of the positive cells was shown on the right. Data are presented as mean ± SD. (n = 5/group, Student t test; $*p < 0.05$, $**p < 0.01$).

osteophytes around the tibial plateau and femoral condyles. Following AFK-PD treatment, the results showed a lower number of osteophytes in AFK-PD-treated OA mice compared to OA mice (Figures 5C, D). So, the above data indicated AFK-PD ameliorated cartilage degeneration and osteophyte formation in OA progression.

3.5 Effect of AFK-PD on chondrocyte metabolism and apoptosis in OA cartilage

To further elucidate the cellular mechanism underlying AFK-PD-mediated alleviation of OA progression, we detected the expression of chondrocyte factors related to OA progression. Immunohistochemistry was subjected to assess chondrocyte anabolic factor Aggrecan in articular cartilage. As seen in Figure 6A, the cartilage of OA mice had lower Aggrecan expression than sham mice, but AFK-PD-treated OA mice showed more robust expression of Aggrecan in articular cartilage than OA mice. Next, IF analysis demonstrated an increased expression level of MMP13 in the cartilage of OA mice compared to sham mice. However, AFK-PD treatment rescued the higher expression of MMP13 in the cartilage of OA mice (Figure 6B). Furthermore, we determined the contribution of AFK-PD to chondrocyte apoptosis in cartilage of OA mice using TUNEL staining. The analysis revealed an increased number of TUNEL-positive cells in the cartilage of OA mice compared to sham mice. However, AFK-PD treatment alleviated the enhanced number of TUNEL-positive cells in the cartilage of OA mice (Figure 6C). The above results suggest that AFK-PD ameliorates cartilage degeneration by inhibiting chondrocyte catabolic metabolism and apoptosis while promoting anabolic metabolism.

3.6 AFK-PD inhibited synovial inflammation by dampening M1 macrophage polarization

Considering the vital contribution of synovial inflammation to initiation and progression of OA (Sanchez-Lopez et al., 2022), H&E staining was carried out to assess synovial inflammation. Synovium of OA mice revealed high levels of synovial hyperplasia and abundant cell infiltration, characteristic of synovitis, along with higher synovitis scores compared to sham mice (Figures 7A, B). However, after AFK-PD treatment, a decrease in synovial hyperplasia and cell infiltration was observed along with lower synovitis scores in the synovium compared to OA mice (Figures 7A, B). Synovitis is mainly characterized by enhancing synovial M1 macrophages (pro-inflammation macrophage) (Zhang et al., 2018). Thus, we detected the expression of M1 macrophage markers (CD80 and iNOS) in the synovium using IF. As shown in Figure 7C,

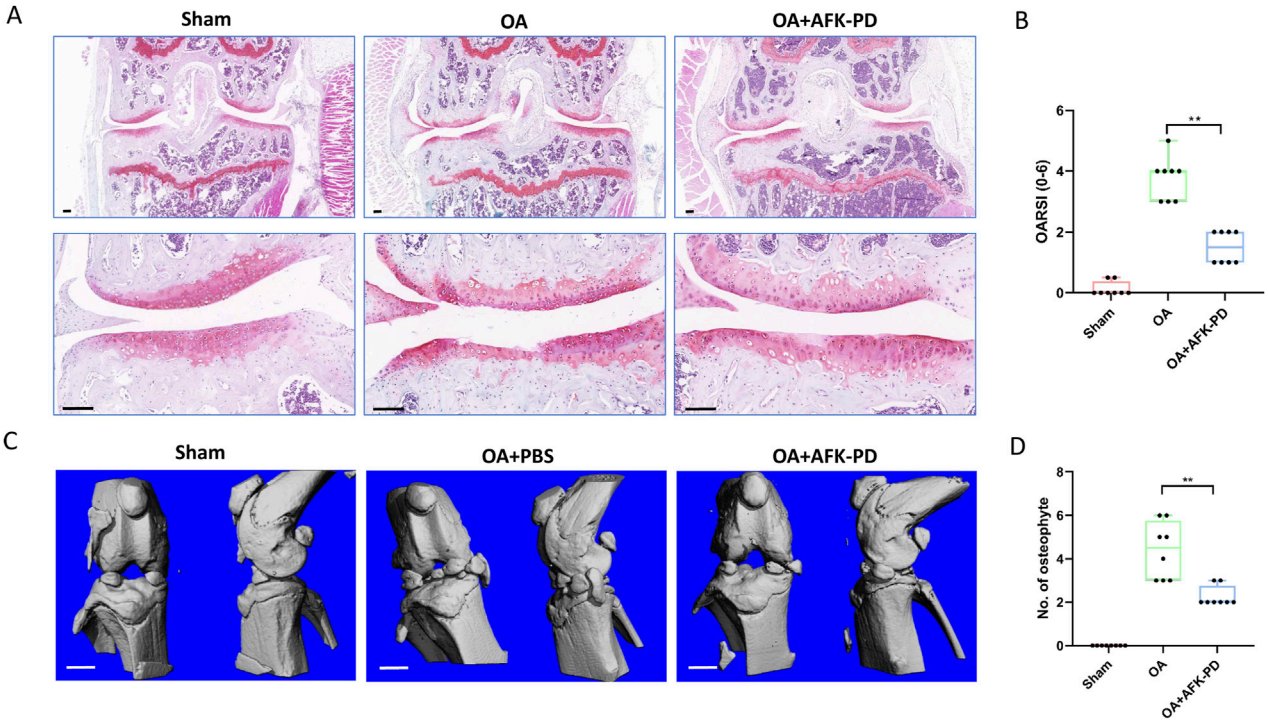

FIGURE 5
AFK-PD inhibited articular cartilage degradation and osteophyte formation at 8 weeks post-OA surgery. **(A)** The safranin O–fast green staining of knee joint in sham, OA and OA + AFK-PD mice (scale bars: 100 μm). **(B)** OARSI scores of the medial femoral condyle and tibial plateau in sham, OA and OA + AFK-PD mice (n = 8). **(C)** 3D reconstructed images of mice knee joints from sham, OA and OA + AFK-PD mice (scale bars: 1 mm). **(D)** Quantified changes in number of osteophytes. Data are presented as mean ± SD (n = 8/group, Student t test; $*p < 0.05$, $**p < 0.01$).

the expression of these markers uncovered more robust in synovium of OA mice compared to sham mice, but AFK-PD treatment partially inhibited their high expression.

Above results indicated AFK-PD inhibited M1 macrophage polarization in OA synovium. We further confirmed the effect of AFK-PD on macrophage M1 polarization in RAW264.7 cells induced by LPS. RT-qPCR results revealed AFK-PD had no effect on M1-related markers (*Il6*, *Inos*, *Il1b* and *Mmp13*) in RAW264.7 cells without LPS. However, AFKP-PD attenuated the LPS-induced high mRNA expression of these M1-related markers in RAW264.7 cells (Supplementary Figure S4AD). IF further confirmed AFK-PD rescued the increased protein expression of iNOS in RAW264.7 cells with LPS (Supplementary Figure S4E). These results indicated that AFK-PD suppresses synovial inflammation by inhibiting M1 macrophage polarization.

4 Discussion

OA is the most prevalent joint disease characterized by cartilage degeneration and low-grade inflammation. The articular inflammatory environment is the key factor contributing to cartilage degeneration (Sanchez-Lopez et al., 2022). Currently, early-stage OA was widely treated with nonsteroidal anti-inflammatory drugs (NSAIDs) to only symptom relief, but these treatments are unable to prevent cartilage degeneration (Liu-Bryan and Terkeltaub, 2015). Consequently, end-stage OA was often submitted to replacement arthroplasty. To date, no effective and available drugs to prevent and treat OA. Therefore, it is an urgent concern to develop new therapeutic drugs that can effectively prevent the deterioration of joint cartilage in osteoarthritis. In our study, we found AFK-PD, a novel pyridone agent, inhibited IL-1β-induced chondrocyte inflammation. And also, AFK-PD improved synovitis in OA mice by inhibiting M1 macrophages polarization. Similar effects were observed as AFK-PD ameliorated lethal endotoxemia in mice by inhibiting the production of TNF-α and IL-1β in M1 macrophages (Tang et al., 2010). Other studies showed AFK-PD restrained inflammation of renal injury by reducing the expression of chemokines, pro-inflammatory cytokines and NLRP3 inflammasome in mouse peritoneal M1 macrophages (Tang et al., 2015; Liao et al., 2021). AFK-PF also mitigated the inflammation of hepatic cirrhosis by inhibiting peritoneal M1 macrophages. Furthermore, AFK-PD inhibits inflammation in acute lung injury by reducing the number of F4/80-labeled macrophages in mice lungs (Lv et al., 2021). Our results indicated that AFK-PD inhibited both chondrocyte and macrophage-mediated inflammation.

As is widely recognized, the imbalance between chondrocyte catabolic and anabolic metabolism is the direct driver of cartilage degeneration during OA progression (Segarra-Queralt et al., 2024). Therefore, we explored the contribution of AFK-PD to chondrocyte's metabolism. Without IL-1β interference, AFK-PD enhanced anabolic metabolism and decreased catabolic metabolism in primary chondrocyte. And AFK-PD rescued

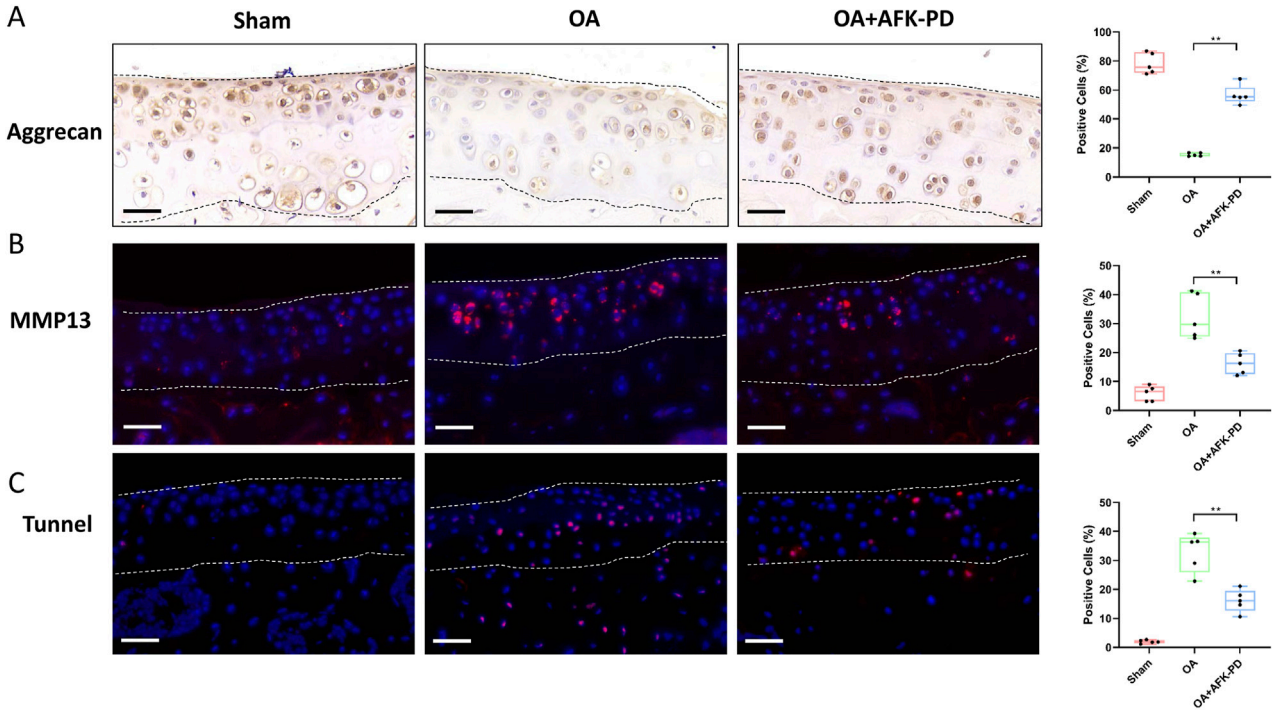

FIGURE 6
AFK-PD enhanced Aggrecan expression and restrained MMP13 and apoptosis of articular cartilage in mice after DMM surgery. **(A)** The Immunohistochemistry for Aggrecan in the articular cartilage in sham, OA and OA + AFK-PD mice at 8 weeks post OA surgery (scale bars: 50 μm), and quantitative analysis of the positive cells was shown on the right. The articular cartilage was marked between two black dotted lines. **(B)** The immunofluorescence for MMP13 expression in the articular cartilage in sham, OA and OA + AFK-PD mice (scale bars: 50 μm), and quantitative analysis of the positive cells was shown on the right. The articular cartilage was marked between two white dotted lines. **(C)** The immunofluorescence for apoptosis marker TUNEL in the articular cartilage in sham, OA and OA + AFK-PD mice (scale bars: 50 μm), and quantitative analysis of the positive cells was shown on the right. The articular cartilage was marked between two white dotted lines. Data are presented as mean ± SD (n = 5/group, Student t test; $*p < 0.05$, $**p < 0.01$).

particially the IL-1β-induced lower anabolic metabolism and higer catabolic metabolism. These results suggested AFK-PD not only regulated chondrocyte's metabolism under physiological status, but also remodeled imbalance of chondrocyte anabolic and catabolic metabolism induced by inflammation. Based on the AFK-PD-promoted chondrocyte diffirentiation *per se*, we wondered whether AFK-PD promotes the chondrogenesis of mesenchymal stem cell (MSC). This is particularly important if AFK-PD promotes cartilage regeneration derived from MSCs to repair cartilage defects.

Chondrocytes, the sole resident cells in articular cartilage, are required for maintaining cartilage structure and homeostasis. Therefore, the survival of chondrocytes is vital for the normal physiological state of the articular cartilage. It is widely recognized that chondrocyte apoptosis is essential for the occurrence and progression of OA (Hosseinzadeh et al., 2016; Li et al., 2024). In our study, we found AFK-PD inhibited the apoptosis of chondrocyte induced by IL-1β *in vitro*. Furthermore, AFK-PD dampened obviously chondrocyte apoptosis in articular cartilage from OA mice. This finding is consistent with previous evidence demonstrating that AFK-PD alleviated apoptosis in acetaminophen-induced acute liver failure (Gu et al., 2023). And AFK-PD also ameliorated cell apoptosis of kidney in cisplatin-induced acute kidney injury mice and cisplatin-treated NRK-52E cells (Jiang et al., 2019). Moreover, AFK-PD attenuated pulmonary apoptosis in LPS-induced acute lung injury mice (Lv et al., 2021). Therefore, our study further expands our understanding of the anti-apoptotic effects of AFK-PD.

The activation of NF-κB and MAPK pathways are closely involved in aggravation of OA, leading to production of pro-inflammatory cytokines and metaloproteinases both in chondrocyte and synovial macrophage. This ultimately results in imbalance of chondrocyte metabolism and cartilage matrix degeneration (Yan et al., 2020; Gratal et al., 2022; Lu et al., 2023). Our study showed NF-κB and MAPK pathways were significantly activated after stimulation with IL-1β. However, AFK-PD demonstrated the ability to inhibit the phosphorylation level of key factors associated with NF-κB and MAPK pathways. This finding suggests that AFK-PD suppresses chondrocyte inflammation and shifts chondrocyte metabolism from catabolism to anabolism in IL-1β-induced chondrocytes by inhibiting NF-κB and MAPK pathways. Consistent with these results, AFK-PD inhibited inflammation in chronic renal failure and acute kidney injury via mitigating NF-κB and MAPK pathways (Tang et al., 2015; Jiang et al., 2019). Moreover, AFK-PD restrained hepatic inflammation in hepatic cirrhosis by blocking the activation of NF-κB pathways (Tu et al., 2021). Moreover, AFK-PD had anti-inflammation effect on acute lung injury through inhibiting MAPK and NF-κB pathway (Lv et al., 2021).

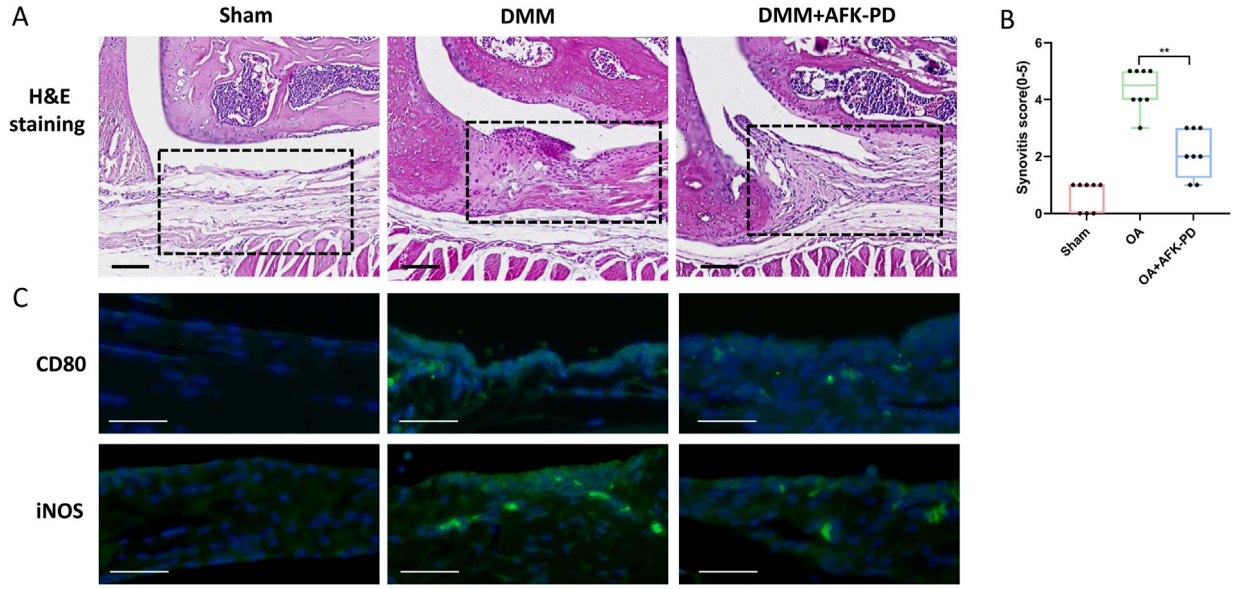

FIGURE 7
AFK-PD relieved synovitis in OA. **(A)** H&E staining of the synovium in sham, OA, and OA + AFK-PD groups at 8 weeks post OA surgery. Scale bars: 100 μm. Black boxed areas showed synovium. **(B)** Quantification of the synovitis scores of samples was shown on the right (n = 8/group). **(C)** The immunofluorescence for CD80 and iNOS in synovium from sham, OA, and OA + AFK-PD mice (scale bars: 100 μm). Data are presented as mean ± SD (Student t test; $*p < 0.05$, $**p < 0.01$).

In conclusion, our findings present AFK-PD as a promising candidate for the treatment of OA. We demonstrated that AFK-PD effectively delayed the development of OA by inhibiting inflammation in chondrocytes and suppressing M1 polarization of synovial macrophages. Furthermore, AFK-PD exhibited positive effects in reducing cartilage degeneration by protecting the chondrocyte functions. Mechanistic investigations revealed that AFK-PD's effects in IL-1β-induced chondrocytes were mediated through the MAPK and NF-κB pathways. Of note, many of risk factors had involved in initiation and development of OA, including biomechanical injury, aging and obesity. In our study, we focused on assessing the impact of AFK-PD on the progression of traumatic osteoarthritis induced by destabilization of the medial meniscus (DMM), a biomechanical injury. However, the specific contribution of AFK-PD to the initiation and development of aging and obesity-related OA remains unclear. Therefore, it is crucial to expand future studies to evaluate the treatment effects of AFK-PD on OA using mouse models that represent aging and obesity-related OA.

Data availability statement

The original contributions presented in the study are included in the article/Supplementary Material, further inquiries can be directed to the corresponding author/s.

Ethics statement

The animal study was approved by Animal Care and Use Committee of Xinxiang Medical University. The study was conducted in accordance with the local legislation and institutional requirements.

Author contributions

ZQ: Funding acquisition, Writing–original draft, Writing–review and editing, Investigation. JX: Writing–original draft, Formal Analysis, Investigation, Methodology. LZ: Writing–original draft, Methodology, Data curation, Investigation. QD: Writing–original draft, Methodology. ZF: Writing–review and editing, Funding acquisition, Visualization. XG: Conceptualization, Data curation, Funding acquisition, Writing–review and editing. ZL: Funding acquisition, Methodology, Software, Writing–original draft. WW: Writing–original draft, Formal Analysis, Funding acquisition, Investigation. LW: Writing–review and editing, Investigation, Project administration, Writing–original draft. XL: Writing–original draft, Writing–review and editing, Investigation, Project administration, Resources. WR: Writing–original draft, Writing–review and editing, Funding acquisition, Investigation, Project administration.

Funding

The author(s) declare that financial support was received for the research, authorship, and/or publication of this article. The study was supported by programs from National Natural Science Foundation of China (No.82302655) for Zhuang Qian; the Natural Science Foundation of Henan province (No. 232300421314) for Zhuang Qian; the Open Project Program of

the Third Affiliated Hospital of Xinxiang Medical University (No.2022KFKTYB07 for Zhuang Qian; No.2022KFKTYB06 for Zhuo Liang); Jiangsu Innovative and Enterpreneurial Talent Project (No.JSSCBS20221853) for Xiaohua Liao; the Henan Provincial Science and Technology Research and Development Joint Fund (Industrial) (No. 235101610001) for Wenjie Ren; National Natural Science Foundation of China (No. 32200754) for Weiyun Wang; the Key Research and Development and Promotion Special (Science and Technology) Project of Henan Province (No. 232102310331 for Xueqiang Guo, No. 242102310321 for Zhenlin Fan; No. 242102230124 for Zhuo Liang); the Open Research Fund of Tissue Engineering and Regenerative Clinical Medical Center of Xinxiang Medical University (No.2022YFYKFKT05 for Xueqiang Guo).

Acknowledgments

We thank Professor Lijian Tao from State Key Laboratory of Medical Genetics of China, Central South University for AFK-PD.

Conflict of interest

The authors declare that the research was conducted in the absence of any commercial or financial relationships that could be construed as a potential conflict of interest.

Publisher's note

Supplementary material

The Supplementary Material for this article can be found online at: https://www.frontiersin.org/articles/10.3389/fphar.2024.1439678/full#supplementary-material

References

Atsuta, Y., Tomizawa, R. R., Levin, M., and Tabin, C. J. (2019). L-type voltage-gated Ca(2+) channel CaV1.2 regulates chondrogenesis during limb development. *Proc. Natl. Acad. Sci. U. S. A.* 116 (43), 21592–21601. doi:10.1073/pnas.1908981116

Gerwin, N., Bendele, A. M., Glasson, S., and Carlson, C. S. (2010). The OARSI histopathology initiative - recommendations for histological assessments of osteoarthritis in the rat. *Osteoarthr. Cartil.* 18 (Suppl. 3), S24–S34. doi:10.1016/j.joca.2010.05.030

Glasson, S. S., Blanchet, T. J., and Morris, E. A. (2007). The surgical destabilization of the medial meniscus (DMM) model of osteoarthritis in the 129/SvEv mouse. *Osteoarthr. Cartil.* 15 (9), 1061–1069. doi:10.1016/j.joca.2007.03.006

Glasson, S. S., Chambers, M. G., Van Den Berg, W. B., and Little, C. B. (2010). The OARSI histopathology initiative - recommendations for histological assessments of osteoarthritis in the mouse. *Osteoarthr. Cartil.* 18 (Suppl. 3), S17–S23. doi:10.1016/j.joca.2010.05.025

Gosset, M., Berenbaum, F., Thirion, S., and Jacques, C. (2008). Primary culture and phenotyping of murine chondrocytes. *Nat. Protoc.* 3 (8), 1253–1260. doi:10.1038/nprot.2008.95

Gratal, P., Mediero, A., Lamuedra, A., Matamoros-Recio, A., Herencia, C., Herrero-Beaumont, G., et al. (2022). 6-Shogaol (enexasogoal) treatment improves experimental knee osteoarthritis exerting a pleiotropic effect over immune innate signalling responses in chondrocytes. *Br. J. Pharmacol.* 179 (22), 5089–5108. doi:10.1111/bph.15908

Gu, L., He, X., Zhang, Y., Li, S., Tang, J., Ma, R., et al. (2023). Fluorofenidone protects against acute liver failure in mice by regulating MKK4/JNK pathway. *Biomed. Pharmacother.* 164, 114844. doi:10.1016/j.biopha.2023.114844

Hashizume, H., Motonari, H., Yamamoto, K., Nakamura, Y., Hisaoka-Nakashima, K., and Morioka, N. (2024). Stimulation of nuclear receptor REV-ERBs alleviates monosodium iodoacetate-induced osteoarthritis pathology of mice and the induction of inflammatory molecules expression in primary cultured chondrocytes. *Int. Immunopharmacol.* 127, 111349. doi:10.1016/j.intimp.2023.111349

Hosseinzadeh, A., Kamrava, S. K., Joghataei, M. T., Darabi, R., Shakeri-Zadeh, A., Shahriari, M., et al. (2016). Apoptosis signaling pathways in osteoarthritis and possible protective role of melatonin. *J. Pineal Res.* 61 (4), 411–425. doi:10.1111/jpi.12362

Jiang, Y., Quan, J., Chen, Y., Liao, X., Dai, Q., Lu, R., et al. (2019). Fluorofenidone protects against acute kidney injury. *FASEB J.* 33 (12), 14325–14336. doi:10.1096/fj.201901468RR

Li, J. W., Wang, R. L., Xu, J., Sun, K. Y., Jiang, H. M., Sun, Z. Y., et al. (2022). Methylene blue prevents osteoarthritis progression and relieves pain in rats via upregulation of Nrf2/PRDX1. *Acta Pharmacol. Sin.* 43 (2), 417–428. doi:10.1038/s41401-021-00646-z

Li, X., Zhao, C., Mao, C., Sun, G., Yang, F., Wang, L., et al. (2024). Oleic and linoleic acids promote chondrocyte apoptosis by inhibiting autophagy via downregulation of SIRT1/FOXO1 signaling. *Biochim. Biophys. Acta Mol. Basis Dis.* 1870 (4), 167090. doi:10.1016/j.bbadis.2024.167090

Liao, X., Jiang, Y., Dai, Q., Yu, Y., Zhang, Y., Hu, G., et al. (2021). Fluorofenidone attenuates renal fibrosis by inhibiting the mtROS-NLRP3 pathway in a murine model of folic acid nephropathy. *Biochem. Biophys. Res. Commun.* 534, 694–701. doi:10.1016/j.bbrc.2020.11.017

Liu-Bryan, R., and Terkeltaub, R. (2015). Emerging regulators of the inflammatory process in osteoarthritis. *Nat. Rev. Rheumatol.* 11 (1), 35–44. doi:10.1038/nrrheum.2014.162

Lou, C., Lin, C., Wang, W., Jiang, H., Cai, T., Lin, S., et al. (2023). Extracts of Oldenlandia diffusa protects chondrocytes via inhibiting apoptosis and associated inflammatory response in osteoarthritis. *J. Ethnopharmacol.* 316, 116744. doi:10.1016/j.jep.2023.116744

Lu, R., Wang, Y. G., Qu, Y., Wang, S. X., Peng, C., You, H., et al. (2023). Dihydrocaffeic acid improves IL-1β-induced inflammation and cartilage degradation via inhibiting NF-κB and MAPK signalling pathways. *Bone Jt. Res.* 12 (4), 259–273. doi:10.1302/2046-3758.124.BJR-2022-0384.R1

Lv, X., Yao, T., He, R., He, Y., Li, M., Han, Y., et al. (2021). Protective effect of fluorofenidone against acute lung injury through suppressing the MAPK/NF-κB pathway. *Front. Pharmacol.* 12, 772031. doi:10.3389/fphar.2021.772031

Peng, Y., Li, L., Zhang, X., Xie, M., Yang, C., Tu, S., et al. (2019). Fluorofenidone affects hepatic stellate cell activation in hepatic fibrosis by targeting the TGF-β1/Smad and MAPK signaling pathways. *Exp. Ther. Med.* 18 (1), 41–48. doi:10.3892/etm.2019.7548

Peng, Y., Yang, H., Zhu, T., Zhao, M., Deng, Y., Liu, B., et al. (2013). The antihepatic fibrotic effects of fluorofenidone via MAPK signalling pathways. *Eur. J. Clin. Invest* 43 (4), 358–368. doi:10.1111/eci.12053

Qian, Z., Gao, X., Jin, X., Kang, X., and Wu, S. (2023). Cartilage-specific deficiency of clock gene Bmal1 accelerated articular cartilage degeneration in osteoarthritis by up-regulation of mTORC1 signaling. *Int. Immunopharmacol.* 115, 109692. doi:10.1016/j.intimp.2023.109692

Qin, J., Mei, W. J., Xie, Y. Y., Huang, L., Yuan, Q. J., Hu, G. Y., et al. (2015). Fluorofenidone attenuates oxidative stress and renal fibrosis in obstructive nephropathy via blocking NOX2 (gp91phox) expression and inhibiting ERK/MAPK signaling pathway. *Kidney Blood Press Res.* 40 (1), 89–99. doi:10.1159/000368485

Saklatvala, J. (2007). Inflammatory signaling in cartilage: MAPK and NF-kappaB pathways in chondrocytes and the use of inhibitors for research into pathogenesis and therapy of osteoarthritis. *Curr. Drug Targets* 8 (2), 305–313. doi:10.2174/138945007779940115

Salvat, C., Pigenet, A., Humbert, L., Berenbaum, F., and Thirion, S. (2005). Immature murine articular chondrocytes in primary culture: a new tool for investigating cartilage. *Osteoarthr. Cartil.* 13 (3), 243–249. doi:10.1016/j.joca.2004.11.008

Sanchez-Lopez, E., Coras, R., Torres, A., Lane, N. E., and Guma, M. (2022). Synovial inflammation in osteoarthritis progression. *Nat. Rev. Rheumatol.* 18 (5), 258–275. doi:10.1038/s41584-022-00749-9

Segarra-Queralt, M., Crump, K., Pascuet-Fontanet, A., Gantenbein, B., and Noailly, J. (2024). The interplay between biochemical mediators and mechanotransduction in chondrocytes: unravelling the differential responses in primary knee osteoarthritis. *Phys. Life Rev.* 48, 205–221. doi:10.1016/j.plrev.2024.02.003

Tang, Y., Li, B., Wang, N., Xie, Y., Wang, L., Yuan, Q., et al. (2010). Fluorofenidone protects mice from lethal endotoxemia through the inhibition of TNF-alpha and IL-1beta release. *Int. Immunopharmacol.* 10 (5), 580–583. doi:10.1016/j.intimp.2010.02.005

Tang, Y., Zhang, F., Huang, L., Yuan, Q., Qin, J., Li, B., et al. (2015). The protective mechanism of fluorofenidone in renal interstitial inflammation and fibrosis. *Am. J. Med. Sci.* 350 (3), 195–203. doi:10.1097/MAJ.0000000000000501

Tu, S., Jiang, Y., Cheng, H., Yuan, X., He, Y., Peng, Y., et al. (2021). Fluorofenidone protects liver against inflammation and fibrosis by blocking the activation of NF-κB pathway. *FASEB J.* 35 (7), e21497. doi:10.1096/fj.202002402R

Wang, L., Xu, H., Li, X., Chen, H., Zhang, H., Zhu, X., et al. (2023). Cucurbitacin E reduces IL-1β-induced inflammation and cartilage degeneration by inhibiting the PI3K/Akt pathway in osteoarthritic chondrocytes. *J. Transl. Med.* 21 (1), 880. doi:10.1186/s12967-023-04771-7

Wei, Q., Kong, N., Liu, X., Tian, R., Jiao, M., Li, Y., et al. (2021). Pirfenidone attenuates synovial fibrosis and postpones the progression of osteoarthritis by anti-fibrotic and anti-inflammatory properties *in vivo* and *in vitro*. *J. Transl. Med.* 19 (1), 157. doi:10.1186/s12967-021-02823-4

Yan, Z., Lin, Z., Wu, Y., Zhan, J., Qi, W., Lin, J., et al. (2020). The protective effect of myricitrin in osteoarthritis: an *in vitro* and *in vivo* study. *Int. Immunopharmacol.* 84, 106511. doi:10.1016/j.intimp.2020.106511

Zhang, H., Cai, D., and Bai, X. (2020). Macrophages regulate the progression of osteoarthritis. *Osteoarthr. Cartil.* 28 (5), 555–561. doi:10.1016/j.joca.2020.01.007

Zhang, H., Lin, C., Zeng, C., Wang, Z., Wang, H., Lu, J., et al. (2018). Synovial macrophage M1 polarisation exacerbates experimental osteoarthritis partially through R-spondin-2. *Ann. Rheum. Dis.* 77 (10), 1524–1534. doi:10.1136/annrheumdis-2018-213450

Zhou, F., Mei, J., Han, X., Li, H., Yang, S., Wang, M., et al. (2019). Kinsenoside attenuates osteoarthritis by repolarizing macrophages through inactivating NF-κB/MAPK signaling and protecting chondrocytes. *Acta Pharm. Sin. B* 9 (5), 973–985. doi:10.1016/j.apsb.2019.01.015

frontiers | Frontiers in Pharmacology

TYPE Mini Review
PUBLISHED 20 September 2024
DOI 10.3389/fphar.2024.1474285

OPEN ACCESS

EDITED BY
Emanuela Ricciotti,
University of Pennsylvania, United States

REVIEWED BY
Alexander Bartelt,
Ludwig Maximilian University of Munich, Germany
Zongde Zhang,
Southwest Medical University, China

*CORRESPONDENCE
Dominik C. Fuhrmann,
fuhrmann@biochem.uni-frankfurt.de

†These authors share first authorship

‡These authors share senior authorship

RECEIVED 01 August 2024
ACCEPTED 12 September 2024
PUBLISHED 20 September 2024

CITATION
Wickert A, Schwantes A, Fuhrmann DC and Brüne B (2024) Inflammation in a ferroptotic environment.
Front. Pharmacol. 15:1474285.
doi: 10.3389/fphar.2024.1474285

Inflammation in a ferroptotic environment

Anja Wickert[1‡], Anna Schwantes[1†], Dominik C. Fuhrmann [1,2‡*] and Bernhard Brüne [1,3,2,4‡]

[1]Institute of Biochemistry I, Faculty of Medicine, Goethe University Frankfurt, Frankfurt, Germany, [3]Frankfurt Cancer Institute, Goethe University Frankfurt, Frankfurt, Germany, [2]German Cancer Consortium (DKTK), Partner Site Frankfurt, Frankfurt, Germany, [4]Fraunhofer Institute for Translational Medicine and Pharmacology ITMP, Frankfurt, Germany

Ferroptosis is an iron-dependent form of cell death, which finally culminates in lipid peroxidation and membrane damage. During the past decade, the interest in ferroptosis increased substantially and various regulatory components were discovered. The role of ferroptosis during inflammation and its impact on different immune cell populations is still under debate. Activation of inflammatory pathways such as nuclear factor kappa-light-chain-enhancer of activated B cells (NF-κB) and hypoxia inducible factors (HIFs) are known to alter the ability of cells to undergo ferroptosis and are closely connected to iron metabolism. During inflammation, iron regulatory systems fundamentally change and cells such as macrophages and neutrophils adapt their metabolism towards iron sequestering phenotypes. In this review, we discuss how ferroptosis alters inflammatory pathways and how iron metabolism under inflammatory conditions affects immune cell ferroptosis.

KEYWORDS

HIF, NF-kB, iron, lipid peroxidation, LCN2

Introduction

Within the last decades, several forms of cell death were discovered. Besides "classic" forms such as apoptosis and necrosis also pyroptosis and ferroptosis were described. More recently, ferroptosis has gained increasing attention in basic science and clinical settings. First hints of this form of cell demise emerged in the 1950s by H. Eagle who showed that amino acid deprivation increased cell death (Eagle, 1955). The term ferroptosis was coined by Dixon and coworkers in 2012 (Dixon et al., 2012). Ferroptosis depends on iron-mediated lipid peroxidation, which disrupts membrane integrity. In the meantime, various cellular pathways were uncovered to contribute to or prevent ferroptosis. Among these glutathione and iron metabolism are most substantial. Besides cell demise, the contribution of ferroptosis to the pathogenesis of cancer and inflammatory diseases emerged. Interestingly, ferroptosis shares features with inflammation such as an altered iron metabolism and increased oxidative stress. Activation of inflammatory pathways upon infection modulates ferroptosis sensitivity of cells. Inflammation frequently is accompanied by hypoxia, which also affects the oxidative machinery and iron homeostasis and thus, must be considered as an additional link between ferroptosis and inflammation. In this review, we report recent findings on basic ferroptotic mechanisms linking them to inflammatory pathways, iron metabolism, and describe the role of ferroptosis under inflammatory conditions.

Mechanisms of ferroptosis

Ferroptosis is an iron-dependent form of cell death occurring due to metabolic imbalances, which result in the extensive production of reactive oxygen species and increased lipid peroxide formation, thereby causing membrane damage and cell death. Lipid peroxidation of polyunsaturated fatty acids (PUFAs) is a hallmark of ferroptosis, which was shown to be prevented by respective inhibitors (Bannai et al., 1977; Zilka et al., 2017). During ferroptosis free-radical initiated fatty acid peroxidation as well as 12-lipoxygenase and/or 15-lipoxygenase (ALOX15) facilitated lipid peroxidation may add to membrane destruction. Besides its harmful capabilities, lipid peroxidation mediated by 15-lipoxygenase type B also affects biological processes such as cholesterol metabolism of human macrophages (Benatzy et al., 2024). Moreover, both lipoxygenases use PUFAs such as arachidonic acid, eicosapentaenoic or decosahexaenoic acid to produce specialized lipid mediators with roles in inflammation and wound healing (Zheng et al., 2020; Benatzy et al., 2022).

In a non-enzymatic manner hydroxyl and hydroperoxyl radicals are generated by the Fenton reaction, where free ferrous ions (Fe^{2+}) catalyzes the decomposition of hydrogen peroxide (Fenton, 1894). Ferrous iron is highly reactive and is accessible for cellular usage in the labile iron pool (LIP). To overcome iron-mediated cytotoxicity, cells developed a well-orchestrated iron uptake, storage, and release system. In brief, iron is bound to transferrin and taken up into cells via internalization of the transferrin receptor (TfR) (Muckenthaler et al., 2017). Inside endosomes, iron is reduced from ferric to ferrous iron by the metalloreductase STEAP3 and released into the cytosol by the divalent metal transporter 1 (DMT1). Iron storage is mediated by ferritins, which oxidize Fe^{2+} to ferric iron (Fe^{3+}) and sequester it. Release of iron from ferritins is achieved by nuclear receptor coactivator 4 (NCOA4) and increases the LIP and thus, sensitized cells towards ferroptosis (Fuhrmann et al., 2020). In turn, cellular export of iron by ferroportin (FPN) protects from ferroptosis (Namgaladze et al., 2022; Geng et al., 2018).

Because of chemical interactions between iron, oxygen, and polyunsaturated lipids, oxidative stress and ROS generation have to be well orchestrated to protect cells from damage. Therefore, defense mechanisms to limit lipid peroxidation are required (Stockwell, 2022). Glutathione peroxidase 4 (GPX4) is a selenoenzyme that directly detoxifies phospholipid hydroperoxides to lipid alcohols in membrane-bound phospholipid peroxides. GPX4 demands glutathione, a cysteine-containing tripeptide, as a cofactor (Ursini et al., 1985). Cells import cystine, the oxidized form of cysteine, through the X_C^- system consisting of solute carrier family 7 member 11 (SLC7A11) mediating cystine/glutamate antiporter activity and solute carrier family 3 member 2, which acts as a chaperone to stabilize the complex in the membrane (Koppula et al., 2021). Further defense mechanisms include ferroptosis suppressor protein 1 (FSP1), which converts phospholipid peroxyl radicals to phospholipid hydroperoxides using ubiquinone and FAD. Thereby FSP1 restricts propagation of lipid peroxidation (Bersuker et al., 2019; Doll et al., 2019). The basic mechanisms of ferroptosis are well reviewed and illustrated, e.g., in ((Berndt et al., 2024), (Stockwell, 2022), (Fuhrmann and Brüne, 2022), (Jiang et al., 2021)).

During the last decade, various inducers and inhibitors of ferroptosis were developed (Figure 1). Ferroptosis inducers are predominantly blocking defense mechanisms, such as the GPX4 inhibitor Ras-selective lethal small molecule 3 (RSL3) or erastin, which lowers cystine supply by inhibiting the X_C^- system. Most inhibitors of ferroptosis antagonize lipid peroxidation, for example, radical-trapping antioxidants, such as liproxstatin-1 and ferrostatin-1 or they reduce the LIP, acting as iron chelators like deferoxamine (Zilka et al., 2017).

Ferroptosis and inflammatory signaling

Under inflammatory conditions multiple signaling cascades affect transcriptional patterns that facilitate cytokine and chemokine expression, modulate resolution of inflammation and regulate ferroptosis-associated pathways (reviewed in (Chen Y. et al., 2023)). While this review focusses on nuclear factor kappa-light-chain-enhancer of activated B cells (NF-κB), hypoxia inducible factors (HIFs), and iron, other inflammatory mediators have been connected to ferroptosis as well. For example, tyrosine-protein kinase JAK (JAK)/signal transducer and activator of transcription (STAT) signaling, regulates the X_C^- system. Activation of JAK/STAT signaling by interferon γ decreased solute carrier family 3 member 2 and SLC7A11 expression, thereby facilitating ferroptosis of adrenocortical and hepatocellular carcinoma cells (Yu et al., 2022; Kong et al., 2021). In addition, interferon γ signals via interferon regulatory factors, which caused expression of SLC7A11 and GPX4, thereby protecting from ferroptosis (Liu et al., 2023). Also, aryl hydrocarbon receptor needs consideration, which regulates SLC7A11 (Kou et al., 2024). Pharmacological and genetic inhibition of aryl hydrocarbon receptor decreased SLC7A11 and sensitized human normal bronchial epithelial cells for erastin-induced ferroptosis. In the following chapters of this review we describe the complex interplay between NF-κB, HIF, iron, and ferroptosis.

Implications of NF-κB for ferroptosis

Ferroptosis plays a role in several physiological and pathophysiological processes such as tumor suppression or aging. Recent studies revealed that ferroptosis is also involved in inflammation. A hallmark regulator of inflammation is the transcription factor NF-κB. The transcription factor is activated by various stimuli such as pathogen antigens, cytokines or genotoxic stress (Perkins, 2007). The active homo- or heterodimeric NF-κB complex consists of p65, p50, and p52. These components are constantly expressed but kept inactive by binding to NF-κB inhibitor alpha (IκBα). To activate the transcriptional activity, IκBα is degraded upon phosphorylation by IκB kinase. Afterwards, NF-κB translocates to the nucleus and induces the expression of pro-inflammatory genes including cytokines and chemokines (Bonizzi and Karin, 2004). Recently, several studies explored how ferroptosis affects NF-κB signaling and whether NF-κB regulates ferroptosis susceptibility (Figure 1). Yao and coworkers show that the loss of leukemia inhibitory factor receptor in liver cancer activated NF-κB, which upregulates the iron-sequestering

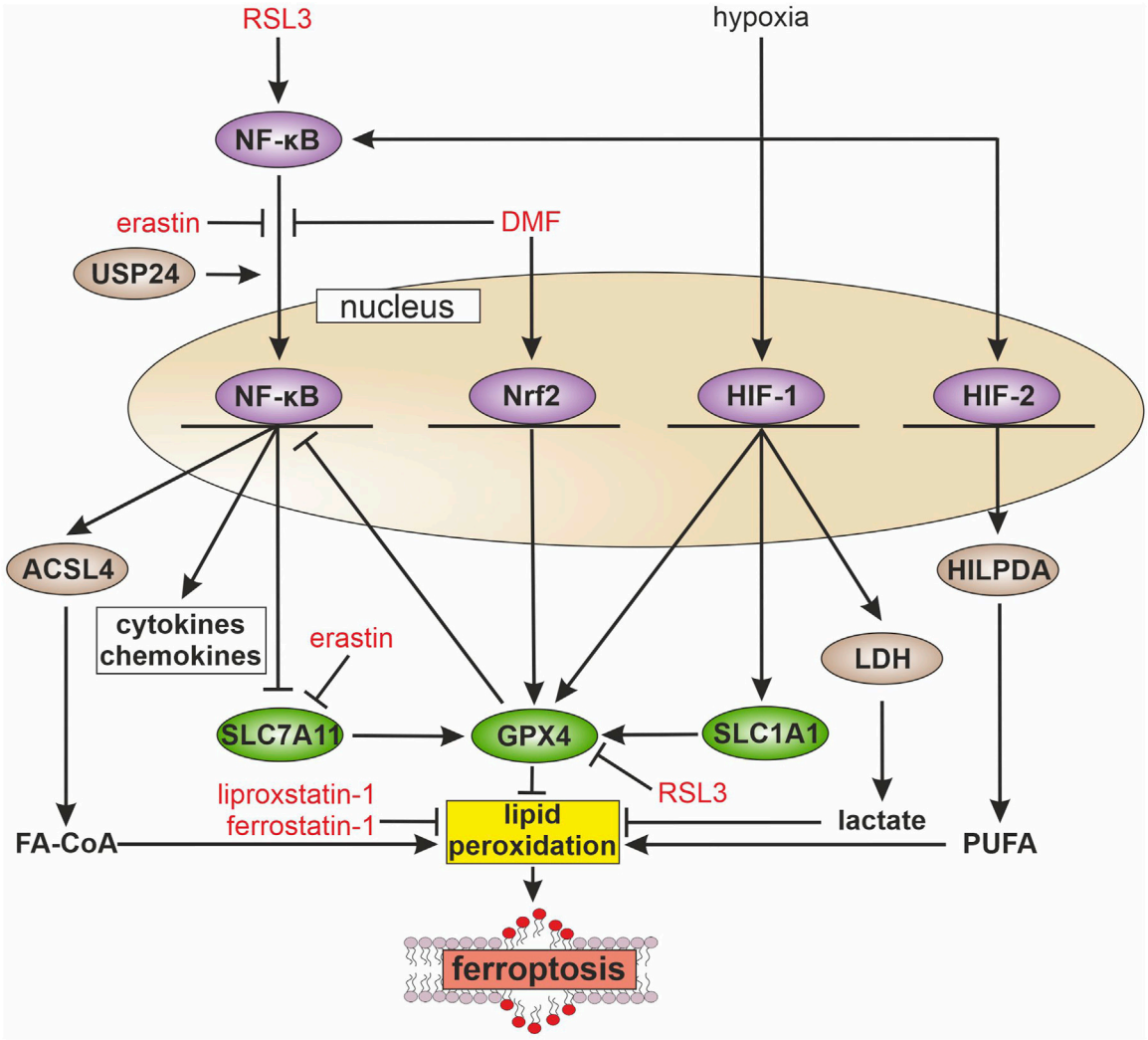

FIGURE 1
Inflammatory pathways and ferroptosis During inflammation multiple signaling cascades are activated, e.g., the transcription factors nuclear factor kappa-light-chain-enhancer of activated B cells (NF-κB), nuclear factor erythroid 2-related factor 2 (Nrf2), and hypoxia-inducible factor (HIF). NF-κB is activated by ras-selective lethal small molecule 3 (RSL3) and the ubiquitin-specific protease 24 (USP24), while erastin and dimethyl fumarate (DMF) block its activation. Activated NF-κB increases the transcription of long-chain-fatty-acid-CoA ligase 4 (ACSL4), which facilitates fatty acyl CoA (FA-CoA) synthesis and ferroptosis. Further, NF-κB blocks the expression of solute carrier family 7 member 11 (SLC7A11), with consequences for glutathione synthesis and glutathione peroxidase 4 (GPX4) activity, which abolishes lipid peroxidation. In contrast, Nrf2 increases GPX4 expression and thus, attenuates ferroptosis. HIF-1 enhances solute carrier family 1 member 1 (SLC1A1) expression, which indirectly supports GPX4 activity. Further, HIF-1 protects from ferroptosis by elevating glycolysis, expression of lactate dehydrogenase (LDH), and facilitating lactate production. HIF-2 acts pro-ferroptotic by increasing hypoxia-inducible lipid droplet-associated protein (HILPDA) and polyunsaturated fatty acid (PUFA) release, which in turn increases lipid peroxidation.

protein lipocalin-2 (LCN2), thereby decreasing ferroptosis sensitivity (Figure 2) (Yao et al., 2021). Vice versa, septic shock in mice is ameliorated by pretreatment with the ferroptosis inducer erastin. Mechanistically, erastin treatment of bone marrow-derived macrophages reduces phosphorylation of IκB kinase β and consequently phosphorylation and degradation of IκBα. This prevents nuclear translocation of NF-κB in lipopolysaccharide (LPS)-stimulated murine macrophages and decreases the production of inflammatory mediators such as nitric oxide, tumor necrosis factor-α, and interleukin-1β (Oh et al., 2019). In some analogy, the group of Li observed that GPX4 activation inhibits TNF-mediated activation of the NF-κB pathway in HEK293T cells (Li et al., 2018). In experiments with chronic cerebral hypoperfusion in mice, treatment with the multiple sclerosis drug dimethyl fumarate (DMF) decreases pro-inflammatory cytokines via the NF-κB pathway and mitigated oxidative stress in the hippocampus (Yan et al., 2021). In parallel, DMF treatment reduces the iron content, likely by elevating ferritin heavy chain (FTH) expression and increasing glutathione levels by enhancing cystine import via the system X_C^- in hippocampus, which potentially protects cells from ferroptosis and reduces hippocampal neuron injury (Figure 2). Inhibition of the NF-κB pathway by DMF is facilitated by activation of the antioxidative transcription factor nuclear factor erythroid 2-related factor 2 (Nrf2), which decreases ferroptosis sensitivity. Besides Nrf2, also Nrf1 protects from ferroptosis by upregulating GPX4. Activation of

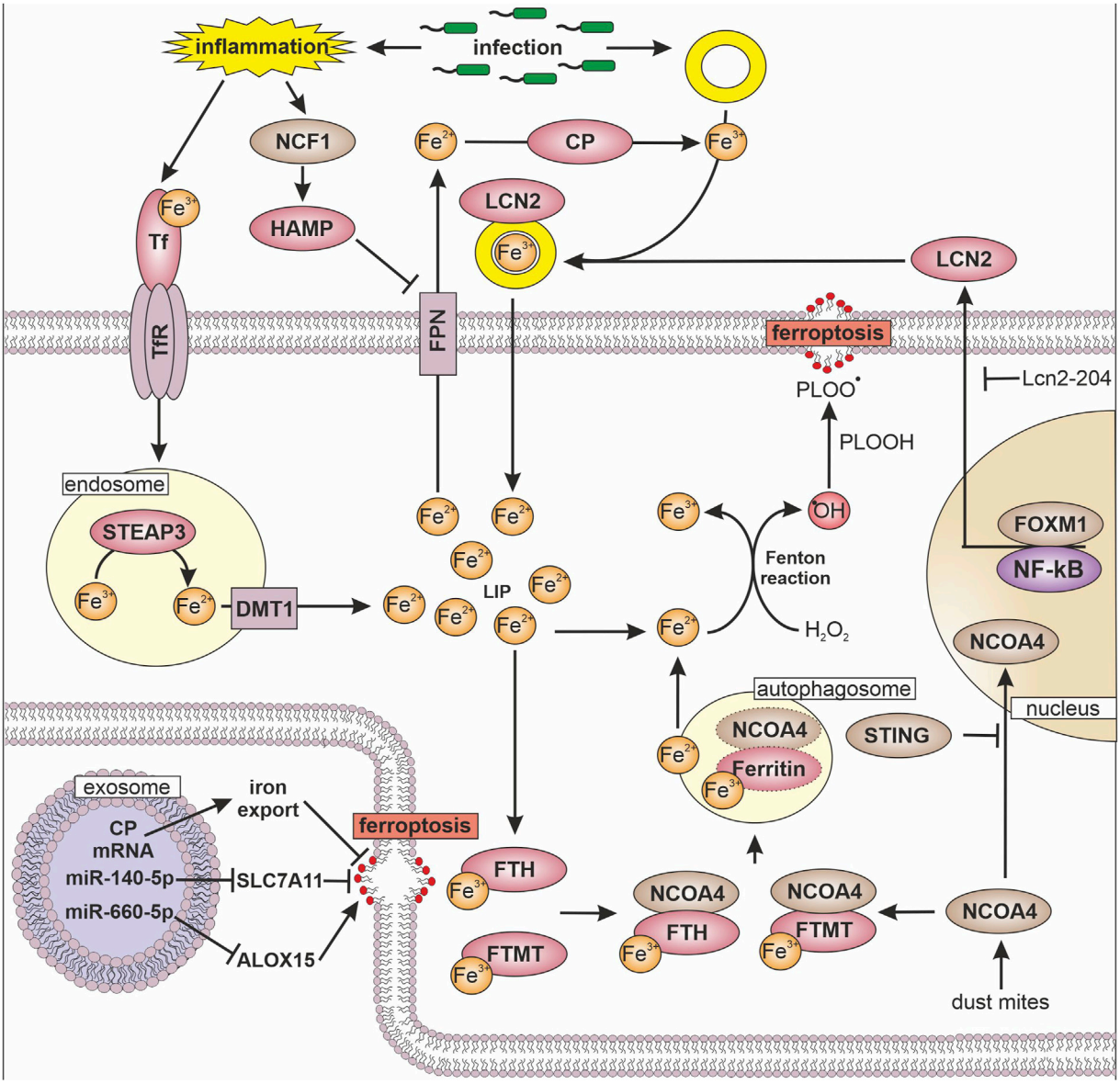

FIGURE 2
Iron, inflammation, and ferroptosis Transferrin (TF) bound iron (Fe) is internalized into the cell via transferrin receptor (TfR). In endosomes metalloreductase STEAP3 reduces iron ($Fe^{3+} \rightarrow Fe^{2+}$) followed by divalent metal transporter 1 (DMT1) mediated release into the cytosol, where it forms the labile iron pool (LIP). To avoid hydrogen peroxide (H_2O_2) mediated formation of hydroxyl radical ($^{\bullet}OH$) and conversion of phospholipid hydroperoxide (PLOOH) to phospholipid hydroperoxyl radicals ($PLOO^{\bullet}$), ferritin heavy chain (FTH) and mitochondrial ferritin (FTMT) oxidize and store iron. To release iron from ferritin, nuclear receptor coactivator 4 (NCOA4) marks FTH and FTMT for autophagosome-mediated degradation, which increases the LIP. The transfer of NCOA4 to the nucleus is inhibited by the stimulator of interferon genes (STING). Another way to sequester iron is via lipoclain 2 (LCN2), which is expressed dependent on forkhead box protein M1 (FOXM1) and nuclear factor kappa-light-chain-enhancer of activated B cells (NF-κB), while long non coding RNA Lcn2-204 inhibits LCN2 expression. LCN2 binds siderophore (yellow ring) bound iron and thereby reduces iron availability for pathogens. Export of iron from cells is facilitated by ferroportin (FPN) in close cooperation with ceruloplasmin (CP), which enables iron binding to TF and siderophores. FPN is regulated by hepcidin (HAMP), which is increased by neutrophil cytosolic factor 1 (NCF1) upon inflammatory stimuli. The ability to undergo ferroptosis can be modulated by exosomes, which transfer micro RNAs (miR) or mRNAs to target cells. Following their uptake miRs regulate the expression of solute carrier family 7 member 11 (SLC7A11) and 15-lipoxignase (ALOX15).

Nrf1 demands a cytosolic peptide:N-glycanase 1, which causes its deglycosylation (Forcina et al., 2022). In addition, Nrf1 sustains proteasomal activity and thereby protects from ferroptosis likely by preventing GPX4 hyper-ubiquitination (Kotschi et al., 2022). Further, interactions between ferroptosis and NF-κB were discovered in glioblastoma cells, where RSL3 activates NF-κB. Moreover, inhibition of NF-κB mitigates RSL3-induced ferroptosis (Li et al., 2021). To explore the impact of NF-κB in executing ferroptosis, GPX4 was silenced but an additional activation of the NF-κB pathway was necessary to effectively induce ferroptosis in glioblastoma cells. These studies indicate an important role of NF-κB in executing ferroptosis. In line, a recent study shows that upregulation of the ubiquitin-specific protease 24 (USP24) in myocardial cells activates the NF-κB pathway in diabetic

cardiomyopathy (Wu et al., 2024). This activation decreases RNA expression of the ferroptosis suppressors SLC7A11 and FTH and increases expression of the ferroptosis promoter long-chain-fatty-acid-CoA ligase 4 (ACSL4), pointing to the involvement of NF-κB and hence ferroptosis in the pathogenesis of diabetic cardiomyopathy.

Interactions between hypoxia inducible factors, inflammation, and ferroptosis

Inflammation is often accompanied by hypoxia, which arises when oxygen demands exceeds its supply (Taylor and Colgan, 2017). To ensure sufficient energy production, cells adapt to hypoxia by activating transcriptional regulators, known as HIFs. HIFs comprise two subunits, HIF-α and HIF-β. While HIF-β is constantly expressed, the HIF-α subunits are hydroxylated by prolyl hydroxylases and degraded under normoxic conditions. Under hypoxia, HIF-α is stabilized, translocates to the nucleus, dimerizes with the β-subunit, and facilitates target gene expression to modulate, e.g., cellular metabolism, angiogenesis, and erythropoiesis (Semenza et al., 1991; Semenza, 2012). Under inflammatory conditions, NF-κB activates hypoxic signaling even under normoxia by increasing the expression of HIF-1α and -1β (van Uden et al., 2008; van Uden et al., 2011). Further, accumulation of metabolites like succinate upon LPS stimulation add to the stabilization of HIF (Fuhrmann et al., 2018). Conversely, HIF-1 facilitated activation of NF-κB in neutrophils (Walmsley et al., 2005). This effect was confirmed in transgenic mice with a gain of HIF-1 function, which increased activation of the NF-κB pathway (Scortegagna et al., 2008). As inflammation and HIF-signaling are closely connected, the question remains whether HIF affects cellular sensitivity towards ferroptosis. Indeed, studies by Yang et al. observe ferroptosis-protecting effects upon HIF-1 activation (Yang et al., 2023). Mechanistically, HIF-1α enhances glycolysis and lactate dehydrogenase (LDH) expression (Figure 1). Thereby, lactate increases and protects the cells from ferroptosis in a pH-dependent manner. Moreover, HIF-1α increases the expression of the glutamate-transporter solute carrier family 1 member 1 (SLC1A1) that promotes cystine uptake and therefore ameliorates ferroptosis resistance. In line with these findings, the ferroptosis-protective effect of HIF-1α was confirmed in non-small cell lung cancer, where HIF-1α was upregulated as seen in many types of cancer. Silencing HIF-1α increases ROS and Fe^{2+} levels and decreases glutathione and GPX4. Furthermore, the absence of HIF-1α enhances cell death, which was partially prevented by the ferroptosis inhibitor ferrotstatin-1 (Zheng et al., 2023). In contrast, HIF activation was also observed to sensitize cells towards ferroptosis. Inhibition of HIF-α degradation increases ferroptosis sensitivity. Distinct inhibition of HIF-1α or HIF-2α reveals that HIF-2α induces genes, which are involved in lipid metabolism, contribute to excessive lipid peroxidation and therefore increase ferroptosis sensitivity (Su et al., 2023). The ferroptosis-sensitizing effect of HIF-2α was also observed in clear cell carcinomas, where HIF-2α selectively enriches polyunsaturated lipids via upregulation of the hypoxia-inducible lipid droplet-associated protein (HILPDA) (Zou et al., 2019). Summarizing these studies, HIF-1α is described to be ferroptosis-suppressive, while HIF-2α sensitizes cells towards ferroptosis. One of the major differences of HIF-2α compared to HIF-1α are increased protein levels upon long-term hypoxia (Holmquist-Mengelbier et al., 2006; Fuhrmann et al., 2015). Thus, under acute hypoxia, HIF-1α plays a more important role than HIF-2α, thereby contributing to decreased ferroptosis. Under chronic hypoxia, HIF-2α levels increase and provoke higher ferroptotic susceptibility.

Recapitulating, under acute inflammation and/or hypoxia NF-κB and HIF-1α activate each other. Predominantly, HIF-1α increases anti-oxidative pathways to enhance ferroptosis resistance. However, NF-κB facilitates ferroptosis-sensitizing effects. Depending on the cell type and stimulus, HIF-1α and NF-κB show either cooperative or contrary effects on ferroptosis susceptibility. This interdependent relationship might regulate the balance between cell survival and cell death in inflammation. However, under chronic hypoxia stabilization of HIF-2α shifts cellular metabolism to a pro-ferroptotic state, which potentially results in excessive tissue damage.

Iron, inflammation, and ferroptosis

Besides its crucial function for cellular integrity, iron represents a link between hypoxia, inflammation, and obviously ferroptosis. Both, hypoxia and inflammation induce an iron scavenging phenotype in macrophages upon their activation by extracellular stimuli, e.g., by inducing or resolving inflammation. Under inflammatory conditions, macrophages reduce blood iron levels to limit the availability of this factor for pathogens (Marques et al., 2022). Inflammatory macrophages sequester iron by increasing iron storage via ferritin and decrease FPN-mediated iron export, while alternatively activated macrophages release iron by elevating the amount of FPN and LCN2 (Jung et al., 2015). In patients with rheumatoid arthritis M2 like macrophages show higher lipid peroxidation and ferroptosis compared to M1 macrophages, which were likely protected by their increased ability to store iron (Liu et al., 2024). Blocking ferroptosis by liproxstatin-1 increases anti-inflammatory M2 macrophage populations and alleviates arthritis progression in mice.

To remove iron during infection, macrophages increase their TfR to facilitate iron uptake. Besides TfR, macrophages and neutrophils express LCN2, which binds to bacteria-derived siderophores and therefore limits iron availability for pathogens by scavenging siderophore-bound iron (Figure 2) (Jung et al., 2017). Under septic conditions, neutrophil-derived LCN2 induces ferroptosis in cardiomyocytes by increasing the labile iron pool and lipid peroxidation (Huang et al., 2022). In part, the long non-coding RNA Lcn2-204 is responsible for ferroptosis in cardiomyocytes in sepsis. Silencing Lcn2-204 reduces LCN2 expression as well as iron overload and provokes a cardioprotective and anti-ferroptotic effect (Huang et al., 2024). Based on a machine learning approach, LCN2 is considered as biomarker for sepsis-induced acute respiratory distress syndrome (Zhan et al., 2024). In ulcerative colitis, LCN2 expression correlates to elevated lipid peroxidation and decreased GPX4 expression (Deng et al., 2023). Silencing LCN2 in this model suppresses ferroptosis. In contrast to inflammatory conditions, LCN2 protects renal and colorectal tumor cells from ferroptosis by decreasing intracellular

iron levels and increasing GPX4 expression as well as causing Nrf2 activation (Chaudhary et al., 2021; Meier et al., 2021). Furthermore, silencing LCN2 sensitizes T-cell acute lymphoblastic leukemia cells to RSL3-mediated ferroptosis (Tian et al., 2023). Expression of LCN2 in endometrial cancer is facilitated by forkhead box protein M1 (FOXM1) (Jiang et al., 2023). Therefore, silencing FOXM1 decreases LCN2 and increases ferroptosis, which is eliminated by LCN2 overexpression. In breast cancer cells, a knockout of LCN2 increases the sensitivity towards cisplatin and stimulates ferroptotic cell death (Valashedi et al., 2022). These studies underscore an ambivalent role of LCN2, which protects cancer cells from ferroptosis, while it acts pro-ferroptotic under inflammatory conditions.

In the blood, most iron is bound to transferrin and is endocytosed upon binding to the transferrin receptor. After internalization, iron is reduced to Fe^{2+} by the metalloreductase STEAP3 and released from endosomes via DMT1. Under inflammatory conditions, iron uptake increases in conjunction with an attenuated release, due to a lower FPN surface expression as a result of hepcidin (HAMP) evoked degradation of the iron exporter (Nemeth and Ganz, 2021). Substantial amounts of HAMP are produced in the liver but also monocytes and macrophages release small quantities to regulate their own FPN expression. These mechanisms favor intracellular iron accumulation and uncontrolled iron-mediated production of reactive oxygen species and potentially, lipid peroxidation. To opt out, macrophages developed efficient iron storage systems. Ferritins increase under inflammatory and hypoxic conditions and can be considered as acute phase proteins during inflammation (Marques et al., 2022). Ferritins oxidize free iron and store it in spheres built of ferritin light chain, FTH, or mitochondrial ferritin (FTMT). FTMT shares high sequence homology with FTH but contains a mitochondrial target sequence, which is removed in macrophages by thrombin-mediated cleavage under hypoxic or oxidative stress, including LPS treatment. Thereby cells increase their ability to scavenge iron and protect themselves from lipid peroxidation (Fuhrmann et al., 2023), a mechanism operating in macrophages to circumvent ferroptosis. Experiments in human macrophages show that the sensitivity towards RSL3-mediated ferroptosis increases after the knockdown of FTH and/or FTMT (Fuhrmann et al., 2020). In this setting, hypoxia decreases NCOA4 expression, which reduces lysosomal degradation of ferritin, a process termed ferritinophagy. Thereby, the release of iron into the labile iron pool was diminished and consequently, protection against ferroptosis increased. A higher rate of ferritinophagy, going in line with enhanced lipid peroxidation and ferroptosis, was evident in a house dust mites-induced asthma model (Zeng et al., 2022). Mice exposed to house dust mites show increased signs of inflammation, which decrease in the presence of deferoxamine and ferrostatin-1. Mechanistically, increased NCOA4 expression goes in line with enhanced free iron, lipid peroxidation, and ferroptosis. Conclusively, ferroptosis of airway cells induces inflammation in mice, which implies that ferroptosis can either result in or be a result of inflammation as seen in another model of acute LPS-induced lung inflammation which induces ferroptosis. In this setting, meteorin-like/meteorin-β protected from ferroptosis by inhibiting p53 and increasing SLC7A11 expression (Chen Z. et al., 2023). Ferritinophagy is also connected to sepsis, where NCOA4-mediated ferroptosis contributes to disease severity by increasing inflammation. Mechanistically, stimulator of interferon genes (STING) blocks nuclear translocation of NCOA4, which facilitates ferritinophagy, iron release, and lipid peroxidation (Wu et al., 2022). Sepsis is often accompanied by cardiac dysfunction caused by the inflammatory response. Ferrostatin-1 suppresses lipid peroxidation and ferroptosis upon LPS-induced cardiac inflammation in rats and improves sepsis-induced cardiac dysfunction (Xiao et al., 2021). Underlining the pivotal role of STING under inflammatory conditions, STING promotes hepatic iron accumulation in mice suffering from autoimmune hepatitis (Zhao et al., 2024). Besides increasing ferritinophagy, STING regulates iron release as shown by a liver-specific knockdown of STING. In this setting STING ameliorates iron accumulation and oxidative stress induced by increased expression of neutrophil cytosolic factor 1 (NCF1), which promotes HAMP expression in liver cells (Zhang et al., 2024). HAMP indirectly, by degrading FPN, provokes an iron overload in Kupffer cells, with consequences for ferroptosis, inflammation, and metabolic dysfunction-associated steatohepatitis (MASH). Another example for the interaction of macrophages with their environment was found in a tumor context, where macrophages invade the tumor and are polarized to tumor-associated macrophages. Apparently, tumor-associated macrophages protect tumor cells from RSL3-mediated ferroptosis (Schwantes et al., 2024) because these macrophages release extracellular vesicles containing ceruloplasmin mRNA. Once taken up by tumor cells, the mRNA is translated into ceruloplasmin protein, which supports iron export with lower rated of lipid peroxidation and ferroptosis. Moreover, tumor-associated macrophages protect tumor cells by an IL-13/IL-4-mediated increase of miR-660-5p, which was packed into exosomes and transferred to tumor cells (Luo et al., 2023). MiR-660-5p blocks ALOX15 expression and reduces lipid peroxidation in tumor cells, which attenuates ferroptosis. In contrast to tumor-associated macrophages, adipose tissue macrophages release exosomes containing miR-140-5p, which reduces SLC7A11 expression (Zhao et al., 2022). A lower amount of SLC7A11 enhances lipid peroxidation and mitochondrial dysfunction by decreasing cystine import and consequently, glutathione synthesis.

Taken together, iron metabolism links inflammation and ferroptosis. Inflammatory conditions alter cellular iron homeostasis and thereby their ferroptotic susceptibility. The other way round, ferroptosis supports inflammation by recruiting and activating immune cells.

Conclusion

During the last decade, ferroptosis gained attention in basic and applied sciences, being connected with various disease conditions. Ferroptosis as of now emerges as a therapeutic target but whether it has to be induced or inhibited strongly depends on the context. To generalize, induction of ferroptosis appears favorable in cancer, while its inhibition attenuates severe inflammation. Under inflammatory conditions, ferroptotic cells evoke immune responses including cytokine production and immune cell attraction. Unfortunately, which immune cells are sensitive to

ferroptosis and to which extent is still under debate. Further, the role of ferroptosis inducers, e.g., erastin or RSL3 in inflammation appears to be ambivalent, which may point to off-target effects. While RSL3 promotes NF-κB signaling, erastin rather causes it inhibition. In the future, analyzing the interplay between lipid peroxidation, ferroptosis, and inflammation will increase our understanding of basic signaling principles. While ferroptosis can easily be studied in cell culture, only a few studies have demonstrated an essential role in humans or mice. Therefore, the impact of ferroptosis towards the cross-communication of immune cells with parenchymal cells needs careful evaluation for its *in vivo* relevance. Still, it is hoped that acquired knowledge may open avenues that help to direct ferroptosis under various disease conditions in either promoting or attenuating this from of cell demise.

Author contributions

AW: Writing–original draft. AS: Writing–original draft. Dominik Christian DF: Visualization, Writing–original draft, Writing–review and editing. BB: Funding acquisition, Writing–review and editing.

Funding

The author(s) declare that financial support was received for the research, authorship, and/or publication of this article. This work was supported by the Deutsche Forschungsgemeinschaft (DFG, German Research Foundation), SFB 1039/TP 04.

Conflict of interest

The authors declare that the research was conducted in the absence of any commercial or financial relationships that could be construed as a potential conflict of interest.

Publisher's note

References

Bannai, S., Tsukeda, H., and Okumura, H. (1977). Effect of antioxidants on cultured human diploid fibroblasts exposed to cystine-free medium. *Biochem. Biophys. Res. Commun.* 74 (4), 1582–1588. doi:10.1016/0006-291x(77)90623-4

Benatzy, Y., Palmer, M. A., and Brüne, B. (2022). Arachidonate 15-lipoxygenase type B: regulation, function, and its role in pathophysiology. *Front. Pharmacol.* 13, 1042420. doi:10.3389/fphar.2022.1042420

Benatzy, Y., Palmer, M. A., Lütjohann, D., Ohno, R.-I., Kampschulte, N., Schebb, N. H., et al. (2024). ALOX15B controls macrophage cholesterol homeostasis via lipid peroxidation, ERK1/2 and SREBP2. *Redox Biol.* 72, 103149. doi:10.1016/j.redox.2024.103149

Berndt, C., Alborzinia, H., Amen, V. S., Ayton, S., Barayeu, U., Bartelt, A., et al. (2024). Ferroptosis in health and disease. *Redox Biol.* 75, 103211. doi:10.1016/j.redox.2024.103211

Bersuker, K., Hendricks, J. M., Li, Z., Magtanong, L., Ford, B., Tang, P. H., et al. (2019). The CoQ oxidoreductase FSP1 acts parallel to GPX4 to inhibit ferroptosis. *Nature* 575 (7784), 688–692. doi:10.1038/s41586-019-1705-2

Bonizzi, G., and Karin, M. (2004). The two NF-kappaB activation pathways and their role in innate and adaptive immunity. *Trends Immunol.* 25 (6), 280–288. doi:10.1016/j.it.2004.03.008

Chaudhary, N., Choudhary, B. S., Shah, S. G., Khapare, N., Dwivedi, N., Gaikwad, A., et al. (2021). Lipocalin 2 expression promotes tumor progression and therapy resistance by inhibiting ferroptosis in colorectal cancer. *Int. J. Cancer* 149 (7), 1495–1511. doi:10.1002/ijc.33711

Chen, Y., Fang, Z.-M., Yi, X., Wei, X., and Jiang, D.-S. (2023a). The interaction between ferroptosis and inflammatory signaling pathways. *Cell Death Dis.* 14 (3), 205. doi:10.1038/s41419-023-05716-0

Chen, Z., Li, J., Peng, H., Zhang, M., Wu, X., Gui, F., et al. (2023b). Meteorin-like/Meteorin-β protects LPS-induced acute lung injury by activating SIRT1-P53-SLC7A11 mediated ferroptosis pathway. *Mol. Med.* 29, 144. doi:10.1186/s10020-023-00714-6

Deng, L., He, S., Li, Y., Ding, R., Li, X., Guo, N., et al. (2023). Identification of lipocalin 2 as a potential ferroptosis-related gene in ulcerative colitis. *Inflamm. Bowel Dis.* 29 (9), 1446–1457. doi:10.1093/ibd/izad050

Dixon, S. J., Lemberg, K. M., Lamprecht, M. R., Skouta, R., Zaitsev, E. M., Gleason, C. E., et al. (2012). Ferroptosis: an iron-dependent form of non-apoptotic cell death. *Cell* 149 (5), 1060–1072. doi:10.1016/j.cell.2012.03.042

Doll, S., Freitas, F. P., Shah, R., Aldrovandi, M., da Silva, M. C., Ingold, I., et al. (2019). FSP1 is a glutathione-independent ferroptosis suppressor. *Nature* 575 (7784), 693–698. doi:10.1038/s41586-019-1707-0

Eagle, H. (1955). The specific amino acid requirements of a human carcinoma cell (Stain HeLa) in tissue culture. *J. Exp. Med.* 102 (1), 37–48. doi:10.1084/jem.102.1.37

Fenton, H. J. H. (1894). LXXIII.—oxidation of tartaric acid in presence of iron. *J. Chem. Soc.* 65, 899–910. doi:10.1039/ct8946500899

Forcina, G. C., Pope, L., Murray, M., Dong, W., Abu-Remaileh, M., Bertozzi, C. R., et al. (2022). Ferroptosis regulation by the NGLY1/NFE2L1 pathway. *Proc. Natl. Acad. Sci. U. S. A.* 119 (11), e2118646119. doi:10.1073/pnas.2118646119

Fuhrmann, D. C., Becker, S., and Brüne, B. (2023). Mitochondrial ferritin expression in human macrophages is facilitated by thrombin-mediated cleavage under hypoxia. *FEBS Lett.* 597 (2), 276–287. doi:10.1002/1873-3468.14545

Fuhrmann, D. C., and Brüne, B. (2022). A graphical journey through iron metabolism, microRNAs, and hypoxia in ferroptosis. *Redox Biol.* 54, 102365. doi:10.1016/j.redox.2022.102365

Fuhrmann, D. C., Mondorf, A., Beifuß, J., Jung, M., and Brüne, B. (2020). Hypoxia inhibits ferritinophagy, increases mitochondrial ferritin, and protects from ferroptosis. *Redox Biol.* 36, 101670. doi:10.1016/j.redox.2020.101670

Fuhrmann, D. C., Tausendschon, M., Wittig, I., Steger, M., Ding, M. G., Schmid, T., et al. (2015). Inactivation of tristetraprolin in chronic hypoxia provokes the expression of cathepsin B. *Mol. Cell. Biol.* 35 (3), 619–630. doi:10.1128/MCB.01034-14

Fuhrmann, D. C., Wittig, I., and Brüne, B. (2018). TMEM126B deficiency reduces mitochondrial SDH oxidation by LPS, attenuating HIF-1α stabilization and IL-1β expression. *Redox Biol.* 20, 204–216. doi:10.1016/j.redox.2018.10.007

Geng, N., Shi, B.-J., Li, S.-L., Zhong, Z.-Y., Li, Y.-C., Xua, W.-L., et al. (2018). Knockdown of ferroportin accelerates erastin-induced ferroptosis in neuroblastoma cells. *Eur. Rev. Med. Pharmacol. Sci.* 22 (12), 3826–3836. doi:10.26355/eurrev_201806_15267

Holmquist-Mengelbier, L., Fredlund, E., Löfstedt, T., Noguera, R., Navarro, S., Nilsson, H., et al. (2006). Recruitment of HIF-1alpha and HIF-2alpha to common target genes is differentially regulated in neuroblastoma: HIF-2alpha promotes an aggressive phenotype. *Cancer Cell* 10 (5), 413–423. doi:10.1016/j.ccr.2006.08.026

Huang, Y., Li, L., Li, Y., Lu, N., Qin, H., Wang, R., et al. (2024). Knockdown of LncRNA Lcn2-204 alleviates sepsis-induced myocardial injury by regulation of iron overload and ferroptosis. *J. Mol. Cell Cardiol.* 192, 79–93. doi:10.1016/j.yjmcc.2024.05.007

Huang, Y., Zhang, N., Xie, C., You, Y., Guo, L., Ye, F., et al. (2022). Lipocalin-2 in neutrophils induces ferroptosis in septic cardiac dysfunction via increasing labile iron pool of cardiomyocytes. *Front. Cardiovasc Med.* 9, 922534. doi:10.3389/fcvm.2022.922534

Jiang, J., Zhu, J., Qiu, P., Ni, J., Zhu, W., and Wang, X. (2023). HNRNPA2B1-mediated m6A modification of FOXM1 promotes drug resistance and inhibits ferroptosis in endometrial cancer via regulation of LCN2. *Funct. Integr. Genomics* 24 (1), 3. doi:10.1007/s10142-023-01279-7

Jiang, X., Stockwell, B. R., and Conrad, M. (2021). Ferroptosis: mechanisms, biology and role in disease. *Nat. Rev. Mol. Cell Biol.* 22 (4), 266–282. doi:10.1038/s41580-020-00324-8

Jung, M., Mertens, C., Bauer, R., Rehwald, C., and Brüne, B. (2017). Lipocalin-2 and iron trafficking in the tumor microenvironment. *Pharmacol. Res.* 120, 146–156. doi:10.1016/j.phrs.2017.03.018

Jung, M., Mertens, C., and Brüne, B. (2015). Macrophage iron homeostasis and polarization in the context of cancer. *Immunobiology* 220 (2), 295–304. doi:10.1016/j.imbio.2014.09.011

Kong, R., Wang, N., Han, W., Bao, W., and Lu, J. (2021). IFNγ-mediated repression of system xc-drives vulnerability to induced ferroptosis in hepatocellular carcinoma cells. *J. Leukoc. Biol.* 110 (2), 301–314. doi:10.1002/JLB.3MA1220-815RRR

Koppula, P., Zhuang, L., and Gan, B. (2021). Cystine transporter SLC7A11/xCT in cancer: ferroptosis, nutrient dependency, and cancer therapy. *Protein Cell* 12 (8), 599–620. doi:10.1007/s13238-020-00789-5

Kotschi, S., Jung, A., Willemsen, N., Ofoghi, A., Proneth, B., Conrad, M., et al. (2022). NFE2L1-mediated proteasome function protects from ferroptosis. *Mol. Metab.* 57, 101436. doi:10.1016/j.molmet.2022.101436

Kou, Z., Tran, F., Colon, T., Shteynfeld, Y., Noh, S., Chen, F., et al. (2024). AhR signaling modulates Ferroptosis by regulating SLC7A11 expression. *Toxicol. Appl. Pharmacol.* 486, 116936. doi:10.1016/j.taap.2024.116936

Li, C., Deng, X., Xie, X., Liu, Y., Friedmann Angeli, J. P., and Lai, L. (2018). Activation of glutathione peroxidase 4 as a novel anti-inflammatory strategy. *Front. Pharmacol.* 9, 1120. doi:10.3389/fphar.2018.01120

Li, S., He, Y., Chen, K., Sun, J., Zhang, L., He, Y., et al. (2021). RSL3 drives ferroptosis through NF-κB pathway activation and GPX4 depletion in glioblastoma. *Oxid. Med. Cell Longev.* 2021, 2915019. doi:10.1155/2021/2915019

Liu, Y., Luo, X., Chen, Y., Dang, J., Zeng, D., Guo, X., et al. (2024). Heterogeneous ferroptosis susceptibility of macrophages caused by focal iron overload exacerbates rheumatoid arthritis. *Redox Biol.* 69, 103008. doi:10.1016/j.redox.2023.103008

Liu, Y., Yang, G., Huo, S., Wu, J., Ren, P., Cao, Y., et al. (2023). Lutein suppresses ferroptosis of cardiac microvascular endothelial cells via positive regulation of IRF in cardiac hypertrophy. *Eur. J. Pharmacol.* 959, 176081. doi:10.1016/j.ejphar.2023.176081

Luo, Y., Chen, Y., Jin, H., Hou, B., Li, H., Li, X., et al. (2023). The suppression of cervical cancer ferroptosis by macrophages: the attenuation of ALOX15 in cancer cells by macrophages-derived exosomes. *Acta Pharm. Sin. B* 13 (6), 2645–2662. doi:10.1016/j.apsb.2023.03.025

Marques, O., Weiss, G., and Muckenthaler, M. U. (2022). The role of iron in chronic inflammatory diseases: from mechanisms to treatment options in anemia of inflammation. *Blood* 140 (19), 2011–2023. doi:10.1182/blood.2021013472

Meier, J. K., Schnetz, M., Beck, S., Schmid, T., Dominguez, M., Kalinovic, S., et al. (2021). Iron-bound lipocalin-2 protects renal cell carcinoma from ferroptosis. *Metabolites* 11 (5), 329. doi:10.3390/metabo11050329

Muckenthaler, M. U., Rivella, S., Hentze, M. W., and Galy, B. (2017). A red carpet for iron metabolism. *Cell* 168 (3), 344–361. doi:10.1016/j.cell.2016.12.034

Namgaladze, D., Fuhrmann, D. C., and Brüne, B. (2022). Interplay of Nrf2 and BACH1 in inducing ferroportin expression and enhancing resistance of human macrophages towards ferroptosis. *Cell Death Discov.* 8, 327. doi:10.1038/s41420-022-01117-y

Nemeth, E., and Ganz, T. (2021). Hepcidin-ferroportin interaction controls systemic iron homeostasis. *Int. J. Mol. Sci.* 22 (12), 6493. doi:10.3390/ijms22126493

Oh, B. M., Lee, S.-J., Park, G. L., Hwang, Y. S., Lim, J., Park, E. S., et al. (2019). Erastin inhibits septic shock and inflammatory gene expression via suppression of the NF-κB pathway. *J. Clin. Med.* 8 (12), 2210. doi:10.3390/jcm8122210

Perkins, N. D. (2007). Integrating cell-signalling pathways with NF-kappaB and IKK function. *Nat. Rev. Mol. cell Biol.* 8 (1), 49–62. doi:10.1038/nrm2083

Schwantes, A., Wickert, A., Becker, S., Baer, P. C., Weigert, A., Brüne, B., et al. (2024). Tumor associated macrophages transfer ceruloplasmin mRNA to fibrosarcoma cells and protect them from ferroptosis. *Redox Biol.* 71, 103093. doi:10.1016/j.redox.2024.103093

Scortegagna, M., Cataisson, C., Martin, R. J., Hicklin, D. J., Schreiber, R. D., Yuspa, S. H., et al. (2008). HIF-1alpha regulates epithelial inflammation by cell autonomous NFkappaB activation and paracrine stromal remodeling. *Blood* 111 (7), 3343–3354. doi:10.1182/blood-2007-10-115758

Semenza, G. L. (2012). Hypoxia-inducible factors in physiology and medicine. *Cell* 148 (3), 399–408. doi:10.1016/j.cell.2012.01.021

Semenza, G. L., Nejfelt, M. K., Chi, S. M., and Antonarakis, S. E. (1991). Hypoxia-inducible nuclear factors bind to an enhancer element located 3' to the human erythropoietin gene. *Proc. Natl. Acad. Sci. U. S. A.* 88 (13), 5680–5684. doi:10.1073/pnas.88.13.5680

Stockwell, B. R. (2022). Ferroptosis turns 10: emerging mechanisms, physiological functions, and therapeutic applications. *Cell* 185 (14), 2401–2421. doi:10.1016/j.cell.2022.06.003

Su, X., Xie, Y., Zhang, J., Li, M., Zhang, Q., Jin, G., et al. (2023). Correction: HIF-α activation by the prolyl hydroxylase inhibitor roxadustat suppresses chemoresistant glioblastoma growth by inducing ferroptosis. *Cell Death Dis.* 14 (1), 31. doi:10.1038/s41419-022-05532-y

Taylor, C. T., and Colgan, S. P. (2017). Regulation of immunity and inflammation by hypoxia in immunological niches. *Nat. Rev. Immunol.* 17 (12), 774–785. doi:10.1038/nri.2017.103

Tian, C., Zheng, M., Lan, X., Liu, L., Ye, Z., and Li, C. (2023). Silencing LCN2 enhances RSL3-induced ferroptosis in T cell acute lymphoblastic leukemia. *Gene* 879, 147597. doi:10.1016/j.gene.2023.147597

Ursini, F., Maiorino, M., and Gregolin, C. (1985). The selenoenzyme phospholipid hydroperoxide glutathione peroxidase. *Biochim. Biophys. Acta* 839 (1), 62–70. doi:10.1016/0304-4165(85)90182-5

Valashedi, M. R., Roushandeh, A. M., Tomita, K., Kuwahara, Y., Pourmohammadi-Bejarpasi, Z., Kozani, P. S., et al. (2022). CRISPR/Cas9-mediated knockout of Lcn2 in human breast cancer cell line MDA-MB-231 ameliorates erastin-mediated ferroptosis and increases cisplatin vulnerability. *Life Sci.* 304, 120704. doi:10.1016/j.lfs.2022.120704

van Uden, P., Kenneth, N. S., and Rocha, S. (2008). Regulation of hypoxia-inducible factor-1alpha by NF-kappaB. *Biochem. J.* 412 (3), 477–484. doi:10.1042/BJ20080476

van Uden, P., Kenneth, N. S., Webster, R., Muller, H. A., Mudie, S., and Rocha, S. (2011). Evolutionary conserved regulation of HIF-1β by NF-κB. *PLoS Genet.* 7 (1), e1001285. doi:10.1371/journal.pgen.1001285

Walmsley, S. R., Print, C., Farahi, N., Peyssonnaux, C., Johnson, R. S., Cramer, T., et al. (2005). Hypoxia-induced neutrophil survival is mediated by HIF-1alpha-dependent NF-kappaB activity. *J. Exp. Med.* 201 (1), 105–115. doi:10.1084/jem.20040624

Wu, J., Liu, Q., Zhang, X., Tan, M., Li, X., Liu, P., et al. (2022). The interaction between STING and NCOA4 exacerbates lethal sepsis by orchestrating ferroptosis and inflammatory responses in macrophages. *Cell Death Dis.* 13 (7), 653. doi:10.1038/s41419-022-05115-x

Wu, S., Zhou, Y., Liang, J., Ying, P., Situ, Q., Tan, X., et al. (2024). Upregulation of NF-κB by USP24 aggravates ferroptosis in diabetic cardiomyopathy. *Free Radic. Biol. Med.* 210, 352–366. doi:10.1016/j.freeradbiomed.2023.11.032

Xiao, Z., Kong, B., Fang, J., Qin, T., Dai, C., Shuai, W., et al. (2021). Ferrostatin-1 alleviates lipopolysaccharide-induced cardiac dysfunction. *Bioengineered* 12 (2), 9367–9376. doi:10.1080/21655979.2021.2001913

Yan, N., Xu, Z., Qu, C., and Zhang, J. (2021). Dimethyl fumarate improves cognitive deficits in chronic cerebral hypoperfusion rats by alleviating inflammation, oxidative stress, and ferroptosis via NRF2/ARE/NF-κB signal pathway. *Int. Immunopharmacol.* 98, 107844. doi:10.1016/j.intimp.2021.107844

Yang, Z., Su, W., Wei, X., Qu, S., Zhao, D., Zhou, J., et al. (2023). HIF-1α drives resistance to ferroptosis in solid tumors by promoting lactate production and activating SLC1A1. *Cell Rep.* 42 (8), 112945. doi:10.1016/j.celrep.2023.112945

Yao, F., Deng, Y., Zhao, Y., Mei, Y., Zhang, Y., Liu, X., et al. (2021). A targetable LIFR-NF-κB-LCN2 axis controls liver tumorigenesis and vulnerability to ferroptosis. *Nat. Commun.* 12 (1), 7333. doi:10.1038/s41467-021-27452-9

Yu, X., Zhu, D., Luo, B., Kou, W., Cheng, Y., and Zhu, Y. (2022). IFNγ enhances ferroptosis by increasing JAK-STAT pathway activation to suppress SLCA711 expression in adrenocortical carcinoma. *Oncol. Rep.* 47 (5), 97. doi:10.3892/or.2022.8308

Zeng, Z., Huang, H., Zhang, J., Liu, Y., Zhong, W., Chen, W., et al. (2022). HDM induce airway epithelial cell ferroptosis and promote inflammation by activating ferritinophagy in asthma. *FASEB J.* 36 (6), e22359. doi:10.1096/fj.202101977RR

Zhan, J., Chen, J., Deng, L., Lu, Y., and Luo, L. (2024). Exploring the ferroptosis-related gene lipocalin 2 as a potential biomarker for sepsis-induced acute respiratory distress syndrome based on machine learning. *Biochim. Biophys. Acta Mol. Basis Dis.* 1870 (4), 167101. doi:10.1016/j.bbadis.2024.167101

Zhang, J., Wang, Y., Fan, M., Guan, Y., Zhang, W., Huang, F., et al. (2024). Reactive oxygen species regulation by NCF1 governs ferroptosis susceptibility of Kupffer cells to MASH. *Cell Metab.* 36, 1745–1763.e6. doi:10.1016/j.cmet.2024.05.008

Zhao, J., Yi, Z., Deng, G., Li, Y., Li, J., Qin, M., et al. (2024). STING modulates iron metabolism to promote liver injury and inflammation in acute immune hepatitis. *Free Radic. Biol. Med.* 210, 367–377. doi:10.1016/j.freeradbiomed.2023.11.038

Zhao, X., Si, L., Bian, J., Pan, C., Guo, W., Qin, P., et al. (2022). Adipose tissue macrophage-derived exosomes induce ferroptosis via glutathione synthesis inhibition by targeting SLC7A11 in obesity-induced cardiac injury. *Free Radic. Biol. Med.* 182, 232–245. doi:10.1016/j.freeradbiomed.2022.02.033

Zheng, S., Mo, J., Zhang, J., and Chen, Y. (2023). HIF-1α inhibits ferroptosis and promotes malignant progression in non-small cell lung cancer by activating the Hippo-YAP signalling pathway. *Oncol. Lett.* 25 (3), 90. doi:10.3892/ol.2023.13676

Zheng, Z., Li, Y., Jin, G., Huang, T., Zou, M., and Duan, S. (2020). The biological role of arachidonic acid 12-lipoxygenase (ALOX12) in various human diseases. *Biomed. Pharmacother.* 129, 110354. doi:10.1016/j.biopha.2020.110354

Zilka, O., Shah, R., Li, B., Friedmann Angeli, J. P., Griesser, M., Conrad, M., et al. (2017). On the mechanism of cytoprotection by ferrostatin-1 and liproxstatin-1 and the role of lipid peroxidation in ferroptotic cell death. *ACS Cent. Sci.* 3 (3), 232–243. doi:10.1021/acscentsci.7b00028

Zou, Y., Palte, M. J., Deik, A. A., Li, H., Eaton, J. K., Wang, W., et al. (2019). A GPX4-dependent cancer cell state underlies the clear-cell morphology and confers sensitivity to ferroptosis. *Nat. Commun.* 10 (1), 1617. doi:10.1038/s41467-019-09277-9

frontiers | Frontiers in Pharmacology

TYPE Original Research
PUBLISHED 21 November 2024
DOI 10.3389/fphar.2024.1503648

OPEN ACCESS

EDITED BY
Angelo Sala,
University of Milan, Italy

REVIEWED BY
Giuseppe Spaziano,
University of Campania Luigi Vanvitelli, Italy
Yago Amigo Pinho Jannini-Sá,
Cedars Sinai Medical Center, United States

*CORRESPONDENCE
Mikael Adner,
mikael.adner@ki.se

RECEIVED 29 September 2024
ACCEPTED 06 November 2024
PUBLISHED 21 November 2024

CITATION
Dong C, Liu J, Quaranta A, Jing X, Nie M, Wheelock CE, Murrell B, Coquet JM, Bowden TM, Engstrand T and Adner M (2024) Polyvinylalcohol-carbazate mitigates acute lung injury caused by hydrochloric acid. *Front. Pharmacol.* 15:1503648. doi: 10.3389/fphar.2024.1503648

Polyvinylalcohol-carbazate mitigates acute lung injury caused by hydrochloric acid

Caijuan Dong[1,2], Jielu Liu[1], Alessandro Quaranta[3], Xu Jing[4], Mu Nie[1], Craig E. Wheelock[3,5], Benjamin Murrell[4], Jonathan M. Coquet[4], Tim Melander Bowden [6], Thomas Engstrand[7] and Mikael Adner[1]*

[1]Experimental Asthma and Allergy Research Unit, Institute of Environmental Medicine (IMM), Karolinska Institutet, Stockholm, Sweden, [2]Department of Cardiology, The First Affiliated Hospital of Soochow University, Suzhou, Jiang Su, China, [3]Unit of Integrative Metabolomics, Institute of Environmental Medicine (IMM), Karolinska Institutet, Stockholm, Sweden, [4]Department of Microbiology, Tumor and Cell Biology, Karolinska Institutet, Stockholm, Sweden, [5]Department of Respiratory Medicine and Allergy, Karolinska University Hospital, Stockholm, Sweden, [6]Department of Chemistry-Ångström Laboratory, Uppsala University, Uppsala, Sweden, [7]Department of Molecular Medicine and Surgery, plastic surgery section, Karolinska University Hospital, Stockholm, Sweden

Background: Acute lung injury (ALI) and acute respiratory distress syndrome (ARDS) are important causes of morbidity and mortality in critically ill patients. Gastric contents aspiration is one of the most common causes of ALI/ARDS. To date, there are still no specific and effective pharmacological treatments for ALI/ARDS. Polyvinylalcohol-carbazate (PVAC), a polymer that can bind endogenous aldehydes, neutralize oxidative stress and inhibit inflammatory factors, may be a potential treatment for ALI/ARDS.

Methods: A hydrochloric acid (HCl) induced mouse model was employed to assess the effect of PVAC. The changes of lung mechanics, pulmonary edema, histology and immune cells, cytokines, and lipid mediators in bronchioalveolar lavage fluid (BALF) were investigated in HCl-challenged mice.

Results: In the HCl model, PVAC administration alleviated airway hyperresponsiveness and improved pulmonary edema and damage. In addition, it decreased the recruitment of neutrophils to the lung, and inhibited the increase of IL-6, TNF-α and leukotriene B_4.

Conclusion: These data indicates that PVAC is a potential candidate for the treatment of ALI/ARDS induced by aspiration of gastric acid or for the control of "asthma-like" symptoms in patients with gastroesophageal reflux.

KEYWORDS

acute respiratory distress syndrome, aspiration pneumonia, oxidative stress, pharmacological treatment, intranasal administration

1 Introduction

Acute lung injury (ALI) and its more severe form, acute respiratory distress syndrome (ARDS), are common causes of morbidity and mortality in critically ill patients. The incidence of ARDS ranges from 4 to 75 cases per 100,000 people per year and the mortality from 40% to 50% (Villar et al., 2016). The main pathophysiological mechanisms of ALI/ARDS include increased vascular permeability, cytokine overproduction, leukocyte recruitment, and

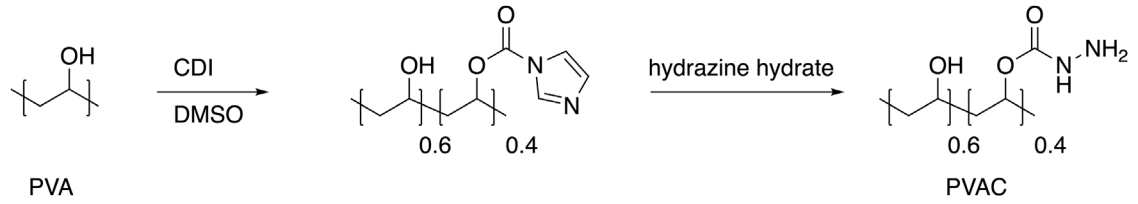

FIGURE 1
Synthesis of PVAC. PVAC is synthesized starting from polyvinyl alcohol (PVA). Activation of the hydroxyl group with carbonyl diimidazole (CDI) in DMSO renders a carbamate intermediate that upon treatment with hydrazine hydrate gives the product polyvinylalcohol-carbazate (PVAC). The degree of substitution of carbazate groups is 0.4.

surfactant dysfunction (Meyer et al., 2021). At present, there is no specific drug for ARDS, so it is of great significance to develop more potential drugs for the treatment of ALI/ARDS.

Gastric contents aspiration is one of the most common causes of ALI/ARDS (Kaku et al., 2020). Aspiration occurs silently but very common in critically ill patients (Metheny et al., 2006). Inhaled substances may include food particles, stomach acid/hydrochloric acid (HCl), blood, or bacteria. Among them, HCl has the greatest effect on lung injury. About one-third of patients with aspiration pneumonia will develop a more severe and prolonged course associated with ALI/ARDS (Raghavendran et al., 2011). The pathogenic mechanisms of HCl-induced ALI/ARDS has shown to relate to reduced levels of anti-oxidating enzymes along with increased levels of lipid peroxidation in lung tissues indicating enhanced oxidative stress (El-Shahat et al., 2021), However, there are no effective pharmacological treatments for ALI/ARDS.

Polyvinylalcohol-carbazate (PVAC) is a highly soluble polymer in aqueous solution (Figure 1), known for its capacity to bind endogenous aldehydes and neutralize oxidative stress (Sellberg et al., 2019). Studies have demonstrated that PVAC gel inhibits inflammation in osteoarthritis joints by quenching reactive oxygen species and lipid peroxidation products such as 4-hydroxynonenal (Fredriksson et al., 2017). Given these properties, it is of interest for investigating whether PVAC can inhibit ALI triggered by oxidative stress. Therefore, our study aimed to evaluate the efficacy of intranasal administration of PVAC in ALI/ARDS animal models induced by HCl.

2 Materials and methods

2.1 Ethical permission

All animal experiments were approved by the Stockholm ethics committee (the permit number:10,712-2020). Animals were housed at Astrid Fagraeus laboratory (KM-F) with 12-h dark/light cycle and had free access to food and water. All the *in vivo* experiments were performed at KM-F after at least 1 week of acclimatization.

2.2 HCl-induced ALI/ARDS mouse model and drug treatment

Male C57BL/6J mice (approximately 25 g, 8–12 weeks old) were ordered from Envigo (Horst, Netherlands). The mice were housed in a biosafety level 1 laboratory at Astrid Fagraeus Laboratory, Karolinska Institutet. Thirty minutes after intranasal administration of PVAC (3 mg/kg), the mice were instilled intratracheally with HCl (pH 1.5; 40 μL). Three hours post HCl exposure, the airway responses to methacholine were assessed followed by bronchoalveolar lavage and sample collections. The left lungs were fixed in 4% formaldehyde and right lungs were snap-frozen for further studies.

The dose rationale for PVAC is based on safety parameters, including molecular behavior and toxicological outcomes (unpublished and proprietary data with permission by T. Bowden and T. Engstrand, PVAC Medical Technologies LTD.). Higher concentrations of PVAC, a polymer, can increase viscosity and cause aggregation. *In vitro* and preclinical studies set the upper concentration limit, with the current study using 3 mg/mL, which is below this limit. Safety studies showed that both rats and rabbits tolerated lower doses of PVAC, but higher doses led to granular material deposition in phagocytic cells. The current study used a dose below the no-observed-adverse-effect-level (NOAEL), with no such depositions observed in the lungs of treated animals.

2.3 Airway responsiveness test

Mice were anesthetized with ketamine hydrochloride (75 mg/kg, Ketaminol® Vet., Intervet, Stockholm, Sweden) and medetomidine hydrochloride (1 mg/kg, Cepetor®Vet., VETMEDIC, Stockholm, Sweden). An 18-gauge blunt metal cannula was inserted into the trachea and secured in place with a nylon suture. Animals were placed on a heating pad and connected to the flexiVent system (flexiVent FX4, SCIREQ Inc., Montreal, Qc, Canada), where airway responses to methacholine (MCh) (1.56 mg/mL to 12.5 mg/mL) were assessed.

2.4 Wet to dry weight ratio

The left lungs were harvested and weighed to obtain the wet weight. The lungs were then placed into a drying oven at 80°C for 24 h to obtain the dry weight. The wet to dry weight ratio was calculated to evaluate the degree of lung edema (Wet to dry ratio = wet weight/dry weight).

2.5 Bronchoalveolar lavage

Bronchoalveolar lavage was performed directly after lung function measurements. 0.8 mL cold PBS was gently lavaged twice in the lung. The bronchoalveolar lavage fluid (BALF) was centrifuged at +4°C, 1,000 rpm, for 10 min and the supernatant was stored at −80°C until use. Total cell number was counted using Turk staining under microscope and expressed as cells·ml^{-1} BALF. Differential cell counts were performed on May-Grünwald/Giemsa stained cytospins, counting a minimum of 300 cells, in a blinded manner.

2.6 H&E histological staining

Hematoxylin and eosin (H&E) staining of paraffin-embedded lung tissue sections were performed to evaluate the lung damage. Lung tissues were fixed with 4% formalin for 24 h, embedded in paraffin, and sectioned at 5-μm thickness. After deparaffinization and dehydration, sections were stained with H&E and were photographed using a light microscope (Nikon Eclipse TS100) equipped with a camera (DS-Fi1; Nikon) and software (NIS-Elements F3.0). Lung injury was scored by assessing the degree of inflammatory cell infiltration, hemorrhage, interstitial and alveolar edema and thickness of the alveolar septum in five randomly selected fields under a light microscope from 0-4 (0: No damage, 1: Mild damage, 2: moderate damage, 3: severe damage and 4: highly severe histological damage).

2.7 ELISA

Enzyme-linked immunosorbent assay (ELISA) was used for determining the protein concentrations of mouse IL-6 (M6000B, R&D Systems), TNF-α (RAB0477, Sigma Aldrich), and Myeloperoxidase (MPO) (RAB0374, Sigma Aldrich). The ELISAs were performed according to the manufacturers' protocols. Absorbance values were detected at 450 nm using a microplate reader and concentrations were calculated according to the standard curves plotted.

2.8 Lipid mediator characterizations

Lipid mediators were extracted and analyzed by following a previously published method (Kolmert et al., 2018). Briefly, 800 μL of BALF were added with an internal standard solution, diluted to 1.5 mL with a solution consisting of 0.2 M Na_2HPO_4/0.1 M citric acid (58/42 v/v, pH 5.6), and extracted on preconditioned ABN Evolute Express solid-phase extraction cartridges (3cc/60 mg, Biotage, Uppsala, Sweden). A total of 110 lipid mediators were quantified by liquid chromatography coupled to tandem mass spectrometry (LC-MS/MS) on an Acquity UPLC coupled to a Xevo TQ-XS mass spectrometer (Waters, Milford, MA, USA).

2.9 Statistical analysis

The experimental results were analyzed using Graphpad Prism 9.0 statistical software (GraphPad, USA). Data were presented as mean ± SEM. Two-group data were analyzed by unpaired t-test, and multiple-group data were analyzed by one-way or two-way ANOVA. Sidak's multiple comparisons test was used for pairwise comparisons in the analysis of variance. *P*-value <0.05 was considered statistically significant.

3 Results

3.1 PVAC improves lung function in HCl mice

To assess airway responsiveness, HCl-challenged mice were connected to the flexiVent system and exposed to increasing concentrations of methacholine (MCh) aerosol. Several parameters were recorded, including the total resistance (Rrs) and elastance (Ers) of the respiratory system, as well as the resistance in the conducting airways (Newtonian resistance; Rn), peripheral lung tissue damping (G), and peripheral tissue elastance (H).

When comparing the saline group and the saline + PVAC group, no significant differences were found in Rrs, Ers, Rn, G, and H ($p > 0.05$) (Figure 2), whereas HCl-challenged caused an increase of these parameters at 6.25 and 12.5 mg/mL MCh ($p < 0.05$). Pretreatment with PVAC dampened the increase induced by HCl in all parameters ($p < 0.05$).

3.2 PVAC improves lung edema and lung damage in HCl mice

Examining whether PVAC affected pulmonary edema, the calculation of the wet to dry weight ratio of the left lung tissue showed that HCl exposure significantly had a significantly higher ratio than the control group ($P< 0.01$), whereas PVAC pretreatment significantly reduced HCl-induced pulmonary edema ($P< 0.01$) (Figures 3A–C).

Lung damage was assessed using H&E-stained slides. Compared to control mice (saline), no histological changes were observed in the lung specimens of saline and PVAC-treated mice (Figure 3D). However, HCl exposure induced massive neutrophil infiltration around the pulmonary vascular and interstitial spaces, marked swelling of the alveolar walls, severe hemorrhage, and significant damage to the alveolar structure (Figure 3E). The lung injury score of the HCl + PVAC group was significantly lower than that of the HCl group ($p < 0.01$), but still higher than that of the control group ($p < 0.001$) (Figure 3D).

3.3 PVAC alleviates inflammation in BALF from HCl mice

To examine inflammation, an analysis of inflammatory cells in bronchoalveolar lavage fluid (BALF) was conducted. Exposure to HCl significantly increased the total number of cells, neutrophils,

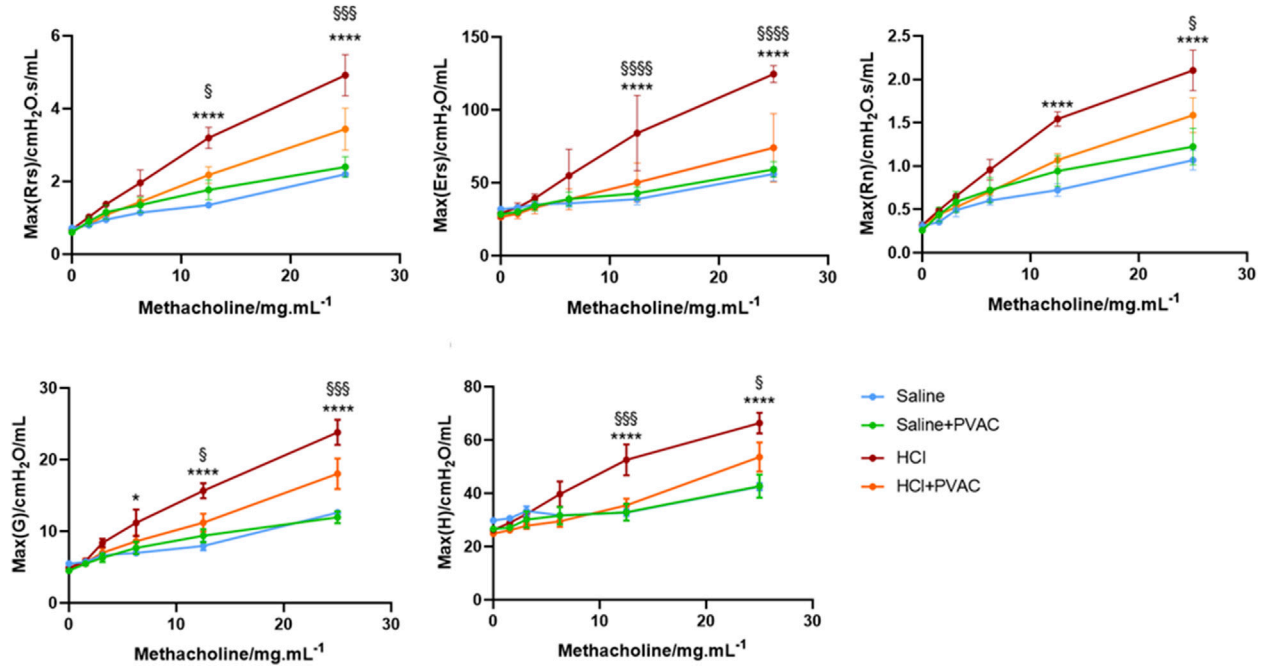

FIGURE 2
Airway responsiveness to Methacholine in HCl-induced ALI/ARDS mice. The AHR was measured with a small animal ventilator (flexiVent; Scireq), as previously described. Resistance of the respiratory system (Rrs), elastance of the respiratory system (Ers), Newtonian Resistance (Rn), tissue damping (G) and tissue elastance (H) were recorded. The results were expressed as mean ± SEM (n = 4–5). saline: animals exposed to saline and received saline pretreatment. saline + PVAC: animals exposed to saline and received PVAC pretreatment. HCl: animals exposed to HCl and received saline pretreatment. HCl + PVAC: animals exposed to HCl and received PVAC pretreatment. *P< 0.05, ****P< 0.0001 vs respective saline, §P< 0.05, §§§P< 0.001, and §§§§P< 0.0001 vs respective HCl + PVAC.

and macrophages compared to the saline group (p < 0.05) (Figures 4A–C). PVAC treatment significantly reduced the number of neutrophils in the BALF of HCl-challenged mice (p < 0.05) (Figure 4B), while the total number of cells and macrophages were not significantly altered. Moreover, HCl significantly increased the total protein levels in BALF (Figure 4D), suggesting that HCl could cause vascular leakage. However, there was no significant change in protein content in BALF in the HCl + PVAC group compared to the HCl group.

As neutrophils is one major important leukocyte in ALI/ARDS (Meyer et al., 2021), the levels of IL-6 and TNF-α associated with neutrophil infiltration and vascular permeability, and MPO as an indicator of neutrophil infiltration were measured in the BALF. Compared with the control group, HCl significantly increased the level of IL-6 in BALF (Figure 4G), whereas TNF-α increased slightly but did not reach statistical significance (Figure 4H). PVAC pretreatment significantly decreased the level of IL-6 in BALF of HCl-challenged mice and the level of TNF-α was also decreased but did not reach statistical significance. For MPO, HCl treatment resulted in a significant increase in MPO activity in BALF which was inhibited by PVAC.

3.4 PVAC modulates lipid mediators in HCl mice

Bioactive lipid mediators are involved in a wide range of physiological and pathological processes, particularly in inflammatory responses (Stables and Gilroy, 2011; Serhan et al., 2014). To investigate the response of lipid mediators in BALF to HCl stimulation and the effect of PVAC on lipid mediators, a broad range of pro- and anti-inflammatory lipid mediators was quantified using LC-MS/MS. HCl treatment increased 42 out of 110 measured lipid mediators, of which 13 were significant. Compared with the control group, HCl caused a significant increase (P< 0.05) of prostaglandin (PG) E_1, PGE_2, 13,14-dihydro-15-keto-PGE_2, leukotriene B_4 (LTB_4), $PGF_{2\alpha}$, 19,20-dihydroxy-docosapentaenoic acid (19(20)-DiHDPA), 12-hydroxy-heptadecatrienoic acid (12-HHTrE), 9-hydroxy-octadecatrienoic acid (HOTrE), 13-HOTrE, 9- hydroxy-octadecadienoic acid (HODE), 13-HODE, 14,15-dihydroxy-eicosatrienoic acid (14,15-DiHETrE), 11-hydroxy-eicosatetraenoic acid (HETE), 20-HETE. Compared with HCl, PVAC could significantly reduce PGE_1 (P<0.05), 13,14-dihydro-15-keto-PGE_2 (P< 0.05) and LTB4 (P< 0.05) (Figures 5B, D, E).

4 Discussion

To our knowledge, this is the first study to evaluate the effect for airway exposure of PVAC. This was assessed on ALI/ARDS animal models. The study revealed the prophylactic effect of PVAC in HCl-induced ALI/ARDS mice. No adverse effects were observed in C57BL/6J mice treated with PVAC, suggesting the safety of PVAC in respiratory diseases. Moreover, pre-treatment of PVAC significantly (i) reduced HCl-induced airway hyperresponsiveness and (ii) improved HCl-induced pulmonary edema and lung

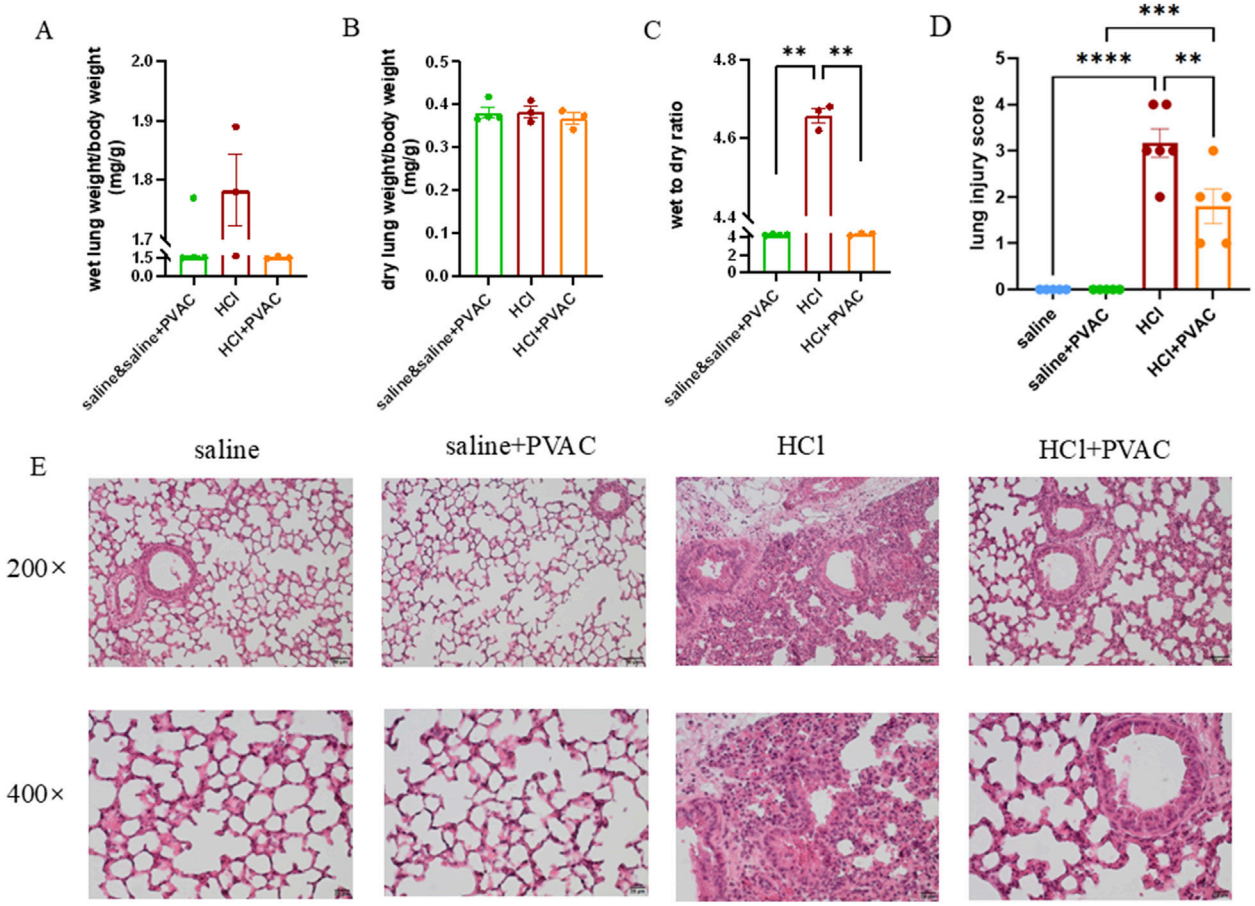

FIGURE 3
HCl-induced lung edema and histological changes in lung tissues. Left lungs were harvested. Some of them were weighed and dried in 80°C oven for 24h to obtain the dry weight. Wet to dry weight ratio was calculated as wet weight/dry weight. The other left lungs were fixed, embedded in paraffin and cut into 5 μm slices. After H&E staining, histological examination was performed by light microscopy and assessed based on the lung injury score. **(A)** Wet weight of left lung (n = 3-4). **(B)** Dry weight of left lung (n = 3-4). **(C)** Wet to dry weight ratio of left lung (n = 3-4). **(D)** lung injuty score (n = 5-6). **(E)** Representative images of H&E-stained lung sections from HCl-challenged mice with and without PVAC pretreatment (bar scale: 50μm and 20 μm). The results were expressed as mean ± SEM. saline: animals exposed to saline and received saline pretreatment. saline + PVAC: animals exposed to saline and received PVAC pretreatment. HCl: animals exposed to HCl and received saline pretreatment. HCl + PVAC: animals exposed to HCl and received PVAC pretreatment. $^{**}P < 0.01$, $^{***}P < 0.001$, and $^{****}p < 0.0001$.

histopathological damage. These effects may be achieved by inhibiting pro-inflammatory cytokines such as IL-6 and TNF-α, and lipid mediators such as LTB_4, thereby reducing neutrophil infiltration and vascular permeability.

Airway hyperresponsiveness is defined as an exaggerated and accelerated constriction of the airway to various stimuli that does not elicit a comparable response in healthy subjects. Consistent with Gilman and colleagues' findings, inhalation of HCl was observed to induce airway hyperresponsiveness in mice (Allen et al., 1985). In the clinic, studies have shown that patients with gastroesophageal reflux suffer airway hyperresponsiveness and "asthma-like" symptoms (Paoletti et al., 2021). There are several possible mechanisms for this such as 1) the barrier disruption caused by HCl facilitates the egress of MCh from the airway lumen to the underlying smooth muscle, resulting in airway hyperresponsiveness, 2) edema within and around the airways that reduces the airway lumen, and 3) elevated cytokines caused by HCl, such as TNF-α, induce calcium influx into airway smooth muscle cells and lead to smooth muscle contraction (Spond et al., 2004). Our study has demonstrated that PVAC can reduce airway hyperresponsiveness in HCl-challenged mice, and a possible mechanism is that PVAC reduces the airway smooth muscle contraction by inhibiting the calcium influx mediated by cytokines such as TNF-α. Moreover, it is possible that PVAC could have important clinical implications for patients with gastroesophageal reflux.

Infiltration and accumulation of leukocytes, especially neutrophils and macrophages in the interstitial and alveolar spaces of the lung, is one of the most important pathological hallmarks of ALI/ARDS (Matthay et al., 2012; Abraham, 2003). Although rapid and appropriate influx of neutrophils from the circulation into the lung is essential for clearance of microbial pathogens and debris from the alveolar space, excessive and persistent sequestration of neutrophils may cause additional damage to the lungs, by releasing several toxic mediators, including proinflammatory cytokines and procoagulant molecules, thereby exacerbating ALI (Abraham, 2003; Bhattacharya and Matthay, 2013). It has been reported that neutrophils in the BALF of ARDS patients is closely related to

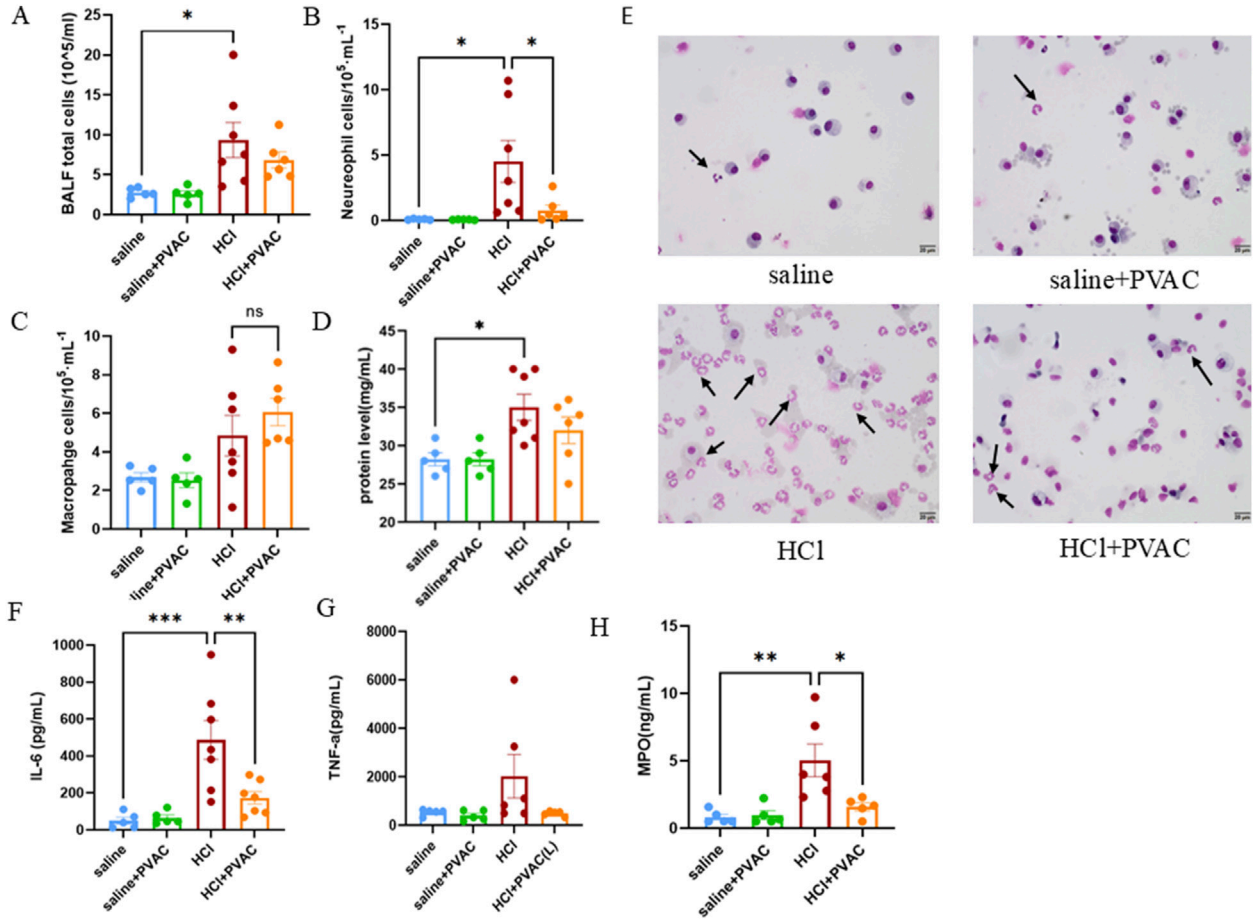

FIGURE 4
Leukocytes, total protein levels and cytokine levels measured in the BALF of HCl-induced ALI/ARDS mice. **(A)** The number of total cells in the BALF. **(B)** The number of neutrophils in the BALF. **(C)** The number of macrophages in the BALF. **(D)** Total protein levels in the BALF. **(E)** Representative images of May-Grünwald/Giemsa-stained cytospin slides from HCl-challenged mice with and without PVAC pretreatment (bar scale: 20 μm). **(F)** IL-6 levels in the BALF. **(G)** TNF-a level in the BALF. **(H)** MPO level in the BALF. The results were expressed as mean ± SEM(n = 5-7). saline: animals exposed to saline and received saline pretreatment. saline + PVAC: animals exposed to saline and received PVAC pretreatment. HCl: animals exposed to HCl and received saline pretreatment. HCl + PVAC: animals exposed to HCl and received PVAC pretreatment. *P< 0.05, **P< 0.01, and ***P< 0.001.

disease severity and poor prognosis (Abraham, 2003). In our study, a significant enhanced neutrophil and macrophage infiltration in BALF were observed in HCl mice. No effects on eosinophils were found suggesting that the effect mainly is T_H1-driven. PVAC pretreatment significantly attenuated HCl-induced neutrophil influx into the lungs without an effect on the macrophages. This selective effect on neutrophils may be due to inhibition of LTB_4 (discussed below). The HCl-induced increase of MPO also indicates neutrophil engagement, a result further corroborated by the results that PVAC also inhibited MPO activity. Edema and protein extravasation are considered indicators of vascular leakage. The wet to dry ratio of left lung tissue and total protein content in the BALF were measured to evaluate the degree of edema and protein leakage. The significantly elevated wet-dry ratio of left lung tissue and total protein content in the BALF were observed in HCl-challenged mice, suggesting HCl increases the pulmonary capillary permeability. However, it can be alleviated by PVAC. These results suggest that PVAC attenuated neutrophil influx and vascular leakage in HCl-challenged mice, thereby ameliorating lung pathology.

IL-6, as a multifunctional cytokine, plays an important role in acute inflammatory responses. Sustained elevation of IL-6 in plasma and BALF in ARDS patients has been shown to be inversely associated with disease outcome and patient survival (Meduri et al., 1995; Casey et al., 1993). Christian et al. confirms that IL-6 mediates neutrophil infiltration and pulmonary edema (Hierholzer et al., 1998). Similar to IL-6, TNF-α, mainly secreted by macrophages, is also involved in the acute inflammatory responses. *In vivo* and *in vitro* experiments have demonstrated that TNF-α increases alveolar capillary wall permeability under pathological conditions (Stephens et al., 1988), causing pulmonary edema. Therefore, we assessed the levels of IL-6 and TNF-α in BALF. It was found that IL-6 was significantly increased in the BALF of HCl mice, and TNF- α was also increased but did not reach statistical significance. Speculating, this result may indicate that TNF-α is involved, which also has been shown previously in a similar model of HCl-induced lung injury (Bastarache and Blackwell, 2009). Decreased IL-6 and TNF-α in BALF were observed in PVAC-treated, HCl-challenged mice. Therefore, PVAC may reduce HCl-induced vascular leakage and neutrophil

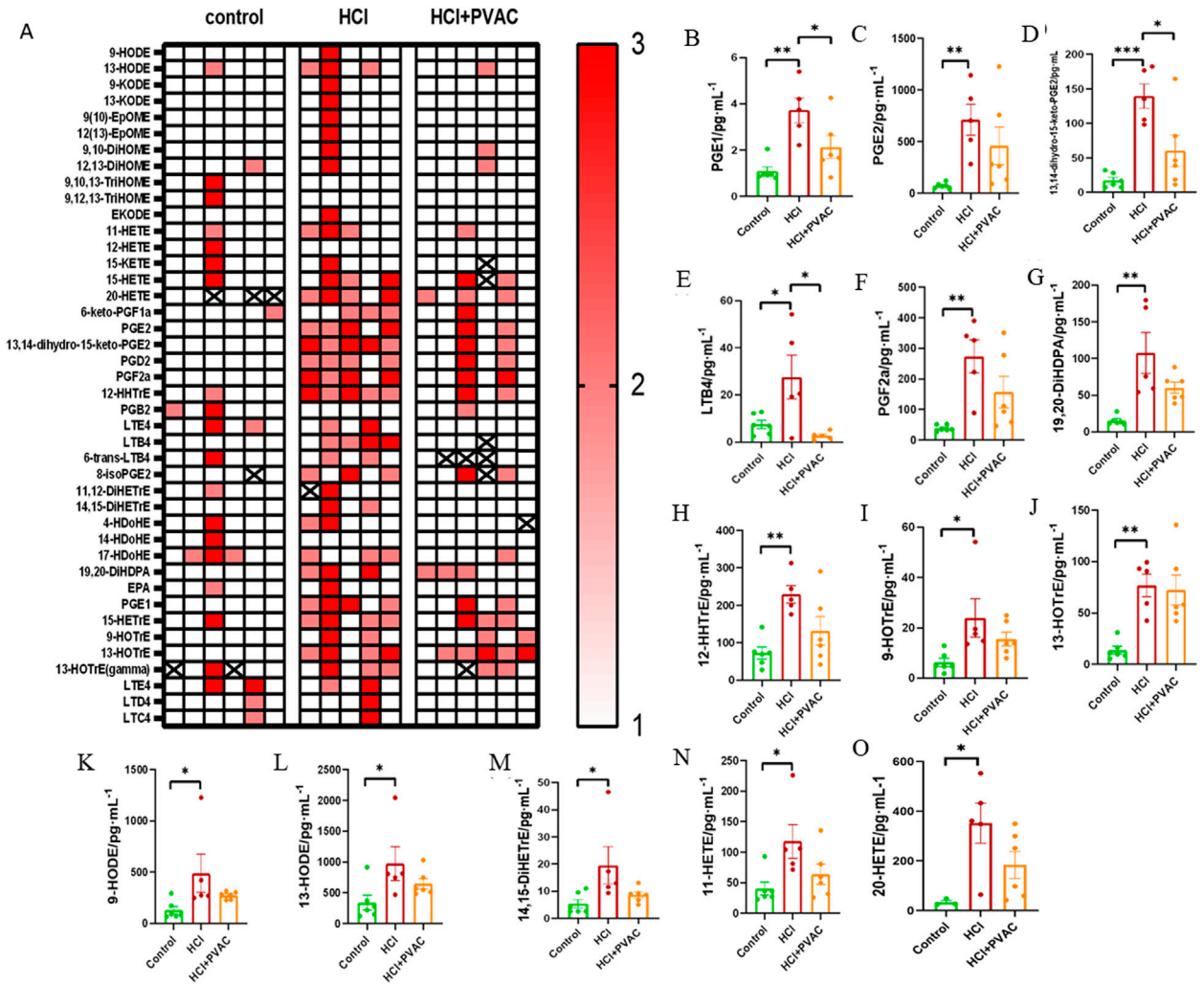

FIGURE 5
Lipid mediators measured in the BALF of HCl-induced ALI/ARDS mice. A broad of pro- and anti-inflammatory lipid mediators were detected using LC-MS/MS method. **(A)** Heat map. 1 (white) indicates concentrations are between the lowest and first tertile, 2 (light red) between the first and second tertile, and 3 (thick red) between the second tertile and maximum concentration; **(B)** PGE1, prostaglandin E1; **(C)** PGE2, prostaglandin E2; **(D)** 13,14-dihydro-15-keto-PGE2, 13,14-dihydro-15-keto prostaglandin E2; **(E)** LTB4, leukotriene B4; **(F)** PGF2α, prostaglandin F2α; **(G)** 19,20-DiHDPA, 19,20-dihydroxy-docosapentaenoic acid; **(H)** 12-HHTrE, 12-hydroxyheptadecatrienoic acid; **(I)** 9-HOTrE, 9-hydroxyoctadecatrienoic acid; **(J)** 13-HOTrE, 13-hydroxyoctadecatrienoic acid; **(K)** 9-HODE, 9-hydroxyoctadecadienoic acid; **(L)** 13-HODE, 13-hydroxyoctadecadienoic acid; **(M)** 14,15-DiHETrE, 14,15-dihydroxyeicosatrienoate; **(N)** 11) -HETE,11-hydroxyeicosatetraenoic acid; **(O)** 20-HETE, 20-hydroxyeicosatetraenoic acid. Results were presented as mean ± SEM (n = 5–6). control: saline and saline + PVAC, HCl: HCl treatment, HCl + PVAC: PVAC pretreatment + HCl treatment. Statistical comparisons between groups were performed using one-way ANOVA, *P< 0.05, **P< 0.01, and ***P< 0.001.

infiltration by inhibiting IL-6 and TNF-α signaling axis, thereby improving pulmonary edema and lung pathological damage. IL-6 and TNF-α have been confirmed to be critical cytokines in the pathogenesis of COVID-19 (Ye et al., 2020), and their levels are correlated with the severity and prognosis of COVID-19. Inhibition of "cytokine storm" has been recognized as an important strategy for the treatment of severe COVID-19. Therefore, PVAC is a potential candidate for the SARS-CoV-2 treatment.

LTB_4 is known to be one of the most potent neutrophil chemotactic agents and plays an important role in host defense against infection by interacting with its high-affinity receptor BLT1 (He et al., 2020). Our study found that HCl caused a significant increase of LTB_4 levels in the BALF, which further corroborated by the results that HCl induced neutrophils influx. PVAC was observed to significantly reduce LTB_4 levels in the BALF of HCl-challenged mice. As PVAC is a potent nucleophilic polymer it can interact with electrophilic molecules (Liu, 2013). The PVAC mode of action is most likely the interaction and inhibition of electrophilic entities in the inflammatory cascade such as hydrogen peroxide, aldehydes and LTA_4 (a LTB_4 precursor). Therefore, PVAC possibly ameliorated lung injury by inhibiting the LTB_4-driven neutrophil infiltration in the lungs of HCl mice. Targeted lipidomic analysis of BALF was performed by LC-MS/MS in 25 healthy controls and 33 COVID-19 patients requiring mechanical ventilation. The study found that fatty acids and inflammatory lipid mediators were increased in the BALF of severe COVID-19 patients. Thromboxane, prostaglandins, leukotrienes (especially LTB_4 and LTE_4) were significantly increased. Monohydroxylated 15-lipoxygenase metabolites from

linoleic, arachidonic, eicosapentaenoic, and docosahexaenoic acids were increased, too. This indicates that the "lipid mediator storm" that occurs in severe COVID-19 involves both pro- and anti-inflammatory lipids (Archambault et al., 2021). Therefore, PVAC is expected to improve the condition of COVID-19 patients by inhibiting the "lipid mediator storm".

This study also has limitations. 1) Human aspiration of gastric fluid is not simply inhalation of HCl, but rather the more complex gastric contents, which include particulate matter, bacterial products, and suspensions of cytokines. Thus, whether PVAC can be used for the treatment of ALI/ARDS caused by acidic substances in humans remains to be further studied. 2) Only the preventive effects of PVAC were investigated. These experiments are the first to study the effect of PVAC on inflammatory challenge in the lung. However, the marked effect of PVAC indicates a potential for promising future studies studying the effect during different time points and therapeutic properties. 3) The mechanisms of action for PVAC are not fully understood. Investigations into how the effect of PVAC is related to oxidative stress will be investigated in future studies.

5 Conclusion

This study shows that administration of PVAC may improve airway hyperresponsiveness, pulmonary edema and pulmonary pathological changes in HCl-induced ALI/ARDS model by reducing the levels of pro-inflammatory cytokines, lipid mediators, and the accumulation of neutrophils in the lungs, making PVAC a potential candidate for the treatment of ALI/ARDS induced by aspiration of gastric acid or for the control of "asthma-like" symptoms in patients with gastroesophageal reflux.

Data availability statement

The raw data supporting the conclusions of this article will be made available by the authors, without undue reservation.

Ethics statement

The animal study was approved by Stockholm ethics committee (the permit number:10,712-2020). The study was conducted in accordance with the local legislation and institutional requirements.

Author contributions

CD: Conceptualization, Data curation, Formal Analysis, Investigation, Methodology, Writing–original draft, Writing–review and editing. JL: Investigation, Methodology, Writing–review and editing. AQ: Data curation, Formal Analysis, Investigation, Methodology, Supervision, Writing–review and editing. XJ: Investigation, Methodology, Writing–review and editing. MN: Investigation, Methodology, Writing–review and editing. CW: Methodology, Project administration, Resources, Supervision, Writing–review and editing. BM: Methodology, Project administration, Resources, Writing–review and editing. JC: Methodology, Project administration, Resources, Writing–review and editing. TB: Conceptualization, Project administration, Resources, Writing–review and editing. TE: Conceptualization, Project administration, Resources, Writing–review and editing. MA: Conceptualization, Funding acquisition, Project administration, Resources, Supervision, Validation, Writing–review and editing.

Funding

The author(s) declare that financial support was received for the research, authorship, and/or publication of this article. The Swedish Heart-Lung foundation (grant numbers 20180514, 20210297); the Swedish Research Council–Medicine and Health (grant number 2019-01630); Cayman Biomedical Research Institute (CABRI), Karolinska Institutet and China Scholarship Council.

Conflict of interest

A patent using PVAC as an anti-inflammatory drug has been granted (Active principle for mitigating undesired medical conditions, WO 2012/105887 A1). The patent is owned by PVAC Medical Technologies Ltd (PMT). TE and TB are shareholders of PMT and have acted as consultants towards the company developing PVAC for clinical applications.

The remaining authors declare that the research was conducted in the absence of any commercial or financial relationships that could be construed as a potential conflict of interest.

Generative AI statement

The author(s) declare that no Generative AI was used in the creation of this manuscript.

Publisher's note

References

Abraham, E. (2003). Neutrophils and acute lung injury. *Crit. Care Med.* 31 (4 Suppl. l), S195–S199. doi:10.1097/01.CCM.0000057843.47705.E8

Allen, G. B., Leclair, T. R., von Reyn, J., Larrabee, Y. C., Cloutier, M. E., Irvin, C. G., et al. (1985)2009). Acid aspiration-induced airways hyperresponsiveness in mice. *J. Appl. Physiol.* 107 (6), 1763–1770. doi:10.1152/japplphysiol.00572.2009

Archambault, A. S., Zaid, Y., Rakotoarivelo, V., Turcotte, C., Dore, E., Dubuc, I., et al. (2021). High levels of eicosanoids and docosanoids in the lungs of intubated COVID-19 patients. *FASEB J.* 35 (6), e21666. doi:10.1096/fj.202100540R

Bastarache, J. A., and Blackwell, T. S. (2009). Development of animal models for the acute respiratory distress syndrome. *Dis. Model Mech.* 2 (5-6), 218–223. doi:10.1242/dmm.001677

Bhattacharya, J., and Matthay, M. A. (2013). Regulation and repair of the alveolar-capillary barrier in acute lung injury. *Annu. Rev. Physiol.* 75, 593–615. doi:10.1146/annurev-physiol-030212-183756

Casey, L. C., Balk, R. A., and Bone, R. C. (1993). Plasma cytokine and endotoxin levels correlate with survival in patients with the sepsis syndrome. *Ann. Intern Med.* 119 (8), 771–778. doi:10.7326/0003-4819-119-8-199310150-00001

El-Shahat, R. A., El-Demerdash, R. S., El Sherbini, E. S., and Saad, E. A. (2021). HCl-induced acute lung injury: a study of the curative role of mesenchymal stem/stromal cells and cobalt protoporphyrin. *J. Genet. Eng. Biotechnol.* 19 (1), 41. doi:10.1186/s43141-021-00139-w

Fredriksson, F., Sellberg, F., Bowden, T., Engstrand, T., Berglund, D., and Lilja, H. E. (2017). Sutures impregnated with carbazate-activated polyvinyl alcohol reduce intraperitoneal adhesions. *J. Pediatr. Surg.* 52 (11), 1853–1858. doi:10.1016/j.jpedsurg.2017.01.058

He, R., Chen, Y., and Cai, Q. (2020). The role of the LTB4-BLT1 axis in health and disease. *Pharmacol. Res.* 158, 104857. doi:10.1016/j.phrs.2020.104857

Hierholzer, C., Kalff, J. C., Omert, L., Tsukada, K., Loeffert, J. E., Watkins, S. C., et al. (1998). Interleukin-6 production in hemorrhagic shock is accompanied by neutrophil recruitment and lung injury. *Am. J. Physiol.* 275 (3), L611–L621. doi:10.1152/ajplung.1998.275.3.L611

Kaku, S., Nguyen, C. D., Htet, N. N., Tutera, D., Barr, J., Paintal, H. S., et al. (2020). Acute respiratory distress syndrome: etiology, pathogenesis, and summary on management. *J. Intensive Care Med.* 35 (8), 723–737. doi:10.1177/0885066619855021

Kolmert, J., Fauland, A., Fuchs, D., Safholm, J., Gomez, C., Adner, M., et al. (2018). Lipid mediator quantification in isolated human and Guinea pig airways: an expanded approach for respiratory research. *Anal. Chem.* 90 (17), 10239–10248. doi:10.1021/acs.analchem.8b01651

Liu, L. (2013). Targeting oxidation stress with functional polymer. *DIVA Degree Proj. Appl. Biotechnol. Upps Univ.*

Matthay, M. A., Ware, L. B., and Zimmerman, G. A. (2012). The acute respiratory distress syndrome. *J. Clin. Invest* 122 (8), 2731–2740. doi:10.1172/JCI60331

Meduri, G. U., Headley, S., Kohler, G., Stentz, F., Tolley, E., Umberger, R., et al. (1995). Persistent elevation of inflammatory cytokines predicts a poor outcome in ARDS. Plasma IL-1 beta and IL-6 levels are consistent and efficient predictors of outcome over time. *Chest* 107 (4), 1062–1073. doi:10.1378/chest.107.4.1062

Metheny, N. A., Clouse, R. E., Chang, Y. H., Stewart, B. J., Oliver, D. A., and Kollef, M. H. (2006). Tracheobronchial aspiration of gastric contents in critically ill tube-fed patients: frequency, outcomes, and risk factors. *Crit. Care Med.* 34 (4), 1007–1015. doi:10.1097/01.CCM.0000206106.65220.59

Meyer, N. J., Gattinoni, L., and Calfee, C. S. (2021). Acute respiratory distress syndrome. *Lancet* 398 (10300), 622–637. doi:10.1016/S0140-6736(21)00439-6

Paoletti, G., Melone, G., Ferri, S., Puggioni, F., Baiardini, I., Racca, F., et al. (2021). Gastroesophageal reflux and asthma: when, how, and why. *Curr. Opin. Allergy Clin. Immunol.* 21 (1), 52–58. doi:10.1097/ACI.0000000000000705

Raghavendran, K., Nemzek, J., Napolitano, L. M., and Knight, P. R. (2011). Aspiration-induced lung injury. *Crit. Care Med.* 39 (4), 818–826. doi:10.1097/CCM.0b013e31820a856b

Sellberg, F., Fredriksson, F., Engstrand, T., Bowden, T. M., Nilsson, B., Hong, J., et al. (2019). Polyvinylalcohol-carbazate (PVAC) reduces red blood cell hemolysis. *PLoS One* 14 (12), e0225777. doi:10.1371/journal.pone.0225777

Serhan, C. N., Chiang, N., Dalli, J., and Levy, B. D. (2014). Lipid mediators in the resolution of inflammation. *Cold Spring Harb. Perspect. Biol.* 7 (2), a016311. doi:10.1101/cshperspect.a016311

Spond, J., Billah, M. M., Chapman, R. W., Egan, R. W., Hey, J. A., House, A., et al. (2004). The role of neutrophils in LPS-induced changes in pulmonary function in conscious rats. *Pulm. Pharmacol. Ther.* 17 (3), 133–140. doi:10.1016/j.pupt.2004.01.003

Stables, M. J., and Gilroy, D. W. (2011). Old and new generation lipid mediators in acute inflammation and resolution. *Prog. Lipid Res.* 50 (1), 35–51. doi:10.1016/j.plipres.2010.07.005

Stephens, K. E., Ishizaka, A., Larrick, J. W., and Raffin, T. A. (1988). Tumor necrosis factor causes increased pulmonary permeability and edema. Comparison to septic acute lung injury. *Am. Rev. Respir. Dis.* 137 (6), 1364–1370. doi:10.1164/ajrccm/137.6.1364

Villar, J., Blanco, J., and Kacmarek, R. M. (2016). Current incidence and outcome of the acute respiratory distress syndrome. *Curr. Opin. Crit. Care* 22 (1), 1–6. doi:10.1097/MCC.0000000000000266

Ye, Q., Wang, B., and Mao, J. (2020). The pathogenesis and treatment of the `Cytokine Storm' in COVID-19. *J. Infect.* 80 (6), 607–613. doi:10.1016/j.jinf.2020.03.037

frontiers | Frontiers in Pharmacology

TYPE Original Research
PUBLISHED 26 November 2024
DOI 10.3389/fphar.2024.1488722

OPEN ACCESS

EDITED BY
Emanuela Ricciotti,
University of Pennsylvania, United States

REVIEWED BY
Atilio Sersun Calefi,
Universidade Cruzeiro do Sul, Brazil
Lucia Trevisi,
University of Padua, Italy

*CORRESPONDENCE
Paola Patrignani,
ppatrignani@unich.it
Antonio Lavecchia,
antonio.lavecchia@unina.it

†These authors have contributed equally to this work and share first authorship

‡These authors have contributed equally to this work and share last authorship

RECEIVED 30 August 2024
ACCEPTED 07 November 2024
PUBLISHED 26 November 2024

CITATION
Ammazzalorso A, Tacconelli S, Contursi A, Hofling U, Cerchia C, Di Berardino S, De Michele A, Amoroso R, Lavecchia A and Patrignani P (2024) A sulfonimide derivative of bezafibrate as a dual inhibitor of cyclooxygenase-2 and PPARα.
Front. Pharmacol. 15:1488722.
doi: 10.3389/fphar.2024.1488722

A sulfonimide derivative of bezafibrate as a dual inhibitor of cyclooxygenase-2 and PPARα

Alessandra Ammazzalorso[1†], Stefania Tacconelli[2†], Annalisa Contursi[2†], Ulrika Hofling[2], Carmen Cerchia[3], Sara Di Berardino[2], Alessandra De Michele[2], Rosa Amoroso[1], Antonio Lavecchia[3*‡] and Paola Patrignani[2*‡]

[1]Department of Pharmacy, "G. d'Annunzio" University, Chieti, Italy, [2]Systems Pharmacology and Translational Therapeutics Laboratory, at the Center for Advanced Studies and Technology (CAST), and Department of Neuroscience, Imaging and Clinical Science, "G. d'Annunzio" University, Chieti, Italy, [3]Department of Pharmaceutical and Toxicological Chemistry, University of Naples "Federico II", Naples, Italy

Background: PPARα and cyclooxygenase (COX)-2 are overexpressed in certain types of cancer. Thus, developing a dual inhibitor that targets both could be more effective as an anticancer agent than single inhibitors. We have previously shown that an analog of the bezafibrate named AA520 is a PPARα antagonist. Herein, we report the identification of AA520 as a potent COX-2 inhibitor using *in silico* approaches. In addition, we performed a thorough pharmacological characterization of AA520 towards COX-1 and COX-2 in different *in vitro* models.

Methods: AA520 was characterized for inhibiting platelet COX-1 and monocyte COX-2 activity in human whole blood (HWB) and for effects on lipidomics of eicosanoids using LC-MS/MS. The kinetics of the interaction of AA520 with COX-2 was assessed in the human colon cancer cell line, HCA-7, expressing only COX-2, by testing the COX-2 activity after extensive washing of the cells. The impact of AA520 on cancer cell viability, metabolic activity, and cytotoxicity was tested using the MTT reagent.

Results: In HWB, AA520 inhibited in a concentration-dependent fashion LPS-stimulated leukocyte prostaglandin (PG) E_2 generation with an IC_{50} of 0.10 (95% CI: 0.05–0.263) μM while platelet COX-1 was not affected up to 300 μM. AA520 did not affect LPS-induced monocyte COX-2 expression, and other eicosanoids generated by enzymatic and nonenzymatic pathways. AA520 inhibited COX-2-dependent PGE_2 generation in the colon cancer cell line HCA7. Comparison of the inhibition of COX-2 and its reversibility by AA520, indomethacin (a time-dependent inhibitor), acetylsalicylic acid (ASA) (an irreversible inhibitor), and ibuprofen (a reversible inhibitor) showed that the compound is acting by forming a tightly bound COX-2 interaction. This was confirmed by docking and molecular dynamics studies. Moreover, AA520 (1 μM) significantly reduced MTT in HCA7 cells.

Conclusion: We have identified a highly selective COX-2 inhibitor with a unique scaffold. This inhibitor retains PPARα antagonism at the same concentration

range. It has the potential to be effective in treating certain types of cancer, such as hepatocellular carcinoma (HCC) and renal cell carcinoma (RCC), where COX-2 and PPARα are overexpressed.

KEYWORDS

COX-2, PPARα, whole blood, NSAIDs, coxibs, lipidomics of eicosanoids, colorectal cancer

1 Introduction

There is strong evidence indicating that inflammation plays a crucial role in both the early stages of cancer development as well as in its progression toward metastasis (Patrignani and Patrono, 2015; Wang and Dubois, 2010a; 2010b). The activity of cyclooxygenase (COX)-2 contributes to inflammation by converting arachidonic acid (AA) into prostanoids, a family of lipid mediators. Among them, prostaglandin E_2(PGE_2) promotes tumorigenesis and metastasis via different mechanisms, and its inhibition causes anti-tumor effects by preventing invasion, proliferation, and angiogenesis and inducing apoptosis. The different biological responses of PGE_2 are mediated by G protein-coupled receptors (EP1-4), expressed in a tissue-specific manner (Wang and Dubois, 2010a; 2010b; Santiso et al., 2024). In

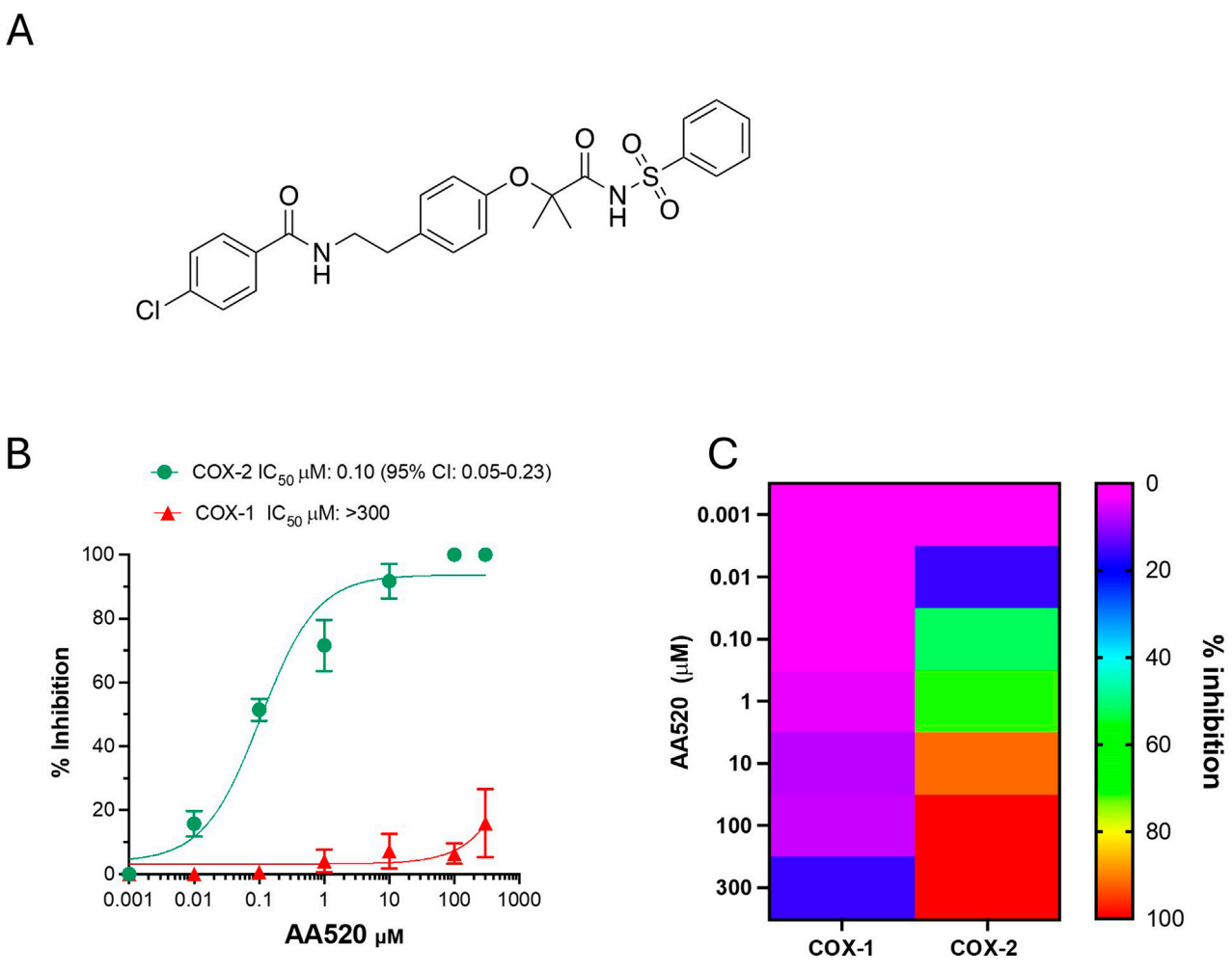

FIGURE 1
Effect of AA520 on the activity of COX-1 and COX-2 in human whole blood. **(A)** Chemical structure of AA520; **(B)** Concentration-response curves of inhibition in human whole blood of platelet COX-1 and LPS-induced monocyte COX-2 activity by AA520. Increasing concentrations of compound AA520 (0.001–300 µM) were incubated with heparinized whole blood samples, withdrawn from 4 healthy volunteers (2 females and 2 males) after suppressing the contribution of platelet COX-1 by adding aspirin (50 µM) *in vitro* solubilized in methanol and then evaporated, in the presence of LPS (10 µg/mL) for 24 h; after centrifugation, PGE_2 levels were analyzed as an index of LPS-induced-COX-2 activity, by a specific RIA. Furthermore, AA520 (0.01–300 µM) was incubated with human whole blood (from the same individuals) and allowed to clot for 1 h at 37°C; after centrifugation, TXB_2 levels were measured as an index of platelet COX-1 activity by a specific immunoassay. Results are depicted as percent inhibition (mean ± SEM, n = 3–4); **(C)** Heat map of % inhibition of COX-1 and COX-2 activities (mean values) versus increasing AA520 concentrations.

particular, EP2 and EP4 subtypes are involved in tumorigenesis, and currently, they represent interesting targets in the development of anticancer drugs (Santiso et al., 2024). Selective COX-2 inhibitors (collectively named coxibs) effectively reduce inflammation and cause anti-tumor effects through PGE_2 biosynthesis inhibition. TPST 1495, a selective dual antagonist of EP2 and EP4, is in clinical development to improve the efficacy of immune checkpoint inhibitors in patients with advanced solid tumors (https://clinicaltrials.gov/study/NCT04344795).

Another important pathway in tumorigenesis is represented by the PPAR (Peroxisome Proliferator-Activated Receptor) family. PPARs are nuclear hormone receptors, including PPARα, PPARδ, and PPARγ, which are important in regulating cancer cell proliferation, survival, apoptosis, and tumor growth (Hong et al., 2019; Kaipainen et al., 2007; Spaner et al., 2013; Messmer et al., 2015). The PPARα subtype represents an interesting anticancer target due to its critical roles in metabolic regulation and immune function. PPARα is involved in several types of cancer through the activation of NF-kB and the regulation of fatty acid oxidation. PPARα promotes tumor cell growth and inhibits anticancer immunity (Tan et al., 2021). TPST-1120 is a first-in-class, oral, small molecule, competitive antagonist of PPARα, with nanomolar potency (IC_{50} 0.04 μM) for human PPARα and high specificity (>250-fold) for PPARα over the other PPAR isoforms (PPAR β/δ and γ). It has been shown to inhibit tumor growth in xenograft and syngeneic tumor models and to improve the efficacy of anti-PD-1 therapy in tumor reduction and durable antitumor immunity (Stock et al., 2017; Yarchoan et al., 2024). Recent First-in-human Phase I Trial results in patients with advanced tumors support its promising anticancer profile (Yarchoan et al., 2024).

In hepatocellular carcinoma (HCC) and renal cell carcinoma (RCC), both COX-2 and PPARα are overexpressed (Chen et al., 2004; Cervello and Montalto, 2006; Abu Aboud et al., 2013). Thus, we have hypothesized that a molecule that inhibits both pathways could lead to improved anticancer effects. We have previously synthesized an analog of the bezafibrate named AA520 (Figure 1A) as a potent PPARα antagonist (Ammazzalorso et al., 2016). This compound was obtained by modifying the carboxyl portion of the bezafibrate and introducing a sulfonimide moiety. Using an *in silico* approach, we have found that AA520 binds COX-2. Here, we performed a thorough pharmacological characterization of AA520 towards COX-1 and COX-2 in different *in vitro* models. AA520 was also characterized for the capacity to interfere with other enzymatic and nonenzymatic pathways of AA by performing targeted lipidomics of eicosanoids by chiral liquid chromatography-mass spectrometry (LC-MS/MS) (Mazaleuskaya et al., 2018; Tacconelli et al., 2020a). The reversibility of the inhibition of COX-2 activity by AA520 was evaluated in the human colon cancer cell line, HCA-7, expressing only COX-2. Moreover, docking and molecular dynamics studies were performed. The impact of AA520 on cancer cell viability, metabolic activity, and cytotoxicity was tested using the MTT viability reagent.

2 Materials and methods

2.1 Materials

Acetonitrile (ACN), water (LC-MS grade), formic acid (FA), *n*-hexane, methanol, acetic acid, and isopropanol were from Carlo Erba Reagents, Milan, Italy. Standards of TXB_2, PGE_2, hydroxyeicosatetraenoic acid (HETE) s, leukotriene (LT) B_4, their deuterated forms, 15R-lipoxin (LX) A_4, and the immunoassay kit for the assessment of TXB_2 (#501020) were from Cayman Chemical (Ann Arbor, Michigan, United States). ECL Western blotting Detection Reagents were from GE Healthcare (Milan, Italy). Dimethyl sulfoxide (DMSO), ethanol (EtOH), bovine serum albumin (BSA), NaCl, Triton X-100, Phenylmethylsulfonyl Fuoride (PMSF), Dulbecco's Modified Eagle's Medium (DMEM), Penicillin-Streptomycin, Fetal Bovine Serum (FBS), arachidonic acid (AA), LPS derived from *Escherichia coli* 026:B6, indomethacin, acetylsalicylic acid (aspirin or ASA), ibuprofen, bezafibrate, and benzenesulfonamide were from Sigma Aldrich, Milan, Italy. AA520 was synthesized as previously reported (Ammazzalorso et al., 2016), starting from bezafibrate and benzenesulfonamide as starting materials. The Lux 3 μm Amylose-1, 150 mm × 3.0 mm chromatographic column was from Phenomenex, Torrance, United States and the ACQUITY UPLC® BEH C18 1.7 μm chromatographic column was from Waters SpA, Milan, Italy. The Bradford protein assay, β-Mercaptoethanol, the PVDF membrane, and the non-fat milk for immunoblot were from Bio-Rad, Milan, Italy. The anti-GAPDH monoclonal antibody (#sc-47724) and the Ficoll-Paque PLUS density gradient media were from Santa Cruz Biotechnology (Dallas, United States). Colon cancer cell line HCA7 colony 29 (HCA7) was from the European Collection of Cell Cultures (ECC, Salisbury, United Kingdom).

2.2 Subjects

Peripheral venous blood samples were drawn from healthy volunteers (n = 10, 7 females, 23–50 years) when they had not taken any non-steroidal anti-inflammatory drug (NSAID) during the 2 weeks preceding the study. This study was carried out following the recommendations of the Declaration of Helsinki after approval by the local Ethics Committee of "G. d' Annunzio" University of Chieti-Pescara (#254), and informed consent was obtained from each subject.

2.3 Effect of AA520 on whole blood COX-1 and COX-2 activities *in vitro*

The compound AA520 was dissolved in DMSO; then 2-μL aliquots of the vehicle or the different solutions of AA520 were added directly into glass test tubes to give the final concentrations of 0.01–300 μM. Duplicate 1-mL aliquots of whole blood drawn from the healthy volunteers were immediately transferred into glass tubes and allowed to clot at 37°C for 1 h. After incubation, serum was immediately separated by centrifugation (1,560 g, 10 min at 4°C) and stored at −80°C until assayed for TXB_2, which reflects platelet COX-1 activity (Patrono et al., 1980) by using a validated immunoassay (Patrignani et al., 2014) (Cayman Chemical, item#501020). At the same time, 2-μL of the vehicle or the different solutions of AA520 were added to duplicate aliquots of heparinized whole blood samples to give the final concentrations of 0.001–300 μM in the presence of LPS (10 μg/mL) for 24 h as previously described (Patrignani et al., 1994). The contribution of platelet COX-1 was

suppressed by adding aspirin *in vitro* at a concentration of 50 μM, solubilized in methanol, and then evaporated through the speed-vac before adding LPS and test-compound. Plasma was separated by centrifugation and kept at −80°C until assayed for PGE_2 levels by using a specific radioimmunoassay (RIA) (Patrignani et al., 1994). Some experiments were performed to test the effect of bezafibrate and benzenesulfonamide (the starting compounds of the synthesis of AA520) on LPS-stimulated whole blood at the final concentrations of 10–300 μM.

2.4 Effects of AA520 on eicosanoid biosynthesis in LPS stimulated whole blood

In LPS-stimulated whole blood, 12R-HETE, 12S-HETE, 15R-HETE, 15S-HETE, 5R-HETE, 5S-HETE, 8R-HETE, 8S-HETE, LTB_4 and 15R-LXA_4, were assessed by a modified LC-MS/MS method (Mazaleuskaya et al., 2018). Briefly, samples were extracted by using a liquid-liquid extraction (Maskrey et al., 2007; Tacconelli et al., 2020a): to 0.3 mL of the sample, phosphate buffer (PBS) was added to give 1 mL; then 2.5 mL of a mixture of acetic acid/isopropanol/hexane (2:20:30, v/v/v) and internal standards (d_8-12S-HETE, d_8-15S-HETE, d_8-5SHETE, d_4-TXB_2 at the final concentration of 5 ng/mL) were added. The extraction was performed by adding 5 mL of *n*-hexane. Then, the samples were centrifuged at 1,500 *g* at 4°C for 5 min. The dried hexane phases were stored at −80°C until LC-MS/MS analysis. Before analysis, dried lipids were resuspended in 0.2 mL of methanol and analyzed by LC-MS/MS as previously described (Tacconelli et al., 2020a). The LC-MS/MS system consisted of ACQUITY UPLC I-Class/Xevo TQS micro IVD System (Waters) equipped with a Z-Spray ESI source under negative ionization conditions. Deuterated and non-deuterated standards (from Cayman Chemical) were analyzed in MS/MS mode to examine the collision-induced fragmentation spectrum to select specific fragments monitored for each eicosanoid (Hofling et al., 2022). Separation of 12R-HETE, 12S-HETE, 15R-HETE, 15S-HETE, 5R-HETE, 5S-HETE, 8R-HETE, 8S-HETE, 15R-LXA_4, LTB_4, PGE_2 and TXB_2 was performed using a chiral chromatographic column (Lux 3 μm Amylose-1, 150 mm × 3.0 mm; Phenomenex, Torrance, CA, United States) eluting a 20-min gradient of 50%–100% solvent B (60% methanol, 40% ACN, 0.1% glacial acetic acid) and solvent A (75% water, 25% ACN, 0.1% glacial acetic acid): 50% solvent B for 5 min; 50%–60% solvent B for 4 min; 60%–80% solvent B for 2 min; 80%–90% solvent B for 2 min; 90%–100% solvent B for 1 min, 100% solvent B for 2 min and 50% of solvent B from 17 to 20 min with a flow rate of 0.2 mL/min). The linear standard curves were obtained by adding constant amounts of internal standards to eight different concentrations of each analyte (0.01–500 ng/mL), then the calibration curves were constructed by linear regression of the ratio of the peak areas of the analytes to the areas of the corresponding internal standards. For 8R- and 8S-HETE and 15R-LXA_4, we used d_8-12S-HETE as their internal standard (Tacconelli et al., 2020a). The eicosanoid concentrations were calculated by interpolation from the calculated regression lines. The eicosanoid peak areas were extracted and analyzed by using MassLynx software (Waters, United Kingdom). The data were normalized to sample volume and expressed as ng/mL. The detection limit of quantification of each eicosanoid was 10 pg/mL.

2.5 Effect of AA520 on COX-1 and COX-2 expression in LPS-stimulated isolated monocytes

Human monocytes were freshly isolated from concentrated buffy coats (obtained from the blood bank of Hospital Renzetti, Lanciano, Chieti, Italy) that were treated *in vitro* with aspirin (50 μM) for 20 min to inhibit the activity of COX-1. As previously described, monocytes were separated from the Ficoll-Paque density gradient media (Patrignani et al., 1994). To characterize the purity of isolated cells, monocytes were incubated with anti-CD14 (1:10) and assessed by FacsVerse cytometer (BD) (Marimuthu et al., 2018). We used four different buffy coats. Assuming an SD of 8 for the % OD values of the COX-1/GAPDH and COX-2/GAPDH immunoreactive bands in LPS-stimulated monocytes, a sample size of 4 would be required to achieve a power of 80% and a significance level of 5% (two-sided) for detecting a difference in means between the LPS-vehicle and AA520 of 20 or more. Cell suspensions routinely contained 90% monocytes (Patrignani et al., 1994). Monocytes (1.5×10^6) grown in RPMI 1640 supplemented with 0.5% FBS, 1% penicillin/streptomycin and 2 mM L-glutamine, were incubated with vehicle (DMSO) or increasing concentrations of AA520 (0.1–10 μM) in the presence of LPS (10 μg/mL) for 24 h. After 24h incubation, monocytes were centrifuged (700 g, 5 min at 4°C); pellets were stored at −80°C until assayed for COX-1 and COX-2 expression by Western blot (Patrignani et al., 2017; Patrignani et al., 1994).

2.6 Western blot

COX-1 and COX-2 expression was assessed in monocytes and PPARα in HCA7 cells by a Western blot technique (Patrignani et al., 2017; Patrignani et al., 1994). Briefly, aliquots of cell lysates were loaded onto 9% Sodium Dodecyl Sulphate-PolyAcrylamide Gel Electrophoresis (SDS-PAGE), transferred to PVDF membrane, and blocked with a solution of 5% blotting grade blocker in tris-buffered saline-0.1% Tween-20 (TBS-Tween-20). The membrane was incubated overnight with COX-2 (mouse) monoclonal antibody (#160112, Cayman Chemical), COX-1 ovine polyclonal antibody (#160108, Cayman Chemical), PPARα rabbit polyclonal antibody (#227074, Abcam) and GAPDH monoclonal antibody (#sc-47724, Santa Cruz Biotechnology) used as the loading control. Membranes were developed using ECL Western blotting Detection Reagents. Results were obtained using a digital imaging system Alliance 4.7 (UVITEC, Cambridge, United Kingdom) (Patrignani et al., 2017).

2.7 Assessment of the inhibition of COX-2 and its reversibility by AA520 in HCA-7 cells

We studied the mechanism of inhibition of COX-2 by AA520 in comparison to aspirin, indomethacin, and ibuprofen in colon cancer cell line HCA-7 colony 29 (HCA-7), selectively expressing only COX-2. The HCA-7 cell line was from the European Collection of Cell Cultures (ECC, Salisbury, United Kingdom). The HCA-7 cells, used at passage levels 11–18, were cultured in DMEM supplemented with 10% FBS, 1% penicillin/streptomycin, and 1% L-glutamine.

Before each experiment, cells were plated at the concentration of 1×10^6 in 5 cm plates (volume 3 mL) containing 2 mL of DMEM supplemented with 0.50% of FBS for 16 h. First, we assessed the inhibition of COX-2 by AA520 by preincubating the cells with vehicle (DMSO) or with different concentrations of the compound (30 min at room temperature); then, AA (0.5 μM) was added for a further 30 min at 37°C, and supernatants were collected and assessed for PGE_2 levels by RIA.

The kinetics of the interaction of AA520 and other NSAIDs with COX-2 was assessed by performing biochemical studies (Vitale et al., 2013) evaluating the residual inhibition of PGE_2 biosynthesis by HCA7 cells after extensive washing of the cells versus the values obtained without washing. Briefly, AA520, indomethacin (a time-dependent inhibitor of COX), aspirin (ASA, an irreversible inhibitor of COX), and ibuprofen (a reversible inhibitor of COX) were incubated with the cells at a concentration of 100 μM for 30 min at room temperature. In some experiments, AA (0.5 μM) was added, and the incubation continued for 30 min at 37°C. In other experiments, cells preincubated with the different compounds were washed three times with 3 mL of DMEM (without FBS), resuspended with medium (without FBS), and stimulated with AA, 0.50 μM for 30 min at 37°C. In both experimental conditions (without or with washing passages), PGE_2 production was determined in the medium by RIA as an index of COX-2 activity (Patrignani et al., 1994). After trypsinization and centrifugation, protein quantification was performed using the Bradford method.

2.8 Development of an LC-MS/MS method for the qualitative assessment of AA520, bezafibrate, and benzenesulfonamide

We have developed a LC-MS/MS method in "Multiple Reaction Monitoring (MRM)" mode (LC/MS/MRM) which allowed qualitative analysis of AA520, bezafibrate and benzenesulfonamide by using an ACQUITY UPLC I-Class/Xevo TQS micro IVD System (Waters) equipped with a Z-Spray ESI source under negative ionization conditions. The three compounds were solubilized in methanol at a final concentration of 1,000 ng/mL and infused into the electrospray ionization source (ESI ZSpray), under negative ionization conditions, at a rate of 50 μL/min, to obtain the MS and MS/MS fragmentation spectra.

Chromatographic separation of the three compounds was performed using an ACQUITY UPLC® BEH C18 1.7 μm chromatography column (Waters) with the following mobile phases: A) water (0.1% FA); B) ACN (0.1% FA). The mobile phases eluted with a flow rate of 0.3 mL/min according to the following gradient: 0–1 min: 100%A; 1–7 min: 10%A; 7–9 min:100% A. The volume injected was 5 μL.

2.9 Qualitative evaluation of AA520, bezafibrate, and benzenesulfonamide by LC-MS/MS in whole blood incubated for 24 h at 37°C with AA520

Aliquots (1 mL) of heparinized whole blood were incubated with AA520 at 37°C for 24 h. At the end of the incubation, the plasma was separated by centrifugation (10 min at 1560 g at 4°C). Then aliquots of 200 μL of plasma were extracted with 1 mL of acetonitrile (Saraner et al., 2019); after vortexing for 30 s, the samples were centrifuged at 1800 *g* for 10 min. Finally, 5 μL of the supernatant was injected into the LC-MS/MS system to determine the presence of AA520 or potential metabolites.

2.10 MTT assay

HCA7 cells were seeded at 4×10^3 cells/well in DMEM supplemented with 0.5% FBS and 1% penicillin/streptomycin at 37°C. Then, cells were treated with AA520 (1–10 μM), rofecoxib (10 μM), GW6471 (a PPARα antagonist, 10 and 25 μM), or vehicle (DMSO), and the viability was assessed up to 72 h of exposure by using the [(3-(4,5-dimethylthiazol-2-yl)-2,5-diphenyltetrazolium bromide] (MTT) assay according to the manufacturer's instructions (CyQUANT™ MTT Cell Viability Assay, Invitrogen).

2.11 Molecular modeling

2.11.1 Protein and ligand preparation

The 2.4 Å resolution X-ray structure of murine COX-2 in complex with celecoxib (PDB 3LN1) (Wang et al., 2010) was downloaded from the Protein Data Bank. The structure of murine COX-2 is highly similar to the human enzyme, with 87% identity and strict sequence conservation in the active site (Kurumbail et al., 1996). The Protein Preparation Wizard in Maestro (Protein Preparation Wizard; Epik, Schrödinger, LLC, New York, NY, 2021; Impact, Schrödinger, LLC, New York, NY, 2021; Prime, Schrödinger, LLC, New York, NY, 2021) was used to prepare the selected structure for docking studies: all the crystallographic water molecules and other chemical components were removed; the right bond orders, charges, and atom types were assigned; and the hydrogen atoms were added. The H-bond network was optimized by exhaustive sampling of rotamers, tautomers, and protonation states of titratable amino acids at neutral pH. Finally, a restrained minimization was performed on the protein structures using the Impref module, by imposing a 0.3 Å RMSD limit from the initial coordinates as constraint. The *in-house* small library of compounds, including AA520 (Ammazzalorso et al., 2016), was prepared for *in silico* studies with LigPrep (LigPrep, Schrödinger, LLC, New York, NY, 2021) in order to generate suitable 3D conformations and tautomerization states at pH 7.

2.11.2 Docking calculations

The virtual screening of the *in-house* library of compounds was accomplished by using Glide (Glide, Schrödinger, LLC, New York, NY, 2021) (Friesner et al., 2004; Halgren et al., 2004) in SP mode.

Docking of AA520 was carried out with the Glide Induced Fit Docking (IFD) protocol (Glide, Schrödinger, LLC, New York, NY, 2021; Prime, Schrödinger, LLC, New York, NY, 2021) (Farid et al., 2006; Sherman et al., 2006a; Sherman et al., 2006b). For both virtual screening and IFD, the docking grid was generated by considering an inner box of 10 Å × 10 Å × 10 Å and an outer box of 30 Å × 30 Å × 30 Å surrounding the bound celecoxib. In the case of IFD, an extended sampling protocol was adopted, which returns up to

80 poses: in the first stage, docking is conducted using a softened potential and removal of side chains, on the basis of solvent-accessible surface areas and B-factors. The results of this procedure are clustered to obtain representative poses. Then, for residues within 5 Å of any ligand pose, a Prime side-chain prediction is carried out, followed by minimization of both residues and ligand. Finally, the ligand is re-docked, using default Glide SP settings, into the induced-fit receptor structure, and each output pose is scored. Both the Glide Emodel and GlideScore lowest-energy values were considered for final pose selection. Before proceeding with the docking simulations of the compound under study, we investigated pose generation quality by re-docking the co-crystalized celecoxib (PDB 3LN1). The above-described IFD protocol well reproduced the experimental geometries, with RMSD value of 0.48 Å.

2.11.3 Molecular dynamics simulations

The protein-ligand complex obtained by the above-described IFD approach was selected for molecular dynamics simulations, carried out by means of Desmond (Bowers et al., 2006). Briefly, the system was solvated in a 10 Å layer orthorhombic box using TIP3P water model, and then neutralized by adding counterions. A salt concentration of 0.15 M of NaCl was also included in the simulation box to reproduce the physiological conditions. OPLS_2005 (Jorgensen et al., 1996) was used as force field. The system was relaxed before the simulation by using the protocol implemented in Desmond; then, the simulation was run for 100 ns under a NTP ensemble using the Nose-Hoover thermostat to maintain a constant temperature of 300 K and Martyna-Tobias-Klein barostat to maintain the pressure at 1 atm. The trajectories were saved at 100 ps intervals for analysis. The obtained trajectory was clustered according to the RMSD matrix of a specified set of atoms (backbone) by employing "Desmond Trajectory Clustering", which uses an affinity propagation clustering method (Frey and Dueck, 2007). A trajectory frame extraction interval of 10 and a maximum output number of clusters to 10 were set. A total of 15 clusters were obtained (Supplementary Table S1), of which the representative structure from the most populated cluster was selected for subsequent analysis. The "Simulation Interactions Diagram" tool was then used for post-MD analysis. The stability of MD simulations was monitored by observing the root mean square deviation (RMSD) of the ligand and protein atom over simulation time.

The representative structure obtained from the clustering procedure was then used to run the calculation of Prime MM-GBSA (Prime, Schrödinger, LLC, New York, NY, 2021). This method can be used to approximate the free energy of binding between a protein and a ligand. The calculations employed predefined dielectric constants, the OPLS_2005 force field, and the VSGB solvation model (Li et al., 2011). A more negative value indicates stronger binding. The obtained values of ΔG_{bind} were compared with those calculated using as reference the COX-2/celecoxib structure obtained from the protein preparation procedure (see above).

All the figures were rendered with PyMOL (The PyMOL Molecular Graphics System, Version 2.0 Schrödinger, LLC).

2.12 Statistical analysis

The data have been reported as mean ± standard error of the mean (SEM) or standard deviation (SD) as specified. The statistical analysis was performed using GraphPad Prism software (version 10.00 for Mac; GraphPad, San Diego, CA). The values of $P < 0.05$ were considered statistically significant. The specific statistical text used in each experiment is reported in the Figure legends. In the experiments assessing the % inhibition of PGE_2 in LPS-stimulated whole blood by AA520, the concentration of PGE_2 produced in LPS-stimulated whole blood was subtracted from that produced without LPS (baseline) The concentration-response curves were obtained using GraphPad Prism software (version 10.00 for Mac). GraphPad Prism software obtained the IC_{50} and 95% confidence interval (CI) values of the sigmoidal concentration-response data.

3 Results

3.1 Identification of COX-2 inhibitors by virtual screening

We virtually screened the in-house small library of compounds described previously (Ammazzalorso et al., 2016) to find novel small molecules targeting PPARα and COX-2. Virtual screening calculations were performed using Glide on COX-2 3D structure in complex with celecoxib (PDB 3LN1). Virtual screening results were sorted based on the docking scores and visual inspection (a more detailed description of the COX-2 binding site is reported in section 3.7). Compounds **1b**, **1e,** and **2b** could not be proficiently docked within the COX-2 active site and were discarded from our analysis. Then, we focused on the top-scoring compounds endowed with potent PPARα antagonistic activity, namely **1d**, **2b**, **6** (hereafter AA520), and **4** (Supplementary Table S2). Finally, we decided to prioritize compound AA520 because of its exquisite selectivity on PPARα concerning PPARγ (Ammazzalorso et al., 2016). In fact, the clinical candidate TPST-1120 possesses high specificity (>250-fold) for PPARα over the other isoforms (Stock et al., 2017).

3.2 Effect of AA520 on eicosanoid generation in human whole blood

In human whole blood allowed to clot at 37°C for 1 h, TXB_2 is generated in serum, and it is mainly derived from platelets in response to endogenously formed thrombin (Patrono et al., 1980). It represents an index of the maximal capacity of platelet COX-1 to generate this prostanoid. Serum TXB_2 at baseline averaged 421 ± 205 ng/mL (n = 10; mean ± SD). In heparinized human whole blood samples, incubated with LPS (10 μg/mL) at 37°C for 24 h, PGE_2 was generated and averaged 19.6 ± 9.8 ng/mL (n = 10; mean ± SD). Under these experimental conditions, it was previously reported that LPS induces COX-2 expression in leukocytes in a time-dependent fashion, and PGE_2 paralleled the COX-2 expression (Patrignani et al., 1994). Aspirin (50 μM) was added at the beginning of the incubation to prevent the contribution of platelets to the generation of PGE_2. Aspirin causes irreversible inhibition of platelet COX-1 that persists throughout the 24 h of incubation due to the limited capacity of the anucleated platelet

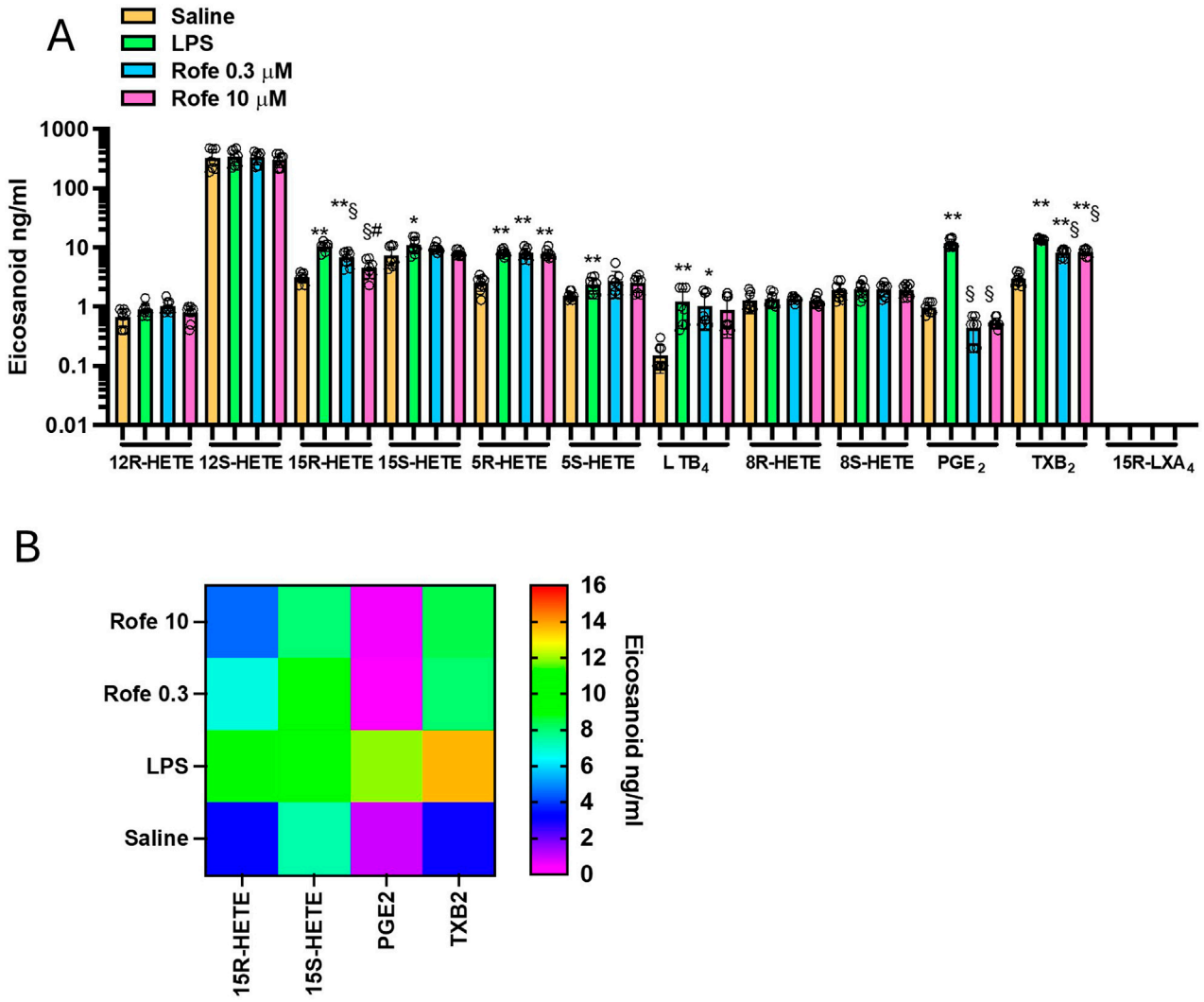

FIGURE 2
Effects of rofecoxib on eicosanoid biosynthesis in LPS-stimulated-whole blood by targeted lipidomics. **(A)** Aliquots (1 mL) of heparinized whole blood drawn from healthy volunteers are incubated with rofecoxib (0.3 and 10 μM) or DMSO (vehicle of rofecoxib) in the presence of NaCl (0.9% w/v, named saline) or LPS (10 μg/mL, dissolved in NaCl 0.9% w/v) for 24 h; after centrifugation, eicosanoid levels (12R-HETE, 12S-HETE, 15R-HETE, 15S-HETE, 5R-HETE, 5S-HETE, 8R-HETE, 8S-HETE, LTB_4, PGE_2, TXB_2 and 15R-LXA_4) were analyzed by using LC-MS/MS. Results are depicted as ng/mL of each eicosanoid [mean ± SEM, n = 8 (5 females and 3 males), and individual values were also reported]. For each eicosanoid, we used one-way ANOVA and Dunnett *post hoc* test (to compare the means of different treatments versus saline or LPS), *P < 0.05, **P < 0.001, versus saline, §P < 0.01 versus LPS; or one-way ANOVA and Tukey *post hoc* test (to compare the mean of each column with the mean of every other column), #P < 0.05, versus 0.3 μM (15R-HETE); **(B)** Heat map of 15R-HETE, 15S-HETE, PGE_2, and TXB_2 (mean values) in saline, LPS and Rofecoxib (0.3 and 10 μM) conditions.

to *de novo* protein synthesis (Evangelista et al., 2006). Aspirin is unstable in plasma and is metabolized to salicylic acid (a weak COX inhibitor) before the induction of COX-2 in leukocytes in response to LPS (Cipollone et al., 1997). Thus, under these experimental conditions, aspirin does not interfere with the activity of COX-2. In unstimulated heparinized whole blood, the PGE_2 levels were 0.34 ± 0.22 ng/mL (n = 10). The assessment of serum TXB_2 and LPS-induced PGE_2 in whole blood is considered the gold standard assay to assess the selectivity of NSAIDs towards COX-2. As shown in Figures 1B, C, AA520 inhibited LPS-induced PGE_2 in a concentration-dependent fashion with an IC_{50} of 0.10 μM (95% CI: 0.05–0.23). The compound only marginally inhibited platelet COX-1 activity at the maximum concentration of 300 μM. The COX-1/COX-2 IC_{50} ratio was >697.

3.3 Targeted lipidomics of LPS-stimulated human whole blood

To verify the impact of AA520 on different enzymatic and nonenzymatic pathways of AA metabolism, we modified a previously published LC-MS/MS method (Mazaleuskaya et al., 2018). To assess 5-lipooxygenase (LOX) activity, we measured 5S-HETE and LTB_4; for the 12S-LOX activity, we assessed 12S-HETE; for 15-LOX-1 activity, we evaluated 15S-HETE and 12S-HETE; for COX-1 and COX-2 activity we measured PGE_2, TXB_2, 15R-HETE and 15S-HETE (these HETEs are minor products of COX activity) (Powell and Rokach, 2015; Mazaleuskaya et al., 2016; 2018; Contursi et al., 2022). We also measured 5R-HETE, 8S-HETE, 8R-HETE, and 12R-HETE as

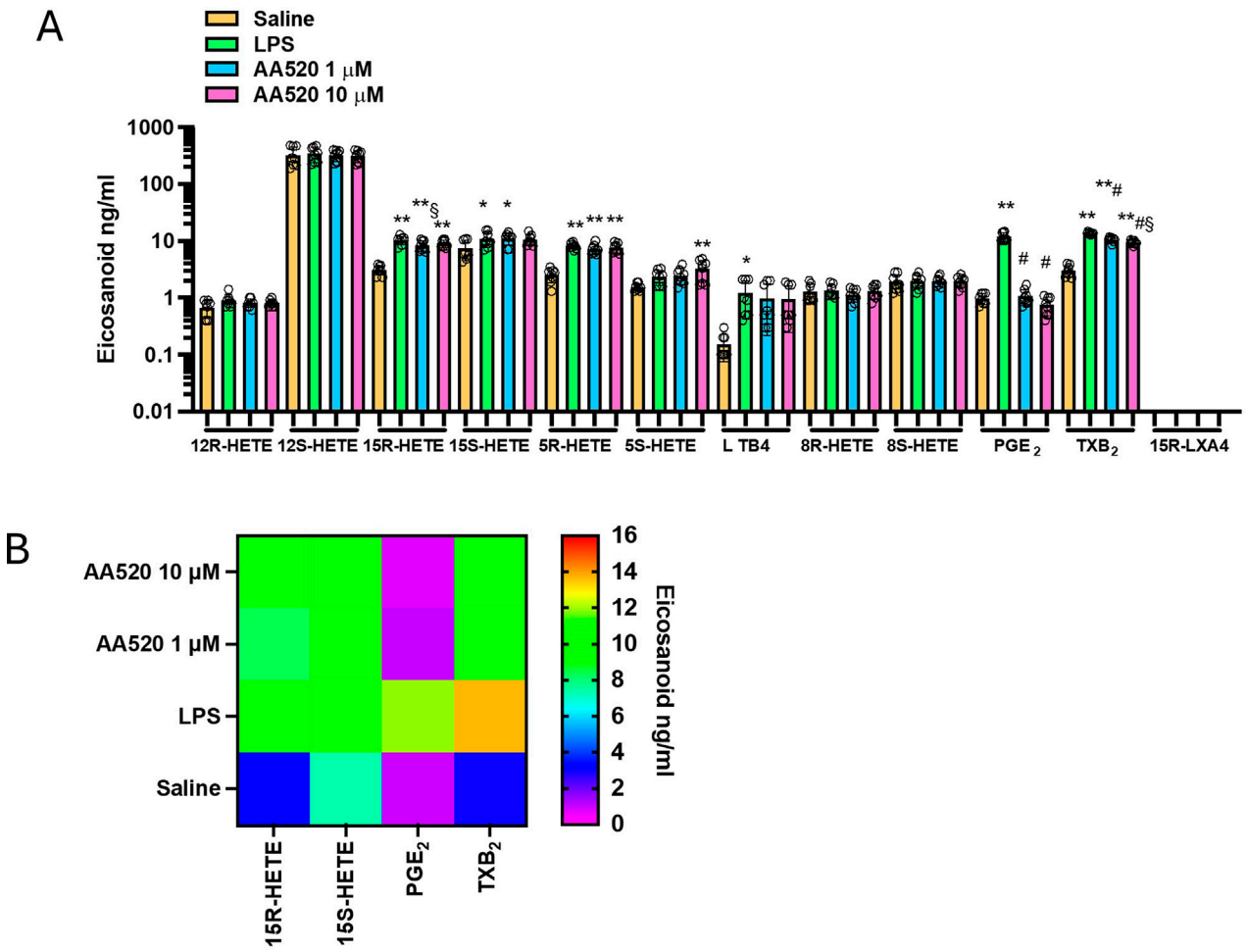

FIGURE 3
Effects of AA520 on eicosanoid biosynthesis in LPS-stimulated whole blood by targeted lipidomics. **(A)** Aliquots (1 mL) of heparinized whole blood drawn from healthy volunteers are incubated with AA520 (1 and 10 μM) or DMSO (vehicle of AA520) in the presence of NaCl (0.9% w/v, named saline) or LPS (10 μg/mL, dissolved in NaCl 0.9% w/v) for 24 h; after centrifugation, eicosanoid levels (12R-HETE, 12S-HETE, 15R-HETE, 15S-HETE, 5R-HETE, 5S-HETE, 8R-HETE, 8S-HETE, LTB_4 PGE_2, TXB_2 and 15R-LXA_4) were analyzed by using LC-MS/MS. Results are depicted as ng/mL of each eicosanoid (mean ± SEM, n = 8, five females and 3 males). For each eicosanoid, we used one-way ANOVA and Dunnett *post hoc* test (to compare the means of different treatments versus saline or LPS), *P < 0.05, **P < 0.01, versus saline, #P < 0.001 versus LPS; or one-way ANOVA and Tukey *post hoc* test (to compare the mean of each column with the mean of every other column), §P< 0.05 versus 10μM; **(B)** Heat map of 15R-HETE, 15S-HETE, PGE_2, and TXB_2 (mean values) in saline, LPS and AA520 (1 and 10 μM) conditions.

markers of nonenzymatic oxidation of AA. Finally, we assessed 15R-LXA_4 (also named aspirin-triggered LXA_4), a product of 15R-HETE and 5-LOX (Serhan, 2002). As shown in Figure 2A and Supplementary Table S3, LPS significantly increased PGE_2, TXB_2, 15R-HETE, 15S-HETE, 5S-HETE, LTB_4, and 5R-HETE vs. unstimulated human whole blood. Noteworthy, 15R-LXA_4 was undetectable (i.e., <10 pg/mL) in unstimulated and LPS-stimulated whole blood.

3.4 Comparison of the effects of rofecoxib and AA520 on targeted lipidomics of LPS-stimulated human whole blood

As shown in Figures 2A, B, the selective COX-2 inhibitor rofecoxib (Patrono et al., 2001; Tacconelli et al., 2002) significantly reduced PGE_2, TXB_2, and 15R-HETE, while the other eicosanoids were not significantly affected. However, the extent of reduction of TXB_2 and 15R-HETE was lower than PGE_2. At 10 μM of rofecoxib, TXB_2, 15R-HETE, and PGE_2 reduction were 39, 56, and 95%, respectively. The lower inhibition of TXB_2 vs. PGE_2 is because TXB_2 can also be generated from leukocyte COX-1. The contribution of platelet COX-1 is excluded since aspirin was added at the beginning of the incubation. 15R-HETE is produced due to AA's different conformational interaction in the COX active site (Thuresson et al., 2001; 2002; Powell and Rokach, 2015), and rofecoxib may be less effective in competing with AA in this conformation.

Next, we tested AA520 on the generation of eicosanoids in LPS-stimulated whole blood (Figures 3A, B). Similarly to rofecoxib, the compound significantly reduced PGE_2, TXB_2, and 15R-HETE, while the other eicosanoids were unaffected. The extent of reduction of TXB_2 and 15R-HETE was lower than PGE_2. At 1 μM of AA520,

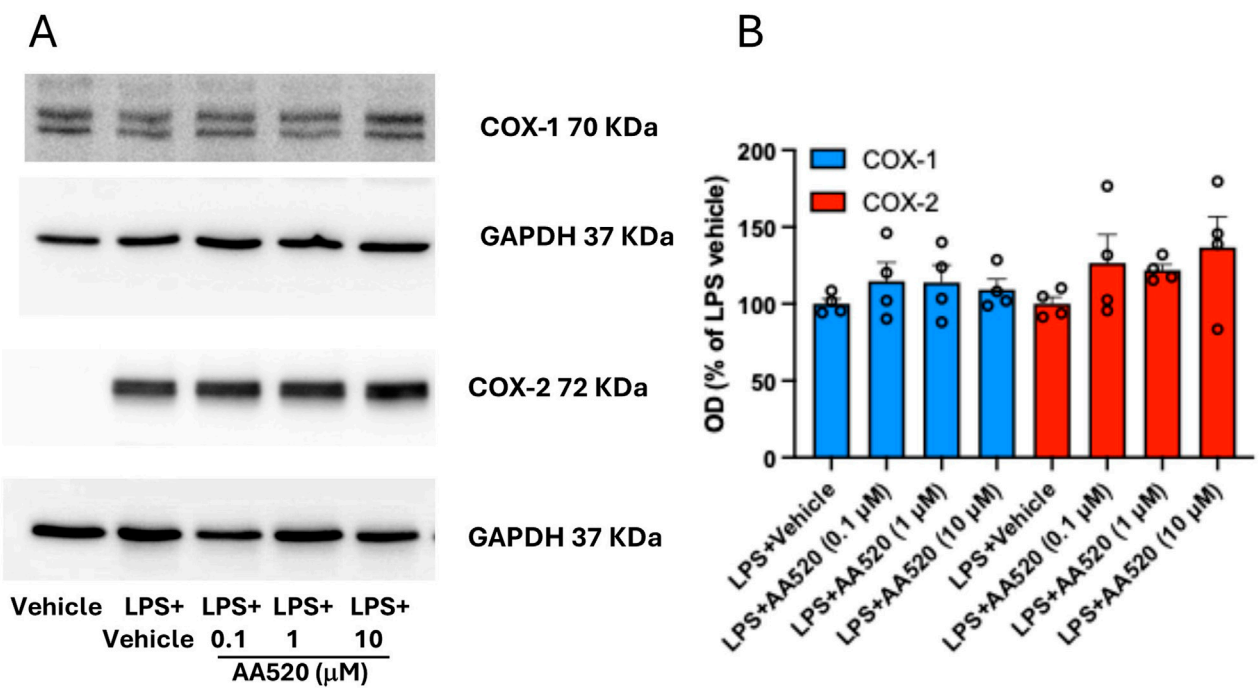

FIGURE 4
Effect of AA520 on COX-1 and COX-2 expression in LPS-stimulated-isolated monocytes. Human monocytes were freshly isolated from concentrated buffy coats. Monocytes (1.5×10^6) grown in RPMI 1640 supplemented with 0.5% FBS, 1% penicillin/streptomycin and 2 mM L-glutamine, were incubated with vehicle (DMSO + NaCl 0.9% w/v) without or with LPS (final 10 μg/mL; vehicle LPS); monocytes were also incubated with LPS in the presence of increasing concentrations of AA520 (0.1–10 μM, dissolved in DMSO) at 37°C for 24 h. After 24 h of incubation, monocytes were centrifuged, and pellets were assayed for COX-1 and COX-2 expression by Western blot **(A)**. The optical density (OD) ratio values of COX-1 and COX-2 immunoreactive bands versus GAPDH bands detected in monocytes treated with LPS vehicle were reported as % of the mean; the effect of increasing concentrations of AA520 (0.1–10 μM) on monocyte COX-1/GAPDH or COX-2/GAPDH were reported as % of LPS vehicle value of each experiment **(B)**. The data were analyzed using one-way ANOVA and Dunnett *post hoc* test (to compare the means of different treatments versus LPS vehicle). The OD values of COX-1/GAPDH or COX-2/GAPDH detected in LPS vehicle were reported as % of the mean + SEM, n = 4.

TXB_2, 15R-HETE, and PGE_2 reduction were 23, 19, and 91%, respectively.

In LPS-isolated human monocytes, AA520 did not significantly affect the protein expression of COX-1 and COX-2 (Figures 4A, B).

Altogether, these findings show that AA520 is a highly selective inhibitor of COX-2 activity.

3.5 Stability of AA520 in LPS-stimulated whole blood and effects of bezafibrate and benzenesulfonamide on PGE_2 generation

Since AA520 was synthesized from the starting products bezafibrate and benzenesulfonamide, we studied the purity of the compound, and a chromatographic LC-MS/MS method was applied to AA520 and its starting compounds bezafibrate and benzenesulfonamide. Figure 5, panels A and B, show the MS and the fragmentation spectra of AA520, respectively. The MS spectrum of AA520 did not display bezafibrate and benzenesulfonamide ions (m/z 360 and m/z 156, respectively, Figure 5A), supporting its purity. From the fragmentation spectra of AA520 (Figure 5B), we have chosen the most abundant fragment to follow for the qualitative analysis of AA520, i.e., m/z 500 > 224 (Figure 5B). For bezafibrate and benzenesulfonamide, the most abundant fragments were m/z360 > 274 and m/z 156 > 79, respectively (not shown).

We assessed the possible metabolization of AA520 (100 μM) to bezafibrate and benzenesulfonamide in heparinized human whole blood incubated for 24 h at 37°C. At the end of the incubation, plasma samples were analyzed for AA520, bezafibrate, and benzenesulfonamide by LC-MS/MS (Figures 5C–E). We detected only tiny amounts of bezafibrate (0.68% of AA520), while benzenesulfonamide was undetectable (<0.1 μM).

We assessed whether benzenesulfonamide and bezafibrate affected COX-2 activity in LPS-stimulated whole blood. As shown in Figure 5, panels F and G, benzenesulfonamide, and bezafibrate reduced PGE_2 generation incompletely (approximately 50%), even at the high concentration of 300 μM.

These data suggest that AA520 is stable in blood up to 24 h and that the possible formation of approximately 1% of bezafibrate did not contribute to COX-2 inhibition by AA520.

3.6 Assessment of the mechanism of inhibition of COX-2 by AA520 in the human colon cancer cell line HCA7

As previously reported (Hofling et al., 2022; Tacconelli et al., 2020b), HCA7 cells express COX-2 but not COX-1. We studied the concentration-dependent inhibition of COX-2-dependent PGE_2 biosynthesis by AA520 in HCA7 cells stimulated with 0.5 μM of

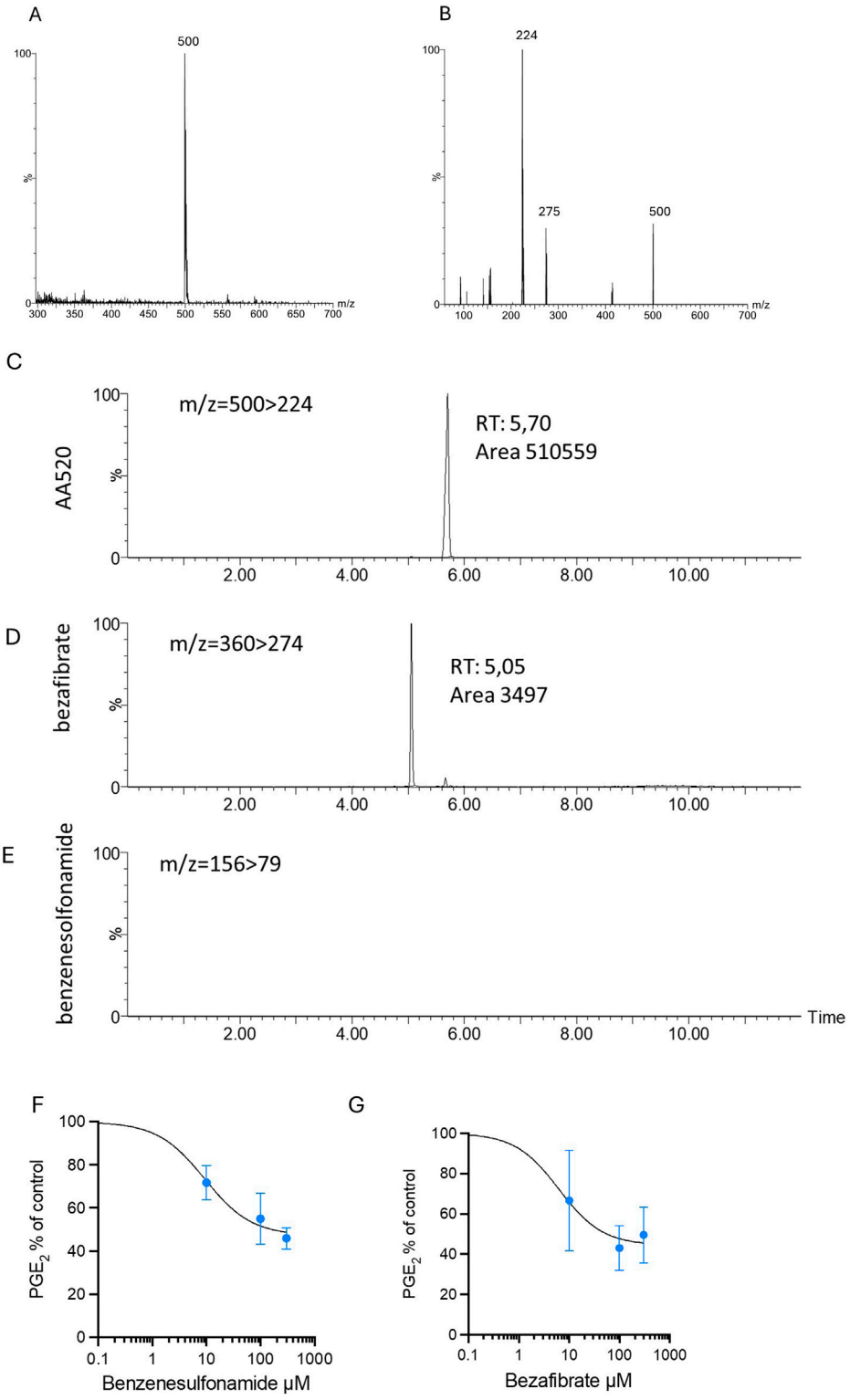

FIGURE 5
Stability of AA520 in LPS-stimulated whole blood and effects of bezafibrate and benzensulfonamide on PGE_2 generation. **(A, B)** Development of a method for the qualitative analysis of AA520: MS **(A)** and MS/MS fragmentation **(B)** spectra of AA520 by triple quadrupole mass spectrometry (MS). AA520 is solubilized in methanol at a final concentration of 1,000 ng/mL and infused into the electrospray ionization source (ESI Z-Spray) under negative ionization conditions at a rate of 50 µL/min. In **(B)**, it is shown the fragmentation spectrum of AA520, obtained with a collision energy of 15 eV; **(C–E)** qualitative evaluation of AA520, bezafibrate, and benzenesulfonamide by LC-MS/MS in whole blood samples incubated for 24 h at 37°C with AA520 (100 µM); a one-mL aliquot of whole blood was incubated with AA520 (100 µM) for 24h at 37°C and after centrifugation and extraction, the sample was injected into the LC-MS/MS system to determine the presence of AA520 and its potential metabolites bezafibrate and benzenesulfonamide; the chromatographic profile of their main fragments m/z 500 > 224 for AA520, m/z360 > 274 for bezafibrate and m/z 156 > 79 for benzenesulfonamide are shown. **(F, G)** Concentration-response curves of inhibition of LPS-induced-PGE_2 biosynthesis by benzenesulfonamide and bezafibrate; increasing

(*Continued*)

FIGURE 5 (Continued)
concentrations of benzenesulfonamide **(F)** and bezafibrate **(G)** (10–300 μM) or vehicle (DMSO + NaCl 0.9% w/v) were incubated with heparinized whole blood samples, withdrawn from healthy volunteers, after suppressing the contribution of platelet COX-1 by adding aspirin (50 μM) *in vitro* solubilized in methanol and then evaporated, in the presence of LPS (10 μg/mL) for 24 h; after centrifugation, PGE_2 levels were analyzed as an index of LPS-induced-COX-2 activity, by specific immunoassay; results are depicted as percent of control (LPS vehicle) (mean ± SEM, n = 3, 2 females and 1 male).

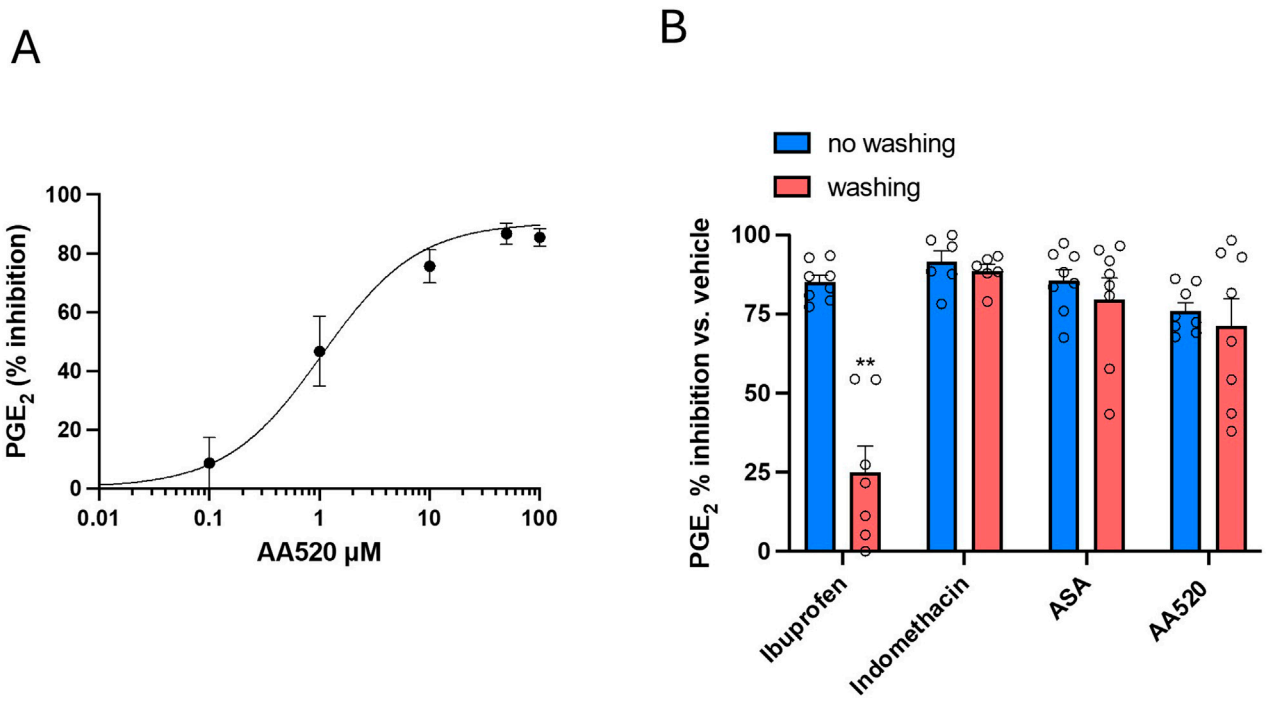

FIGURE 6
Assessment of the inhibition of COX-2 and its reversibility by AA520 in HCA-7 Cells. **(A)** Concentration-dependent inhibition of PGE_2 biosynthesis by AA520 in HCA-7 colony 29 cell line (HCA-7 cells). HCA-7 cells were incubated with DMSO or increasing concentrations of AA520 (0.01–100 μM) for 30min; then, cells were incubated with AA (0.5 μM) for a further 30 min at 37°C, and the levels of PGE_2 were assessed in the conditioned medium by a validated immunoassay. Data are reported as mean ± SEM, n = 4, and represented as % inhibition of PGE_2 generated without the compounds (vehicle). **(B)** Kinetics of the interaction of AA520 and other NSAIDs on COX-2 of HCA-7 cells; the inhibition of COX-2-dependent PGE_2 biosynthesis was assessed by preincubating HCA-7 cells with AA520 (10 μM), indomethacin (a time-dependent inhibitor of COX, 100 μM), aspirin (acetylsalicylic acid, ASA, 100 μM) (an irreversible inhibitor of COX, 100 μM), or ibuprofen (a reversible inhibitor of COX, 100 μM) for 30 min; then, AA (0.5 μM) was added, and the incubation continued for 30 min at 37°C. In other experiments, cells preincubated with the different compounds were washed three times with 3 mL of DMEM (without FBS), resuspended with medium (without FBS), and stimulated with AA, 0.50 μM for 30 min at 37°C. In both experimental conditions (without or with washing passages), PGE_2 production was determined in the medium by a validated immunoassay as an index of COX-2 activity. Data are shown as % inhibition (versus vehicle), mean ± SEM, n = 6–8. The data were analyzed using a two-way ANOVA and Šídák's multiple comparisons test; **P< 0.01 versus no washing condition.

AA. As shown in Figure 6A, AA520 inhibited in a concentration-dependent fashion COX-2-dependent PGE_2 with an IC_{50} of 1.05 (95% CI: 0.58–1.97) μM.

We determined the kinetics of the interaction of AA520 on HCA7 cell COX-2. This involved assessing whether the interaction is rapidly reversible, time-dependent reversible, or irreversible. To achieve this, we compared the extent of PGE_2 biosynthesis inhibition in cells exposed to the compound for 30 min and subsequently washed versus those not washed. Similar experiments were performed with ASA, an irreversible inhibitor of COX; indomethacin, a time-dependent/slowly reversible inhibitor of COX; and ibuprofen, a time-independent/rapidly reversible inhibitor of COX (Walker et al., 2001; Blobaum and Marnett, 2007; Vitale et al., 2013). As shown in Figure 6B, the inhibition of COX-2 activity by AA520 was not significantly affected by the washing of cells similar to ASA and indomethacin.

In contrast, washing the cells almost completely reversed the inhibition of ibuprofen. These results suggest that AA520 tightly interacts with COX-2, resembling the mechanism of indomethacin, i.e., slowly reversible inhibition. However, these results cannot exclude an irreversible interaction with the enzyme similar to the mechanism of inhibition by ASA. To clarify this issue, we performed docking studies.

3.7 Molecular basis of AA520 inhibitory activity on COX-2

To elucidate the molecular basis of the activity of AA520, computational studies were performed using the crystal structure

of COX-2 in complex with celecoxib (PDB 3LN1) (Wang et al., 2010).

The COX active site comprises a predominantly hydrophobic channel that penetrates deeply into the catalytic domain. Although amino acid numbering for COX-1 is usually applied to COX-2, herein, we will retain the numbering of the selected COX-2 X-ray structure (PDB 3LN1). It is worth noting that the numbers of the amino acids in COX-2 are lower by 14 than those of the corresponding residues in COX-1. For instance, the catalytic tyrosine residue is 385 in COX-1 and 371 in COX-2. Based on AA binding, it is possible to divide the active site into different pockets. Residues R106, Y341, and E510 define a "constriction site" (Figure 7A), which opens up the so-called "lobby" (Rouzer and Marnett, 2020). These residues frequently interact with fatty acids or other polar functional groups of substrates or inhibitors. The central binding pocket, instead, contains the residues directly involved in catalysis (Y334, L338, Y371, W373, G512, and S516). COX-2 is known to have a larger binding cavity (Ahmadi et al., 2022), with a "side pocket" next to the active site comprising the amino acids V509, V420, L489, and R499 compared with COX-1, in which such amino acids are changed to I523, I434, F503, and H513, respectively. In particular, the smaller valine residue V509 in COX-2 is primarily responsible for the larger size of its active site. The side pocket is a key binding site exploited by many COX-2 selective inhibitors, including coxibs.

The results of the IFD approach showed that AA520 fitted well within the COX-2 active site, stabilized by several interactions (Figure 7B; Supplementary Figure S1): the oxygen atom of the sulfonimide moiety was H-bonded with the side chain of R499, whereas the carbonyl oxygen accepted an H-bond from the side chain of Y101. In addition, R106 engaged a salt bridge with the negatively charged nitrogen atom of the sulfonimide moiety and a further H-bond with the oxygen atom of the phenoxy moiety. The ligand's tail formed mainly hydrophobic interactions, with the distal *p*-chlorobenzoyl moiety establishing π–π stacking interactions with Y371 and W373. As described above, Y371 is a key catalytic residue that, during enzyme activation, donates an atom of hydrogen to heme (Rouzer and Marnett, 2020). On the other hand, W373 has been reported to possess a role in the correct positioning of AA within the active site by mutagenesis studies, suggesting that both steric bulk and hydrophobicity at this position are important (Thuresson et al., 2001).

The results of the MD simulations and clustering carried out on the COX-2/AA520 complex obtained by the IFD approach showed that the compound is well stabilized within the COX-2 binding site, assuming a horseshoe-shaped conformation within the constriction site and the central binding cavity (Figure 8A). The RMSD analysis of both protein and ligand revealed stable trajectories (Figure 8B). AA520 was further stabilized by a water molecule in its interaction with R106; also, a very strong H-bond with Y341 emerged during the simulation. The benzenesulfonamide head group slightly rearranged to form a cation-π interaction with R499, whereas the ligand's tail group also engaged water-mediated H-bonds with Y371 and S516 through the carbonyl group.

In addition, in order to roughly estimate the binding affinity of AA520 with COX-2, we employed the Prime MMGBSA approach, which provides a useful method to approximate the free energy of binding between a protein and a ligand (Li et al., 2011). The above-described representative structure was used to run the calculation of Prime MM-GBSA; for AA520 we obtained a ΔG_{bind} = −97.20 kcal/mol, suggesting a very favorable binding affinity, considering that for celecoxib we obtained a ΔG_{bind} = −100.53 kcal/mol.

The binding mode of AA520 allowed us to shed some light on the exquisite COX-2 selectivity shown in inhibition assays. A primary determinant for selectivity seems to reside in the interactions formed by the benzenesulfonamide group with R499, which is replaced by histidine in COX-1. This latter would not be able to extend sufficiently to interact with this crucial ligand's moiety. Worthy of note is the tight interactions formed with R106 (Figure 8C), a residue that is critical for the binding of classical NSAIDs bearing carboxylic acid moieties, such as indomethacin and flurbiprofen. In this regard, the binding mode of AA520 is very peculiar because it has, from one side, the key molecular interactions in common with selective COX-2 inhibitors, but still, some features recall the classical NSAIDs. For instance, NS-398 (Supplementary Figure S2A), one of the earliest COX-2 selective inhibitors, possesses a methanesulfonamide moiety interacting with the side chain of R120 (R106 according to the numbering employed herein), which has been indicated as a molecular determinant for time-dependent inhibition of COX-2 (Vecchio and Malkowski, 2011). NS-398 was initially expected to insert the methanesulfonamide moiety into the side pocket, similarly to the methylsulfone moiety of rofecoxib (Supplementary Figure S2B) however structural data proved that this group was, instead, positioned towards the constriction site. Compound AA520, thus, seems to recapitulate such behavior. In addition, the ability of AA520 to interact with R499, as observed for rofecoxib and other members of the coxib class, makes this ligand exquisitely selective. A good overlap between the phenyl ring, the lactone moiety of rofecoxib, and the *p*-chlorobenzoyl of AA520 within the central binding pocket could also be observed (Supplementary Figure S2B).

Lumiracoxib, reported to be the most potent COX-2-selective inhibitor *in vivo* (Blobaum and Marnett, 2007) lies within the central binding pocket. It has been found to interact with S516 and Y371 through its carboxylate moiety. These latter contacts have emerged from the MD simulation of AA520, highlighting the ability of this ligand to engage many critical interactions observed for potent and selective COX-2 inhibitors but also shared by classical NSAIDs.

The overlay of AA520 and indomethacin showed a certain overlap of their *p*-chlorobenzoyl groups (Supplementary Figures S2D, S3) as well as the 2′-methyl of indomethacin and the phenethyl linker of AA520. A hallmark of indomethacin inhibitory activity of COX enzymes is that it appears to be functionally irreversible; reversibility assays carried out by us in HCA7 cells confirmed this finding and displayed, for compound AA520, a behavior like indomethacin. Interestingly, the 2′-methyl group of indomethacin is projected in a pocket formed by V335, A513, S516, and L517 (Supplementary Figure S3). Mutations reducing the size of this pocket or removal of the 2′-methyl group convert indomethacin from a potent tight binding inhibitor to a rapidly reversible, weaker inhibitor (Prusakiewicz et al., 2004), suggesting that the interactions formed within this small and rather hydrophobic pocket may be involved in the formation of a tightly bound enzyme-inhibitor complex. Therefore, it is tempting to speculate that such a mechanism might also apply to AA520, being able to recapitulate such interaction patterns.

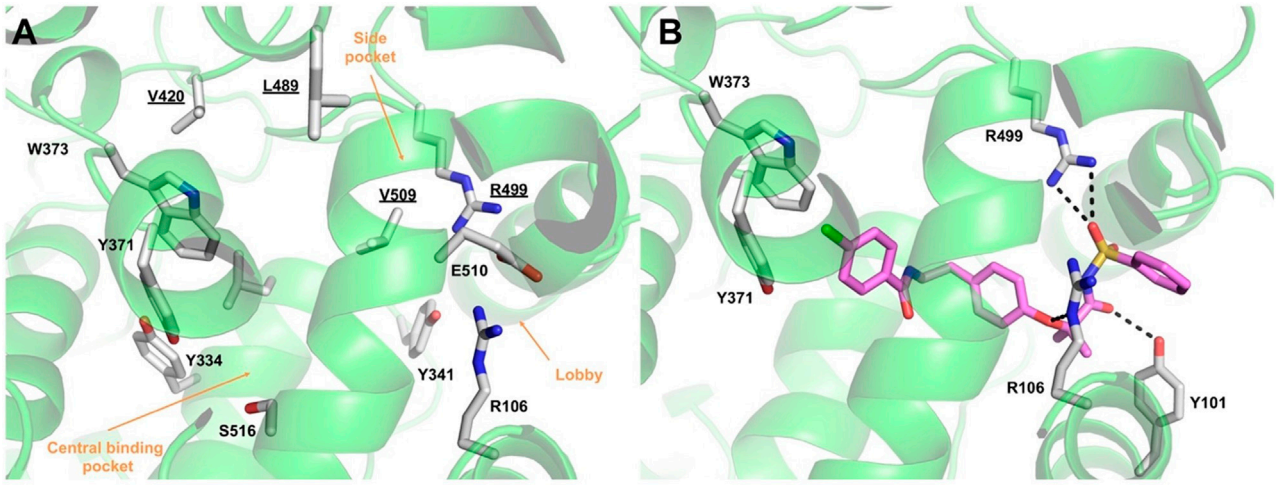

FIGURE 7
(A) Overview of the COX-2 (green ribbons) active site. Amino acids lining the different pockets are shown as white sticks and labeled. Amino acids lining the COX-2 "side pocket" are underlined. **(B)** Binding mode of compound AA520 (violet sticks) into COX-2 (green ribbons, PDB 3LN1), as predicted by IFD calculations. Only amino acids involved in pivotal contacts are displayed (white sticks) and labeled. H-bonds discussed in the text are depicted as dashed black lines.

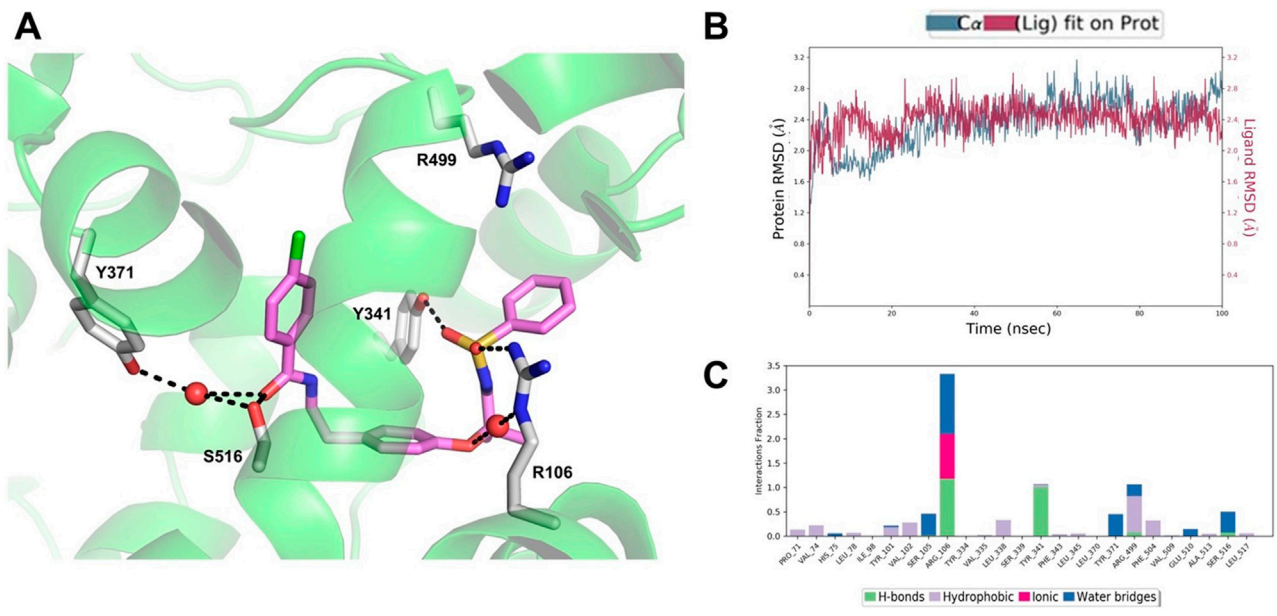

FIGURE 8
(A) Binding mode of AA520 (violet sticks) into COX-2 after 100 ns MD. The representative structure from the most populated cluster is shown. Only amino acids involved in pivotal contacts are displayed (white sticks) and labeled. Waters that engage stable interactions are displayed as red spheres. **(B)** RMSD plot of the protein Ca (blue line) and ligand heavy atoms (red line) with respect to the initial MD frame taken as reference. **(C)** Histogram plot showing the protein interactions with the ligand monitored throughout the simulation.

To sum up, AA520 selectivity and potency could mainly be ascribed to the benzenesulfonamide head group, which can engage both R106 and R499 (a key residue for COX-2 selectivity); the remainder of the ligand extends towards the central binding pocket, where it is stabilized by additional interactions, including the H-bonds with S516 and Y371, which are critical for binding of selective and potent inhibitors such as lumiracoxib.

3.8 Effects of AA520, GW6741 and rofecoxib on cell viability

We have previously demonstrated that AA520 exhibits antagonistic effects on PPARα using *in vitro* transactivation assay, with an IC_{50} of 0.80 ± 0.08 μM (mean ± SEM) (Ammazzalorso et al., 2016). Thus, we aimed to compare the

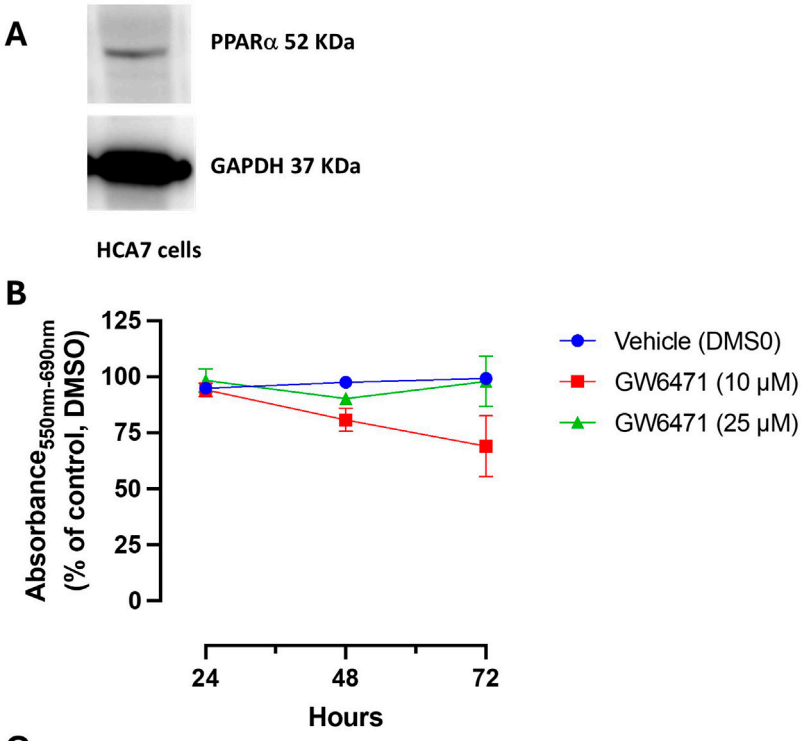

C

AUC	Vehicle (DMS0)	GW6471 (10 μM)	GW6471 (25 μM)
Mean	4668	3895	4520
95% CI	4524 to 4812	3525 to 4265	4214 to 4827

FIGURE 9
(A) Western blot analysis of PPARα in HCA7 cells. **(B, C)** Effect of GW6471 (a PPARα antagonist) on HCA7 cell viability. **(B)** GW6471 (10 and 25 μM) was added to HCA7 cells (4×10^3 cells/well), and an MTT assay was performed for up to 72 h of incubation; results are expressed as a percent of control (DMSO) (mean ± SEM, n = 10). **(C)** AUC values were assessed from 24 to 72 h, providing the mean and 95% CI.

effect of AA520 with a PPARα antagonist GW6471 (Xu et al., 2002) on the MTT cell viability/toxicity assay in HCA7 cancer cells. Moreover, we aimed to verify the contribution of COX-2 inhibition to this effect by coincubating GW6471 with rofecoxib.

As shown in Figure 9A, HCA7 cells express PPARα, and we have previously shown that the cells also express COX-2 (Hofling et al., 2022; Tacconelli et al., 2020b) and generate PGE_2. GW6471, at 10 μM, reduced MTT in a time-dependent fashion. A nonsignificant effect on MTT response was found at higher concentrations of the compound (Figures 9B, C).

The MTT reduction by GW6471 (10 μM) was not influenced by the coincubation with rofecoxib. We used a concentration of 10 μM of rofecoxib, which caused a selective maximal inhibition of COX-2 activity (Figure 3). The selective COX-2 inhibitor incubated alone did not affect MTT (Figures 10A, B).

AA520 caused a maximal time-dependent MTT reduction at 1 μM, a concentration that inhibits PPARα and COX-2, at 72 h. This effect was reduced at higher concentrations (Figures 11A, B).

Figure 12 reports the data found at 72 h of incubation. AA520 at 1 μM caused a more profound reduction of MTT than GW6471 (10 μM). Rofecoxib did not potentiate the MTT effect of the PPARα antagonism by GW6471. These data suggest that the contribution of PPARα antagonism is involved in the cytotoxic effect of AA520 in HCA7 cancer cells.

4 Discussion

With an *in silico* approach, we identified a novel chemical scaffold that is highly selective and potent in inhibiting COX-2 activity in inflammatory and cancer cells. AA520 is a sulfonamide derivative of bezafibrate, and we have previously shown that it is also a potent antagonist of PPARα (Ammazzalorso et al., 2016). Thus, our compound is a unique molecule with dual inhibitory effects on COX-2 and PPARα at the same concentration range.

To characterize the pharmacological effects of AA520 on COX-isozymes, we have used human whole-blood assays (Patrignani et al., 1994; Tacconelli et al., 2020a). We also evaluated whether the compound inhibits other enzymatic and nonenzymatic pathways involved in AA metabolism (Mazaleuskaya et al., 2018). To this aim, we assessed the main prostanoids PGE_2 and TXB_2 and some of the HETEs in both the R and S configurations in LPS-stimulated whole

A

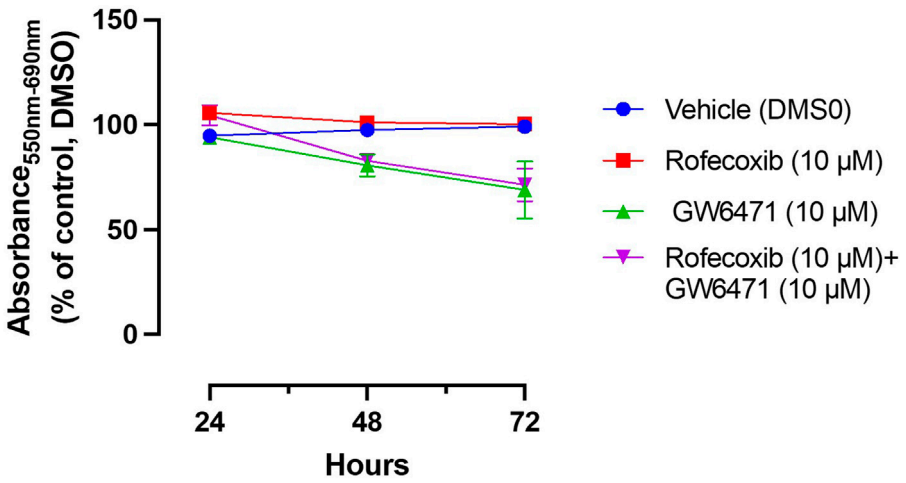

B

AUC	Vehicle (DMS0)	Rofecoxib (10 μM)	GW6471 (10 μM)	Rofecoxib (10 μM)+GW6471 (10 μM)
Mean	4668	4901	3895	4101
95% CI	4524 to 4812	4692 to 5110	3525 to 4265	3857 to 4345

FIGURE 10
Effect of Rofecoxib and GW6471 on HCA7 cell viability. **(A)** Rofecoxib 10 μM, GW6471 10 μM, or both compounds were added to HCA7 cells (4×10^3 cells/well), and an MTT viability assay was performed for up to 72 h of incubation; results are expressed as percent of control (DMSO) (mean ± SEM, n = 10). **(B)** AUC values were assessed from 24 to 72 h, providing the mean and 95% CI.

blood using LC-MS/MS. Human whole blood associated with LC-MS/MS is appropriate for the characterization of the effect of drugs on bioactive eicosanoid lipidomics *in vitro* and *ex vivo*, and it is ideal for drug screening (Mazaleuskaya et al., 2018). It allows small sample sizes and reproducible measures of a broad spectrum of eicosanoids in human blood. This assay can capture drug-induced substrate rediversion and unexpected shifts in product formation by blocking microsomal prostaglandin E synthase-1 (mPGES-1) inhibitors (Cheng et al., 2006). It can identify drug off-target effects. It can detect an antioxidant effect by assessing the levels of HETEs generated from AA by auto-oxidation (Powell and Rokach, 2015).

AA520 resulted in a highly selective and potent inhibitory effect on leukocyte COX-2 activity. The compound was >697-fold more potent towards leukocyte COX-2 than platelet COX-1. The AA520s highly selective inhibitory effect on COX-2 is due to its bulky molecular structure, which makes it difficult to bind the narrow active site of COX-1. Our study examined how AA520 interacts with COX-2 in the human colon cancer cell line HCA7, which does not express COX-1 (Hofling et al., 2022; Tacconelli et al., 2020b). We found that the compound strongly binds to the active site of COX-2, and this binding persists even after extensive washing. This type of binding is like the slow, time-dependent inhibition kinetics seen with COX inhibitors like indomethacin (Blobaum and Marnett, 2007). The docking and molecular dynamics experiments further supported the results from our biochemical characterization studies. The main determinants of AA520 selectivity and potency reside in the benzenesulfonamide head group, which can interact with R106 and R499 (a key residue for COX-2 selectivity). In addition, the hydrophobic contacts with V335, A513, S516, and L517 (Supplementary Figure S3) are likely to form a tightly bound enzyme-inhibitor complex, recapitulating the indomethacin interaction pattern. Interestingly, the benzenesulfonamide head group of AA520 is also a key structural requirement for the antagonistic activity of PPARα, as shown by previous molecular modeling studies (Ammazzalorso et al., 2016). AA520, thus, might be able to induce a receptor's conformation, which is prone to co-repressor recruitment. While derivatives bearing benzothiazole (Ammazzalorso et al., 2016) or benzoxazole (Moreno-Rodríguez et al., 2024) rings present a dual α/γ inhibitory profile, AA520 is selective for PPARα.

As AA520 acts with a dual action mechanism, the antagonism of PPARα and the inhibition of COX-2, it may present potential immunomodulating and antineoplastic activities (Wagner and Wagner, 2022; Wang and Dubois, 2010). The antitumor effects of COX-2 inhibition are well documented since PGE_2 is involved in

A

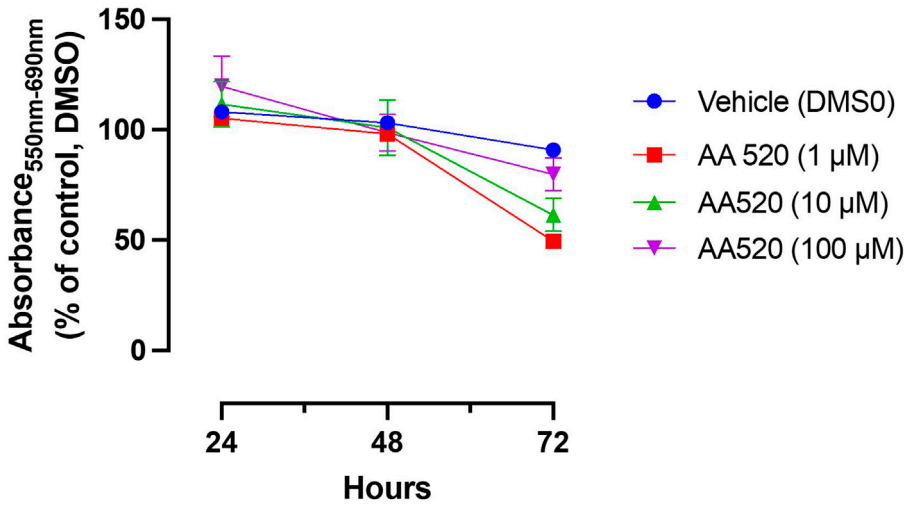

B

AUC	Vehicle (DMS0)	AA520 (1 μM)	AA520 (10 μM)	AA520 (100 μM)
Mean	4867	4213	4501	4765
95% CI	4310 to 5424	3970 to 4457	3990 to 5012	4307 to 5222

FIGURE 11
Effect of AA520 on HCA7 cell viability. **(A)** AA520 (1–100 μM) was added to HCA7 cells (4×10^3 cells/well), and an MTT viability assay was performed for up to 72 h of incubation; results are expressed as a percent of control (DMSO) (mean ± SEM, n = 10). **(B)** AUC values were assessed from 24 to 72 h, providing the mean and 95% CI.

proliferation, migration, and immune escape (Patrignani and Patrono, 2015). A PPARα antagonism action can improve the anticancer effect of COX-2 inhibition. PPARα transcription factor regulates fatty acid oxidation and inflammation in many cancers (Varga et al., 2011). TPST-1120, an orally bioavailable, small molecule, selective, and competitive antagonist of PPARα, is in clinical development by Tempests Therapeutics (Stock 2017). TPST-1120 has shown promise in killing tumor cells and promoting tumor-specific immunity (Whiting et al., 2019). In an ongoing Phase Ib/II, open-label, multicenter, randomized umbrella study in participants with advanced liver cancers, positive results were obtained in combination with atezolizumab (an immune checkpoint inhibitor) and bevacizumab (an antiangiogenic drug) (https://clinicaltrials.gov/study/NCT04524871).

We have tested the impact of AA520 on the MTT assay, which evaluates cell metabolism by estimating mitochondrial NAD(P) H oxidoreductases or cytoplasmic esterase activities (Braissant et al., 2020). This assay assesses the reduction in the number of viable cells. However, we did not study whether the reduction of MTT was due to inhibition of cell metabolism and/or proliferation (cytostatic effect) or actual cell death (cytotoxic effect). Further studies should clarify this issue using different cancer cell lines.

AA520 at 1 μM at 72 h caused an approximately 50% reduction of the MTT response in HCA7 cells, which was significantly higher than that of PPARα antagonist GW6471 (10 μM) (Xu et al., 2002). Both AA520 and GW6471 decreased the effect on MTT when used at higher concentrations. Several explanations can be suggested, such as the antagonists' loss of specificity towards PPARα at higher concentrations. However, AA520 effectively reduced cellular metabolic activity as an indicator of cell viability, proliferation, and cytotoxicity at the appropriate low concentration, affecting PPARα and COX-2 activity.

AA520 can reduce inflammation and pain associated with tumors that exhibit high expression of both PPARα and COX-2, such as advanced RCC (Chen et al., 2004; Abu Aboud et al., 2013), for which there are no effective therapies that prevent its progression. The compound can help alleviate pain linked to tumor metastases, whether used alone or in combination with antiangiogenic and immune checkpoint inhibitors (Song et al., 2020).

AA520 demonstrates high selectivity in inhibiting COX-2, leading to a gastrointestinal safety profile. However, further investigation is needed to understand the impact of the dual inhibitory activity against COX-2 and PPARα on the cardiovascular system. Ongoing studies aim to characterize its effect on the biosynthesis of vascular prostacyclin in experimental models.

In conclusion, considering the synergistic effect between PPARα and COX-2 inhibitors in limiting tumorigenesis, the development of molecules with a dual pharmacological target, i.e., COX-2 inhibitors and PPARα antagonists, is of clinical relevance. This strategy can provide several advantages over single-target inhibitors (Löscher,

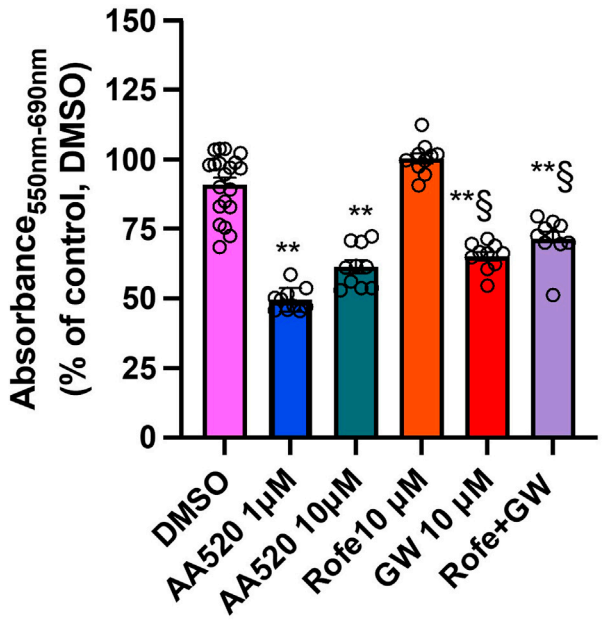

FIGURE 12
Comparison of the effects of AA520, rofecoxib, and GW6471 on HCA7 cell viability at 72 h. AA520 (1 or 10 μM), rofecoxib (10 μM), GW6471 (10 μM), or both rofecoxib and GW6471 were added to HCA7 cells (4×10^3 cells/well) for 72 h, and an MTT viability assay was performed; results are expressed as a percent of control (DMSO) (mean ± SEM, n = 10–20). The data were analyzed using a one-way ANOVA, followed by Dunnett's or Tukey's test; **P < 0.01 versus vehicle; §P< 0.01 vs. AA520 1 μM.

2021): it can reduce the risk of drug resistance, achieve greater anti-tumor efficacy, and minimize adverse events by possibly requiring lower drug dosing during treatment.

Data availability statement

The raw data supporting the conclusions of this article will be made available by the authors, without undue reservation.

Ethics statement

The studies involving humans were approved by Local Ethics Committee of "G. d' Annunzio" University of Chieti-Pescara. The studies were conducted in accordance with the local legislation and institutional requirements. The participants provided their written informed consent to participate in this study.

Author contributions

AA: Writing–review and editing, Writing–original draft, Supervision, Methodology, Conceptualization. ST: Writing–review and editing, Writing–original draft, Project administration, Methodology, Funding acquisition. AC: Writing–review and editing, Writing–original draft, Methodology, Investigation, Funding acquisition. UH: Writing–review and editing, Writing–original draft, Methodology, Investigation. CC: Writing–review and editing, Writing–original draft, Methodology, Investigation. SD: Writing–review and editing, Writing–original draft, Investigation. AD: Writing–review and editing, Writing–original draft, Investigation. RA: Writing–review and editing, Writing–original draft, Project administration. AL: Writing–review and editing, Writing–original draft, Supervision, Data curation. PP: Writing–review and editing, Writing–original draft, Supervision, Funding acquisition, Formal Analysis, Data curation, Conceptualization.

Funding

The author(s) declare that financial support was received for the research, authorship, and/or publication of this article. This original article was funded by Associazione Italiana per la Ricerca sul Cancro (AIRC) [under IG 2017- ID. 20365 Project; Principal Investigator PP], and by Ministero dell'Istruzione, dell'Università e della Ricerca (MIUR) [Fondi per la Ricerca Scientifica di Ateneo, (ex 60%)] to PP and ST. In addition, this work was conducted on behalf of the Aspirin for Cancer Prevention Group, Wolfson Institute of Preventive Medicine, Queen Mary School of Medicine and Dentistry, University of London (UK). Moreover, it was funded by the European Union - European Social Fund - PON Research and Innovation 2014–2020 to AC.

Acknowledgments

We thank the undergraduate students Serena Deliallisi, Giulia Mele, Andrea Di Lorenzo and Cristina Fretta, "G. d'Annunzio" University, for enthusiasm, dedication, and exceptional technical assistance.

Conflict of interest

The authors declare that the research was conducted in the absence of any commercial or financial relationships that could be construed as a potential conflict of interest.

The author(s) declared that they were an editorial board member of Frontiers, at the time of submission. This had no impact on the peer review process and the final decision.

Publisher's note

Supplementary material

The Supplementary Material for this article can be found online at: https://www.frontiersin.org/articles/10.3389/fphar.2024.1488722/full#supplementary-material

References

Abu Aboud, O., Wettersten, H. I., and Weiss, R. H. (2013). Inhibition of PPARα induces cell cycle arrest and apoptosis and synergizes with glycolysis inhibition in kidney cancer cells. *PLoS One* 8 (8), e71115. doi:10.1371/journal.pone.0071115

Ahmadi, M., Bekeschus, S., Weltmann, K. D., von Woedtke, T., and Wende, K. (2022). Non-steroidal anti-inflammatory drugs: recent advances in the use of synthetic COX-2 inhibitors. *RSC Med. Chem.* 13 (5), 471–496. doi:10.1039/d1md00280e

Ammazzalorso, A., Carrieri, A., Verginelli, F., Bruno, I., Carbonara, G., D'Angelo, A., et al. (2016). Synthesis, *in vitro* evaluation, and molecular modeling investigation of benzenesulfonimide peroxisome proliferator-activated receptors α antagonists. *Eur. J. Med. Chem.* 114, 191–200. doi:10.1016/j.ejmech.2016.02.064

Blobaum, A., and Marnett, L. (2007). Structural and functional basis of cyclooxygenase inhibition. *J. Med. Chem.* 50, 1425–1441. doi:10.1021/jm0613166

Blobaum, A. L., and Marnett, L. J. (2007). Molecular determinants for the selective inhibition of cyclooxygenase-2 by lumiracoxib. *J. Biol. Chem.* 282 (22), 16379–16390. doi:10.1074/jbc.M609883200

Bowers, K. J., Chow, D. E., Xu, H., Dror, R. O., Eastwood, M. P., Gregersen, B. A., et al. (2006). Scalable algorithms for molecular dynamics simulations on commodity clusters. *Proc. 2006 ACM/IEEE Conf. Supercomput.*, 43. doi:10.1109/SC.2006.54

Braissant, O., Astasov-Frauenhoffer, M., Waltimo, T., and Bonkat, G. (2020). A review of methods to determine viability, vitality, and metabolic rates in microbiology. *Front. Microbiol.* 11, 547458. doi:10.3389/fmicb.2020.547458

Cervello, M., and Montalto, G. (2006). Cyclooxygenases in hepatocellular carcinoma. *World J. Gastroenterol.* 12 (32), 5113–5121. doi:10.3748/wjg.v12.i32.5113

Chen, Q., Shinohara, N., Abe, T., Watanabe, T., Nonomura, K., and Koyanagi, T. (2004). Significance of COX-2 expression in human renal cell carcinoma cell lines. *Int. J. Cancer* 108 (6), 825–832. doi:10.1002/ijc.11646

Cheng, Y., Wang, M., Yu, Y., Lawson, J., Funk, C. D., and Fitzgerald, G. A. (2006). Cyclooxygenases, microsomal prostaglandin E synthase-1, and cardiovascular function. *J. Clin. Invest* 116 (5), 1391–1399. doi:10.1172/JCI27540

Cipollone, F., Patrignani, P., Greco, A., Panara, M. R., Padovano, R., Cuccurullo, F., et al. (1997). Differential suppression of thromboxane biosynthesis by indobufen and aspirin in patients with unstable angina. *Circulation* 96 (4), 1109–1116. doi:10.1161/01.cir.96.4.1109

Contursi, A., Tacconelli, S., Hofling, U., Bruno, A., Dovizio, M., Ballerini, P., et al. (2022). Biology and pharmacology of platelet-type 12-lipoxygenase in platelets, cancer cells, and their crosstalk. *Biochem. Pharmacol.* 205, 115252. doi:10.1016/j.bcp.2022.115252

Evangelista, V., Manarini, S., Di Santo, A., Capone, M. L., Ricciotti, E., Di Francesco, L., et al. (2006). *De novo* synthesis of cyclooxygenase-1 counteracts the suppression of platelet thromboxane biosynthesis by aspirin. *Circ. Res.* 98 (5), 593–595. doi:10.1161/01.RES.0000214553.37930.3e

Farid, R., Day, T., Friesner, R. A., and Pearlstein, R. A. (2006). New insights about HERG blockade obtained from protein modeling, potential energy mapping, and docking studies. *Bioorg Med. Chem.* 14 (9), 3160–3173. doi:10.1016/j.bmc.2005.12.032

Frey, B. J., and Dueck, D. (2007). Clustering by passing messages between data points. *Science* 315 (5814), 972–976. doi:10.1126/science.1136800

Friesner, R. A., Banks, J. L., Murphy, R. B., Halgren, T. A., Klicic, J. J., Mainz, D. T., et al. (2004). Glide: a new approach for rapid, accurate docking and scoring. 1. Method and assessment of docking accuracy. *J. Med. Chem.* 47 (7), 1739–1749. doi:10.1021/jm0306430

Halgren, T. A., Murphy, R. B., Friesner, R. A., Beard, H. S., Frye, L. L., Pollard, W. T., et al. (2004). Glide: a new approach for rapid, accurate docking and scoring. 2. Enrichment factors in database screening. *J. Med. Chem.* 47 (7), 1750–1759. doi:10.1021/jm030644s

Hofling, U., Tacconelli, S., Contursi, A., Bruno, A., Mucci, M., Ballerini, P., et al. (2022). Characterization of the acetylation of cyclooxygenase-isozymes and targeted lipidomics of eicosanoids in serum and colon cancer cells by the new aspirin formulation IP1867B *versus* aspirin *in vitro*. *Front. Pharmacol.* 13, 1070277. doi:10.3389/fphar.2022.1070277

Hong, F., Pan, S., Guo, Y., Xu, P., and Zhai, Y. (2019). PPARs as nuclear receptors for nutrient and energy metabolism. *Molecules* 24 (14), 2545. doi:10.3390/molecules24142545

Jorgensen, W. L., Maxwell, D. S., and Tirado-Rives, J. (1996). Development and testing of the OPLS all-atom force field on conformational energetics and properties of organic liquids. *J. Am. Chem. Soc.* 118, 11225–11236. doi:10.1021/ja9621760

Kaipainen, A., Kieran, M. W., Huang, S., Butterfield, C., Bielenberg, D., Mostoslavsky, G., et al. (2007). PPARalpha deficiency in inflammatory cells suppresses tumor growth. *PLoS One* 2, e260. doi:10.1371/journal.pone.0000260

Kurumbail, R. G., Stevens, A. M., Gierse, J. K., McDonald, J. J., Stegeman, R. A., Pak, J. Y., et al. (1996). Structural basis for selective inhibition of cyclooxygenase-2 by anti-inflammatory agents. *Nature* 384 (6610), 644–648. doi:10.1038/384644a0

Li, J., Abel, R., Zhu, K., Cao, Y., Zhao, S., and Friesner, R. A. (2011). The VSGB 2.0 model: a next generation energy model for high resolution protein structure modeling. *Proteins* 79 (10), 2794–2812. doi:10.1002/prot.23106

Löscher, W. (2021). Single-target versus multi-target drugs versus combinations of drugs with multiple targets: preclinical and clinical evidence for the treatment or prevention of epilepsy. *Front. Pharmacol.* 12, 730257. doi:10.3389/fphar.2021.730257

Marimuthu, R., Francis, H., Dervish, S., Li, S. C. H., Medbury, H., and Williams, H. (2018). Characterization of human monocyte subsets by whole blood. Flow cytometry analysis. *J. Vis. Exp.* 140, 57941. doi:10.3791/57941

Maskrey, B. H., Bermúdez-Fajardo, A., Morgan, A. H., Stewart-Jones, E., Dioszeghy, V., Taylor, G. W., et al. (2007). Activated platelets and monocytes generate four hydroxyphosphatidylethanolamines via lipoxygenase. *J. Biol. Chem.* 282 (28), 20151–20163. doi:10.1074/jbc.M611776200

Mazaleuskaya, L. L., Lawson, J. A., Li, X., Grant, G., Mesaros, C., Grosser, T., et al. (2016). A broad-spectrum lipidomics screen of antiinflammatory drug combinations in human blood. *JCI Insight* 1 (12), e87031. doi:10.1172/jci.insight.87031

Mazaleuskaya, L. L., Salamatipour, A., Sarantopoulou, D., Weng, L., FitzGerald, G. A., Blair, I. A., et al. (2018). Analysis of HETEs in human whole blood by chiral UHPLC-ECAPCI/HRMS. *J. Lipid Res.* 59 (3), 564–575. doi:10.1194/jlr.D081414

Messmer, D., Lorrain, K., Stebbins, K., Bravo, Y., Stock, N., Cabrera, G., et al. (2015). A selective novel peroxisome proliferator-activated receptor (PPAR)-α antagonist induces apoptosis and inhibits proliferation of CLL cells *in vitro* and *in vivo*. *Mol. Med.* 21, 410–419. doi:10.2119/molmed.2015.00139

Moreno-Rodríguez, N., Laghezza, A., Cerchia, C., Sokolova, D. V., Spirina, T. S., De Filippis, B., et al. (2024). Synthesis and *in vitro* cytotoxicity of benzoxazole-based PPARα/γ antagonists in colorectal cancer cell lines. *Arch. Pharm. Weinh.* 357, e2400086. doi:10.1002/ardp.202400086

Patrignani, P., and Patrono, C. (2015). Cyclooxygenase inhibitors: from pharmacology to clinical read-outs. *Biochim. Biophys. Acta* 1851 (4), 422–432. doi:10.1016/j.bbalip.2014.09.016

Patrignani, P., Sacco, A., Sostres, C., Bruno, A., Dovizio, M., Piazuelo, E., et al. (2017). Low-Dose aspirin acetylates cyclooxygenase-1 in human colorectal mucosa: implications for the chemoprevention of colorectal cancer. *Clin. Pharmacol. Ther.* 102 (1), 52–61. doi:10.1002/cpt.639

Patrignani, P., Panara, M. R., Greco, A., Fusco, O., Natoli, C., Iacobelli, S., et al. (1994). Biochemical and pharmacological characterization of the cyclooxygenase activity of human blood prostaglandin endoperoxide synthases. *J. Pharmacol. Exp. Ther.* 27 (3), 1705–1712. doi:10.1002/(SICI)1097-0193(1996)4:1<58::AID-HBM4>3.0.CO;2-O

Patrignani, P., Tacconelli, S., Piazuelo, E., Di Francesco, L., Dovizio, M., Sostres, C., et al. (2014). Reappraisal of the clinical pharmacology of low-dose aspirin by comparing novel direct and traditional indirect biomarkers of drug action. *J. Thromb. Haemost.* 12 (8), 1320–1330. doi:10.1111/jth.12637

Patrono, C., Ciabattoni, G., Pinca, E., Pugliese, F., Castrucci, G., De Salvo, A., et al. (1980). Low dose aspirin and inhibition of thromboxane B2 production in healthy subjects. *Thromb. Res.* 17 (3-4), 317–327. doi:10.1016/0049-3848(80)90066-3

Patrono, C., Patrignani, P., and García Rodríguez, L. A. (2001). Cyclooxygenase-selective inhibition of prostanoid formation: transducing biochemical selectivity into clinical read-outs. *J. Clin. Invest* 108 (1), 7–13. doi:10.1172/JCI13418

Powell, W. S., and Rokach, J. (2015). Biosynthesis, biological effects, and receptors of hydroxyeicosatetraenoic acids (HETEs) and oxoeicosatetraenoic acids (oxo-ETEs) derived from arachidonic acid. *Biochim. Biophys. Acta* 1851 (4), 340–355. doi:10.1016/j.bbalip.2014.10.008

Prusakiewicz, J. J., Felts, A. S., Mackenzie, B. S., and Marnett, L. J. (2004). Molecular basis of the time-dependent inhibition of cyclooxygenases by indomethacin. *Biochemistry* 43 (49), 15439–15445. doi:10.1021/bi048534q

Rouzer, C. A., and Marnett, L. J. (2020). Structural and chemical biology of the interaction of cyclooxygenase with substrates and non-steroidal anti-inflammatory drugs. *Chem. Rev.* 120 (15), 7592–7641. doi:10.1021/acs.chemrev.0c00215

Santiso, A., Heinemann, A., and Kargl, J. (2024). Prostaglandin E2 in the tumor microenvironment, a convoluted affair mediated by EP receptors 2 and 4. *Pharmacol. Rev.* 76 (3), 388–413. doi:10.1124/pharmrev.123.000901

Saraner, N., Fikirdesici, E., Guney, B., and Saglam, O. (2019). Determination of bezafibrate in human plasma by using liquid chromatography-tandem mass spectrometry. *Biomed. Res. Rev.* 3, 2–4. doi:10.15761/brr.1000124

Serhan, C. N. (2002). Lipoxins and aspirin-triggered 15-epi-lipoxin biosynthesis: an update and role in anti-inflammation and pro-resolution. *Prostagl. Other Lipid Mediat* 68-69, 433–455. doi:10.1016/s0090-6980(02)00047-3

Sherman, W., Beard, H. S., and Farid, R. (2006a). Use of an induced fit receptor structure in virtual screening. *Chem. Biol. Drug Des.* 67 (1), 83–84. doi:10.1111/j.1747-0285.2005.00327.x

Sherman, W., Day, T., Jacobson, M. P., Friesner, R. A., and Farid, R. (2006b). Novel procedure for modeling ligand/receptor induced fit effects. *J. Med. Chem.* 49 (2), 534–553. doi:10.1021/jm050540c

Song, Y., Fu, Y., Xie, Q., Zhu, B., Wang, J., and Zhang, B. (2020). Anti-angiogenic agents in combination with immune checkpoint inhibitors: a promising strategy for cancer treatment. *Front. Immunol.* 11, 1956. doi:10.3389/fimmu.2020.01956

Spaner, D. E., Lee, E., Shi, Y., Wen, F., Li, Y., Tung, S., et al. (2013). PPAR-alpha is a therapeutic target for chronic lymphocytic leukemia. *Leukemia* 27, 1090–1099. doi:10.1038/leu.2012.329

Stock, N. S., Chih-Yu, C. A., Mostofi, B. Y., Duarte, J. J., Melissa, B. J., Andrew, S. B., et al. (2017). US patent No.676,754 B2. *Triazolone Compd. uses thereof*.

Tacconelli, S., Capone, M. L., Sciulli, M. G., Ricciotti, E., and Patrignani, P. (2002). The biochemical selectivity of novel COX-2 inhibitors in whole blood assays of COX-isozyme activity. *Curr. Med. Res. Opin.* 18 (8), 503–511. doi:10.1185/030079902125001335

Tacconelli, S., Contursi, A., Falcone, L., Mucci, M., D'Agostino, I., Fullone, R., et al. (2020b). Characterization of cyclooxygenase-2 acetylation and prostanoid inhibition by aspirin in cellular systems. *Biochem. Pharmacol.* 178, 114094. doi:10.1016/j.bcp.2020.114094

Tacconelli, S., Fullone, R., Dovizio, M., Pizzicoli, G., Marschler, S., Bruno, A., et al. (2020a). Pharmacological characterization of the biosynthesis of prostanoids and hydroxyeicosatetraenoic acids in human whole blood and platelets by targeted chiral lipidomics analysis. *Biochim. Biophys. Acta Mol. Cell Biol. Lipids* 1865 (12), 158804. doi:10.1016/j.bbalip.2020.158804

Tan, Y., Wang, M., Yang, K., Chi, T., Liao, Z., and Wei, P. (2021). PPAR-A modulators as current and potential cancer treatments. *Front. Oncol.* 11, 599995. doi:10.3389/fonc.2021.599995

Thuresson, E. D., Lakkides, K. M., Rieke, C. J., Sun, Y., Wingerd, B. A., Micielli, R., et al. (2001). Prostaglandin endoperoxide H synthase-1: the functions of cyclooxygenase active site residues in the binding, positioning, and oxygenation of arachidonic acid. *J. Biol. Chem.* 276 (13), 10347–10357. doi:10.1074/jbc.M009377200

Thuresson, E. D., Lakkides, K. M., and Smith, W. L. (2002). PGG2, 11R-HPETE and 15R/S-HPETE are formed from different conformers of arachidonic acid in the prostaglandin endoperoxide H synthase-1 cyclooxygenase site. *Adv. Exp. Med. Biol.* 507, 67–72. doi:10.1007/978-1-4615-0193-0_11

Varga, T., Czimmerer, Z., and Nagy, L. (2011). PPARs are a unique set of fatty acid regulated transcription factors controlling both lipid metabolism and inflammation. *Biochim. Biophys. Acta* 1812 (8), 1007–1022. doi:10.1016/j.bbadis.2011.02.014

Vecchio, A. J., and Malkowski, M. G. (2011). The structure of NS-398 bound to cyclooxygenase-2. *J. Struct. Biol.* 176 (2), 254–258. doi:10.1016/j.jsb.2011.07.019

Vitale, P., Tacconelli, S., Perrone, M. G., Malerba, P., Simone, L., Scilimati, A., et al. (2013). Synthesis, pharmacological characterization, and docking analysis of a novel family of diarylisoxazoles as highly selective cyclooxygenase-1 (COX-1) inhibitors. *J. Med. Chem.* 56 (11), 4277–4299. doi:10.1021/jm301905a

Wagner, N., and Wagner, K. D. (2022). Peroxisome proliferator-activated receptors and the hallmarks of cancer. *Cells* 11 (15), 2432. doi:10.3390/cells11152432

Walker, M. C., Kurumbail, R. G., Kiefer, J. R., Moreland, K. T., Koboldt, C. M., Isakson, P. C., et al. (2001). A three-step kinetic mechanism for selective inhibition of cyclo-oxygenase-2 by diarylheterocyclic inhibitors. *Biochem. J.* 357, 709–718. doi:10.1042/0264-6021:3570709

Wang, D., and Dubois, R. N. (2010a). Eicosanoids and cancer. *Nat. Rev. Cancer* 10 (3), 181–193. doi:10.1038/nrc2809

Wang, D., and Dubois, R. N. (2010b). The role of COX-2 in intestinal inflammation and colorectal cancer. *Oncogene* 29 (6), 781–788. doi:10.1038/onc.2009.421

Wang, J. L., Limburg, D., Graneto, M. J., Springer, J., Hamper, J. R., Liao, S., et al. (2010). The novel benzopyran class of selective cyclooxygenase-2 inhibitors. Part 2: the second clinical candidate having a shorter and favorable human half-life. *Bioorg Med. Chem. Lett.* 20 (23), 7159–7163. doi:10.1016/j.bmcl.2010.07.054

Whiting, C., Stock, N., Messmer, D., Olafson, T., Metzger, D., Enstrom, A., et al. (2019). "Blockade of the PPARα metabolic checkpoint with TPST-1120 suppresses tumor growth and stimulates anti-tumor immunity," in Proceedings of the American Association for Cancer Research Annual Meeting, Atlanta, GA. Philadelphia (PA), March 29–April 3, 2019. AACR; Cancer Res79 (13(suppl)).

Xu, H. E., Stanley, T. B., Montana, V. G., Lambert, M. H., Shearer, B. G., Cobb, J. E., et al. (2002). Structural basis for antagonist-mediated recruitment of nuclear co-repressors by PPARalpha. *Nature* 415 (6873), 813–817. doi:10.1038/415813a

Yarchoan, M., Powderly, J. D., Bastos, B. R., Karasic, T. B., Crysler, O. V., Munster, P. N., et al. (2024). First-in-human phase I trial of TPST-1120, an inhibitor of PPARα, as monotherapy or in combination with nivolumab, in patients with advanced solid tumors. *Cancer Res. Commun.* 4 (4), 1100–1110. doi:10.1158/2767-9764.CRC-24-0082

frontiers | Frontiers in Pharmacology

TYPE Original Research
PUBLISHED 20 December 2024
DOI 10.3389/fphar.2024.1528759

OPEN ACCESS

EDITED BY
Paola Patrignani,
University of Studies G. d'Annunzio Chieti and Pescara, Italy

REVIEWED BY
Luciana Mucci,
Italian Medicines Agency (AIFA), Italy
Stefania Tacconelli,
University of Studies G. d'Annunzio Chieti and Pescara, Italy

*CORRESPONDENCE
Ralf P. Brandes,
brandes@vrc.uni-frankfurt.de
Andreas Weigert,
weigert@biochem.uni-frankfurt.de

‡These authors share first authorship

RECEIVED 15 November 2024
ACCEPTED 04 December 2024
PUBLISHED 20 December 2024

CITATION
Kiprina A, Teichmann T, Martín Giménez VM, Xu W, Sailer F, Windbergs M, Manucha W, Weigert A and Brandes RP (2024) The endocannabinoid anandamide prevents TH17 programming of activated T lymphocytes while preserving TH1 responses.
Front. Pharmacol. 15:1528759.
doi: 10.3389/fphar.2024.1528759

The endocannabinoid anandamide prevents TH17 programming of activated T lymphocytes while preserving TH1 responses

Anastasiia Kiprina [1‡], Tom Teichmann [2,3‡], Virna Margarita Martín Giménez[4], Wenqing Xu[1], Fiona Sailer[1], Maike Windbergs[5], Walter Manucha[6,7], Andreas Weigert [1*] and Ralf P. Brandes[2,3*]

[1]Institute of Biochemistry I, Faculty of Medicine, Goethe University Frankfurt, Frankfurt, Germany, [2]Institute for Cardiovascular Physiology, Goethe University Frankfurt, Frankfurt, Germany, [3]German Centre of Cardiovascular Research (DZHK), Partner site RheinMain, Frankfurt, Germany, [4]Instituto de Investigaciones en Ciencias Químicas, Facultad de Ciencias Químicas y Tecnológicas, Universidad Católica de Cuyo, San Juan, Argentina, [5]Institute of Pharmaceutical Technology, Goethe University Frankfurt, Frankfurt, Germany, [6]Instituto de Medicina y Biología Experimental de Cuyo (IMBECU), Consejo Nacional de Investigaciones Científicas y Tecnológicas (CONICET), Mendoza, Argentina, [7]Departamento de Patología, Área de Farmacología, Facultad de Ciencias Médicas, Universidad Nacional de Cuyo, Mendoza, Argentina

Introduction: Anandamide (AEA) is an endocannabinoid that has recently been recognized as a regulator of various inflammatory diseases as well as cancer. While AEA was thought to predominantly engage cannabinoid (CB) receptors, recent findings suggest that, given its protective anti-inflammatory role in pathological conditions, anandamide may engage not only CB receptors.

Methods: In this study, we studied the role of exogenous AEA in a mouse AirPouch model of acute inflammation by examining immune cell infiltrates by flow cytometry. Human primary immune cells were used to validate findings towards immune cell activation and migration by flow cytometry and bead-based ELISA.

Results: We found that AEA decreases the acute infiltration of myeloid cells including granulocytes and monocytes into the inflamed area, but unexpectedly increases the number of T cells at the site of inflammation. This was related to AEA signaling through nuclear receptor subfamily 4A (NR4A) transcription factors rather than CB receptors. Exploring regulatory mechanisms in the human system, we found that AEA broadly inhibits the migratory capacity of immune cells, arguing for blocked emigration of T cells from the inflamed tissue. Taking a closer look at the impact of AEA on T cells revealed that AEA profoundly alters the activation and exhaustion status of $CD4^+$ T and $CD8^+$ T cells, thereby strongly inhibiting TH17 responses, while not altering TH1 differentiation.

Discussion: These data suggest that AEA has the potential to block chronic inflammation without influencing crucial anti-viral and anti-microbial immune defense mechanisms, and may therefore be an attractive molecule to interfere with the establishment of chronic inflammation.

KEYWORDS

AEA, endocannabinoids, T cells, inflammation, lipids

Introduction

Endocannabinoids are ligands of the G-protein-coupled endocannabinoid receptors CB1 and CB2 (Lu and Mackie, 2021). The most studied endocannabinoid is N-arachidonoylethanolamine (anandamide, AEA), which is synthesized *de novo* by cells in response to activation (Lu and Mackie, 2016). AEA has a low half-life in tissue as it is rapidly degraded by fatty acid amide hydrolase (FAAH), cyclooxygenase 2 (COX2), lipoxygenases (LOX) and cytochrome P450 (CYP) enzymes (Maccarrone, 2017).

CB receptors are also expressed outside the brain and elicit a broad spectrum of effects, among them modulation of inflammatory activity. In fact, genetic deletion of CB1 in mice has been shown to promote chronic heart failure (Liao et al., 2013), whereas CB2 results in an increased risk of atherosclerosis (Netherland et al., 2010) as well as cardiomyopathy (Duerr et al., 2014). Deletion of CB1 receptors in myeloid cells limits atherosclerosis development in male mice (Wang et al., 2024) and CB1 receptor activation promotes vascular smooth muscle cell proliferation and neo-intima formation (Molica et al., 2013). Although CB receptors are considered the predominant mediators of AEA signaling, it became clear that they are not the only signaling receptors responding to this nitro-lipid. In fact, extracellular AEA can also bind and activate the transient receptor potential vanilloid type-1 (TRPV1) and transient receptor potential ankyrin type-1 (TRPA1) channels as well as the G-protein coupled receptors GPR55 and GPR119 (Ligresti et al., 2016; Maccarrone, 2017; Pertwee et al., 2010; Zygmunt et al., 1999).

AEA is produced within the central nervous system (CNS), where it was shown to have anti-inflammatory and neuroprotective effects in the context of neuroinflammation (Eljaschewitsch et al., 2006). Moreover, AEA is known to reduce vascular, skin and endotoxin-induced inflammation (Martín Giménez et al., 2022; McCormick et al., 2023; Tomczyk et al., 2021) by acting on CB receptors, but also by triggering epigenetic changes (Martín Giménez et al., 2022). Various studies have demonstrated that AEA has oncoprotective activity against breast, prostate and non-melanoma skin cancers (Sarfaraz et al., 2008; Soliman and van Dross, 2016).

We recently identified that AEA elicits a strong anti-inflammatory effect in vascular smooth muscle cells (VSMCs), which was mediated by an epigenetic modulation through NCoR1 (Pflüger-Müller et al., 2020). Interestingly, we also observed that these effects of AEA require high concentrations and were not mediated by classic AEA receptors, like CB1 and CB2. This constellation may suggest an action of AEA through nuclear receptors (NR). NRs are proteins with transcription factor properties that are typically activated by lipophilic compounds (Frigo et al., 2021). After ligand binding and, if required, nuclear translocation, nuclear receptors, acting as mono or hetero- and homo-dimer, activate gene expression (Martínez-González et al., 2021). In addition to these classic hormone receptors, a broad spectrum of lipid receptors like peroxisome proliferator-activated receptor (PPARs) alter gene expression in response to some poly unsaturated fatty acids (PUFAs) and other ligands (O'Sullivan, 2007). Finally, orphan NRs exist and and some of them even lack a ligand binding site rendering their activity controlled through phosphorylation or abundance and subcellular localization (Mullican et al., 2013). Receptors of the NR4 class belong to the latter group, although more and more compounds are being identified, which appear to bind these receptors and increase their activity. Among them are signaling lipids like prostaglandin A2 or pharmacological compounds like CDIM12 or cytosporone B (Hammond et al., 2015; Rajan et al., 2020; Zhan et al., 2008). We recently reported that AEA binds and activates NR4A1 and NR4A2 to mediate an anti-inflammatory effect in vascular smooth muscle cells (VSMCs) (Teichmann et al., 2024). In fact, there is a good amount of data linking NR4 receptors to inflammatory control: In inflamed human synovial tissue, multiple sclerosis or atherosclerotic lesions, their expression is drastically increased (McMorrow and Murphy, 2011), while in mice, both loss of NR4A1 or NR4A2 was associated with increased inflammation (Bonta et al., 2006; Hamers et al., 2013). Moreover, NR4A receptors are rapidly and strongly induced by various inflammatory cytokines, suggesting a protective role in an acute scenario by helping to resolve inflammation through a negative feedback mechanism, aiming to restore homeostasis in the later stages of inflammation (Rodríguez-Calvo et al., 2017).

A limitation of our previous study on the AEA-mediated activation of NR4 receptors was, that the physiological relevance of the anti-inflammatory effect was only determined in organ culture of the isolated mouse aorta and cultured VSMC. In the present study we therefore set out to determine whether AEA also limits inflammation *in vivo*. Unexpectedly, we observed a strong, NR4-dependent effect of AEA on T-lymphocytes, which, among others, resulted in a prevention of differentiation towards a TH17 phenotype and rather maintained competence of the cells to respond to acute inflammatory stimulation.

Materials and methods

Animals

Global knockout mice for NR4A1$^{-/-}$(Nur77), NR4A2$^{-/-}$ (Nur1) and double knockout for NR4A1/2$^{-/-}$ were generated by crossing NR4A1$^{flox/flox}$ (obtained from the Jackson Laboratory) or NR4A2$^{flox/flox}$ mice (kindly provided by Pierre Chambon (Sekiya

et al., 2011), with CMV-GT-Rosa-CreERT2$^{TG/0}$. All knockout animals were generated on the C57BL/6 background. Global deletion of NR4A1 (A1KO) and/or NR4A2 (A2KO) was induced by administering tamoxifen (400 mg/kg in chow) for 10 days, followed by a 14-day tamoxifen-free "wash-out" period. In this study, control animals (WT) are defined as littermates, which did not receive tamoxifen treatment with the chow. All animals had free access to chow and water in a specified pathogen-free facility with a 12 h light/dark cycle and all animal experiments were performed in accordance with the German animal protection law and were carried out after approval by the local authorities (Regierungspräsidium Darmstadt, approval number FU1268). Every mouse received an identification number for each experiment and the experimenter was blinded for the genotype. Animal group sizes differed due to number of available littermates.

Preparation of AEA micellar nanoformulations

AEA is an oily substance, which limits application *in vivo* and controlled absorption. Therefore, the compound was applied as nanoformulation. The preparation of the AEA micellar nanoformulations was carried out as previously described (Martín Giménez et al., 2023). Briefly, 30 mg of the commercial co-polymer Pluronic® F127 (PF127; BASF, CABA, Buenos Aires, Argentina) was accurately weighed and dissolved in 1 mL of Milli-Q water (Sigma-Aldrich, St. Louis, MO, USA) each. The mixture was continuously stirred at RT until homogeneous and a transparent dispersion was obtained. Subsequently, 750 µg of AEA, dissolved in absolute ethanol (using 15 µL of a commercial AEA ethanolic solution from Cayman Chemical, Ann Arbor, MI, USA), was incorporated (drop by drop) into the polymeric dispersion. Stirring was maintained until complete ethanol evaporation. AEA-free micellar nanoformulations of the PF127 polymer (Pluronic) served as control (CTL).

AirPouch model of acute inflammation

The AirPouch model (Paul-Clark et al., 2012; Pierron et al., 2023) was conducted on both tamoxifen-treated mice following intake and washout, as well as on untreated mice (CTL) that did not receive tamoxifen. Mice were anesthetized using isoflurane inhalation and placed on a heating pad to maintain body temperature. The dorsal skin region was shaved, and the skin was sterilized with 70% ethanol. An AirPouch was created by subcutaneous injection of 5 mL sterile air using a 23-gauge needle, followed by additional injects of 3 mL after 3 days to maintain the pouch. On day 6, 30 µg diclofenac and 10 µg AEA-Pluronic nanoparticles or Pluronic control nanoparticles without AEA (in 0.5 mL 0.9% NaCl) were injected into the pouch. Diclofenac was administered to avoid degradation of AEA by cyclooxygenases. After 1 h of pre-incubation, 1 mL of a 1% zymosan solution was injected into the pouch. After 6 h the pouch content was recovered by injection of 1 mL PBS into the pouch, massage and aspiration of the contained liquids. The concentration used for the final experiments was the result of a dose-escalation study on individual animals to determine an effective concentration.

Primary human macrophage generation, activation, and treatment

Human peripheral blood mononuclear cells were isolated from commercially available buffy coats from anonymous donors (DRK-Blutspendedienst Baden-Württemberg-Hessen, Institut für Transfusionsmedizin und Immunhämatologie, Frankfurt, Germany) using Ficoll density centrifugation. Peripheral blood mononuclear cells were washed twice with PBS containing 2 mM EDTA and thereafter incubated for 2 h under growth conditions in RPMI 1640 media supplemented with penicillin (100 U/mL) and streptomycin (100 µg/mL) to enable adherence to culture dishes (Sarstedt, Nümbrecht, Germany). Non-adherent cells were removed. Monocytes were differentiated into naïve macrophages with RPMI 1640 media (Gibco) containing 3% AB-positive human serum (DRK-Blutspendedienst Baden-Württemberg-Hessen, Frankfurt, Germany) for at least 7 days. Differentiated macrophages were exposed to media with 1% FCS overnight. The next day, cells were incubated in RPMI 1640 media with 1% FCS alone, with EtOH as solvent for 2 h, with 10 µM diclofenac (Sigma Aldrich) for 1 h, and treated with 10 µM AEA or EtOH as solvent for 2 h. Diclofenac was used to arrest the cyclooxygenase-mediated breakdown of AEA. After treatment, macrophages were incubated with 10 µg/mL Zymosan (Sigma Aldrich) for 6 h.

T cell isolation, activation and treatment

Primary human peripheral blood cells were isolated from buffy coats of anonymous donors (DRK-Blutspendedienst Baden-Württemberg-Hessen, Institut für Transfusionsmedizin und Immunhämatologie, Frankfurt am Main). T cells were isolated using the EasySep™ Human T Cell Isolation Kit (Stemcell Technologies) through negative selection. The purity of T cells was greater than 95%, as confirmed by flow cytometry. The cells were cultured at concentration 1×10^6 cells/mL in T-cell medium (RPMI 1640, penicillin (100 U/mL), streptomycin (100 µg/mL), FCS (10%), non-essential and essential amino acids (1%), sodium pyruvate (1%) and 1% 4-(2-hydroxyethyl)-1 piperazineethanesulfonic acid (HEPES)). Cells were supplemented with human recombinant IL-2 (10 ng/mL; PrepoTech) at days 0, 2, and 4 and β-mercaptoethanol (50 µM; Gibco). Cells were cultured for up to 6 days. T cells were treated with Diclofenac for 1 h, Diclofenac and ethanol for 2 h, and Diclofenac and AEA for 2 h. After treatment, T cells were left unstimulated and stimulated with an anti-CD3/CD28/CD2 T cell activator (Stemcell) for up to 6 days. At the endpoint, supernatants were collected for cytokine measurement, and cells were analyzed by flow cytometry.

PBMC migration assay

The migration assay was performed using 6.5 mm diameter transwell cell culture inserts (5 µm pore size; Costar). Human PBMCs were isolated from the buffy coats by Ficoll density centrifugation, washed, counted, and incubated overnight in RPMI 1640 media with 10% FCS, human recombinant IL-2 (10 ng/mL), and β-mercaptoethanol (50 µM). The next day, 10^5

TABLE 1 Antibodies used for FACS analysis of AirPouch samples.

Antigen	Fluorochrome	Clone	Dilution used	Manufacturer	Cat. No.
CD3	PE-CF594	145-2C11	1:100	BD Biosciences	562286
CD4	V500	RM4-5	1:75	BD Biosciences	560782
CD8	BV650	53–6.7	1:100	Biolegend	100742
CD11b	BV605	M170	1:200	Biolegend	101257
CD11c	AlexaFluor700	N418	1:200	Biolegend	117320
CD19	APC/Fire 750	6D5	1:100	Biolegend	115558
CD45	VioBlue	30F11	1:50	Miltenyi Biotec	130-118-953
CD206	FITC	C068C2	1:100	Biolegend	141704
F4/80	PE-Cy7	BM8	1:200	Biolegend	123114
HLA-DR (MHC II)	APC	M5/114.15.2	1:100	Biolegend	107614
Ly-6C	PerCP-Cy5.5	HK1.4	1:200	Biolegend	128012
Ly-6G	APC-CTy7	1A8	1:100	Biolegend	127624
CD80	PE	16-10A1	1:50	Biolegend	104708

cells were seeded in the insert in serum-free medium. Prior to the migration assay, PBMCs were treated with AEA and Diclofenac or left untreated. Treated cells were used to migrate toward the medium with FCS. PBMCs that did not receive treatment were used for migration toward macrophage-derived supernatants, medium with AEA (EtOH as control), Diclofenac, and Zymosan (10 μg/mL). Cells were allowed to migrate for 3 h in cell culture. Afterwards, migrated and non-migrated cells were analyzed by flow cytometry. The percentage of migrated immune cells was determined by the ratio of migrated/non-migrated cells.

LegendPlex

The concentrations of CCL2, CCL20, CCL4, CCL17, CCL5, IL-8, CXCL1, CXCL10, and CXCL9 in macrophage supernatants were quantified using LegendPlex (BioLegend). Samples were analyzed via flow cytometry. Data were analyzed using FlowJo V.10 (Tree Star).

Cytometric bead array

IFN-γ, IL-10, IL-13, and IL-17A concentrations in the T cell-derived supernatants were quantified using Cytometric Bead Array flex sets (BD Bioscience). Samples were analyzed via flow cytometry. Data were analyzed using FlowJo V.10 (Tree Star).

Flow cytometry

Single-cell suspensions from air pouches were blocked with FcR blocking reagent (Miltenyi Biotec) in 0.5% PBS-BSA for 10 min, stained with fluorochrome-conjugated antibodies (Table 1) and analyzed on a FACSSymphony A5 flow cytometer (BD

TABLE 2 Antibodies used for FACS analysis of migration and T-cell activation assays.

Antibody	Clone	Provider
CD192-PE-Cy7	K036C2	BioLegend
CD184-BV750	12G5	BD Biosciences
CD183-APC	G025H7	BioLegend
CD279-BUV737	EH12.1	BD Biosciences
CD223-AlexaFlour488	11C3C65	BioLegend
CD69-BUV395	FN50	BD Biosciences
CD4-BB630	SK3	BD Biosciences
CD8-BV650	RPA-T8	BD Biosciences
CD196-PE	G034E3	BioLegend
CD38-BUV615	HIT2	BD Biosciences
TIGIT-PE-CF594	A15153G	BioLegend
CD194-BV421	L291H4	BioLegend
CD25-BUV661	2A3	BD Biosciences
CD3-BUV805	SK7	BD Biosciences
CD20-APC-H7	2H7	BD Biosciences
HLA-DR-APC Fire750	L243	BioLegend
CD56-BV605	HCD56	BioLegend
CD16-BV650	3G8	BD Biosciences
CD195-BUV395	3A9	BD Biosciences
CD198- PE-CF594	433H	BD Biosciences
CD14-BB700	MΦP9	BD Biosciences
CD33-BV510	WM53	BD Biosciences

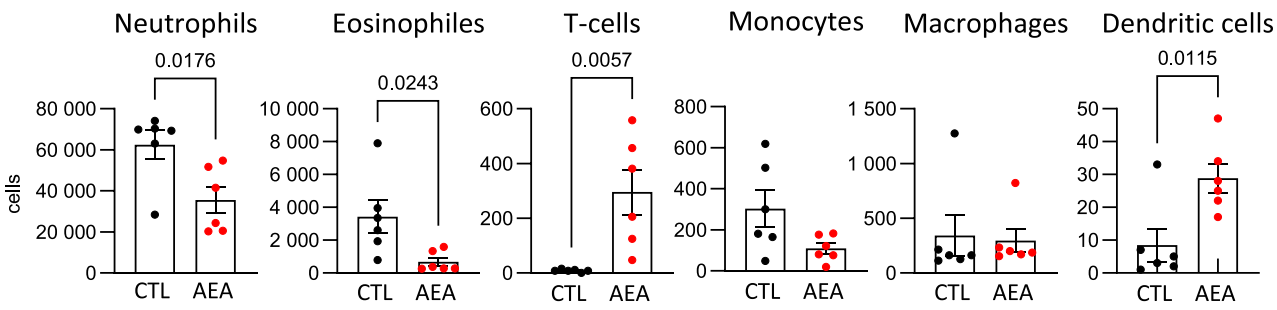

FIGURE 1
AEA increases T-cell number in AirPouch exudates in response to zymosan. Analysis of cellular infiltrate in murine AirPouch exudates after control (CTL) or AEA nanoformulation (AEA) pre-treatment (1 h) followed by zymosan stimulation (6 h) in mice. Each data point represents an animal showing the total number of cells recovered by FACS analysis. Mann-Whitney test. n = 4–8. *$p < 0.05$.

Biosciences). Live single cells were identified by FSC/SSC characteristics. Data were analyzed using FlowJo V10 (TreeStar).

T cells and PBMCs were harvested, pelleted by centrifugation, blocked with an FcR blocking reagent (Miltenyi Biotec) in 0.5% PBS-BSA, stained with fluorochrome-conjugated antibodies (Tables 1, 2), and analyzed on a FACSymphony A5 flow cytometer (BD Biosciences). Data were analyzed using FlowJo V.10 (TreeStar).

All antibodies and secondary reagents were titrated to determine optimal concentrations. Comp-Beads (BD) were used for single-color compensation to create multicolor compensation matrices. For gating, fluorescence minus one controls were used. The instrument calibration was controlled daily using Cytometer Setup and Tracking beads (BD Biosciences). To determine the actual number of cells, counting beads were used (Bangs Laboratories).

Statistical analysis

All experiments were independently performed at least three times as indicated by the number (n) in the respective figure legend. Statistical analysis was performed using Prism 10.1.2. Shapiro-Wilk tests were used to test for normal Gaussian distribution. A paired two-tailed Student's t-test was used to calculate statistically significant differences between two groups of human immune cells. A one-sample Student's t-test was used to calculate statistically significant differences between normalized data. ANOVA followed by Tukey's test or Student's t-test was used to evaluate statistical significance in murine data. Values of $p \leq 0.05$ were considered significant. All data are expressed as mean ± standard error of mean (SEM).

Results

Anandamide increases T-cell but reduced granulocyte infiltration in the airpouch model

To determine a potential anti-inflammatory effect of AEA *in vivo* the AirPouch model of acute inflammation was used. AEA nanoformulations or nanoformulation control were injected into the pouch followed by Zymosan stimulation. Subsequently accumulation of inflammatory cells in the pouch was determined. As compared to control, the number of neutrophils and eosinophils was significantly lower in the AEA group. A similar trend existed for monocytes, but did not reach statistical significance. In contrast to this, the number of T cells as well as dendritic cells (DCs) recovered from the pouch was significantly higher in the AEA group as compared to the control group (Figure 1). Thus, AEA treatment reduced myeloid cell infiltration in the pouches, while the number of invaded T cells, which are typically involved in the later immune response, was increased by AEA.

Anandamide directly decreases chemokine levels in Zymosan treated human macrophages

To determine potential mechanisms explaining the findings in the AirPouch model, human primary immune cells were used. First, the impact of AEA on chemokine production by Zymosan-activated primary human macrophages was tested, since local macrophages are the first responders to Zymosan and affect recruitment of further immune cells, among other mechanisms by producing chemokines. Human macrophages were exposed to a medium containing 1% FCS overnight, followed by AEA treatment and activation with Zymosan. Initially, AEA was used at a concentration of 10 nM or 10 µM. However, 10 nM AEA did not have any impact on chemokine levels. When looking at overall chemokine levels, AEA at 10 µM did not significantly change the chemokine production in Zymosan-activated human macrophages (Figure 2; Supplementary Figure S1) due to high variability in chemokine levels between donors. However, when data were normalized, a decreased expression of CCL2 (Figure 2A), CCL4 (Figure 2B), and CCL20 (Figure 2C) in the presence of AEA compared to the Diclofenac and solvent controls (CCL2, CCL4, and CCL20), or only compared to solvent control (CCL20), was noted. Additionally, AEA decreased the production of CCL17 (Figure 2D) compared to Diclofenac and the solvent, even though the changes were minor. The expression of the remaining chemokines was consistent among control and treated groups (Supplementary Figure S1). These data suggest that high concentrations of AEA reduce the expression of chemokines, which participate in attracting cells to the site of inflammation. These findings, while being in line with reduced myeloid cell

10.3389/fphar.2024.1528759

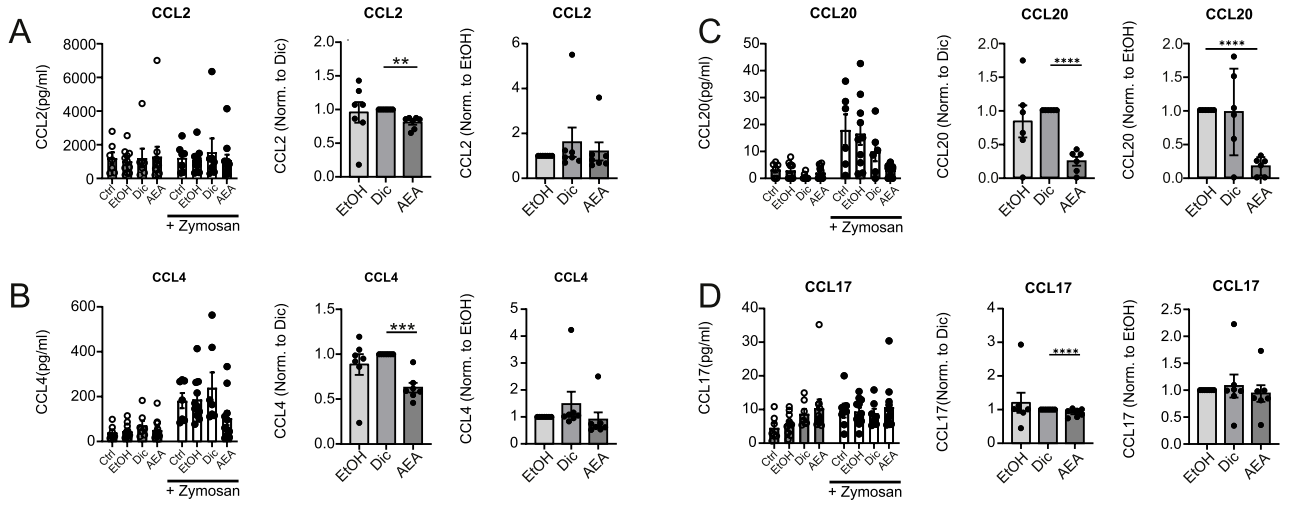

FIGURE 2
AEA reduces chemokine production in Zymosan-activated Macrophages. Human primary macrophages were treated with ethanol (EtOH), Diclofenac and EtOH (Dic), or and AEA (10 μM) with Diclofenac (AEA), and were subsequently stimulated with Zymosan for 6 h. The concentrations of CCL2 **(A)**, CCL4 **(B)**, CCL20 **(C)**, and CCL17 **(D)** were determined by LegendPlex assay. Besides raw data, normalized data of Zymosan-activated cells is shown. Data are from three independent experiments, with at least 2 donors each. Each data point corresponds to a single donor (n = 7). Data are shown as mean ± SEM. *$p < 0.05$, **$p < 0.01$, ***$p < 0.001$, ****$p < 0.0001$; p-values were calculated using two-way ANOVA or one-sample t-test.

numbers, did not explain increased T cell numbers in the AirPouch model after AEA treatment. To investigate, whether changes in chemokine production directly alter the migratory capacity of immune cells, a boyden chamber assay was performed in which human PBMCs were allowed to migrate towards a supernatant derived from Zymosan-activated macrophages macrophages that were treated with either solvent controls or AEA. However, leukocyte migration towards supernatants derived from macrophages was not affect, whether they were treated with AEA or left untreated (data not shown). Unexpectedly, also CCR6+ $CD4^+$ T cells and CCR6+ $CD8^+$ T cells, as responders to CCL20, did not show altered migration towards supernatants from the AEA-treated as compared to control-treated macrophages. In addition, conditioned media of AEA-treated macrophages as compared to control conditions did not alter the migration capability of CCR2+ cells (data not shown). Taken together, AEA reduced the levels of the chemokines CCL20, CCL4, CCL2, and CCL17 in Zymosan-activated macrophages, but this did not directly impact immune cell migration.

The presence of AEA suppresses the migration of human immune cells

To explore a direct effect of AEA on human PBMC migration, the Boyden chamber migration assay was employed to allow PBMCs to migrate towards media containing solvent (CTL), AEA, Zymosan, and AEA + Zymosan. Diclofenac was present in each group to prevent cyclooxygenase-mediated breakdown of AEA. Media with and without FCS were used as positive and negative controls respectively, and the proportion between migrated and non-migrated immune cells was determined by flow cytometry (Supplementary Figure S2). The presence of AEA alone decreased the migration rate of immune cells, while AEA in combination with Zymosan increased the percentage of migrated cells (Figures 3A, B). These data suggest that AEA can have a multifaceted role in immune cell migration. Similarly, the presence of AEA alone in the bottom chamber also decreased the migration rate of B cells (Figure 3C). AEA alone and in combination with Zymosan reduced the migration of NK cells (Figure 3D) and the cytotoxic NK cell subset (CD56dim CD16hi) (Figure 3E). However, there was no difference between groups in the migration rate of the CD56hi CD16dim NK cell subpopulation (Figure 3F). Importantly, the addition of AEA alone or together with Zymosan did not alter the migration rate of T cells *per se* (Figure 3G). However, there was a tendency for a reduced number of migrated $CD4^+$ T cells (Figure 3H) towards AEA in combination with Zymosan, while AEA did not have impact on the migration rate of $CD8^+$ T cells (Figure 3I) and CCR6+ $CD4^+$ T cells (Figure 3J). When looking at myeloid cells, AEA did not affect the migration of myeloid cells *per se* (Figure 3K), as well as that of myeloid subsets such as classical monocytes (Figure 3L), intermediate monocytes (Figure 3M), mDCs (Figure 3N), and activated mDCs (Figure 3O). The migration of myeloid CD33low cells (Figure 3P), and CD195 (CCR5)+ myeloid CD33low cells (Figure 3Q), which may correspond to $CD33^+$ NK cells, was decreased by AEA without the presence of Zymosan. Together, these data demonstrated that AEA directly affects migration of certain immune cell subsets, despite being applied at the site towards which the cells migrate.

Anandamide stimulation alters the migratory capacity of human immune cells

Next, we tested whether or not pre-incubation of PBMCs with AEA would affect their ability to migrate towards FCS. Cells were pre-treated for 1 h with Diclofenac and for 2 h with AEA. Again, media with and without FCS were used as positive and negative

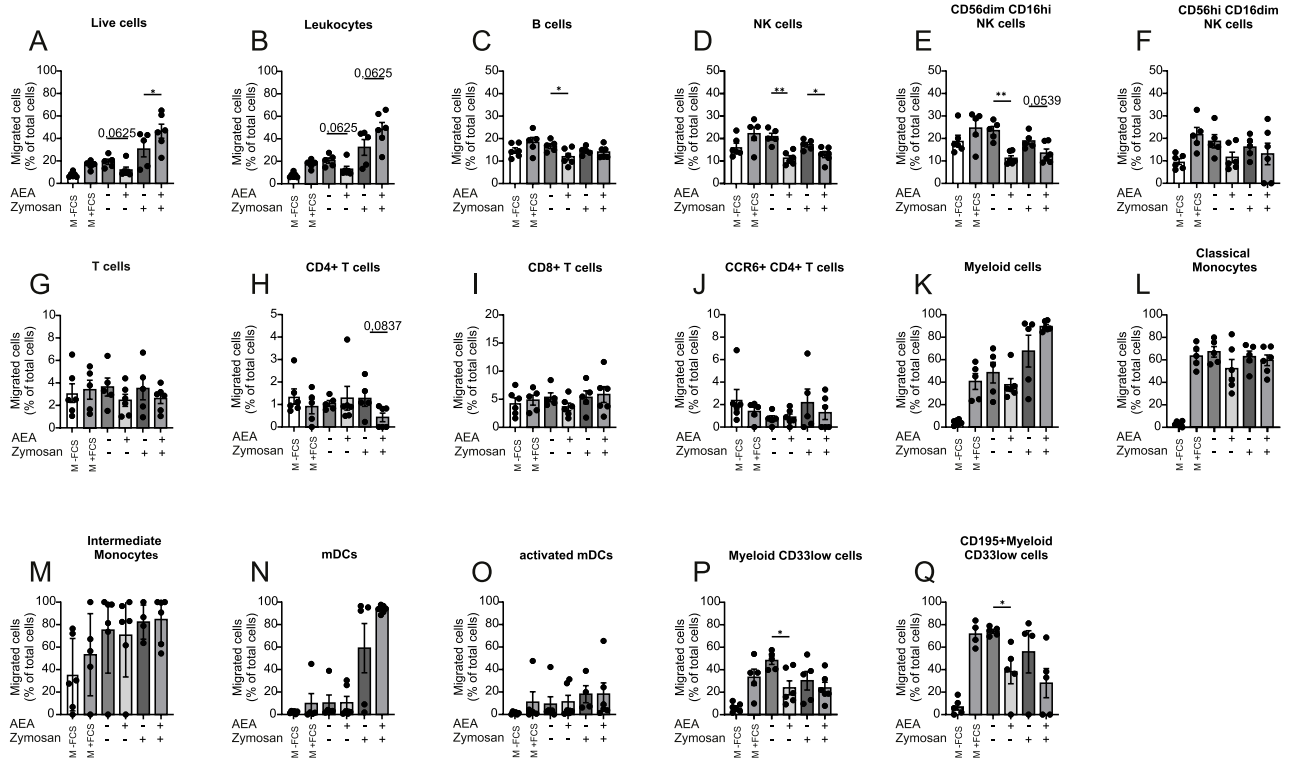

FIGURE 3
AEA and Zymosan together alter immune cell migration. Human PBMCs were kept for 3 h to migrate toward media without FCS (-FCS), with FCS (+FCS), AEA (10 μM), Zymosan, or AEA (10 μM) and Zymosan. All groups except positive and negative controls contained Diclofenac (10 μM). The numbers of migrated cells were measured by flow cytometry. The percentage of migrated live cells **(A)**, leukocytes **(B)**, B cells **(C)**, NK cells **(D)**, CD56dim CD16hi NK cells **(E)**, CD56hi CD16dim NK cells **(F)**, T cells **(G)**, $CD4^+$ T cells **(H)**, $CD8^+$ T cells **(I)**, CCR6+ $CD4^+$ T cells **(J)**, myeloid cells **(K)**, classical Monocytes **(L)**, intermediate Monocytes **(M)**, mDCs **(N)**, activated mDCs **(O)**, myeloid CD33low cells **(P)**, and $CD195^+$ myeloid CD33low cells **(Q)** was calculated by the ratio of migrated/non-migrated cells. Data are from three independent experiments, with 2 donors each. Each data point corresponds to a single donor (n = 6). Data are shown as mean ± SEM. $*p < 0.05$, $**p < 0.01$, $***p < 0.001$, $****p < 0.0001$; *p*-values were calculated using one-way ANOVA with Tukey correction, paired *t*-test and Wilcoxon signed-rank test for non-parametric data.

controls respectively, and flow cytometry was employed to measure the migration rate of major immune cell populations. AEA dramatically reduced the migration rate of the cells studied including leukocytes (Figures 4A, B), B cells (Figure 4C), NK cells (Figure 4D) and cytotoxic NK cells (Figure 4E), while NK cell precursors treated with AEA demonstrated a tendency to reduced migration rate (Figure 4F). Importantly, pretreatment with AEA reduced migration of T cells (Figure 4G), where particularly the migration of $CD8^+$ T cells (Figure 4I) treated with AEA was significantly reduced, while $CD4^+$ T cells (Figure 4H) and CCR6+ $CD4^+$ T cells (Figure 4J) did not respond to AEA treatment. Similarly, classical monocytes (Figure 4K), activated mDCs (Figure 4L), mDCs (Figure 4N), and myeloid CD33low cells (Figure 4O) treated with AEA showed a tendency towards lower migration rates. There was no difference in migrated cell number in myeloid cells (Figure 4M), CD195+ myeloid CD33low cells (Figure 4P), and intermediate monocytes (Figure 4Q) between groups. Collectively, these data indicate that AEA has a direct impact on immune cells and impairs their migration ability. Moreover, the data suggest that the increase in T cells in the animal model is not a consequence of an increased recruitment by AEA. Rather, AEA might block emigration of cells towards the lymphatics.

AEA substantially affects proliferation, activation, and exhaustion status of $CD4^+$ T cells

Following the findings that AEA altered T cell migration in mouse and human systems, the question whether or not AEA may affect the T cell phenotype at sites of inflammation was studied. Bead-isolated human T cells were treated with AEA or control and were afterward activated with CD3/CD28/CD2 activator cocktail for 5 days. Using flow cytometry, the expression levels of chemokine receptors (CCR6, CCR2, CXCR3, CXCR4), activation markers (CD25, CD38, CD69), and exhaustion markers (TIGIT, LAG3, PD1) were measured (Supplementary Figures S3, S4). Similar to the macrophage experiments, AEA was tested at concentrations 10 nM and 10 μM. Anandamide at lower concentrations did not have any impact on T cell activation, proliferation, and maturation status. However, a marked reduction in T cell cluster formation was observed (Figure 5A) when the cells were treated with 10 μM AEA. In contrast, the percentage of live T cells increased in the presence of AEA (Figure 5B). Both parameters indicate reduced T cell activation. There was no difference in clusters and live cell numbers between groups in non-activated T cells. Addition of AEA decreased percentage of $CD4^+$ T cell among non and activated cells

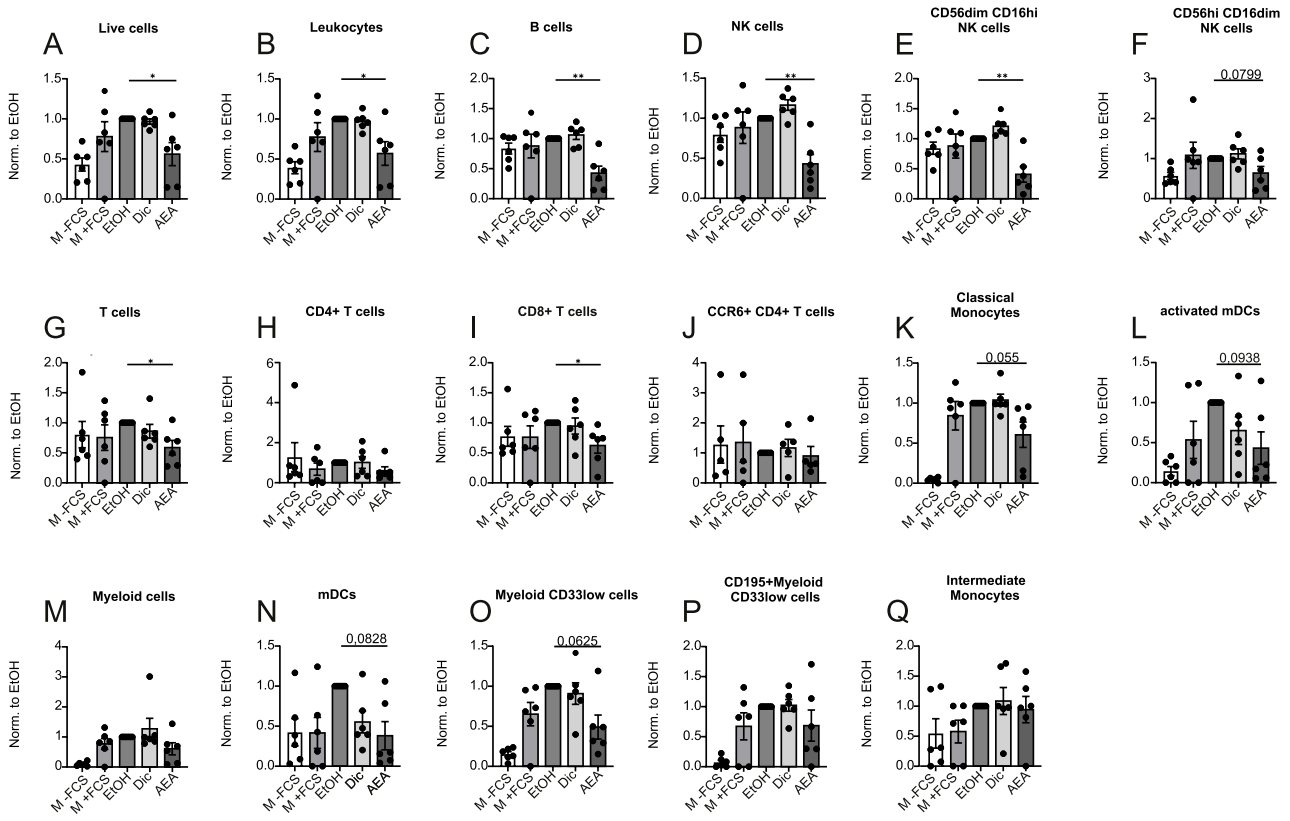

FIGURE 4
AEA treatment reduces immune cell migration. Human PBMCs were pre-treated with ethanol (EtOH), Diclofenac and EtOH (Dic), and AEA (10 μM) with Diclofenac (AEA). Medium without (-FCS) and with FCS (+FCS) were used as negative and positive controls. The numbers of migrated cells were measured by flow cytometry and represent three independent experiments. The numbers of live cells **(A)**, leukocytes **(B)**, B cells **(C)**, NK cells **(D)**, CD56dimCD16hi NK cells **(E)**, CD56hiCD16dim NK cells **(F)**, T cells **(G)**, $CD4^+$ T cells **(H)**, $CD8^+$ T cells **(I)**, CCR6+ $CD4^+$ T cells **(J)**, classical monocytes **(K)**, activated mDCs **(L)**, myeloid cells **(M)**, mDCs **(N)**, myeloid CD33low cells **(O)**, CD195+myeloid CD33low cells **(P)**, and intermediate monocytes **(Q)** was calculated by the ratio of migrated/non-migrated cells and normalized to EtOH. Data are from three independent experiments, with 2 donors each. Each data point corresponds to a single donor (n = 6). Data are shown as mean ± SEM. *$p < 0.05$, **$p < 0.01$, ***$p < 0.001$, ****$p < 0.0001$; p-values were calculated using one-sample t-test.

(Figure 5C). Surprisingly, a significant reduction in non-activated Th17 cells treated was observed in the AEA treated group (Figure 5D). Additionally, AEA decreased the percentage of activated TIGIT+$CD4^+$ T cells (Figure 5E). AEA also reduced the expression of CD38 and CD25, both in activated and non-activated $CD4^+$ T cells (Figures 5F, G). No alterations were identified in CCR2+ $CD4^+$ T cells, LAG3+ $CD4^+$ T cells, Th1 cells, and Th2 cells (Supplementary Figure S5). These data demonstrated that AEA decreases the activation and exhaustion status of $CD4^+$ T cells and reduces the number of Th17 cells.

AEA alters the proliferation, activation and exhaustion status of $CD8^+$ T cells

The impact of AEA on $CD8^+$ T cells was measured alongside $CD4^+$ T cells. By contrast, AEA was found not to alter the percentage of $CD8^+$ T cells (Figure 6A). When looking closer at $CD8^+$ T cell activation and exhaustion status, PD1+ $CD8^+$ T cells (Figure 6B), TIGIT+ $CD8^+$ T cells (Figure 6C), $CD38^+$ $CD8^+$ T cells (Figures 6F, H), and $CD69^+$ $CD8^+$ T cells (Figures 6G, H) populations were significantly decreased following AEA and activator addition. Similarly, to $CD4^+$ T cells, a reduced Tc17 cells percentage in the AEA group in non-activated cells was observed (Figure 6D). Moreover, AEA presence decreased the Tc1 percentage in the non-activated group (Figure 6E). There was no observable effect on CCR2+ $CD8^+$ T cells, LAG3+ $CD8^+$ T cells, and Tc2 cells (Supplementary Figure S5). Taken together, these data demonstrated that AEA reduces the number of activated and exhausted $CD8^+$ T cells and limits $CD8^+$ T cell subsets such as Tc1 and Tc17 cells.

Anandamide reduces the expression of IL-10, IL-17a, and IL-13 in activated human T cells

Based on Anandamide altering T cell activation surface markers, we further investigated if it would affect T cell cytokine production. To test this, we collected supernatants after T cells were treated with AEA and activated for 6 days. Despite reduced activation observed by flow cytometry, there was no significant difference in interferon-γ (IFN-γ) secretion (Figure 7A). However, we found a dramatic reduction in IL-10, IL-13, and IL-17A cytokine production

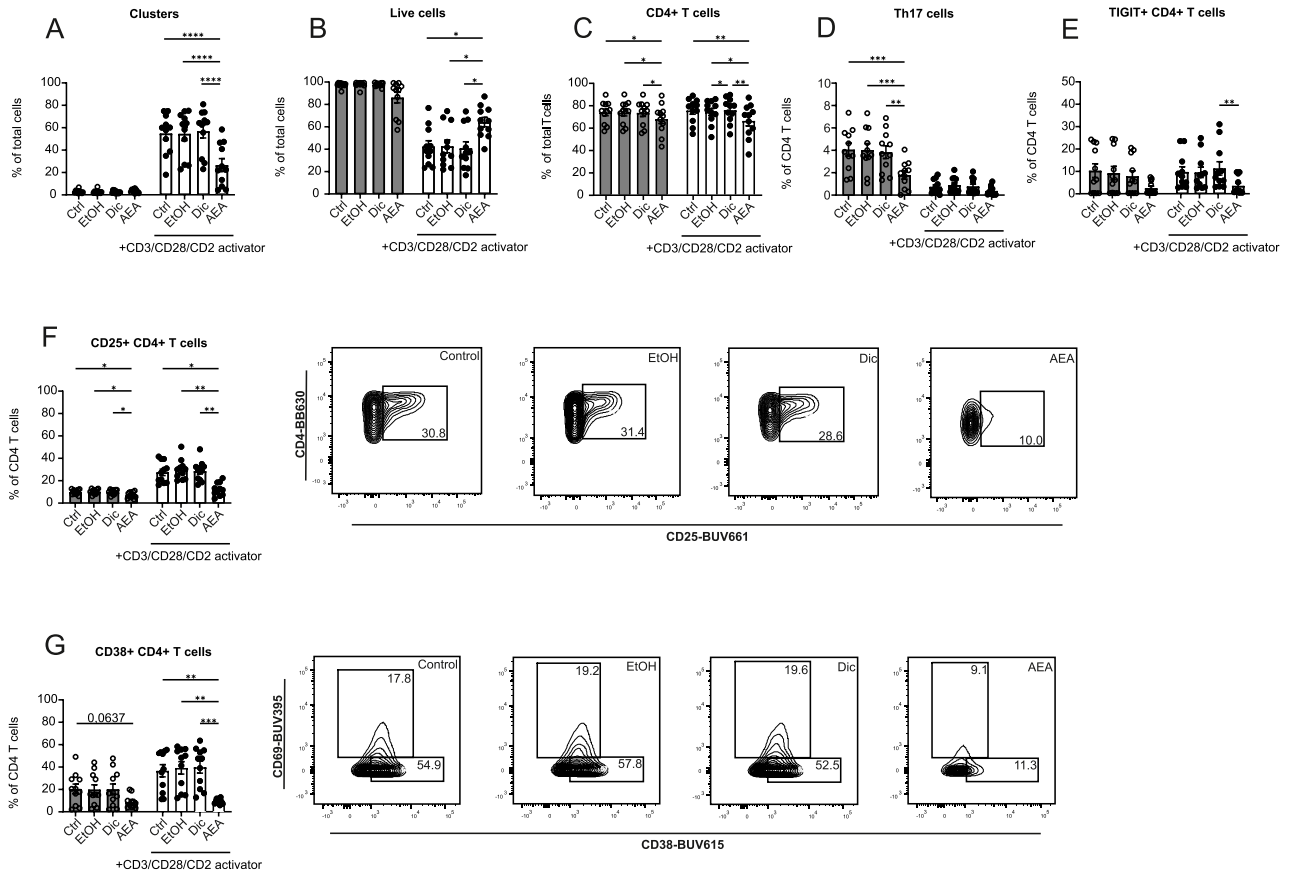

FIGURE 5
AEA dramatically alters the proliferation, activation and exhaustion profiles of CD4⁺ T cells. Human isolated T cells were pre-treated with ethanol (EtOH), Diclofenac and EtOH (Dic), and AEA (10 μM) with Diclofenac (AEA), and were activated or remained inactivated for up to 6 days. Cells were measured by flow cytometry. Percentage of cell clusters **(A)**, live cells **(B)**, CD4⁺ T cells **(C)**, Th17 cells **(D)**, TIGIT+CD4⁺ T cells **(E)**, CD25⁺ CD4⁺ T cells **(F)**, and CD38⁺CD4⁺ T cells **(G)** are shown. Data are from three independent experiments, with at least 3 donors each. Each data point corresponds to a single donor (n = 11). Data are shown as mean ± SEM. *$p < 0.05$, **$p < 0.01$, ***$p < 0.001$, ****$p < 0.0001$; p-values were calculated using two-way ANOVA with Tukey correction.

following AEA and activator addition (Figures 7B–D). These data confirmed that AEA has an impact on T cell activation. Particularly, AEA decreases the production of Th2 and Th17 cytokines, but does not alter the Th1 cytokine IFN-γ. Previous studies showed that AEA at already low concentrations engages CB2 receptors in immune cells altering cell activation and differentiation (Cencioni et al., 2010). Therefore, we measured IL-10, IL-17A, IL-13, and IFN-γ cytokine production in activated T cells treated with AEA at concentrations of 10 nM, 100 nM, and 1 μM (data not shown), which would be sufficient for CB receptor engagement. However, we did not observe any effect in cytokine production when T cell were treated with lower concentrations of AEA. These data suggest a shift in T cell activation profiles rather than a global suppression of T cell activation by AEA. While AEA exhibits its central effects primarily through Gi-coupled cannabinoid receptors CB1 and CB2 receptors which are activated already at nanomolar concentrations (Munro et al., 1993), the lack of an anti-inflammatory effect at such a low concentration suggests alternative receptors with lower sensitivity like intracellular receptors. These require efficient cellular uptake and thus particularly high extracellular concentrations (Teichmann et al., 2024).

Anandamide increases T-cell through NR4A1

Based on our previous study suggesting that NR4A1 and NR4A2 may contribute to the signaling of AEA, and the importance of the NR4A family in T cell biology (Odagiu et al., 2020), the effect of genetic deletion of each receptor or both in combination was determined in the AirPouch model. Deletion of any of the two receptors blocked the effect of AEA. NR4A1 and NR4A2 deficient, as well as double knockout mice, did not exhibit a significant decrease in neutrophil or eosinophil accumulation. Although not statistically significant, it appeared that knockout of each receptor partially attenuated the response of AEA with the double knockout mouse exhibiting the strongest, indicating additive reduction (Figure 8).

Double knockout of NR4A1 and NR4A2 also prevented the AEA-induced increase in T cell and dendritic cells. A similar effect was observed in NR4A1 KO mice. In NR4A2 KO mice, AEA still induced an increase in T cells and dendritic cells, which for T cells did, however, not reach the significance level with the group size present (Figure 8). Collectively, these data suggest that AEA elicits

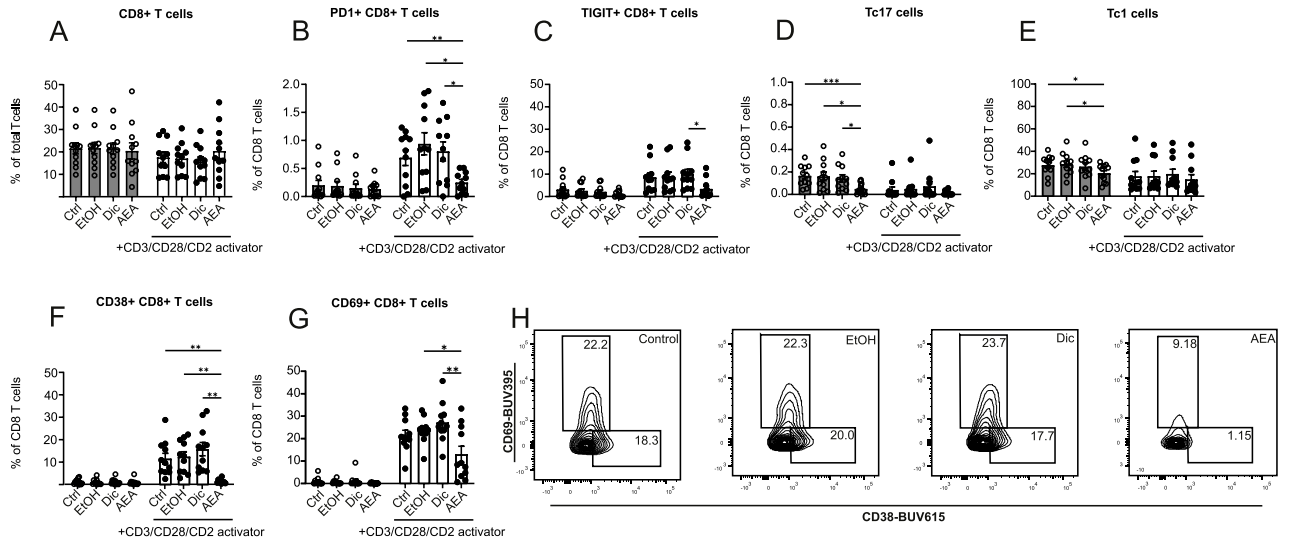

FIGURE 6
AEA has an impact on the proliferation, activation and exhaustion profiles of CD8 T cells. Human isolated T cells were pre-treated with ethanol (EtOH), Diclofenac and EtOH (Dic), and AEA (10 μM) with Diclofenac (AEA), and were activated or remained inactivated for up to 6 days. Cells were measured by flow cytometry. Percentage of $CD8^+$ T cells **(A)**, PD1+ $CD8^+$ T cells **(B)**, TIGIT+ $CD8^+$ T cells **(C)**, Tc17 cells **(D)**, Tc1 cells **(E)**, $CD38^+$ $CD8^+$ T cells **(F)**, and $CD69^+CD8^+$ T cells **(G)** are shown. **(H)** Representative FACS plot of $CD69^+CD8^+$ T and $CD38^+CD8^+$ T cells. Data are from three independent experiments, with at least 3 donors each. Each data point corresponds to a single donor (n = 11). Data are shown as mean ± SEM. $*p < 0.05$, $**p < 0.01$, $***p < 0.001$, $****p < 0.0001$; p-values were calculated using two-way ANOVA with Tukey correction.

an inhibitor effect on granulocyte accumulation in the AirPouch model by NR4A1 and NRA2, whereas it increases T cell and dendritic cell accumulation through NR4A.

Discussion

Anandamide was the first endocannabinoid described to activate CB1 and CB2 receptors. AEA is pivotal in regulating inflammation as indicated by recent studies showing that AEA administration lessens inflammation and improves survival scores in various inflammatory murine models (Berg et al., 2023; Sultan et al., 2021). Nevertheless, its impact on immune cell migration and activation in murine and human systems remain controversial. We found in this study that AEA application in the Zymosan AirPouch mouse model decreases the infiltration of neutrophils, eosinophils, and monocytes to the site of inflammation, and elevates the number of T cells in the Zymosan-enriched area. To explore this issue, we employed a human *in vitro* system to gain a better understanding of the immune cell migration process.

It was shown that cannabinoids can have anti-inflammatory effects on primary human macrophages (Gojani et al., 2023) and activated microglial cells (Rodrigues et al., 2024). Moreover, Leuti *et al.* showed that AEA promotes pro-resolving mechanisms in human macrophages by binding to CB2 and GPR18 receptors (Leuti et al., 2024). In our study AEA impaired chemokine production in Zymosan-activated macrophages, particularly of CCL2, CCL4, CCL17, and CCL20. Together, these chemokines are responsible for myeloid and lymphocyte cell infiltration into the sites of inflammation, suggesting that AEA can reduce severity in the acute phase of inflammatory diseases. In particular, CCL2 plays a crucial role in the attraction of various immune cell subsets (monocytes, memory T cells, and DCs) to the inflamed region by engaging the CCR2 receptor (Gschwandtner et al., 2019). CCL4 is known to be a pro-inflammatory chemokine and one of the main chemoattractants for $CD8^+$ T cells (Castellino et al., 2006). Similarly, Th2 cells accumulate in response to CCL17 via the CCR4 receptor, contributing to allergic pathological conditions (McIlroy et al., 2006). The reduced level of CCL20 upon AEA treatment is of particular interest, given that CCL20 is the major chemokine for Th17 migration to the inflammatory milieu by engaging its receptor CCR6 on the Th17 cell surface, and the CCR6-CCL20 axis is involved in the pathogenesis of various chronic inflammatory and autoimmune diseases (Meitei et al., 2021). It was previously shown that AEA is responsible for keratinocyte-dependent inhibition of Th1 and Th17 polarization (Chiurchiù et al., 2016). An inhibitory role of AEA on chemokine production was described previously. AEA reduced the production of CXCL8 in monocyte-derived Langerhans cells induced by TLR7/8 (Pénzes et al., 2024), and CCL2 levels in vascular smooth muscle cells (Pflüger-Müller et al., 2020) and keratinocytes (McCormick et al., 2023). The current study adds to these data by showing that AEA alters the expression of CCL2, CCL4, CCL17, and CCL20 in human macrophages that are activated via TLR2 and TLR6 signaling pathways.

AEA alone or in combination with Zymosan was found to inhibit the migration of B cells and NK cell subsets. Based on the observations that B cells and NK cells exposed to AEA exhibit reduced migration, we can conclude that AEA directly influences these lymphocyte populations by impairing their motility. Previous studies have shown that lower concentrations of AEA decrease NK cell cytotoxic activity *in vitro* (Lissoni et al., 2008), but did not affect NK cell line motility (Kishimoto et al., 2005). Research on the effect of cannabinoids and ECS on B cells is limited. A recent study showed that cannabinoids have a dramatic effect on the cytokine profile of

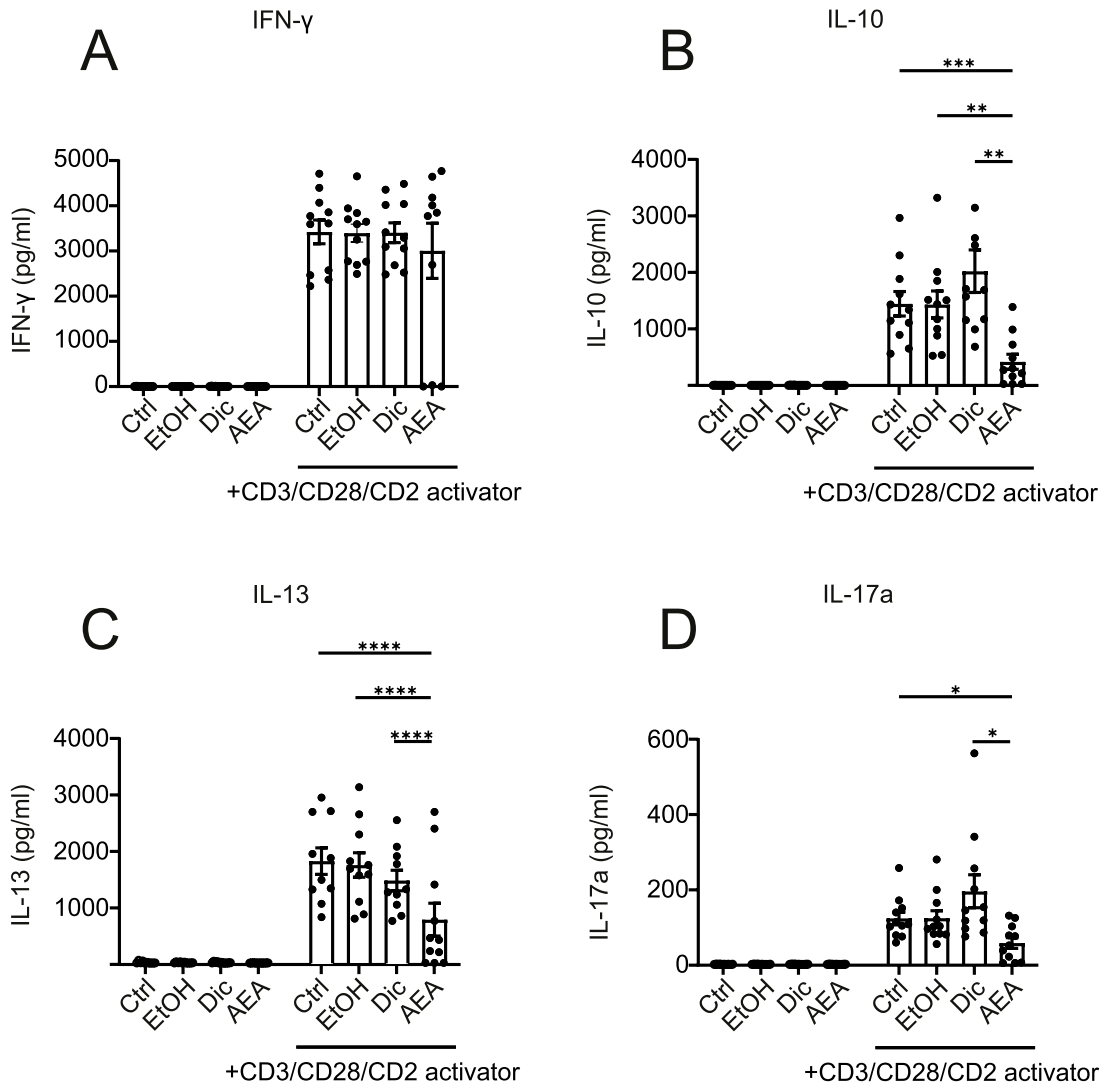

FIGURE 7
AEA reduces the levels of IL-10, IL-13, and IL-17A in activated human T cells. Human isolated T cells were pre-treated with ethanol (EtOH), Diclofenac and EtOH (Dic), and AEA (10 μM) with Diclofenac (AEA), and were activated or remained inactivated for up to 6 days. Supernatant was harvested and cytokines were measured using Cytometric Bead Array by flow cytometry. The concentrations of IFN-γ **(A)** IL-10 **(B)**, IL-13 **(C)**, and IL-17A **(D)** are shown. Data are from three independent experiments, with at least 3 donors each. Each data point corresponds to a single donor (n = 11). Data are shown as mean ± SEM. *$p < 0.05$, **$p < 0.01$, ***$p < 0.001$, ****$p < 0.0001$; p-values were calculated using two-way ANOVA with Tukey correction.

B cells, and reduce the number of IgM+/IgG+ cells (Lampron et al., 2023). Also, Tetrahydrocannabinol (THC) and AEA were shown to decrease antibody formation in plaque-forming cell assays (Eisenstein et al., 2007). Intriguingly, the endocannabinoid 2-AG induced B cell migration among murine splenocytes *in vitro* (Alberich Jordà et al., 2002). The present data add to these findings, by showing that AEA directly influences NK and B cell migration, which can be important to further investigate the impact of AEA in the fields of autoimmune disease and cancer.

Previous studies have investigated an impact of AEA on T cell activation and cytokine production *in vitro* both in human and murine settings (Cencioni et al., 2010; Ribeiro et al., 2010; Sultan et al., 2021). Similar to prior findings (Cencioni et al., 2010), we confirm that AEA decreased the production of IL-17A in activated human T cells. Nevertheless, we did not observe reduced levels of IFN-γ upon AEA treatment. By contrast, we determined that AEA does not have any impact on IFN-γ production, while it dramatically decreased IL-10 and IL-13 in T cell-derived supernatants. This indicates that AEA possibly alters Th2, Th17, and Treg differentiation, while Th1 differentiation remains unchanged. Differences to previous studies can be explained due to the different functional read-outs. The present study focused on T cell differentiation (culture of activated T cells for 6 days) rather than acute cytokine production in activated T cells triggered by protein kinase C activation as determined before (Cencioni et al., 2010). Previously, it was shown that AEA is oxidized by COX-2 (Yu et al., 1997). Here, the COX-2-dependent breakdown of AEA was blocked, enabling longer culture protocols.

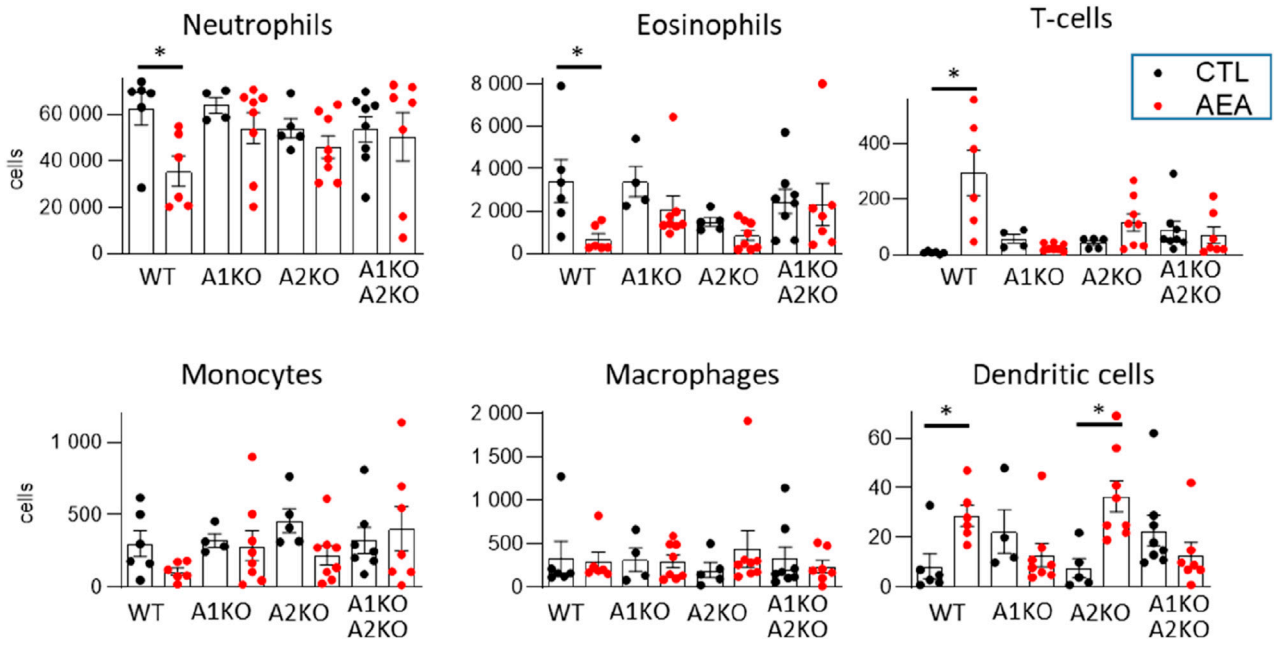

FIGURE 8
AEA increases T-cell number through NR4A receptors in the AirPouch Zymosan model. Analysis of cellular infiltrate in murine AirPouch exudates after control (CTL) or AEA nanoformulation (AEA) pre-treatment (1 h) followed by zymosan stimulation (6 h) in mice inheriting a knockout for NR4A1$^{-/-}$ (A1KO), NR4A2$^{-/-}$ (A2KO) or double knockout for NR4A1/2$^{-/-}$, compared to control mice (also shown in Figure 1). Mice without knockout on the floxed/cre background served as control (WT). Each data point represents an animal showing the total number of cells recovered by FACS analysis. 1-way ANOVA and Mann-Whitney test. n = 4–8. *$p < 0.05$.

Surprisingly, given the selected changes in cytokine production, T cell activation as determined by cell cluster formation and increased numbers of live activated T cells death (Green et al., 2003) was broadly reduced upon AEA administration. Additionally, the expression of activation receptors on the T cell surface was dramatically decreased in the presence of AEA. Decreased CD25, but not CD69 expression on CD4$^+$ T cells treated with AEA was described before (Sultan et al., 2021). The findings described in here add that AEA also decreased CD38 expression on CD4$^+$ T cells, as well as CD38 and CD69 expression on CD8$^+$ T cells.

Recently, there has been a growing interest in the role of endocannabinoids and cannabinoids in tumor progression and their impact on the efficacy of immunotherapeutic drugs (Sarsembayeva and Schicho, 2023). AEA was previously shown to reduce the effect of PD-1 antibodies in tumor mouse models (Xiong et al., 2022). This work shows that AEA decreases the expression of PD-1 on the surface of activated CD8$^+$ T cells, and TIGIT on the surface of activated CD4$^+$ T and CD8$^+$ T cells. TIGIT is known to inhibit anti-tumor immunity (Tang et al., 2023). Thus, these data may shed light on the involvement of endocannabinoids and possible therapeutic approaches for cancer treatment.

Beside cancer, the data present here provide insights into a potential role of AEA in acute and chronic inflammatory settings. Given the contrast between murine data and results derived from migration assays and T cell activation, the increased number of T cells in the AirPouch model can be explained by their reduced activation status and motility, which causes the T cells to be retained at the site of inflammation, instead of remigrating towards lymphatics. This is consistent with data on DCs in the AirPouch model since these cells follow comparable chemokine gradients towards the lymphatics compared to T cells (Johnson and Jackson, 2014). Granulocytes and myeloid cells are recruited to an inflamed region before lymphocyte recruitment, since these cells are responsible for the first line defense. Thus, AEA would act on recruitment of these myeloid cells from the circulation at the early time point employed in the AirPouch model in this study, but not on lymphocyte recruitment, rather acting on tissue-resident lymphocytes (Ziessman et al., 2006). T cells accumulating locally upon AEA treatment likely experience altered activation and, subsequently exhaustion due to AEA. Previously, it was shown that proliferation of T cells toward Th17 cells is inhibited by AEA (Cencioni et al., 2010). By contrast, polarization toward the Th1 phenotype was facilitated indirectly via AEA (Pénzes et al., 2024). These findings of a preserved Th1, but blocked Th17 differentiation are supported by the data presented herein. Thus, T cells accumulating locally under the influence of AEA appear to remain competent in fighting infection, while chronic inflammatory responses are prevented. These features position AEA as a player promoting resolution of infection and inflammation, by ensuring the removal of the inflammatory trigger but blocking chronification of inflammation. This is supported by the findings that AEA blocked the expression of CCL20, a major Th17 chemokine. Overall, AEA emerges as a negative regulator of chronic inflammatory T cell activation and recruitment.

The following experiments with NR4A1 and NR4A2 KO mice in the AirPouch model demonstrated that AEA engaging NR4A1 and NR4A2 receptors is responsible for decreased

eosinophils and via NR4A1 increased T-cell and DC accumulation. Previous data showed that NR4A1 upregulation caused T cell dysfunction (Liu et al., 2019). Whether this is connected to the action of AEA remains to be determined in future studies. Taken together, the data presented here demonstrate that AEA has a strong inhibitory effect on T cell activation, while increasing the number of T cells at the site of inflammation via the NR4A1 receptor. A deeper understanding of the mechanisms underlying the interaction between AEA and nuclear receptors in T cells may shed light on therapeutic uses for AEA in chronic inflammatory disease settings.

Data availability statement

The original contributions presented in the study are included in the article/Supplementary Material, further inquiries can be directed to the corresponding authors.

Ethics statement

The requirement of ethical approval was waived by Ethics Committee of Goethe University Frankfurt for the studies on humans because Buffy Coats from anonymous blood donors were used. The studies were conducted in accordance with the local legislation and institutional requirements. Written informed consent for participation was not required from the participants or the participants' legal guardians/next of kin in accordance with the national legislation and institutional requirements. The human samples used in this study were acquired from a by-product of routine care or industry. The animal study was approved by the Regierungspräsidium Darmstadt, approval number FU1268. The study was conducted in accordance with the local legislation and institutional requirements.

Author contributions

AK: Conceptualization, Formal Analysis, Investigation, Methodology, Visualization, Writing–original draft, Writing–review and editing. TT: Formal Analysis, Investigation, Methodology, Visualization, Writing–original draft, Writing–review and editing. VM: Investigation, Writing–original draft, Writing–review and editing. WX: Investigation, Writing–original draft, Writing–review and editing. FS: Investigation, Writing–original draft, Writing–review and editing. MW: Resources, Writing–original draft, Writing–review and editing. WM: Resources, Writing–original draft, Writing–review and editing. AW: Conceptualization, Formal Analysis, Funding acquisition, Supervision, Visualization, Writing–original draft, Writing–review and editing. RB: Conceptualization, Funding acquisition, Supervision, Visualization, Writing–original draft, Writing–review and editing.

Funding

The author(s) declare that financial support was received for the research, authorship, and/or publication of this article. This study was supported by the US National Institutes of Health (NIH) grant R01AG070719 from the National Institute on Aging (DJK); the Leistungszentrum Innovative Therapeutics (TheraNova) funded by the Fraunhofer Society and the Hessian Ministry of Science and Arts and Deutsche Forschungsgemeinschaft (DFG) projects: GRK2336 (AVE), Projektnummer 321115009; SFB1039 Projektnummer 204083920; SFB1531, Projektnummer 456687919; Cardio-Pulmonary Institute (CPI) (EXC2026, Projektnummer 390649896); the Goethe-University Frankfurt and the DZHK (Deutsches Zentrum für Herz-Kreislauf-Erkrankungen) and the Dr. Rolf Schwiete-Stiftung. This study was also supported by the Agencia Nacional de Promoción Científica y Tecnológica with PICT 2020 Serie A 4000 and was also funded by a stipend of the German Academic Exchange Service (DAAD).

Acknowledgments

The authors are grateful for the excellent technical assistance of Margarete Mijatovic.

Conflict of interest

The authors declare that the research was conducted in the absence of any commercial or financial relationships that could be construed as a potential conflict of interest.

Generative AI statement

The author(s) declare that no Generative AI was used in the creation of this manuscript.

Publisher's note

Supplementary material

The Supplementary Material for this article can be found online at: https://www.frontiersin.org/articles/10.3389/fphar.2024.1528759/full#supplementary-material

References

Alberich Jordà, M., Verbakel, S. E., Valk, P. J. M., Vankan-Berkhoudt, Y. V., Maccarrone, M., Finazzi-Agrò, A., et al. (2002). Hematopoietic cells expressing the peripheral cannabinoid receptor migrate in response to the endocannabinoid 2-arachidonoylglycerol. *Blood* 99 (8), 2786–2793. doi:10.1182/blood.V99.8.2786

Berg, B. B., Linhares, A. F. S., Martins, D. M., Rachid, M. A., Cau, S. B. de A., Souza, G. G. d., et al. (2023). Anandamide reduces the migration of lymphocytes to the intestine by CB2 activation and reduces TNF-α in the target organs, protecting mice from graft-versus-host disease. *Eur. J. Pharmacol.* 956, 175932. doi:10.1016/j.ejphar.2023.175932

Bonta, P. I., van Tiel, C. M., Vos, M., Pols, T. W. H., van Thienen, J. V., Ferreira, V., et al. (2006). Nuclear receptors Nur77, Nurr1, and NOR-1 expressed in atherosclerotic lesion macrophages reduce lipid loading and inflammatory responses. *Arterioscler. Thrombosis, Vasc. Biol.* 26 (10), 2288–2294. doi:10.1161/01.ATV.0000238346.84458.5d

Castellino, F., Huang, A. Y., Altan-Bonnet, G., Stoll, S., Scheinecker, C., and Germain, R. N. (2006). Chemokines enhance immunity by guiding naive CD8+ T cells to sites of CD4+ T cell–dendritic cell interaction. *Nature* 440 (7086), 890–895. doi:10.1038/nature04651

Cencioni, M. T., Chiurchiù, V., Catanzaro, G., Borsellino, G., Bernardi, G., Battistini, L., et al. (2010). Anandamide suppresses proliferation and cytokine release from primary human T-lymphocytes mainly via CB2 receptors. *PLOS ONE* 5 (1), e8688. doi:10.1371/journal.pone.0008688

Chiurchiù, V., Rapino, C., Talamonti, E., Leuti, A., Lanuti, M., Gueniche, A., et al. (2016). Anandamide suppresses proinflammatory T cell responses *in vitro* through type-1 cannabinoid receptor–mediated mTOR inhibition in human keratinocytes. *J. Immunol.* 197 (9), 3545–3553. doi:10.4049/jimmunol.1500546

Duerr, G. D., Heinemann, J. C., Suchan, G., Kolobara, E., Wenzel, D., Geisen, C., et al. (2014). The endocannabinoid-CB2 receptor axis protects the ischemic heart at the early stage of cardiomyopathy. *Basic Res. Cardiol.* 109 (4), 425. doi:10.1007/s00395-014-0425-x

Eisenstein, T. K., Meissler, J. J., Wilson, Q., Gaughan, J. P., and Adler, M. W. (2007). Anandamide and Delta9-tetrahydrocannabinol directly inhibit cells of the immune system via CB2 receptors. *J. Neuroimmunol.* 189 (1), 17–22. doi:10.1016/j.jneuroim.2007.06.001

Eljaschewitsch, E., Witting, A., Mawrin, C., Lee, T., Schmidt, P. M., Wolf, S., et al. (2006). The endocannabinoid anandamide protects neurons during CNS inflammation by induction of MKP-1 in microglial cells. *Neuron* 49 (1), 67–79. doi:10.1016/j.neuron.2005.11.027

Frigo, D. E., Bondesson, M., and Williams, C. (2021). Nuclear receptors: from molecular mechanisms to therapeutics. *Essays Biochem.* 65 (6), 847–856. doi:10.1042/EBC20210020

Gojani, E. G., Wang, B., Li, D.-P., Kovalchuk, O., and Kovalchuk, I. (2023). Anti-inflammatory effects of minor cannabinoids CBC, THCV, and CBN in human macrophages. *Molecules* 28 (18), 6487. doi:10.3390/molecules28186487

Green, D. R., Droin, N., and Pinkoski, M. (2003). Activation-induced cell death in T cells. *Immunol. Rev.* 193 (1), 70–81. doi:10.1034/j.1600-065X.2003.00051.x

Gschwandtner, M., Derler, R., and Midwood, K. S. (2019). More than just attractive: how CCL2 influences myeloid cell behavior beyond chemotaxis. *Front. Immunol.* 10, 2759. doi:10.3389/fimmu.2019.02759

Hamers, A. A. J., Hanna, R. N., Nowyhed, H., Hedrick, C. C., and Vries, C. J. M. de (2013). Nr4a nuclear receptors in immunity and atherosclerosis. *Curr. Opin. Lipidol.* 24 (5), 381–385. doi:10.1097/MOL.0b013e3283643eac

Hammond, S. L., Safe, S., and Tjalkens, R. B. (2015). A novel synthetic activator of Nurr1 induces dopaminergic gene expression and protects against 6-hydroxydopamine neurotoxicity *in vitro*. *Neurosci. Lett.* 607, 83–89. doi:10.1016/j.neulet.2015.09.015

Johnson, L. A., and Jackson, D. G. (2014). Control of dendritic cell trafficking in lymphatics by chemokines. *Angiogenesis* 17 (2), 335–345. doi:10.1007/s10456-013-9407-0

Kishimoto, S., Muramatsu, M., Gokoh, M., Oka, S., Waku, K., and Sugiura, T. (2005). Endogenous cannabinoid receptor ligand induces the migration of human natural killer cells. *J. Biochem.* 137 (2), 217–223. doi:10.1093/jb/mvi021

Lampron, M.-C., Paré, I., Al-Zharani, M., Semlali, A., and Loubaki, L. (2023). Cannabinoid mixture affects the fate and functions of B cells through the modulation of the caspase and MAP kinase pathways. *Cells* 12 (4), 588. doi:10.3390/cells12040588

Leuti, A., Fava, M., Forte, G., Pellegrini, N., Oddi, S., Scipioni, L., et al. (2024). The endocannabinoid anandamide activates pro-resolving pathways in human primary macrophages by engaging both CB_2 and GPR18 receptors. *FASEB J.* 38 (10), e23675. doi:10.1096/fj.202301325R

Liao, Y., Bin, J., Luo, T., Zhao, H., Ledent, C., Asakura, M., et al. (2013). Cb1 cannabinoid receptor deficiency promotes cardiac remodeling induced by pressure overload in mice. *Int. J. Cardiol.* 167 (5), 1936–1944. doi:10.1016/j.ijcard.2012.05.033

Ligresti, A., Petrocellis, L. de, and Di Marzo, V. (2016). From phytocannabinoids to cannabinoid receptors and endocannabinoids: pleiotropic physiological and pathological roles through complex pharmacology. *Physiol. Rev.* 96 (4), 1593–1659. doi:10.1152/physrev.00002.2016

Lissoni, P., Tintori, A., Fumagalli, L., Brivio, F., Messina, G., Parolini, D., et al. (2008). The endocannabinoid anandamide neither impairs *in vitro* T-cell function nor induces regulatory T-cell generation. *ANTICANCER Res.* 28, 3743–3748.

Liu, X., Wang, Y., Lu, H., Li, J., Yan, X., Xiao, M., et al. (2019). Genome-wide analysis identifies NR4A1 as a key mediator of T cell dysfunction. *Nature* 567 (7749), 525–529. doi:10.1038/s41586-019-0979-8

Lu, H.-C., and Mackie, K. (2016). An introduction to the endogenous cannabinoid system. *Biol. Psychiatry* 79 (7), 516–525. doi:10.1016/j.biopsych.2015.07.028

Lu, H.-C., and Mackie, K. (2021). Review of the endocannabinoid system. *Biol. Psychiatry. Cognitive Neurosci. Neuroimaging* 6 (6), 607–615. doi:10.1016/j.bpsc.2020.07.016

Maccarrone, M. (2017). Metabolism of the endocannabinoid anandamide: open questions after 25 years. *Front. Mol. Neurosci.* 10, 166. doi:10.3389/fnmol.2017.00166

Martínez-González, J., Cañes, L., Alonso, J., Ballester-Servera, C., Rodríguez-Sinovas, A., Corrales, I., et al. (2021). NR4A3: a key nuclear receptor in vascular biology, cardiovascular remodeling, and beyond. *Int. J. Mol. Sci.* 22 (21), 11371. doi:10.3390/ijms222111371

Martín Giménez, V. M., Chuffa, L. G. A., Simão, V. A., Reiter, R. J., and Manucha, W. (2022). Protective actions of vitamin D, anandamide and melatonin during vascular inflammation: epigenetic mechanisms involved. *Life Sci.* 288, 120191. doi:10.1016/j.lfs.2021.120191

Martín Giménez, V. M., Moretton, M. A., Chiappetta, D. A., Salgueiro, M. J., Fornés, M. W., and Manucha, W. (2023). Polymeric nanomicelles loaded with anandamide and their renal effects as a therapeutic alternative for hypertension treatment by passive targeting. *Pharmaceutics* 15 (1), 176. doi:10.3390/pharmaceutics15010176

McCormick, E. T., Draganski, A., Chalmers, S., Zahn, J., Garcia, S., Nussbaum, D., et al. (2023). Nano-encapsulated anandamide reduces inflammatory cytokines *in vitro* and lesion severity in a murine model of cutaneous lupus erythematosus. *Exp. Dermatol.* 32 (12), 2072–2083. doi:10.1111/exd.14935

McIlroy, A., Caron, G., Blanchard, S., Frémaux, I., Duluc, D., Delneste, Y., et al. (2006). Histamine and prostaglandin E up-regulate the production of Th2-attracting chemokines (CCL17 and CCL22) and down-regulate IFN-gamma-induced CXCL10 production by immature human dendritic cells. *Immunology* 117 (4), 507–516. doi:10.1111/j.1365-2567.2006.02326.x

McMorrow, J. P., and Murphy, E. P. (2011). Inflammation: a role for NR4A orphan nuclear receptors? *Biochem. Soc. Trans.* 39 (2), 688–693. doi:10.1042/BST0390688

Meitei, H. T., Jadhav, N., and Lal, G. (2021). CCR6-CCL20 axis as a therapeutic target for autoimmune diseases. *Autoimmun. Rev.* 20 (7), 102846. doi:10.1016/j.autrev.2021.102846

Molica, F., Burger, F., Thomas, A., Staub, C., Tailleux, A., Staels, B., et al. (2013). Endogenous cannabinoid receptor CB1 activation promotes vascular smooth-muscle cell proliferation and neointima formation. *J. Lipid Res.* 54 (5), 1360–1368. doi:10.1194/jlr.M035147

Mullican, S. E., Dispirito, J. R., and Lazar, M. A. (2013). The orphan nuclear receptors at their 25-year reunion. *J. Mol. Endocrinol.* 51 (3), T115–T140. doi:10.1530/JME-13-0212

Munro, S., Thomas, K. L., and Abu-Shaar, M. (1993). Molecular characterization of a peripheral receptor for cannabinoids. *Nature* 365 (6441), 61–65. doi:10.1038/365061a0

Netherland, C. D., Pickle, T. G., Bales, A., and Thewke, D. P. (2010). Cannabinoid receptor type 2 (CB2) deficiency alters atherosclerotic lesion formation in hyperlipidemic Ldlr-null mice. *Atherosclerosis* 213 (1), 102–108. doi:10.1016/j.atherosclerosis.2010.07.060

Odagiu, L., May, J., Boulet, S., Baldwin, T. A., and Labrecque, N. (2020). Role of the orphan nuclear receptor NR4A family in T-cell biology. *Front. Endocrinol.* 11, 624122. doi:10.3389/fendo.2020.624122

O'Sullivan, S. E. (2007). Cannabinoids go nuclear: evidence for activation of peroxisome proliferator-activated receptors. *Br. J. Pharmacol.* 152 (5), 576–582. doi:10.1038/sj.bjp.0707423

Paul-Clark, M. J., George, P. M., Gatheral, T., Parzych, K., Wright, W. R., Crawford, D., et al. (2012). Pharmacology and therapeutic potential of pattern recognition receptors. *Pharmacol. and Ther.* 135 (2), 200–215. doi:10.1016/j.pharmthera.2012.05.007

Pénzes, Z., Horváth, D., Molnár, P., Fekete, T., Pázmándi, K., Bácsi, A., et al. (2024). Anandamide modulation of monocyte-derived Langerhans cells: implications for immune homeostasis and skin inflammation. *Front. Immunol.* 15, 1423776. doi:10.3389/fimmu.2024.1423776

Pertwee, R. G., Howlett, A. C., Abood, M. E., Alexander, S. P. H., Di Marzo, V., Elphick, M. R., et al. (2010). International union of basic and clinical pharmacology Lxxix Cannabinoid receptors and their ligands: beyond CB_1 and CB_2. *Pharmacol. Rev.* 62 (4), 588–631. doi:10.1124/pr.110.003004

Pflüger-Müller, B., Oo, J. A., Heering, J., Warwick, T., Proschak, E., Günther, S., et al. (2020). The endocannabinoid anandamide has an anti-inflammatory effect on CCL2 expression in vascular smooth muscle cells. *Basic Res. Cardiol.* 115 (3), 34. doi:10.1007/s00395-020-0793-3

Pierron, A., Guzylack-Piriou, L., Tardieu, D., Foucras, G., and Guerre, P. (2023). Zymosan-induced murine peritonitis is associated with an increased sphingolipid synthesis without changing the long to very long chain ceramide ratio. *Int. J. Mol. Sci.* 24 (3), 2773. doi:10.3390/ijms24032773

Rajan, S., Jang, Y., Kim, C.-H., Kim, W., Toh, H. T., Jeon, J., et al. (2020). Pge1 and PGA1 bind to Nurr1 and activate its transcriptional function. *Nat. Chem. Biol.* 16 (8), 876–886. doi:10.1038/s41589-020-0553-6

Ribeiro, A., Ferraz-de-Paula, V., Pinheiro, M. L., Sakai, M., Costa-Pinto, F. A., and Palermo-Neto, J. (2010). Anandamide prior to sensitization increases cell-mediated immunity in mice. *Int. Immunopharmacol.* 10 (4), 431–439. doi:10.1016/j.intimp.2009.12.017

Rodrigues, F. d. S., Newton, W. R., Tassinari, I. D. 'Á., da, C. X., Felipe, H., Marx, A., et al. (2024). Cannabidiol prevents LPS-induced inflammation by inhibiting the NLRP3 inflammasome and iNOS activity in BV2 microglia cells via CB2 receptors and PPARγ. *Neurochem. Int.* 177, 105769. doi:10.1016/j.neuint.2024.105769

Rodríguez-Calvo, R., Tajes, M., and Vázquez-Carrera, M. (2017). The NR4A subfamily of nuclear receptors: potential new therapeutic targets for the treatment of inflammatory diseases. *Expert Opin. Ther. Targets* 21 (3), 291–304. doi:10.1080/14728222.2017.1279146

Sarfaraz, S., Adhami, V. M., Syed, D. N., Afaq, F., and Mukhtar, H. (2008). Cannabinoids for cancer treatment: progress and promise. *Cancer Res.* 68 (2), 339–342. doi:10.1158/0008-5472.CAN-07-2785

Sarsembayeva, A., and Schicho, R. (2023). Cannabinoids and the endocannabinoid system in immunotherapy: helpful or harmful? *Front. Oncol.* 13, 1296906. doi:10.3389/fonc.2023.1296906

Sekiya, T., Kashiwagi, I., Inoue, N., Morita, R., Hori, S., Waldmann, H., et al. (2011). The nuclear orphan receptor Nr4a2 induces Foxp3 and regulates differentiation of CD4+ T cells. *Nat. Commun.* 2, 269. doi:10.1038/ncomms1272

Soliman, E., and van Dross, R. (2016). Anandamide-induced endoplasmic reticulum stress and apoptosis are mediated by oxidative stress in non-melanoma skin cancer: receptor-independent endocannabinoid signaling. *Mol. Carcinog.* 55 (11), 1807–1821. doi:10.1002/mc.22429

Sultan, M., Alghetaa, H., Mohammed, A., Abdulla, O. A., Wisniewski, P. J., Singh, N., et al. (2021). The endocannabinoid anandamide attenuates acute respiratory distress syndrome by downregulating miRNA that target inflammatory pathways. *Front. Pharmacol.* 12, 644281. doi:10.3389/fphar.2021.644281

Tang, W., Chen, J., Ji, T., and Cong, X. (2023). Tigit, a novel immune checkpoint therapy for melanoma. *Cell Death and Dis.* 14 (7), 466–469. doi:10.1038/s41419-023-05961-3

Teichmann, T., Pflüger-Müller, B., Giménez, V. M. M., Sailer, F., Dirks, H., Zehr, S., et al. (2024). The endocannabinoid anandamide mediates anti-inflammatory effects through activation of NR4A nuclear receptors. *Br J Pharmacol Adv online Publ*. doi:10.1111/bph.17366

Tomczyk, M., Tomaszewska-Zaremba, D., Bochenek, J., Herman, A., and Herman, A. P. (2021). Anandamide influences interleukin-1β synthesis and IL-1 system gene expressions in the ovine hypothalamus during endo-toxin-induced inflammation. *Animals An Open Access J. MDPI* 11 (2), 484. doi:10.3390/ani11020484

Wang, Y., Li, G., Chen, B., Shakir, G., Volz, M., van der Vorst, E. P. C., et al. (2024). Myeloid cannabinoid CB1 receptor deletion confers atheroprotection in male mice by reducing macrophage proliferation in a sex-dependent manner. *Cardiovasc. Res.* 120 (12), 1411–1426. doi:10.1093/cvr/cvae125

Xiong, X., Chen, S., Shen, J., You, H., Yang, H., Yan, C., et al. (2022). Cannabis suppresses antitumor immunity by inhibiting JAK/STAT signaling in T cells through CNR2. *Signal Transduct. Target. Ther.* 7 (1), 99–13. doi:10.1038/s41392-022-00918-y

Yu, M., Ives, D., and Ramesha, C. S. (1997). Synthesis of prostaglandin E2 ethanolamide from anandamide by cyclooxygenase-2. *J. Biol. Chem.* 272 (34), 21181–21186. doi:10.1074/jbc.272.34.21181

Zhan, Y., Du, X., Chen, H., Liu, J., Zhao, B., Huang, D., et al. (2008). Cytosporone B is an agonist for nuclear orphan receptor Nur77. *Nat. Chem. Biol.* 4 (9), 548–556. doi:10.1038/nchembio.106

Ziessman, H. A., O'Malley, J. P., and Thrall, J. H. (2006). "Chapter 12 - infection and inflammation," in *The requisites in radiology. Nuclear medicine*. Editors H. A. Ziessman, J. P. O'Malley, and J. H. Thrall Third Edition (Mosby), 384–418. doi:10.1016/B978-0-323-02946-9.50017-9

Zygmunt, P. M., Petersson, J., Andersson, D. A., Chuang, H., Sørgård, M., Di Marzo, V., et al. (1999). Vanilloid receptors on sensory nerves mediate the vasodilator action of anandamide. *Nature* 400 (6743), 452–457. doi:10.1038/22761

frontiers | Frontiers in Pharmacology

TYPE Review
PUBLISHED 23 December 2024
DOI 10.3389/fphar.2024.1520488

OPEN ACCESS

EDITED BY
Galina Sud'ina,
Lomonosov Moscow State University, Russia

REVIEWED BY
Luciana Mucci,
Italian Medicines Agency (AIFA), Italy
Nadji Hannachi,
University Ferhat Abbas of Setif, Algeria

*CORRESPONDENCE
Paola Patrignani,
ppatrignani@unich.it

†These authors have contributed equally to this work and share first authorship

RECEIVED 31 October 2024
ACCEPTED 04 December 2024
PUBLISHED 23 December 2024

CITATION
Contursi A, Tacconelli S, Di Berardino S, De Michele A and Patrignani P (2024) Platelets as crucial players in the dynamic interplay of inflammation, immunity, and cancer: unveiling new strategies for cancer prevention. *Front. Pharmacol.* 15:1520488. doi: 10.3389/fphar.2024.1520488

Platelets as crucial players in the dynamic interplay of inflammation, immunity, and cancer: unveiling new strategies for cancer prevention

Annalisa Contursi[1,2†], Stefania Tacconelli[1,2†], Sara Di Berardino[1,2], Alessandra De Michele[1,2] and Paola Patrignani[1,2*]

[1]Systems Pharmacology and Translational Therapeutics Laboratory, The Center for Advanced Studies and Technology (CAST), "G. d'Annunzio" University, Chieti, Italy, [2]Department of Neuroscience, Imaging and Clinical Science, "G. d'Annunzio" University Medical School, Chieti, Italy

Inflammation plays a critical role in the pathogenesis of various diseases by promoting the acquisition of new functional traits by different cell types. Shared risk factors between cardiovascular disease and cancer, including smoking, obesity, diabetes, high-fat diet, low physical activity, and alcohol consumption, contribute to inflammation linked to platelet activation. Platelets contribute to an inflammatory state by activating various normal cells, such as fibroblasts, immune cells, and vascular cells. This activation is achieved by releasing diverse molecules from platelets, including lipids (eicosanoids), growth and angiogenic factors, and extracellular vesicles (EVs) rich in various RNA species. Antiplatelet agents like low-dose aspirin can prevent cardiovascular disease and cancer by inhibiting platelet functions beyond the antithrombotic action. Throughout the initial phases of tumorigenesis, the activation of platelets induces the overexpression of cyclooxygenase (COX)-2 in stromal cells, leading to increased biosynthesis of prostaglandin (PG)E_2. This prostanoid can contribute to tumor development by inhibiting apoptosis, promoting cancer cell proliferation and migration, and immune evasion. Notably, platelets induce the epithelial-mesenchymal transition (EMT) in tumor cells, enhancing their metastatic potential. Two platelet eicosanoids, PGE_2 (generated as a minor product of COX-1) and 12S-hydroxyeicosatetraenoic acid (HETE) [derived from the platelet-type 12-lipoxygenase (LOX)], contribute to EMT. In addition to the pharmacological inhibition of eicosanoid biosynthesis, a potential strategy for mitigating platelet-induced metastasis might encompass the inhibition of direct interactions between platelets and cancer cells. For example, there is promise in utilizing revacept to inhibit the interaction between platelet collagen receptors (particularly GPVI) and galectin-3 in cancer cells. Identifying these novel platelet functions suggests the potential application of antiplatelet agents, such as low-dose aspirin, in mitigating cancer risk, particularly in the case of colorectal cancer. It is necessary to investigate the effectiveness of other antiplatelet drugs, such as ADP $P2Y_{12}$ receptor antagonists, in cancer prevention. Other new antiplatelet drugs, such as revacept and selective 12-LOX inhibitors, currently under clinical development, are of interest due to their low risk of bleeding. Platelets and EVs carry important clinical information

because they contain specific proteins and RNAs associated with disease conditions. Their analysis can improve the accuracy of liquid biopsies for early cancer detection, monitoring progression, and assessing drug response.

KEYWORDS

platelets, cancer, aspirin, antiplatelet agents, inflammation, revacept, 12-lipoxygenase, extracellular vesicles

Introduction

The cellular components involved in the process of inflammation

Acute inflammation is a highly regulated physiological process essential in defending the body against various external and internal threats. Any disruption in tissue homeostasis triggers the activation of innate immune cells, which form the first line of defense intended to restore the affected tissue (Delves and Roitt, 2000). The primary inflammatory cells that mediate acute inflammation are the polymorphonuclear leukocytes (PMN). The production of chemotactic molecules induces the migration from the venous system to the damaged site of monocytes/macrophages, mast cells, dendritic cells, and natural killer (NK) cells. They amplify the inflammatory response, leading to pathogen elimination and tissue repair by releasing cytokines, chemokines, matrix-remodeling proteases, and reactive oxygen and nitrogen species (Coussens and Werb, 2002; Chitu and Stanley, 2006). Like that associated with wound healing, physiological inflammation is a strictly controlled and self-limiting process (Martin and Leibovich, 2005). However, losing control over immune components can lead to chronic inflammation.

Multiple factors can contribute to an excessive burden of inflammation, encompassing lifestyle factors such as smoking and dietary habits, along with conditions like obesity, diabetes, and exposure to environmental pollutants (Libby, 2012). The development of chronic inflammation is associated with a range of diseases, including fatty liver disease, inflammatory bowel disease (IBD), Alzheimer's, Parkinson's, atherosclerosis, and cancer (Chen et al., 2017). Current studies indicate that the trigger signaling of chronic inflammation is associated with enhanced platelet activation (Gawaz et al., 2005; Dovizio et al., 2014). It is now acknowledged that platelets are mediators of intercellular communication and propagation of the cellular activation response through the release and transfer of their molecular cargo to numerous cell types implicated in inflammation (Rondina et al., 2013; Varon and Shai, 2015). Consequently, this insight opens doors to innovative approaches to curbing chronic inflammation-related diseases (Gawaz et al., 2023; Patrignani and Patrono, 2015; 2018).

In atherosclerosis, the damage of vascular endothelial cells induces a rapid adhering to the vascular wall of activated platelets; this event contributes to the development of vascular inflammation through leukocyte chemoattraction and their subsequent infiltration into the vessel wall associated with the proliferation of smooth muscle cells (Ross et al., 1985; Gawaz et al., 2005). Interactions between platelets and leukocytes occur via PSGL-1-P-selectin (Evangelista et al., 1999; Yang et al., 1999), followed by the binding between Mac-1 (CD11b/CD18, αMb2) and GPIbα (Simon et al., 2000), JAM-3 (Santoso et al., 2002), or ICAM-2 (Diacovo et al., 1994). The binding facilitates the release of inflammatory molecules from platelets, triggering monocyte inflammatory cascades (Weyrich et al., 1996).

Platelets promote plaque formation by accelerating foam cell formation upon binding to oxidized LDL (Coenen et al., 2021). Platelet-derived matrix metalloproteinases (MMPs), a family of proteolytic enzymes that mediate physiological and pathophysiological extracellular matrix turnover (Gresele et al., 2021), such as MMP-1 and -2 can cleave protease-activated receptors (PARs). Among them, PAR-1 is a G protein-coupled receptor with important roles in hemostasis and inflammation (Willis Fox and Preston, 2020). Rana et al. (2018) demonstrated a role for MMP-1 in plaque formation in mice, mediated via interaction with endothelial PAR-1. Momi et al. (2022) discovered that platelet MMP-2 plays a role in mice's early formation of arterial plaque. This occurs by activating endothelial PAR-1, which leads to endothelial activation and monocyte intravasation. They also found that in patients with coronary artery disease (CAD) and human immunodeficiency virus (HIV), MMP-2 is overexpressed on the surface of platelets compared to healthy individuals of similar age and sex. Furthermore, it was noted that platelet MMP-2 levels are positively associated with the severity of carotid artery stenosis in humans. These findings indicate that inhibiting PAR-1 activities could be a promising way to reduce atherothrombosis. New strategies may involve targeting the signaling downstream of PAR-1 activated by MMP-1 and -2 to specifically inhibit the proinflammatory activity of PAR-1 (Willis Fox and Preston, 2020).

The release of platelet-derived CD40 ligand (CD40L, CD154) fosters inflammation within the endothelium. The binding of CD40 on endothelial cells to CD40L on activated platelets boosts the release of IL-8 and monocyte chemoattractant protein-1 (MCP-1), major attractants for neutrophils and monocytes (Henn et al., 1998). The interaction also prompts smooth muscle cells and macrophages to release MMPs, facilitating the degradation and remodeling of inflamed tissues.

A persistent inflammatory microenvironment continuously provides various factors—such as cytokines, chemokines, and growth factors—that oppose cell death and repair mechanisms, causing genomic instability and predisposing tissues to cancer (Mantovani and Pierotti, 2008; Hussain and Harris, 2007). Consequently, mediators and cellular effectors of inflammation play a crucial role in the local tumor milieu. It was estimated that 20% of all cancers are linked to chronic infections and inflammation (Mantovani et al., 2008), highlighting inflammation as the seventh hallmark of cancer. The unrestrained nature of cancer-related inflammation promotes tumor growth, supports angiogenesis and metastasis, undermines adaptive immune

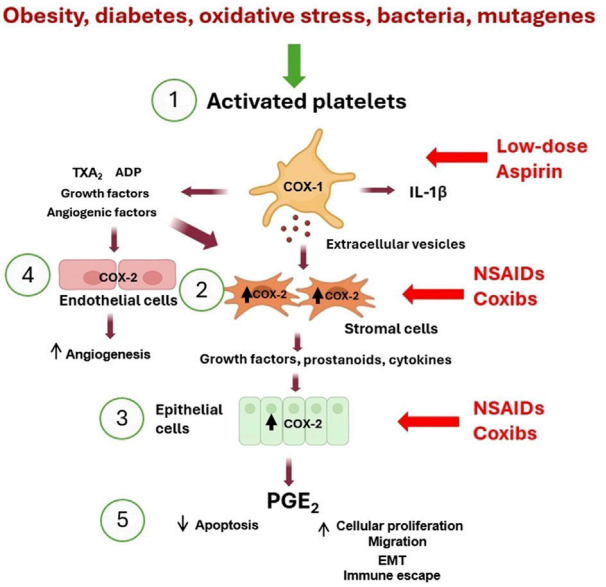

FIGURE 1
Platelet activation triggers the early phases of tumorigenesis. (1) Activated platelets release many mediators [including eicosanoids (such as TXA_2), ADP, cytokines (such as IL-1β), growth and angiogenic factors, and extracellular vesicles (EVs) containing genetic material (such as mRNAs and microRNAs)] that contribute to (2) COX-2 overexpression in stromal cells (including macrophages and fibroblasts). (3) The crosstalk with epithelial cells leads to COX-2 induction. (4) Additionally, COX-2 is overexpressed in endothelial cells, leading to angiogenesis. (5) These events lead to the release of PGE_2, which translates to inhibition of apoptosis, an increase in proliferation and migration, and induction of epithelial-mesenchymal transition (EMT). The inhibition of platelet COX-1 by low-dose aspirin prevents the downstream signaling pathways involved in the early events of tumorigenesis and indirectly inhibits COX-2 induction. In contrast, NSAIDs and coxibs have an antitumorigenic effect by directly inhibiting COX-2 activity and prostanoid generation in stromal cells, epithelial cells, and endothelial cells.

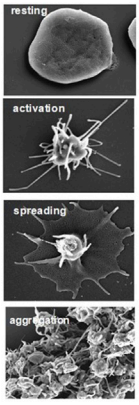

The Multiple Roles of Blood Platelets

Primary hemostasis: vascular integrity, cessation of bleeding
Tissue repair
Angiogenesis
Innate and adaptive immunity
Embryonic development
Arterial thrombosis
Inflammation
Atherosclerosis
Cancer metastasis

FIGURE 2
Different stages of platelet activation from resting to aggregation, by high resolution scanning electron microscopy. Platelets possess multifaceted functions beyond thrombosis contributing to inflammation, atherosclerosis and cancer metastasis.

responses, and modifies responses to chemotherapy (Balkwill et al., 2005; Mantovani et al., 2008). Although genetic studies in mouse models have shown that innate immune cells can get an adaptive immune response capable of eradicating nascent tumors (Negus et al., 1997), the genetic, epigenetic, and metabolic instability characteristic of neoplastic cells allows new variants to escape immune surveillance, leading to tumor establishment and progression (immunoediting process) (Dunn et al., 2002).

Notably, leukocyte infiltration observed in tumor tissues and the anticancer efficacy of antiinflammatory agents support the role of chronic inflammation in cancer development and progression (Menter et al., 2010; Wong et al., 2020; Li et al., 2020).

In the last decade, experimental evidence has supported platelets' pivotal role in developing chronic inflammation beyond their roles in hemostasis and thrombosis (Davì and Patrono, 2007; Smyth et al., 2009; Patrignani and Patrono, 2015; 2018). Platelets transduce inflammation-related signals, contributing to the variable microenvironment facilitating cell plasticity and heterogeneity. Platelets interact directly with target cells and release numerous mediators, including eicosanoids [thromboxane $(TX)A_2$ and prostaglandin $(PG)E_2$], angiogenic and growth factors from α-granules, ADP from dense granules, and extracellular vesicles (EVs) containing genetic material such as mRNA and microRNAs (miRs) (Patrono et al., 2001; Patrignani and Patrono, 2015; 2018). These phenomena can contribute to developing the early events of tumorigenesis triggered by platelet activation (Figure 1).

Platelet extravasation and the development of an inflammatory microenvironment

Platelets possess multifaceted functions beyond thrombosis (Figure 2), significantly contributing to various pathological conditions, including atherosclerosis, restenosis, cardiac fibrosis, airway hyperresponsiveness, airway wall remodeling, intestinal colitis, and tumor metastasis (Patrignani and Patrono, 2018; Rumbaut and Thiyagaraja, 2010; Golebiewska and Poole, 2015). An important function of platelets is the capacity to extravasate at sites of inflammation, thus interacting and activating other cells that constitute the cellular stromal compartment of different tissues. Platelets activate other cell types via direct interaction or through the release of many mediators with a wide range of activities and the capacity to release EVs that transfer platelet cargo far from the platelet. These events are associated with inflammation, tissue injury, and organ failure severity.

Platelet recruitment to post-capillary venules at sites of acute inflammation has been shown in various experimental models, often associated with PMN-endothelial interactions. In a mouse model of corneal epithelial abrasion, an acute inflammatory response is necessary for effective wound healing (De La Cruz et al., 2021). In this model, PMNs and platelets are recruited to the small blood vessels surrounding the cornea in a mutually dependent manner. Depleting either cell type systemically inhibits the recruitment of the other. The mechanisms responsible for platelet extravasation in inflammation need to be clarified. However, the data suggest that in this model of corneal inflammation, platelet extravasation depends on CD18, mast cells, and PMNs, with a central role for mast cell degranulation in the responses. Platelet extravasation is

accompanied by red blood cell (RBC) extravasation, with evidence of disruption of microvascular integrity (De La Cruz et al., 2021).

It has been reported that platelets influence leukocyte trafficking from blood vessels into lung tissue because platelets are necessary for the pulmonary recruitment of eosinophils and lymphocytes in murine allergic inflammation (Pitchford et al., 2003; Pitchford et al., 2005; Pitchford et al., 2008).

In hypertensive mice with prostacyclin (PGI_2) receptor (IP) deletion (IPKO) fed with a high-salt diet associated with hypertension and cardiac fibrosis, enhanced systemic biosynthesis of TXA_2 and left ventricular TXA_2 receptor (TP) expression were detected (D'Agostino et al., 2021). Increased cardiac collagen deposition, profibrotic gene expression (including TGF-β), number of myofibroblasts at perivascular levels, and extravasated platelets were detected compared to WT mice treated with the same diet. The antiplatelet agent low-dose aspirin caused a selective inhibition of platelet TXA_2 biosynthesis and mitigated enhanced blood pressure, cardiac fibrosis, and left ventricular profibrotic gene expression in IPKO but not WT mice. Moreover, the number of myofibroblasts and extravasated platelets in the heart was reduced (D'Agostino et al., 2021).

Platelets have been detected to extravasate and accumulate in the colonic lamina propria of chronic inflammation-associated fibrosis (Sacco et al., 2019) and intestinal adenomas in mice (Bruno et al., 2022), associated with an enhanced number of myofibroblasts.

Platelet-myofibroblast crosstalk: a key mechanism of intestinal inflammation-linked tumorigenesis

Under normal physiological conditions, the stroma comprises fibroblasts, smooth muscle cells, immune cells, endothelial cells, nerve cells, and the extracellular matrix (ECM) (Barron and Rowley, 2012). The stroma is a structural and functional support system for epithelial cells, regulating their behavior and enabling tissue repair in response to injury (Tuxhorn et al., 2001). Stromal activation during wound healing, characterized by myofibroblast activation, type I collagen deposition, and angiogenesis, is also observed in the tumor microenvironment, referred to as reactive stroma (Kalluri and Zeisberg, 2006; Tuxhorn et al., 2002).

In intestinal inflammation resulting from epithelial damage, such as experimentally induced colitis in mice or inflammatory bowel disease (IBD) in humans, platelets are observed to migrate from the bloodstream into the interstitial tissue of the colon (Danese et al., 2004; Petito et al., 2017). This extravasation may contribute to the persistence of chronic inflammation, leading to fibrosis and facilitating tumorigenesis through intercellular communication with myofibroblasts.

Sacco et al. (2019) conducted a study revealing that when human platelets are cocultured with intestinal myofibroblasts, the platelets undergo activation, resulting in increased production of TXA_2, a major oxylipin derived from arachidonic acid (AA) through cyclooxygenase (COX)-1 activity. Subsequently, TXA_2 induces phenotypic and functional alterations in myofibroblasts. In the presence of platelets, the characteristic spindle-shaped myofibroblasts turn towards a polarized phenotype, accompanied by elongation of the cellular body associated with enhanced proliferation and migratory) properties. The changes in myofibroblast morphology and functions induced by platelets were accompanied by reduced α-SMA, vimentin, fibronectin, and RhoA expression. These changes were prevented when platelets were exposed to aspirin, an irreversible inhibitor of platelet COX-1, and then washed away before incubation with myofibroblasts. Similar effects were observed when using an antagonist of the TP receptors, indicating that COX-1-dependent TXA_2 is a crucial mediator released by platelets to activate myofibroblasts via TP receptors (Sacco et al., 2019). In the coculture of human platelets and myofibroblasts, platelet-derived TXA_2 was involved in the induction of COX-2 in myofibroblasts since it was prevented by the selective inhibition of platelet COX-1 by aspirin or by a specific antagonist of TXA_2 receptors (TP) (SQ 29,548) (Bruno et al., 2022). Enhanced COX-2-dependent PGE_2 was detected under these experimental conditions. Interestingly, both TXA_2 and PGE_2 contribute to COX-2 induction in the coculture of platelet and myofibroblasts. The activation of TP by the TXA_2 mimetic U46619 caused a rapid expression of COX-2 in myofibroblasts cultured alone, but PGE_2 was required for the sustained expression of COX-2 (Bruno et al., 2022). Faour et al. (2001) reported that in IL-1β-treated human synovial fibroblasts, PGE_2 stabilizes COX-2 mRNA and stimulates translation via EP4 receptor and the downstream kinases p38MAPK and cAMP-dependent protein kinase.

Enhanced COX-2-dependent PGE_2 in the tumor microenvironment promotes tumor growth and inhibition of immunosurveillance and induces angiogenesis. Moreover, PGE_2 can activate tumor epithelial cells, causing proliferation, survival, migration/invasion, and epigenetic changes (Wang and DuBois, 2013). However, it was found that TXA_2 and PGE_2 contribute to COX-2 induction in the coculture of platelet and myofibroblasts. The activation of TP by the TXA_2 mimetic U46619 caused a rapid expression of COX-2 in myofibroblasts cultured alone, but PGE_2 was required for the sustained expression of COX-2 (Bruno et al., 2022). Faour et al. (2001) reported that in IL-1β-treated human synovial fibroblasts, PGE_2 stabilizes COX-2 mRNA and stimulates translation via EP4 receptor and the downstream kinases p38MAPK and cAMP-dependent protein kinase.

Proinflammatory stimuli, such as IL-1β, have been shown to upregulate COX-2 signaling in human colonic fibroblasts, modulating the proliferation and invasiveness of human colonic epithelial cancer cells (Zhu et al., 2012). Moreover, COX-2 expression has been detected in the stromal compartment of polyps from $Apc^{Min/+}$ mice (Oshima et al., 1996).

These findings demonstrate the potential contribution of platelets to the development of an inflammatory microenvironment, thereby promoting the early stages of tumorigenesis through the upregulation of COX-2 and the increased production of PGE_2 (Figure 1). Platelet-derived TXA_2 is a pivotal trigger and sustainer of the cascade of events induced by platelet activation leading to intestinal tumorigenesis. Notably, antiplatelet agents can indirectly disrupt this cascade of downstream events (Patrignani and Patrono, 2015). Direct inhibition of COX-2 activity can achieve similar efficacy. Selective COX-2 inhibitors (coxibs) reduce tumor development by targeting COX-2 and PGE_2. (Bertagnolli et al., 2006; Patrignani and Patrono, 2015; Wang and DuBois, 2013) (Figure 1). However, the heightened risk of cardiovascular side effects by COX-2 inhibitors hinders the

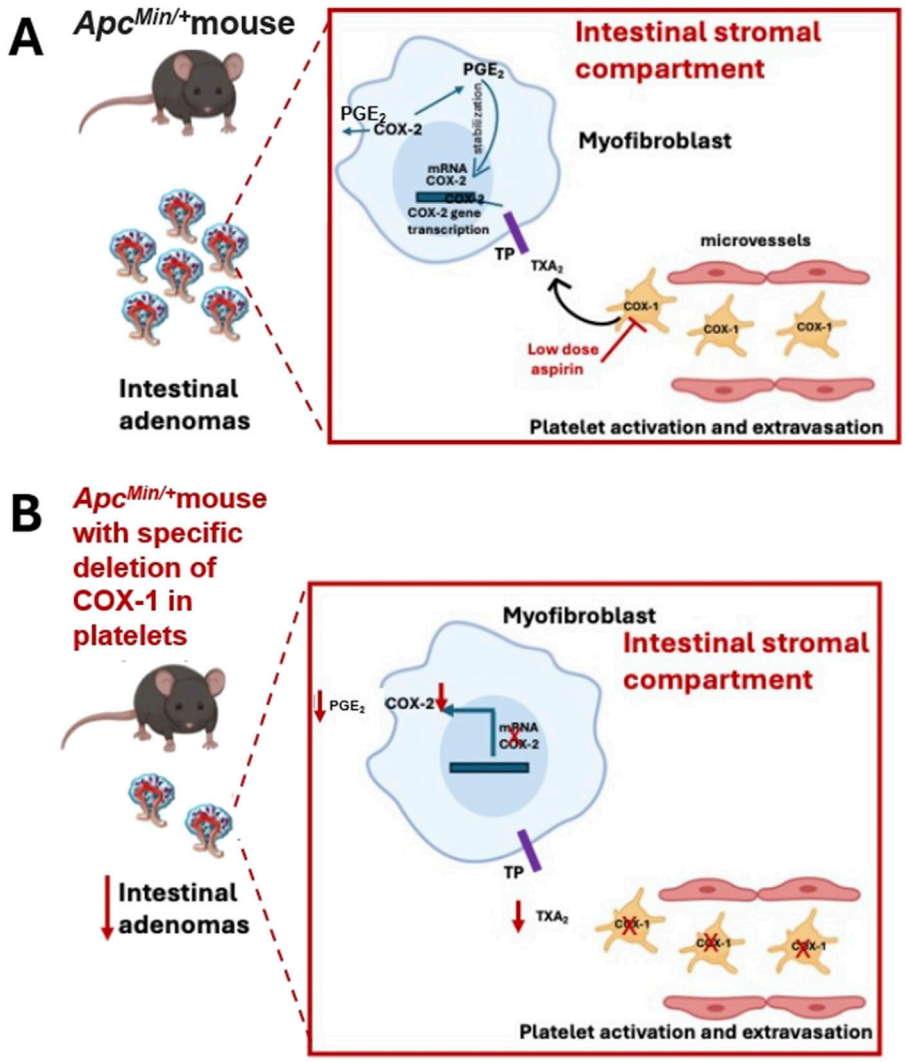

FIGURE 3
The role of platelet COX-1 in intestinal tumorigenesis of *Apc*$^{Min/+}$ mice. **(A)** The platelet COX-1-dependent TXA_2 (also from extravasated platelets) can contribute to intestinal neoplasia by triggering the expression of COX-2 in stromal cells, which is involved in the biosynthesis of PGE_2; the selective inhibition of COX-1 in platelets by aspirin can prevent the biosynthesis of TXA_2 and indirectly the upregulation of COX-2. **(B)** In *Apc*$^{Min/+}$ mice, the specific deletion of platelet COX-1 caused a profound reduction in platelet TXA_2 biosynthesis *in vivo*, which was associated with decreased COX-2 expression and PGE_2 biosynthesis, and a reduced number and size of intestinal adenomas.

utilization of these drugs for long-term cancer prevention regimens (Grosser et al., 2006).

The role of platelets in the development of intestinal tumorigenesis: a lesson from conditional COX-1 knockout mice in megakaryocytes/platelets

The role of platelet TXA_2 in intestinal inflammation and tumorigenesis has been convincingly demonstrated by generating mice with the specific deletion of COX-1 in megakaryocytes/platelets (Sacco et al., 2019; Bruno et al., 2022).

We generated a mouse with floxed Ptgs1 (COX-1) (Sacco et al., 2019), in which exons 6 and 7 were flanked by loxP sites using transcription activator-like effector nucleases as a genome-editing tool, which significantly boosts genomic modification efficiency (Joung and Sander, 2013). These mice were bred with platelet factor 4 (Pf4)-Cre transgenic C57BL/6 mice [obtained from Jackson Laboratories (Bar Harbor, ME)] expressing a codon-improved Cre recombinase (iCre) under the control of the mouse Pf4 promoter, resulting in Cre recombinase expression in most megakaryocytes (Sacco et al., 2019). In these mice, the synthesis of TXA_2 by platelet COX-1 was almost completely inhibited. The systemic biosynthesis of TXA_2, as assessed by the enzymatic urinary metabolites of TXB_2, was also profoundly reduced. However, COX-2-dependent markers of prostanoid biosynthesis (such as the urinary metabolite of PGE_2 and PGI_2) were not significantly affected (Sacco et al., 2019; Bruno et al., 2022). These effects observed in mice with the COX-1 specific deletion in platelets are similar to the impact of low-dose aspirin in humans, which is an antiplatelet agent that selectively inhibits COX-1 in platelets (Patrignani et al., 2014; Patrono et al., 2005).

In mice with experimental intestinal colitis treated with dextran sulfate sodium (DSS), there is increased biosynthesis of TXA_2 from platelets (Sacco et al., 2019). TXA_2 contributes to increased microvascular permeability (Turnage et al., 1985) and inflammatory, immune cells, and platelets' movement, leading to colon accumulation (Vitiello et al., 2014). Deletion of COX-1 in platelets inhibits the chronic inflammatory response linked to the reversal of intestinal colitis symptoms in DSS-induced colitis. Furthermore, the specific deletion of COX-1 in platelets prevented intestinal inflammation-associated fibrosis (Sacco et al., 2019).

In $Apc^{Min/+}$ mice that develop multiple intestinal neoplasia due to a nonsense mutation at codon 850 of the *Apc* gene, like humans with germline mutations in the *APC* gene (Moser et al., 1995), enhanced systemic TXA_2 biosynthesis was detected deriving mainly from activated platelets (Bruno et al., 2022). The specific deletion of platelet COX-1 in $Apc^{Min/+}$ mice was associated with a reduced systemic biosynthesis of TXA_2 and a reduced number of intestinal adenomas (Figures 3A, B). $Apc^{Min/+}$mice developed multiple sessile tubular adenomas with marked nuclear enlargement with hyperchromasia, denoting a lower grade of differentiation than $Apc^{Min/+}$ mice with the specific deletion of platelet COX-1, as confirmed by the higher number of mitotic elements (Bruno et al., 2022). The adenomas of $Apc^{Min/+}$mice showed higher staining of PCNA (proliferating cell nuclear antigen) than $Apc^{Min/+}$mice with specific deletion of COX-1 in the platelet; PCNA is an auxiliary protein for DNA polymerase that reaches maximal expression during the S phase of the cell cycle (Celis et al., 1987). In polyps of $Apc^{Min/+}$mice, enhanced expression of COX-2 and mPGES-1 (i.e., microsomal prostaglandin E synthase-1, the downstream enzyme responsible for PGE_2 biosynthesis from COX-2 product PGH_2) was detected in association with the downregulation of 15-prostaglandin dehydrogenase (15-PGDH, an enzyme oxidizing and degrading PGE_2). These changes could contribute to enhanced biosynthesis of PGE_2 in the tumor, which can reflect the increased systemic biosynthesis of PGE_2 found in $Apc^{Min/+}$ mice (Bruno et al., 2022). Deleting platelet COX-1 prevented the upregulation of COX-2 in the intestinal adenomas associated with reduced systemic biosynthesis of PGE_2 (Figure 3B). The results of this study demonstrate that activated platelets can contribute to enhanced PGE_2 generation in intestinal tumors, and inhibition of platelet function can indirectly prevent it, thus interfering with adenoma formation (Figures 3A, B).

Platelets and the immune system

It is increasingly evident that platelets play a pivotal role in various immunological processes beyond their conventional function in hemostasis and thrombosis (Ali et al., 2015). Platelets can contribute to 1) defending against microbial threats, 2) recruiting and augmenting innate effector cell functions, 3) regulating antigen presentation, and 4) enhancing adaptive immune responses.

Platelets interact with immune complexes (ICs), which are associations of antibodies with their antigens. The presence of ICs in the bloodstream is documented in many pathological conditions characterized by chronic or acute inflammation

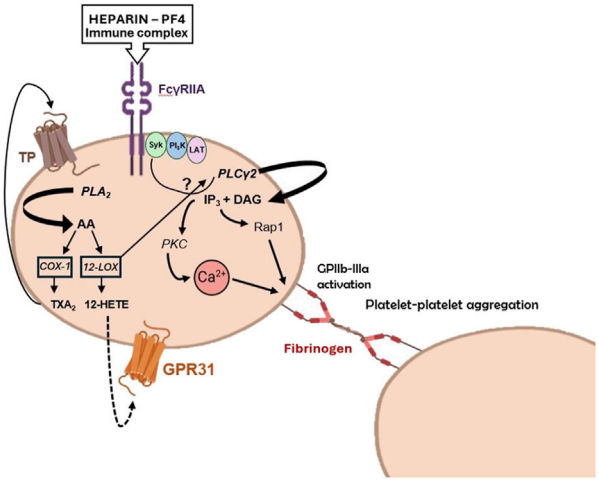

FIGURE 4
Potential roles of 12-lipoxygenase (LOX) in platelet activation by heparin-platelet factor 4 (PF4) immune complexes. PF4 is a chemokine released from platelet a-granules upon activation. It can form immune complexes with negatively charged substances, such as heparin. The formation of PF4-heparin complexes leads to the synthesis of antibodies, which activate platelets via FcγRIIa receptors. 12-LOX can amplify platelet activation through FcγRIIa via three different pathways: i) the arachidonic acid (AA)-derived compound 12S-HETE generated by 12-LOX, ii) the 12S-HETE receptor GPR31, and iii) the interaction with PLCγ2 or upstream signaling and adaptor molecules, such as Syk (spleen tyrosine kinase), PI3K (phosphoinositide 3-kinase), and LAT (T-cell activation linker). Modified from Alison H. Goodal et al. Blood 2014; 124 (14): 2166–2168 (comment on Yeung et al., Blood 2014; 124:2271-2279).

(Cloutier et al., 2018). Platelets become activated when ICs bind to the IgG Fc receptor on human platelets, known as FcγRIIa (CD32) (Arman and Krauel, 2015). FcγRIIa is one of the three immunoreceptor-based activation motif (ITAM) family members of tyrosine kinase signaling receptors in human platelets (Boylan et al., 2008). The other two members are the collagen receptor glycoprotein (GP) VI and C-type lectin receptor 2. These receptors have a different signaling pathway from the G protein-coupled receptors (GPCRs) for other platelet agonists such as thrombin, adenosine 5′-diphosphate (ADP), and TXA_2 (Boulaftali et al., 2014). Upon activation via ITAMs, platelets undergo aggregation and degranulation and are transformed into procoagulant platelets, which release procoagulant EVs (Puhm et al., 2021). Platelets express COX-1, crucial in converting AA released from membrane phospholipids following activation to the platelet agonist TXA_2 (Patrignani and Patrono, 2015; 2018) that activates platelets through their TP receptors (Rovati et al., 2022). The selective and irreversible inhibition of COX-1 by aspirin is a fundamental aspect of antiplatelet therapy (Patrignani and Patrono, 2015). However, platelets also express 12-lipoxygenase (12S-LOX) (Contursi et al., 2022; Yoshimoto et al., 1992), and its specific role in platelet biology is not fully elucidated. AA released from cellular phospholipids in platelets can undergo a metabolic pathway involving 12-LOX (Figure 4), resulting in the generation of 12S-HpETE (hydroperoxyeicosatetraenoic acid), which subsequently undergoes rapid conversion to 12S-HETE (hydroxyeicosatetraenoic acid). The functional implications of 12-

HETE in platelet physiology were hindered by the lack of specific 12-LOX inhibitors (Contursi et al., 2022). However, inhibitors that are selective for 12S-LOX over other LOXs and COXs have recently been developed (Luci et al., 2014). Their use showed the involvement of 12-LOX in the aggregation and degranulation of platelets activated by collagen, ADP, and thrombin, the latter via the PAR4 receptor, but interestingly, not via PAR1 (Tourdot and Holinstat, 2017). Using one of these new 12-LOX inhibitors (ML355), it was evidenced that 12-LOX also plays an important role in activating platelets through FcγRIIa (Yeung et al., 2014; Luci et al., 2014).

Heparin-induced thrombocytopenia (HIT) is a condition where platelet count decreases due to the disintegration and release of platelet-derived EVs into the bloodstream, promoting thrombin generation (Ahmed et al., 2007). It can be life-threatening and is caused by heparin binding to platelet factor 4 (PF4) released from platelets, which in some patients can result in immune recognition of the structurally modified heparin-PF4 complexes (Arepally and Padmanabhan, 2021). In HIT, 12-LOX is important in stimulating platelets through FcγRIIa leading to GPIIb-IIIa (the platelet fibrinogen receptor) activation (Goodall, 2014) (Figure 4). Thus, ML355 attenuates aggregation and degranulation via a mechanism that also affects phosphorylation of phospholipase Cγ2 (PLCγ2), calcium mobilization, and phosphorylation of protein kinase C (PKC) and Ras-proximate-1 or Ras-related protein 1 (Rap1involved in activation of GPIIb-IIIa) (Figure 4), while having no direct effect on phosphorylation of FcγRIIa itself (Yeung et al., 2014). The decreased phosphorylation of Rap1 was confirmed in platelets from 12-LOX$^{-/-}$ mice, indicating that the effects were specific to 12-LOX. The data suggests that targeting 12-LOX could be a promising treatment for patients with HIT. Preclinical studies have shown that ML355 has a good safety profile (Adili et al., 2017). As 12-LOX enhances platelet activation by other agonists like TXA_2 and ADP, selectively inhibiting 12-LOX may reduce the platelet response without completely blocking it. This indicates a favorable balance between the risk of clotting and bleeding. ML355 (also known as VLX-1005) is currently in phase 2 clinical trials for treating HIT and thrombosis (Stanger and Holinstat, 2023).

Due to immune surveillance, tumor cells face significant challenges surviving in the bloodstream. Consequently, metastasis and subsequent extravasation involve intricate mechanisms facilitating cancer cell survival in the systemic circulation. Fundamental to this process is the recruitment of monocytes, neutrophils, and platelets, which protect tumor cells from immune surveillance and facilitate the formation of metastases (Kitamura et al., 2015). In addition to these mechanisms, platelets have been found to impair the immune response through various other avenues. They play a pivotal role in regulating innate and adaptive immunity, particularly T cells. Furthermore, platelets can serve as antigen-presenting cells (APCs), as demonstrated by the expression of MHC class I proteins on their surface, initiating the adaptive immune response (Ali et al., 2015). It has been reported that platelets can transfer MHC class I proteins to tumor cells, resulting in a tumor cell phenotype termed the "phenotype of false pretenses." This allows platelets to disrupt the self from non-self-recognition by NK cells, ultimately failing to protect the host by producing IFN-γ (Placke et al., 2012).

Emerging evidence indicates that platelets express the immune checkpoint molecule PD-L1 (Programmed Death-Ligand 1), which interacts with PD-1 (Programmed Cell Death Protein 1) on T cells, leading to their exhaustion (Figure 5). Notably, platelets from cancer patients with non-small cell lung cancer (NSCLC) showed significant levels of PD-L1 (Hinterleitner et al., 2021). Using specific antibodies, such as pembrolizumab, to block the PD-L1/PD-1 interaction has resulted in long-term responses in patients with metastatic NSCLC (Dang et al., 2016). Some tumor cells also express high levels of PD-L1, aiding in immune system evasion (Juneja et al., 2017).

Interestingly, Rachidi and colleagues (2017) identified a potential role for the non-signaling TGF-β-docking receptor glycoprotein A repetitions predominant (GARP), constitutively expressed on the platelet surface. Platelets are the primary source of TGF-β in systemic circulation and the tumor microenvironment. Platelet TGF-β production and secretion occur through GARP expression and the secretion of TGF-β itself (Tran et al., 2009). It has been shown that platelet-derived TGF-β has an immunosuppressive effect, primarily affecting T cells, and that the deletion of Lrrc32 (the gene encoding GARP) enhances the protective effect of the immune system against both melanoma and colon cancer. Combining immunotherapy with antiplatelet agents is an effective therapeutic strategy in mouse models. This effectiveness is attributed to the interruption of the GARP-TGF-β axis (Rachidi et al., 2017). Thus, antiplatelet agents may interfere with cancer cells' capacity to evade immune surveillance (Patrignani and Patrono, 2018).

Platelets appear to be involved in the pathogenesis of hepatocellular carcinoma (HCC), a potential complication of chronic HBV infection (Sitia et al., 2012). During chronic hepatitis B virus (HBV) infection, HBV-specific CD8$^+$ T cells fail to eradicate the infection, leading to necrosis, regeneration, inflammation, and ultimately HCC development (Guidotti and Chisari, 2006). It was reported that administering aspirin and clopidogrel (two antiplatelet agents) reduces the number of HBV-specific CD8$^+$ T cells and secondary nonspecific infiltrates, preventing liver injury and fibrosis (Sitia et al., 2012). The pathophysiology of HBV infection and the role of platelet/T cell crosstalk are not fully understood. It has been proposed that interaction through platelet-CD40L and lymphocyte-CD40 (Elzey et al., 2003) could trigger an inflammatory endothelial response (Henn et al., 1998). Studies have shown an increased number of thrombotic events in patients with liver diseases (Tripodi and Mannucci, 2011), suggesting the potential for investigating antiplatelet drugs in further randomized clinical trials (RCTs) to assess their effects on HCC development in patients with chronic HBV infection.

Platelets fuel cancer metastasis

Cancer metastasis, which involves the spread of cancer cells from a primary lesion to distant organs, is the main cause of cancer-related deaths (Massagué and Obenauf, 2016). Numerous studies have highlighted the crucial role platelets play in this process. Clinical observations have underlined the potential link between cancer cell diffusion via the bloodstream and platelet involvement in coagulation (Gay and Felding-Habermann, 2011; Contursi et al., 2017). Once cancer cells enter systemic circulation, they interact

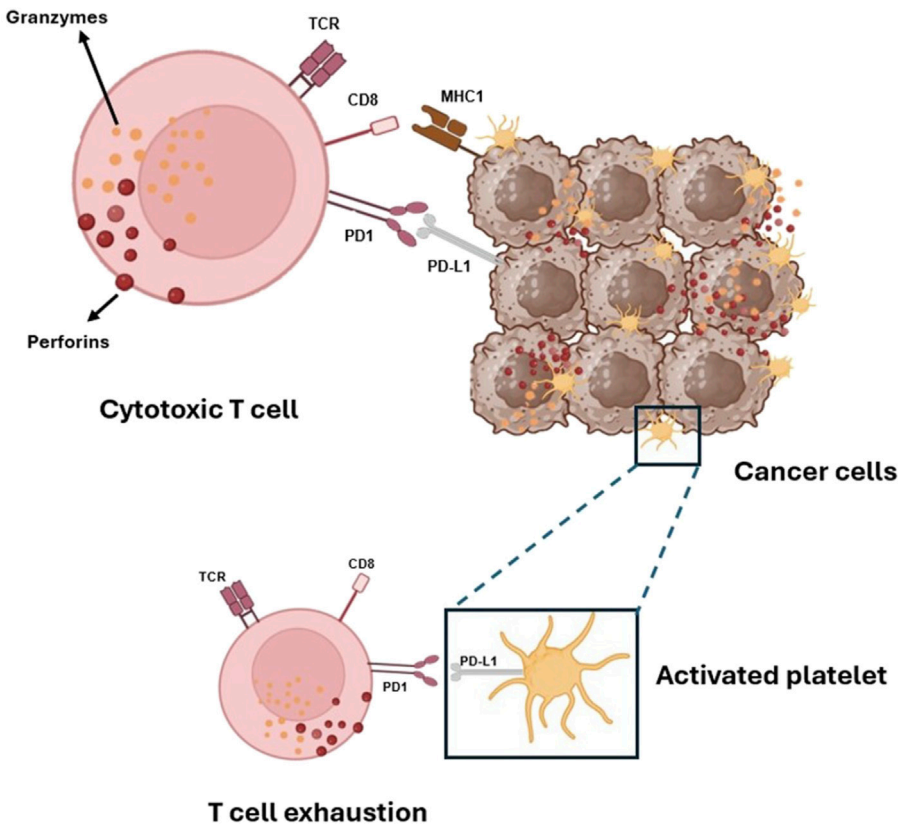

FIGURE 5
Platelets and tumor cells' immune evasion via activation of PD-1 on T-cells by its ligands PD-L1. Platelets, like cancer cells, can activate the immune checkpoint protein PD-1, which controls the immune response of cytotoxic CD^{8+} T cells that carry out their killing function by releasing two types of preformed cytotoxic proteins: the granzymes, which seem able to induce apoptosis in any target cell, and the pore-forming protein perforin, which punches holes in the target cell membrane through which the granzymes can enter.

with platelets. Platelets can surround cancer cells, forming aggregates that promote survival, protect them from immune responses, and enhance their capacity to adhere to the endothelium, arrest, and exit blood vessels (Gay and Felding-Habermann, 2011).

Recent findings have shown that platelets induce a more malignant phenotype in cancer cells by enhancing their migratory properties (Labelle et al., 2011; Dovizio et al., 2013; Guillem-Llobat et al., 2016). Platelets release mediators such as PDGF, TGF-β, and PGE_2, which promote EMT, that endows cancer cells with mesenchymal markers like vimentin and fibronectin and transcription factors such as Twist, Snail, and Zeb while downregulating epithelial markers like E-cadherin, thereby enabling these cells to acquire migratory properties and colonize distant organs (Kalluri and Weinberg, 2009). Labelle et al. (2011) demonstrated that EMT is induced in colon and breast cancer cells via platelet-derived TGF-β1, which activates the TGF-β/Smad pathway, thus promoting the metastatic potential of tumor cells. Dovizio et al. (2013) demonstrated that platelets trigger EMT and COX-2 overexpression in human adenocarcinoma cells (such as HT29 cells) through direct contact and PDGF release. The direct interaction involves the platelet collagen receptor GPVI and cancer cell galectin-3, unique among galectins due to its collagen-like domain. Inhibition of galectin-3 function [using β-lactose, a dominant-negative form of galectin-3, Gal-3C (Yang et al., 2008), or anti-galectin-3 antibody M3/38] or the inhibition of platelet adhesion to collagen-like binding sites on cancer cells by revacept, the soluble dimeric GPVI receptor fusion protein (GPVI-Fc) (Ungerer et al., 2011), prevented abnormal COX-2 expression. Revacept, which prevents the interaction between platelets and cancer cells, and the inhibition of COX-2 by rofecoxib, a highly selective COX-2 inhibitor, avoided platelet-induced changes in mRNA levels of EMT markers. This suggests that the direct platelet-cancer cell interaction and abnormal COX-2 expression contribute to the modifications in gene expression associated with EMT. Mammadova-Bach et al. (2020) found that genetic deficiency of platelet GPVI in mice reduced both experimental and spontaneous colon and breast cancer cell metastasis. Similar results were observed in mice lacking the spleen-tyrosine kinase Syk in platelets, a crucial component of the ITAM-signaling cascade. Both *in vitro* and *in vivo* analyses confirmed that mouse and human GPVI facilitated platelet adhesion to colon and breast cancer cells. Through a CRISPR/Cas9-based gene knockout approach, galectin-3 was identified as the primary counterreceptor of GPVI on tumor cells. Further, *in vivo* studies revealed that the interaction between platelet GPVI and tumor cell–expressed galectin-3 involves ITAM-signaling components in platelets and promotes the extravasation of tumor cells.

Additionally, it was demonstrated that inhibiting GPVI by JAQ1 F (ab′) 2 antibody efficiently impairs platelet–tumor cell interaction and tumor metastasis (Mammadova-Bach et al., 2020).

Guillem-Llobat et al. (2016) studied the impact of platelets on the spread of colorectal cancer cells (HT29 cells) to the lungs and the effect of the antiplatelet agent low-dose aspirin. When HT-29 cells were exposed to platelets *in vitro*, they were more likely to cause lung metastasis once injected in humanized immunodeficient mice than untreated HT29 cells. This effect was linked to the development of mesenchymal-like cancer cells by platelets associated with acquiring migratory properties and EMT. Mesenchymal-like cancer cells had an enhanced capacity to activate platelets, thus promoting the formation of platelet aggregates surrounding tumor cells, and this event is central in the development of cancer metastases. Administering a low dose of aspirin to the mice, prevented the increased rate of lung metastasis associated with the prevention of platelet activation *in vivo* in response to the injection of mesenchymal-like cancer cells. These results provide a mechanistic understanding of the reported antimetastatic properties of low-dose aspirin in posthoc analyses of randomized trials for cardiovascular prevention (Patrignani and Patrono, 2016) and reinforce the rationale for performing adjuvant trials of low-dose aspirin and possibly other antiplatelet agents, in colorectal cancer patients. *In vitro* studies of cocultures of platelets and HT29 cells showed that platelet-derived PGE_2 activated the EP4 receptor on cancer cells, promoting EMT (Guillem-Llobat et al., 2016). Different antiplatelet agents, such as aspirin DG-041 (an EP3 receptor antagonist), and ticagrelor (a $P2Y_{12}$ receptor antagonist), prevented EMT of cancer cells by inhibiting platelet activation and platelet-derived PGE_2 release involved in cancer cell EP4-dependent migration (Guillem-Llobat et al., 2016).

Further studies investigated the potential of anticoagulant agents to disrupt communication between platelets and cancer cells. Battinelli et al. (2014) discovered that the interaction between breast cancer cells (MCF-7) and platelets stimulated the secretion of VEGF from platelets, a process that was prevented by the administration of low molecular weight heparin (LMWH) or fondaparinux. This suggests a thrombin-dependent release of angiogenic molecules by platelets after interaction with tumor cells. Human adenocarcinoma cell lines (such as HCT-8 and LoVo) and anaplastic murine tumor cells (such as Hut-20) can generate thrombin, which in turn activates platelets (Nierodzik and Karpatkin, 2006). Mitrugno et al. (2014) found that the colorectal cancer cell line Caco-2 and the prostate carcinoma cell line PC3M-luc induce platelet activation and granule secretion. They showed that the platelet immune receptor FcγRIIa plays a crucial role in this process by activating the FcγRIIa-spleen tyrosine kinase (Syk)-PLCγ signaling pathway, resulting in further platelet activation and granule secretion. This enhanced platelet recruitment and protection of circulating tumor cells from the immune system promote tumor cell survival and metastasis (Mitrugno et al., 2014), suggesting FcγRIIa as a target for antimetastatic therapy. Mannori et al. (1995) highlighted interactions between platelets and colon cancer cells (LS 180, T84, COLO 205, COLO 320, and HT-29) involving P-selectin on platelets and mucin-type glycoproteins on the cancer cell surface. Other studies reported the role of the platelet GPIIb/IIIa receptor in platelet/cancer cell crosstalk. In the melanoma cell line M3Dau, the interaction between the platelet receptor GPIIb/IIIa and a similar complex on tumor cells led to larger platelet-tumor aggregates (Boukerche et al., 1989). Mammadova-Bach et al. (2016) reported interactions between platelets and breast or colon tumor cells via platelet integrin α6β1 and ADAM-9 on tumor cells. This interaction promotes platelet activation, granule secretion, and endothelial transmigration, thus promoting metastasis. Genetic deletion of platelet α6β1 or an integrin α6-blocking antibody (GoH3) reduced lung metastasis by preventing platelet-tumor cell crosstalk (Mammadova-Bach et al., 2016). Lysophosphatidic acid (LPA), a platelet-derived mediator, plays a significant role in cancer development (Mills and Moolenaar, 2003). LPA acts through GPCRs, promoting platelet shape change and aggregation (Williams et al., 2009). Platelet-derived LPA promotes bone metastasis in ovarian and breast cancers by binding to LPA1 on tumor cells, and a specific LPA1 antagonist can inhibit this interaction without affecting normal platelet function (Boucharaba et al., 2004; 2006). Platelets also contribute to LPA biosynthesis via the enzyme autotaxin (ATX), which hydrolyzes LPA precursors to form LPA, binding to its receptors on cancer cells to promote invasion and metastasis (Leblanc et al., 2014). LPA can induce EMT in ovarian cancer cells by promoting nuclear translocation of β-catenin, activating Wnt/β-catenin target genes and hypoxia-induced factor-1α (HIF1α), leading to mesenchymal marker expression (Burkhalter et al., 2015; Ha et al., 2016).

The metabolite 12S-HETE, generated by platelet 12S-LOX, plays a crucial role in cancer development and metastasis through various mechanisms (Contursi et al., 2022). The involvement of 12S-LOX in cancer development has been demonstrated in human gastric cancer cells with *ALOX12* overexpression, and it is suggested as a marker of cancer progression in melanoma (Timár et al., 1999). 12-HETE is generated as a free acyl and is found in esterified form in membrane phospholipids, particularly in platelets where it is involved in coagulation (Thomas et al., 2010; Slatter et al., 2018; Lauder et al., 2017). HT29 cells do not express 12-LOX or synthesize 12-HETE when cultured alone, but in coculture with platelets, they express the protein and synthesize 12-HETE (Contursi et al., 2021). The interaction with cancer cells activates platelets that release EVs containing catalytically active 12S-LOX, quickly transferred to cancer cells. The cancer cells then acquire the capacity to generate 12-HETE, which is esterified rapidly, mainly in plasmalogen phospholipids. In cancer cells exposed to platelets, endogenous but not exogenous 12S-HETE contributed to changes in EMT gene expression by modifying cancer cell phospholipids by 12-HETE (Contursi et al., 2021). Modifying cancer cell phospholipids by 12S-HETE may functionally impact cancer cell biology, and the pharmacological inhibition of 12-LOX represents a novel anticancer strategy.

Platelet-derived extracellular vesicles in cancer

Platelets secrete medium-size EVs (mEVs) (Gasecka et al., 2019; Kailashiya, 2018) ranging from 100 to 1,000 nm, released under various physiological and pathological conditions (Kailashiya, 2018). They are characterized by the inversion of membrane phospholipids, exposure of phosphatidylserine (PS) on the outer

membrane—rendering them 50 to 100 times more procoagulant than platelets—and the expression of various integrins and enzymes (Janowska-Wieczorek et al., 2005; Italiano et al., 2010). These mEVs promote the communication between platelets and various cell types (Italiano et al., 2010). They act by (1) stimulating target cells through their surface ligands, (2) transferring surface receptors, and (3) delivering their cargo, i.e., proteins, bioactive lipids, mRNAs, transcription factors, and miRs, which can significantly alter cellular phenotypes. mEVs can also transfer infectious particles (e.g., HIV, prions) and intact organelles (e.g., mitochondria) (Ratajczak et al., 2006). Due to their carrier role, mEVs are involved in various biological processes, including hemostasis, thrombosis, inflammation, tumorigenesis, angiogenesis, and immunity (Italiano et al., 2010). For instance, platelet-derived EVs transfer receptors to both normal and cancer cells, enhancing adhesion, proliferation, and survival (e.g., CD41, CD61, CD62, CXCR4, PAR-1) (Baj-Krzyworzeka et al., 2002). mEVs also carry bioactive lipids like sphingosine-1-phosphate (S1P) and AA. Barry and colleagues demonstrated the transfer of platelet AA via mEVs to monocytes and endothelial cells, inducing COX-2 expression and prostanoid synthesis (Barry et al., 1997; 1999). Platelet mEVs transfer mRNA to monocytic THP-1 cells, increasing gamma-globin transcripts and hemoglobin subunits (Risitano et al., 2012). Additionally, platelet-derived mEVs contribute to tumorigenesis through miR transfer. For instance, the transfer of miR-223 to endothelial cells downregulates tumor-suppressor genes (Laffont et al., 2013), while the transfer of miR-939 to ovarian cancer cells promotes EMT (Tang et al., 2017). Conversely, mEVs carrying miR-24 induce apoptosis and suppress tumor growth (Michael et al., 2017). Platelet mEVs interact with monocytes/macrophages in inflammatory contexts, influencing proinflammatory cytokine release (Linke et al., 2017; Vasina et al., 2011).

Platelets contain important RNA biomarkers [mRNAs, miRs, circular (circ) RNAs, long non-coding (lnc) RNAs, mitochondrial-RNAs] and have a protein translation machinery for processing the RNA transcripts (Harrison and Goodall, 2008). CircRNAs, generated from exons of protein-coding genes through back-splicing, are abundant in platelets. They have received increasing attention for their potential role as cancer biomarkers due to their high stability and spatiotemporal-specific expression (Bach et al., 2019). In addition, lncRNAs (Dahariya et al., 2019) and miRs (Nagalla et al., 2011) represent important cancer biomarkers. Boerrigter et al. (2020) reported that the measurement of these molecules in prostate cancer (PCa) offers promising prospects because they are highly tumor-specific and relatively easy to detect. Through their crosstalk with other cells, including cancer cells, platelets can uptake these RNAs. These molecules can be found in isolated platelets. Analyzing RNAs from patients' platelets offers significant promise for accurately distinguishing between metastatic and non-metastatic tumors. Additionally, RNA sequencing from platelets could identify the primary tumor location of six distinct tumor types with an accuracy of 71% (Hu et al., 2024).

Liquid biopsy involves analyzing biomarkers found in non-solid biological tissues, primarily blood. It offers significant advantages over traditional methods: it is risk-free, non-invasive, painless, does not necessitate surgery, and lowers costs and diagnostic time. The most extensively studied non-invasive cancer biomarkers include circulating tumor cells (CTCs), circulating tumor DNA (ctDNA), and EV cargo (Marrugo-Ramírez et al., 2018). They offer several advantages, including the ability for early detection, assessment of an individual patient's prognosis, such as cancer stage and spread, identification of new targets for personalized treatments, and predict therapy responses. Currently, blood-based biopsy measurements focus on the evaluation of biomarker biosources, including circulating tumor DNA (ctDNA), circulating tumor cells (CTCs), EVs (i.e., exosomes, mEVs and oncosomes), and tumor-educated platelets (TEPs) (Marrugo-Ramírez et al., 2018; Best et al., 2015; Nilsson et al., 2011; 2016; Skog et al., 2008).

Contursi et al. (2023) studied platelet-derived mEVs collected from non-metastatic CRC patients at initial diagnosis versus healthy controls (HCs). The aim was to address how these mEVs can change the expression of genes related to the process of EMT in four different human colorectal cancer cell lines: HCA7, HCT116, HT29, and Caco2. These cell lines have different genetic features and metastatic potentials. The study found that platelet-derived mEVs from CRC patients affect colorectal cancer cells differently depending on their genetic makeup and behavior. Specifically, the mEVs from CRC patients caused an increase in the expression of *TWIST1* and *VIM* (protein name: vimentin) in all the studied cancer cell lines, while those from healthy subjects did not. In HCA7 cells, the expression of *CDH1* (protein name, E-cadherin) was not affected by the mEVs from either CRC patients or HCs. However, the HCT116, HT29, and Caco2 cells showed decreased *CDH1* expression when cultured with mEVs from CRC patients, with the HCT116 cells (which have high metastatic potential) showing decreased expression after just 4 hours of exposure. Moreover, the mEVs from CRC patients and HCs induced the expression of COX-2 in colorectal cancer cell lines at 24 but not at 4 hours, suggesting that this effect may be due to post-transcriptional regulation (Contursi et al., 2023).

Cancer-associated thrombosis is a leading cause of death in cancer patients (Mahajan A. et al., 2022). Contursi et al. (2023) explored whether platelet-derived mEVs collected from CRC patients affected the TXB_2 biosynthesis of 4 CRC cell lines *in vitro*. Proteomic analysis revealed that COX-1 and TXA_2 synthase were expressed similarly in mEVs collected from CRC patients and healthy controls (HC). HCA7 cells can generate endogenously TXB_2, and when exposed to mEVs, the TXB_2 levels were unchanged. Other CRC cell lines have very limited capacity to generate TXB_2, but when cocultured with mEVs from both CRC patients and HCs, TXB_2 was detectable. This may suggest that platelet-derived mEVs could provide AA to cancer cells, leading to TXB_2 generation. Alternatively, platelet-derived mEVs might transfer COX-1 and/or TXA_2 synthase to cancer cells, allowing them to produce TXB_2.

A comparison of the proteomic profiles of mEVs from CRC patients and HCs revealed 208 significantly altered proteins. High expression of HLA-B class I and PSMD2 in CRC patient mEVs was detected. The human leukocyte antigen (HLA) system or complex is a group of related proteins encoded by the major histocompatibility complex (MHC) gene; it has been reported that cell surface expression of HLA I/MHC I molecules is a marker of young, reactive platelets (Angénieux et al., 2019). PSMD2 is part of the ubiquitin-proteasome system and plays a role in immune modulation (Colberg et al., 2020). Platelets contain proteasome

and immunoproteasome components, allowing them to process foreign proteins into peptide fragments. These fragments are then loaded onto MHC I molecules and presented on the surface of the platelets as peptide-MHC I complexes. Immunoproteasomes may regulate platelets' involvement in innate and adaptive immunity, highlighting the connection between hemostasis and inflammation. The increased protein levels of HLA-B class I and PSMD2 found in platelet-derived mEVs from CRC patients by Contursi et al. (2023) suggest that platelet-derived mEVs are modulators of the immune response in CRC. A comprehensive examination of the protein composition and its alterations associated with cancer underscores the potential of platelet-derived mEV proteomics to facilitate early diagnosis, provide continuous monitoring, and support personalized treatment strategies, ultimately enhancing patient outcomes.

Conclusion

The complex and intricate interplay between inflammation and platelets in the development of tumors presents exciting opportunities for pioneering new avenues in cancer prevention and treatment strategies. A wealth of clinical and experimental evidence underscores platelets' pivotal and multifaceted role in fostering an inflammatory microenvironment that fuels tumor growth and progression. Moreover, platelets play a key role in the development of cancer metastasis. This huge amount of knowledge opens the way to using antiplatelet agents, such as low-dose aspirin, which exhibit considerable potential in dampening platelet activation and consequent inflammatory processes, thereby lowering cancer risk, particularly in cases of CRC (Patrignani and Patrono, 2016; 2018). It is necessary to investigate further the effectiveness of alternative antiplatelet medications, such as ADP $P2Y_{12}$ receptor antagonists (Ballerini et al., 2018). Other potential new antiplatelet drugs, such as revacept (Ungerer et al., 2011; Mayer et al., 2021) and selective 12-LOX inhibitors (Tourdot and Holinstat, 2017), currently under clinical development, are of interest due to their lower risk of bleeding (Sim et al., 2023).

The role of platelets in promoting the initial stages of cancer development is supported by various evidence, including studies using knockout mouse models and clinical research (Bruno et al., 2022; Patrignani and Patrono, 2016). Platelets contribute to inflammation by releasing various molecules and EVs. The molecules delivered by platelets activate different signaling pathways in the cells involved in inflammation and immunity (Patrignani and Patrono, 2018). Platelets are essential for cell-cell communication and significantly influence the phenotype of cellular components within the stromal compartment of tissues. An emerging and continuously evolving paradigm underscores the synergistic connection between cardiovascular disease (CVD) and cancer, elucidated by their shared modifiable risk factors, which encompass tobacco use, obesity, diabetes mellitus, dietary patterns, physical activity, and alcohol consumption. It is important to note that all these factors contribute to the activation of platelets, making this response a key event in both cancer and cardiovascular disease (Patrignani and Patrono, 2016; Davì and Patrono, 2007). This helps explain why using antiplatelet agents like low-dose aspirin effectively prevents cardiovascular disease and possibly cancer (Patrignani and Patrono, 2016). Platelet activation results in an increased generation of TXA_2 and PGE_2, subsequently triggering the activation of immune cells, fibroblasts, and endothelial cells. Thus, the inhibition of platelet function effectively impedes the release of molecules from platelets involved in initial events linked to tumorigenesis (Patrignani and Patrono, 2016). In cases where cancer has already developed, antiplatelet agents are likely less effective because they have limited capacity to directly affect the cellular component of a cancerous lesion (Patrignani et al., 2024). However, platelets can infiltrate cancerous tissues (Bruno et al., 2022), which can lead to tumor immune evasion, inflammation, and EMT (Patrignani and Patrono, 2016; 2018). This suggests that antiplatelet agents could indirectly cause antitumor effects by reducing platelet accumulation in tumors.

Genetic alterations may affect an individual's response to aspirin. However, Frouws et al. (2017) reported that the mutation status of the BRAF and KRAS genes should not be regarded as reliable indicators for personalized aspirin therapy. In contrast, Liao et al. (2012) showed that tumors with mutations in the PIK3CA gene (which codes for the protein phosphatidylinositol 4,5-bisphosphate 3-kinase catalytic subunit alpha isoform) exhibit increased sensitivity to the effects of aspirin. Nonetheless, the underlying mechanisms explaining this association remain to be elucidated.

Ongoing clinical trials investigate aspirin's potential as an adjuvant cancer therapy in various doses and durations in CRC patients (Table 1). Some of these trials are targeting patients based on specific biomarkers. These trials are part of the Prospective Aspirin Meta-analysis, registered on PROSPERO in October 2023. The main objective of this meta-analysis is to ascertain the potential moderate effects of aspirin, both overall and within different subgroups. These subgroups include those defined by tumor location (right-sided versus left-sided) and specific biomarkers.

At long follow-up, aspirin (300 mg BID) has been shown to prevent Lynch Syndrome (LS) cancers, including CRC (Burn et al., 2008; 2011; 2020). LS is a dominantly inherited cancer predisposition syndrome characterized by an increased risk of numerous cancers. LS-associated tumors are mismatch repair deficient (Engel et al., 2020). Aspirin is now recommended in NICE guidelines to prevent CRC in LS (National Institute for Health and Care, 2020; Serrano et al., 2022). CaPP3 trial (https://www.capp3.org/) is ongoing to define the most appropriate aspirin dose in LS. The trial is a non-inferiority study comparing daily aspirin of 600, 300, and 100 mg (100 mg/d is the dose recommended for preventing CVD). The finding of comparable efficacy of the higher doses versus the low dose of aspirin (100 mg/d) would support the platelet hypothesis in tumorigenesis (Patrignani and Patrono, 2016; 2018), thus opening the way to its use for cancer prevention in LS.

However, chronic aspirin use, even at low doses, can be associated with increased bleeding (Patrono and Baigent, 2019), especially in older individuals. Therefore, the decision to treat individual patients with low-dose aspirin should consider the bleeding risk weighed against CVD prevention and cancer benefits.

In the current era of precision medicine, developing treatment protocols involving the safe utilization of antiplatelet agents to prevent cancer and cardiovascular disease necessitates adopting a

TABLE 1 Ongoing Phase III placebo-controlled trials for aspirin in adjuvant colorectal cancer.

Trial (Clinical trials ID)	Patients (number)	Aspirin dose (duration)	Primary/Secondary endpoint	Actual status
Add-Aspirin (NCT02804815)	Stage II/III or IV CRC with completely resected liver metastasis (2332)	100 mg and 300 mg (5 years)	DFS/OS	Recruiting
ASCOLT (NCT00565708)	Dukes C and high-risk B colon and rectal cancers (1587)	200 mg (3 years)	DFS/OS	Active, not recruiting
EPISODE-III (Japan Registry of Clinical Trials as jRCTs031180009)	Stage III CRC following curative resection (880)	100 mg (3 years)	DFS/OS	Recruiting
ASPIRIN (NCT02301286, NCT03464305)	Stage II/III colon cancer in Netherlands and Belgium (770)	80 mg (5years)	DFS/OS	Active, not recruiting
ALASCCA (NCT02647099)	Stage II-III CRC with PI3K mutation (627)	160 mg (3 years)	DFS/OS	Active, not recruiting
ASAC (NCT03326791)	CRC with resected liver metastasis (446)	160 mg (3years)	DFS/OS	Active, not recruiting
ASPIK (NCT02945033)	Stage II-III CRC with PI3K mutation (134)	100 mg (3 years)	DFS/OS	Recruiting
SAKK 41/13 (NCT02467582)	Stage II-III CRC with PI3K mutation (113)	300 mg (3years)	DFS/OS	Active, not recruiting

Aspirin for Dukes' C and high-risk Dukes' B colorectal cancers (ASCOLT); Efficacy of aspirin for stage III, colorectal cancer: a randomized double-blind placebo-controlled trial (EPISODE III); Adjuvant Low Dose Aspirin in Colorectal Cancer (ALASCCA); Aspirin in Colorectal Cancer Liver Metastases (ASAC); Aspirin Versus Placebo in Resected Colon Cancer With PI3K Mutation Stage III, or II, High Risk (ASPIK); Colorectal cancer (CRC); Disease free survival (DFS); Overall survival (OS).

systems biology approach. This strategy entails a comprehensive analysis of heterogeneous datasets, including genomics, epigenomics, proteomics, lipidomics, and clinical data, at the level of the individual patient. This procedure involves dynamic systems modeling to identify candidate pathways that contribute to the benefits and harms of aspirin and possibly other antiplatelet agents. Additionally, this strategy will help identify susceptibility profiles for CRC and possibly other types of cancer, verifying whether platelet- and EV-based liquid biopsy can predict the onset and recurrence of cancer.

Author contributions

AC: Funding acquisition, Writing–review and editing, Writing–original draft. ST: Funding acquisition, Writing–review and editing, Writing–original draft. SDB: Writing–review and editing. ADM: Writing–review and editing. PP: Writing–review and editing, Conceptualization, Funding acquisition, Writing–original draft.

Funding

The author(s) declare that financial support was received for the research, authorship, and/or publication of this article. This review was funded by Associazione Italiana per la Ricerca sul Cancro (AIRC) [under IG 2017- ID. 20365 Project; Principal Investigator PP], and by Ministero dell'Istruzione, dell'Università e della Ricerca (MIUR) [Fondi per la Ricerca Scientifica di Ateneo, (ex 60%)] to PP and ST. In addition, this work was conducted on behalf of the Aspirin for Cancer Prevention Group, Wolfson Institute of Preventive Medicine, Queen Mary School of Medicine and Dentistry, University of London (United Kingdom). Moreover, it was funded by the European Union - European Social Fund - PON Research and Innovation 2014–2020 to AC.

Conflict of interest

The authors declare that the research was conducted in the absence of any commercial or financial relationships that could be construed as a potential conflict of interest.

The author(s) declared that they were an editorial board member of Frontiers, at the time of submission. This had no impact on the peer review process and the final decision.

Generative AI statement

The author(s) declare that no Generative AI was used in the creation of this manuscript.

Publisher's note

References

Adili, B. E. T., Mast, K., Yeung, J., Freedman, J. C., Green, A., Luci, D. K., et al. (2017). First selective 12-LOX inhibitor, ML355, impairs thrombus formation and vessel occlusion *in vivo* with minimal effects on hemostasis. *Arterioscler. Thromb. Vasc. Biol.* 37, 1828–1839. doi:10.1161/ATVBAHA.117.309868

Ahmed, I., Majeed, A., and Powell, R. (2007). Heparin induced thrombocytopenia: diagnosis and management update. *Postgrad. Med. J.* 83 (983), 575–582. doi:10.1136/pgmj.2007.059188

Ali, R. A., Wuescher, L. M., and Worth, R. G. (2015). Platelets: essential components of the immune system. *Curr. Trends Immunol.* 16, 65–78.

Angénieux, C., Dupuis, A., Gachet, C., de la Salle, H., and Maître, B. (2019). Cell surface expression of HLA I molecules as a marker of young platelets. *J. Thromb. Haemost.* 17 (9), 1511–1521. doi:10.1111/jth.14537

Arepally, G. M., and Padmanabhan, A. (2021). Heparin-induced thrombocytopenia: a focus on thrombosis. *Arterioscler. Thromb. Vasc. Biol.* 41 (1), 141–152. doi:10.1161/ATVBAHA.120.315445

Arman, M., and Krauel, K. (2015). Human platelet IgG Fc receptor FcγRIIA in immunity and thrombosis. *J. Thromb. Haemost.* 13 (6), 893–908. doi:10.1111/jth.12905

Bach, D. H., Lee, S. K., and Sood, A. K. (2019). Circular RNAs in cancer. *Mol. Ther. Nucleic Acids* 16, 118–129. doi:10.1016/j.omtn.2019.02.005

Baj-Krzyworzeka, M., Majka, M., Pratico, D., Ratajczak, J., Vilaire, G., Kijowski, J., et al. (2002). Platelet-derived microparticles stimulate proliferation, survival, adhesion, and chemotaxis of hematopoietic cells. *Exp. Hematol.* 30, 450–459. doi:10.1016/s0301-472x(02)00791-9

Balkwill, F., Charles, K. A., and Mantovani, A. (2005). Smoldering and polarized inflammation in the initiation and promotion of malignant disease. *Cancer Cell* 7 (3), 211–217. doi:10.1016/j.ccr.2005.02.013

Ballerini, P., Dovizio, M., Bruno, A., Tacconelli, S., and Patrignani, P. (2018). $P2Y_{12}$ receptors in tumorigenesis and metastasis. *Front. Pharmacol.* 9, 66. doi:10.3389/fphar.2018.00066

Barron, D. A., and Rowley, D. R. (2012). The reactive stroma microenvironment and prostate cancer progression. *Endocr. Relat. Cancer* 19 (6), R187–R204. doi:10.1530/ERC-12-0085

Barry, O. P., Kazanietz, M. G., Praticò, D., and FitzGerald, G. A. (1999). Arachidonic acid in platelet microparticles up-regulates cyclooxygenase-2-dependent prostaglandin formation via a protein kinase C/mitogen-activated protein kinase-dependent pathway. *J. Biol. Chem.* 274, 7545–7556. doi:10.1074/jbc.274.11.7545

Barry, O. P., Pratico, D., Lawson, J. A., and FitzGerald, G. A. (1997). Transcellular activation of platelets and endothelial cells by bioactive lipids in platelet microparticles. *J. Clin. Investigation* 99, 2118–2127. doi:10.1172/JCI119385

Battinelli, E. M., Markens, B. A., Kulenthirarajan, R. A., Machlus, K. R., Flaumenhaft, R., and Italiano, J. E., Jr (2014). Anticoagulation inhibits tumor cell-mediated release of platelet angiogenic proteins and diminishes platelet angiogenic response. *Blood* 123 (1), 101–112. doi:10.1182/blood-2013-02-485011

Bertagnolli, M. M., Eagle, C. J., Zauber, A. G., Redston, M., Solomon, S. D., Kim, K., et al. (2006). Celecoxib for the prevention of sporadic colorectal adenomas. *N. Engl. J. Med.* 355 (9), 873–884. doi:10.1056/NEJMoa061355

Best, M. G., Sol, N., Kooi, I., Tannous, J., Westerman, B. A., Rustenburg, F., et al. (2015). RNA-seq of tumor-educated platelets enables blood-based pan-cancer, multiclass, and molecular pathway cancer diagnostics. *Cancer Cell* 28 (5), 666–676. doi:10.1016/j.ccell.2015.09.018

Boerrigter, E., Groen, L. N., Van Erp, N. P., Verhaegh, G. W., and Schalken, J. A. (2020). Clinical utility of emerging biomarkers in prostate cancer liquid biopsies. *Expert Rev. Mol. Diagn* 20 (2), 219–230. doi:10.1080/14737159.2019.1675515

Boucharaba, A., Serre, C. M., Grès, S., Saulnier-Blache, J. S., Bordet, J. C., Guglielmi, J., et al. (2004). Platelet-derived lysophosphatidic acid supports the progression of osteolytic bone metastases in breast cancer. *J. Clin. Invest* 114, 1714–1725. doi:10.1172/JCI22123

Boucharaba, A., Serre, C. M., Guglielmi, J., Bordet, J. C., Clézardin, P., and Peyruchaud, O. (2006). The type 1 lysophosphatidic acid receptor is a target for therapy in bone metastases. *Proc. Natl. Acad. Sci. U. S. A.* 103, 9643–9648. doi:10.1073/pnas.0600979103

Boukerche, H., Berthier-Vergnes, O., Tabone, E., Doré, J. F., Leung, L. L., and McGregor, J. L. (1989). Platelet-melanoma cell interaction is mediated by the glycoprotein IIb-IIIa complex. *Blood* 74, 658–663. doi:10.1182/blood.v74.2.658.bloodjournal742658

Boulaftali, Y., Hess, P. R., Kahn, M. L., and Bergmeier, W. (2014). Platelet immunoreceptor tyrosine-based activation motif (ITAM) signaling and vascular integrity. *Circ. Res.* 114 (7), 1174–1184. doi:10.1161/CIRCRESAHA.114.301611

Boylan, B., Gao, C., Rathore, V., Gill, J. C., Newman, D. K., and Newman, P. J. (2008). Identification of FcgammaRIIa as the ITAM-bearing receptor mediating alphaIIbbeta3 outside-in integrin signaling in human platelets. *Blood* 112 (7), 2780–2786. doi:10.1182/blood-2008-02-142125

Bruno, A., Contursi, A., Tacconelli, S., Sacco, A., Hofling, U., Mucci, M., et al. (2022). The specific deletion of cyclooxygenase-1 in megakaryocytes/platelets reduces intestinal polyposis in $Apc^{Min/+}$ mice. *Pharmacol. Res.* 185, 106506. doi:10.1016/j.phrs.2022.106506

Burkhalter, R. J., Westfall, S. D., Liu, Y., and Stack, M. S. (2015). Lysophosphatidic acid initiates epithelial to mesenchymal transition and induces β-Catenin-mediated transcription in epithelial ovarian carcinoma. *J. Biol. Chem.* 290, 22143–22154. doi:10.1074/jbc.M115.641092

Burn, J., Bishop, D. T., Mecklin, J. P., Macrae, F., Möslein, G., Olschwang, S., et al. (2008). Effect of aspirin or resistant starch on colorectal neoplasia in the Lynch syndrome. *N. Engl. J. Med.* 359 (24), 2567–2578. doi:10.1056/NEJMoa0801297

Burn, J., Gerdes, A. M., Macrae, F., Mecklin, J. P., Moeslein, G., Olschwang, S., et al. (2011). Long-term effect of aspirin on cancer risk in carriers of hereditary colorectal cancer: an analysis from the CAPP2 randomised controlled trial. *Lancet* 378 (9809), 2081–2087. doi:10.1016/S0140-6736(11)61049-0

Burn, J., Sheth, H., Elliott, F., Reed, L., Macrae, F., Mecklin, J. P., et al. (2020). Cancer prevention with aspirin in hereditary colorectal cancer (Lynch syndrome), 10-year follow-up and registry-based 20-year data in the CAPP2 study: a double-blind, randomised, placebo-controlled trial. *Lancet* 395 (10240), 1855–1863. doi:10.1016/S0140-6736(20)30366-4

Celis, P. M., Celis, A., Nielsen, H. V., and Gesser, B. (1987). Cyclin (PCNA, auxiliary protein of DNA polymerase delta) is a central component of the pathway(s) leading to DNA replication and cell division. *FEBS Lett.* 220, 1–7. doi:10.1016/0014-5793(87)80865-7

Chen, L., Deng, H., Cui, H., Fang, J., Zuo, Z., Deng, J., et al. (2017). Inflammatory responses and inflammation-associated diseases in organs. *Oncotarget* 9 (6), 7204–7218. doi:10.18632/oncotarget.23208

Chitu, V., and Stanley, E. R. (2006). Colony-stimulating factor-1 in immunity and inflammation. *Curr. Opin. Immunol.* 18 (1), 39–48. doi:10.1016/j.coi.2005.11.006

Cloutier, N., Allaeys, I., Marcoux, G., Machlus, K. R., Mailhot, B., Zufferey, A., et al. (2018). Platelets release pathogenic serotonin and return to circulation after immune complex-mediated sequestration. *PNAS* 115, E1550-E1559–E1559. doi:10.1073/pnas.1720553115

Coenen, D. M., Heinzmann, A. C. A., Karel, M. F. A., Cosemans, JMEM, and Koenen, R. R. (2021). The multifaceted contribution of platelets in the emergence and aftermath of acute cardiovascular events. *Atherosclerosis* 319, 132–141. doi:10.1016/j.atherosclerosis.2020.12.017

Colberg, L., Cammann, C., Greinacher, A., and Seifert, U. (2020). Structure and function of the ubiquitin-proteasome system in platelets. *J. Thromb. Haemost.* 18, 771–780. doi:10.1111/jth.14730

Contursi, A., Fullone, R., Szklanna-Koszalinska, P., Marcone, S., Lanuti, P., Taus, F., et al. (2023). Tumor-educated platelet extracellular vesicles: proteomic profiling and crosstalk with colorectal cancer cells. *Cancers (Basel)* 15 (2), 350. doi:10.3390/cancers15020350

Contursi, A., Sacco, A., Grande, R., Dovizio, M., and Patrignani, P. (2017). Platelets as crucial partners for tumor metastasis: from mechanistic aspects to pharmacological targeting. *Cell. Mol. Life Sci.* 74, 3491–3507. doi:10.1007/s00018-017-2536-7

Contursi, A., Schiavone, S., Dovizio, M., Hinz, C., Fullone, R., Tacconelli, S., et al. (2021). Platelets induce free and phospholipid-esterified 12-hydroxyeicosatetraenoic acid generation in colon cancer cells by delivering 12-lipoxygenase. *J. Lipid Res.* 62, 100109. doi:10.1016/j.jlr.2021.100109

Contursi, A., Tacconelli, S., Hofling, U., Bruno, A., Dovizio, M., Ballerini, P., et al. (2022). Biology and pharmacology of platelet-type 12-lipoxygenase in platelets, cancer cells, and their crosstalk. *Biochem. Pharmacol.* 205, 115252. doi:10.1016/j.bcp.2022.115252

Coussens, L. M., and Werb, Z. (2002). Inflammation and cancer. *Nature* 420 (6917), 860–867. doi:10.1038/nature01322

D'Agostino, I., Tacconelli, S., Bruno, A., Contursi, A., Mucci, L., Hu, X., et al. (2021). Low-dose Aspirin prevents hypertension and cardiac fibrosis when thromboxane A_2 is unrestrained. *Pharmacol. Res.* 170, 105744. doi:10.1016/j.phrs.2021.105744

Dahariya, S., Paddibhatla, I., Kumar, S., Raghuwanshi, S., Pallepati, A., and Gutti, R. K. (2019). Long non-coding RNA: classification, biogenesis and functions in blood cells. *Mol. Immunol.* 112, 82–92. doi:10.1016/j.molimm.2019.04.011

Danese, S., Motte, Cd C., and Fiocchi, C. (2004). Platelets in inflammatory bowel disease:clinical, pathogenic, and therapeutic implications. *Am. J. Gastroenterol.* 99, 938–945. doi:10.1111/j.1572-0241.2004.04129.x

Dang, T. O., Ogunniyi, A., Barbee, M. S., and Drilon, A. (2016). Pembrolizumab for the treatment of PD-L1 positive advanced or metastatic non-small cell lung cancer. *Expert Rev. Anticancer Ther.* 16 (1), 13–20. doi:10.1586/14737140.2016.1123626

Davì, G., and Patrono, C. (2007). Platelet activation and atherothrombosis. *N. Engl. J. Med.* 357 (24), 2482–2494. doi:10.1056/NEJMra071014

De La Cruz, A., Hargrave, A., Magadi, S., Courson, J. A., Landry, P. T., Zhang, W., et al. (2021). Platelet and erythrocyte extravasation across inflamed corneal venules

depend on CD18, neutrophils, and mast cell degranulation. *Int. J. Mol. Sci.* 22 (14), 7360. doi:10.3390/ijms22147360

Delves, P. J., and Roitt, I. M. (2000). The immune system First of two parts. *N. Engl. J. Med.* 343 (1), 37–49. doi:10.1056/NEJM200007063430107

Diacovo, T. G., deFougerolles, A. R., Bainton, D. F., and Springer, T. A. (1994). A functional integrin ligand on the surface of platelets: intercellular adhesion molecule-2. *J. Clin. Invest* 94 (3), 1243–1251. doi:10.1172/JCI117442

Dovizio, M., Alberti, S., Guillem-Llobat, P., and Patrignani, P. (2014). Role of platelets in inflammation and cancer: novel therapeutic strategies. *Basic Clin. Pharmacol. Toxicol.* 114 (1), 118–127. doi:10.1111/bcpt.12156

Dovizio, M., Maier, T. J., Alberti, S., Di Francesco, L., Marcantoni, E., Munch, G., et al. (2013). Pharmacological inhibition of platelet-tumor cell cross-talk prevents platelet-induced overexpression of cyclooxygenase-2 in HT29 human colon carcinoma cells. *Mol. Pharmacol.* 84, 25–40. doi:10.1124/mol.113.084988

Dunn, G. P., Bruce, A. T., Ikeda, H., Old, L. J., and Schreiber, R. D. (2002). Cancer immunoediting: from immunosurveillance to tumor escape. *Nat. Immunol.* 3 (11), 991–998. doi:10.1038/ni1102-991

Elzey, B. D., Tian, J., Jensen, R. J., Swanson, A. K., Lees, J. R., Lentz, S. R., et al. (2003). Platelet-mediated modulation of adaptive immunity. A communication link between innate and adaptive immune compartments. *Immunity* 19, 9–19. doi:10.1016/s1074-7613(03)00177-8

Engel, C., Ahadova, A., Seppälä, T. T., Aretz, S., Bigirwamungu-Bargeman, M., Bläker, H., and German HNPCC Consortium, the Dutch Lynch Syndrome Collaborative Group (2020). Associations of pathogenic variants in MLH1, MSH2, and MSH6 with risk of colorectal adenomas and tumors and with somatic mutations in patients with Lynch syndrome. *Gastroenterology* 158 (5), 1326–1333. doi:10.1053/j.gastro.2019.12.032

Evangelista, V., Manarini, S., Sideri, R., Rotondo, S., Martelli, N., Piccoli, A., et al. (1999). Platelet/polymorphonuclear leukocyte interaction: P-selectin triggers protein-tyrosine phosphorylation-dependent CD11b/CD18 adhesion: role of PSGL-1 as a signaling molecule. *Blood* 93 (3), 876–885. doi:10.1182/blood.v93.3.876.403k25_876_885

Faour, W. H., He, Y., He, Q. W., de Ladurantaye, M., Quintero, M., Mancini, A., et al. (2001). Prostaglandin E(2) regulates the level and stability of cyclooxygenase-2 mRNA through activation of p38 mitogen-activated protein kinase in interleukin-1 beta-treated human synovial fibroblasts. *J. Biol. Chem.* 276 (34), 31720–31731. doi:10.1074/jbc.M104036200

Frouws, M. A., Reimers, M. S., Swets, M., Bastiaannet, E., Prinse, B., van Eijk, R., et al. (2017). The influence of BRAF and KRAS mutation status on the association between aspirin use and survival after colon cancer diagnosis. *PLoS One* 12 (1), e0170775. doi:10.1371/journal.pone.0170775

Gasecka, A., Nieuwland, R., van der Pol, E., Hajji, N., Ćwiek, A., Pluta, K., et al. (2019). P2Y12 antagonist ticagrelor inhibits the release of procoagulant extracellular vesicles from activated platelets. *Cardiol. J.* 26 (6), 782–789. doi:10.5603/CJ.a2018.0045

Gawaz, M., Geisler, T., and Borst, O. (2023). Current concepts and novel targets for antiplatelet therapy. *Nat. Rev. Cardiol.* 20 (9), 583–599. doi:10.1038/s41569-023-00854-6

Gawaz, M., Langer, H., and May, A. E. (2005). Platelets in inflammation and atherogenesis. *J. Clin. Invest* 115, 3378–3384. doi:10.1172/JCI27196

Gay, L. J., and Felding-Habermann, B. (2011). Contribution of platelets to tumour metastasis. *Nat. Rev. Cancer* 11, 123–134. doi:10.1038/nrc3004

Golebiewska, and Poole, A. W. (2015). Platelet secretion: from haemostasis to wound healing and beyond. *Blood Rev.* 29, 153–162. doi:10.1016/j.blre.2014.10.003

Goodall, A. H. (2014). Platelet 12-LOX scores a HIT. *Blood* 124 (14), 2166–2168. doi:10.1182/blood-2014-08-595652

Gresele, P., Falcinelli, E., Momi, S., Petito, E., and Sebastiano, M. (2021). Platelets and matrix metalloproteinases: a bidirectional interaction with multiple pathophysiologic implications. *Hamostaseologie* 41 (2), 136–145. doi:10.1055/a-1393-8339

Grosser, T., Fries, S., and FitzGerald, G. A. (2006). Biological basis for the cardiovascular consequences of COX-2 inhibition: therapeutic challenges and opportunities. *J. Clin. Invest* 116 (1), 4–15. doi:10.1172/JCI27291

Guidotti, L. G., and Chisari, F. V. (2006). Immunobiology and pathogenesis of viral hepatitis. *Annu. Rev. Pathology* 1, 23–61. doi:10.1146/annurev.pathol.1.110304.100230

Guillem-Llobat, P., Dovizio, M., Bruno, A., Ricciotti, E., Cufino, V., Sacco, A., et al. (2016). Aspirin prevents colorectal cancer metastasis in mice by splitting the crosstalk between platelets and tumor cells. *Oncotarget* 7, 32462–32477. doi:10.18632/oncotarget.8655

Ha, J. H., Ward, J. D., Radhakrishnan, R., Jayaraman, M., Song, Y. S., and Dhanasekaran, D. N. (2016). Lysophosphatidic acid stimulates epithelial to mesenchymal transition marker Slug/Snail2 in ovarian cancer cells via Gαi2, Src, and HIF1α signaling nexus. *Oncotarget* 7, 37664–37679. doi:10.18632/oncotarget.9224

Harrison, P., and Goodall, A. H. (2008). Message in the platelet-more than just vestigial mRNA. *Platelets* 19 (6), 395–404. doi:10.1080/09537100801990582

Henn, V., Slupsky, J. R., Gräfe, M., Anagnostopoulos, I., Förster, R., Müller-Berghaus, G., et al. (1998). CD40 ligand on activated platelets triggers an inflammatory reaction of endothelial cells. *Nature* 391, 591–594. doi:10.1038/35393

Hinterleitner, C., Strähle, J., Malenke, E., Hinterleitner, M., Henning, M., Seehawer, M., et al. (2021). Platelet PD-L1 reflects collective intratumoral PD-L1 expression and predicts immunotherapy response in non-small cell lung cancer. *Nat. Commun.* 12 (1), 7005. doi:10.1038/s41467-021-27303-7

Hu, H., Song, H., Han, B., Zhao, H., and He, J. (2024). Tumor-educated platelet RNA and circulating free RNA: emerging liquid biopsy markers for different tumor types. *Front. Biosci. Landmark Ed.* 29 (2), 80. doi:10.31083/j.fbl2902080

Hussain, S. P., and Harris, C. C. (2007). Inflammation and cancer: an ancient link with novel potentials. *Int. J. Cancer* 121 (11), 2373–2380. doi:10.1002/ijc.23173

Italiano, J. E., Jr, Mairuhu, A. T., and Flaumenhaft, R. (2010). Clinical relevance of microparticles from platelets and megakaryocytes. *Curr. Opin. Hematol.* 17, 578–584. doi:10.1097/MOH.0b013e32833e77ee

Janowska-Wieczorek, A., Wysoczynski, M., Kijowski, J., Marquez-Curtis, L., Machalinski, B., Ratajczak, J., et al. (2005). Microvesicles derived from activated platelets induce metastasis and angiogenesis in lung cancer. *Int. J. Cancer* 113, 752–760. doi:10.1002/ijc.20657

Joung, J. K., and Sander, J. D. (2013). TALENs: a widely applicable technology for targeted genome editing. *Nat. Rev. Mol. Cell Biol.* 14, 49–55. doi:10.1038/nrm3486

Juneja, V. R., McGuire, K. A., Manguso, R. T., LaFleur, M. W., Collins, N., Haining, W. N., et al. (2017). PD-L1 on tumor cells is sufficient for immune evasion in immunogenic tumors and inhibits CD8 T cell cytotoxicity. *J. Exp. Med.* 214, 895–904. doi:10.1084/jem.20160801

Kailashiya, J. (2018). Platelet-derived microparticles analysis: techniques, challenges and recommendations. *Anal. Biochem.* 546, 78–85. doi:10.1016/j.ab.2018.01.030

Kalluri, R., and Weinberg, R. A. (2009). The basics of epithelial-mesenchymal transition. *J. Clin. Investigation* 119, 1420–1428. doi:10.1172/JCI39104

Kalluri, R., and Zeisberg, M. (2006). Fibroblasts in cancer. *Nat. Rev. Cancer* 6 (5), 392–401. doi:10.1038/nrc1877

Kitamura, T., Qian, B. Z., and Pollard, J. W. (2015). Immune cell promotion of metastasis. *Nat. Rev. Immunol.* 15, 73–86. doi:10.1038/nri3789

Labelle, M., Begum, S., and Hynes, R. O. (2011). Direct signaling between platelets and cancer cells induces an epithelial-mesenchymal-like transition and promotes metastasis. *Cancer Cell* 20, 576–590. doi:10.1016/j.ccr.2011.09.009

Laffont, B., Corduan, A., Plé, H., Duchez, A. C., Cloutier, N., Boilard, E., et al. (2013). Activated platelets can deliver mRNA regulatory Ago2·microRNA complexes to endothelial cells via microparticles. *Blood* 122, 253–261. doi:10.1182/blood-2013-03-492801

Lauder, S. N., Allen-Redpath, K., Slatter, D. A., Aldrovandi, M., O'Connor, A., Farewell, D., et al. (2017). Networks of enzymatically oxidized membranelipids support calcium-dependent coagulation factor binding to maintain hemostasis. *Sci. Signal.* 10, eaan2787. doi:10.1126/scisignal.aan2787

Leblanc, R., Lee, S. C., David, M., Bordet, J. C., Norman, D. D., Patil, R., et al. (2014). Interaction of platelet-derived autotaxin with tumor integrin αVβ3 controls metastasis of breast cancer cells to bone. *Blood* 124, 3141–3150. doi:10.1182/blood-2014-04-568683

Li, S., Jiang, M., Wang, L., and Yu, S. (2020). Combined chemotherapy with cyclooxygenase-2 (COX-2) inhibitors in treating human cancers: recent advancement. *Biomed. Pharmacother.* 129, 110389. doi:10.1016/j.biopha.2020.110389

Liao, X., Lochhead, P., Nishihara, R., Morikawa, T., Kuchiba, A., Yamauchi, M., et al. (2012). Aspirin use, tumor PIK3CA mutation, and colorectal-cancer survival. *N. Engl. J. Med.* 367 (17), 1596–1606. doi:10.1056/NEJMoa1207756

Libby, P. (2012). Inflammation in atherosclerosis. *Arterioscler. Thromb. Vasc. Biol.* 32 (9), 2045–2051. doi:10.1161/ATVBAHA.108.179705

Linke, B., Schreiber, Y., Picard-Willems, B., Slattery, P., Nüsing, R. M., Harder, S., et al. (2017). Activated platelets induce an anti-inflammatory response of monocytes/macrophages through cross-regulation of PGE2 and cytokines. *Mediat. Inflamm.* 2017, 1463216. doi:10.1155/2017/1463216

Luci, D. K., Jameson, J. B. 2nd, Yasgar, A., Diaz, G., Joshi, N., Kantz, A., et al. (2014). Synthesis and structure-activity relationship studies of 4-((2-hydroxy-3-methoxybenzyl)amino)benzenesulfonamide derivatives as potent and selective inhibitors of 12-lipoxygenase. *J. Med. Chem.* 57 (2), 495–506. doi:10.1021/jm4016476

Mahajan, A., Brunson, A., Adesina, O., Keegan, T. H. M., and Wun, T. (2022). The incidence of cancer-associated thrombosis is increasing over time. *Blood Adv.* 6, 307–320. doi:10.1182/bloodadvances.2021005590

Mammadova-Bach, E., Gil-Pulido, J., Sarukhanyan, E., Burkard, P., Shityakov, S., Schonhart, C., et al. (2020). Platelet glycoprotein VI promotes metastasis through interaction with cancer cell-derived galectin-3. *Blood* 135 (14), 1146–1160. doi:10.1182/blood.2019002649

Mammadova-Bach, E., Zigrino, P., Brucker, C., Bourdon, C., Freund, M., De Arcangelis, A., et al. (2016). Platelet integrin α6β1 controls lung metastasis through direct binding to cancer cell-derived ADAM9. *JCI Insight* 1, e88245. doi:10.1172/jci.insight.88245

Mannori, G., Crottet, P., Cecconi, O., Hanasaki, K., Aruffo, A., Nelson, R. M., et al. (1995). Differential colon cancer cell adhesion to E-P-and L-selectin: role of mucin-type glycoproteins. *Cancer Res.* 55 (19), 4425–4431.

Mantovani, A., Allavena, P., Sica, A., and Balkwill, F. (2008). Cancer-related inflammation. *Nature* 454 (7203), 436–444. doi:10.1038/nature07205

Mantovani, A., and Pierotti, M. A. (2008). Cancer and inflammation: a complex relationship. *Cancer Lett.* 267 (2), 180–181. doi:10.1016/j.canlet.2008.05.003

Marrugo-Ramírez, J., Mir, M., and Samitier, J. (2018). Blood-based cancer biomarkers in liquid biopsy: a promising non-invasive alternative to tissue biopsy. *Int. J. Mol. Sci.* 19 (10), 2877. doi:10.3390/ijms19102877

Martin, P., and Leibovich, S. J. (2005). Inflammatory cells during wound repair: the good, the bad and the ugly. *Trends Cell Biol.* 15 (11), 599–607. doi:10.1016/j.tcb.2005.09.002

Massagué, J., and Obenauf, A. C. (2016). Metastatic colonization by circulating tumour cells. *Nature* 529 (7586), 298–306. doi:10.1038/nature17038

Mayer, K., Hein-Rothweiler, R., Schüpke, S., Janisch, M., Bernlochner, I., Ndrepepa, G., et al. (2021). Efficacy and safety of revacept, a novel lesion-directed competitive antagonist to platelet glycoprotein VI, in patients undergoing elective percutaneous coronary intervention for stable ischemic heart disease: the randomized, double-blind, placebo-controlled ISAR-PLASTER phase 2 trial. *JAMA Cardiol.* 6 (7), 753–761. doi:10.1001/jamacardio.2021.0475

Menter, D. G., Schilsky, R. L., and DuBois, R. N. (2010). Cyclooxygenase-2 and cancer treatment: understanding the risk should be worth the reward. *Clin. Cancer Res.* 16 (5), 1384–1390. doi:10.1158/1078-0432.CCR-09-0788

Michael, J. V., Wurtzel, J. G. T., Mao, G. F., Rao, A. K., Kolpakov, M. A., Sabri, A., et al. (2017). Platelet microparticles infiltrating solid tumors transfer miRNAs that suppress tumor growth. *Blood* 130 (5), 567–580. doi:10.1182/blood-2016-11-751099

Mills, G. B., and Moolenaar, W. H. (2003). The emerging role of lysophosphatidic acid in cancer. *Nat. Rev. Cancer* 3, 582–591. doi:10.1038/nrc1143

Mitrugno, A., Williams, D., Kerrigan, S. W., and Moran, N. (2014). A novel and essential role for FcγRIIa in cancer cell-induced platelet activation. *Blood* 123, 249–260. doi:10.1182/blood-2013-03-492447

Momi, S., Falcinelli, E., Petito, E., Ciarrocca Taranta, G., Ossoli, A., and Gresele, P. (2022). Matrix metalloproteinase-2 on activated platelets triggers endothelial PAR-1 initiating atherosclerosis. *Eur. Heart J.* 43 (6), 504–514. doi:10.1093/eurheartj/ehab631

Moser, C. L., Gould, K. A., McNeley, M. K., Shoemaker, A. R., and Dove, W. F. (1995). ApcMin: a mouse model for intestinal and mammary tumorigenesis. *Eur. J. Cancer 31A*, 1061–1064. doi:10.1016/0959-8049(95)00181-h

Nagalla, S., Shaw, C., Kong, X., Kondkar, A. A., Edelstein, L. C., Ma, L., et al. (2011). Platelet microRNA-mRNA coexpression profiles correlate with platelet reactivity. *Blood* 117 (19), 5189–5197. doi:10.1182/blood-2010-09-299719

National Institute for Health and Care (2020). *Excellence NICE-effectiveness of aspirin in the prevention of colorectal cancer in people with Lynch syndrome*. London, UK: National Institute for Health and Care.

Negus, R. P., Stamp, G. W., Hadley, J., and Balkwill, F. R. (1997). Quantitative assessment of the leukocyte infiltrate in ovarian cancer and its relationship to the expression of C-C chemokines. *Am. J. Pathol.* 150 (5), 1723–1734.

Nierodzik, M. L., and Karpatkin, S. (2006). Thrombin induces tumor growth, metastasis, and angiogenesis: evidence for a thrombin-regulated dormant tumor phenotype. *Cancer Cell* 10 (5), 355–362. doi:10.1016/j.ccr.2006.10.002

Nilsson, R. J., Balaj, L., Hulleman, E., van Rijn, S., Pegtel, D. M., Walraven, M., et al. (2011). Blood platelets contain tumor-derived RNA biomarkers. *Blood* 118 (13), 3680–3683. doi:10.1182/blood-2011-03-344408

Nilsson, R. J., Karachaliou, N., Berenguer, J., Gimenez-Capitan, A., Schellen, P., Teixido, C., et al. (2016). Rearranged EML4-ALK fusion transcripts sequester in circulating blood platelets and enable blood-based crizotinib response monitoring in non-small-cell lung cancer. *Oncotarget* 7 (1), 1066–1075. doi:10.18632/oncotarget.6279

Oshima, M., Dinchuk, J. E., Kargman, S. L., Oshima, H., Hancock, B., Kwong, E., et al. (1996). Suppression of intestinal polyposis in Apc delta716 knockout mice by inhibition of cyclooxygenase 2 (COX-2). *Cell* 87 (5), 803–809. doi:10.1016/s0092-8674(00)81988-1

Patrignani, P., and Patrono, C. (2015). Cyclooxygenase inhibitors: from pharmacology to clinical read-outs. *Biochim. Biophys. Acta* 1851, 422–432. doi:10.1016/j.bbalip.2014.09.016

Patrignani, P., and Patrono, C. (2016). Aspirin and cancer. *J. Am. Coll. Cardiol.* 68, 967–976. doi:10.1016/j.jacc.2016.05.083

Patrignani, P., and Patrono, C. (2018). Aspirin, platelet inhibition and cancer prevention. *Platelets* 29 (8), 779–785. doi:10.1080/09537104.2018.1492105

Patrignani, P., Tacconelli, S., Piazuelo, E., Di Francesco, L., Dovizio, M., Sostres, C., et al. (2014). Reappraisal of the clinical pharmacology of low-dose aspirin by comparing novel direct and traditional indirect biomarkers of drug action. *J. Thromb. Haemost.* 12 (8), 1320–1330. doi:10.1111/jth.12637

Patrignani, P., Tacconelli, S., Contursi, A., Piazuelo, E., Bruno, A., Nobili, S., et al. (2024). Optimizing aspirin dose for colorectal cancer patients through deep phenotyping using novel biomarkers of drug action. *Front. Pharmacol.* 29;15, 1362217. doi:10.3389/fphar.2024.1362217

Patrono, C., and Baigent, C. (2019). Role of aspirin in primary prevention of cardiovascular disease. *Nat. Rev. Cardiol.* 16 (11), 675–686. doi:10.1038/s41569-019-0225-y

Patrono, C., García Rodríguez, L. A., Landolfi, R., and Baigent, C. (2005). Low-dose aspirin for the prevention of atherothrombosis. *N. Engl. J. Med.* 353 (22), 2373–2383. doi:10.1056/NEJMra052717

Patrono, C., Patrignani, P., and García Rodríguez, L. A. (2001). Cyclooxygenase selective inhibition of prostanoid formation: transducing biochemical selectivity into clinical read-outs. *J. Clin. Invest* 108, 7–13. doi:10.1172/JCI13418

Petito, E., Momi, S., and Gresele, P. (2017). "The migration of platelets and their interaction with other migrating cells," in *Platelets in thrombotic and non-thrombotic disorders*. Editors P. Gresele, N. Kleiman, J. Lopez, and C. Page (Cham, Switzerland: Springer), 337–351. Ray MK, Fagan SP, and Brunicardi.

Pitchford, S. C., Momi, S., Baglioni, S., Casali, L., Giannini, S., Rossi, R., et al. (2008). Allergen induces the migration of platelets to lung tissue in allergic asthma. *Am. J. Respir. Crit. Care Med.* 177 (6), 604–612. doi:10.1164/rccm.200702-214OC

Pitchford, S. C., Momi, S., Giannini, S., Casali, L., Spina, D., Page, C. P., et al. (2005). Platelet P-selectin is required for pulmonary eosinophil and lymphocyte recruitment in a murine model of allergic inflammation. *Blood* 105 (5), 2074–2081. doi:10.1182/blood-2004-06-2282

Pitchford, S. C., Yano, H., Lever, R., Riffo-Vasquez, Y., Ciferri, S., Rose, M. J., et al. (2003). Platelets are essential for leukocyte recruitment in allergic inflammation. *J. Allergy Clin. Immunol.* 112 (1), 109–118. doi:10.1067/mai.2003.1514

Placke, T., Örgel, M., Schaller, M., Jung, G., Rammensee, H. G., Kopp, H. G., et al. (2012). Platelet-derived MHC class I confers a pseudonormal phenotype to cancer cells that subverts the antitumor reactivity of natural killer immune cells. *Cancer Res.* 72, 440–448. doi:10.1158/0008-5472.CAN-11-1872

Puhm, F., Boilard, E., and Machlus, K. R. (2021). Platelet extracellular vesicles: beyond the blood. *Arterioscler. Thromb. Vasc. Biol.* 41 (1), 87–96. doi:10.1161/ATVBAHA.120.314644

Rachidi, S., Metelli, A., Riesenberg, B., Wu, B. X., Nelson, M. H., Wallace, C., et al. (2017). Platelets subvert T cell immunity against cancer via GARP-TGFβ axis. *Sci. Immunol.* 2 (11), eaai7911. doi:10.1126/sciimmunol.aai7911

Rana, R., Huang, T., Koukos, G., Fletcher, E. K., Turner, S. E., Shearer, A., et al. (2018). Noncanonical matrix metalloprotease 1–protease-activated receptor 1 signaling drives progression of atherosclerosis. *Arterioscler. Thromb. Vasc. Biol.* 38, 1368–1380. doi:10.1161/ATVBAHA.118.310967

Ratajczak, J., Wysoczynski, M., Hayek, F., Janowska-Wieczorek, A., and Ratajczak, M. Z. (2006). Membrane-derived microvesicles: important and underappreciated mediators of cell-to-cell communication. *Leukemia* 20, 1487–1495. doi:10.1038/sj.leu.2404296

Risitano, A., Beaulieu, L. M., Vitseva, O., and Freedman, J. E. (2012). Platelets and platelet-like particles mediate intercellular RNA transfer. *Blood* 119, 6288–6295. doi:10.1182/blood-2011-12-396440

Rondina, M. T., Weyrich, A. S., and Zimmerman, G. A. (2013). Platelets as cellular effectors of inflammation in vascular diseases. *Circ. Res.* 112 (11), 1506–1519. doi:10.1161/CIRCRESAHA.113.300512

Ross, R., Bowen-Pope, D. F., and Raines, E. W. (1985). Platelets, macrophages, endothelium, and growth factors. Their effects upon cells and their possible roles in atherogenesis. *Ann. N. Y. Acad. Sci.* 454, 254–260. doi:10.1111/j.1749-6632.1985.tb11865.x

Rovati, G., Contursi, A., Bruno, A., Tacconelli, S., Ballerini, P., and Patrignani, P. (2022). Antiplatelet agents affecting GPCR signaling implicated in tumor metastasis. *Cells* 11 (4), 725. doi:10.3390/cells11040725

Rumbaut, R. E., and Thiagarajan, P. (2010). Platelet-vessel wall interactions in hemostasis and thrombosis. *San. Rafael Morgan Claypool Life Sci.* 2, 1–75. doi:10.4199/C00007ED1V01Y201002ISP004

Sacco, A., Bruno, A., Contursi, A., Dovizio, M., Tacconelli, S., Ricciotti, E., et al. (2019). Platelet-specific deletion of cyclooxygenase-1 ameliorates dextran sulfate sodium-induced colitis in mice. *J. Pharmacol. Exp. Ther.* 370 (3), 416–426. doi:10.1124/jpet.119.259382

Santoso, S., Sachs, U. J., Kroll, H., Linder, M., Ruf, A., Preissner, K. T., et al. (2002). The junctional adhesion molecule 3 (JAM-3) on human platelets is a counterreceptor for the leukocyte integrin Mac-1. *J. Exp. Med.* 196 (5), 679–691. doi:10.1084/jem.20020267

Serrano, D., Patrignani, P., Stigliano, V., Turchetti, D., Sciallero, S., Roviello, F., et al. (2022). Aspirin colorectal cancer prevention in Lynch syndrome: recommendations in the era of precision medicine. *Genes (Basel)* 13 (3), 460. doi:10.3390/genes13030460

Sim, M. M. S., Shiferawe, S., and Wood, J. P. (2023). Novel strategies in antithrombotic therapy: targeting thrombosis while preserving hemostasis. *Front. Cardiovasc Med.* 10, 1272971. doi:10.3389/fcvm.2023.1272971

Simon, D. I., Chen, Z., Xu, H., Li, C. Q., Dong, Jf, McIntire, L. V., et al. (2000). Platelet glycoprotein ibalpha is a counterreceptor for the leukocyte integrin Mac-1 (CD11b/CD18). *J. Exp. Med.* 192 (2), 193–204. doi:10.1084/jem.192.2.193

Sitia, G., Aiolfi, R., Di Lucia, P., Mainetti, M., Fiocchi, A., Mingozzi, F., et al. (2012). Antiplatelet therapy prevents hepatocellular carcinoma and improves survival in a mouse model of chronic hepatitis B. *Proc. Natl. Acad. Sci. U. S. A.* 109, E2165–E2172. doi:10.1073/pnas.1209182109

Skog, J., Würdinger, T., van Rijn, S., Meijer, D. H., Gainche, L., Sena-Esteves, M., et al. (2008). Glioblastoma microvesicles transport RNA and proteins that promote tumour growth and provide diagnostic biomarkers. *Nat. Cell Biol.* 10 (12), 1470–1476. doi:10.1038/ncb1800

Slatter, D. A., Percy, C. L., Allen-Redpath, K., Gajsiewicz, J. M., Brooks, N. J., Clayton, A., et al. (2018). Enzymatically oxidized phospholipids restore thrombin generation in coagulation factor deficiencies. *JCI Insight* 3 (6), e98459. doi:10.1172/jci.insight.98459

Smyth, S. S., McEver, R. P., Weyrich, A. S., Morrell, C. N., Hoffman, M. R., Arepally, G. M., et al. (2009). Platelet functions beyond hemostasis. *J. Thromb. Haemost.* 7 (11), 1759–1766. doi:10.1111/j.1538-7836.2009.03586.x

Stanger, L., and Holinstat, M. (2023). Bioactive lipid regulation of platelet function, hemostasis, and thrombosis. *Pharmacol. Ther.* 246, 108420. doi:10.1016/j.pharmthera.2023.108420

Tang, M., Jiang, L., Lin, Y., Wu, X., Wang, K., He, Q., et al. (2017). Platelet microparticle-mediated transfer of miR-939 to epithelial ovarian cancer cells promotes epithelial to mesenchymal transition. *Oncotarget* 8, 97464–97475. doi:10.18632/oncotarget.22136

Thomas, C. P., Morgan, L. T., Maskrey, B. H., Murphy, R. C., Kühn, H., Hazen, S. L., et al. (2010). Phospholipid-esterified eicosanoids are generated in agonist-activated human platelets and enhance tissue factor-dependent thrombin generation. *J. Biol. Chem.* 285 (10), 6891–6903. doi:10.1074/jbc.M109.078428

Timár, J., Rásó, E., Honn, K. V., and Hagmann, W. (1999). 12-lipoxygenase expression in human melanoma cell lines. *Adv. Exp. Med. Biol.* 469, 617–622. doi:10.1007/978-1-4615-4793-8_89

Tourdot, B. E., and Holinstat, M. (2017). Targeting 12-lipoxygenase as a potential novel antiplatelet therapy. *Trends Pharmacol. Sci.* 38 (11), 1006–1015. doi:10.1016/j.tips.2017.08.001

Tran, D. Q., Andersson, J., Wang, R., Ramsey, H., Unutmaz, D., and Shevach, E. M. (2009). GARP (LRRC32) is essential for the surface expression of latent TGF-beta on platelets and activated FOXP3+ regulatory T cells. *Proc. Natl. Acad. Sci. U. S. A.* 106 (32), 13445–13450. doi:10.1073/pnas.0901944106

Tripodi, A., and Mannucci, P. M. (2011). The coagulopathy of chronic liver disease. *N. Engl. J. Med.* 365, 147–156. doi:10.1056/NEJMra1011170

Turnage, R. H., LaNoue, J. L., Kadesky, K. M., Meng, Y., and Myers, S. I. (1985). Thromboxane A2 mediates increased pulmonary microvascular permeability after intestinal reperfusion. *J. Appl. Physiol.* 82 (2), 592–598. doi:10.1152/jappl.1997.82.2.592

Tuxhorn, J. A., Ayala, G. E., and Rowley, D. R. (2001). Reactive stroma in prostate cancer progression. *J. Urol.* 166 (6), 2472–2483. doi:10.1016/s0022-5347(05)65620-0

Tuxhorn, J. A., Ayala, G. E., Smith, M. J., Smith, V. C., Dang, T. D., and Rowley, D. R. (2002). Reactive stroma in human prostate cancer: induction of myofibroblast phenotype and extracellular matrix remodeling. *Clin. Cancer Res.* 8 (9), 2912–2923.

Ungerer, M., Rosport, K., Bültmann, A., Piechatzek, R., Uhland, K., Schlieper, P., et al. (2011). Novel antiplatelet drug revacept (Dimeric Glycoprotein VI-Fc) specifically and efficiently inhibited collagen-induced platelet aggregation without affecting general hemostasis in humans. *Circulation* 123, 1891–1899. doi:10.1161/CIRCULATIONAHA.110.980623

Varon, D., and Shai, E. (2015). Platelets and their microparticles as key players in pathophysiological responses. *J. Thromb. Haemost.* 13 (Suppl. 1), S40–S46. doi:10.1111/jth.12976

Vasina, E. M., Cauwenberghs, S., Feijge, M. A., Heemskerk, J. W., Weber, C., and Koenen, R. R. (2011). Microparticles from apoptotic platelets promote resident macrophage differentiation. *Cell Death and Dis.* 2, e211. doi:10.1038/cddis.2011.94

Vitiello, L., Spoletini, I., Gorini, S., Pontecorvo, L., Ferrari, D., Ferraro, E., et al. (2014). Microvascular inflammation in atherosclerosis. *IJC Metab. Endocr.* 3, 1–7. doi:10.1016/j.ijcme.2014.03.002

Wang, D., and DuBois, R. N. (2013). An inflammatory mediator, prostaglandin E2, in colorectal cancer. *Cancer J.* 19 (6), 502–510. doi:10.1097/PPO.0000000000000003

Weyrich, A. S., Elstad, M. R., McEver, R. P., McIntyre, T. M., Moore, K. L., Morrissey, J. H., et al. (1996). Activated platelets signal chemokine synthesis by human monocytes. *J. Clin. Invest* 97 (6), 1525–1534. doi:10.1172/JCI118575

Williams, J. R., Khandoga, A. L., Goyal, P., Fells, J. I., Perygin, D. H., Siess, W., et al. (2009). Unique ligand selectivity of the GPR92/LPA5 lysophosphatidate receptor indicates role in human platelet activation. *J. Biol. Chem.* 284, 17304–17319. doi:10.1074/jbc.M109.003194

Willis Fox, O., and Preston, R. J. S. (2020). Molecular basis of protease-activated receptor 1 signaling diversity. *J. Thromb. Haemost.* 18, 6–16. doi:10.1111/jth.14643

Wong, C. C., Baum, J., Silvestro, A., Beste, M. T., Bharani-Dharan, B., Xu, S., et al. (2020). Inhibition of IL-1β by canakinumab may be effective against diverse molecular subtypes of lung cancer: an exploratory analysis of the CANTOS trial. *Cancer Res.* 80 (24), 5597–5605. doi:10.1158/0008-5472.CAN-19-3176

Yang, J., Hirata, T., Croce, K., Merrill-Skoloff, G., Tchernychev, B., Williams, E., et al. (1999). Targeted gene disruption demonstrates that P-selectin glycoprotein ligand 1 (PSGL-1) is required for P-selectin-mediated but not E-selectin-mediated neutrophil rolling and migration. *J. Exp. Med.* 190 (12), 1769–1782. doi:10.1084/jem.190.12.1769

Yang, R. Y., Rabinovich, G. A., and Liu, F. T. (2008). Galectins: structure, function and therapeutic potential. *Expert Rev. Mol. Med.* 10, e17. doi:10.1017/S1462399408000719

Yeung, J., Tourdot, B. E., Fernandez-Perez, P., Vesci, J., Ren, J., Smyrniotis, C. J., et al. (2014). Platelet 12-LOX is essential for FcγRIIa-mediated platelet activation. *Blood* 124 (14), 2271–2279. doi:10.1182/blood-2014-05-575878

Yoshimoto, T., Arakawa, T., Hada, T., Yamamoto, S., and Takahashi, E. (1992). Structure and chromosomal localization of human arachidonate 12-lipoxygenase gene. *J. Biol. Chem.* 267, 24805–24809. doi:10.1016/s0021-9258(18)35835-6

Zhu, Y., Zhu, M., and Lance, P. (2012). IL1β-mediated Stromal COX-2 signaling mediates proliferation and invasiveness of colonic epithelial cancer cells. *Exp. Cell Res.* 318 (19), 2520–2530. doi:10.1016/j.yexcr.2012.07.021

frontiers | Frontiers in Pharmacology

TYPE Original Research
PUBLISHED 23 December 2024
DOI 10.3389/fphar.2024.1485915

OPEN ACCESS

EDITED BY
Angelo Sala,
University of Milan, Italy

REVIEWED BY
Venkatesh Pooladanda,
Massachusetts General Hospital and Harvard Medical School, United States
Anil Kumar Banothu,
P.V. Narsimha Rao Telangana Veterinary University, India

*CORRESPONDENCE
Wen Huang,
huangwen@scu.edu.cn
Guang Xin,
xinguang@scu.edu.cn

†These authors have contributed equally to this work and share first authorship

RECEIVED 25 August 2024
ACCEPTED 09 December 2024
PUBLISHED 23 December 2024

CITATION
Zhao X, Li F, Wen A, Yu X, Xu X, Wan C, Cao Y, Xin G and Huang W (2024) Elucidating the mechanism of stigmasterol in acute pancreatitis treatment: insights from network pharmacology and *in vitro*/*in vivo* experiments. *Front. Pharmacol.* 15:1485915. doi: 10.3389/fphar.2024.1485915

Elucidating the mechanism of stigmasterol in acute pancreatitis treatment: insights from network pharmacology and *in vitro*/*in vivo* experiments

Xuanlin Zhao[1†], Fan Li[1†], Ao Wen[1†], Xiuxian Yu[1], Xinrui Xu[1], Chengyu Wan[1], Yu Cao[2], Guang Xin[1*] and Wen Huang[1*]

[1]West China Center of Excellence for Pancreatitis, Institute of Integrated Traditional Chinese and Western Medicine, Natural and Biomimetic Medicine Research Center, Tissue-Orientated Property of Chinese Medicine Key Laboratory of Sichuan Province, West China School of Medicine, West China Hospital, Sichuan University, Chengdu, China, [2]Department of Emergency Medicine, West China School of Medicine, West China Hospital, Sichuan University, Chengdu, China

Introduction: Acute pancreatitis (AP) is a severe inflammatory disease of the pancreas that could trigger a systemic inflammation and multi-organ dysfunction. Stigmasterol, a natural plant sterol found in various herbs and vegetables, exhibits a significant anti-inflammatory, antioxidant, and cholesterol-lowering effects. However, its therapeutic potential in AP have not been thoroughly investigated.

Methods: The present study employed network pharmacology combined with experimental verification to explore the protective effect of stigmasterol on AP and its molecular mechanism in a sodium taurocholate (STC)-induced AP mouse model.

Results: Protein-protein interaction (PPI) analysis pinpointed out MAPK3, also named as ERK1, as a promising stigmasterol target in AP therapy. Molecular docking analysis further revealed a strong binding capacity of stigmasterol to ERK1 (−6.57 kL/mol). Furthermore, both *in vivo* and *in vitro* studies demonstrated that stigmasterol treatment notably attenuated STC-induced pancreatic injury, as evidented by decreased serum levels of lipase and amylase, improved systemic inflammation, and reduced acinar cell necrosis. At the molecular level, stigmasterol treatment exhibited a significant inhibition on STC-induced activation of ERK signaling pathway in pancreatic acinar cells, leading to the transition of acinar cell death from necrosis to apoptosis, thereby preventing acinar cell necrosis-induced systemic inflammation.

Conclusion: This study demonstrated that stigmasterol exhibits a significant protective effect aganist AP, at least in part through enhancing acinar cell apoptosis via modulating the ERK signaling pathways.

KEYWORDS

stigmasterol, acute pancreatitis, apoptosis, network pharmacology, molecular docking

1 Introduction

Acute pancreatitis (AP) is a potentially life-threatening condition characterized by acute inflammation of the pancreas (Xiao et al., 2016; Dambrauskas et al., 2010; Akinosoglou and Gogos, 2014), often accompanied by a systemic inflammatory response and, in severe cases, multi-organ dysfunction (Mederos et al., 2021; Mayerle et al., 2019). The pathophysiology of AP is complex, involving a cascade of events that begin with the activation of digestive enzymes within the pancreas, leading to autodigestion and subsequent inflammation. Nevertheless, the AP pathogenesis remains elusive, necessitating further clarification. The outcome of AP is determined by the type of acinar cell death. The type of cell death including inflammatory death (ferroptosis, pyroptosis) and non-inflammatory death (apoptosis, autophagy) (Mayerle et al., 2019) Previous studies have confirmed that apoptosis plays a role of self-protection in pancreatitis, mainly due to the fact that apoptosis activation can inhibit other inflammatory death processes and thus avoid the occurrence of systemic inflammation, but the specific mechanism of action is still unclear (Kaiser et al., 1995; Bhatia et al., 1998; Chen et al., 2019). Therefore, it is important to explore the mechanism of inflammatory response and acinar cells apoptosis.

Natural products, including plant-derived compounds, have long been recognized as sources of potential therapeutic agents due to their diverse biological activities and relatively low toxicity (Ma et al., 2011; Zhang et al., 2021), providing numerous new avenues for AP treatment. Phytosterols, naturally occurring steroids abundant in plant tissues, are renowned for their health-bolstering attributes. Consumption of phytosterol-rich diets curbs cardiovascular risk and displays potent anti-inflammatory (Garcia-Llatas and Rodriguez-Estrada, 2011; Moreau et al., 2002) and antioxidant capacities effects (Moreau et al., 2002; Ramu et al., 2016). Stigmasterol (Stigma), a natural plant sterol widely distributed in various herbs and vegetables (Ramu et al., 2016; Aboobucker and Suza, 2019), has garnered attention for its anti-inflammatory, antioxidant, and cholesterol-lowering properties (Liang et al., 2020; Yuan et al., 2019; Sun et al., 2019; Zhang et al., 2023). The multifaceted nature of stigmasterol's biological activities suggests that it may have potential in the treatment of inflammatory diseases, including AP. Recent studies show that the anti-oxidation and anti-inflammatory effects of Stigma may be related to its regulation of apoptosis (Lu et al., 2023), such as induced the activity of apoptotic proteins, including cleaved caspase-3, cleaved caspase-9, cytochrome c, and BAX. In view of the self-protective role of apoptosis in the progression of pancreatitis, we hypothesize that Stigma might promote the transformation of pancreatic acinar cells from necrosis to modulation, providing therapeutic potential in AP.

This study aims to explore the potential of stigmasterol in the context of AP using a combination of network pharmacology and experimental validation. Network pharmacology is an integrative approach that applies systems biology principles to analyze the interactions between drugs and biological systems, offering a comprehensive understanding of drug action (Xiong et al., 2020; Huang et al., 2017). This methodology is particularly well-suited for complex diseases like AP, where multiple pathways and targets are implicated in the disease process (Feng et al., 2024; Zhang et al., 2024). Specifically, we employed PPI analysis to identify potential stigmasterol targets in AP and then conducted molecular docking analysis to predict the binding affinity of stigmasterol to these targets. Using PPI and molecular docking, we found that MAPK3 (ERK1) is an effective target for the treatment of acute pancreatitis. Extracellular signal-regulated kinase 1 (ERK1) has been shown to play a crucial role in the pathogenesis of AP. As a member of the MAPK family, ERK1 is involved in cell proliferation, differentiation, and apoptosis. Modulating MAPK signaling pathways has been shown to promote the apoptosis of acinar cells while reducing inflammatory damage to the pancreas. However, it is unclear whether Stigma treatment would affect the ERK1 signaling pathway and result in the modulation of acinar cell apoptosis.

In this study we hypothesized that Stigma treatment could protect mice from pancreatic injury through enhancing cell apoptosis via modulating ERK1 signaling pathway. To address this hypothesis, we evaluated changes in pancreatic histology, serum amylase and lipase activities to elucidate the impact of Stigma on AP-induced damage at both cellular and systemic levels. Moreover, Western blotting, Immunohistochemical, and TUNEL Staining were conducted to determine the regulatory role of Stigma on cell apoptosis and ERK1 signaling pathway. The research route is illustrated in Figure 1.

2 Materials and methods

2.1 Chemicals and reagents

Stigmasterol (HY-N0131) were acquired from MCE (Shanghai, China). Cell counting kit-8 (MA0218-1) and Propidium Iodide (MB2920-1) was obtained from meilunbio (Dalian, China). Hoechst 33342 (40731ES10) were purchased from Yeasen Biotechnology Co, Ltd. (Shanghai, China). Calcein AM (C2012) was obtained from Beyotime Biotechnology (Shanghai, China). DeadEnd™ Fluorometric TUNEL System (G3250) were purchased from Promega (America).

2.2 Data collection

The PubChem database furnished the generic name, CID, and 3D configuration of Stigma. SwissTargetPrediction database contributed Stigma-derived target sets, while GeneCards sourced AP-associated targets. Commonality analysis among these targets was executed utilizing Venny 2.1.0 software.

2.3 Network analysis

Network analyses were conducted with Cytoscape 3.9.1, where nodes' significance was quantified by scores, inversely correlated with color intensity. STRING facilitated the construction of a PPI network for shared targets, revealing interconnected target clusters. Within these clusters, the most significant node, designated SEED, emerged as a potential cluster key target. Consequently, the top 15 genes and SEEDs were prioritized as crucial hubs from the PPI landscape.

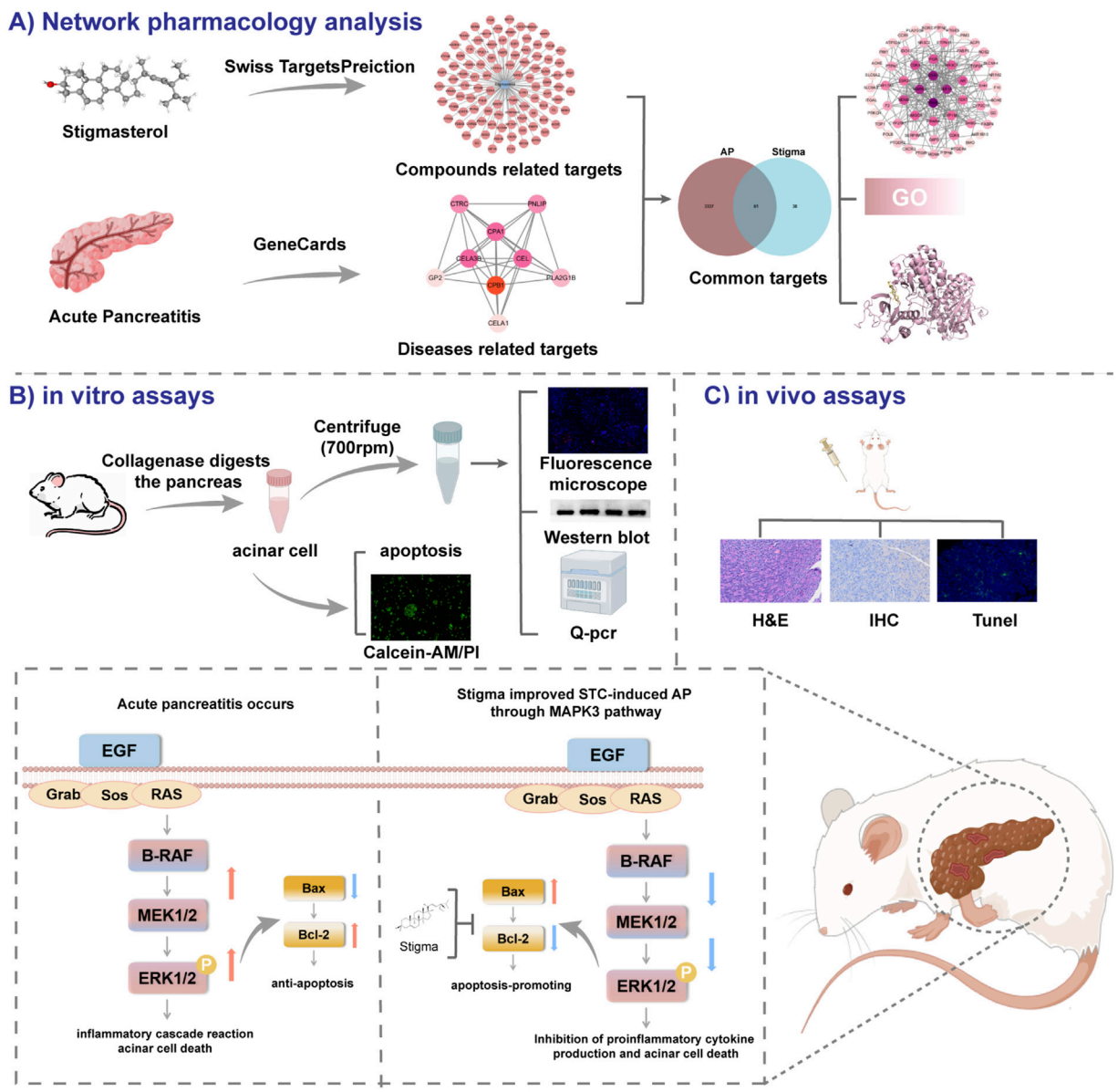

FIGURE 1
All technical approaches rely on network pharmacology and experimental verification. **(A)** Network Pharmacology Analysis. **(B)** *in vitro* assays. **(C)** *in vivo* assays.

2.4 Gene ontology enrichment analysis

We employed the KOBAS 3.0 platform to execute GO enrichment investigations on shared targets and hub genes, applying a p-value threshold of <0.05 for result filtration. The top 15 enriched GO terms were visually represented using Omicshare via circular, histogram, and bubble diagrams.

2.5 Molecular docking

The RSCB PDB database facilitated the retrieval of gene structures, while PubChem sourced the SDF format of compounds. PyMOL software was instrumental in docking, visualizing protein residues and binding interactions, creating 3D structures, and displaying the intricate molecular interactions.

2.6 Experimental animals

Ethical clearance for the study's entirety was granted by the Ethics Review Board of West China Hospital, Sichuan University (Approval ID: 20220221068). Male C57BL/6 mice, weighing 23–25 g and aged 6–8 weeks, were procured from SPF Biotechnology Co., Ltd. (Chengdu, China). The mice underwent a week-long acclimatization period in a pathogen-free environment, with temperature regulated at 20°C–22°C, humidity maintained at 55%, and a standard 12-h light-dark cycle.

2.7 AP model establishment and experimental design

Prior to surgery, animals underwent a 12 h fasting period. Mice were randomly divided into four groups, each containing 5-8 animals. STC-induced AP mouse model: After anesthesia with 1% pentobarbital sodium, AP was induced through retrograde injection into the pancreatic duct using 3.5% sodium taurocholate (STC). Stigma was administered intraperitoneally at doses of 50 mg/kg or 100 mg/kg, with saline serving as the control, given 1 hour after model induction. Stigma was dissolved in saline. 24 h after administration, mice were anesthetized with an intraperitoneal injection of 1% pentobarbital, then euthanized by cervical dislocation, and serum, pancreas, and lung tissues were collected.

2.8 Primary pancreatic acinar cells isolation

Primary pancreatic acinar cell are prepared with modification of the technique developed by Delia Menozzi (Menozzi et al., 1990) and Zhao et al. (Zhao et al., 2018). Fresh pancreas was infused with buffer A (140 mM NaCl, 4.7 mM KCl, 1.13 mM $MgCl_2$, 1 mM $CaCl_2$, 10 mM glucose, 10 mM HEPES, and 0.5 mg/mL soybean trypsin inhibitor [pH 7.3]) containing 0.3 mg/mL collagenase, minced and digested (19 min, 100 rpm/min shaking, 37°C). Mechanical disruption separated the cells, which were then passed through a 100-μm cell strainer. Cell precipitation was achieved by centrifugation at 700 rpm for 2 minutes, and the cell pellet was resuspended in HEPES buffer, and complete the follow-up experiment within 5 hours.

2.9 Histological examination

Pancreatic tissues were fixed in 10% formalin, dehydrated and embedded in paraffin. Tissue sections were cut and stained with hematoxylin and eosin (H&E) for histological examination.

2.10 TUNEL staining

Pancreatic tissues were fixed in 10% formalin, dehydrated, and paraffin embedded. Tissue sections were excised, followed by TUNEL staining. The specific methods are as follows (Kyrylkova et al., 2012): 1) Wash sections 2× with PBS, 5 min each time (to remove OCT); 2) Fix sections with 4% paraformaldehyde in PBS for 15 min; 3) Wash the sections 2× with PBS, 5 min each time; 4) Treat sections with 1 μg/mL proteinase K in PBS for 10–20 min; 5) Wash sections with PBS for 5 min; 6) Refix sections with 4% paraformaldehyde in PBS for 5 min; 7) Wash sections 2× with PBS, 5 min each time; 8) Prepare a positive control; 9) Remove excess liquid from the slides. Add 100 μL per slide of equilibration buffer. Cover slides with plastic coverslips -carefully and incubate for 5–10 min; 10) Carefully remove plastic coverslips and excess buffer from the slides. Add 100 μL per slide of TdT reaction mix. Meanwhile, prepare a negative control (optional): Add -negative control mix instead of TdT reaction mix. Cover the slides with plastic coverslips carefully. Incubate the slides at 37°C for 60 min; 11) Wash sections with 2× SSC for 15 min; 12) Wash sections 3× with PBS, 5 min each time; 13) Add 120 μL per slide of SA–Cy3 diluted in PBS (1:500). Cover the slides with plastic coverslips carefully. Incubate the slides for 30–45 min; 14) Wash sections 3× with PBST, 10 min each time; 15) Transfer slides to a slide rack. Wash the sections 2× with dH2O, 3 min each time; 16) Dehydrate sections 1× in 50, 70, and 95% ethanol in water, and 2× in 100% ethanol, 3 min each time; 17) Incubate sections 2× in xylene, 3 min each time; 18) Mount slides with DPX and apply micro cover glasses, being careful not to trap any air bubbles. Let slides dry overnight.

2.11 Cell culture and cytotoxicity study

266–6 cell were cultured in Dulbecco's modified Eagle's medium (DMEM) with 10% fetal bovine serum (FBS) and 1% penicillin/streptomycin at 37°C and 5% CO2 humidity. Inoculation of 266–6 cell in 96-well plates at a concentration of approximately 1.5*104/100 μL per well (n = 3). 24 h later, the plates were incubated with different concentrations of Stigma (25, 50, 100, and 200 μM) in the well plates for 24 h. After 24 h, 10 μ of CCK-8 solution was added to each well. The cytotoxicity assay was measured with the Cell Counting Kit-8 (CCK-8) assay.

2.12 Serum amylase and lipase measurement

Blood collected post-anesthesia via cardiac puncture into serum separator tubes was centrifuged at 3,000 rpm for 10 min to obtain serum. A 50 μL aliquot of serum was diluted with distilled water to a final volume of 300 μL, and serum amylase and lipase levels were measured using a fully automated biochemical analyzer (Roche, Mannheim, Germany) following the manufacturer's instructions.

2.13 Propidium iodide (PI) staining

Freshly isolated primary pancreatic acinar cells were treated with STC (final concentration 5 mM) and co-incubated with Stigma at 37°C for 50 min. Cells were subsequently stained with Hoechst 33342 (50 μg/mL) and propidium iodide (PI, 1 μmol/mL). Images were captured using an upright fluorescence microscope (Axio Imager Z2, Zeiss, Oberkochen, Germany), and displaying Hoechst 33342/PI fluorescence. Upon analyzing each stained preparation, 3 randomly selected fields of view per group were counted using ImageJ to count all live cells and all pi-positive (necrotic) cells in the area.

2.14 Microscale thermophoresis (MST) assays

The dye was first incubated (Entzian and Schubert, 2016) with ERK1 recombinant protein for 30 min and placed on ice to

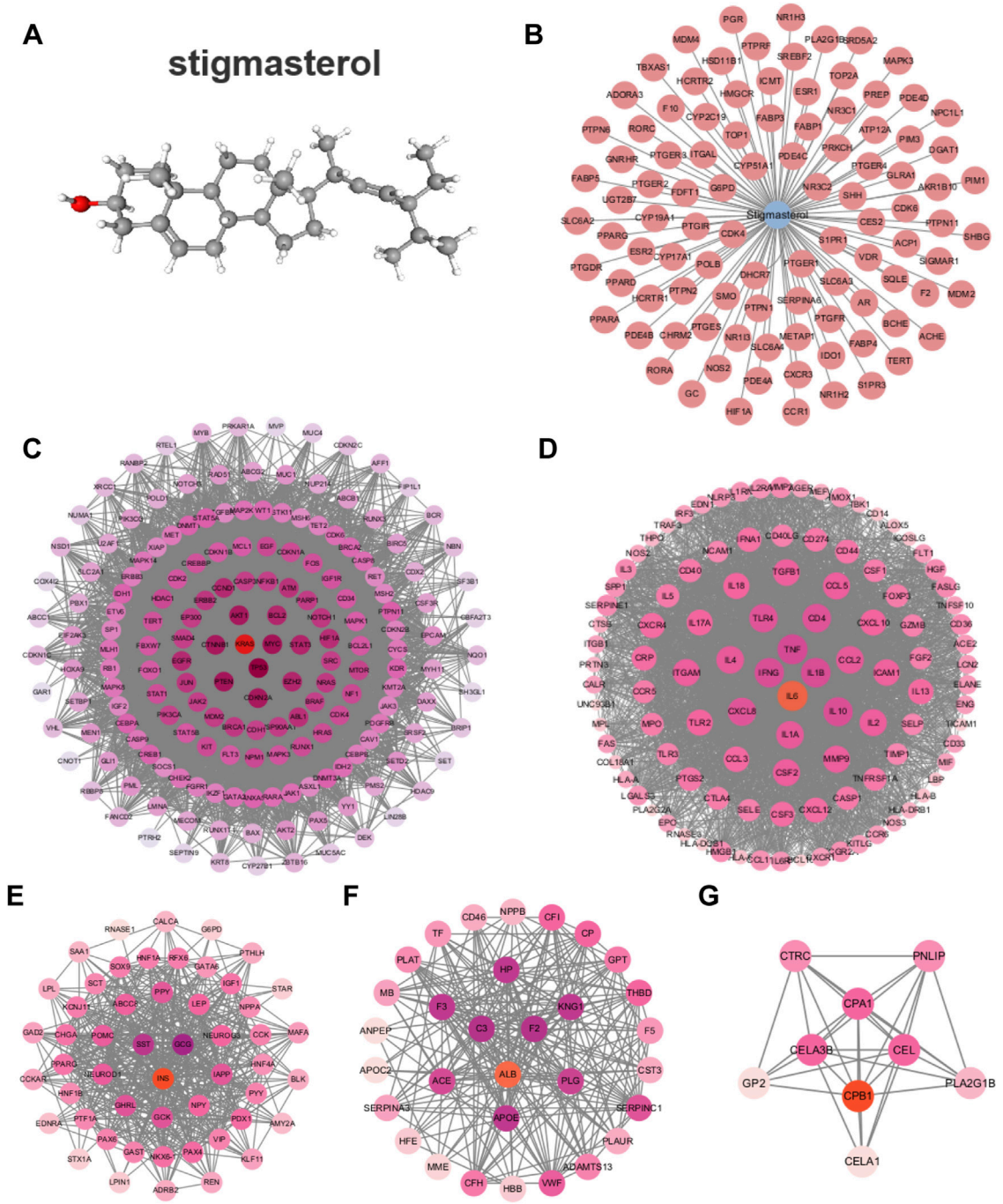

FIGURE 2
Network analysis of predict targets for Stigma compound and AP. **(A)** Structure of the Stigma. **(B)** Potential targets for Stigma. **(C–G)** Cluster analysis identified the top 5 core seed nodes involved in AP in the corresponding clusters. The seed nodes in each cluster were marked with red circles.

be assayed. A starting concentration of 100 μm was selected for Stigma, which was then 2-fold gradient diluted to 16 concentrations. 10 μL of 200 nM aptamer working solution was added to 10 μL of each ligand dilution and the samples were mixed by pipetting. Incubate the samples at room temperature for 5 min, then fill a standard capillary with the sample. Place the capillary on the capillary tray and insert it into the MST device.

2.15 Q-PCR analysis

The total RNA of was isolated using TRIzol™ reagent (Invitrogen, Carlsbad, CA, United States) according to the manufacturer's instructions. Total RNA was reverse-transcribed using Hifair III first Strand cDNA Synthesis SuperMix (Yeasen, Shanghai, China). Real-time qPCR was performed using Hieff® qPCR SYBR Green Master Mix Kit (Yeasen, Shanghai, China) on

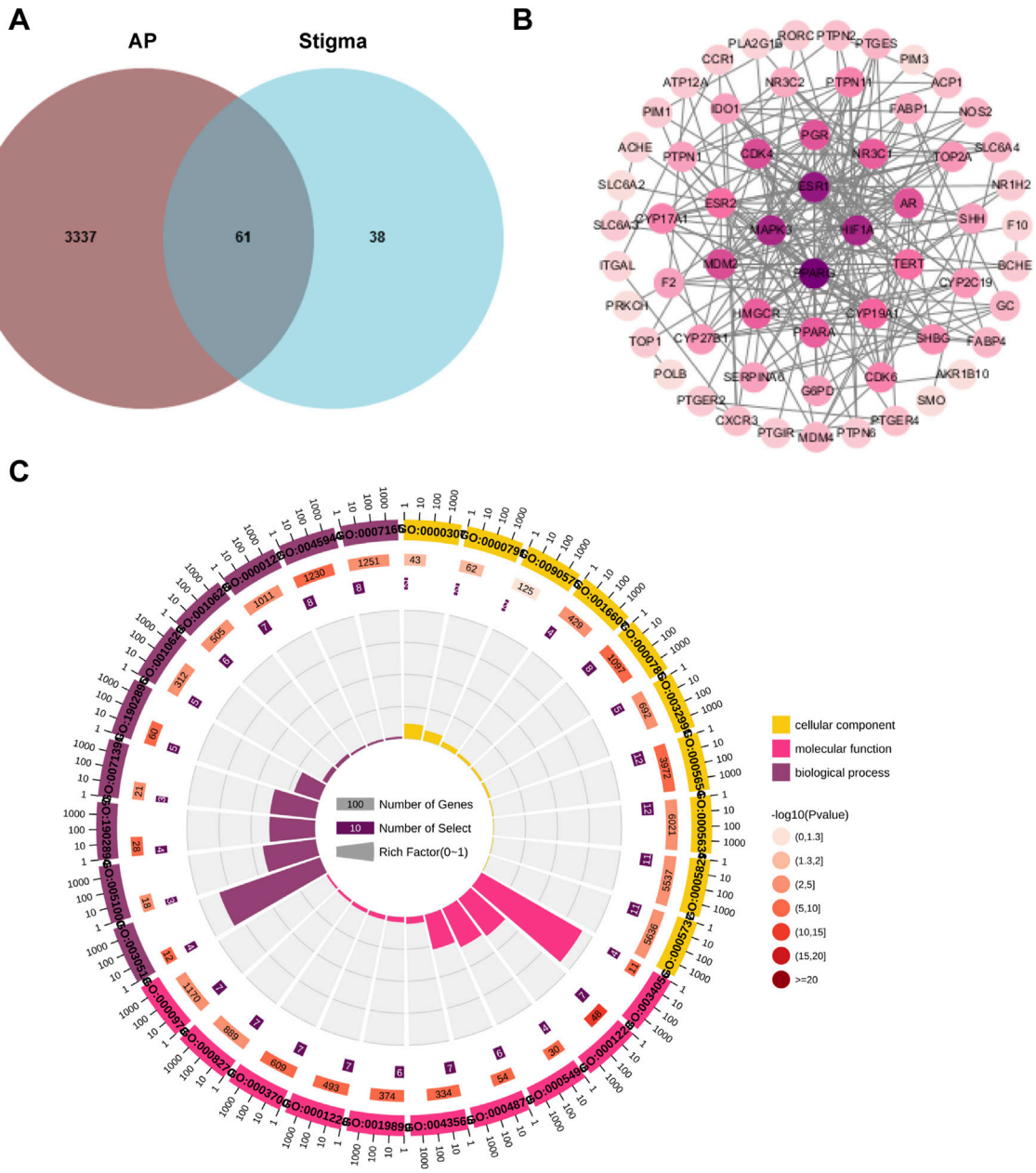

FIGURE 3
Cluster analysis of PPI network with compound-disease common targets. **(A)** Venny diagram of 61 targets, which was intersection of the Stigma compound predicted targets and AP-related targets. **(B)** The PPI network of 61 common targets. **(C)** Top 15 BP, CC and MF in GO analysis of the common 61 targets.

a Thermo Q6 Real-Time System, according to the manufacturer's instructions. Gene expression relative to that of β-actin was analyzed for each sample using the $2^{-\Delta\Delta CT}$ method. The primers were designed and synthesized as follows:

TNF-α-F: 5′-CCTGTAGCCCACGTCGTAG-3′;
TNF-α-R: 5′-GGGAGTAGACAAGGTACAACCC-3′;
IL-1β-F: 5′-GAAATGCCACCTTTTGACAGTG-3′;
IL-1β-R:5′- TGGATGCTCTCATCAGGACAG-3′;
IL-6-F: 5′-AGTTGCCTTCTTGGGACTGA-3′;
IL-6-R:5′-TCCACGATTTCCCAGAGAAC-3′;
β-actin-F:5′-GTGACGTTGACATCCGTAAAGA-3′;
β-actin-R:5′-GCCGGACTCATCGTACTCC-3′.

2.16 Western blot analysis

Similar to the accepted experimental procedure, in simple terms, the protein was separated by SDS-PAGE gels, then transported to PVDF membrane, and finally incubated with primary antibody and HRPlabeled secondary antibody, and the final blot image was observed.

2.17 Statistical analysis

Data are presented as the mean ± standard deviation (SD). Statistical analysis were conducted using GraphPad Prism 8.0, employing two-sided Student's unpaired t-tests or one-way analysis of variance (ANOVA) as appropriate. We did a G-power on all our results based on the sample sizes and test levels of the study results, which confirmed that all statistical power were greater than 0.8.

3 Results

3.1 Screening of potential targets

Stigma is a phytosterol with anti-inflammatory properties, its chemical structure formula is shown in Figure 2A (Haque et al., 2021). In this study, the SwissTargetPrediction database was utilized to predict targets for Stigma, and a total of 99 potential targets were obtained (Figure 2B). GeneCards was used to screen 3,398 potential targets which related to AP. Cluster analysis was conducted using the MCODE plug-in, yielding five clusters including KRAS, IL-6, INS, ALB, CPB1. Each cluster was marked by a red circle representing a seed node (Figures 2C–G).

3.2 Cluster analysis of PPI network with compound-disease common targets

The Venny diagram showed that 61 common targets were identified by matching 99 drug targets and 3,398 disease targets (Figure 3A), which are potential therapeutic targets of Stigma for acute pancreatitis. The 61 targets are imported into the STRING database to obtain the PPI network. There are 61 Nodes and 221 Edges in the PPI network. The "Cytoscape" plug-in can be used to analyze the Degree value of the targets, and the analyzed topological parameters can be used to visualize the PPI network, the larger the shape and the darker the color, the larger the Degree value of the node (Figure 3B). The top 15 core targets were selected: PPARG, ESR1, HIF1A, MAPK3, MDM2, CDK4, PGR, AR, PPARA, HMGCR, NR3C1, CYP19A1, ESR2, TERT, CYP17A1.

GO analysis and KEGG analysis were performed on the intersecting targets, including biological processes, cellular components and molecular functions, The enrich circle plot were used to visualize the enrichment results of the top 15 GO terms. The outermost circle showed the classification of GO enrichment, and the purple represents BP, the pink represents MF, the yellow represents CC. The second circle showed the P-value, the smaller the value, the darker the color. The third circle showed the total number of foreground genes. The fourth circle showed the RichFactor value of each classification. The results showed that BP was most related to positive regulation of nitric-oxide synthase activity, CC was most related to RNA polymerase II transcription factor complex, and MF was most related to RNA polymerase II core promoter proximal region sequence-specific DNA binding (Figure 3C).

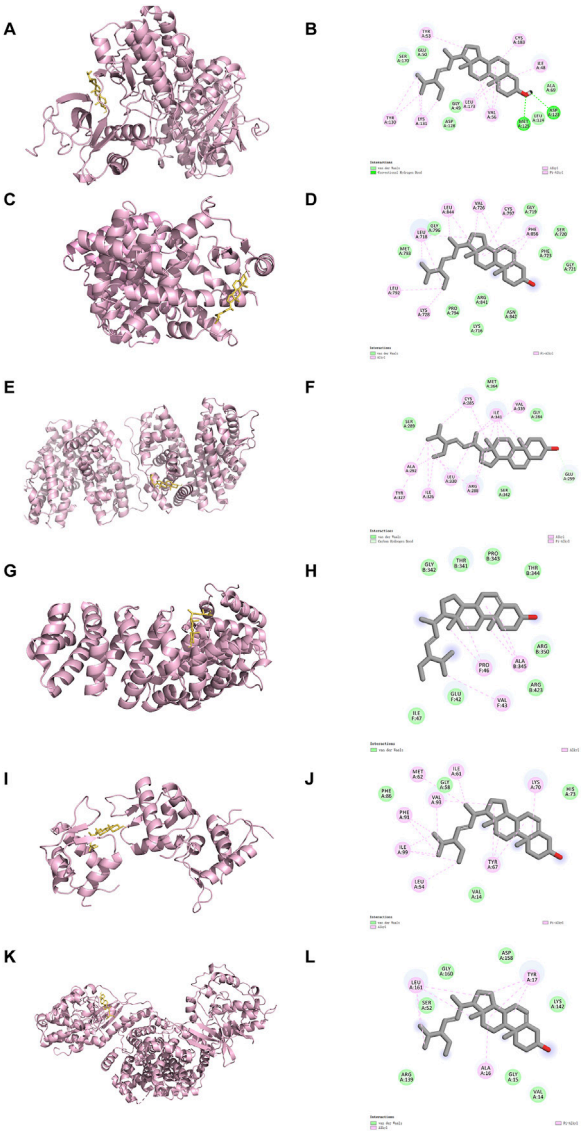

FIGURE 4
Results of molecular docking and the 2D docking diagram of Stigma. **(A, B)** MAPK3, **(C, D)** EGFR, **(E, F)** PPARG, **(G, H)** HIF1A, **(I, J)** MDM2 and **(K, L)** CDK4.

3.3 The binding studies of ERK1 and stigma

We next select the top 6 targets of Stigma to conduct molecular docking analysis to confirm the interaction between Stigma and its potential targets. A reduced docking score correlates positively with enhanced ligand-receptor binding strength, predictive of heightened interaction potential. Binding energies for all targets against Stigma fell below −5.0 kJ/mol. MAPK3 was rated as low as −6.57, suggesting which may be an important target for Stigma in the treatment of AP. 3D binding configurations are visualized in Figure 4, revealing probable intermolecular engagements between core compounds and their protein targets, as depicted in the docking analyses. Furthermore, we introduce microscale thermophoresis (MST) as a tool to characterize protein-small molecule interactions in

10.3389/fphar.2024.1485915

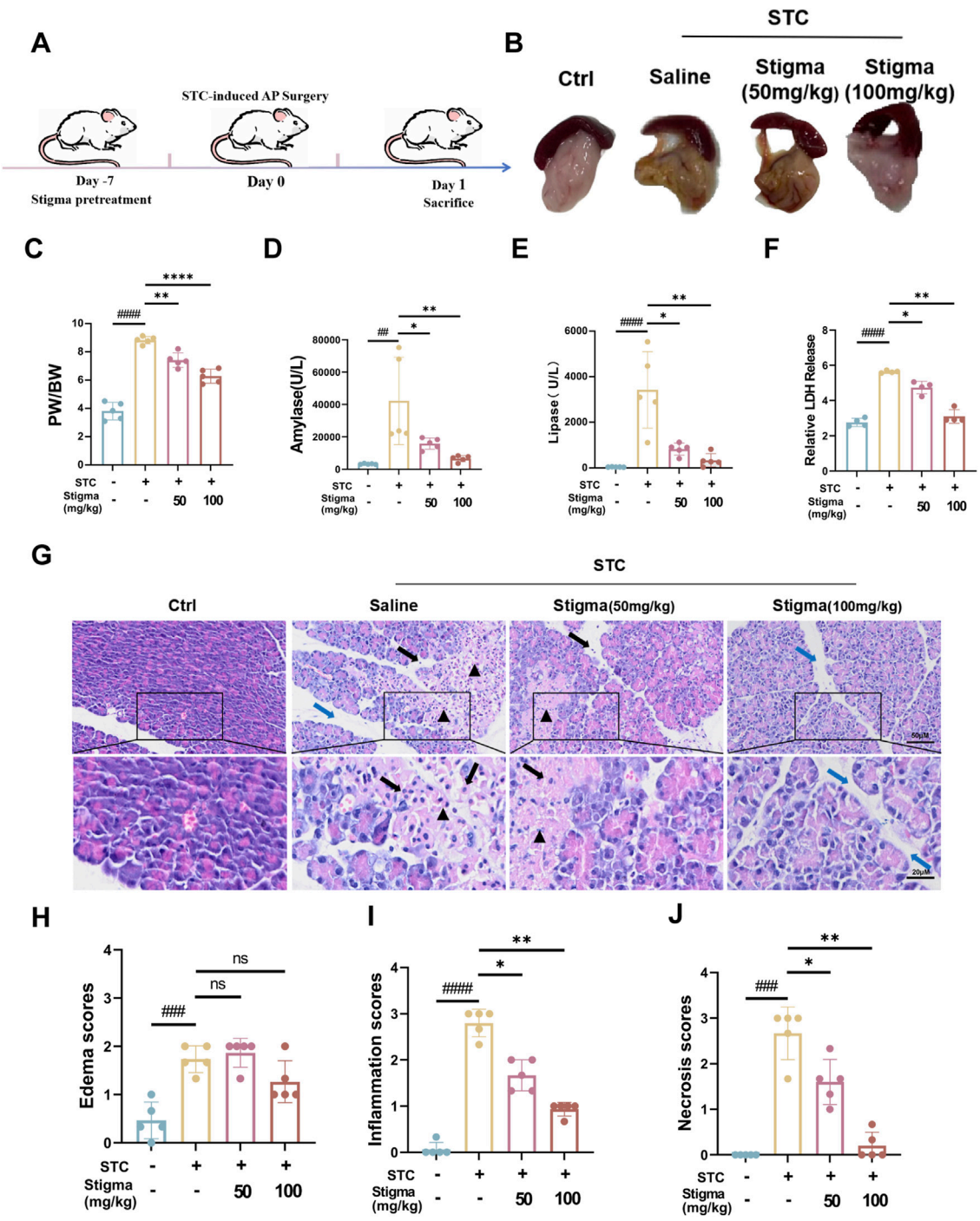

FIGURE 5
Stigma relieves STC-induced AP in mice. **(A)** Schematic diagram of the establishment of STC-induced AP mouse model and the therapeutic process via i v. (intravenous) injection. **(B)** Representative images of pancreatic morphology. **(C)** Ratio of pancreas to body weight in mice. **(D, E)** Serum levels of amylase and lipase in mice. **(F)** LDH Release levels in mouse serum. **(G)** H&E staining of mice pancreatic sections. Stained sections were taken at magnification of 50 μm and 20 μm. **(H–J)** Histopathological scoring of pancreatic tissue involving three assessment indices: edema, inflammatory infiltration and parenchymal necrosis. Black arrows point to inflammatory cells, triangles mark areas of necrosis, and blue arrows point to the width of the pancreatic lobular space, representing the degree of edema. All data are expressed as mean ± SD. n = 5. All the *p < 0.05. ns: not significant.

biological liquids. Notably, the results of MST assays indicate that ERK1 and Stigma may directly interact with each other (Supplementary Figure S1). Taken together with other data, these results suggest that Stigma may exert its pharmacological activity through ERK1.

3.4 Stigma treatment relieved the severity of STC-induced AP in mice

To verify the therapeutic activity of Stigma *in vivo*, we established a STC-induced AP mouse model and treated the mice

10.3389/fphar.2024.1485915

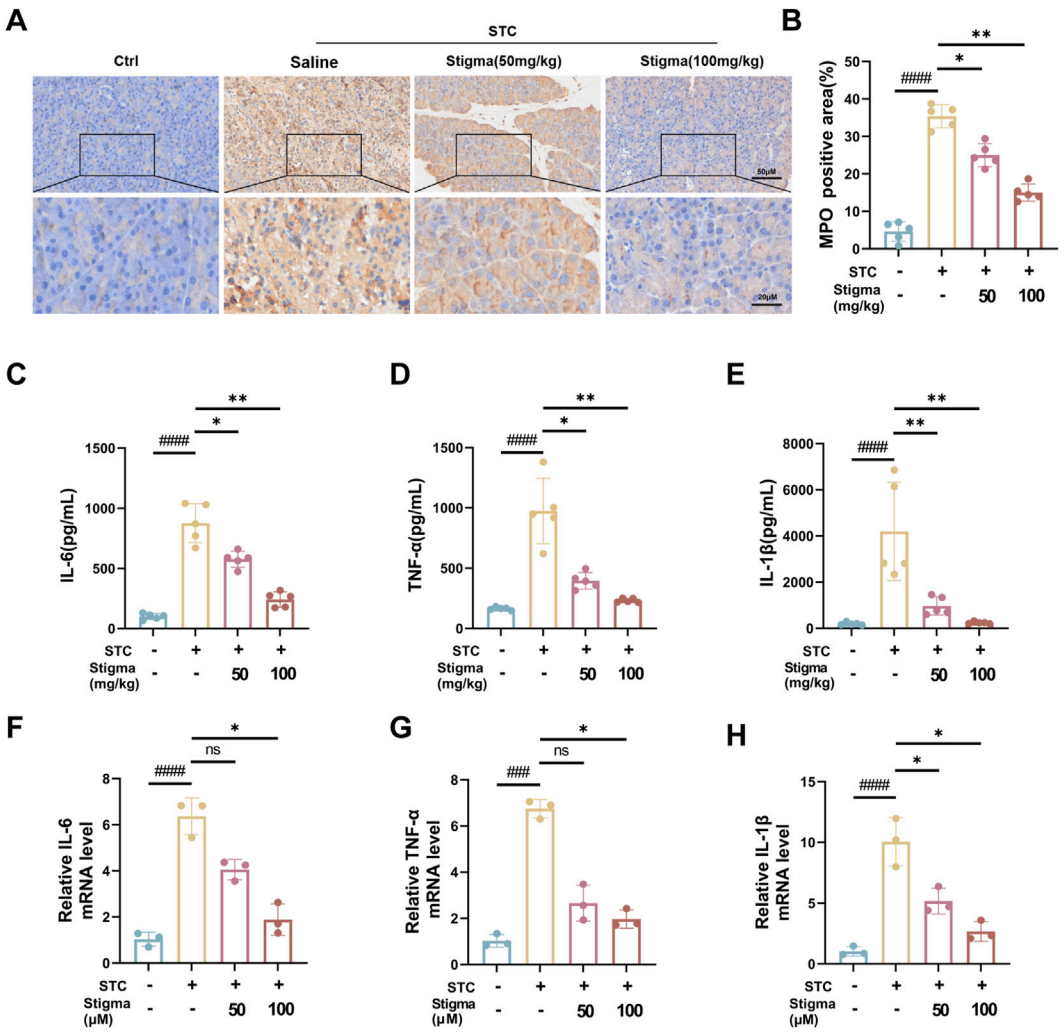

FIGURE 6
Stigma reduces inflammation in AP mice. **(A, B)** Representative immunohistochemistry images and quantitative analysis of MPO on the pancreas sections in STC-induced AP model mice treated with or without Stigma (i.g, 50 or 100 mg/kg/d, 7d). Stained sections were taken at magnification of 50 μm and 20 μm. **(C–E)** Levels of IL-6, TNF-α and IL-1β in mouse serum were determined by ELISA. **(F–H)** IL-6, TNF-α and IL-1β levels in STC stimulated primary pancreatic acinar cells were measured by quantitative PCR assay. All data are expressed as mean ± SD. n = 3 or 5. All the *$p < 0.05$. ns: not significant.

according to the drug regimen designed in Figure 5A. The results indicated that the pancreatic tissues of mice in the AP group exhibited obvious edema, inflammatory infiltration. Notably, compared to the AP group, both 50 mg/kg and 100 mg/kg Stigma ameliorated the pancreatic tissue pathological damage, with the higher dose demonstrating a more pronounced improvement effect (Figure 5B). We statistically analyzed the ratio of pancreatic weight to body weight to assess the degree of pancreatic edema in each group of mice, and the results were shown in Figure 5C. The pancreas/body weight ratio was significantly higher in the STC group compared with that of the Sham group, and the pancreas/body weight ratio in the 100 mg/kg Stigma group was significantly lower than that of the STC group. Furthermore, serum lipase and amylase levels were found to be significantly elevated in STC mice, while treatment of Stigma reduced these indicators, with the 100 mg/kg Stigma group exhibiting a more significant therapeutic effect (Figures 5D, E). Moreover, Stigma intervention markedly decreased LDH leakage into the serum of AP mice subjected to STC challenge, indicative of its protective role in acinar cell necrosis (Figure 5F). Notably, H&E staining revealed that Stigma administered intraperitoneally mitigated STC-induced pancreatic tissue injury, including edema, inflammatory cell infiltration, and acinar necrosis, with the 100 mg/kg dose yielding a superior therapeutic response (Figures 5G–J). Collectively, these findings underscore the protective potential of Stigma against STC-induced AP in mice.

3.5 Stigma reduces inflammation in mice with AP

Myeloperoxidase (MPO), an established marker of neutrophil activation, offers valuable insights into neutrophil infiltration assessment. Immunohistochemical (IHC) analysis was employed

10.3389/fphar.2024.1485915

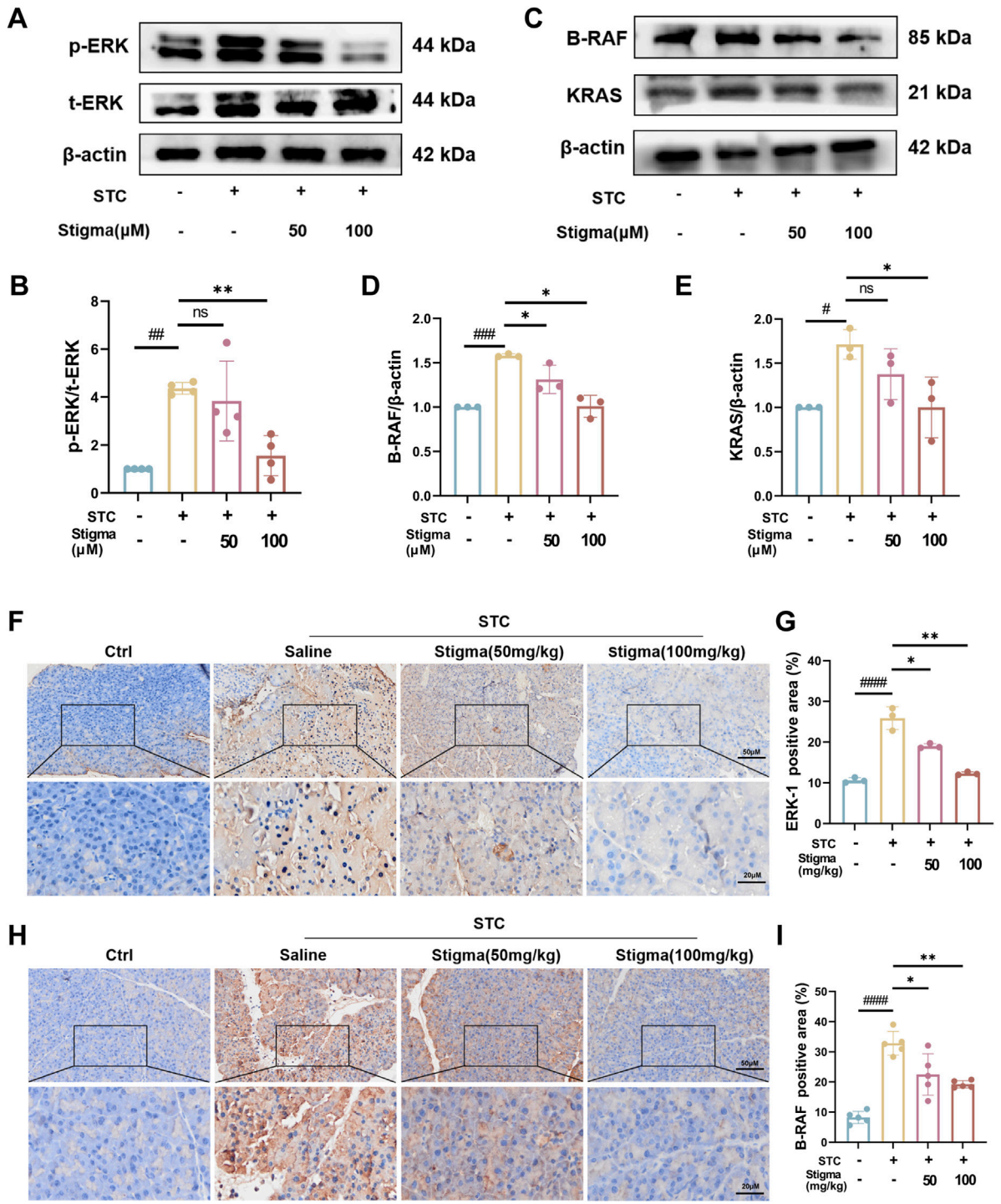

FIGURE 7
Stigma inhibits p-ERK/B-RAF/KRAS pathway with STC-induced AP in mice. **(A, B)** Representative Western blotting and quantitative analysis of p-ERK proteins in primary pancreatic acinar cells. **(C–E)** Representative Western blotting and quantitative analysis of B-RAF and KRAS proteins in primary pancreatic acinar cells. **(F, G)** Representative immunohistochemistry images and quantitative analysis of p-ERK on the pancreas sections in sodium taurocholate (STC)-induced AP model mice treated with or without Stigma (i.g, 50 or 100 mg/kg/d, 7d) **(G–I)** Representative immunohistochemistry images and quantitative analysis of B-RAF and KRAS on the pancreas sections in sodium taurocholate (STC)-induced AP model mice treated with or without Stigma (i.g, 50 or 100 mg/kg/d, 7d). Stained sections were taken at magnification of 50 μm and 20 μm. All data are expressed as mean ± SD. n = 3 or 5. All the *$p < 0.05$. ns: not significant.

to quantify MPO expressions. Notably, strong MPO immunostaining was discernible in pancreatic acinar cell of the AP group. Stigma, administered at varying concentrations, significantly attenuated MPO levels, with the 100 mg/kg dose exhibiting superior efficacy over 50 mg/kg (Figures 6A, B). This finding aligns with HE staining outcomes, suggesting that Stigma

mitigates acinar cell damage in STC-induced acute pancreatitis. Cytokine-driven inflammatory responses, including those mediated by tumor necrosis factor-α (TNF-α), IL-1β, and IL-6, play a pivotal role in the progression of AP (Papachristou, 2008). As shown in Figures 6C–E, the AP group showed significantly raised levels of serum TNF-α, IL-6, and IL-1β in comparison with the sham group. To determine whether Stigma treatment could downregulate the transcription levels of inflammatory cytokines in STC-induced acute pancreatitis, we investigated these inflammatory cytokines using q-PCR. In the AP groups, the levels of TNF-α, IL-6 and IL-1β was significantly increased, whereas Stigma treatment reduced their production (Figures 6F–H). These results demonstrate that Stigma treatment effectively mitigates the production of inflammatory cytokines in STC-induced acute pancreatitis.

3.6 Stigma inhibits STC-induced AP through ERK1 pathway

Based on the hub targets and pathway predictions from network pharmacology, the therapeutic effect of Stigma appears to be associated with ERK1 signaling pathway. To validate these results, we performed Western blotting (WB) analysis, which revealed a significant increase in the expression of p-ERK in pancreatic acinar cell stimulated by STC (Figure 7A). Moreover, Stigma mitigated the upregulation of p-ERK expression observed in STC-induced AP, consistent with the results derived from network pharmacology (Figure 7B), indicating that ERK related pathways are crucial for the therapeutic effect of Stigma in AP. Subsequently, leveraging the results from Cluster analysis and KEGG, we performed Western blotting analysis on the upstream and downstream proteins of p-ERK in the AP pathway. The results showed that the expression of B-RAF and KRAS was upregulated in STC-induced AP, but this upregulation was reversed by Stigma treatment (Figures 7C–E). To deepen our understanding of the connection between STC-induced AP and the ERK1 signaling cascade, we delved into the expressions of p-ERK and B-RAF via IHC analysis. Our findings indicated an increase in the IHC staining for p-ERK and B-RAF in the AP group. In contrast, Stigma intervention mitigated this positivity, with a more discernible decline noted in the high-dose regimen. (Figures 7F–I).

Collectively, these results demonstrate that Stigma mitigates acinar cell injury in STC-induced AP may be by modulating ERK1-related pathways.

3.7 Stigma relieves primary pancreatic acinar cells injury in STC-induced AP

In deeply explore the potential protective effect of Stigma in STC-induced necrosis in primary pancreatic acinar cell, we first examined the cytotoxicity of various concentrations of Stigma using the CCK-8 assay kit, along with Hoechst and PI live-dead cell staining. The CCK-8 assay (Figure 8A) and Hoechst and PI live-dead cell staining results (Figures 8B, C) indicated that after 24 h of incubation with 200 μM of the drug, the survival rate of 266–6 cells exceeded 80%. Subsequently, we extracted primary pancreatic acinar cells and used STC stimulation to establish a *in vitro* model of AP, with interventions of Stigma at concentrations of 50 μM and 100 μM. The results showed that STC stimulation led to a significant increase in cell necrosis, with the proportion of necrotic cells rising from 8.5% in the control group to 69.3% in the model group. Treatment with Stigma significantly reduced the proportion of necrotic cells, with the most pronounced inhibitory effect observed at 100 μM Stigma (Figures 8D, E). This data suggests the potential protective role of Stigma against STC-induced necrosis in pancreatic acinar cells.

3.8 Stigma promotes acinar cells apoptosis in STC-induced AP

Typically, apoptosis is regarded as advantageous upon the initiation of AP, as it effectively averts the propagation of the inflammatory cascade, thereby mitigating deleterious consequences. TUNEL staining was used to analyze apoptosis of acinar cells, and our results revealed pancreatic acinar cells underwent apoptosis upon the induction of STC, as depicted in Figure 9A. After Stigma treatment, the incidence of TUNEL-positive cells has significantly increased (Figure 9B). Calcein-AM/Propidium Iodide (PI) Staining shows increased number of PI-Positive cells after Stigma treatment (Figures 9C, D). We investigated the expression of Bcl-2 and Bax by WB in acinar cells. The WB analysis demonstrated that Stigma exhibited markedly elevated the ratio of Bcl-2/Bax in comparison to both the sham and AP groups. WB analysis showed that Stigma exhibited a significantly elevated Bcl-2/Bax ratio compared to the sham and AP groups (Figures 9E, F). This indicates that Stigma significantly enhanced the apoptosis of pancreatic acinar cells in AP.

4 Discussion

AP is manifested by pancreatic damage and inflammatory responses, leading to local and systemic complications, with high morbidity and mortality worldwide (Tarasiuk and Fichna, 2019; Lodewijkx et al., 2016; Yadav and Lowenfels, 2013). Current treatment guidelines for AP include intravenous fluids, dietary changes, analgesics, pancreatic secretory inhibitors (somatostatin and its analogues octreotide) (Dimagno, 2015). Specific therapeutic modalities, including trypsin inhibition to reduce necrosis of pancreatic tissue, such as the use of ustekinumab with mebeverine and octreotide, have shown limited efficacy. There is a lack of drugs that can significantly inhibit necrosis of pancreatic cells and uncontrolled inflammatory responses. As a result, there is renewed interest in botanicals, which have no serious adverse effects and are beneficial not only for symptoms but also for disease evolution. In addition, dietary preparations such as phytochemicals, which generally remain non-toxic even at relatively high doses and are inexpensive, have great potential. Recent studies have shown that some phytochemical components have been proven to have good pharmacological effects in the treatment of AP, such as lycopene, curcumin, cinnamin B-1, capsaicin, piperine, lycopene, resveratrol (Thorat et al., 1995; Sidhu et al., 2011; Wang et al., 2014; Bae et al., 2011; Ozkan

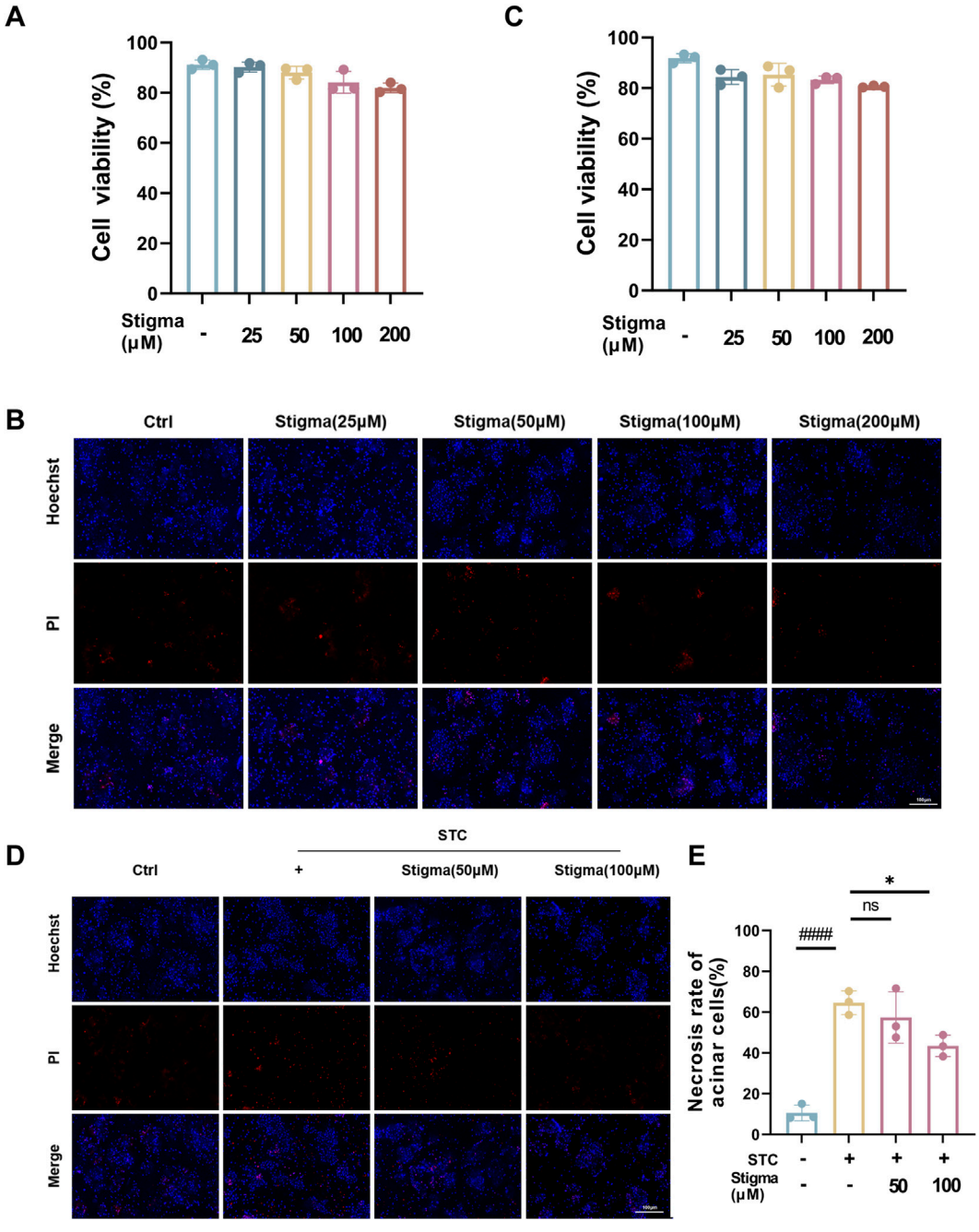

FIGURE 8
Stigma relieves primary pancreatic acinar cells injury in STC-induced AP. **(A)** The cytotoxicity of Stigma is evaluated with CCK-8 assay. **(B, C)** Representative images and quantitative analysis of Hoechst 33,342 and PI staining in primary pancreatic acinar cells. 1 - (number of PI stained cells (necrotic) divided by number of Hoechst 33,342 positive cells) to calculate cell viability percentage (%), 100 μm scale bar. **(D)** Representative images of Hoechst 33,342 and PI staining in STC stimulated primary pancreatic acinar cells treated with or without Stigma. 100 μm scale bar. **(E)** Quantitative analysis of STC-induced primary pancreatic acinar cell necrosis. The number of PI-stained cells (necrotic) was divided by the number of Hoechst 33,342-positive cells to calculate the percentage of necrosis (%). All data are expressed as mean ± SD. n = 3. All the $*p < 0.05$. ns: not significant.

et al., 2012). But so far, there are no studies exploring the therapeutic effect of Stigma on AP. This study represents the first exploration into the role of Stigma in the AP process.

Stigma is a natural sterol that features a double bond at the C-22 position (Mora-Ranjeva et al., 2006). It belongs to a larger class of plant compounds known as phytosterols, which are widely found in plant-based foods and common medicinal plants across the globe (Ryan et al., 2007). Research has shown that Stigma possesses a variety of pharmacological activities, including anti-inflammatory and anti-oxidative stress properties (Antwi et al., 2017; Feng et al., 2017; Morgan et al., 2021; Sampath et al., 2021a). Specifically, Liang et al. discovered that Stigma could reduce the production of free radicals and lipid peroxidation, demonstrating its effectiveness in combating oxidative damage (Sampath et al., 2021b). Fan J et al.

10.3389/fphar.2024.1485915

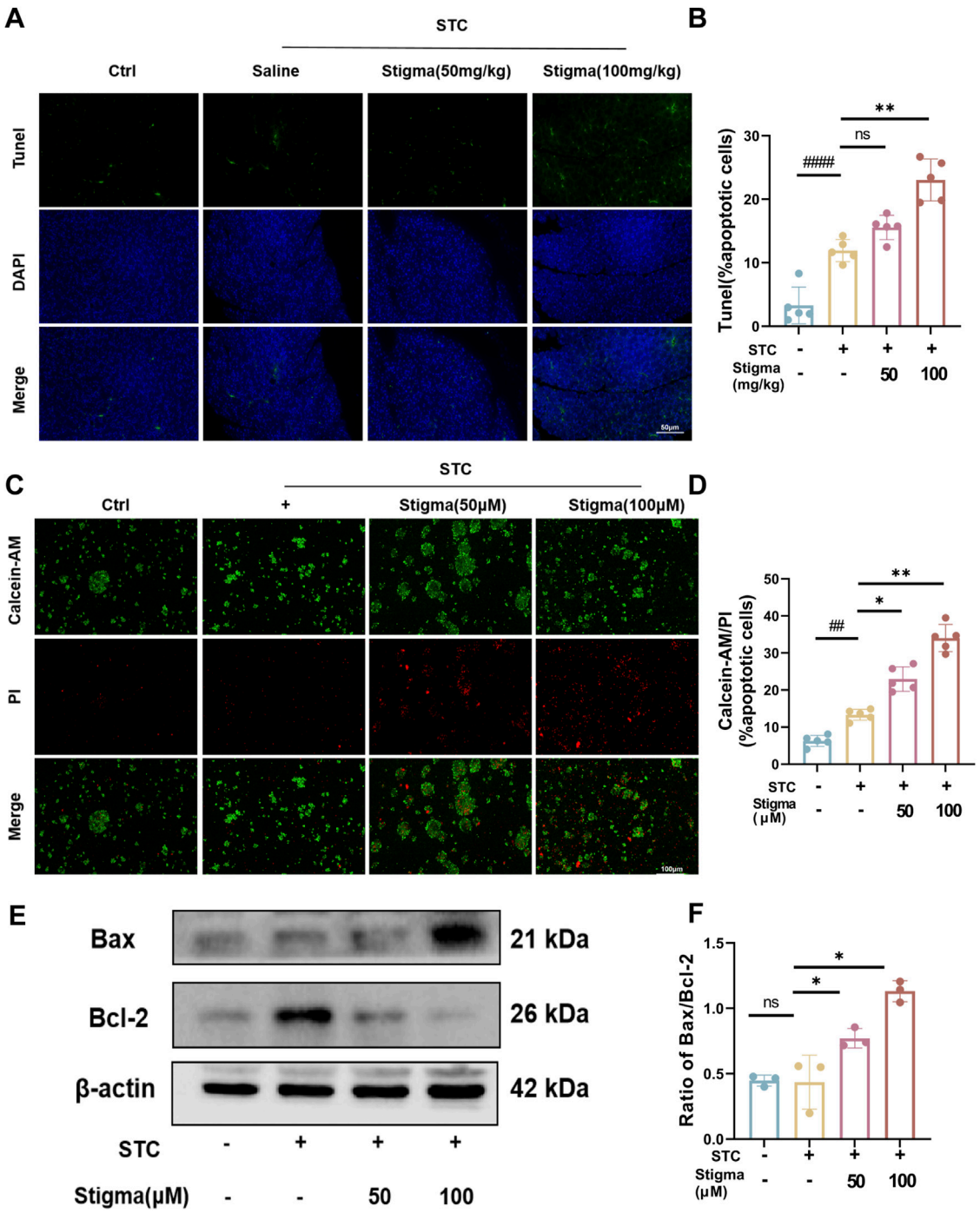

FIGURE 9
Stigma promotes acinar cell apoptosis in STC-induced AP. **(A)** Representative images of TUNEL staining for the evaluation of apoptotic acinar cells in mice with STC-induced AP 50 μm scale bar. **(B)** Statistical results on the proportion of pancreatic acinar cells undergoing apoptosis in each group. **(C)** Representative images of Calcein-AM/PI staining from pancreatic acinar cells, 100 μm scale bar. **(D)** Statistical results on the proportion of pancreatic acinar cells undergoing apoptosis in each group. **(E, F)** Representative images and quantitative analysis of Bax as well Bcl-2 proteins in STC-stimulated primary pancreatic acinar cells treated with or without Stigma. All data are expressed as mean ± SD. n = 3 or 5. All the *$p < 0.05$. ns: not significant.

demonstrated that Stigma could mediate the secretion of inflammatory cytokines by regulating NF-κB signaling or the NLRP3 inflammatome (Feng et al., 2017). Liang et al. found that Stigma can relieve oxidative stress, inflammation, and apoptotic responses to a certain extent to protect the brain from brain I/R damage (Liang et al., 2020). However, the anti-inflammatory effects of Stigma have yet to be studied in the context of the STC-induced AP model. Our study demonstrates that, compared to existing treatments for AP, Stigma significantly reduces acinar cell necrosis and inflammatory factor release, inhibits the secretion of

amylase and lipase in experimental pancreatitis models *in vitro* and *in vivo*, providing a substantial anti-pancreatitis effect. Additionally, its analog, the isospirostanol analog diosgenin, has therapeutic effects on AP (Zhang et al., 2016). However, diosgenin has cell perforation, hemolysis and hormone-like side effects such as gonadotropin hyperplasia and reproductive toxicity, which seriously limits its clinical application (Lin and Wang, 2010; Gao et al., 2024). While, Stigma exhibits no such side effects and has weaker hormone-like effects during the anti-inflammatory process, making it a more advantageous candidate as an anti-pancreatitis drug.

Network pharmacology is a powerful approach for identifying bioactive compounds and predicting drug targets using advanced computational simulations. Through molecular docking studies, we have identified that Stigma exhibits the strongest binding affinity with ERK1, suggesting that ERK1 is a promising target for Stigma. Furthermore, and the interaction between Stigma and ERK1 was directly verified by MST, which combined with WB and IHC to detect the phosphorylation level of ERK1, providing evidence that Stigma is actively involved in regulating the activation of ERK1 signaling pathway.

The MAPK signaling pathway plays a central role in regulating cellular behavior and the signaling of inflammatory factors, thereby influencing immune cell function and enhancing the activation of the immune system to combat foreign pathogens. This pathway also plays a key role in modulating and reducing the body's inflammatory response (Zhou et al., 2020; Ma et al., 2018). Among the MAPK family members, ERK1 (MAPK3) is particularly significant in controlling inflammatory responses and apoptotic pathways. The Raf/MEK/ERK1 axis represents a classic signaling cascade within the MAPK subfamily. Phosphorylated Raf (p-Raf), the initiator of this pathway, triggers the phosphorylation of downstream MEK (p-MEK), which in turn activates and phosphorylates ERK1 (p-ERK), thereby influencing the expression of downstream inflammatory mediators. This cascade ultimately modulates the overall inflammatory response (He et al., 2024). By integrating network pharmacology with previous research findings, we analyzed the expression and mRNA levels of the ERK1 pathway-associated proteins RAS, RAF, and ERK1 in mouse acinar cells. The results from qPCR, WB, and IHC revealed a significant downregulation of ERK1, KRAS, and B-RAF mRNA and protein expression levels compared to the model group. These findings suggest that Stigma may alleviate AP inflammation by promoting apoptosis and inhibiting ERK1 expression.

Apoptosis, initially defined as a physiological or programmed form of cell death, is characterized by distinct morphological changes such as cell atrophy, retention of organelles, and nuclear chromatin condensation, all of which occur in response to various stress-related stimuli. The regulation of apoptosis is primarily governed by the Bax and Bcl-2 genes, with the Bax/Bcl-2 ratio, rather than the absolute levels of these proteins, serving as a critical determinant of a cell's susceptibility to apoptosis (Hou et al., 2017; Vucicevic et al., 2016). The present study demonstrated that the therapeutic mechanism of Stigma in treating AP was closely linked to ERK1, which plays a pivotal role in regulating the expression of apoptosis-related molecules such as Bcl-2 and Bcl-XL. These molecules are essential for cell growth, development, and proliferation (Chang et al., 2003). ERK1 activation can upregulate anti-apoptotic proteins like Bcl-2 and induce its activation, which in turn promotes Bcl-2 expression, inhibits cytochrome c (Cyt-c) release, preserves mitochondrial function, and suppresses apoptosis (Romerio and Zella, 2002). Additionally, ERK1 can inhibit the pro-apoptotic activity of Bim by preventing its binding to Bax through phosphorylation (Harada et al., 2004). Recent studies showed that the degree of apoptosis in pancreatic acinar cells was inversely correlated with the severity of acute pancreatitis, suggesting that apoptosis may serve as a protective mechanism in this condition (Fuchs and Steller, 2011; Bhatia, 2004). In this study, apoptosis was assessed using TUNEL and Calcein-AM/PI staining, and the results showed that Stigma treatment promoted apoptosis. Specifically, we observed an increase in Bax expression and a decrease in Bcl-2 expression, leading to a significant elevation in the Bax/Bcl-2 ratio. These findings suggest that Stigma-induced cell death is regulated by the Bax/Bcl-2 pathway.

The comprehensive approach employed in this study establishes a solid foundation for further exploration of natural product components, their associated targets, and potential mechanisms of action in the treatment of AP. While these findings offer valuable insights into the therapeutic potential of Stigma for treating AP, there are still a series of defects. First, our research model STC-induced AP is to simulate cholestatic pancreatitis (Chen et al., 2018), in addition to cholestatic pancreatitis, there are other types of clinical AP, such as alcohol-origin pancreatitis, hypertrig lyceridemia-AP, etc., whether Stigma can protect against other types of remains to be further studied. Meanwhile, the STC-induced pancreatitis model is widely regarded as closely mimicking SAP due to the significant tissue damage and systemic inflammatory response it generates. While, this model is unsuitable for studying mild pancreatitis, which presents with less severe symptoms. In addition, STC-AP is still different from real clinical cholestasis and cannot completely replicate human disease, and the AP-related mechanisms discovered based on these modeling studies must be interpreted with caution, and the future translation of Stigma still needs clinical support. Network pharmacology utilizes computer simulations and various databases to screen drug molecular targets and predict their signaling pathways and mechanisms of action, but the network pharmacology approach still has inherent limitations in predicting *in vivo* outcomes. To compensate for these shortcomings, we first used MST to provide direct evidence for the binding of Stigma and ERK1, and then our *in vitro* and *in vivo* experimental results further solidified the effect of Stigma on the ERK1 signaling pathway. Additional fundamental research and clinical trials are essential to validate these conclusions and address any safety concerns related to Stigma.

5 Conclusion

This study represents the first attempt to integrate network pharmacology with experimental validation to explore the mechanism of Stigma in treating AP. The results confirmed that Stigma can mitigate the severity of AP by inhibiting the RAS/RAF/MEK/ERK1 signaling pathway and promoting the apoptosis of

acinar cells. These findings suggest that Stigma could be a promising therapeutic agent for AP, offering a novel and effective approach to managing this condition.

Data availability statement

The raw data supporting the conclusions of this article will be made available by the authors, without undue reservation.

Ethics statement

The animal study was approved by West China Hospital, Sichuan University. The study was conducted in accordance with the local legislation and institutional requirements.

Author contributions

XZ: Conceptualization, Data curation, Formal Analysis, Writing–original draft, Writing–review and editing, Investigation, Methodology. FL: Conceptualization, Data curation, Writing–original draft, Visualization. AW: Writing–review and editing, Validation. XY: Validation, Writing–review and editing. XX: Investigation, Writing–original draft. CW: Methodology, Writing–review and editing. YC: Investigation, Writing–original draft. GX: Funding acquisition, Resources, Writing–review and editing. WH: Funding acquisition, Resources, Writing–review and editing.

Funding

The author(s) declare that financial support was received for the research, authorship, and/or publication of this article. We thank the Innovative Chinese Medicine and Health Products Research Academician Workstation of Academician Boli Zhang and Academician Beiwei Zhu, West China Hospital, Sichuan University (Grant No. HXYS19001, HXYS19002), the 135 Project for Disciplines of Excellence, West China Hospital, Sichuan University (No. ZYXY21002), and the Innovative Chinese Medicine Preclinical Research Fund of "Liqing No.2", West China Hospital, Sichuan University (No. 161200012).

Acknowledgments

The authors sincerely appreciate the editors and peer reviewers for their careful reading and valuable comments, which have significantly contributed to improving our manuscript. We sincerely appreciate Dan Zhou, Jingyao Zhang, and Fangfang Wang and from the Core Facilities of West China Hospital, Sichuan University for helping us perform SPR and cell studies.

Conflict of interest

The authors declare that this research was conducted without any commercial or financial relationships that could be perceived as potential conflicts of interest.

Publisher's note

All claims expressed in this article are solely those of the authors and do not necessarily represent those of their affiliated organizations, or those of the publisher, the editors and the reviewers. Any product that may be evaluated in this article, or claim that may be made by its manufacturer, is not guaranteed or endorsed by the publisher.

Supplementary material

The Supplementary Material for this article can be found online at: https://www.frontiersin.org/articles/10.3389/fphar.2024.1485915/full#supplementary-material

References

Aboobucker, S. I., and Suza, W. P. (2019). Why do plants convert sitosterol to stigmasterol? *Front. Plant Sci.* 10, 354. doi:10.3389/fpls.2019.00354

Akinosoglou, K., and Gogos, C. (2014). Immune-modulating therapy in acute pancreatitis: fact or fiction. *World J. Gastroenterol.* 20 (41), 15200–15215. doi:10.3748/wjg.v20.i41.15200

Antwi, A. O., Obiri, D. D., and Osafo, N. (2017). Stigmasterol modulates allergic airway inflammation in Guinea pig model of ovalbumin-induced asthma. *Mediat. Inflamm.* 2017, 2953930. doi:10.1155/2017/2953930

Bae, G. S., Kim, M. S., Jeong, J., Lee, H. Y., Park, K. C., Koo, B. S., et al. (2011). Piperine ameliorates the severity of cerulein-induced acute pancreatitis by inhibiting the activation of mitogen activated protein kinases. *Biochem. Biophys. Res. Commun.* 410 (3), 382–388. doi:10.1016/j.bbrc.2011.05.136

Bhatia, M. (2004). Apoptosis of pancreatic acinar cells in acute pancreatitis: is it good or bad? *J. Cell Mol. Med.* 8 (3), 402–409. doi:10.1111/j.1582-4934.2004.tb00330.x

Bhatia, M., Wallig, M. A., Hofbauer, B., Lee, H. S., Frossard, J. L., Steer, M. L., et al. (1998). Induction of apoptosis in pancreatic acinar cells reduces the severity of acute pancreatitis. *Biochem. Biophys. Res. Commun.* 246 (2), 476–483. doi:10.1006/bbrc.1998.8519

Chang, F., Steelman, L. S., Lee, J. T., Shelton, J. G., Navolanic, P. M., Blalock, W. L., et al. (2003). Signal transduction mediated by the ras/raf/mek/erk pathway from cytokine receptors to transcription factors: potential targeting for therapeutic intervention. *Leukemia* 17 (7), 1263–1293. doi:10.1038/sj.leu.2402945

Chen, K. L., Chen, J. L., Chi, J. L., Zhou, Z. G., and Li, Y. (2018). An improved acute pancreatitis apoptosis/necrosis *in vitro* model of acinar cells. *Sichuan Da Xue Xue Bao Yi Xue Ban.* 49 (5), 765–770.

Chen, L., Chen, Y., Yun, H., and Jianli, Z. (2019). Tetramethylpyrazine (TMP) protects rats against acute pancreatitis through NF-κB pathway. *Bioengineered* 10 (1), 172–181. doi:10.1080/21655979.2019.1613103

Dambrauskas, Z., Giese, N., Gulbinas, A., Giese, T., Berberat, P. O., Pundzius, J., et al. (2010). Different profiles of cytokine expression during mild and severe acute pancreatitis. *World J. Gastroenterol.* 16 (15), 1845–1853. doi:10.3748/wjg.v16.i15.1845

Dimagno, M. J. (2015). Clinical update on fluid therapy and nutritional support in acute pancreatitis. *Pancreatology* 15 (6), 583–588. doi:10.1016/j.pan.2015.09.005

Entzian, C., and Schubert, T. (2016). Studying small molecule-aptamer interactions using microscale thermophoresis (mst). *Methods* 97, 27–34. doi:10.1016/j.ymeth.2015.08.023

Feng, M. C., Luo, F., Huang, L. J., Li, K., Chen, Z. M., Li, H., et al. (2024). Rheum palmatum l. And salvia miltiorrhiza bge. Alleviates acute pancreatitis by regulating th17 cell differentiation: an integrated network pharmacology analysis, molecular

dynamics simulation and experimental validation. *Chin. J. Integr. Med.* 30 (5), 408–420. doi:10.1007/s11655-023-3559-6

Feng, S., Dai, Z., Liu, A., Wang, H., Chen, J., Luo, Z., et al. (2017). β-Sitosterol and stigmasterol ameliorate dextran sulfate sodium-induced colitis in mice fed a high fat Western-style diet. *Food Funct.* 8 (11), 4179–4186. doi:10.1039/c7fo00375g

Fuchs, Y., and Steller, H. (2011). Programmed cell death in animal development and disease. *Cell* 147 (4), 742–758. doi:10.1016/j.cell.2011.10.033

Gao, H., Wang, Z., Zhu, D., Zhao, L., and Xiao, W. (2024). Dioscin: therapeutic potential for diabetes and complications. *Biomed. Pharmacother.* 170, 116051. doi:10.1016/j.biopha.2023.116051

Garcia-Llatas, G., and Rodriguez-Estrada, M. T. (2011). Current and new insights on phytosterol oxides in plant sterol-enriched food. *Chem. Phys. Lipids* 164 (6), 607–624. doi:10.1016/j.chemphyslip.2011.06.005

Haque, M. N., Hannan, M. A., Dash, R., Choi, S. M., and Moon, I. S. (2021). The potential LXRβ agonist stigmasterol protects against hypoxia/reoxygenation injury by modulating mitophagy in primary hippocampal neurons. *Phytomedicine* 81, 153415. doi:10.1016/j.phymed.2020.153415

Harada, H., Quearry, B., Ruiz-Vela, A., and Korsmeyer, S. J. (2004). Survival factor-induced extracellular signal-regulated kinase phosphorylates bim, inhibiting its association with bax and proapoptotic activity. *Proc. Natl. Acad. Sci. U. S. A.* 101 (43), 15313–15317. doi:10.1073/pnas.0406837101

He, Y. X., Li, Y. Y., Wu, Y. Q., Ren, L. Z., Wang, Y., Wang, Y. M., et al. (2024). Huanglian ganjiang decoction alleviates ulcerative colitis by restoring gut barrier via apoc1-jnk/p38 mapk signal pathway based on proteomic analysis. *J. Ethnopharmacol.* 318 (Pt B), 116994. doi:10.1016/j.jep.2023.116994

Hou, W. C., Miao, X. H., Ma, L. J., Bai, X. X., Liu, Q., and Song, L. (2017). Withaferin a induces apoptosis in rat c6 glioma cells through regulating nf-kb nuclear translocation and activation of caspase cascade. *Afr. J. Tradit. Complement. Altern. Med.* 14 (2), 319–324. doi:10.21010/ajtcam.v14i2.33

Huang, J., Li, L., Cheung, F., Wang, N., Li, Y., Fan, Z., et al. (2017). Network pharmacology-based approach to investigate the analgesic efficacy and molecular targets of xuangui dropping pill for treating primary dysmenorrhea. *Evid. Based Complement. Altern. Med.* 2017, 7525179. doi:10.1155/2017/7525179

Kaiser, A. M., Saluja, A. K., Sengupta, A., Saluja, M., and Steer, M. L. (1995). Relationship between severity, necrosis, and apoptosis in five models of experimental acute pancreatitis. *Am. J. Physiol.* 269 (5 Pt 1), C1295–C1304. doi:10.1152/ajpcell.1995.269.5.C1295

Kyrylkova, K., Kyryachenko, S., Leid, M., and Kioussi, C. (2012). Detection of apoptosis by tunel assay. *Methods Mol. Biol.* 887, 41–47. doi:10.1007/978-1-61779-860-3_5

Liang, Q., Yang, J., He, J., Chen, X., Zhang, H., Jia, M., et al. (2020). Stigmasterol alleviates cerebral ischemia/reperfusion injury by attenuating inflammation and improving antioxidant defenses in rats. *Biosci. Rep.* 40 (4). doi:10.1042/BSR20192133

Lin, F., and Wang, R. (2010). Hemolytic mechanism of dioscin proposed by molecular dynamics simulations. *J. Mol. Model* 16 (1), 107–118. doi:10.1007/s00894-009-0523-0

Lodewijkx, P. J., Besselink, M. G., Witteman, B. J., Schepers, N. J., Gooszen, H. G., van Santvoort, H. C., et al. (2016). Nutrition in acute pancreatitis: a critical review. *Expert Rev. Gastroenterol. Hepatol.* 10 (5), 571–580. doi:10.1586/17474124.2016.1141048

Lu, D., Yang, Y., Ma, W., Yao, X., Ling, Y., Huang, Y., et al. (2023). Stigmasterol depresses the proliferation and facilitates the apoptosis of fibroblast-like synoviocytes via the pi3k/akt signaling pathway in collagen-induced arthritis rats. *Altern. Ther. Health Med.* 30, 338–345.

Ma, Q., Zhang, M., Wang, Z., Ma, Z., and Sha, H. (2011). The beneficial effect of resveratrol on severe acute pancreatitis. *Ann. N. Y. Acad. Sci.* 1215, 96–102. doi:10.1111/j.1749-6632.2010.05847.x

Ma, S. Q., Wei, H. L., and Zhang, X. (2018). TLR2 regulates allergic airway inflammation through NF-κB and MAPK signaling pathways in asthmatic mice. *Eur. Rev. Med. Pharmacol. Sci.* 22 (10), 3138–3146. doi:10.26355/eurrev_201805_15073

Mayerle, J., Sendler, M., Hegyi, E., Beyer, G., Lerch, M. M., and Sahin-Toth, M. (2019). Genetics, cell biology, and pathophysiology of pancreatitis. *Gastroenterology* 156 (7), 1951–1968. doi:10.1053/j.gastro.2018.11.081

Mederos, M. A., Reber, H. A., and Girgis, M. D. (2021). Acute pancreatitis: a review. *JAMA* 325 (4), 382–390. doi:10.1001/jama.2020.20317

Menozzi, D., Jensen, R. T., and Gardner, J. D. (1990). Dispersed pancreatic acinar cells and pancreatic acini. *Methods Enzymol.* 192, 271–279. doi:10.1016/0076-6879(90)92076-p

Mora-Ranjeva, M. P., Charveron, M., Fabre, B., Milon, A., and Muller, I. (2006). Incorporation of phytosterols in human keratinocytes. Consequences on uva-induced lipid peroxidation and calcium ionophore-induced prostaglandin release. *Chem. Phys. Lipids* 141 (1-2), 216–224. doi:10.1016/j.chemphyslip.2006.03.005

Moreau, R. A., Whitaker, B. D., and Hicks, K. B. (2002). Phytosterols, phytostanols, and their conjugates in foods: structural diversity, quantitative analysis, and health-promoting uses. *Prog. Lipid Res.* 41 (6), 457–500. doi:10.1016/s0163-7827(02)00006-1

Morgan, L. V., Petry, F., Scatolin, M., de Oliveira, P. V., Alves, B. O., Zilli, G., et al. (2021). Investigation of the anti-inflammatory effects of stigmasterol in mice: insight into its mechanism of action. *Behav. Pharmacol.* 32 (8), 640–651. doi:10.1097/FBP.0000000000000658

Ozkan, E., Akyuz, C., Dulundu, E., Topaloglu, U., Sehirli, A. O., Ercan, F., et al. (2012). Protective effects of lycopene on cerulein-induced experimental acute pancreatitis in rats. *J. Surg. Res.* 176 (1), 232–238. doi:10.1016/j.jss.2011.09.005

Papachristou, G. I. (2008). Prediction of severe acute pancreatitis: current knowledge and novel insights. *World J. Gastroenterol.* 14 (41), 6273–6275. doi:10.3748/wjg.14.6273

Ramu, R., Shirahatti, P. S., Nayakavadi, S., R, V., Zameer, F., Dhananjaya, B. L., et al. (2016). The effect of a plant extract enriched in stigmasterol and β-sitosterol on glycaemic status and glucose metabolism in alloxan-induced diabetic rats. *Food Funct.* 7 (9), 3999–4011. doi:10.1039/c6fo00343e

Romerio, F., and Zella, D. (2002). Mek and erk inhibitors enhance the anti-proliferative effect of interferon-alpha2b. *FASEB J.* 16 (12), 1680–1682. doi:10.1096/fj.02-0120fje

Ryan, E., Galvin, K., O'Connor, T. P., Maguire, A. R., and O'Brien, N. M. (2007). Phytosterol, squalene, tocopherol content and fatty acid profile of selected seeds, grains, and legumes. *Plant Foods Hum. Nutr.* 62 (3), 85–91. doi:10.1007/s11130-007-0046-8

Sampath, S., Kotikalapudi, N., and Venkatesan, V. (2021a). A novel therapeutic combination of mesenchymal stem cells and stigmasterol to attenuate osteoarthritis in rodent model system-a proof of concept study. *Stem Cell Investig.* 8, 5. doi:10.21037/sci-2020-048

Sampath, S., Rath, S. N., Kotikalapudi, N., and Venkatesan, V. (2021b). Beneficial effects of secretome derived from mesenchymal stem cells with stigmasterol to negate IL-1β-induced inflammation *in-vitro* using rat chondrocytes-OA management. *Inflammopharmacology* 29 (6), 1701–1717. doi:10.1007/s10787-021-00874-z

Sidhu, S., Pandhi, P., Malhotra, S., Vaiphei, K., and Khanduja, K. L. (2011). Beneficial effects of emblica officinalis in l-arginine-induced acute pancreatitis in rats. *J. Med. Food* 14 (1-2), 147–155. doi:10.1089/jmf.2010.1108

Sun, J., Li, X., Liu, J., Pan, X., and Zhao, Q. (2019). Stigmasterol exerts neuro-protective effect against ischemic/reperfusion injury through reduction of oxidative stress and inactivation of autophagy. *Neuropsychiatr. Dis. Treat.* 15, 2991–3001. doi:10.2147/NDT.S220224

Tarasiuk, A., and Fichna, J. (2019). Effectiveness and therapeutic value of phytochemicals in acute pancreatitis: a review. *Pancreatology* 19 (4), 481–487. doi:10.1016/j.pan.2019.04.010

Thorat, S. P., Rege, N. N., Naik, A. S., Thatte, U. M., Joshi, A., Panicker, K. N., et al. (1995). Emblica officinalis: a novel therapy for acute pancreatitis--an experimental study. *HPB Surg.* 9 (1), 25–30. doi:10.1155/1995/51310

Vucicevic, K., Jakovljevic, V., Colovic, N., Tosic, N., Kostic, T., Glumac, I., et al. (2016). Association of bax expression and bcl2/bax ratio with clinical and molecular prognostic markers in chronic lymphocytic leukemia. *J. Med. Biochem.* 35 (2), 150–157. doi:10.1515/jomb-2015-0017

Wang, H., Wang, S., Tang, A., Gong, H., Ma, P., and Chen, L. (2014). Combined effects of sivelestat and resveratrol on severe acute pancreatitis-associated lung injury in rats. *Exp. Lung Res.* 40 (6), 288–297. doi:10.3109/01902148.2014.908249

Xiao, A. Y., Tan, M. L., Wu, L. M., Asrani, V. M., Windsor, J. A., Yadav, D., et al. (2016). Global incidence and mortality of pancreatic diseases: a systematic review, meta-analysis, and meta-regression of population-based cohort studies. *Lancet Gastroenterol. Hepatol.* 1 (1), 45–55. doi:10.1016/S2468-1253(16)30004-8

Xiong, W. C., Wu, H. Z., Xiong, Y. Y., Liu, B., Xie, Z. T., Wu, S. T., et al. (2020). Network pharmacology-based research of active components of albiziae flos and mechanisms of its antidepressant effect. *Curr. Med. Sci.* 40 (1), 123–129. doi:10.1007/s11596-020-2155-7

Yadav, D., and Lowenfels, A. B. (2013). The epidemiology of pancreatitis and pancreatic cancer. *Gastroenterology* 144 (6), 1252–1261. doi:10.1053/j.gastro.2013.01.068

Yuan, L., Zhang, F., Shen, M., Jia, S., and Xie, J. (2019). Phytosterols suppress phagocytosis and inhibit inflammatory mediators via erk pathway on lps-triggered inflammatory responses in raw264.7 macrophages and the correlation with their structure. *Foods* 8 (11), 582. doi:10.3390/foods8110582

Zhang, J., Zhang, C., Miao, L., Meng, Z., Gu, N., and Song, G. (2023). Stigmasterol alleviates allergic airway inflammation and airway hyperresponsiveness in asthma mice through inhibiting substance-p receptor. *Pharm. Biol.* 61 (1), 449–458. doi:10.1080/13880209.2023.2173252

Zhang, Q., Zhao, C., Zhang, L., Sun, K., Yu, L., Wang, X., et al. (2021). Escin sodium improves the prognosis of acute pancreatitis via promoting cell apoptosis by suppression of the erk/stat3 signaling pathway. *Oxid. Med. Cell Longev.* 2021, 9921839. doi:10.1155/2021/9921839

Zhang, R., Asikaer, A., Chen, Q., Wang, F., Lan, J., Liu, Y., et al. (2024). Network pharmacology and *in vitro* experimental verification unveil glycyrrhizin from glycyrrhiza glabra alleviates acute pancreatitis via modulation of mapk and stat3 signaling pathways. *BMC Complement. Med. Ther.* 24 (1), 58. doi:10.1186/s12906-024-04372-x

Zhang, R., Wen, L., Shen, Y., Shi, N., Xing, Z., Xia, Q., et al. (2016). One compound of saponins from disocorea zingiberensis protected against experimental acute pancreatitis by preventing mitochondria-mediated necrosis. *Sci. Rep.* 6, 35965. doi:10.1038/srep35965

Zhao, Q., Wei, Y., Pandol, S. J., Li, L., and Habtezion, A. (2018). Sting signaling promotes inflammation in experimental acute pancreatitis. *Gastroenterology* 154 (6), 1822–1835. doi:10.1053/j.gastro.2018.01.065

Zhou, Q., Sun, H. J., Liu, S. M., Jiang, X. H., Wang, Q. Y., Zhang, S., et al. (2020). Anti-inflammation effects of the total saponin fraction from dioscorea nipponica makino on rats with gouty arthritis by influencing mapk signalling pathway. *BMC Complement. Med. Ther.* 20 (1), 261. doi:10.1186/s12906-020-03055-7

frontiers | Frontiers in Pharmacology

TYPE Original Research
PUBLISHED 14 January 2025
DOI 10.3389/fphar.2024.1520507

OPEN ACCESS

EDITED BY
Galina Sud'ina,
Lomonosov Moscow State University, Russia

REVIEWED BY
Hans-Erik Claesson,
Karolinska Institutet and Karolinska University Hospital Solna, Sweden
Yana Toporkova,
Kazan Institute of Biochemistry and Biophysics (RAS), Russia

*CORRESPONDENCE
Dieter Steinhilber,
steinhilber@em.uni-frankfurt.de

RECEIVED 31 October 2024
ACCEPTED 24 December 2024
PUBLISHED 14 January 2025

CITATION
Hyprath M, Molitor M, Schweighöfer I, Marschalek R and Steinhilber D (2025) MLL-AF4 upregulates 5-lipoxygenase expression in t(4;11) leukemia cells via the ALOX5 core promoter. *Front. Pharmacol.* 15:1520507. doi: 10.3389/fphar.2024.1520507

MLL-AF4 upregulates 5-lipoxygenase expression in t(4;11) leukemia cells via the ALOX5 core promoter

Marius Hyprath[1], Maximilian Molitor[1], Ilona Schweighöfer[1], Rolf Marschalek[2] and Dieter Steinhilber[1]*

[1]Institute of Pharmaceutical Chemistry, Goethe University, Frankfurt, Germany, [2]Institute of Pharmaceutical Biology, Goethe University, Frankfurt, Germany

5-Lipoxygenase (5-LO), encoded by the gene *ALOX5*, is implicated in several pathologies. As key enzyme in leukotriene biosynthesis, 5-LO plays a central role in inflammatory diseases, but the 5-LO pathway has also been linked to development of certain hematological and solid tumor malignancies. Of note, previous studies have shown that the leukemogenic fusion protein MLL-AF4 strongly increases *ALOX5* gene promoter activity. Here, we investigate the upregulation of *ALOX5* gene expression by MLL-AF4. Using reporter assays, we first identified the tandem GC box within the *ALOX5* promotor sequence as the main target of MLL-AF4. Subsequently, we narrowed down the domains within the MLL-AF4 protein responsible for *ALOX5* promoter activation. Our findings indicate that MLL-AF4 binds to the *ALOX5* promoter via its CXXC domain and that the AF9ID, pSER and CHD domains redundantly activate transcriptional elongation. Knockdown of the MLL-AF4 gene in the human B cell line SEM revealed that MLL-AF4 is an inducer of *ALOX5* gene expression in leukemic cells with lymphoid properties. Finally, we found that the MLL-AF4-related protein MLL-AF9, a driver of acute myeloid leukemia, similarly acts on the *ALOX5* promoter. Taken together, we show that two prominent MLL fusion proteins are *ALOX5* gene inducers in cells with lymphoid features.

KEYWORDS

5-lipoxygenase, MLL, MLL-AF4, leukemia, leukocyte, leukotriene

Introduction

The 5-lipoxygenase (5-LO) enzyme fulfills several cellular functions. First, it is well known as the pivotal enzyme in the biosynthesis of leukotrienes (Rådmark et al., 2015). Moreover, recent studies have shown that the protein elicits further non-canonical cellular functions as regulator of gene expression which interferes with β-catenin/Wnt and TGFβ signaling (Rådmark et al., 2007; Brand et al., 2018; Kreiß et al., 2022). Moreover, 5-LO can interact with the RNA-processing enzyme dicer, and thus, interferes with microRNA maturation and processing (Provost et al., 1999; Uebbing et al., 2021). Pathophysiologically, the 5-LO pathway is implicated in inflammatory reactions, but it is also known that high 5-LO expression correlates with the development of solid tumors as well as leukemogenesis (Moore and Pidgeon, 2017; Göbel et al., 2023; Claesson et al., 2024). Obviously, canonical and non-canonical 5-LO functions provide advantages for tumors regarding growth and progression (Kahnt et al., 2024).

The *ALOX5* gene is located on chromosome 10 and spans a genomic range of around 82 kilobases (kb). The *ALOX5* promoter structure has been analyzed in several studies, and binding sites for several proteins in transcriptional regulation have been found within a core region ~800 bp from the translation start site (TSS) (Funk et al., 1989; In et al., 1997). In summary, *ALOX5* gene expression is regulated in a complex manner via regulatory sequences controlling the initiation of transcription and others in distal gene regions regulating transcription elongation (Stoffers et al., 2010). Reporter gene studies revealed that the fusion protein MLL-AF4, a product of the leukemogenic chromosomal rearrangement of the genes KMT2A (MLL1) and AFF1 (AF4), induces *ALOX5* core promoter activity by more than 40-fold (Ahmad et al., 2014; Ahmad et al., 2015). The MLL1 (mixed lineage leukemia, MLL) protein is a histone lysine N-methyltransferase and is encoded by the KMT2A gene (histone-lysine N-methyltransferase 2A) on chromosome 11q23. It serves as a platform for protein complexes involved in reading and writing of chromatin epigenetic modifications that regulate gene transcription. AF4 is encoded by the AFF1 gene (ALF transcription elongation factor 1) on chromosome 4 and serves again as a platform to form the multi-protein super elongation complex (SEC) (Benedikt et al., 2011; Marschalek, 2016). The rearrangements of chromosomes 4 and 11 results in two mutant chromosomes known as derivative chromosome 4 (der4) and derivative chromosome 11 (der11), encoding the fusion proteins MLL-AF4 and AF4-MLL, respectively. This rearrangement is one of the most prominent events in the onset of acute lymphoblastic leukemia (ALL) which is found in 5%–10% of all leukemia patients (Behm et al., 1996; Winters and Bernt, 2017). In addition, it is diagnosed as sole genetic aberration in 80% of all infant ALL cases (Meyer et al., 2023).

Given the prominent role of MLL-AF4 in leukemogenesis and its known activating potential on the *ALOX5* promoter, the present study elucidates the mechanism of this interplay.

Materials and methods

Cell lines and culture conditions

If not stated otherwise, all cell culture materials have been purchased from Thermo Fisher Scientific™ (Thermo Fisher Scientific™ Waltham, Massachusetts, United States). The adherent cell lines: HeLa (ACC 57, DSMZ, Hannover, Germany), HT-29 (ACC 299, DSMZ) and U-2 OS (HTB-96, ATCC, Manassas, United States) were cultured in a humidified atmosphere with 5% CO_2 at 37°C in Dulbecco's modified Eagle´s medium without phenol red (wDMEM). The medium was supplemented with 10% fetal bovine serum (FBS, Capricorn Scientific GmbH, Ebsdorfegrund, Germany), 1 mM sodium pyruvate, GlutaMAX™, 100 U/mL penicillin and 100 µg/mL streptomycin. Cells were grown to 70%–90% confluency before being passaged (twice a week). The suspension cell lines MV4-11 (ACC 102, DSMZ) and SEM (ACC 546, DSMZ) were cultured in a humidified atmosphere with 5% CO_2, at 37°C in RPMI 1,640 medium supplemented with 10% FBS, 100 U/mL penicillin and 100 µg/mL streptomycin. Cultures were split twice a week. Both cell lines were seeded at a concentration of 0.3×10^6 cells/mL and 1.0×10^6 cells/mL for routine culture, respectively.

Plasmid design and cloning

A list of all DNA primer sequences and restriction enzymes used for cloning is provided in the supplementary materials. Restriction enzymes were purchased from New England Biolabs (New England Biolabs GmbH, Frankfurt am Main, Germany), DNA primers were received from Eurofins (Ebersberg, Germany). Promotor constructs were cloned using the NEBuilder HiFi DNA Assembly kit (New England Biolabs GmbH, Frankfurt am Main, Germany) and were introduced into DH5α *E. coli*. Vectors pGL3B and pRL-SV40 were purchased from Promega (Promega GmbH, Walldorf, Germany). The reporter construct containing 800 bp of the *ALOX5* core promoter (pGL3-ALOX5-0.8) and a corresponding deletion construct lacking a characteristic five-fold tandem GC-Box (pGL3-ALOX5-0.8-ΔGC) were designed by our group and previously referred to as pN10 and pN10ΔGC0 (Klan et al., 2003). MLL-AF4 expression vectors are based on the empty vector pTarget (Ahmad et al., 2014), which is referred to in the present study as VC (vector control). The MLL-AF4 domain constructs contained the following amino acid positions (AA) of the wildtype protein sequence: MLL-AF4_ΔCHD AA 1–1,869 (ΔAA 1,870–226); MLL_ALFpSER AA 1–1,537 (ΔAA 1,538–2,226); MLL_ALF AA 1–1455 (ΔAA 1,456–2,226); MLL_CHD AA 1–1,362, 1,871–2,226 (ΔAA 1,363–1,870); N-MLL AA 1–1,362 (ΔAA 1,363–2,226); MLL-AF4_CXXCmut AA 1,188 C→D; MLL-AF4_ΔAT AA 1–169, AA 309–2,226 (ΔAA 170–308); MLL-AF4_ΔMenΔAT AA 1-1, AA 309–2,226 (ΔAA 2–308); Men-CXXC-CHD AA 1–18, AA 1,148–1,203, AA 1,871–2,226 (ΔAA 19–1147, ΔAA 1,204–1,870). The expression vector for MLL-AF9 (pT-MLL-AF9) was cloned using the described plasmid N-MLL. The C-terminal part of the AF9 sequence, containing the last 193 amino acids of the protein, were amplified from cDNA generated from the cell line MonoMac 6 that carries a translocation t (9;11) (p22;q23) (Super et al., 1995). Plasmids pSBtetGH and pSB100X were obtained from Eric Kowarz (Goethe University, Frankfurt, Germany) and were used for the generation of stably transfected cell lines overexpressing an inserted transgene after incubation with doxycycline (Kowarz et al., 2015). The coding sequence for MLL-AF4 was inserted into the pSBtetGH construct to generate the pSBtetGH_MLL-AF4 plasmid. The C-terminal tagged GFP constructs (Men-CXXC-CHD-GFP, N-MLL-GFP, MLL_CHD-GFP, MLL-AF4_CXXCmut-GFP or MLL-AF4-GFP) were cloned by using the mentioned untagged constructs and the coding sequence for EGFP. The sequence was obtained by using the Lonza (Basel, Switzerland) pMAX-GFP control vector.

Generation of cell lines with inducible expression of MLL-AF4

Cell lines carrying a stably integrated, doxycycline-inducible expression system encoding MLL-AF4 were generated using the Sleeping Beauty transposon system (Kowarz et al., 2015). Plasmids employed were pSBtet-GH_MLL-AF4, encoding MLL-AF4, GFP and a hygromycin resistance marker, as described under plasmid design and cloning and SB100X encoding transposase (Kowarz et al., 2015). For transfection, HT-29 cells and U-2 OS cells (1×10^6 and

0.3×10^6 per well, respectively) were seeded into 6-well plates in 5 mL wDMEM. A total of 1900 ng pSBtet-GH_MLL-AF4, 100 ng SB100X and Lipofectamine™ LTX with Plus Reagent (Thermo Fisher Scientific™) were added to each well (4:1 ratio of Lipofectamine:DNA according to manufacturer's protocol). After 24 h, the medium was replaced by selection medium, consisting of wDMEM supplemented with 500 µg/mL hygromycin B (Thermo Fisher Scientific™). Transfected cells were selected with hygromycin B under standard culture conditions (see cell lines and cell culture) for 3 weeks. Cells were sub cultured twice a week at 80% confluence. The cellular GFP signal was used to monitor the selection progress via fluorescence microscopy.

Transient reporter gene assays

HeLa cells were seeded in 24-well plates at (0.5 mL wDMEM; density of 4×10^4 cells/well) 24 h before transfection. Polyethyleneimine (PEI, Sigma-Aldrich, St. Louis, United States) was used as transfection agent. The DNA-PEI mix was prepared in medium free from serum and antibiotics (DNA:PEI ratio of 4:1). Each transfection mix contained 400 ng reporter plasmid (either pGL3B, pGL3-ALOX5-0.8, pGL3B-ALOX5-0.8-Δ5GC, pGL3-TK or pGL3-TK-5GC), 200 ng expression plasmid or the corresponding empty vector (either VC, pT-MLL-AF4, pT-MLL_CHD, pT-N-MLL, pT-MLL-AF4_CXXCmut, pT-MLL-AF4_ΔAT, pT-MLL-AF4_ΔMenΔAT or pT-Men-CXXC-CHD) and 20 ng Renilla luciferase control plasmid (pRL-SV40). The transfection mix was incubated for 20 min at room temperature (RT) before adding 50 µL to the cells. After 16 h of incubation in a humidified atmosphere with 5% CO_2, at 37°C, medium was replaced by fresh wDMEM. After further 24 h of incubation, the medium was removed and the cells were washed once with PBS. Luciferase luminescence was measured using the Dual-Glo® Luciferase assay system (Promega Corporation, Fitchburg, United States) in Lumitrac™ 96 well plates (Greiner AG, Kremsmünster, Österreich) with a TECAN Spark® plate reader (Tecan Group, Männedorf, Switzerland). Relative luminescence units (RLU) were calculated by normalizing Firefly luciferase LU to Renilla luciferase LU.

Reporter gene assays with stably transfected cells

Stably transfected HT-29 or U-2 OS cells expressing MLL-AF4 (U-2 OS_MLL-AF4; HT-29_MLL-AF4) or the corresponding wildtype cells (U-2 OS_wt; HT-29_wt) were seeded in 24-well plates (0.5 mL wDMEM, 1.2×10^4 cells/well for U-2 OS and 1.2×10^5 cells/well for HT-29). After 24 h, cells were transfected with 600 ng reporter plasmid (either pGL3B, pGL3-ALOX5-0.8 or pGL3B-ALOX5-0.8-Δ5GC) and 20 ng Renilla luciferase control plasmid (pRL-SV40) using Lipofectamine® LTX&PLUS™ Reagent (Thermo Fisher Scientific™) at a LTX to Plus reagent ratio of 4:1. After 16 h, the medium was removed and replaced with wDMEM containing 1 µg/mL doxycycline. wDMEM without doxycycline served as a control. The cells were incubated for another 24 h, the medium was removed, and the cells were washed once with PBS. Luciferase activities were measured as described above for transient reporter assays.

Analysis of subcellular localization

HeLa cells were seeded in 24-well plates (0.5 mL wDMEM; 1.5×10^4 cells). After 24 h, cells were transfected with 620 ng of one of the following expressions constructs which encode full length MLL-AF4 or deletion mutants thereof (see "Cell lines and cell culture"), each fused with a C-terminal GFP tag (Men-CXXC-CHD-GFP, N-MLL-GFP, MLL_CHD-GFP, MLL-AF4_CXXCmut-GFP or MLL-AF4-GFP). The mentioned pMAX-GFP plasmid expressing GFP was used as a control. PEI reagent was used for transfection with a DNA: PEI ratio of 1:4. After 16 h, the medium was replaced with maintenance medium and cells were incubated for additional 24 h. Subsequently, cells were washed with PBS and were fixated with 4% paraformaldehyde (PFA, Sigma Aldrich) in PBS for 20 min at RT. PFA was removed, cells were washed with PBS and stained with 1 µg/mL 4′,6-diamidino-2-phenylindole (DAPI, Sigma Aldrich) in PBS for 20 min at RT. After a final washing step, cells were stored in PBS at 4°C until image acquisition. Pictures were captured with a Zeiss AX10 microscope attached to a Zeiss Axiocam 305 color imaging system (Carl Zeiss AG, Jena, Germany). An image overlay was generated using the ImageJ software (Schneider et al., 2012).

cDNA synthesis and RT-qPCR

MV4-11 and SEM cells (0.2×10^6 each) were harvested and RNA was isolated with the NucleoSpin RNA/Protein Mini Kit (Macherey-Nagel GmbH and Co. KG, Düren, Germany) following the manufacturer´s protocol. The RNA amount was determined by measuring the absorbance at 260 nm with a NanoDrop 2000 spectrophotometer (Thermo Fisher Scientific™). cDNA synthesis was performed using the HighCapacity RNA to cDNA kit (Thermo Fisher Scientific™) from 400 ng of RNA. qPCR was performed with 10 ng cDNA equivalents per well in MicroAMP® FastAMP 96-well reaction plates (Thermo Fisher Scientific™) with PowerUP SYBR Green Master Mix (Thermo Fisher Scientific™). mRNA expression levels of the following target genes were analyzed by qPCR on a StepOnePlus™ Real-Time PCR-System (Thermo Fisher Scientific™) using the corresponding primer pairs (from Eurofins, Ebersberg, Germany): *ALOX5* (fwd: CTCAAGCAACAC CGACGTAAA, rev: CCTTGTGGCATTTGGCATCG), *UBC* (fwd: CTGGAAGATGGTCGTACCCTG rev: GGTCTTGCCAGTGAG TGTCT), *GAPDH* (fwd: GCATCCTGGGCTACACTGA, rev: CCACCACCCTGTTGCTGTA), *MLL-AF4* (fwd: GGTCCAGAG CAGAGCAAACAG, rev: TGTATTGCTGTCAAAGGAGGCG), *MLL-AF9* (fwd: TGGTTTGCTTTCTCTGTCGC, rev: GGACCT TGTTGCCTGGTCTG. GAPDH served as housekeeping control, which was used to normalize the measured CT values and data are shown as relative induction compared to negative control ($2^{(-\Delta\Delta CT)}$).

Western blot analysis

For the analysis of cellular 5-LO protein expression, cells were seeded in 10 cm petri dishes in 10 mL DMEM supplemented with 1 µg/mL doxycycline at a density of 5×10^6 cells per dish for HT-29_ wt, and HT-29_MLL-AF4 and 2.5×10^6 cells for U-2 OS_wt and U-2

OS_MLL-AF4. Parallel cultures without doxycycline served as a control. After 48 h of incubation, cells were harvested, suspended in SDS lysis buffer (77 mM SDS, 1.5 M Glycerol, 56 mM Tris, pH 6.8) and sonicated with an ultrasonic homogenizer at 10% of maximum amplitude (Sonopuls HD 200 with Sonopuls microtip MS72, BANDELIN electronic GmBH and Co. KG, Berlin, Germany). Cell lysates were centrifuged (10 min, 12,000 rcf, 4°C) and the supernatant was transferred to a fresh tube. Protein concentration was determined using the Pierce™ BCA Protein Assay Kit (Thermo Fisher Scientific™) and a Tecan Infinite M200 plate reader (Tecan Group Ltd.). 30 µg of total cellular protein per sample were separated by SDS-PAGE (10% running gel, 80 V for 15 min and 130 V for 100 min). Purified recombinant 5-LO protein served as a positive control and Precision Plus Protein™ All Blue Prestained Protein Standard (Bio-Rad, Hercules, United States) was used for size estimation. Separated proteins were transferred to 0.2 µm nitrocellulose membranes (Bio-Rad) with a wet tank method using a Mini Trans-Blot® cell (Bio-Rad) (125 mA for 85 min). Membranes were blocked for 1 h using EveryBlot Blocking Buffer (Bio-Rad) at RT before being probed with an anti-5-LO primary antibody (66326-1-Ig Proteintech Group, Inc., Rosemont, United States) and an anti-GAPDH antibody as control (PLA0302, Merck, Darmstadt, Germany). Matching fluorescence-conjugated secondary antibodies donkey-anti-mouse (for 5-LO antibody) donkey-anti-goat (for GAPDH antibody) IRDye, LI-COR Biosciences, Bad Homburg, Germany) were used for detection with the Odyssey Infrared Imaging System (LI-COR Biosciences). For the analysis of cellular 5-LO protein expression in MV4-11 and SEM cells, 7.5×10^6 cells were seeded in 15 mL RPMI (with or without 1 ng/mL TGFβ, 50 nM $1.25(OH)_2D_3$ ($VitD_3$), or the combination of both) in 10 cm dishes. After 72 h incubation cells were harvested, lysed and western blot analysis was performed as already described. The membrane was probed with an anti-5-LO primary antibody (66326-1-Ig Proteintech Group) and an anti-β-actin antibody as control (ab8229, Abcam, Cambridge, UK). Secondary antibodies used were donkey-anti-mouse for the 5-LO antibody and donkey-anti-goat for the β-actin antibody (IRDye, LI-COR Biosciences).

Analysis of 5-LO product formation

Analysis of 5-LO activity was performed with SEM cells or MV4-11 cells after differentiation with 1 ng/mL transforming growth factor-β (TGFβ, PeproTech, Cranbury, United States), 50 nM $1,25(OH)_2D_3$ (Cayman Chemical Company, Ann Arbor, United States) or both agents at 37°C in a humidified atmosphere with 6% CO_2 for 72 h in cell culture flasks. To determine the 5-LO activity in intact cells, 3×10^6 MV4–11 and 6×10^6 SEM cells for each treatment group were harvested, and the pellet was resuspended in PBS containing 1 mg/mL glucose. 5-LO activity was stimulated by the addition of 20 µM arachidonic acid (Cayman Chemical Company, Ann Arbor, United States) and 2.5 µM calcium ionophore (A23187, Sigma Aldrich). To measure 5-LO activity in cell homogenates, 3×10^6 MV4–11 and 6×10^6 SEM cells were harvested, and the pellet was resuspended in PBS containing 1 mM EDTA and 1 mM ATP. The cell suspension was sonicated three times for 10 s at 10% of the maximal amplitude (Sonopuls HD 200 with Sonopuls microtip MS72). The reaction was started by the addition of 2 mM Ca^{2+} and 20 µM arachidonic acid (Cayman Chemical Company). Both, intact cells and homogenates, were incubated for 10 min at 37°C before stopping the reaction by the addition of 1 mL of ice-cold methanol (LC-MS grade, Carl Roth, Karlsruhe, Germany). Extraction of 5-LO products followed by LC-MS analysis was performed as originally described by Werz and Steinhilber, modified by Goebel and Kreiß (Werz and Steinhilber, 1996; Kreiß et al., 2022).

siRNA-mediated gene silencing of MLL-AF4

For siRNA-mediated gene silencing of MLL-AF4 in MV4-11 and SEM cells, 0.2×10^6 cells/well were seeded in 96-well cell culture plates (Greiner AG, Kremsmünster, Austria) in 200 µL Accell™ siRNA Delivery Medium (Horizon Discovery Group plc, Waterbeach, United Kingdom). Accell™ siRNA (Horizon Discovery Group plc) targeting MLL-AF4 was dissolved in siRNA buffer (Horizon Discovery Group plc) and added to the cells according to manufacturer's protocol (final concentration of 1 µM). The following siRNA sequences were used: sense 5′-CCA AAAGAAAAGGAAAUGAUU-3′, antisense 5′-UCAUUUCCU UUUCUUUUGGUU-3′ (MV4-11) and sense 5′-CAAAAGAAA AGCAGACCUAUU-3′, antisense 5′-UAGGUCUGCUUUUCU UUUGUU-3′ (SEM). The sequences were designed to target the cell line-specific MLL-AF4 exon-exon junctions of the two cell lines. Accell™ non-targeting control siRNA pool or Accell™ GAPD control siRNA pool cells treated analogously were used as control. MV4-11 and SEM cells were incubated with siRNA containing media for 72 h under standard culture conditions. After 72 h, cells were harvested and resuspended in PBS for further use.

Results

Activation of the ALOX5 promoter by MLL-AF4 is mediated by pSER, AF9-ID, CHD and CXXC domain and a five-fold tandem GC box in the ALOX5 promoter

In previous studies, it was shown by reporter gene analysis that MLL-AF4 is able to prominently induce activity of the *ALOX5* core promoter by a factor of up to 47-fold. The reporter construct employed in this analysis contained 0.8 kb of the proximal *ALOX5* promoter (plasmid pGL3-ALOX5-0.8) (Ahmad et al., 2014). In order to identify the specific sequences within this promoter region that are responsible for MLL-AF4-mediated activation, we investigated the activity of the 5-fold tandem GC box proximal to the transcriptional start site (formerly referred to as GC0-element (Schnur et al., 2007)), which is known to be crucial for basal *ALOX5* promoter activity (Schnur et al., 2007). To this end, we deleted the tandem GC element from the *ALOX5* core promoter reporter construct pGL3-ALOX5-0.8, leading to plasmid pGL3-ALOX5-0.8_ΔGC. As shown in Figure 1A, coexpression of MLL-AF4 did not lead to a significant induction of the *ALOX5* promoter lacking the tandem GC box (~1.7-fold increase), compared to the ~5-fold upregulation when the promoter contains

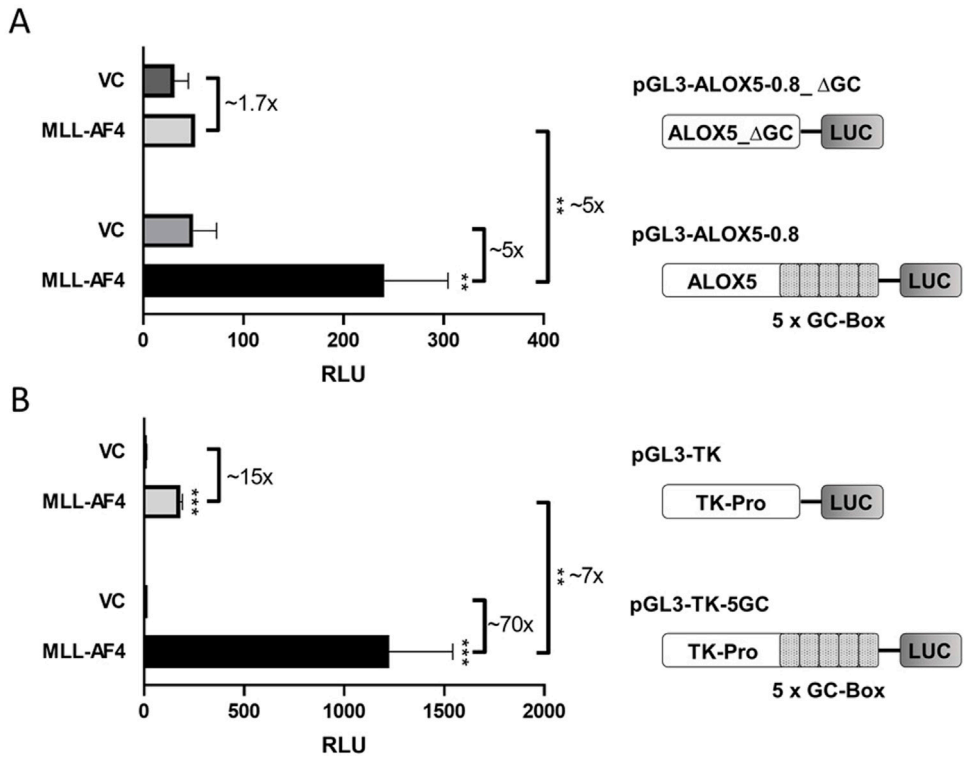

FIGURE 1
Reporter gene analysis shows GC box-dependency of MLL-AF4 activity. **(A)** HeLa cells were transfected with one of the reporter vectors pGL3-ALOX5-0.8 or pGL3-ALOX5-0.8_ΔGC and with the empty expression vector control (VC) or the expression plasmid for MLL-AF4 (MLL-AF4). **(B)** HeLa cells were transfected with one of the reporter vectors pGL3-TK or pGL3-TK-5GC and with the empty expression vector control (VC) or the expression plasmid for MLL-AF4. Results are shown as relative luminescence units (RLU) normalized to the Renilla control. The values are presented as mean ± S.E.M. of three independent experiments. An unpaired *t*-test was used to determine the significance of the influence of the MLL-AF4 expression compared to VC on the according reporter construct. Asterisks indicate significant changes of MLL-AF4 compared to VC transfected cells. *$p \leq 0.05$, **$p \leq 0.01$, ***$p \leq 0.001$.

the GC element. In order to further investigate the activating function of the GC box, we cloned the GC element in front of the viral thymidine kinase (TK) promoter (plasmid pGL3-TK), leading to plasmid pGL3-TK-5GC. Figure 1B shows that the coexpression of MLL-AF4 as a general transcriptional activator already led to a ~15-fold increase in reporter activity from the control plasmid pGL3-TK. An even stronger activation of ~70-fold was observed from the plasmid carrying the tandem GC box. This approximately ~7-fold increase in activation clearly demonstrates that the tandem repeat is the key element for MLL-AF4-mediated upregulation of *ALOX5* promoter activity.

In a next step, we aimed to identify the regions of the multi-domain MLL-AF4 protein structure (Figure 2) that play a pivotal role in the activation of the 5-LO core promoter. To investigate this, we designed a series of expression constructs which contain either mutations or deletions of individual domains or of multi-domain segments of full-length MLL-AF4. The data indicate that several domains of MLL-AF4 play a crucial role in GC-box-dependent activation of the *ALOX5* promoter. Obviously, some domains originating from the AF4 gene locus are indispensable for MLL-AF4 effects, as shown by the strong reduction of reporter activity after deletion of the complete C-terminal part (construct N-MLL) which reduced the activity level to ~30%. However, neither the single deletion of the CH domain (MLL-AF4_ΔCHD) which is known to dimerize with wt-AF4 (Mueller et al., 2007; Benedikt et al., 2011), nor the 5′-flanking domains including the serine rich pSer domain (MLL-AF4_ΔpSER) which can interact with the selectivity factor 1 (SL1) protein and the AF9-ID (MLL-AF4_ΔAF9-ID) (Okuda et al., 2015; Siemund et al., 2022), result in a loss of activity (Supplementary Figure S1). The deletion of the C-terminus, including CHD and AF9-ID (MLL_ALFpSER) results in a significant reduction of activity to ~69% (Figure 2). Finally, the additional deletion of the pSER domain (MLL_ALF) reduced the activity even further to ~37%. Interestingly, the addition of the CH domain to the inactive N-MLL (MLL_CHD) restored full activity. In contrast, the mutation of only one amino acid within the C-terminal CXXC domain (MLL-AF4_CXXCmut) which has been described to bind hemi-methylated CpG rich DNA (Birke et al., 2002), led to a prominent reduction of the reporter signal to ~28% residual activity compared to full-length MLL-AF4, pointing to a central role of this domain. As shown in Supplementary Figure S2 the constructs with diminished activity (N-MLL and MLL-AF4_CXXCmut) only show a ~1.4-fold activation compared to the empty expression vector control. Regarding the MLL part of the fusion protein, we investigated the influence of a domain with AT-hooks, which was shown to be a binding motif for the DNA backbone (Aravind and Landsman, 1998), and a larger N-terminal part of MLL encompassing the AT-hooks and the N-terminal Menin binding domain (Yokoyama et al., 2005) which is known to interact with Menin-1 and Lens Epithelium-Derived Growth Factor (LEDGF) (El Ashkar et al., 2017). Both constructs, MLL-AF4_

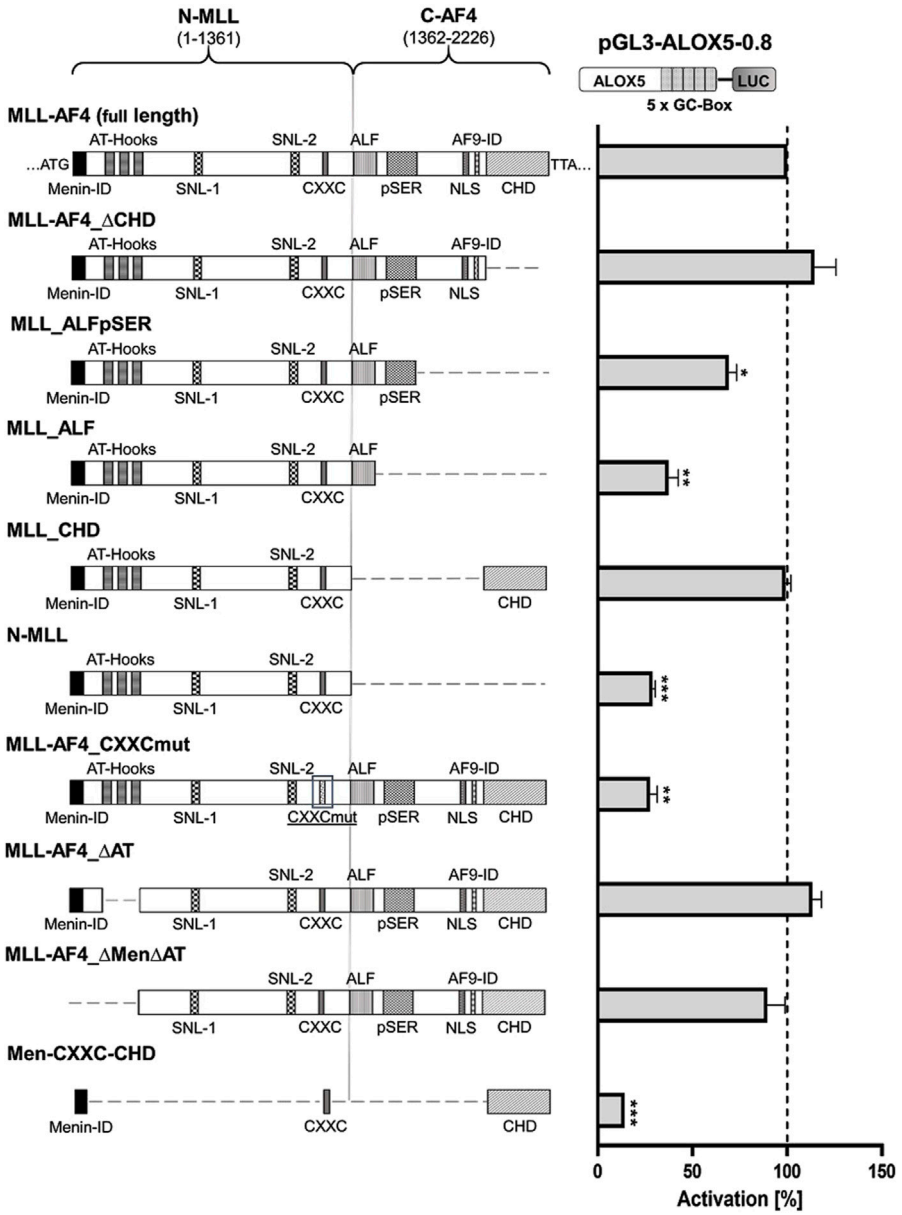

FIGURE 2
Reporter gene assay to determine GC-box-dependent transcriptional activity of MLL-AF4 mutants. HeLa cells were transfected with the full-length construct (MLL-AF4) or with one of the mutants (MLL-AF4_ΔCHD, MLL_ALFpSER, MLL_ALF, MLL_CHD, N-MLL, MLL-AF4_CXXCmut, MLL-AF4_ΔAT, MLL-AF4_ΔMenΔAT, Men-CXXC-CHD) and a reporter plasmid containing the *ALOX5* promoter (pGL3-ALOX5-0.8). Additionally, a pRL-SV40 Renilla plasmid was cotransfected to normalize the luminescence. N-MLL: N-terminal fusion part of MLL protein, C-AF4: C-terminal fusion part of AF4, numbers represent amino acid range, Menin-ID: Menin interaction domain (El Ashkar et al., 2017; Slany, 2020), AT-Hooks: DNA binding motif (Aravind and Landsman, 1998), SNL-1, SNL-2: Speckled nuclear localization domain 1 and 2 (Yano et al., 1997), CXXC: binding motif for CpG DNA elements (MT domain) (Birke et al., 2002), ALF: family specific conserved domain (Nilson et al., 1997), pSER: Serine rich domain (Okuda et al., 2015; Siemund et al., 2022), NLS: Nuclear localization signal (Domer et al., 1993), AF9-ID: AF9 interaction domain (Bitoun et al., 2007), CHD: C-terminal homology domain (Benedikt et al., 2011; Slany, 2020). Promoter activity is displayed as % activation compared activation of pGL3-ALOX5-0.8 by full length MLL-AF4. Results (RLU) are presented as mean ± S.E.M. of three independent experiments. An unpaired *t*-test with Welch´s correction was used to determine the significance of the influence of the MLL-AF4 expression on the reporter construct compared to the mutants. $*p \leq 0.05$, $**p \leq 0.01$, $***p \leq 0.001$.

ΔAT and MLL-AF4_ΔMenΔAT, only led to a minor reduction in activity, which was statistically not significant (Figure 2). Based on these results, we finally attempted to design a construct of minimal size with the ability to activate the *ALOX5* promoter. We included regions of the protein that have shown to be necessary for its activity in our analysis, or are considered to be of special importance in the literature, namely, the Menin binding, CXXC and CH domains (construct Men-CXXC-CHD) (Slany, 2020). However, the Men-CXXC-CHD construct did not exhibit any significant activity on the 5-LO promoter, leading to only ~14% residual activity. Taken together, the reporter gene data show that the CXXC domain is absolutely essential for the MLL-AF4 activity. The CHD, AF9-ID and the pSER domains are involved in mediating MLL-AF4 transcriptional elongation activity as well with redundant functions regarding *ALOX5* promoter activation.

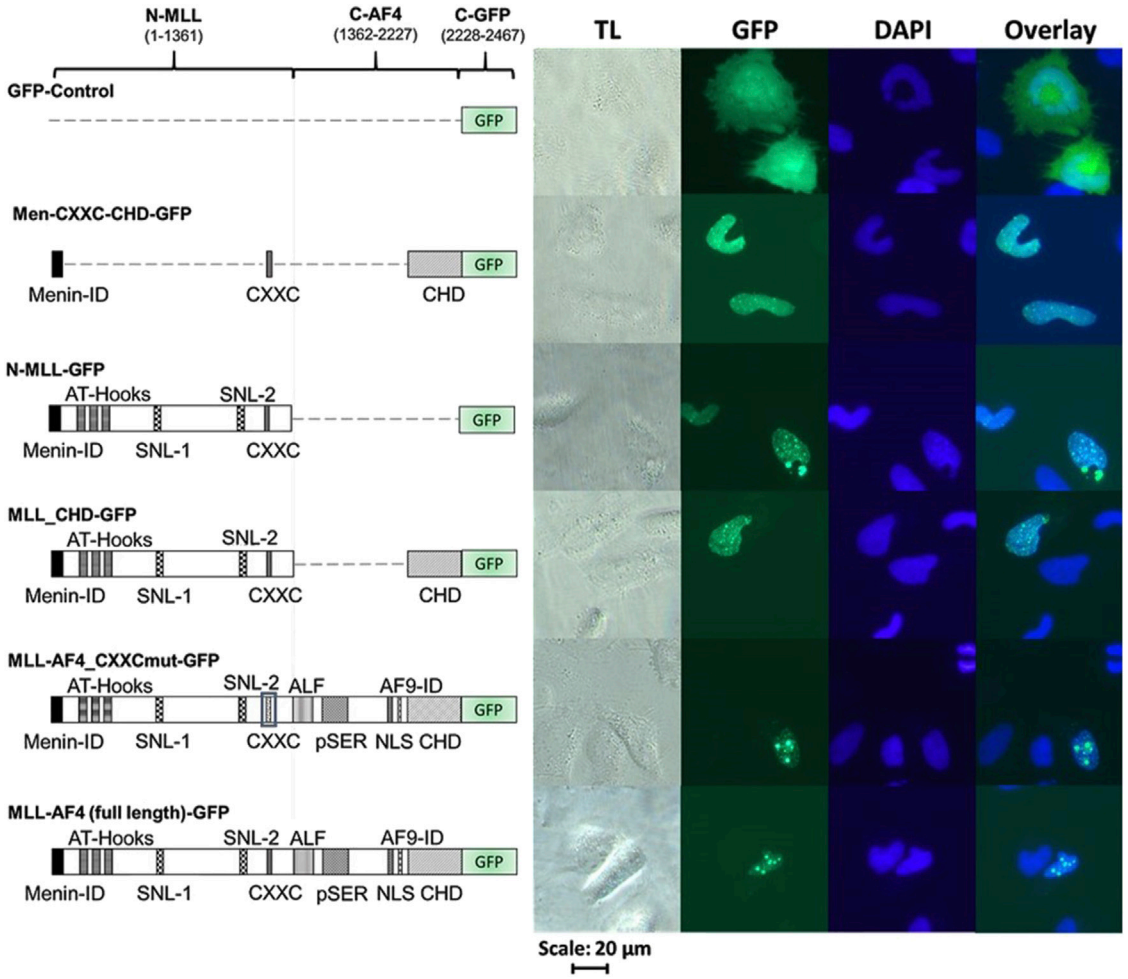

FIGURE 3
Cellular localization of MLL derivatives. Images of HeLa cells transfected with different C-terminally GFP-tagged MLL constructs or GFP protein (as control). HeLa cells were grown for 24 h and then transfected with one of the GFP-tagged constructs (GFP, Men-CXXC-CHD-GFP, N-MLL-GFP, MLL_CHD-GFP, MLL-AF4_CXXCmut-GFP, MLL-AF4-GFP) and incubated for additional 24 h. Cells were fixed with paraformaldehyde and stained with DAPI (TL = transmitted light, GFP, DAPI). Every image represents the result of one of three independent experiments.

Various MLL-AF4 domains determine nuclear localization

In order to validate the correct expression and localization of the inactive constructs from Figure 2 (MLL-AF4_CXXCmut, Men-CXXC-CHD and N-MLL), fluorescence imaging was performed with the respective GFP-tagged constructs (MLL-AF4_CXXCmut-GFP, Men-CXXC-CHD-GFP, N-MLL-GFP). The constructs encoding GFP-tagged proteins with full activity in the reporter assays (MLL-AF4-GFP, MLL-CHD-GFP, Figure 2) served as positive controls. Furthermore, a plasmid expressing only GFP (GFP-Control) was used as a control for the fluorescence pattern obtained by a protein with known cytoplasmic localization such as GFP (Kitamura et al., 2015). The analysis of the microscopic images in Figure 3 revealed that stable proteins are produced from all constructs and that all proteins, with the exception of GFP alone, were localized in the nucleus. We noticed that cells transfected with N-MLL-GFP, MLL_CHD-GFP, MLL-AF4_CXXCmut-GFP and MLL-AF4-GFP exhibit a distinctly punctuated distribution of signals in the nucleus. A similar signal, however not as pronounced, was seen in some areas of the nucleus, most prominently after transfection within constructs MLL-AF4_CXXC-GFP and MLL-AF4-GFP. We can conclude that all constructs are fully expressed and exclusively localized in the nucleus.

Heterologous expression of MLL-AF4 in 5-LO positive solid tumor cell lines HT-29 and U-2 OS does not affect ALOX5 gene expression

The two tumor cell lines HT-29 and U-2 OS, which are derived from a colorectal tumor and an osteosarcoma, have both been shown to prominently express 5-LO (Weisser et al., 2023). This allowed us to use these cells as model systems to analyze the effect of heterologously expressed MLL-AF4 on *ALOX5* gene expression on mRNA and protein level. For this purpose, cells were stably transfected with a doxycycline-inducible MLL-AF4 expression construct. To further validate the cell model, we checked for

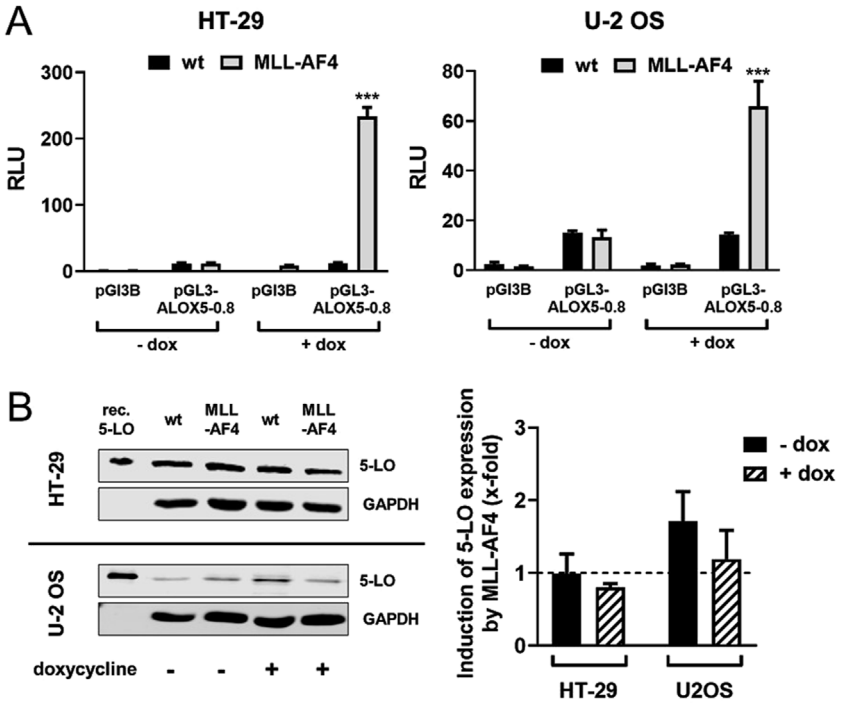

FIGURE 4
Effect of MLL-AF4 on 5-LO expression in HT-29 and U-2 OS cells. **(A)** Reporter gene analysis of HT-29 and U-2 OS wild type cells (wt) and cells stably transfected with MLL-AF4. Cells were transfected with reporter gene constructs containing the 5-LO core promoter (pGL3-ALOX5-0.8) or empty reporter vector as control (pGL3B). The activity was measured 24 h after transfection and incubation with or without doxycycline as emitted luminescence. The values were normalized to Renilla control and displayed as RLU. Results are presented as mean ± S.E.M. of three independent experiments. An unpaired *t*-test was used to determine the significance of the influence of the MLL-AF4 expressing cells compared to wild type cells. Asterisks indicate significant changes of wt cells compared to MLL-AF4 expressing cells. *$p \leq 0.05$, **$p \leq 0.01$, ***$p \leq 0.001$. **(B)** Western blot and densitometric analysis of 5-LO expression in wild type (wt) and stably transfected and inducible MLL-AF4 positive HT-29 and U-2 OS cells with or without doxycycline (dox) treatment. Quantitative evaluation of Western blot results presented as relative 5-LO expression normalized to GAPDH and 5-LO expression in wildtype cells. Results are presented as mean ± S.E.M. of three independent experiments.

expression of functional MLL-AF4 protein in reporter gene assays. As can be seen from Figure 4A, induction of MLL-AF4 expression with doxycycline treatment resulted in a 60- and 220-fold increase in *ALOX5* promoter activity in the MLL-AF4 transfected cells, but not in wild type controls. No activation of reporter activity was observed with the empty vector control. These results confirm the presence of doxycycline-dependent expression of functional MLL-AF4 in these cells. To study the influence of MLL-AF4 on the activity of the genomic *ALOX5* locus, both cell lines were treated with doxycycline, or left untreated before *ALOX5* mRNA and 5-LO protein expression were analyzed by qPCR and immunoblotting, respectively. As shown in Figure 4B, induction of MLL-AF4 expression by doxycycline treatment does not affect *ALOX5* mRNA and 5-LO protein expression in these cell lines.

siRNA-mediated knockdown of MLL-AF4 significantly represses ALOX5 gene expression in the B cell line SEM but not in the monocytic cell line MV4-11

In a next step we wanted to investigate the effect of a MLL-AF4 knockdown in cells with native MLL-AF4 and ALOX5 expression. For this purpose, the leukemic B cell line SEM and the myelomonocytic leukemia cell line MV4-11 were used for a siRNA mediated MLL-AF4 knockdown and the 5-LO mRNA expression was investigated. Knockdown of MLL-AF4 was performed by modified, self-delivering siRNA targeting the genomic t(4,11) breakpoint junctions. In order to ensure the correct design of the siRNAs, we first confirmed the sequences of the breakpoint junctions reported in the literature for these cells (Jansen et al., 2005; Gessner et al., 2010) by qPCR (data not shown). For method validation, we used self-delivering siRNA directed against glyceraldehyde-3-phosphate dehydrogenase (GAPDH) to ensure efficient siRNA uptake in these cells, while a pool of non-targeting siRNA served as a negative control. As depicted in Figure 5, incubation of SEM and MV4-11 cells with siRNA against GAPDH resulted in a residual level of ~13% (SEM) and ~45% (MV4-11) of GAPDH expression, confirming successful siRNA delivery. The mRNA expression levels could be significantly reduced by the siRNAs to ~29% (SEM) and to ~40% (MV4-11) of non-targeting siRNA controls. However, with respect to the effects of MLL-AF4 knockdown on *ALOX5* mRNA expression, the two cell lines were differently affected. In SEM cells, *ALOX5* mRNA expression was significantly downregulated to ~19% of the control, whereas in MV4-11 cells, although also statistically significant, the reduction of the mRNA level was only ~74% of the control.

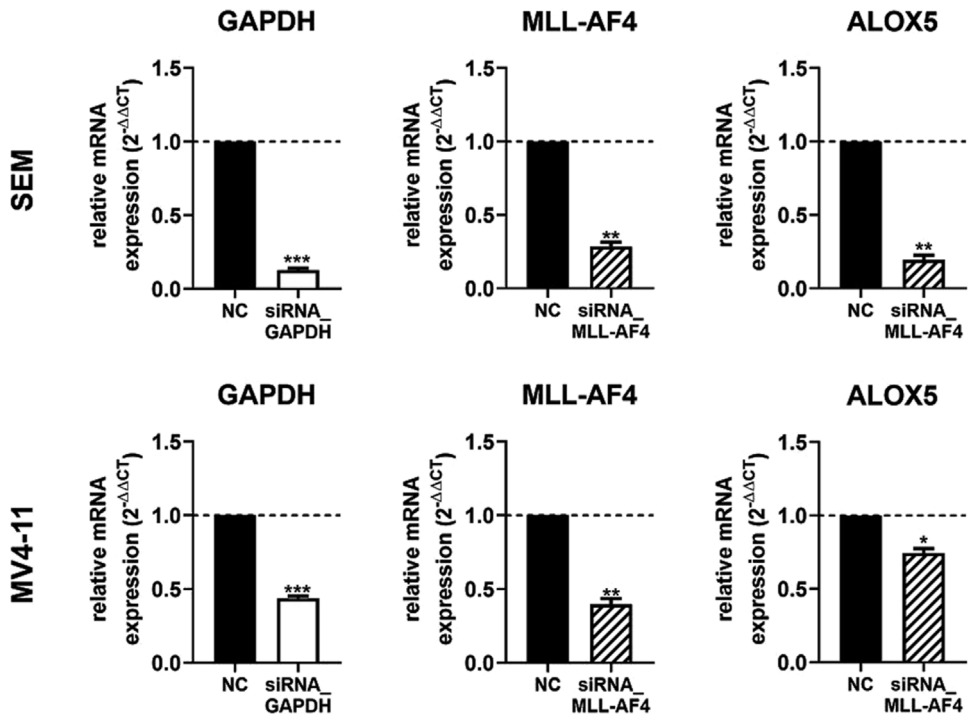

FIGURE 5
RT-qPCR analysis of 5-LO mRNA expression in siRNA-mediated MLL-AF4 knockdown cells (SEM, MV4-11). MV4-11 or SEM cells were incubated with 1 μM Accell® non targeting siRNA (NC) or target siRNA (GAPDH siRNA or MLL-AF4 siRNA). Results are presented as the mean of relative mRNA expression (normalized to UBC (housekeeping gene) and compared to NC treated cells ($2^{-\Delta\Delta CT}$)) ± S.E.M. of three independent experiments. An unpaired *t*-test with Welch´s correction was used to determine the significance. Asterisks indicate significant changes of target siRNA treated cells to NC treated cells. *$p \leq 0.05$, **$p \leq 0.01$, ***$p \leq 0.001$.

ALOX5 expression by TGFβ and 1,25(OH)$_2$D$_3$ is induced in MV4-11 cells but not in SEM cells

In conjunction with our finding that knockdown of MLL-AF4 affects *ALOX5* mRNA expression in MV4-11 and SEM cells differently (Figure 5), we analyzed whether the two cell lines display differential responsiveness of *ALOX5* gene expression and protein activity to TGFβ and 1,25(OH)$_2$D$_3$ that has been reported for B-cells and cells with monocytic properties (Jakobsson et al., 1992; Kreiß et al., 2022). We found that differentiation with TGFβ and 1,25(OH)$_2$D$_3$ induced marked morphological changes and reduced cell proliferation in MV4-11 cells, whereas SEM cells did not react to the treatment. Western blot analysis revealed a strong upregulation of 5-LO protein expression in MV4-11 cells after differentiation with TGFβ and 1,25(OH)$_2$D$_3$, but very low 5-LO protein expression was detected in SEM cells (Figure 6B; Supplementary Figure S3). Analysis of 5-LO activity was conducted in intact cells and cell homogenates (Figure 6A). In intact MV4-11 cells, differentiation with TGFβ and 1,25(OH)$_2$D$_3$ led to an upregulation of 5-LO product formation by 6-fold as compared to undifferentiated cells, whereas no 5-LO activity could be detected in differentiated and undifferentiated SEM cells. In SEM cell homogenates, we could not detect any 5-LO product formation. In contrast, 5-LO product formation in MV4-11 cell homogenates was increased ~213-fold by treatment with TGFβ and 1,25(OH)$_2$D$_3$ relative to undifferentiated cells. Since the combination of TGFβ and 1,25(OH)$_2$D$_3$ can act synergistically on myeloid cells, whereas TGFβ and 1,25(OH)$_2$D$_3$ alone produce less pronounced effects, we finally tested the influence of the individual treatments. We found that differentiation with TGFβ or 1,25(OH)$_2$D$_3$ alone led to an increase in 5-LO activity by ~21-fold and ~6-fold in MV4-11 cell homogenates, respectively.

MLL-AF9 also activates the ALOX5 promoter

Our finding that the chromosomal translocation product MLL-AF4 activates the *ALOX5* promoter prompted us to investigate if related MLL rearrangement proteins act in a similar fashion. To test this hypothesis, we investigated the fusion protein MLL-AF9 (Figure 7A) that is present in the monocytic cell lines MonoMac-6 and THP-1, which are frequently used model cell lines for studies on *ALOX5* expression and activity (Super et al., 1997; Pession et al., 2003). Thus, we amplified the MLL-AF9 coding sequence from MonoMac-6 cDNA and created the expression plasmid pT-MLL-AF9 which was employed in transient reporter gene assays. Interestingly, while MLL-AF4 increased 5-LO promoter activity by ~4.7-fold compared to VC, MLL-AF9 even led to an increase of ~7.2-fold (Figure 7B). Finally, we checked for a possible link between our findings that the fusion protein MLL-AF9 activates the *ALOX5* promoter and the long-known observation that *ALOX5* expression is strongly upregulated by TGFβ and 1.25(OH)$_2$D$_3$ in MonoMac-6 and THP-1 cells (Kreiß et al., 2022). However, no significant differences could be found, as shown in Figure 7C, suggesting that the strong induction of *ALOX5* expression by TGFβ and 1,25(OH)$_2$D$_3$ is not due to the induction of MLL rearrangement products.

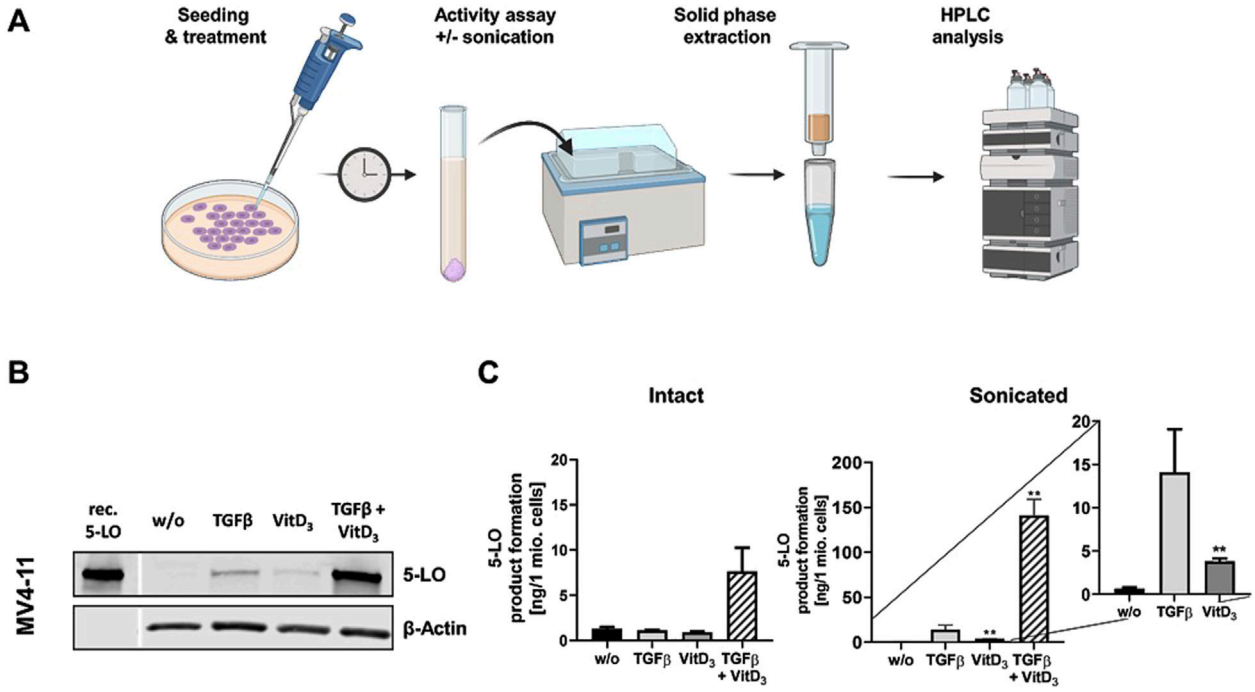

FIGURE 6
Incubation of MV4-11 cells with differentiation reagents. **(A)** Illustration of the workflow of 5-LO activity assay. **(B)** Western blot analysis of 5-LO expression in MV4-11 cells. Cells were incubated without (w/o) or with TGFβ, 1,25(OH)$_2$D$_3$ (VitD$_3$), or the combination of both. Each blot represents the results of three independent experiments. **(C)** 5-LO product formation in MV4-11 cells after treatment with TGFβ or 1,25(OH)$_2$D$_3$ (VitD$_3$), the combination of both or untreated cells (w/o). After 72 h 5-LO product formation was determined. Results are presented as mean ± S.E.M. of three independent experiments. Dunnet´s multiple comparison test was used to determine the significance of the influence of treated cells compared to untreated cells. Asterisks indicate significancy. *$p \leq 0.05$, **$p \leq 0.01$, ***$p \leq 0.001$.

Discussion

Previous studies have shown that the fusion protein MLL-AF4 is able to induce the *ALOX5* promoter in reporter gene assays (Ahmad et al., 2014). This observation suggested a potential link between the strong leukemogenic driver protein MLL-AF4 and 5-lipoxygenase. Apart from its prominent role in inflammation (Rådmark et al., 2007; Brand et al., 2018; Kreiß et al., 2022), 5-lipoxygenase has also been associated with tumorigenesis (Kennedy and Harris, 2023; Kahnt et al., 2024) as well as with survival advantages and the aggressiveness of tumor cells (Runarsson et al., 2005; Guriec et al., 2014). As discussed, subsequently, we provide evidence on the mechanism and the cell specificity of MLL-AF4-mediated *ALOX5* gene regulation.

The tandem GC-box of the ALOX5 promoter and the CXXC domain of MLL-AF4 are crucial for MLL-AF4-mediated ALOX5 promoter activation

The proximal *ALOX5* promoter contains a five-fold tandem consensus SP1 binding motif, which is considered the core element of the promoter responsible for basal activity (Hoshiko et al., 1990). Concomitantly, it is known that the CXXC domain of MLL-AF4 binds to hemi-methylated CpG-rich elements (Birke et al., 2002), pointing to an interaction between MLL-AF4 and the *ALOX5* promoter via GC boxes. In line with this, we could show by reporter analysis that the five-fold tandem GC-box into the viral thymidine kinase promoter renders this promoter inducible by MLL-AF4. Second, we found that deletion of the GC-box from the *ALOX5* promoter sequence significantly decreases its responsiveness to MLL-AF4. Conversely, we show through targeted mutation of the CXXC domain that MLL-AF4 activation of the *ALOX5* promoter depends on this element, as CXXC mutation dramatically reduces the induction of reporter gene activity by the CXXC mutant. This suggests a crucial role of the GC-boxes and the CXXC domain. It is noteworthy that the tandem GC-box which serves as the primary binding motif for MLL-AF4 is subject to naturally occurring polymorphisms. In a study, 6% of asthma patients exhibited mutations within this GC-box arrangement, leading to an unresponsiveness to treatment with 5-LO targeting medications like zileuton. Thus, it would be interesting, whether alterations in the GC box of *ALOX5* is of relevance in the context of leukemias carrying MLL-containing fusion proteins such as MLL-AF4 (Drazen et al., 1999).

pSER, AF9-ID and CH domains of MLL-AF4 redundantly mediate ALOX5 promoter activation

MLL-AF4, as a prominent leukemogenic product of MLL-r (MLL gene rearrangements), contains a multitude of protein

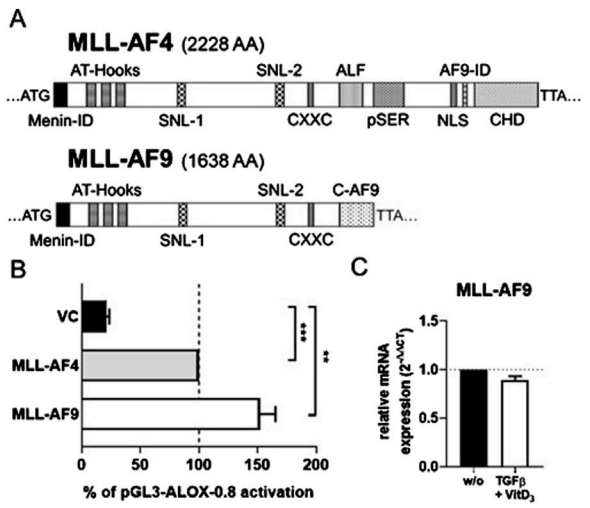

FIGURE 7
Comparison of MLL-AF4 and MLL-AF9. **(A)** MLL-AF4 and MLL-AF9 protein size in amino acids (AA). **(B)** Transcriptional activation of the *ALOX5* promoter by MLL-AF4 and MLL-AF9. HeLa cells were transfected with the expression plasmid for MLL-AF4 or MLL-AF9 and with a reporter plasmid containing the *ALOX5* promoter (pGL3-ALOX5-0.8). Promoter activity is displayed as % activation compared to activation of pGL3-ALOX5-0.8 by full length MLL-AF4, the Renilla signal was used for normalization. Results are presented as mean ± S.E.M. of three independent experiments. Welch´s *t*-test was used to determine the significance of the influence of the MLL-AF9 and VC compared to MLL-AF4 activation of pGL3-ALOX5-0.8. Asterisks indicate significant changes vs. control vector cells. $*p \leq 0.05$, $**p \leq 0.01$, $***p \leq 0.001$. **(C)** qPCR analysis of MLL-AF9 mRNA expression after differentiation of MonoMac-6 cells with TGFβ and $1,25(OH)_2D_3$ for 72 h or without treatment (w/o). Results are presented as relative MLL-AF9 mRNA expression (normalized to the housekeeping gene UBC and compared to NC treated cells ($2^{-\Delta\Delta CT}$)).

domains whose functions are not yet fully understood (Lavau et al., 1997). We found that in addition to the CXXC domain, distinct domains of the AF4-part of MLL-AF4 are essential for the *ALOX5* promoter activation (see below) but that the deletion of the Menin binding domain and thus the interaction with LEDGF is of minor importance and that the DNA binding AT-hooks do not play a significant role in *ALOX5* promoter activation (Figure 2) (Yokoyama et al., 2005; El Ashkar et al., 2017). In contrast, complete deletion of the AF4 fragment (construct N-MLL) strongly diminished the transactivation potency of the mutants to levels comparable with the CXXC mutant, which shows that at least one of the redundantly acting AF4 segments is necessary for the activity of the fusion protein. The deletion analysis of the AF4 part suggests that the pSer, AF9-ID and CH domains have redundant functions in 5-LO promoter activation (Figure 2). In addition, a deletion of both CHD and AF9-ID (construct MLL_ALFpSER) results in a moderately active fusion protein that is only ~69% active compared to the full-length construct. This suggests that either the interaction with ENL or AF9 via AF9-ID or the interaction with the AF4 wild-type complex via CHD may be sufficient to recruit the P-TEFb/SEC (super elongation complex) and initiate transcriptional elongation of promoter-proximal arrested RNA polymerase (POL A) via conversion into elongating RNA polymerase (POL E) (Mueller et al., 2009; Luo et al., 2012; Slany, 2020). This would explain why there is no simultaneous requirement for both domains to interact with their protein partners, provided that there is at least one interaction of the MLL-AF4 fusion protein with P-TEFb/SEC (Lin et al., 2010; He et al., 2011; Luo et al., 2012; Fujinaga et al., 2023). The remaining activity of MLL_ALFpSER could be explained by the fact, that the pSER domain can still fulfil a transactivation function via recruitment of the selective factor 1 complex (Okuda et al., 2015; Siemund et al., 2022). Our findings are summarized in Figure 8. Finally, to find a minimal functional MLL-AF4 mutant, we designed a construct (Men-CXXC-CHD), containing the putative essential domains based on our reporter gene assays. Surprisingly, the construct remained inactive for an as yet unknown reason.

Nuclear localization of mutated MLL-AF4 constructs

For the inactive MLL-AF4 mutants (N-MLL, MLL-AF4_CXXCmut, Men-CXXC-CHD) we found that all constructs are expressed and located in the nucleus so that the lack of activity is not due to a failure of protein expression and a lacking import into the nucleus, rather to a loss of function (Figure 3). The observation that MLL-AF4-GFP and MLL-AF4_CXXCmut-GFP exhibit a highly punctuated distribution within the nucleus is in agreement with findings of previously published studies on the N-MLL protein, where it was suggested that this punctuated pattern is likely to be associated with wt-MLL binding DNA (Yano et al., 1997) and a formation of transcriptional, highly active micro compartments (Rasouli et al., 2024). However, even the construct with a mutated CXXC domain (MLL-AF4_CXXCmut-GFP), exhibits this speckled nuclear distribution, although the mutated CXXC domain should no longer be able to bind to DNA. This could indicate that the DNA binding is transmitted through an additional protein region (e.g., AT-hooks) which is not able to substitute for the CXXC domain binding towards GC boxes but can mediate interaction with DNA (Reeves and Nissen, 1990; Aravind and Landsman, 1998). Furthermore, it is worth mentioning that even the smallest construct (Men-CXXC-CHD) is located in the nucleus, even though it does not contain nuclear localization sequences. This could be a hint for a shuttling mechanism which could be transmitted through the CH domain, working as an interaction platform for ENL and with this for AF9. It is known that both proteins, ENL and AF9, are located in the nucleus and could shuttle Men-CXXC-CHD to the same destination (Rubnitz et al., 1994; Erfurth et al., 2004; Kabra and Bushweller, 2022).

Regulation of ALOX5 gene in solid tumor cells is not affected by MLL-AF4 co-expression

The knock-in and the expression of the MLL-AF4 fusion gene into the colorectal cancer cell line HT-29 and the osteosarcoma cell line U-2 OS did not result in a significant change in the expression of the 5-LO (Figure 4B). Despite demonstrating that MLL-AF4 is expressed and active following the induction with doxycycline and the followed induction of the *ALOX5* reporter system, we did not see any change in 5-LO protein levels, when the cells

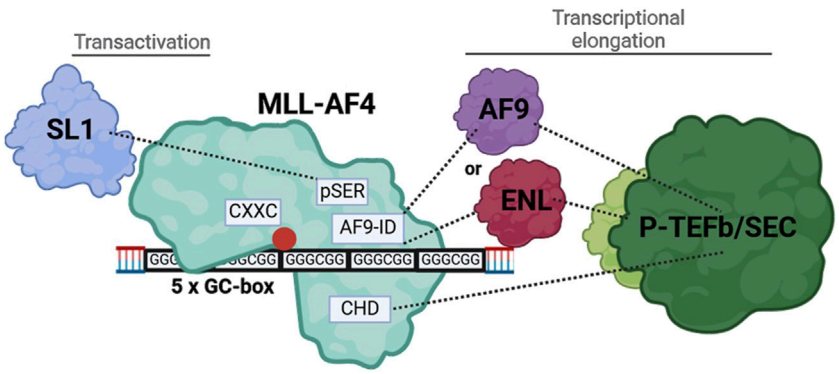

FIGURE 8
Illustration of the interaction of MLL-AF4 with the tandem GC-box within the *ALOX5* promoter and the recruitment of interaction partners, resulting in increased gene expression.

express MLL-AF4 (Figure 4A). This indicates that the native *ALOX5* promoter is regulated differently in these solid tumor cell lines, compared to the transiently transfected pGL3-ALOX5-0.8 reporter construct.

Differential regulation of ALOX5 expression by MLL-AF4 as well as TGFβ and 1,25(OH)$_2$D$_3$ in SEM and MV4-11 cells

So far, the mechanisms involved in 5-LO pathway activation in lymphoid and myeloid leukemia is very limited. It was reported that a loss of the ALOX5 gene prevents the outbreak of leukemia in a mouse model (Chen et al., 2009). Even though this study needs independent reproduction it is clear evidence, that 5-LO could play a major role in the development and progression of malignant blood diseases. To get a better insight into the mechanisms behind the ALOX5 activation, we used SEM and MV4-11 cells which both carry the chromosomal translocation t(4;11)(q21;q23), resulting in the expression of two reciprocal fusion proteins, MLL-AF4 and AF4-MLL, and performed MLL-AF4 knockdown experiments. It is known that malignant B-cells can over express 5-LO, but so far this regulation does not lead to increased 5-LO metabolite formation suggesting that 5-LO might have non-canonical functions in these cell lines (Jakobsson et al., 1992; Kahnt et al., 2024). However, 5-LO mRNA and protein expression in SEM cells is not upregulated (Karlsson et al., 2021; Proteinatlas, 2024). Interestingly, *ALOX5* gene expression in SEM cells is significantly downregulated by the MLL-AF4 knockdown (Figure 5 SEM). However, we were not able to detect MLL-AF4 or 5-LO via Western blotting due to low expression levels. Interestingly, another study in 1995 encompassing eight samples of B-ALL patients, showed that only four of the tested cells expressed 5-LO (Feltenmark et al., 1995). In contrast to SEM cells, the knockdown of MLL-AF4 only slightly affected *ALOX5* mRNA expression in MV4-11 cells in our study (Figure 5, MV4-11), indicating that the *ALOX5* regulation is different in both cell lines. This is supported by the observation that 5-LO expression and activity is strongly induced by TGFβ and 1,25(OH)$_2$D$_3$ in MV4-11 cells but not in SEM cells (Figure 6). The elevated formation of 5-LO pathway metabolites is an interesting finding, as it was already published that the expression and the formation of 5-LO products can contribute to an inflammatory environment that promotes malignant progression and chemotherapeutic resistance in myeloid leukemia (Runarsson et al., 2007; Vincent et al., 2008; Stranahan et al., 2022). We could previously show that induction of 5-LO gene expression in myeloid cells by TGFβ and 1,25(OH)$_2$D$_3$ is mainly due to transcript elongation (Sorg et al., 2006; Rådmark et al., 2007; Stoffers et al., 2010; Ahmad et al., 2015). Our data on the MLL-AF4 fusion protein and its dependence on the tandem GC box in the *ALOX5* promoter as well as the CXXC domain suggests that its activity is related to transcriptional initiation. Interestingly, previous studies showed that the reciprocal fusion protein of MLL-AF4, AF4-MLL (N-terminal AF4 fused with C-terminal MLL) mediates the responsiveness of the ALOX5 gene to induction by TGFβ and 1,25(OH)$_2$D$_3$ which is associated with regulatory elements in the distal parts of the *ALOX5* gene and related to transcriptional elongation (Ahmad et al., 2015). Thus, the *ALOX5* gene in SEM cells appears to be more promoter driven by MLL-AF4 whereas in MV4-11 cells induction of transcriptional elongation by TGFβ and 1,25(OH)$_2$D$_3$ mainly drives *ALOX5* expression. Whereas 5-LO expression and activity is high in differentiated myeloid cells and in the majority of B cell lines, the low 5-LO expression in SEM cells and the lack of cellular activity could point to a role of 5-LO as transcriptional regulator and regulator of cell proliferation in this cell line (Jakobsson et al., 1995; Mahshid et al., 2009; Kreiß et al., 2022; Claesson et al., 2024).

MLL-AF9 and MLL-AF4 similarly activate the ALOX5 promoter

MLL-AF9 is the translocation product of the KMT2A gene and the MLLT3 Super Elongation Complex Subunit gene (MLLT3). This fusion occurs much more prominent in acute myeloid leukemias (Meyer et al., 2013). The resulting fusion protein MLL-AF9 contains the same N-terminal MLL domains as MLL-AF4 but has a different C-terminus. The finding that MLL-AF9 induces the *ALOX5* even stronger compared to MLL-AF4 is of high interest taking the fact that the C-terminal AF9 portion in MLL-AF9 is much smaller than C-terminal AF4 in MLL-AF4 which provides a much smaller

interaction surface for other proteins of the P-TEFb/SEC (Figure 7A). It is known that MLL-AF9 interacts with members of the super elongation complex such as wt-AF4 and PAF1 via its C-terminal ANC1 homology and YEATS domain (AHD) (Pession et al., 2003; He et al., 2011). Thus, a common mechanism of MLL-AF4 and MLL-AF9 could be the recruitment of the AF4 super elongation complex (SEC) via the AF9-ID or CHD portion of the protein (Steinhilber and Marschalek, 2018). This finding is in line with our observation that only one C-terminal interactive domain in MLL-AF4 is needed to recruit the P-TEFb/SEC elongation complex, pointing towards a similarity between the activation mechanism of MLL-AF4 and MLL-AF9. AML cells, such as MonoMac-6 and THP-1, carrying the MLL-AF9 translocation, show strong *ALOX5* induction by TGFβ and $1,25(OH)_2D_3$ (Brungs et al., 1995; Kreiß et al., 2022), similar to our findings with MV4-11 cells (Figure 6C). However, we did not observe significant changes in MLL-AF9 expression suggesting that the effects of TGFβ and $1,25(OH)_2D$ are not due to induction of MLL-AF9 but are related to different, yet unknown mechanisms. Of note, it will be interesting to study ALOX5 expression in freshly isolated AML cells carrying MLL translocations.

Taken together, we could show that MLL-AF4 and MLL-AF9 strongly activate the *ALOX5* promoter in B-lymphocytic cells and that the MLL-AF4 effects are mediated by the tandem GC box in the *ALOX5* promoter. Furthermore, we could identify several AF4 domains known to bind the super elongation complex that are essential for the induction of *ALOX5* promoter activity.

Data availability statement

The raw data supporting the conclusions of this article will be made available by the authors, without undue reservation.

Ethics statement

Ethical approval was not required for the studies on humans in accordance with the local legislation and institutional requirements because only commercially available established cell lines were used. Ethical approval was not required for the studies on animals in accordance with the local legislation and institutional requirements because only commercially available established cell lines were used.

Author contributions

MH: Conceptualization, Formal Analysis, Methodology, Validation, Visualization, Writing–original draft, Writing–review and editing. MM: Methodology, Writing–original draft. IS: Methodology, Writing–original draft. RM: Supervision, Writing–review and editing. DS: Conceptualization, Funding acquisition, Supervision, Visualization, Writing–review and editing.

Funding

The author(s) declare that financial support was received for the research, authorship, and/or publication of this article. DS was supported by the Deutsche Forschungsgemeinschaft (SFB 1039, TP A02; GRK 2336, TP4), the LOEWE project TRABITA and the Fraunhofer Leistungszentrum Innovative Therapeutics (TheraNova).

Acknowledgments

We would like to express our sincerest gratitude to Bernd Sorg for his invaluable support, insightful discussions, and professional consultation. Figures 6a, 8 were created with BioRender.

Conflict of interest

The authors declare that the research was conducted in the absence of any commercial or financial relationships that could be construed as a potential conflict of interest.

The author(s) declared that they were an editorial board member of Frontiers, at the time of submission. This had no impact on the peer review process and the final decision.

Generative AI statement

The author(s) declare that no Generative AI was used in the creation of this manuscript.

Publisher's note

Supplementary material

The Supplementary Material for this article can be found online at: https://www.frontiersin.org/articles/10.3389/fphar.2024.1520507/full#supplementary-material

References

Ahmad, K., Katryniok, C., Scholz, B., Merkens, J., Löscher, D., Marschalek, R., et al. (2014). Inhibition of class I HDACs abrogates the dominant effect of MLL-AF4 by activation of wild-type MLL. *Oncogenesis* 3, e127. doi:10.1038/oncsis.2014.39

Ahmad, K., Scholz, B., Capelo, R., Schweighöfer, I., Kahnt, A. S., Marschalek, R., et al. (2015). AF4 and AF4-MLL mediate transcriptional elongation of 5-lipoxygenase mRNA by 1, 25-dihydroxyvitamin D3. *Oncotarget* 6, 25784–25800. doi:10.18632/oncotarget.4703

Aravind, L., and Landsman, D. (1998). AT-hook motifs identified in a wide variety of DNA-binding proteins. *Nucleic Acids Res.* 26, 4413–4421. doi:10.1093/nar/26.19.4413

Behm, F., Raimondi, S., Frestedt, J., Liu, Q., Crist, W., Downing, J., et al. (1996). Rearrangement of the MLL gene confers a poor prognosis in childhood acute lymphoblastic leukemia, regardless of presenting age. *Blood* 87, 2870–2877. doi:10.1182/blood.V87.7.2870.bloodjournal8772870

Benedikt, A., Baltruschat, S., Scholz, B., Bursen, A., Arrey, T. N., Meyer, B., et al. (2011). The leukemogenic AF4–MLL fusion protein causes P-TEFb kinase activation and altered epigenetic signatures. *Leukemia* 25, 135–144. doi:10.1038/leu.2010.249

Birke, M., Schreiner, S., García-Cuéllar, M.-P., Mahr, K., Titgemeyer, F., and Slany, R. K. (2002). The MT domain of the proto-oncoprotein MLL binds to CpG-containing DNA and discriminates against methylation. *Nucleic Acids Res.* 30, 958–965. doi:10.1093/nar/30.4.958

Bitoun, E., Oliver, P. L., and Davies, K. E. (2007). The mixed-lineage leukemia fusion partner AF4 stimulates RNA polymerase II transcriptional elongation and mediates coordinated chromatin remodeling. *Hum. Mol. Genet.* 16, 92–106. doi:10.1093/hmg/ddl444

Brand, S., Roy, S., Schröder, P., Rathmer, B., Roos, J., Kapoor, S., et al. (2018). Combined proteomic and *in silico* target identification reveal a role for 5-lipoxygenase in developmental signaling pathways. *Cell Chem. Biol.* 25, 1095–1106. doi:10.1016/j.chembiol.2018.05.016

Brungs, M., Rådmark, O., Samuelsson, B., and Steinhilber, D. (1995). Sequential induction of 5-lipoxygenase gene expression and activity in Mono Mac 6 cells by transforming growth factor beta and 1,25-dihydroxyvitamin D3. *Proc. Natl. Acad. Sci.* 92, 107–111. doi:10.1073/pnas.92.1.107

Chen, Y., Hu, Y., Zhang, H., Peng, C., and Li, S. (2009). Loss of the Alox5 gene impairs leukemia stem cells and prevents chronic myeloid leukemia. *Nat. Genet.* 41, 783–792. doi:10.1038/ng.389

Claesson, H.-E., Sjöberg, J., Xu, D., and Björkholm, M. (2024). Expression and putative biological roles of lipoxygenases and leukotriene receptors in leukemia and lymphoma. *Prostagl. Other Lipid Mediat* 174, 106871. doi:10.1016/j.prostaglandins.2024.106871

Drazen, J. M., Yandava, C. N., Dubé, L., Szczerback, N., Hippensteel, R., Pillari, A., et al. (1999). Pharmacogenetic association between ALOX5 promoter genotype and the response to anti-asthma treatment. *Nat. Genet.* 22, 168–170. doi:10.1038/9680

Domer, P. H., Fakharzadeh, S. S., Chen, C. S., Jockel, J., Johansen, L., Silverman, G. A., et al. (1993). Acute mixed-lineage leukemia t(4;11)(q21;q23) generates an MLL-AF4 fusion product. *Proc. Natl. Acad. Sci.* 90, 7884–7888. doi:10.1073/pnas.90.16.7884

El Ashkar, S., Schwaller, J., Pieters, T., Goossens, S., Demeulemeester, J., Christ, F., et al. (2017). LEDGF/p75 is dispensable for hematopoiesis but essential for MLL-rearranged leukemogenesis. *Blood* 131, 95–107. blood-2017-05-786962. doi:10.1182/blood-2017-05-786962

Erfurth, F., Hemenway, C. S., de Erkenez, A. C., and Domer, P. H. (2004). MLL fusion partners AF4 and AF9 interact at subnuclear foci. *Leukemia* 18, 92–102. doi:10.1038/sj.leu.2403200

Feltenmark, S., Runarsson, G., Larsson, P., Jakobsson, P.-J., Bjorkholm, M., and Claesson, H.-E. (1995). Diverse expression of cytosolic phospholipase A 2, 5-lipoxygenase and prostaglandin H synthase 2 in acute pre-B-lymphocytic leukaemia cells. *Br. J. Haematol.* 90, 585–594. doi:10.1111/j.1365-2141.1995.tb05588.x

Fujinaga, K., Huang, F., and Peterlin, B. M. (2023). P-TEFb: the master regulator of transcription elongation. *Mol. Cell* 83, 393–403. doi:10.1016/j.molcel.2022.12.006

Funk, C. D., Hoshiko, S., Matsumoto, T., Rdmark, O., and Samuelsson, B. (1989). Characterization of the human 5-lipoxygenase gene. *Proc. Natl. Acad. Sci.* 86, 2587–2591. doi:10.1073/pnas.86.8.2587

Gessner, A., Thomas, M., Garrido Castro, P., Büchler, L., Scholz, A., Brümmendorf, T. H., et al. (2010). Leukemic fusion genes MLL/AF4 and AML1/MTG8 support leukemic self-renewal by controlling expression of the telomerase subunit TERT. *Leukemia* 24, 1751–1759. doi:10.1038/leu.2010.155

Göbel, T., Goebel, B., Hyprath, M., Lamminger, I., Weisser, H., Angioni, C., et al. (2023). Three-dimensional growth reveals fine-tuning of 5-lipoxygenase by proliferative pathways in cancer. *Life Sci. Alliance* 6, e202201804. doi:10.26508/lsa.202201804

Guriec, N., Le Jossic- Corcos, C., Simon, B., Ianotto, J. C., Tempescul, A., Dréano, Y., et al. (2014). The arachidonic acid-LTB4-BLT2 pathway enhances human B-CLL aggressiveness. *Biochim. Biophys. Acta Mol. Basis Dis.* 1842, 2096–2105. doi:10.1016/j.bbadis.2014.07.016

He, N., Chan, C. K., Sobhian, B., Chou, S., Xue, Y., Liu, M., et al. (2011). Human polymerase-associated factor complex (PAFc) connects the super elongation complex (SEC) to RNA polymerase II on chromatin. *Proc. Natl. Acad. Sci.* 108, E636–E645. doi:10.1073/pnas.1107107108

Hoshiko, S., Rådmark, O., and Samuelsson, B. (1990). Characterization of the human 5-lipoxygenase gene promoter. *Proc. Natl. Acad. Sci.* 87, 9073–9077. doi:10.1073/pnas.87.23.9073

In, K. H., Asano, K., Beier, D., Grobholz, J., Finn, P. W., Silverman, E. K., et al. (1997). Naturally occurring mutations in the human 5-lipoxygenase gene promoter that modify transcription factor binding and reporter gene transcription. *J. Clin. Investigation* 99, 1130–1137. doi:10.1172/JCI119241

Jakobsson, P., Shaskin, P., Larsson, P., Feltenmark, S., Odlander, B., Aguilar-Santelises, M., et al. (1995). Studies on the regulation and localization of 5-lipoxygenase in human B-lymphocytes. *Eur. J. Biochem.* 232, 37–46. doi:10.1111/j.1432-1033.1995.tb20778.x

Jakobsson, P. J., Steinhilber, D., Odlander, B., Rådmark, O., Claesson, H. E., and Samuelsson, B. (1992). On the expression and regulation of 5-lipoxygenase in human lymphocytes. *Proc. Natl. Acad. Sci.* 89, 3521–3525. doi:10.1073/pnas.89.8.3521

Jansen, M. W. J. C., van der Velden, V. H. J., and van Dongen, J. J. M. (2005). Efficient and easy detection of MLL-AF4, MLL-AF9 and MLL-ENL fusion gene transcripts by multiplex real-time quantitative RT-PCR in TaqMan and LightCycler. *Leukemia* 19, 2016–2018. doi:10.1038/sj.leu.2403939

Kabra, A., and Bushweller, J. (2022). The intrinsically disordered proteins MLLT3 (AF9) and MLLT1 (ENL) – multimodal transcriptional switches with roles in normal hematopoiesis, MLL fusion leukemia, and kidney cancer. *J. Mol. Biol.* 434, 167117. doi:10.1016/j.jmb.2021.167117

Kahnt, A. S., Häfner, A.-K., and Steinhilber, D. (2024). The role of human 5-Lipoxygenase (5-LO) in carcinogenesis - a question of canonical and non-canonical functions. *Oncogene* 43, 1319–1327. doi:10.1038/s41388-024-03016-1

Karlsson, M., Zhang, C., Méar, L., Zhong, W., Digre, A., Katona, B., et al. (2021). A single–cell type transcriptomics map of human tissues. *Sci. Adv.* 7, eabh2169–9. doi:10.1126/sciadv.abh2169

Kennedy, B. M., and Harris, R. E. (2023). Cyclooxygenase and lipoxygenase gene expression in the inflammogenesis of colorectal cancer: correlated expression of EGFR, JAK STAT and src genes, and a natural antisense transcript, RP11-C67.2.2. *Cancers (Basel)* 15, 2380. doi:10.3390/cancers15082380

Kitamura, A., Nakayama, Y., and Kinjo, M. (2015). Efficient and dynamic nuclear localization of green fluorescent protein via RNA binding. *Biochem. Biophys. Res. Commun.* 463, 401–406. doi:10.1016/j.bbrc.2015.05.084

Klan, N., Seuter, S., Schnur, N., Jung, M., and Steinhilber, D. (2003). Trichostatin A and structurally related histone deacetylase inhibitors induce 5-lipoxygenase promoter activity. *Biol. Chem.* 384, 777–785. doi:10.1515/BC.2003.086

Kowarz, E., Löscher, D., and Marschalek, R. (2015). Optimized Sleeping Beauty transposons rapidly generate stable transgenic cell lines. *Biotechnol. J.* 10, 647–653. doi:10.1002/biot.201400821

Kreiß, M., Oberlis, J. H., Seuter, S., Bischoff-Kont, I., Sürün, D., Thomas, D., et al. (2022). Human 5-lipoxygenase regulates transcription by association to euchromatin. *Biochem. Pharmacol.* 203, 115187. doi:10.1016/j.bcp.2022.115187

Lavau, C., Szilvassy, S. J., Slany, R., and Cleary, M. L. (1997). Immortalization and leukemic transformation of a myelomonocytic precursor by retrovirally transduced HRX-ENL. *EMBO J.* 16, 4226–4237. doi:10.1093/emboj/16.14.4226

Lin, C., Smith, E. R., Takahashi, H., Lai, K. C., Martin-Brown, S., Florens, L., et al. (2010). AFF4, a component of the ELL/P-TEFb elongation complex and a shared subunit of MLL chimeras, can link transcription elongation to leukemia. *Mol. Cell* 37, 429–437. doi:10.1016/j.molcel.2010.01.026

Luo, Z., Lin, C., and Shilatifard, A. (2012). The super elongation complex (SEC) family in transcriptional control. *Nat. Rev. Mol. Cell Biol.* 13, 543–547. doi:10.1038/nrm3417

Mahshid, Y., Lisy, M.-R., Wang, X., Spanbroek, R., Flygare, J., Christensson, B., et al. (2009). High expression of 5-lipoxygenase in normal and malignant mantle zone B lymphocytes. *BMC Immunol.* 10, 2. doi:10.1186/1471-2172-10-2

Marschalek, R. (2016). Systematic classification of mixed-lineage leukemia fusion partners predicts additional cancer pathways. *Ann. Lab. Med.* 36, 85–100. doi:10.3343/alm.2016.36.2.85

Meyer, C., Hofmann, J., Burmeister, T., Gröger, D., Park, T. S., Emerenciano, M., et al. (2013). The MLL recombinome of acute leukemias in 2013. *Leukemia* 27, 2165–2176. doi:10.1038/leu.2013.135

Meyer, C., Larghero, P., Almeida Lopes, B., Burmeister, T., Gröger, D., Sutton, R., et al. (2023). The KMT2A recombinome of acute leukemias in 2023. *Leukemia* 37, 988–1005. doi:10.1038/s41375-023-01877-1

Moore, G., and Pidgeon, G. (2017). Cross-talk between cancer cells and the tumour microenvironment: the role of the 5-lipoxygenase pathway. *Int. J. Mol. Sci.* 18, 236. doi:10.3390/ijms18020236

Mueller, D., Bach, C., Zeisig, D., Garcia-Cuellar, M.-P., Monroe, S., Sreekumar, A., et al. (2007). A role for the MLL fusion partner ENL in transcriptional elongation and chromatin modification. *Blood* 110, 4445–4454. doi:10.1182/blood-2007-05-090514

Mueller, D., García-Cuéllar, M. P., Bach, C., Buhl, S., Maethner, E., and Slany, R. K. (2009). Misguided transcriptional elongation causes mixed lineage leukemia. *PLoS Biol.* 7, e1000249. doi:10.1371/journal.pbio.1000249

Nilson, I., Reichel, M., Ennas, M. G., Greim, R., Knörr, C., Siegler, G., et al. (1997). Exon/intron structure of the human AF-4 gene, a member of the AF -4/LAF -4/FMR -2 gene family coding for a nuclear protein with structural alterations in acute leukaemia. *Br. J. Haematol.* 98, 157–169. doi:10.1046/j.1365-2141.1997.1522966.x

Okuda, H., Kanai, A., Ito, S., Matsui, H., and Yokoyama, A. (2015). AF4 uses the SL1 components of RNAP1 machinery to initiate MLL fusion- and AEP-dependent transcription. *Nat. Commun.* 6, 8869. doi:10.1038/ncomms9869

Pession, A., Martino, V., Tonelli, R., Beltramini, C., Locatelli, F., Biserni, G., et al. (2003). MLL-AF9 oncogene expression affects cell growth but not terminal differentiation and is downregulated during monocyte-macrophage maturation in AML-M5 THP-1 cells. *Oncogene* 22, 8671–8676. doi:10.1038/sj.onc.1207125

Proteinatlas (2024). Proteinatlas.org: data available from v23.0.proteinatlas.org. Available at: https://www.proteinatlas.org/ENSG00000012779-ALOX5/cell+line#leukemia (Accessed August 28, 2024).

Provost, P., Samuelsson, B., and Rådmark, O. (1999). Interaction of 5-lipoxygenase with cellular proteins. *Proc. Natl. Acad. Sci.* 96, 1881–1885. doi:10.1073/pnas.96.5.1881

Rådmark, O., Werz, O., Steinhilber, D., and Samuelsson, B. (2007). 5-Lipoxygenase: regulation of expression and enzyme activity. *Trends Biochem. Sci.* 32, 332–341. doi:10.1016/j.tibs.2007.06.002

Rådmark, O., Werz, O., Steinhilber, D., and Samuelsson, B. (2015). 5-Lipoxygenase, a key enzyme for leukotriene biosynthesis in health and disease. *Biochimica Biophysica Acta (BBA) - Mol. Cell Biol. Lipids* 1851, 331–339. doi:10.1016/j.bbalip.2014.08.012

Rasouli, M., Troester, S., Grebien, F., Goemans, B. F., Zwaan, C. M., and Heidenreich, O. (2024). NUP98 oncofusions in myeloid malignancies: an update on molecular mechanisms and therapeutic opportunities. *Hemasphere* 8, e70013. doi:10.1002/hem3.70013

Reeves, R., and Nissen, M. S. (1990). The A·T-DNA-binding domain of mammalian high mobility group I chromosomal proteins: a novel peptide motif for recognizing DNA structure. *J. Biol. Chem.* 265, 8573–8582. doi:10.1016/s0021-9258(19)38926-4

Rubnitz, J., Morrissey, J., Savage, P., and Cleary, M. (1994). ENL, the gene fused with HRX in t(11;19) leukemias, encodes a nuclear protein with transcriptional activation potential in lymphoid and myeloid cells. *Blood* 84, 1747–1752. doi:10.1182/blood.V84.6.1747.1747

Runarsson, G., Feltenmark, S., Forsell, P. K. A., Sjöberg, J., Björkholm, M., and Claesson, H. (2007). The expression of cytosolic phospholipase A 2 and biosynthesis of leukotriene B 4 in acute myeloid leukemia cells. *Eur. J. Haematol.* 79, 468–476. doi:10.1111/j.1600-0609.2007.00967.x

Runarsson, G., Liu, A., Mahshid, Y., Feltenmark, S., Pettersson, A., Klein, E., et al. (2005). Leukotriene B4 plays a pivotal role in CD40-dependent activation of chronic B lymphocytic leukemia cells. *Blood* 105, 1274–1279. doi:10.1182/blood-2004-07-2546

Schneider, C. A., Rasband, W. S., and Eliceiri, K. W. (2012). NIH Image to ImageJ: 25 years of image analysis. *Nat. Methods* 9, 671–675. doi:10.1038/nmeth.2089

Schnur, N., Seuter, S., Katryniok, C., Rådmark, O., and Steinhilber, D. (2007). The histone deacetylase inhibitor trichostatin A mediates upregulation of 5-lipoxygenase promoter activity by recruitment of Sp1 to distinct GC-boxes. *Biochimica Biophysica Acta (BBA) - Mol. Cell Biol. Lipids* 1771, 1271–1282. doi:10.1016/j.bbalip.2007.08.003

Siemund, A. L., Hanewald, T., Kowarz, E., and Marschalek, R. (2022). MLL-AF4 and a murinized pSer-variant thereof are turning on the nucleolar stress pathway. *Cell Biosci.* 12, 47. doi:10.1186/s13578-022-00781-y

Slany, R. K. (2020). MLL fusion proteins and transcriptional control. *Biochimica Biophysica Acta (BBA) - Gene Regul. Mech.* 1863, 194503. doi:10.1016/j.bbagrm.2020.194503

Sorg, B. L., Klan, N., Seuter, S., Dishart, D., Rådmark, O., Habenicht, A., et al. (2006). Analysis of the 5-lipoxygenase promoter and characterization of a vitamin D receptor binding site. *Biochimica Biophysica Acta (BBA) - Mol. Cell Biol. Lipids* 1761, 686–697. doi:10.1016/j.bbalip.2006.04.005

Steinhilber, D., and Marschalek, R. (2018). How to effectively treat acute leukemia patients bearing MLL-rearrangements. *Biochem. Pharmacol.* 147, 183–190. doi:10.1016/j.bcp.2017.09.007

Stoffers, K. L., Sorg, B. L., Seuter, S., Rau, O., Rådmark, O., and Steinhilber, D. (2010). Calcitriol upregulates open chromatin and elongation markers at functional vitamin D response elements in the distal part of the 5-lipoxygenase gene. *J. Mol. Biol.* 395, 884–896. doi:10.1016/j.jmb.2009.10.022

Stranahan, A. W., Berezniuk, I., Chakraborty, S., Feller, F., Khalaj, M., and Park, C. Y. (2022). Leukotrienes promote stem cell self-renewal and chemoresistance in acute myeloid leukemia. *Leukemia* 36, 1575–1584. doi:10.1038/s41375-022-01579-0

Super, H., Martinez-Climent, J., and Rowley, J. (1995). Molecular analysis of the Mono Mac 6 cell line: detection of an MLL-AF9 fusion transcript [letter; comment]. *Blood* 85, 855–856. doi:10.1182/blood.V85.3.855.bloodjournal853855

Super, H. G., Strissel, P. L., Sobulo, O. M., Burian, D., Reshmi, S. C., Roe, B., et al. (1997). Identification of complex genomic breakpoint junctions in the t(9;11) MLL-AF9 fusion gene in acute leukemia. *Genes Chromosom. Cancer* 20, 185–195. doi:10.1002/(sici)1098-2264(199710)20:2<185::aid-gcc9>3.0.co;2-#

Uebbing, S., Kreiß, M., Scholl, F., Häfner, A., Sürün, D., Garscha, U., et al. (2021). Modulation of microRNA processing by 5-lipoxygenase. *Faseb J.* 35, 211933–e21215. doi:10.1096/fj.202002108R

Vincent, C., Fiancette, R., Donnard, M., Bordessoule, D., Turlure, P., Trimoreau, F., et al. (2008). 5-LOX, 12-LOX and 15-LOX in immature forms of human leukemic blasts. *Leuk. Res.* 32, 1756–1762. doi:10.1016/j.leukres.2008.05.005

Weisser, H., Göbel, T., Melissa Krishnathas, G., Kreiß, M., Angioni, C., Sürün, D., et al. (2023). Knock-out of 5-lipoxygenase in overexpressing tumor cells—consequences on gene expression and cellular function. *Cancer Gene Ther.* 30, 108–123. doi:10.1038/s41417-022-00531-9

Werz, O., and Steinhilber, D. (1996). Selenium-dependent peroxidases suppress 5-lipoxygenase activity in B-lymphocytes and immature myeloid cells. The presence of peroxidase-insensitive 5-lipoxygenase activity in differentiated myeloid cells. *Eur. J. Biochem.* 242, 90–97. doi:10.1111/j.1432-1033.1996.0090r.x

Winters, A. C., and Bernt, K. M. (2017). MLL-rearranged leukemias—an update on science and clinical approaches. *Front. Pediatr.* 5, 4–13. doi:10.3389/fped.2017.00004

Yano, T., Nakamura, T., Blechman, J., Sorio, C., Dang, C. V., Geiger, B., et al. (1997). Nuclear punctate distribution of ALL-1 is conferred by distinct elements at the N terminus of the protein. *Proc. Natl. Acad. Sci.* 94, 7286–7291. doi:10.1073/pnas.94.14.7286

Yokoyama, A., Somervaille, T. C. P., Smith, K. S., Rozenblatt-Rosen, O., Meyerson, M., and Cleary, M. L. (2005). The menin tumor suppressor protein is an essential oncogenic cofactor for MLL-associated leukemogenesis. *Cell* 123, 207–218. doi:10.1016/j.cell.2005.09.025

frontiers | Frontiers in Pharmacology

TYPE Original Research
PUBLISHED 25 February 2025
DOI 10.3389/fphar.2025.1524980

OPEN ACCESS

EDITED BY
Thorsten Jürgen Maier,
Paul-Ehrlich-Institut (PEI), Germany

REVIEWED BY
Sidharth Mehan,
Indo-Soviet Friendship College of Pharmacy, India
Thangavel Muthusamy,
Sree Balaji Medical College and Hospital, India

*CORRESPONDENCE
A. Sala,
angelo.sala@unimi.it
C. Bolego,
chiara.bolego@unipd.it

†PRESENT ADDRESSES
E. Zulato, Surgical Pathology Unit, University Hospital of Padua, Padua, Italy
M. Vara-Messler, Sanofi Belgium, Zwijnaarde, Belgium

RECEIVED 08 November 2024
ACCEPTED 04 February 2025
PUBLISHED 25 February 2025

CITATION
Vara-Messler M, Trevisi L, Zulato E, Ramaschi GE, Risé P, Pinna C, Indraccolo S, Sala A and Bolego C (2025) Aspirin-triggered DHA metabolites inhibit angiogenesis. *Front. Pharmacol.* 16:1524980. doi: 10.3389/fphar.2025.1524980

Aspirin-triggered DHA metabolites inhibit angiogenesis

M. Vara-Messler[1,2†], L. Trevisi[1], E. Zulato[3†], G. E. Ramaschi[1], P. Risé[4], C. Pinna[4], S. Indraccolo[3,5], A. Sala[4]* and C. Bolego[1]*

[1]Department of Pharmaceutical and Pharmacological Sciences, University of Padova, Padova, Italy, [2]Pole of Pharmacology and Therapeutics (FATH), Institut de Recherche Expérimentale et Clinique (IREC), Université Catholique de Louvain (UC Louvain), Brussels, Belgium, [3]Basic and Translational Oncology Unit, Istituto Oncologico Veneto IOV-IRCCS, Padova, Italy, [4]Department of Pharmaceutical Sciences, University of Milan, Milan, Italy, [5]Department of Surgery Oncology and Gastroenterology, University of Padova, Padova, Italy

Background and aim: Blood vessels supply oxygen, nutrients and provide gateways for immune surveillance. Since this network nourishes all tissues, vessel abnormalities contribute to many diseases, such as cancer. One of the potential targets for Docosahexaenoic Acid (DHA) in cancer is suppressing angiogenesis, a process of new blood vessel formation within tumors. In addition, aspirin (ASA) has antineoplastic effects that may be mediated, at least in part, by metabolites derived from acetylated COX-2. We aimed at determining the effect of DHA as well as its metabolites in angiogenesis, using *in vitro* as well as *in vivo* models.

Methods: Endothelial cell (EC) proliferation, motility and capillary-like tube formation were determined by MTT, wound healing, Boyden and Matrigel assays, respectively. In vivo angiogenesis was measured by the Matrigel sponge model in mice. The biosynthesis of proresolving lipid mediators by ECs was determined by LC-MS-MS.

Results and conclusion: DHA, but not arachidonic acid (AA), at concentrations consistent with those reached in blood after fish oil supplementation, decreased EC migration in a time- and concentration-dependent manner. Pretreatment with ASA modulated cell migration already after 24 h, while both DHA and ASA decreased migration at longer incubation times without affecting viability. 17-hydroxy-DHA was detected upon incubation with DHA, and increased amounts were observed upon combined treatment with DHA and ASA, an increase that was associated to a synergic effect on EC migration. 17(R)-hydroxy-DHA (17R-HDHA), the metabolite resulting from acetylated COX-2 activity of DHA, reduced EC migration in a concentration-dependent manner. DHA in the presence of ASA, as well as 17R-HDHA, also reduced EC tube formation. These results were confirmed *in vivo* where both 17R-HDHA or its downstream metabolite 17RResolvinD1 were able to decrease microvessels density in a Matrigel sponge model. Overall, we demonstrated that DHA in the presence of ASA-dependent acetylation of COX-2 showed increased antiangiogenic effects, possibly resulting from its conversion to its hydroxylated derivatives.

KEYWORDS

angiogenesis, docosahexaenoic acid (DHA), aspirin (ASA), 17(R)-hydroxy-docosahexaenoic acid (17(R)-HDHA), human umbilical vein endothelial cells (HUVEC)

1 Introduction

Angiogenesis is a tightly regulated process occurring through dynamic functions of endothelial cells including migration, proliferation and formation of capillary-like structures. The angiogenic process is a necessary step in tumour growth and metastasis (Folkman, 1995), but is also a key feature of many pathological conditions such as chronic inflammatory disease, supporting the occurrence of a link between cancer and unresolved inflammation (Fishbein et al., 2020; Fishbein et al., 2021).

Angiogenesis is affected by several pro-angiogenic growth factors and cytokines, but a growing body of evidence is suggesting a potential role for fatty acids (He et al., 2023). Ω-6 and ω-3 polyunsaturated fatty acids (PUFAs) can affect angiogenesis through multiple and opposite mechanisms including their oxidation and the formation of PUFA-derived metabolites (Frömel et al., 2022; Kang and Liu, 2013; Quinlivan et al., 2024). PUFAs are substrates for enzymes such as cyclooxygenases (COXs), lipoxygenases (LOXs) and cytochrome P450 (CYP450s) that generate potent bioactive lipid mediators (Calder, 2020; Serhan et al., 2020). In particular, several COX-2- and/or COX-1-derived arachidonic acid (AA, 20:4 ω-6) metabolites promote angiogenesis (Salvado et al., 2012), whereas ω-3 PUFAs such as docosahexaenoic acid (DHA, 22:6 ω-3) have anti-angiogenic and anti-tumor properties (Kelly et al., 2024; Rose and Connolly, 1999), by serving as alternative substrates to generate ω-3 lipid mediators endowed with anti-inflammatory and pro-resolution activities (Gilligan et al., 2019; Quinlivan et al., 2024) and suppressing the formation of several pro-angiogenic factors (Spencer et al., 2009). Of note, DHA metabolites generated by LOXs mainly expressed in inflammatory cells have been shown to have a beneficial role in pathological retinal angiogenesis (Connor et al., 2007; Maisto et al., 2020) as well as in cancer-associated angiogenesis (Prevete et al., 2017; Sulciner et al., 2018a; Sulciner et al., 2018b).

Epidemiological studies showed that aspirin has the unique ability to reduce the risk of several cancers (Elwood et al., 2024; Skriver et al., 2024) but the mechanisms underlying this effect are only partially understood (Patrignani and Patrono, 2018). The pharmacological activity of aspirin (ASA) is linked to the irreversible acetylation of COXs, but whereas COX-1 acetylation results in the loss of enzymatic activity, ASA-acetylated COX-2 is unable to generate prostanoids but remains active as a 15(R)-lipoxygenase (Lecomte et al., 1994; Mancini et al., 1994), and has been shown to contribute to the biosynthesis of anti-inflammatory and pro-resolving lipid mediators known as aspirin triggered (AT)-lipoxins (Clària and Serhan, 1995). In addition to metabolizing AA, 15-lipoxygenases enzymatic activities can easily convert DHA into 17-hydroxy-DHA (Dobson et al., 2013), and treatment with ASA and DHA resulted in the novel formation of 17-hydroxy-DHA *in vivo* in mice (Serhan et al., 2002). 17(R) hydroxy-DHA (17R-HDHA) generated by ASA-acetylated COX-2 from DHA, can be further oxygenated by 5-LOX in inflammatory cells through transcellular metabolism, resulting in the formation of 17(R)-resolvin D1 (17R-RvD1), also referred to as Aspirin Triggered-resolvin D1 (Serhan et al., 2002). Aspirin-Triggered lipid metabolites belong to the superfamily of specialized pro-resolving lipid mediators (SPMs) (Serhan et al., 2020), and a growing body of evidence suggests that SPMs supplementation may be beneficial in several diseases, including cancer, by promoting resolution over time of disease-associated inflammation (Serhan and Levy, 2018). Gilligan et al. recently showed that the production of AT-SPMs (17R-RvD1 and AT-LXA_4) may contribute to the antitumor activity of aspirin by promoting macrophage phagocytosis of tumor cell debris and functionally antagonizing macrophage secretion of proinflammatory cytokines (Gilligan et al., 2019). Given that inflammation and angiogenesis are strictly related processes (Mantovani et al., 2008; Trenti et al., 2018), AT-metabolites may affect angiogenesis, thus contributing to explain their pro-resolving potential in pathological conditions characterized by sustained low-grade phlogosis, such as cancer. The direct *in vitro* antiangiogenic effect of stable AA-derived AT-SPMs such as 15(R)-lipoxin A_4 has been well characterized (Cezar-De-Mello et al., 2006; Cezar-De-Mello et al., 2008), but whether DHA metabolites from ASA-acetylated COX-2, and in particular 17R-HDHA, may affect angiogenesis is still substantially unexplored, with evidence available focusing on 17R-RvD1 (Maisto et al., 2020).

Based on this background, we tested (a) the antiangiogenic activity of PUFAs (AA or DHA) or aspirin alone or in combination, and (b) the effect of specific Aspirin Triggered-metabolites in *in vitro* and *in vivo* models of angiogenesis.

2 Results

2.1 Effects of DHA and AA on HUVEC viability and migration

We first evaluated the effects of DHA on human umbilical vein endothelial cells (HUVECs) viability and migration at concentrations consistent with those reached in blood after fish oil supplementation (Yurko-Mauro et al., 2015). HUVEC viability was not significantly affected by treatment with 1–30 μM DHA for up to 72 h (Figures 1A–C), while 50 μM DHA, significantly decreased cell viability upon incubation for 48 h or 72 h (Figures 1B, C). Similarly, treatment of HUVECs with 1–50 μM AA for 48 h did not significantly affect cell viability (Figure 1D).

Then, in order to evaluate the effect of DHA on collective HUVEC migration, we used a wound healing assay. As shown in Figure 2, treatment with DHA time- and dose-dependently decreased HUVEC collective migration when compared to untreated control cells, with significant effects already observed at the concentration of 1 μM DHA after 72 h pre-treatment (Figure 2C).

2.2 DHA in the presence of ASA decreased endothelial cell migration without affecting viability

In the presence of 50 μM ASA, 10 μM DHA significantly inhibited HUVEC migration already after 24 h (Figures 3A, B), without affecting viability (data not shown), while neither DHA nor ASA alone resulted effective. No modifications of HUVEC migration were observed in cells treated with 10 μM AA in the presence of ASA for 24 h (Figures 3C, D). Both DHA and ASA caused a decrease in cell migration at longer incubation times of 48 and 72h, but the effect of their combination at both 48 h (Figures

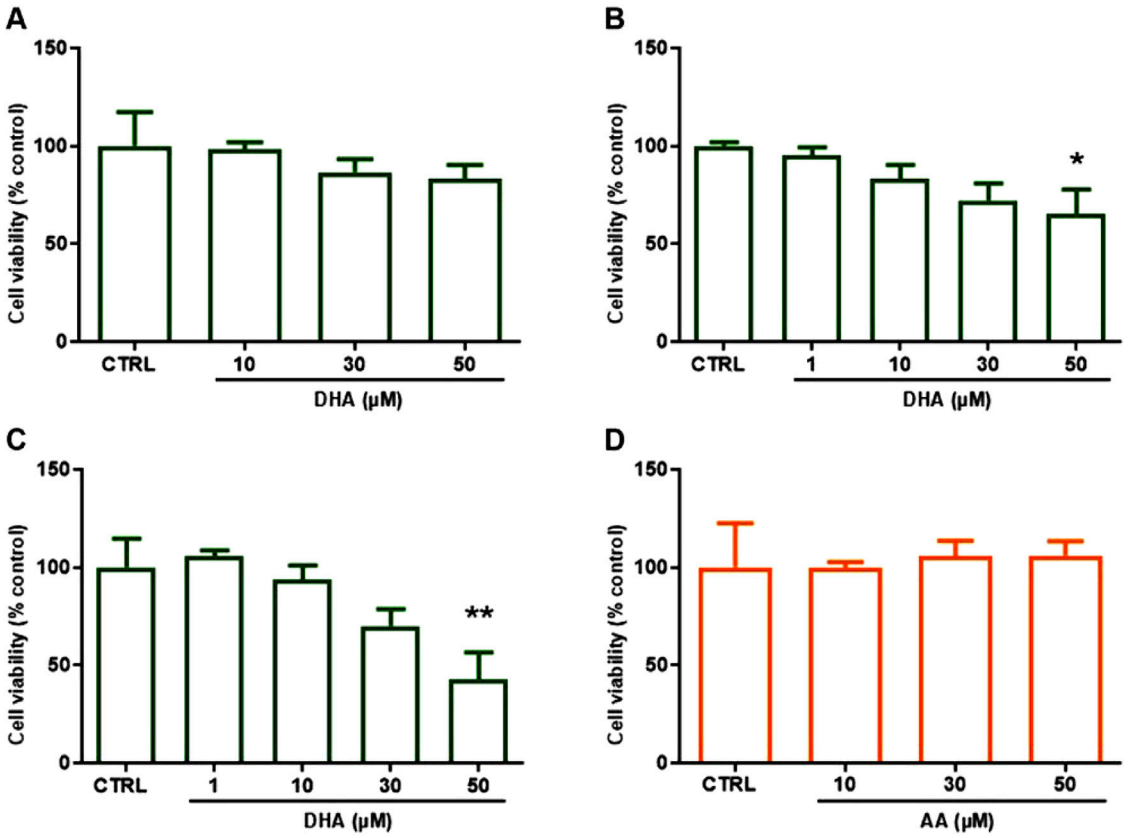

FIGURE 1
Effects of DHA (ω-3) and AA (ω-6) on HUVEC viability after 24–72 h. HUVECs were grown in 96-well plates and incubated in complete culture medium with DHA (1–50 μM) for **(A)** 24, **(B)** 48, **(C)** 72 h or **(D)** with AA (10–50 μM) for 48 h. Cell viability was assessed by MTT assay and expressed as % of control (untreated cells, CTRL). Bars show the mean ± SEM of 3 **(A)** or 4 **(B–D)** independent experiments performed in quadruplicate. One-way analysis of variance followed by Dunnett's *post hoc* test: *p < 0.05, **p < 0.01 vs. control.

4A, B) or 72 h (Figures 4C, D), exceeded the simple sum of the two separate activities.

Viability of treated cells was not different with respect to control cells at any time or concentration tested (Figure 4E).

2.3 17-HDHA production by endothelial cells is enhanced by incubation with ASA

We analyzed the supernatants of cells pre-treated with DHA (10 μM), ASA (50 μM) or DHA (10 μM) + ASA (50 μM) for 24 h by liquid chromatography-tandem mass spectrometry (LC/MS/MS), showing that HUVECs biosynthesize nanomolar concentrations of 17-HDHA upon incubation with exogenous DHA, and that the production is further increased in cells treated with ASA (Figure 5).

2.4 The aspirin-triggered DHA metabolite 17(R)-HDHA decreased the HUVEC proangiogenic potential

17(R)-HDHA (0.1–3 μM), showed a significant, time-dependent effect on HUVEC migration after 24–48 h (Figures 6A–C), without effects on HUVEC viability (Figure 6D).

Furthermore, using a microchemotaxis chamber, we assessed the effect of 17(R)-HDHA on HUVEC chemotaxis, an essential step in tumor angiogenesis (Trenti et al., 2018), showing that already after 6h, 17(R)-HDHA reduced FBS-induced EC migration in a concentration-dependent manner (0.3–3 μM) (Figures 7A, B), while DHA alone resulted ineffective (data not shown).

Finally, we studied the effect of 17(R)-HDHA on tubularization, the process of organization of endothelial cells in capillary tube-like structures when cultured onto extracellular matrix proteins.

In HUVECs treated with either DHA + ASA or 17(R)-HDHA for 6 h a decreased formation of specific parameters of HUVEC tubularization was observed. DHA (10 μM) in the presence of ASA (50 μM) as well as 17(R)-HDHA (0.3–3 μM) decreased nodes, meshes and mesh area. The number of junctions and the total tubule length also showed a tendency to decrease even if the difference did not reach statistical significance with respect to control cells (Figures 8A, B).

2.5 Aspirin-triggered DHA metabolites inhibited *in vivo* angiogenesis

To confirm *in vitro* data, we tested the effect of 17R-HDHA (3 μM) and its downstream metabolite 17R-RvD1 (50 nM) on *in*

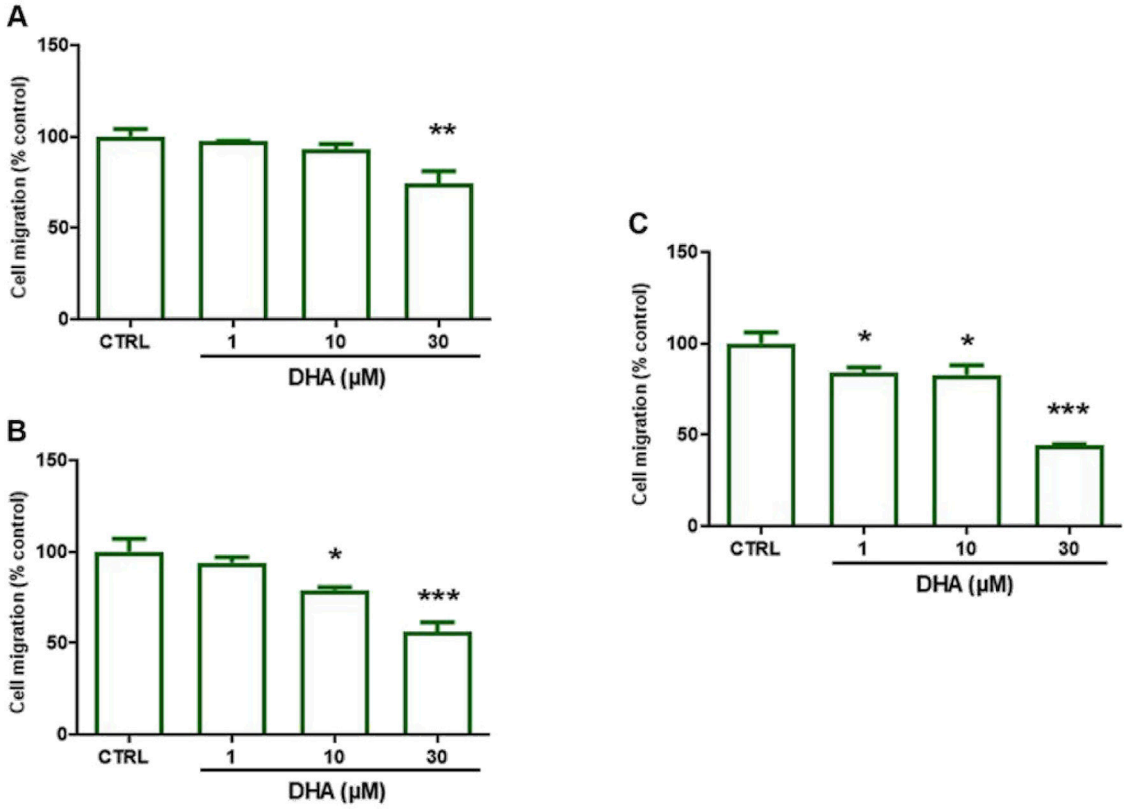

FIGURE 2
Effect of DHA on HUVEC migration after 24–72 h. HUVECs were grown in 24 well plates and the assay was performed in confluent cells. Cells were pre-treated with DHA (1–30 μM) for: **(A)** 24, **(B)** 48 or **(C)** 72 h. Thereafter, monolayers were wounded (t0), washed and treated as above for 16 h (t16). For each experimental condition 3 images were taken at t0 and t16; wound closure was calculated as described in Methods. Data are reported as % of control (untreated cells, CTRL). Bars show the mean ± SEM of 3 independent experiments. One-way analysis of variance followed by Dunnett's *post hoc* test. *p < 0.05, **p < 0.01, ***p < 0.001 vs. control.

vivo angiogenesis using the Matrigel sponge model enriched with SKOV3 ovarian cells. SKOV3 cells were chosen to avoid misleading results due to potential cytotoxic effects of AT-lipid mediators on cancer cells. Indeed, *in vitro* tests of cell viability showed a higher resistance of SKOV3 compared to other ovarian cancer cells tested (CaOV and A2870) to 17R-HDHA and 17R-RvD1 treatment (data not shown).

Microvessel density (MVD) was significantly reduced in mice treated with either 17R-HDHA or 17R-RvD1, when compared with controls (Figure 9), lending additional support to the results obtained *in vitro*.

3 Discussion

In the present study we provide initial evidence that combined treatment with DHA and ASA results in larger effects on endothelial cell migration and angiogenesis than the simple sum of the effects resulting from DHA or ASA treatments. The increased effects on angiogenesis are associated with increased amounts of 17-HDHA being produced in the presence of ASA + DHA, as the result of acetylated COX-2 acting as a 15R-lipoxygenase (Mancini et al., 1994). Administration of both exogenous 17R-HDHA and the trihydroxylated DHA derivative 17R-RvD1 were also able to modulate angiogenesis, reducing vessel formation in a model of angiogenesis *in vivo*, providing support to the hypothesis of a causal relationship between the formation of Aspirin Triggered DHA metabolites and the effects on angiogenesis.

Angiogenesis is a stepwise process requiring proliferation and migration of endothelial cells (Conway et al., 2001; Lee et al., 2021). Several studies have shown that AA and DHA may affect tumor angiogenesis in opposite ways either directly or through their oxygenated metabolites (Kang and Liu, 2013). In particular, ω3-PUFAs may act by inhibiting the production of several pro-angiogenic metabolites, including mediators derived from AA such as PGE_2 (Spencer et al., 2009), or by directly modulating angiogenesis through the conversion into bioactive lipid mediators arising from the activities of acetylated-COX-2, LOXs and CYP450s (Gilligan et al., 2019; Kelly et al., 2024; Sulciner et al., 2018b).

ASA possesses antitumor properties that may be ascribed, at least in part, to its antiplatelet activity (Contursi et al., 2024), as well as to the ability to affect angiogenesis by inhibiting the formation of PGE_2 (Salvado et al., 2013), a potent, COX-2 derived eicosanoid contributing to VEGF-dependent and -independent angiogenesis (Santiso et al., 2024; Xu and Croix, 2014). While ASA inhibits the biosynthesis of prostanoids both from COX-1 and COX-2, acetylation of the latter converts COX-2 into a 15-lipoxygenase, capable of metabolizing both AA and DHA into 15(R)-

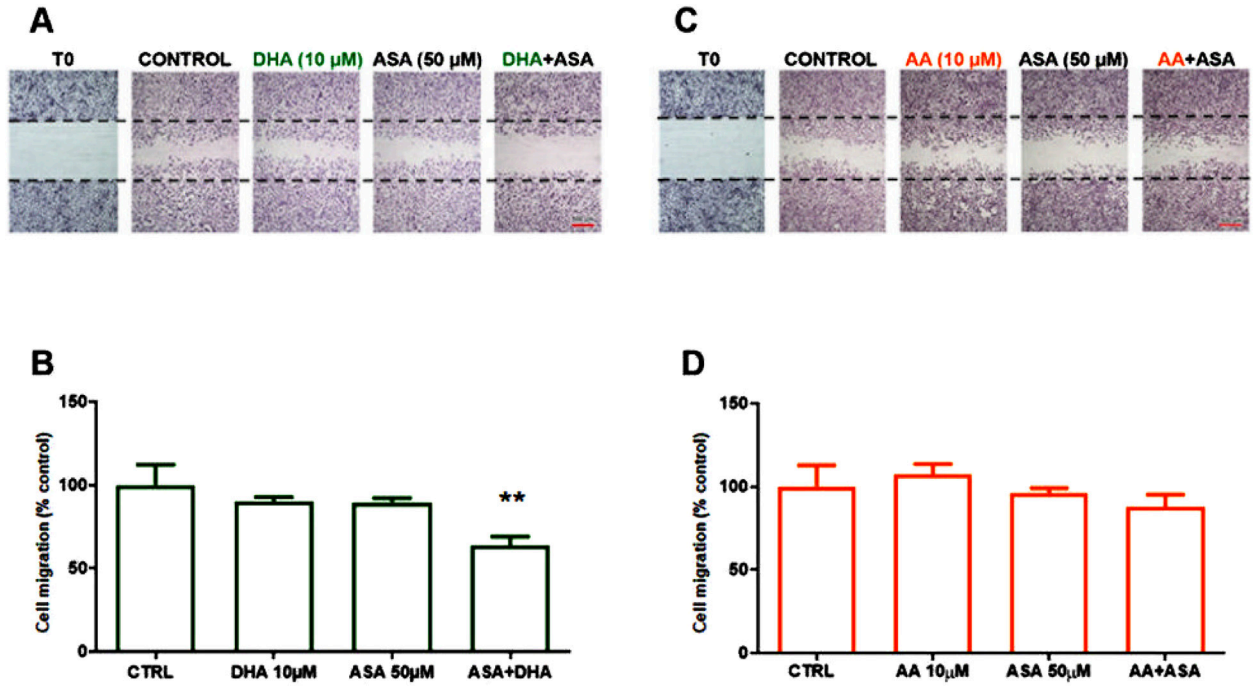

FIGURE 3
Effect of DHA ± ASA and AA ± ASA on HUVEC migration after 24h. HUVECs were grown in 24 well plates and the assay was performed in confluent cells. Cells were pre-treated with DHA (10 μM) **(A, B)** or with AA (10 μM) **(C, D)** in the presence or absence of ASA (50 μM) for 24 h. Thereafter, monolayers were wounded (t0), washed and treated as above for 16 h (t16). For each experimental condition 3 images were taken at t0 and t16; wound closure was calculated as described in Methods. **(A, C)** Representative images of a wound healing experiment in hematoxylin-eosin stained cells (scale bar: 500 μm). **(B, D)** Quantitative analysis of wound healing experiments. Data are reported as % of control (untreated cells, CTRL). Bars show the mean ± SEM of 3 **(D)** or 4 **(B)** independent experiments. One-way analysis of variance followed by Dunnet's *post hoc* test. **p < 0.01 vs. control.

hydroxyeicosatetraenoic acid (15R-HETE) and 17R-HDHA, respectively (Mancini et al., 1994; Serhan et al., 2002); both compounds also serves as the substrate for the 5-LOX-dependent formation of specific Aspirin-Triggered (AT)-lipid mediators possessing protective effects in inflammatory diseases (Romano et al., 2015; Serhan et al., 2002). A limited number of studies investigated the antiangiogenic properties of AT-lipid mediators, mainly focusing on AA-metabolites (Cezar-De-Mello et al., 2006; 2008) or RvD1 (Maisto et al., 2020) but little is known about the potential role of 17R-HDHA.

Normal plasma concentrations of DHA, assessed by GC/FID or GC/MS in humans, range between 70 and 160 μg/mL, that is 150–500 μM (Buchanan et al., 2021; Lv and Yang, 2012). Nevertheless, free fatty acids account for a small fraction of plasmatic fatty acids, with concentrations ranging from 200 to 600 μM in total, that is between 2 and 6 μM for DHA (Yli-Jama et al., 2002), values that we showed can increase by 2-3 folds upon DHA supplementation with either a fish-rich diet or fish-oil capsules (Visioli et al., 2003). We therefore assessed the effects of ω3-PUFAs at the concentration of 10 μM, and their potential positive interaction with ASA on collective HUVEC migration using a wound healing migration assay, showing that both treatments decrease EC migration, without affecting cell viability. Moreover, the effect observed in the presence of both ASA and DHA was more than additive, suggesting that ASA may potentiate the activity of DHA or vice-versa. Acetylation of COX-2 by ASA prevents the formation of pro-angiogenic PGE_2 prostanoids in HUVECs (Mulligan et al., 2010; Tamura et al., 2006), but in the presence of DHA the acetylated enzyme may still synthesize 17R-HDHA that can either act on its own or be further metabolized by 5-LO into 17R-resolvins (Serhan and Levy, 2018).

Detection of 17-HDHA in supernatants from HUVECs incubated with DHA is in agreement with results previously obtained using vascular tissues (Chatterjee et al., 2017), and the increased amounts observed in the presence of ASA suggest that acetylated COX-2 in HUVECs may contribute to the final production of 17-HDHA. It must be noted that we did not carry out chiral analysis of the observed hydroxylated metabolite of DHA, and therefore it is possible that in the presence of DHA alone the stereochemistry of the 17-hydroxyl may be S or a combination of S and R, while the additional formation of 17-HDHA observed in the presence of ASA could be referred to the formation of the R epimer, according to the stereochemistry of the product resulting from acetylation of COX-2.

17S-HDHA, the epimer of 17R-HDHA, is metabolized within 4 h to generate Rv-D1 and this conversion *in vivo* is mainly mediated by transcellular metabolism involving interaction between inflammatory (e.g. macrophage or neutrophils) and endothelial cells (Serhan et al., 2002; Chatterjee et al., 2017). Although it is known that R epimers resist rapid inactivation by oxidoreductases and have longer half-lives with respect to the S epimers, limited evidence is available about the *in vivo* biological activity of 17R-HDHA. The assessment of the direct activity of 17R-HDHA on HUVECs, showed that this metabolite is clearly effective in

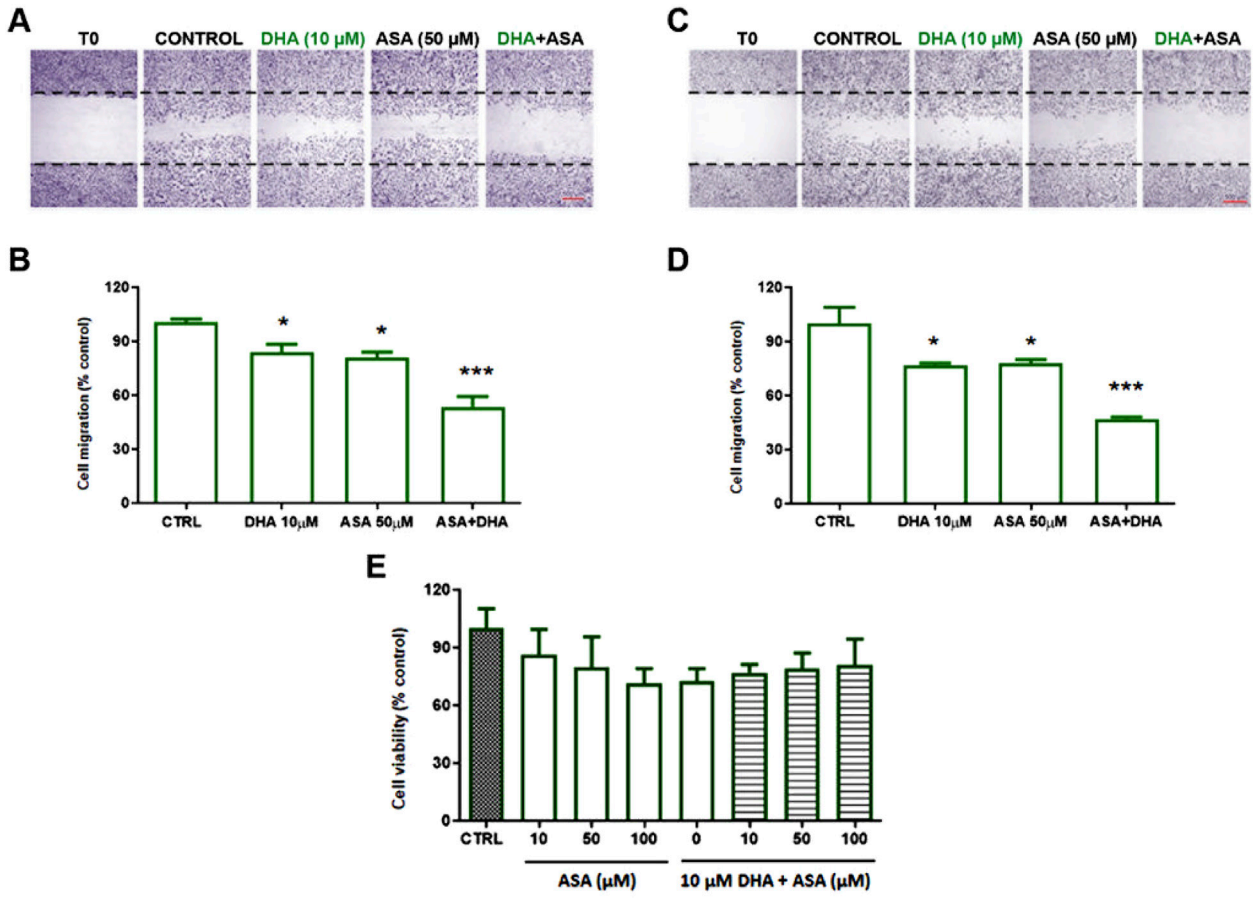

FIGURE 4
Effect of DHA ± ASA on HUVEC migration or viability after 48–72 h. HUVECs were grown in 24 well plates and the assay was performed in confluent cells. Cells were pre-treated with DHA (10 μM) in the presence or absence of ASA (50 μM) for 48 h **(A, B)** or 72 h **(C, D)**. Thereafter, monolayers were wounded (t0), washed and treated as above for 16 h (t16). For each experimental condition 3 images were taken at t0 and t16; wound closure was calculated as described in Methods. **(A, C)** representative images of a wound healing experiment in hematoxylin eosin stained cells (scale bar: 500 μm). **(B, D)** quantitative analysis of wound healing experiments. Data are reported as % of control (untreated cells, CTRL). Bars show the mean ± SEM of 3 independent experiments. One-way analysis of variance followed by Dunnet's *post hoc* test. *$p < 0.05$, ***$p < 0.001$ vs. control. **(E)** HUVECs were grown in 96-well plates in complete medium and treated with ASA (10–100 μM) or DHA (10 μM) + ASA (10–100 μM) for 72 h. Cell viability was assessed by MTT assay and expressed as % of control (untreated cells, CTRL). Bars show the mean ± SEM of 3 independent experiments performed in quadruplicate. One-way analysis of variance followed by Dunnet's *post hoc* test, n. s.

modulating their pro-angiogenic potential, an effect that was confirmed also by *in vivo* administration in an animal model of angiogenesis. While 17R-RvD1 was also able to affect microvessel formation *in vivo* (and at lower concentrations), it must be noted that *in vivo* formation of di- and tri-hydroxylated DHA derivatives (such as the 17R-RvD1) has been questioned over the last few years (O'Donnell et al., 2023; Schebb et al., 2022). Undetectable levels of SPMs were reported under different conditions, including supplementation with high doses of DHA and *in vivo* challenge with LPS in humans (Skarke et al., 2015), while *in vitro* formation of monohydroxylated DHA derivatives in human leukocytes vastly exceeded that of (if any) di- and tri-hydroxylated metabolites (Kahnt et al., 2023).

Indeed, we have been able to consistently report the *in vivo* formation of 14-hydroxy and 17-hydroxy-docosahexaenoic acid in different pathological conditions (Teopompi et al., 2019; Terranova et al., 2022), and we believe that monohydroxy derivative of DHA may play an important role in mediating the biological effects of DHA and DHA supplementation. Almost 40 years ago, we reported that the 12-lipoxygenase derived DHA metabolite, namely the 14-hydroxy-docosahexaenoic acid, is a potent receptor antagonist of Thromboxane A2 (Croset et al., 1988), and the present results support another relevant activity for a DHA monohydroxy-derivative.

It must be noted that our study has limitations: while the effects observed on isolated endothelial cells may support the activity observed *in vivo,* the specific contribution of direct effects on these cells and indirect systemic effects will require additional investigation. The use of the Matrigel sponge also may have a limited relevance with respect to specific tumor angiogenesis, but it must be noted that this experimental model is still widely accepted for the evaluation of the angiogenic potential or anti-angiogenic activity of various compounds in experimental animals (Benton et al., 2014; Kastana et al., 2019).

Overall, the data presented are showing that DHA and ASA may synergistically affect endothelial cell migration and angiogenesis,

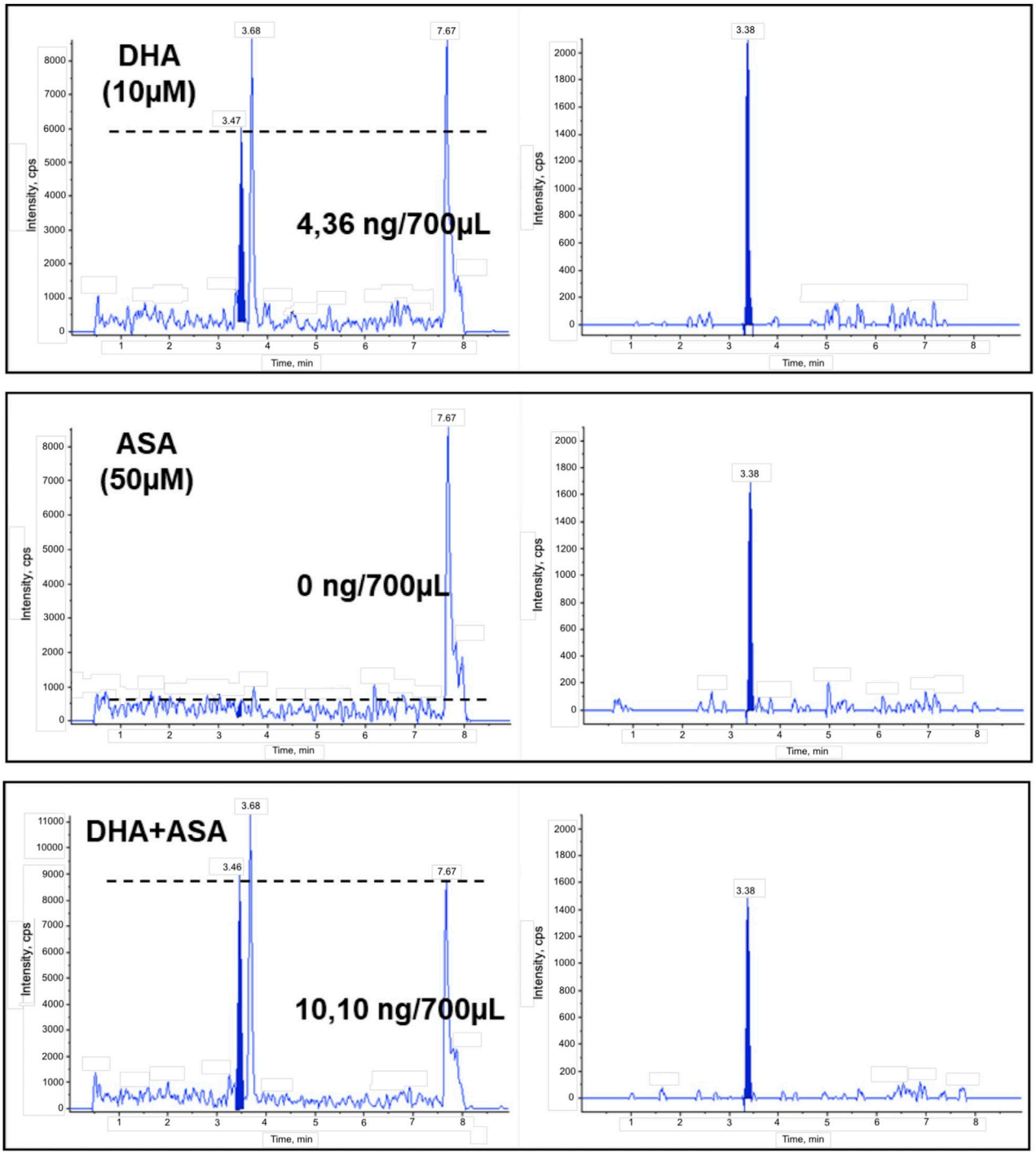

FIGURE 5
Synthesis of 17-HDHA in HUVEC treated with DHA, ASA or DHA + ASA. Representative chromatograms of the ion current for the specific transition of 17-HDHA (m/z 343 > 281) in supernatants from HUVECs treated with DHA (10 μM), ASA (50 μM) or DHA + ASA for 24 h as described in Methods (left panels). Quantitation was performed with [d^8]15-HETE as internal standard (m/z 327 > 226, right panels) and standard curves of synthetic 17R-HDHA.

and that 17R-HDHA can contribute to these activities, as also shown by its ability to affect invasion and microvessels formation *in vivo*. While additional research is necessary to establish the molecular mechanisms of these activities, the evidence obtained may contribute to explain the beneficial effects of aspirin and ω-3 FA in the context of cancer.

4 Materials and methods

4.1 HUVEC isolation and culture

Human umbilical vein endothelial cells (HUVECs) were isolated as previously published (Bolego et al., 2006). Briefly, umbilical cords

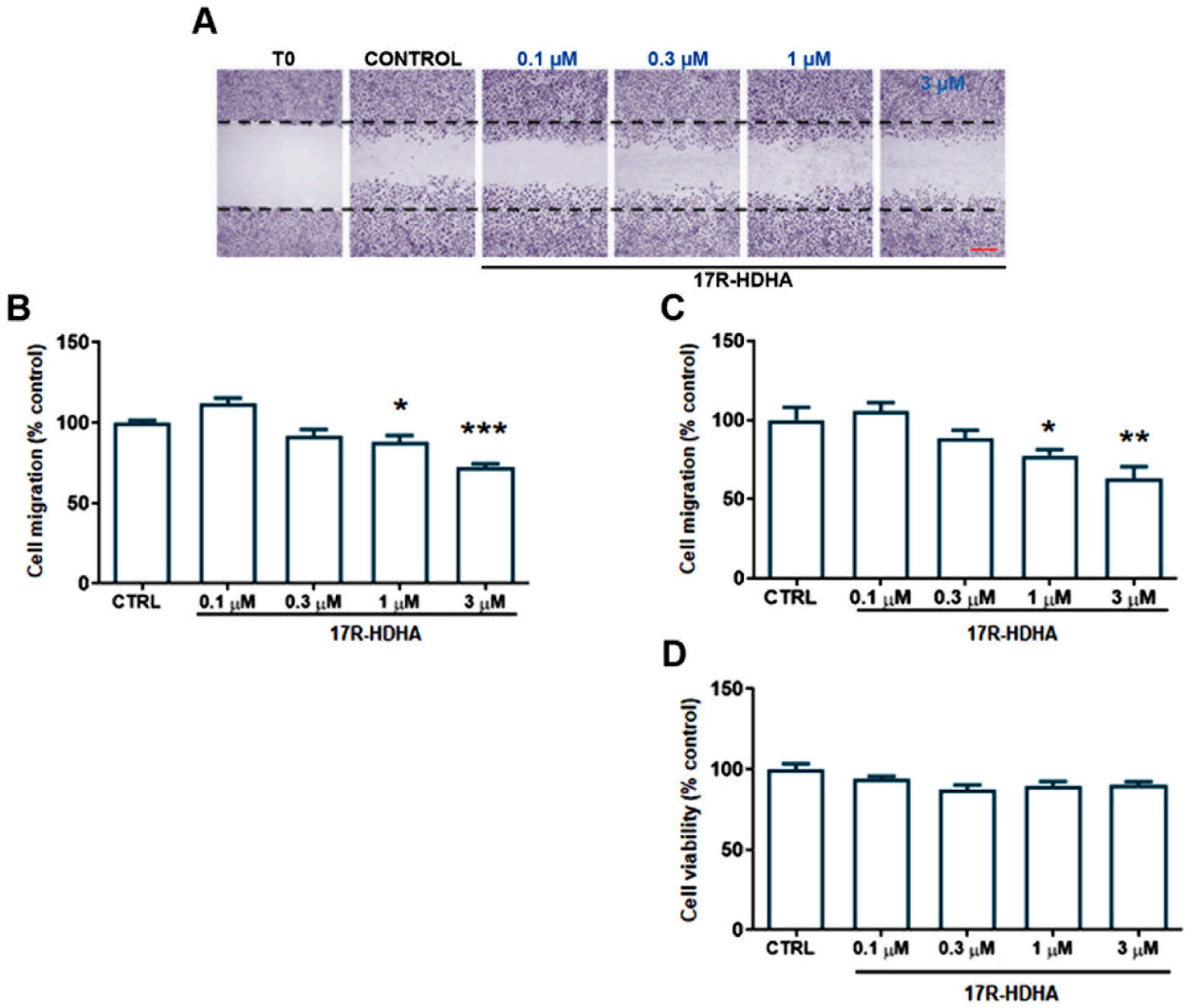

FIGURE 6
Effect of 17R-HDHA on HUVEC migration and viability after 24 or 48 h. HUVECs were grown in 24 well plates and the assay was performed in confluent cells. Cells were pre-treated with 17R-HDHA (0.1–3 μM) for 24 h **(B)** or 48 h **(A, C)**. Thereafter, monolayers were wounded (t0), washed and treated as above for 16 h (t16). For each experimental condition 3 images were taken at t0 and t16; wound closure was calculated as described in Methods. **(A)** Representative images of a wound healing experiment in hematoxylin eosin-stained cells after 48 h (scale bar: 500 μm). **(B, C)** Quantitative analysis of wound healing experiments at 24 **(B)** or 48 h **(C)**. Data are reported as % of control (untreated cells, CTRL). Bars show the mean ± SEM of 4 independent experiments. One-way analysis of variance followed by Dunnett's *post hoc* test. *$p < 0.05$, **$p < 0.01$, ***$p < 0.001$ vs. control. **(D)** HUVECs were grown in 96-well plates in complete medium and treated with 17R-HDHA (0.1–3 μM) for 48 h. Cell viability was assessed by MTT assay and expressed as % of control (untreated cells, CTRL). Bars show the mean ± SEM of 3 independent experiments performed in quadruplicate. One-way analysis of variance followed by Dunnett's *post hoc* test, n. s.

were collected after delivery, from full-term normal pregnancies at the Obstetrics and Gynaecological Unit of Padua University Hospital. The donors gave their informed consent, and the collected cords were non-identifiable. The procedure was approved by the local Ethics Committee (Comitato Etico per la Sperimentazione Clinica della Provincia di Padova). Each HUVEC preparation was derived from at least three donors and cells were pooled after isolation. Cells were grown in medium M199 (Thermo Fisher Scientific, Waltham, MA, United States) supplemented with 15% fetal calf serum (FCS, Thermo Fisher Scientific), gentamicin (40 μg/mL, Thermo Fisher Scientific), endothelial cell growth supplement (ECGS, 100 μg/mL), and heparin (100 UI/mL, Sigma-Aldrich, Saint Louis, MO) at 37°C in a humidified 5% CO_2 atmosphere. HUVECs were identified by their morphology and the expression of CD31-related antigen and used for experiments from passages 2 through 6.

4.2 MTT assay

HUVECs were seeded in complete medium at different cell densities considering the duration of the treatment (2×10^4, 1.5×10^4 or 10^4 cells for 24, 48 and 72 h of treatment, respectively) in 96-well plates. The next day, cells were treated in fresh medium containing DHA or AA (Cayman Chemical, Ann Arbor, United States), or with ASA in the presence or absence of DHA (Sigma-Aldrich), as detailed

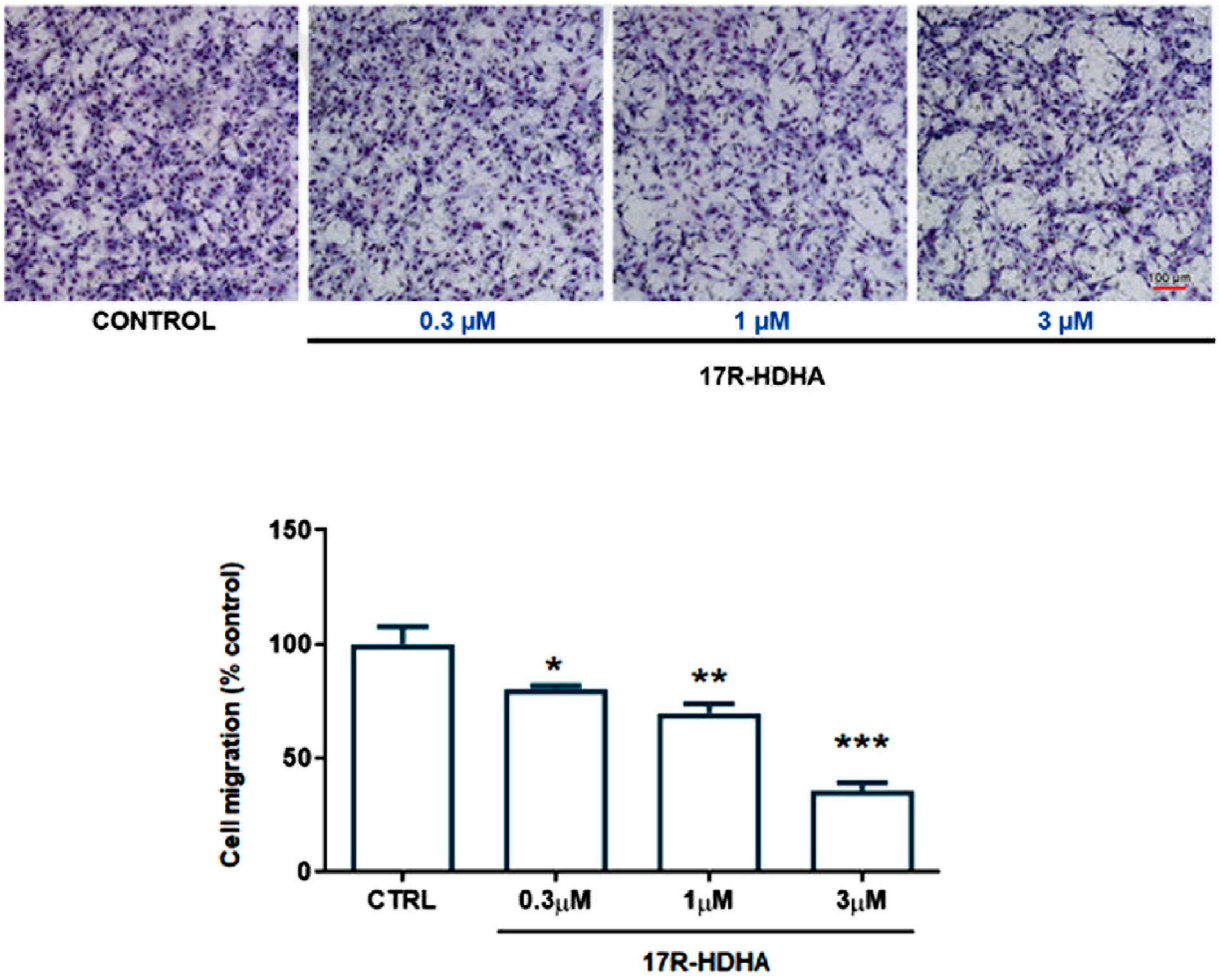

FIGURE 7
Effect of 17R-HDHA on HUVEC chemotaxis. HUVEC migration toward 15% FBS (control, CTRL) was measured in a microchemotaxis chamber in the presence or absence of increasing concentrations of 17R-HDHA (0.3–3 μM). *Upper panels*: representative images of migrated cells on the bottom of a filter membrane stained with Diff-Quick solution as detailed in Methods (scale bar: 100 μm). *Lower panel*: quantitative analysis of cell migration expressed as % of control. Bars show the mean ± SEM of 3 independent experiments performed in sextuplicate. One-way analysis of variance followed by Dunnett's *post hoc* test. **p < 0.01, **p < 0.001 vs. control.

in the Results section. Selected experiments were performed by treating cells with increasing concentrations of 17R-HDHA (Cayman Chemical) for 72 h. Four hours before the end of incubation, 10 μL of 3-[4,5 dimethylthiazol-2-yl]-2,5 diphenyltetrazolium bromide (MTT, 5 mg/mL in phosphate-buffered saline, Sigma Aldrich) was added to each well. Then, the medium was removed and formazan crystals were dissolved in 100 μL dimethylsulfoxide. MTT reduction was quantified by measuring light absorbance with a Wallac Victor^2 plate reader (PerkinElmer, Waltham, MA, United States) at 570–630 nm. Background absorbance values from control wells (cell-free media) were subtracted. Cell viability is expressed as percent of controls.

4.3 Chemotaxis assay

Chemotaxis experiments were performed in a 48-well microchemotaxis chamber (Neuro Probe, Gaithersburg, MD, United States) using 8 μm polyvinylpyrrolidone-free polycarbonate filters coated with 10 μg mL^{-1} of collagen (rat tail, Roche, Basel, Switzerland). Upper chambers were filled with 50 μL HUVEC suspension (1.6 × 10^5 cells per mL in M199 supplemented with 1% FBS and 100 UmL^{-1} heparin). Lower chambers were filled with 28 μL of complete M199 supplemented with 100 UmL^{-1} heparin in presence of 15% FBS plus 100 μg mL^{-1} ECGS. Cell migration towards complete medium with 15% FBS was taken as control. For the evaluation of the basal motility, M199 supplemented with 1% FBS and 100 UmL^{-1} heparin was added in the lower chamber. 17R-HDHA (0.3–3 μM) was added both in the upper and lower compartment. After 6 h of incubation at 37°C, the non-migrated HUVECs on the upper surface of the filter were removed by scraping. The cells that migrated to the lower side of the filter were stained with Diff-Quick stain (vWR Scientific Products, Bridgeport, NJ). Five images per well were acquired with a phase contrast inverted microscope (Nikon Eclipse Ti, Shinagawa, Tokyo, Japan) equipped with a digital camera using a ×20 objective. Cells were counted using a Cell Counter plugging developed by ImageJ

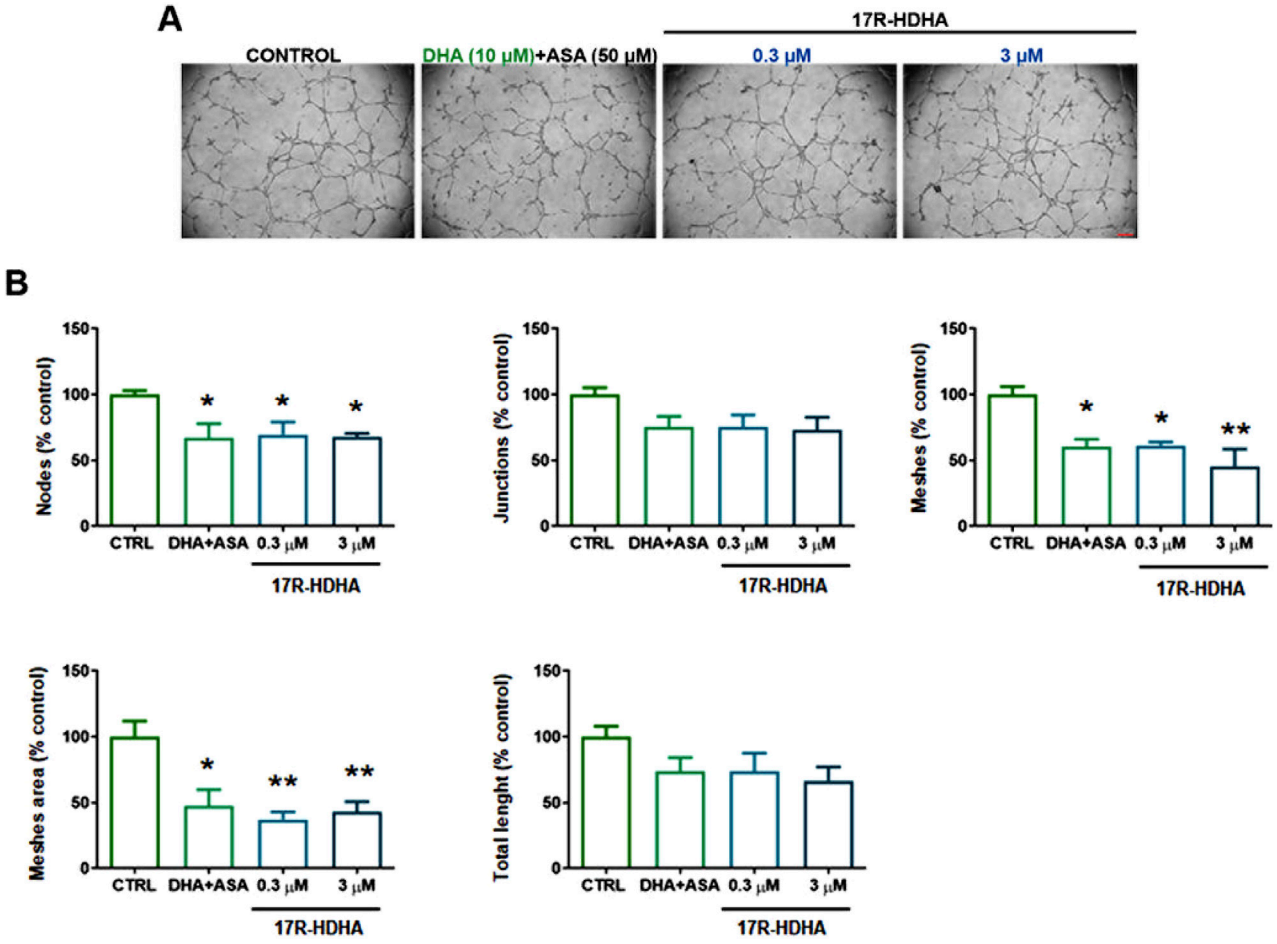

FIGURE 8
Effect of DHA in the presence of ASA or 17R-HDHA on HUVEC capillary tube formation. HUVECs were seeded onto Matrigel-coated 48-well plates in complete culture medium and treated with DHA (10 μM) +ASA (50 μM) or 17R-HDHA (0.3–3 μM) for 6 h. Complete medium with 15%FBS was taken as control (CTRL). **(A)** Representative images (scale bar: 200 μm). **(B)** Quantitative analysis of specific parameters of capillary tube as determined using Angiogenesis Analyzer (ImageJ). Bars show the mean ± SEM of 3 independent experiments expressed as % of cotrol. One-way analysis of variance followed by Dunnet's *post hoc* test. *p < 0.05, **p < 0.01 vs. control.

version 1.47 software (National Institute of Health, United States). Each experimental condition was performed in sextuplicate. Results are expressed as percent of control.

4.4 Collective migration assay

HUVECs were seeded in complete medium at different cell densities considering the duration of the treatment (2×10^5, 1.5×10^5 or 10^5 cells for 24, 48 and 72 h of treatment, respectively) in 12-well plates. The next day the media was replaced with fresh complete medium containing AA or DHA in the presence or absence of ASA for up to 72 h as detailed in the Results section. Selected experiments were performed treating cells with 17R-HDHA for 24 or 48 h. After that, one scratch was made and cells were incubated in fresh medium containing the tested compounds for additional 16 h. At the end of the experiment, three images of each well were acquired with a phase contrast inverted microscope (Nikon Eclipse Ti) equipped with a digital camera using a ×4 objective immediately after the scratch was made (time 0) and after 16 h of incubation. The wound area of each image was measured using ImageJ, and the average wound area of three images was determined for each sample. Quantitative analysis of cell migration was performed as the percentage of area change using the following formula: %change = [(average wound area at t0 – average wound area at t16) ÷ average wound area at t0] × 100. Values are expressed as % change from control (untreated cells).

4.5 Capillary-like tube formation assay

HUVECs (2×10^4 cells) were plated onto a thin layer (120 μL) of a basement membrane matrix (Matrigel™, Corning Corp., Corning, NY, United States) in 48-well plates, and incubated at 37°C for 6 h in complete cell culture medium in the presence or absence of test compounds as indicated in the Results. Complete cell culture medium with 15% FBS was taken as control. Three images per well were acquired with a phase contrast inverted microscope (Nikon Eclipse Ti) equipped with a digital camera using a ×4 objective. Images were analyzed using Angiogenesis Analyzer, a plugin developed for the ImageJ software. The data

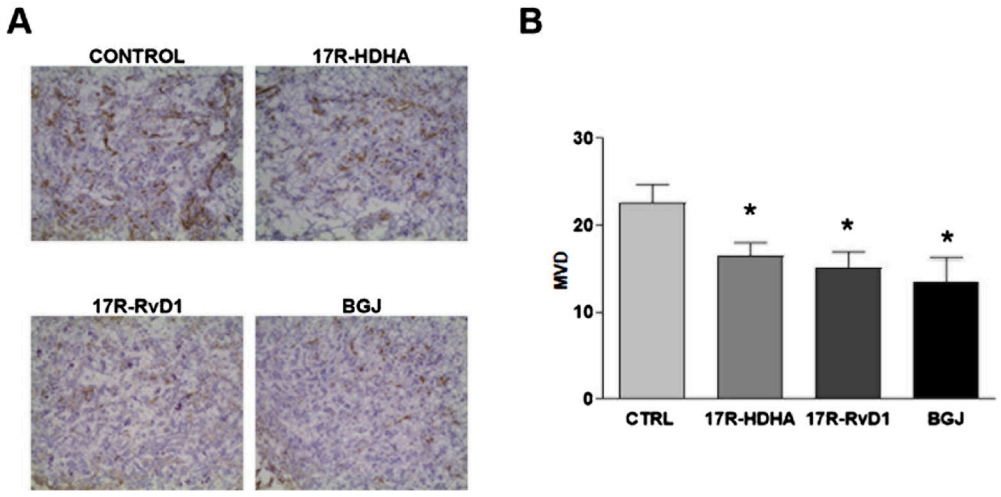

FIGURE 9
Effect of 17R-HDHA and 17R-Resolvin D1 on bFGF-induced angiogenesis *in vivo*. Vascularization of Matrigel pellets by staining with anti-CD31 mAb and calculation of microvessel density (MVD). For angiogenesis to be induced, on day 0 NOD/SCID-$\gamma^{-/-}$(NSG) mice were injected s. c. with Matrigel (400 µL per injection) supplemented with bFGF (500 ng) and SKOV-3 tumor cells (5 × 10^5cells per injection), along with 17R-HDHA (3 µM), 17R-Resolvin D1 (50 nM) or vehicle (EtOH). The pan FGFR inhibitor BGJ398 (1 µM) was used as a positive control. Seven days later, animals were killed and Matrigel pellets obtained, frozen and processed for immunohistochemical analysis. **(A)** Representative microphotographs are shown (original magnification: ×200). **(B)** Quantitative analysis of MVD. Bars show the mean ± SEM values of n = 5 animals per group. T-test *p < 0.05 vs. coltrol (vehicle, CTRL).

on dimensional parameters (total tubule length) and topological parameters (number of junctions, nodes and meshes, and total mesh area) of the capillary-like network (Trenti et al., 2017) were analyzed in all the images obtained from control and treated wells. Data are expressed as percent change from controls.

4.6 Biosynthesis of proresolving lipid mediators by LC-MS-MS

HUVECs (2 × 10^5 cells) were seeded in complete medium in 12-well plates and treated with DHA or ASA or DHA + ASA for 24 h. At the end of the experiment, cell medium was harvested and analyzed by Liquid chromatography-tandem mass spectrometry as previously published (Teopompi et al., 2019) with modifications. Briefly, samples were centrifuged to remove any cellular material. 50 µL of internal standard ([d^8]15-HETE, Cayman Chemical) were added to 700 µL of sample and immediately applied to polymeric SPE cartridges (Strata-X, 33 µm Polymeric Reversed Phase; Phenomenex, Torrance, CA) that had been preconditioned with 1 mL methanol and 1 mL water. After washing with 1 mL of water, the hydroxy-fatty acids were eluted using 400 µL of a acetonitrile: methanol (65%:35%). Samples were evaporated to dryness by centrifugation under vacuum (SpeedVac; Thermo Scientific, Waltham, MA) and reconstituted in 100 µL of a solution 70% (v/v) phase A (water, acetic acid 0.05%, pH: 5.7) and 30% (v/v) phase B (65% acetonitrile and 35% methanol). 10 µL of each sample were injected in an HPLC (Agilent 1,100) equipped with a reverse phase column (Kinetex 5 µm C18, 50 × 2.1 mm, Phenomenex, Castel Maggiore, BO, Italy). The column was eluted with a linear gradient from 30% to 100% solvent B over 9 min. The effluent from the high-performance liquid chromatography (HPLC) column was directly infused into the electro spray source of an API4000 triple quadrupole (ABSciex, Framingham, MA) operated in negative ion mode. Quantitation was performed using standard curves obtained with synthetic standard (17R-HDHA, Cayman Chemical) and stable isotope dilution.

4.7 *In vivo* angiogenesis

4.7.1 Animals and treatment

All procedures involving animals and their care conformed to institutional guidelines that comply with national and international laws and policies (EEC Council Directive 86/609, OJ L 358, 12 December 1987) and were authorized by the Italian Ministry of Health (Authorization n. 129/2017-PR). Animal studies are reported in compliance with the ARRIVE guidelines (Kilkenny et al., 2010; McGrath et al., 2015). During *in vivo* experiments, animals in all experimental groups were examined daily for a decrease in physical activity and other signs of disease or drug toxicity. Six to eight-week-old female NOD/SCID-$\gamma^{-/-}$ (NSG) mice were purchased from Charles River Laboratories (Wilmington, MA, United States) and housed in our specific pathogen-free animal facility in Allentown IVC cages (floor area 542 cm^2) with a maximum of six mice per cage. All mice received water and food *ad libitum* and were kept under a 12 h light/dark cycle in a well-ventilated room at an approximate temperature of 22°C. Mice acclimatized for a minimum of 7 days and a maximum of 15 days before being randomly assigned to treatment or vehicle groups.

The Matrigel sponge model of *in vivo* angiogenesis introduced by Albini et al. (1994), Passaniti et al. (1992) was used. For angiogenesis to be induced, NSG mice were randomly divided into four groups of five animals each and injected s. c. into both flanks with 400 µL Matrigel supplemented with 500 ng bFGF and SKOV-3 tumor cells (5 × 10^5 cells per injection), along with either 17-R-HDHA (3 µM), 17-R-RvD1 (50 nM, Cayman Chemical) or

vehicle (EtOH). The pan FGFR inhibitor BGJ398 (Selleck Chemicals GmbH, Cologne, Germany) was used as positive control (Rezzola et al., 2021). Seven days after injection, mice were anaesthetized with isoflurane/oxygen and killed via cervical dislocation, and Matrigel pellets (two pellets per mouse) were collected.

4.7.2 Evaluation of MVD

Four-μm-thick frozen sections of Matrigel pellets were processed for immunohistochemistry as previously reported (Nardo et al., 2011). Microvessels were stained by rat anti-CD31 mAb (1:50 dilution; Becton Dickinson, East Rutherford, NJ, United States); immunostaining was performed using the avidin–biotin–peroxidase complex technique and 3–3′ diaminobenzidine as chromogen (Vector Laboratories, Burlingame, CA, United States), and the sections were then lightly counterstained with Mayer's haematoxylin. Parallel negative controls, obtained by replacing primary Abs with PBS, were run. Microvessel density (MVD) was quantified by screening the CD31-stained sections for the areas of highest vascularity. The number of fields analyzed varied between 5 and 10 per sample, depending on the sample size. Images were collected at a total magnification of ×200. For each animal, the mean value of replicates was used for statistical analysis; five animals per group were analyzed.

5 Statistical analysis

All data represent the results of at least three independent experiments. Results are expressed as mean ± standard error of the mean (SEM). GraphPad Prism Software, version 8.4 (San Diego, CA, United States) was used for plotting of the data and statistical analysis. Data were analyzed by one-way ANOVA followed by Dunnett's *post hoc* test or T-test as detailed in the figure legends. Differences were considered statistically significant for $p < 0.05$.

Data availability statement

The raw data supporting the conclusions of this article will be made available by the authors, without undue reservation.

Ethics statement

The animal study was approved by Institutional Review Board for Animal Research of the University of Padua and the Italian Ministry of Health. The study was conducted in accordance with the local legislation and institutional requirements.

Author contributions

MV-M: Conceptualization, Investigation, Methodology, Visualization, Writing–review and editing, Formal Analysis. LT: Formal Analysis, Visualization, Writing–review and editing. EZ: Formal Analysis, Investigation, Visualization, Writing–review and editing. GR: Investigation, Visualization, Writing–review and editing. PR: Investigation, Visualization, Writing–review and editing. CP: Visualization, Writing–review and editing. SI: Formal Analysis, Methodology, Visualization, Writing–review and editing. AS: Conceptualization, Investigation, Methodology, Visualization, Writing–original draft, Writing–review and editing. CB: Conceptualization, Formal Analysis, Funding acquisition, Methodology, Project administration, Supervision, Writing–original draft, Writing–review and editing.

Funding

The author(s) declare that financial support was received for the research, authorship, and/or publication of this article. This work was supported by institutional funding from the University of Padova, Padova, Italy to CB.

Acknowledgments

We wish to thank Fabiola Modenese and the delivery room staff of the Obstetrics and Gynaecological Unit of Padova University Hospital (Padova, Italy) for the precious collaboration.

Conflict of interest

The authors declare that the research was conducted in the absence of any commercial or financial relationships that could be construed as a potential conflict of interest.

The author(s) declared that they were an editorial board member of Frontiers, at the time of submission. This had no impact on the peer review process and the final decision.

Generative AI statement

The author(s) declare that no Generative AI was used in the creation of this manuscript.

Publisher's note

References

Albini, A., Fontanini, G., Masiello, L., Tacchetti, C., Bigini, D., Luzzi, P., et al. (1994). Angiogenic potential *in vivo* by Kaposi's sarcoma cell-free supernatants and HIV-1 tat product: inhibition of KS-like lesions by tissue inhibitor of metalloproteinase-2. *AIDS Lond. Engl.* 8 (9), 1237–1244. doi:10.1097/00002030-199409000-00004

Benton, G., Arnaoutova, I., George, J., Kleinman, H. K., and Koblinski, J. (2014). Matrigel: from discovery and ECM mimicry to assays and models for cancer research. *Adv. Drug Deliv. Rev.* 79–80, 3–18. doi:10.1016/j.addr.2014.06.005

Bolego, C., Buccellati, C., Radaelli, T., Cetin, I., Puglisi, L., Folco, G., et al. (2006). eNOS, COX-2, and prostacyclin production are impaired in endothelial cells from diabetics. *Biochem. Biophysical Res. Commun.* 339 (1), 188–190. doi:10.1016/j.bbrc.2005.11.017

Buchanan, C. D. C., Lust, C. A. C., Burns, J. L., Hillyer, L. M., Martin, S. A., Wittert, G. A., et al. (2021). Analysis of major fatty acids from matched plasma and serum samples reveals highly comparable absolute and relative levels. *Prostagl. Leukot. Essent. Fat. Acids* 168, 102268. doi:10.1016/j.plefa.2021.102268

Calder, P. C. (2020). Eicosanoids. *Essays Biochem.* 64 (3), 423–441. doi:10.1042/EBC20190083

Cezar-De-Mello, P. F. T., Nascimento-Silva, V., Villela, C. G., and Fierro, I. M. (2006). Aspirin-triggered Lipoxin A4 inhibition of VEGF-induced endothelial cell migration involves actin polymerization and focal adhesion assembly. *Oncogene* 25 (1), 122–129. doi:10.1038/sj.onc.1209002

Cezar-De-Mello, P. F. T., Vieira, A. M., Nascimento-Silva, V., Villela, C. G., Barja-Fidalgo, C., and Fierro, I. M. (2008). ATL-1, an analogue of aspirin-triggered lipoxin A 4, is a potent inhibitor of several steps in angiogenesis induced by vascular endothelial growth factor. *Br. J. Pharmacol.* 153 (5), 956–965. doi:10.1038/sj.bjp.0707650

Chatterjee, A., Komshian, S., Sansbury, B. E., Wu, B., Mottola, G., Chen, M., et al. (2017). Biosynthesis of proresolving lipid mediators by vascular cells and tissues. *FASEB J.* 31 (8), 3393–3402. doi:10.1096/fj.201700082R

Clària, J., and Serhan, C. N. (1995). Aspirin triggers previously undescribed bioactive eicosanoids by human endothelial cell-leukocyte interactions. *Proc. Natl. Acad. Sci. U. S. A.* 92 (21), 9475–9479. doi:10.1073/pnas.92.21.9475

Connor, K. M., Sangiovanni, J. P., Lofqvist, C., Aderman, C. M., Chen, J., Higuchi, A., et al. (2007). Increased dietary intake of ω-3-polyunsaturated fatty acids reduces pathological retinal angiogenesis. *Nat. Med.* 13 (7), 868–873. doi:10.1038/nm1591

Contursi, A., Tacconelli, S., Di Berardino, S., De Michele, A., and Patrignani, P. (2024). Platelets as crucial players in the dynamic interplay of inflammation, immunity, and cancer: unveiling new strategies for cancer prevention. *Front. Pharmacol.* 15, 1520488. doi:10.3389/FPHAR.2024.1520488

Conway, E. M., Collen, D., and Carmeliet, P. (2001). Molecular mechanisms of blood vessel growth. *Cardiovasc. Res.* 49 (3), 507–521. doi:10.1016/s0008-6363(00)00281-9

Croset, M., Sala, A., Folco, G., and Lagarde, M. (1988). Inhibition by lipoxygenase products of TXA_2-like responses of platelets and vascular smooth muscle. 14-Hydroxy from 22:6N-3 is more potent than 12-HETE. *Biochem. Pharmacol.* 37 (7), 1275–1280. doi:10.1016/0006-2952(88)90782-4

Dobson, E. P., Barrow, C. J., Kralovec, J. A., and Adcock, J. L. (2013). Controlled formation of mono- and dihydroxy-resolvins from EPA and DHA using soybean 15-lipoxygenase. *J. Lipid Res.* 54 (5), 1439–1447. doi:10.1194/jlr.M036186

Elwood, P., Morgan, G., Watkins, J., Protty, M., Mason, M., Adams, R., et al. (2024). Aspirin and cancer treatment: systematic reviews and meta-analyses of evidence: for and against. *Br. J. Cancer* 130 (1), 3–8. doi:10.1038/S41416-023-02506-5

Fishbein, A., Hammock, B. D., Serhan, C. N., and Panigrahy, D. (2021). Carcinogenesis: failure of resolution of inflammation? *Pharmacol. and Ther.* 218, 107670. doi:10.1016/J.PHARMTHERA.2020.107670

Fishbein, A., Wang, W., Yang, H., Yang, J., Hallisey, V. M., Deng, J., et al. (2020). Resolution of eicosanoid/cytokine storm prevents carcinogen and inflammation-initiated hepatocellular cancer progression. *Proc. Natl. Acad. Sci. U. S. A.* 117 (35), 21576–21587. doi:10.1073/pnas.2007412117

Folkman, J. (1995). Angiogenesis in cancer, vascular, rheumatoid and other disease. *Nat. Med.* 1 (1), 27–31. doi:10.1038/nm0195-27

Frömel, T., Naeem, Z., Pirzeh, L., and Fleming, I. (2022). Cytochrome P450-derived fatty acid epoxides and diols in angiogenesis and stem cell biology. *Pharmacol. and Ther.* 234, 108049. doi:10.1016/J.PHARMTHERA.2021.108049

Gilligan, M. M., Gartung, A., Sulciner, M. L., Norris, P. C., Sukhatme, V. P., Bielenberg, D. R., et al. (2019). Aspirin-triggered proresolving mediators stimulate resolution in cancer. *Proc. Natl. Acad. Sci. U. S. A.* 116 (13), 6292–6297. doi:10.1073/pnas.1804000116

He, M., Xu, S., Yan, F., Ruan, J., and Zhang, X. (2023). Fatty acid metabolism: a new perspective in breast cancer precision therapy. *Front. Biosci. Landmark Ed.* 28 (12), 348. doi:10.31083/J.FBL2812348

Kahnt, A. S., Schebb, N. H., and Steinhilber, D. (2023). Formation of lipoxins and resolvins in human leukocytes. In *Prostagl. Other Lipid Mediat.*, 166. 106726. doi:10.1016/j.prostaglandins.2023.106726

Kang, J. X., and Liu, A. (2013). The role of the tissue omega-6/omega-3 fatty acid ratio in regulating tumor angiogenesis. *Cancer Metastasis Rev.* 32 (1–2), 201–210. doi:10.1007/s10555-012-9401-9

Kastana, P., Zahra, F. T., Ntenekou, D., Katraki-Pavlou, S., Beis, D., Lionakis, M. S., et al. (2019). Matrigel plug assay for *in vivo* evaluation of angiogenesis. *Methods Mol. Biol. Clift. N.J.* 1952, 219–232. doi:10.1007/978-1-4939-9133-4_18

Kelly, A. G., Wang, W., Rothenberger, E., Yang, J., Gilligan, M. M., Kipper, F. C., et al. (2024). Enhancing cancer immunotherapy via inhibition of soluble epoxide hydrolase. *Proc. Natl. Acad. Sci. U. S. A.* 121 (7), e2314085121. doi:10.1073/PNAS.2314085121

Kilkenny, C., Browne, W. J., Cuthill, I. C., Emerson, M., and Altman, D. G. (2010). Improving bioscience research reporting: the ARRIVE guidelines for reporting animal research. *PLoS Biol.* 8 (6), e1000412. doi:10.1371/journal.pbio.1000412

Lecomte, M., Laneuville, O., Ji, C., DeWitt, D. L., and Smith, W. L. (1994). Acetylation of human prostaglandin endoperoxide synthase-2 (cyclooxygenase-2) by aspirin. *J. Biol. Chem.* 269 (18), 13207–13215. doi:10.1016/s0021-9258(17)36820-5

Lee, H. W., Xu, Y., He, L., Choi, W., Gonzalez, D., Jin, S. W., et al. (2021). Role of venous endothelial cells in developmental and pathologic angiogenesis. *Circulation* 144 (16), 1308–1322. doi:10.1161/CIRCULATIONAHA.121.054071

Lv, W., and Yang, T. (2012). Identification of possible biomarkers for breast cancer from free fatty acid profiles determined by GC–MS and multivariate statistical analysis. *Clin. Biochem.* 45 (1–2), 127–133. doi:10.1016/j.clinbiochem.2011.10.011

Maisto, R., Trotta, M. C., Petrillo, F., Izzo, S., Cuomo, G., Alfano, R., et al. (2020). Corrigendum: resolvin D1 modulates the intracellular VEGF-related miRNAs of retinal photoreceptors challenged with high glucose. *Front. Pharmacol.* 11, 871. doi:10.3389/fphar.2020.00871

Mancini, J. A., O'Neill, G. P., Bayly, C., and Vickers, P. J. (1994). Mutation of serine-516 in human prostaglandin G/H synthase-2 to methionine or aspirin acetylation of this residue stimulates 15-R-HETE synthesis. *FEBS Lett.* 342 (1), 33–37. doi:10.1016/0014-5793(94)80579-2

Mantovani, A., Allavena, P., Sica, A., and Balkwill, F. (2008). Cancer-related inflammation. *Nature* 454 (7203), 436–444. doi:10.1038/nature07205

McGrath, J. C., McLachlan, E. M., and Zeller, R. (2015). Transparency in Research involving Animals: the Basel Declaration and new principles for reporting research in BJP manuscripts. *Br. J. Pharmacol.* 172 (10), 2427–2432. doi:10.1111/bph.12956

Mulligan, J. K., Rosenzweig, S. A., and Young, M. R. I. (2010). Tumor secretion of VEGF induces endothelial cells to suppress T cell functions through the production of PGE2. *J. Immunother.* 33 (2), 126–135. doi:10.1097/CJI.0b013e3181b91c9c

Nardo, G., Favaro, E., Curtarello, M., Moserle, L., Zulato, E., Persano, L., et al. (2011). Glycolytic phenotype and AMP kinase modify the pathologic response of tumor xenografts to VEGF neutralization. *Cancer. Research.* 71 (12), 4214–4225. doi:10.1158/0008-5472.CAN-11-0242

O'Donnell, V. B., Schebb, N. H., Milne, G. L., Murphy, M. P., Thomas, C. P., Steinhilber, D., et al. (2023). Failure to apply standard limit-of-detection or limit-of-quantitation criteria to specialized pro-resolving mediator analysis incorrectly characterizes their presence in biological samples. *Nat. Commun.* 14 (1), 7172. doi:10.1038/s41467-023-41766-w

Passaniti, A., Taylor, R. M., Pili, R., Guo, Y., Long, P. V., Haney, J. A., et al. (1992). A simple, quantitative method for assessing angiogenesis and antiangiogenic agents using reconstituted basement membrane, heparin, and fibroblast growth factor. *Laboratory Investigation; a J. Tech. Methods Pathology* 67 (4), 519–528. Available at: http://www.ncbi.nlm.nih.gov/pubmed/1279270.

Patrignani, P., and Patrono, C. (2018). Aspirin, platelet inhibition and cancer prevention. *Platelets* 29 (8), 779–785. doi:10.1080/09537104.2018.1492105

Prevete, N., Liotti, F., Illiano, A., Amoresano, A., Pucci, P., de Paulis, A., et al. (2017). Formyl peptide receptor 1 suppresses gastric cancer angiogenesis and growth by exploiting inflammation resolution pathways. *OncoImmunology* 6 (4), e1293213. doi:10.1080/2162402X.2017.1293213

Quinlivan, K. M., Howard, I. V., Southan, F., Bayer, R. L., Torres, K. L., Serhan, C. N., et al. (2024). Exploring the unique role of specialized pro-resolving mediators in cancer therapeutics. *Prostagl. and Other Lipid Mediat.*, 106944. doi:10.1016/j.prostaglandins.2024.106944

Rezzola, S., Guerra, J., Chandran, A. M. K., Loda, A., Cancarini, A., Sacristani, P., et al. (2021). Vegf-independent activation of müller cells by the vitreous from proliferative diabetic retinopathy patients. *Int. J. Mol. Sci.* 22 (4), 1–16. doi:10.3390/ijms22042179

Romano, M., Cianci, E., Simiele, F., and Recchiuti, A. (2015). Lipoxins and aspirin-triggered lipoxins in resolution of inflammation. *Eur. J. Pharmacol.* 760, 49–63. doi:10.1016/j.ejphar.2015.03.083

Rose, D. P., and Connolly, J. M. (1999). Omega-3 fatty acids as cancer chemopreventive agents. *Pharmacol. Ther.* 83 (3), 217–244. doi:10.1016/S0163-7258(99)00026-1

Salvado, M. D., Alfranca, A., Haeggström, J. Z., and Redondo, J. M. (2012). Prostanoids in tumor angiogenesis: therapeutic intervention beyond COX-2. *Trends Mol. Med.* 18 (4), 233–243. doi:10.1016/j.molmed.2012.02.002

Salvado, M. D., Di Gennaro, A., Lindbom, L., Agerberth, B., and Haeggström, J. Z. (2013). Cathelicidin LL-37 induces angiogenesis via PGE2-EP3 signaling in endothelial cells, *in vivo* inhibition by aspirin. *Arteriosclerosis, Thrombosis, Vasc. Biol.* 33 (8), 1965–1972. doi:10.1161/ATVBAHA.113.301851

Santiso, A., Heinemann, A., and Kargl, J. (2024). Prostaglandin E2 in the tumor microenvironment, a convoluted affair mediated by EP receptors 2 and 4. *Pharmacol. Rev.* 76 (3), 388–413. doi:10.1124/pharmrev.123.000901

Schebb, N. H., Kühn, H., Kahnt, A. S., Rund, K. M., O'Donnell, V. B., Flamand, N., et al. (2022). Formation, signaling and occurrence of specialized pro-resolving lipid mediators-what is the evidence so far? *Front. Pharmacol.* 13, 838782. doi:10.3389/FPHAR.2022.838782

Serhan, C. N., Gupta, S. K., Perretti, M., Godson, C., Brennan, E., Li, Y., et al. (2020). The atlas of inflammation resolution (AIR). *Mol. Aspects Med.* 74, 100894. doi:10.1016/j.mam.2020.100894

Serhan, C. N., Hong, S., Gronert, K., Colgan, S. P., Devchand, P. R., Mirick, G., et al. (2002). Resolvins: a family of bioactive products of omega-3 fatty acid transformation circuits initiated by aspirin treatment that counter proinflammation signals. *J. Exp. Med.* 196 (8), 1025–1037. doi:10.1084/jem.20020760

Serhan, C. N., and Levy, B. D. (2018). Resolvins in inflammation: emergence of the pro-resolving superfamily of mediators. *J. Clin. Investigation* 128 (7), 2657–2669. doi:10.1172/JCI97943

Skarke, C., Alamuddin, N., Lawson, J. A., Li, X., Ferguson, J. F., Reilly, M. P., et al. (2015). Bioactive products formed in humans from fish oils. *J. Lipid Res.* 56 (9), 1808–1820. doi:10.1194/jlr.M060392

Skriver, C., Maltesen, T., Dehlendorff, C., Wessel Skovlund, C., Schmidt, M., Toft Sørensen, H., et al. (2024). Long-term aspirin use and cancer risk: a 20-year cohort study. *J. Natl. Cancer Inst.* 116 (4), 530–538. doi:10.1093/jnci/djad231

Spencer, L., Mann, C., Metcalfe, M., Webb, M., Pollard, C., Spencer, D., et al. (2009). The effect of omega-3 FAs on tumour angiogenesis and their therapeutic potential. *Eur. J. Cancer* 45 (12), 2077–2086. doi:10.1016/j.ejca.2009.04.026

Sulciner, M. L., Gartung, A., Gilligan, M. M., Serhan, C. N., and Panigrahy, D. (2018a). Targeting lipid mediators in cancer biology. *Cancer Metastasis Rev.* 37 (2–3), 557–572. doi:10.1007/s10555-018-9754-9

Sulciner, M. L., Serhan, C. N., Gilligan, M. M., Mudge, D. K., Chang, J., Gartung, A., et al. (2018b). Resolvins suppress tumor growth and enhance cancer therapy. *J. Exp. Med.* 215 (1), 115–140. doi:10.1084/jem.20170681

Tamura, K., Sakurai, T., and Kogo, H. (2006). Relationship between prostaglandin E2 and vascular endothelial growth factor (VEGF) in angiogenesis in human vascular endothelial cells. *Vasc. Pharmacol.* 44 (6), 411–416. doi:10.1016/j.vph.2006.02.009

Teopompi, E., Risé, P., Pisi, R., Buccellati, C., Aiello, M., Pisi, G., et al. (2019). Arachidonic acid and docosahexaenoic acid metabolites in the airways of adults with cystic fibrosis: effect of docosahexaenoic acid supplementation. *Front. Pharmacol.* 10, 938. doi:10.3389/fphar.2019.00938

Terranova, L., Risé, P., Gramegna, A., Pinna, C., Agostoni, C., Syrén, M. L., et al. (2022). Pro-resolving and pro-inflammatory fatty acid-derived mediators in sputum of stable state bronchiectasis patients. *Respir. Res.* 23 (1), 363. doi:10.1186/s12931-022-02301-5

Trenti, A., Tedesco, S., Boscaro, C., Trevisi, L., Bolego, C., and Cignarella, A. (2018). Estrogen, angiogenesis, immunity and cell metabolism: solving the puzzle. *Int. J. Mol. Sci.* 19 (3), 859. doi:10.3390/ijms19030859

Trenti, A., Zulato, E., Pasqualini, L., Indraccolo, S., Bolego, C., and Trevisi, L. (2017). Therapeutic concentrations of digitoxin inhibit endothelial focal adhesion kinase and angiogenesis induced by different growth factors. *Br. J. Pharmacol.* 174 (18), 3094–3106. doi:10.1111/bph.13944

Visioli, F., Risé, P., Barassi, M. C., Marangoni, F., and Galli, C. (2003). Dietary intake of fish vs. formulations leads to higher plasma concentrations of n−3 fatty acids. *Lipids* 38 (4), 415–418. doi:10.1007/s11745-003-1077-x

Xu, L., and Croix, B. S. (2014). Improving VEGF-targeted therapies through inhibition of COX-2/PGE2 signaling. *Mol. and Cell. Oncol.* 1 (4), e969154. doi:10.4161/23723548.2014.969154

Yli-Jama, P., Meyer, H. E., Ringstad, J., and Pedersen, J. I. (2002). Serum free fatty acid pattern and risk of myocardial infarction: a case-control study. *J. Intern. Med.* 251 (1), 19–28. doi:10.1046/j.1365-2796.2002.00922.x

Yurko-Mauro, K., Kralovec, J., Bailey-Hall, E., Smeberg, V., Stark, J. G., and Salem, N. (2015). Similar eicosapentaenoic acid and docosahexaenoic acid plasma levels achieved with fish oil or krill oil in a randomized double-blind four-week bioavailability study. *Lipids Health Dis.* 14 (1), 99. doi:10.1186/s12944-015-0109-z

frontiers | Frontiers in Pharmacology

TYPE Original Research
PUBLISHED 18 March 2025
DOI 10.3389/fphar.2025.1480844

OPEN ACCESS

EDITED BY
Angelo Sala,
University of Milan, Italy

REVIEWED BY
Emira Bousoik,
University of Derna, Libya
Lei Liu,
The Second affiliated Hospital of Zhejiang University, School of Medicine, China
Xinwei Wu,
National Institutes of Health (NIH), United States

*CORRESPONDENCE
Quanbo Zhang,
quanbozhang@126.com
Yufeng Qing,
qingyufengqq@163.com

†These authors have contributed equally to this work

RECEIVED 14 August 2024
ACCEPTED 26 February 2025
PUBLISHED 18 March 2025

CITATION
Zhang Z, Wang P, Lei T, Guo J, Jiang Y, Li Y, Zheng J, Wang S, Xu H, Jian G, Zhang Q and Qing Y (2025) The role and impact of the IL-6 mediated JAK2-STAT1/3 signaling pathway in the pathogenesis of gout.
Front. Pharmacol. 16:1480844.
doi: 10.3389/fphar.2025.1480844

The role and impact of the IL-6 mediated JAK2-STAT1/3 signaling pathway in the pathogenesis of gout

Zeng Zhang[1,2,3,4†], Peng Wang[1,2†], Tianyi Lei[1,3†], Jianwei Guo[1,2], Yi Jiang[1,3], Yanhui Li[1,3], Jianxiong Zheng[1,3], Shunbing Wang[1,3], Haimuzi Xu[1,3], Guilin Jian[1,4], Quanbo Zhang[1,2,3*] and Yufeng Qing[1,2,3*]

[1]Hyperuricaemia and Gout Research Centre, Affiliated Hospital of North Sichuan Medical College, Nanchong, Sichuan, China, [2]Department of Geriatrics, Affiliated Hospital of North Sichuan Medical College, Nanchong, Sichuan, China, [3]Department of Rheumatology and Immunology, Affiliated Hospital of North Sichuan Medical College, Nanchong, Sichuan, China, [4]The Third People's Hospital of Suining, Suining, Sichuan, China

Background: Interleukin-6 (IL-6) is a pleiotropic cytokine, with specific effects depending on the immune microenvironment. Extensive research has confirmed the pathological roles of the IL-6/JAK2/STAT1/3 signaling pathway in inflammation, autoimmunity, and cancer, as well as its involvement in the pathogenesis of various rheumatic diseases. However, the role and impact of IL-6 as an upstream regulator of the JAK2-STAT1/3 pathway in gout have seldom been reported. This study explores the influence and role of upstream IL-6 in regulating the JAK2-STAT1/3 signaling pathway on gout inflammation, offering new insights for targeted therapeutic interventions and drug development in gout management.

Methods and Results: Clinical data and peripheral blood specimens were collected from gout patients and healthy individuals. In vitro and in vivo models of acute gout inflammation were established by stimulating PBMCs, THP-1 cells, and mice with MSU crystals. IL-6 expression was manipulated using IL-6 agonists and IL-6 knockout (KO) mouse technology to investigate the role and impact of the IL-6-mediated JAK2-STAT1/3 signaling pathway in gout models. RT-qPCR, WB, and ELISA were utilized to assess gene and protein expression levels. Paw swelling in mice was measured using a caliper gauge, while HE and IHC staining were conducted to evaluate the inflammatory status of mouse paw pad synovial tissues and detect the positive expression of relevant proteins. Serum IL-6 protein expression levels were significantly elevated in patients with gouty arthritis (GA) compared to healthy individuals, with multifactor logistic regression revealing an odds ratio (OR) of 2.175 for IL-6. In GA patients, mRNA expression of IL-6, JAK2, STAT1/3, and IL-1β was notably lower in the gout group compared to the healthy control (HC) group. Moreover, IL-6, JAK2, STAT1/3, p-JAK2, p-STAT1/3, and IL-1β proteins were markedly higher in the acute gout (AG) group compared to the intercritical gout (IG) and HC groups. Within the IG group, IL-6, JAK2, STAT3, and IL-1β proteins were significantly elevated compared to the HC group, whereas STAT1, p-JAK2, and p-STAT1/3 proteins were significantly lower. The expression of IL-6 protein and JAK2 mRNA showed positive correlations with certain inflammatory markers. In

the 2h human blood in vitro gout inflammation model, expressions of IL-1β, IL-6, JAK2 mRNA, and IL-1β, IL-6, JAK2, STAT1/3, p-JAK2, p-STAT1/3 proteins were significantly higher compared to both the blank control and PBS-negative control groups. In the acute gout THP-1 cell model, The 6-hour model group showed significantly higher levels of IL-1β, IL-6, JAK2, STAT1/3 mRNA, and corresponding proteins, including their phosphorylated forms, compared to the blank control group. Additionally, treatment with an IL-6 agonist further increased these expression levels compared to the untreated model group. In the acute gout mouse model, IL-6 KO mice exhibited significantly reduced footpad swelling and swelling index compared to wild-type (WT) mice. HE staining revealed decreased inflammatory cell infiltration in IL-6 KO mice. Furthermore, Compared to 12-hour gout model WT mice, IL-1β, IL-6, JAK2, STAT1/3 mRNA, protein expression, and phosphorylated protein levels were notably decreased in IL-6 KO mice. IHC staining showed reduced positive expression of p-JAK2 and p-STAT1/3 in IL-6 KO mice. At the 24-hour mark, IL-6 mRNA and protein expression levels did not differ significantly between IL-6 KO and WT mice; however, IL-1β mRNA and protein expression, as well as JAK2 and STAT3 mRNA expression, were reduced in IL-6 KO mice, while STAT1 mRNA expression remained similar.

Conclusion: IL-6 emerges as a potential risk factor for acute gout attacks, with its involvement in the JAK2-STAT1/3 signaling pathway contributing to the inflammation and pathogenesis process of acute gout through positive feedback mechanisms.

KEYWORDS

gout, IL-6, JAK2, STAT1, stat3, inflammation

Introduction

Gouty arthritis (GA) is an inflammatory disorder caused by disrupted purine metabolism, leading to abnormal deposition of monosodium urate (MSU) crystals in joints and surrounding tissues. It presents with joint redness, swelling, heat, pain, and functional impairment, potentially resulting in severe complications such as joint disability, uric acid nephropathy, and renal failure (He et al., 2023). In China, the number of gout patients was 16.2 million in 2019, with an age-standardized prevalence rate (ASPR) of 12.3% in males and 3.9% in females. The ASPR of gout has been increasing from 1990 to 2019, and projections indicate it will reach 11.7% in males and 4.0% in females by 2029, posing a significant burden on society and healthcare systems (Zhu et al., 2022). The inflammatory response in gout involves various cytokines such as IL-6, IL-1β, and TNF-α, pivotal in the amplification cascade of inflammation. Overproduction of these cytokines can lead to systemic manifestations like hemodynamic instability and metabolic disorders, contributing to pain syndromes (Pinto et al., 2021). Research (Zhang et al., 2021) has identified that both acute and chronic inflammation, alongside immune dysregulation, are significant factors in the pathogenesis of gout. Toll-like receptors and the NLRP3 inflammasome have been highlighted as crucial mechanisms underlying gout (Zhang et al., 2021), yet the *in vivo* self-regulation mechanism remains unclear. The JAK2-STAT1/3 signaling pathway, modulated by IL-6, is an intracellular pathway crucial for immune regulation. IL-6 mediates inflammation occurrence and progression through this pathway. Increasing evidence indicates (Hu et al., 2021) that dysregulation of the JAK2-STAT1/3 pathway is linked to various cancers, autoimmune disorders, and inflammatory conditions, and it plays a critical role in vivo self-regulation mechanisms.

The primary treatment goals for acute gout focus on alleviating inflammation, managing pain, and relieving symptoms. Common therapeutic approaches include non-steroidal anti-inflammatory drugs (NSAIDs), glucocorticoids, colchicine, and IL-1 antagonists to counteract acute inflammation. Chronic management of gout primarily revolves around lowering uric acid levels, often using medications such as allopurinol, to prevent recurrence and disease progression. However, these conventional therapies frequently lead to varying degrees of adverse reactions and complications (Keysser, 2020). In recent years, IL-6 has emerged as a pivotal factor in several inflammatory diseases (Kaneko and Takeuchi, 2021), including rheumatoid arthritis, systemic juvenile idiopathic arthritis, and vasculitis. The efficacy of tocilizumab, the first approved anti-IL-6 biologic, has been validated in treating these conditions (Kaneko and Takeuchi, 2021). Notably, studies by Mokuda et al. (2014) and Pinto et al. (2013) have reported the effectiveness of tocilizumab in treating a resistant case of severe tophaceous gout in a female patient and a severe tophaceous gout case in a male patient. Furthermore, research suggests that tocilizumab or baricitinib can inhibit IL-6 or its mediated JAK/STAT signaling pathway-induced inflammation in MSU-induced neutrophils (Temmoku et al., 2021). The JAK/STAT pathway functions as a central signaling hub for numerous inflammatory cytokines and plays a crucial role in the pathogenesis and progression of rheumatic diseases. Consequently, an increasing number of JAK inhibitors are being utilized in the treatment of rheumatic immune disorders (Tzeng et al., 2021). Currently, there is significant progress in clinical trials involving candidate molecules targeting the IL-6 and IL-6 signaling pathways across various diseases (Rose-John et al., 2023; Yao et al., 2014). Advancing biological understanding of the IL-6 and JAK/STAT signaling pathways enables clinical practitioners to better

grasp how these insights influence the treatment strategies for autoimmune and inflammatory conditions. This study employs clinical analysis and establishes both *in vitro* and *in vivo* models of acute gouty arthritis (AGA) to investigate the role and impact of upstream IL-6 regulation of the JAK2-STAT1/3 signaling pathway on gout inflammation, while exploring potential underlying mechanisms. The objective is to enhance understanding of the self-regulatory mechanisms in gout and to offer new perspectives or theoretical foundations for clinical treatment strategies.

Materials and methods

Preparation of MSU crystals

One Gram of uric acid was dissolved in 200 mL of boiling water containing 6 mL of 1N NaOH. Hydrochloric acid was added to adjust the pH of the solution to 7.2. The solution was cooled with stirring at room temperature and then incubated overnight at 4°C. The precipitate was separated from the solution by filtration and dried under low temperature conditions. The crystals were weighed under sterile conditions and suspended in PBS at concentrations of 80 mg/mL and 25 mg/mL.

Patient samples and clinical data

A total of 111 cases were included in this study, comprising 55 cases of acute-phase gout (AG group) and 56 cases of intermittent gout (IG group), all male patients attending the Department of Rheumatology and Immunology at the Affiliated Hospital of Chuanbei Medical College from January 2023 to June 2023. All patients met the diagnostic criteria for gout established by ACR/EULAR in 2015, and complete clinical data were available. During the same period, blood specimens and data were collected from 57 male individuals undergoing health check-ups (HC group) in the hospital's medical examination department. Peripheral blood mononuclear cells (PBMCs) and serum were obtained from these participants. Informed consent was obtained from all participants, and the study was approved by the Medical Ethics Committee (approval number: 2022ER376-1).

Human blood *in vitro* function experiment

Peripheral venous blood (32 mL each from 5 cases of HC) was collected and divided into eight groups. PBMCs were isolated using lymphocyte isolation solution in an ultra-clean environment. The cells were cultured in RPMI-1640 medium supplemented with 10% fetal bovine serum at a density of 5×10^5 cells/mL in 6-well plates. MSU crystals at a concentration of 100 μg/mL were used to stimulate cells at time points of 0, 1, 2, 4, 6, 8, 10, and 12 h. Incubation was conducted under standard conditions in a CO2 incubator (5 mL/L CO2). The concentrations of IL-1β and IL-6 proteins in plasma were measured using ELISA. Additionally, three tubes (4 mL each) of peripheral venous blood from 19 HC cases were collected, and PBMCs were isolated and cultured as described above. These cells were stimulated with 100 μg/mL MSU crystals for 2 h. A blank control group and a negative control group (PBS stimulation for 2 h) were included. Supernatants and cells were collected after treatment.

THP-1 cell experiments

Human myeloid leukemia mononuclear cells (THP1) were obtained from the cell bank of the Chinese Academy of Sciences. Cells were cultured in RPMI-1640 medium supplemented with 10% fetal bovine serum (ThermoFisher Scientific, USA) and 1% penicillin-streptomycin, and maintained in a humidified incubator at 37°C with 5% CO2. THP1 cells were differentiated using 100 ng/mL phorbol ester (Sigma, USA) for 48 h. Subsequently, cells were stimulated with 100 μg/mL MSU for 0, 3, 6, 9, and 12 h and maintained in a 37°C incubator with 5% CO2. For specific experiments, cells were stimulated with 100 μg/mL MSU for 6 h alone, or with 100 μg/mL MSU in combination with IL-6R alpha [MedChemExpress (MCE) Catalogue No: HY-P7223, USA] for a total of 6 h. A blank control was included for comparison. Supernatants and cells were collected after treatment.

Animal experiments

Heterozygous IL-6 knockout (IL-6+/−) mice were generated by breeding IL-6+/+ and IL-6−/− mice, followed by genotyping of the offspring within the same litter to identify IL-6+/+, IL-6+/−, and IL-6−/− genotypes. The IL-6 KO mice [obtained from the Max Planck Institute for Immunobiology, Freiburg, Germany; B6; 129S2 (Stock No. 002254)] and wild-type (WT) mice [purchased from SPF (Beijing) Biotechnology Co., Ltd.; SCXK (Jing) 2019–0,010] weighed 20–25 g. All mice were housed in pathogen-free facilities at the North Sichuan Medical College Animal Center under a 12-h light/dark cycle, with a relative humidity of 50%–70% and a temperature of 24°C ± 2°C. All animal handling and experimental procedures complied with the guidelines of the Institutional Animal Care and Use Committee (IACUC), and the study was approved by the Animal Ethics Committee of North Sichuan Medical College [Approval No. NSMC-IACUC-2023–082]. Each group, consisting of 6–8 mice, received an injection of 150 μL MSU (80 mg/mL) into the synovial space of the right foot pad of WT and IL-6 KO mice. The swelling index was calculated as (thickness of footpad injected with MSU - initial footpad thickness)/initial footpad thickness, with a ratio >0.15 indicating inflammation. Footpad thickness was measured at specified time points using electronic calipers. Subsequently, mice were anesthetized and euthanized in batches, and footpad tissues were processed for total RNA extraction using Trizol, total protein extraction *via* RIPA homogenization, and supernatant collection for cytokine analysis. Synovial tissues were fixed in 4% paraformaldehyde. Sections were subjected to Hematoxylin-eosin (HE) staining for histological analysis of inflammatory cell infiltration under a light microscope (×40 objective lens). Immunohistochemistry (IHC) staining was performed to observe p-JAK2 and p-STAT1/3 positive areas, following the kit instructions and high-pressure antigen retrieval method. Primary antibodies included rabbit anti-mouse p-JAK2, p-STAT1, and p-STAT3 antibodies (diluted 1:200). Slides were examined at ×400 magnification using a BA400Digital

TABLE 1 Primer sequences for human internal reference and target genes.

Gene name	Forward primer(5′-3′)	Reverse primer(5′-3′)
β-Actin	5′GAGCTACGAGCTGCCTGACG3′	5′GTAGTTTCGTGGATGCCACAG3′
GAPDH	5′ATCGCCCACTTGATTTTGG3′	5′GGATTTGGTCGTATTGGGCG3′
IL-1β	5′ATGATGGCTTATTACAGTGGCAA3′	5′GTCGGAGATTCGTAGCTGGA3′
IL-6	5′ACTCACCTCTTCAGAACGAATTG3′	5′CCATCTTTGGAAGGTTCAGGTTG3′
JAK2	5′TCTGGGGAGTATGTTGCAGAA3′	5′AGACATGGTTGGGTGGATACC3′
STAT1	5′ATCAGGCTCAGTCGGGGAATA3′	5′TGGTCTCGTGTTCTCTGTTCT3′
STAT3	5′ACCAGCAGTATAGCCGCTTC3′	5′GCCACAATCCGGGCAATCT3′

TABLE 2 Primer sequences for mouse internal reference and target genes.

Gene name	Forward primer(5′-3′)	Reverse primer(5′-3′)
β-Actin	5′GAGCTACGAGCTGCCTGACG3′	5′GTAGTTTCGTGGATGCCACAG3′
GAPDH	5′AGGTCGGTGTGAACGGATTTG3′	5′GGGGTCGTTGATGGCAACA3′
IL-1β	5′GAAATGCCACCTTTTGACAGTG3′	5′TGGATGCTCTCATCAGGACAG3′
IL-6	5′TCTATACCACTTCACAAGTCGGA3′	5′GAATTGCCATTGCACAACTCTTT3′
JAK2	5′GGAATGGCCTGCCTTACAATG3′	5′TGGCTCTATCTGCTTCACAGAAT3′
STAT1	5′GCTGCCTATGATGTCTCGTTT3′	5′TGCTTTTCCGTATGTTGTGCT3′
STAT3	5′AGAACCTCCAGGACGACTTTG3′	5′TCACAATGCTTCTCCGCATCT3′

microscope and analyzed with the Halo 101-WL-HALO-1 Data Image Acquisition System.

Primer design and synthesis

The primers for human and mouse β-Actin, GAPDH, IL-1β, IL-6, JAK2, STAT1, and STAT3 genes were designed based on their gene sequences obtained from PubMed Gene. The primers were synthesized by Shanghai Shenggong Bioengineering Company, and the gene sequences are detailed in Table 1 and Table 2.

Total RNA extraction and quantitative reverse transcription PCR (qRT-PCR)

Total RNA was extracted from PBMCs, THP-1 cells, and mouse synovial tissues using the Trizol method. The RNA concentration was determined by UV spectrophotometry, with optimal absorbance values ranging between 1.8 and 2.0. Subsequently, cDNA synthesis was performed through reverse transcription. RT-qPCR was conducted using the SYBR Green PCR Mix kit (Takara, Japan) and the StepOnePlus Real-Time PCR System (CFXconnect, BIO-RAD, USA). The reaction volume for RT-qPCR was set at 10 μL, comprising 5 μL of Power SYBR Green PCR Mix, 3.4 μL of deionized water, 0.3 μL of each primer (forward and reverse), and 1 μL of cDNA. Reaction conditions: first step: 95°C 30s one cycle→95°C 5s→60°C 34s 40 cycles. Step 2: 95°C 5s→60°C 60s→95°C 15s one cycle. Specimens were arranged in duplicate wells, and lysis curves were analyzed upon reaction completion. The ΔCt value, calculated as the difference between the Ct value of the target gene and the Ct value of the internal reference, was used to represent the mRNA expression level of the target gene through the $2^{-\Delta Ct}$ method.

Western blotting (WB) and protein blot analysis

Cells were lysed using the RIPA method, and protein concentrations were determined using the BCA assay. Samples were separated by 8%–10% SDS-PAGE and transferred onto polyvinylidene difluoride (PVDF) membranes (Sigma-Aldrich, USA) at 250 V. The membranes were blocked with BSA or IBlockTM for 30–60 min at room temperature and then incubated overnight at 4°C with primary antibodies. After extensive washing with TBST, the membranes were incubated with secondary antibodies at room temperature for 1 h. Protein signals were detected using an ultra-sensitive chemiluminescence method (Affinity ECL Reagent: FG-level) and captured with a Tanon-5200 chemiluminescence image analysis system. Primary antibodies used included rabbit antibodies against JAK2, p-JAK2, STAT1/3, p-STAT1/3 (Abcam, UK), rabbit antibodies against murine IL-1β, GAPDH, and rabbit antibodies against IL-6 (Affinity Biosciences, USA). Secondary antibodies used were goat anti-rabbit or anti-mouse antibodies (CST, USA). Grey values were quantified using ImageJ software, and the ratio to GAPDH was used for semi-quantitative analysis.

TABLE 3 Comparison of clinical data and laboratory indicators between groups.

Items	Gout group(n = 111)	AG group(n = 55)	IG group(n = 56)	HC group(n = 57)	*F/H* value	*P* Value
Age(years) ($\bar{x}$±SD)	40.09 ± 10.02	39.73 ± 10.34	40.45 ± 9.78	39.11 ± 11.86	0.22	0.801
Gender F/M	0/111	0/55	0/56	0/57	—	—
sUA(umol/L) ($\bar{x}$±SD)	502.0 ± 125.0[a]	529.3 ± 138.9[a,b]	475.2 ± 103.9[a]	347.8 ± 42.4	46.36	<0.001
Crea(mmol/L) ($\bar{x}$±SD)	86.05 ± 14.15[a]	84.99 ± 14.54[a]	87.09 ± 13.82[a]	70.99 ± 10.49	7.55	<0.001
eGFR($ml \cdot min^{-1} \cdot 1.73min^{-2}$) ($\bar{x}$±SD)	89.20 ± 13.83[a]	90.51 ± 14.95[a]	87.91 ± 12.64[a]	100.10 ± 15.81	11.02	<0.001
Cysc(mg/L) ($\bar{x}$±SD)	1.11 ± 0.31[a]	1.04 ± 0.22[a,b]	1.18 ± 0.36[a]	0.82 ± 0.13	28.56	<0.001
GLU(mmol/L) ($\bar{x}$±SD)	5.62 ± 0.62[a]	5.57 ± 0.67[a]	5.68 ± 0.57[a]	4.75 ± 0.70	34.35	<0.001
Globulin(g/L) ($\bar{x}$±SD)	32.76 ± 3.48[a]	33.53 ± 2.54[a,b]	32.00 ± 4.09[a]	29.14 ± 2.93	26.22	<0.001
ESR(mm/1 h) [M(Q_1,Q3)]	14.00(8.00.17.00)	17.00(14.00.22.00)[b]	10.00(6.00.13.00)	—	6.39	<0.001
hsCRP(mg/L) [M(Q_1,Q3)]	8.39(2.29.28.39)	28.39(16.64.41.54)[b]	2.33(1.15.4.21)	—	9.05	<0.001
WBC($\times 10^9$/L) ($\bar{x}$±SD)	7.62 ± 1.98[a]	8.76 ± 1.87[a,b]	6.51 ± 1.36[a]	6.02 ± 1.10	54.76	<0.001
GR($\times 10^9$/L) ($\bar{x}$±SD)	4.66 ± 1.14[a]	5.26 ± 0.80[a,b]	4.07 ± 1.12[a]	3.52 ± 0.82	51.70	<0.001
LY($\times 10^9$/L) ($\bar{x}$±SD)	2.07 ± 0.57[a]	2.06 ± 0.64	2.07 ± 0.50[a]	1.89 ± 0.57	2.27	0.106
Mo($\times 10^9$/L) ($\bar{x}$±SD)	0.48 ± 0.14[a]	0.54 ± 0.13[a,b]	0.41 ± 0.12[a]	0.33 ± 0.10	47.66	<0.001
TG(mmol/L) ($\bar{x}$±SD)	2.05 ± 0.81[a]	1.94 ± 0.85[a]	2.15 ± 0.77[a]	1.15 ± 0.44	31.41	<0.001
TC(mmol/L) ($\bar{x}$±SD)	4.77 ± 1.05[a]	4.61 ± 0.94[a]	4.92 ± 1.13[a]	4.32 ± 0.54	6.17	0.003
HDL(mmol/L) ($\bar{x}$±SD)	1.16 ± 0.28	1.14 ± 0.26	1.18 ± 0.29	1.23 ± 0.30	1.37	0.257
LDLC(mmol/L) ($\bar{x}$±SD)	2.59 ± 0.63	2.50 ± 0.66	2.68 ± 0.60	2.52 ± 0.46	1.72	0.182
VLDL(mmol/L) ($\bar{x}$±SD)	0.88 ± 0.28[a]	0.88 ± 0.28[a]	0.97 ± 0.42[a]	0.63 ± 0.21	18.06	<0.001
apoA1(mmol/L) ($\bar{x}$±SD)	1.14 ± 0.22[a]	1.10 ± 0.22[a,b]	1.18 ± 0.20[a]	1.34 ± 0.20	20.05	<0.001
apoB100(mmol/L) ($\bar{x}$±SD)	0.89 ± 0.20[a]	0.86 ± 0.19[a]	0.91 ± 0.23[a]	0.75 ± 0.12	12.62	<0.001
IL-6(pg/mL)	16.61(7.57.40.98)[a]	40.98(26.71.61.68)[a,b]	7.67(6.04.9.55)[a]	4.02(2.12.5.63)	199.90	<0.001

[a]$P < 0.05$ vs. HC group.
[b]$P < 0.05$ vs. IG group.

Enzyme-linked immunosorbent assay (ELISA)

Cytokine levels in serum, cell culture supernatant, and mouse tissue supernatant were measured using ELISA kits from Xinbosheng Reagent Kit (Beijing, China), Signalway Antibody (SAB, USA), and R&D Systems (USA), following the manufacturer's protocols.

Statistical analysis

SPSS 26.0 and GraphPad Prism 8 software were utilized for statistical analyses. For normally distributed data, t-tests or one-way ANOVA followed by LSD *post hoc* tests were employed. Non-normally distributed data were analyzed using Kruskal–Wallis H tests and Mann-Whitney tests. Spearman correlation analysis was used to assess relationships between variables. Receiver Operating Characteristic (ROC) curves were constructed to evaluate diagnostic accuracy, and logistic regression was employed to assess risk factors. Statistical significance was set at $P < 0.05$.

Results

Clinical data and laboratory test indices

Table 3 presents the general data and clinical characteristics of the subjects. Age, gender, LY, HDL, and LDLC did not differ significantly among the three groups ($P > 0.05$). Compared to the HC group, the AG group showed significantly higher levels of IL-6, sUA, Crea, eGFR, Cysc, GLU, Globulin, WBC, GR, MO, TG, TC, VLDL, apoA1, and apoB100. Similarly, the IG group exhibited

TABLE 4 Univariate and multivariate logistic regression analysis of acute gouty attacks.

Variables	AG group (n = 55)	Combined group (n = 113)	Univariate analysis	Multivariate analysis	
			P_1-value	P_2-value	OR(95%CI)
IL-6(pg/mL)	40.98(26.71.61.68)	5.72(4.00.7.86)	0.009	0.009	2.175(1.219.3.881)
sUA(umol/L)	529.3 ± 138.9	410.9 ± 101.5	<0.001	0.179	
Globulin(g/L)	33.53 ± 2.54	30.56 ± 3.82	<0.001	0.171	
ESR(mm/1 h)	17.00(14.00.22.00)	10.00(6.00.13.00)	<0.001	0.765	
WBC($\times10^9$/L)	8.76 ± 1.87	6.26 ± 1.25	<0.001	0.492	
GR($\times10^9$/L)	5.26 ± 0.80	3.79 ± 1.02	<0.001	0.564	
Mo($\times10^9$/L)	0.54 ± 0.13	0.37 ± 0.11	<0.001	0.088	
TG(mmol/L)	1.94 ± 0.85	1.65 ± 0.80	0.035	0.134	
apoA1(mmol/L)	1.10 ± 0.22	1.26 ± 0.21	<0.001	0.165	

Note: Multifactorial Logistic Regression for Acute Gouty Attacks. The combined group consists of the IG, and HC, groups. *P*1 values were obtained through unifactorial logistic regression, while *P*2 and OR, values were derived from multifactorial logistic regression.

higher levels of IL-6, sUA, Crea, eGFR, Cysc, GLU, Globulin, WBC, GR, LY, MO, TG, TC, VLDL, apoA1, and apoB100 compared to the HC group (all $P < 0.05$). Within the AG group, IL-6, sUA, Cysc, Globulin, ESR, hsCRP, WBC, GR, MO, and apoA1 levels were significantly higher than those in the IG group (all $P < 0.05$).

Multifactorial logistic regression of acute gouty attacks

To enhance model stability, the IG and HC groups were consolidated. Subsequently, all clinical data and serum IL-6 concentrations from the AG and combined groups were subjected to univariate regression analysis. Variables with a significance level of $P < 0.05$ and a Variance Inflation Factor (VIF) less than 10 were selected for inclusion in logistic regression, as detailed in Table 4. Using the forward stepwise regression method with an entry SLE of 0.05 and stay of 0.1, the final logistic regression results identified IL-6 as a significant risk factor for acute gouty attacks.

Comparative analysis of transcriptional and translational expression of IL-1β, IL-6, JAK2, and STAT1/3 in PBMCs from gout patients and healthy controls

The expression levels of IL-1β, IL-6, JAK2, and STAT1/3 mRNA were significantly lower in the gout group compared to the HC group (all $P < 0.001$). Subgroup analysis further revealed statistically significant differences in expression among all three groups (all $P < 0.001$). Specifically, IL-6 mRNA expression was significantly lower in both the AG and IG groups compared to the HC group, with lower levels observed in the AG group compared to the IG group (all $P < 0.05$). The expression of JAK2, STAT3, and IL-1β mRNA was significantly lower in both the AG and IG groups compared to the HC group, and levels were higher in the AG group than the IG group ($P < 0.05$). STAT1 mRNA expression was significantly lower in both the AG and IG groups compared to the HC group ($P < 0.001$), with no statistically significant difference between the AG and IG groups ($P > 0.05$) (Figure 1a). Protein levels of IL-6, JAK2, STAT1/3, p-JAK2, p-STAT1/3, and IL-1β among the three groups showed statistically significant differences ($P < 0.001$). Specifically, the AG group exhibited significantly higher levels compared to the IG and HC groups. Compared to the HC group, the IG group showed significant increases in IL-6, JAK2, STAT3, and IL-1β protein levels, while STAT1, p-JAK2, and p-STAT1/3 protein levels were significantly decreased ($P < 0.05$) (Figure 1b). These findings underscore elevated serum IL-6 levels and dysregulated expression of IL-6/JAK2/STAT1/3 signaling pathway-related genes in gout patients.

Correlation analysis and ROC curves of IL-6 and JAK2 mRNA or protein expression with inflammatory markers in gout patients

ESR, CRP, WBC, GR, Mo, and LY serve as inflammation-related indicators crucial for assessing disease activity in gouty arthritis. Spearman correlation analysis revealed significant positive associations between ESR, CRP, WBC, GR, Mo, and serum IL-6 protein expression (all $P < 0.05$). Additionally, CRP, WBC, GR, Mo, and JAK2 mRNA expression showed significant positive correlations ($P < 0.05$) (Figure 2a). The Area Under the Curve (AUC) values (95% CI) for IL-6 and JAK2 mRNA expression in GA were 0.709 (0.632, 0.786) and 0.711 (0.631, 0.791), respectively, while for AG, the AUC (95% CI) of IL-6 mRNA expression was 0.781 (0.697, 0.865) (Figure 2b). These findings suggest that IL-6 and JAK2 are linked to both clinical and laboratory aspects of GA and offer additional diagnostic value in the evaluation of gout.

Changes in the expression levels of IL-1β, IL-6, JAK2 and STAT1/3 in an *in vitro* gouty inflammation model in human blood

PBMCs from healthy individuals were stimulated with MSU to establish an *in vitro* model of gout using human blood. The

10.3389/fphar.2025.1480844

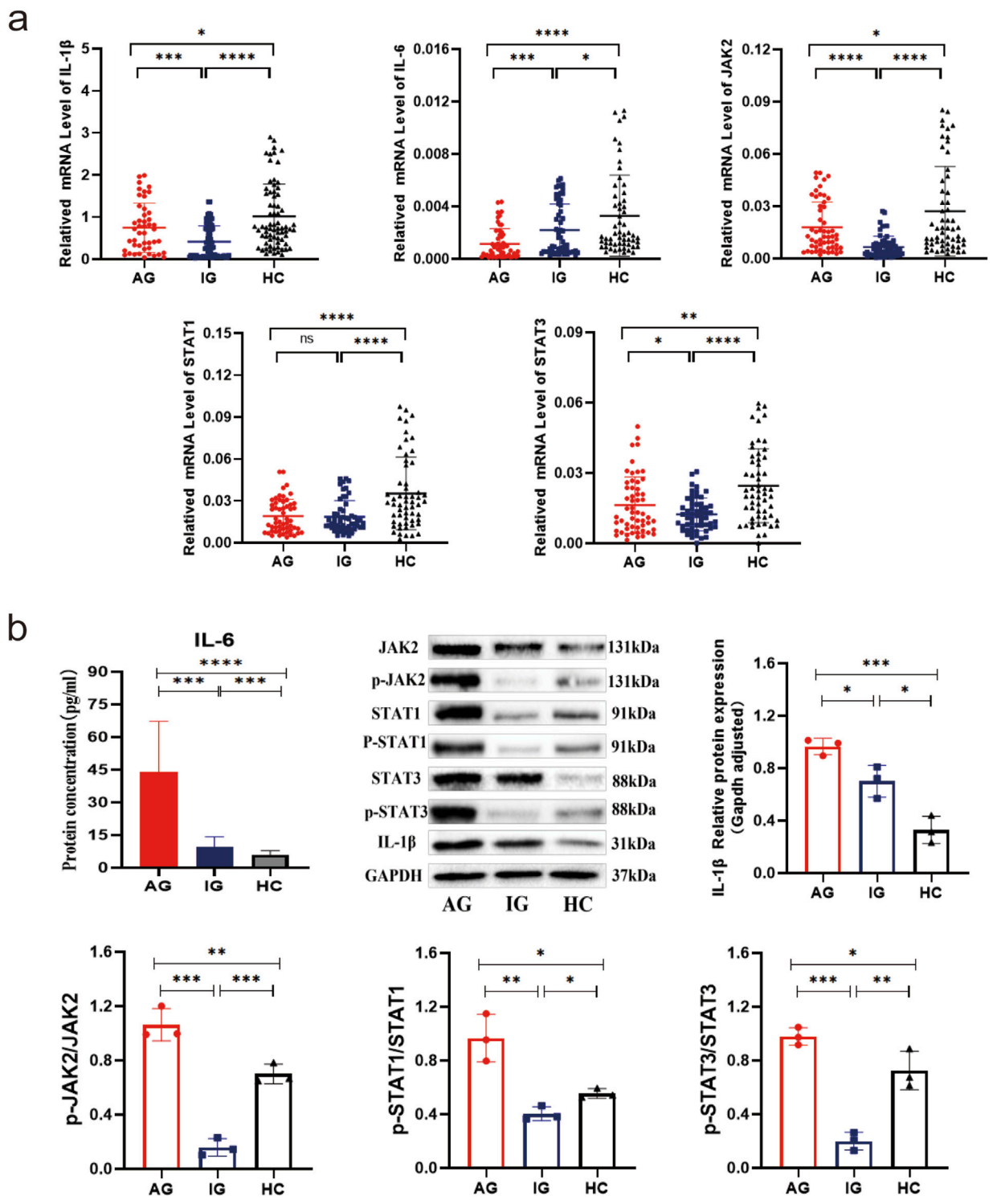

FIGURE 1
Transcriptional and translational expression of IL-1β, IL-6, JAK2, and STAT1/3 in PBMCs of gout patients and healthy controls. **(a)** Scatter plot showing mRNA expression levels of IL-1β, IL-6, JAK2, and STAT1/3. **(b)** IL-6 serum ELISA results, as well as protein bands and expression histograms for JAK2, STAT1/3, p-JAK2, p-STAT1/3, and IL-1β. Data are expressed as mean ± SD from three independent experiments. *p < 0.05, **p < 0.01, ***p < 0.001, ****p < 0.0001, ns p > 0.05.

expression of relevant genes was monitored at various time points. Compared to baseline (0 h), both IL-1β and IL-6 protein levels were significantly elevated after 1 h (both $P <$ 0.05), with peak inflammation observed at 4–6 h, indicating successful establishment of the acute gout inflammation model (Figure 3a). In the 2-h *in vitro* gout inflammation model using

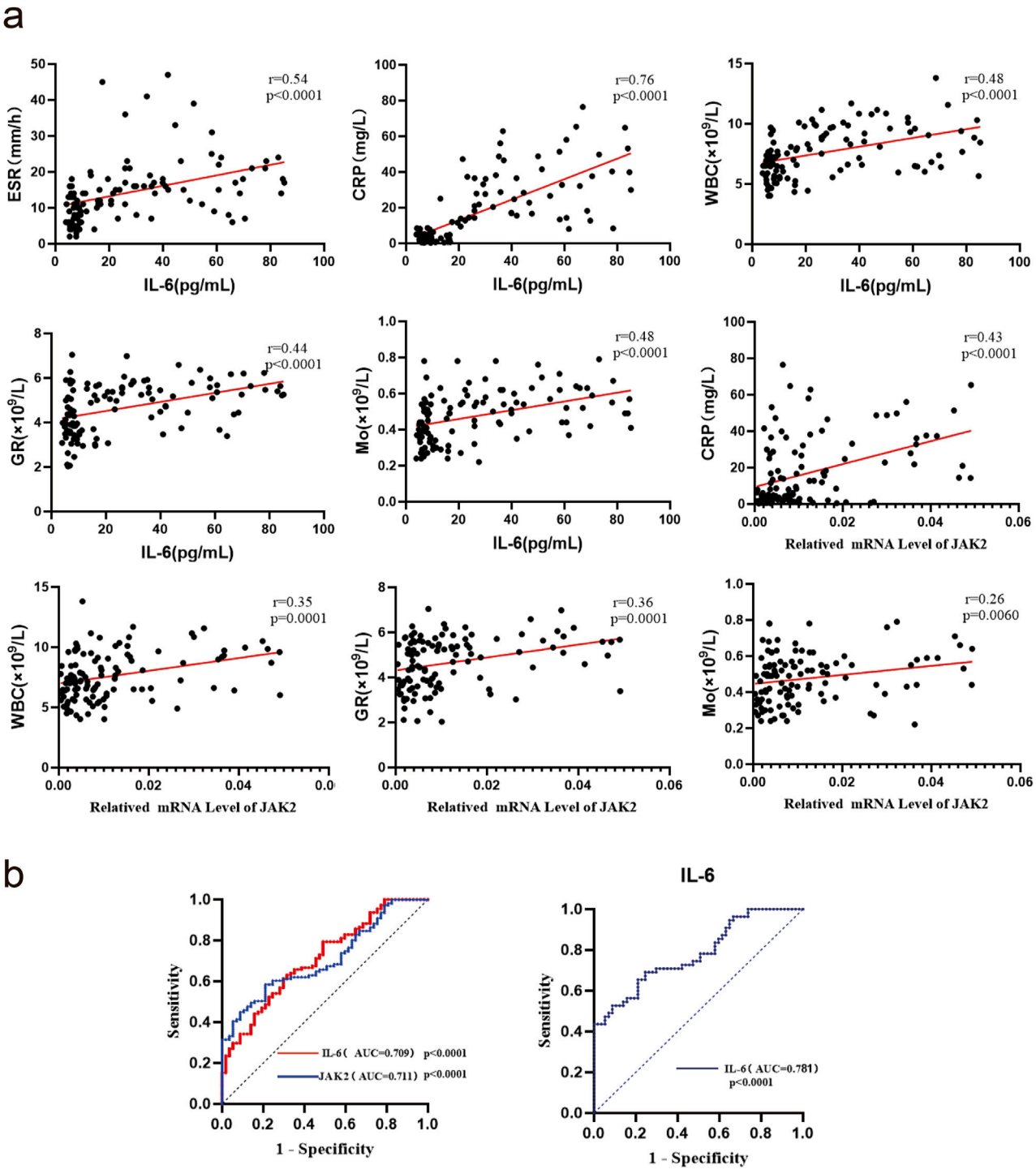

FIGURE 2
Correlation analysis and ROC curves of IL-6 and JAK2 mRNA or protein expression with inflammatory markers in gout patients. **(a)** Correlation analysis(n = 111). **(b)** ROC curve analysis:the AUC analysis for IL-6 and JAK2 is based on mRNA expression data.

human blood, mRNA expression of IL-1β, IL-6, and JAK2, as well as protein expression of IL-1β, IL-6, JAK2, STAT1/3, p-JAK2, and p-STAT1/3, were significantly higher in the model group compared to both the blank control group and the PBS-negative control group (all $P < 0.05$). No statistically significant differences were observed between the blank control group and the PBS-negative control group (both $P > 0.05$) (Figures 3b, c). These findings suggest that the IL-6-JAK2-STAT1/3 signaling pathway may be involved in the activation of acute gout inflammation or its pathogenesis process.

10.3389/fphar.2025.1480844

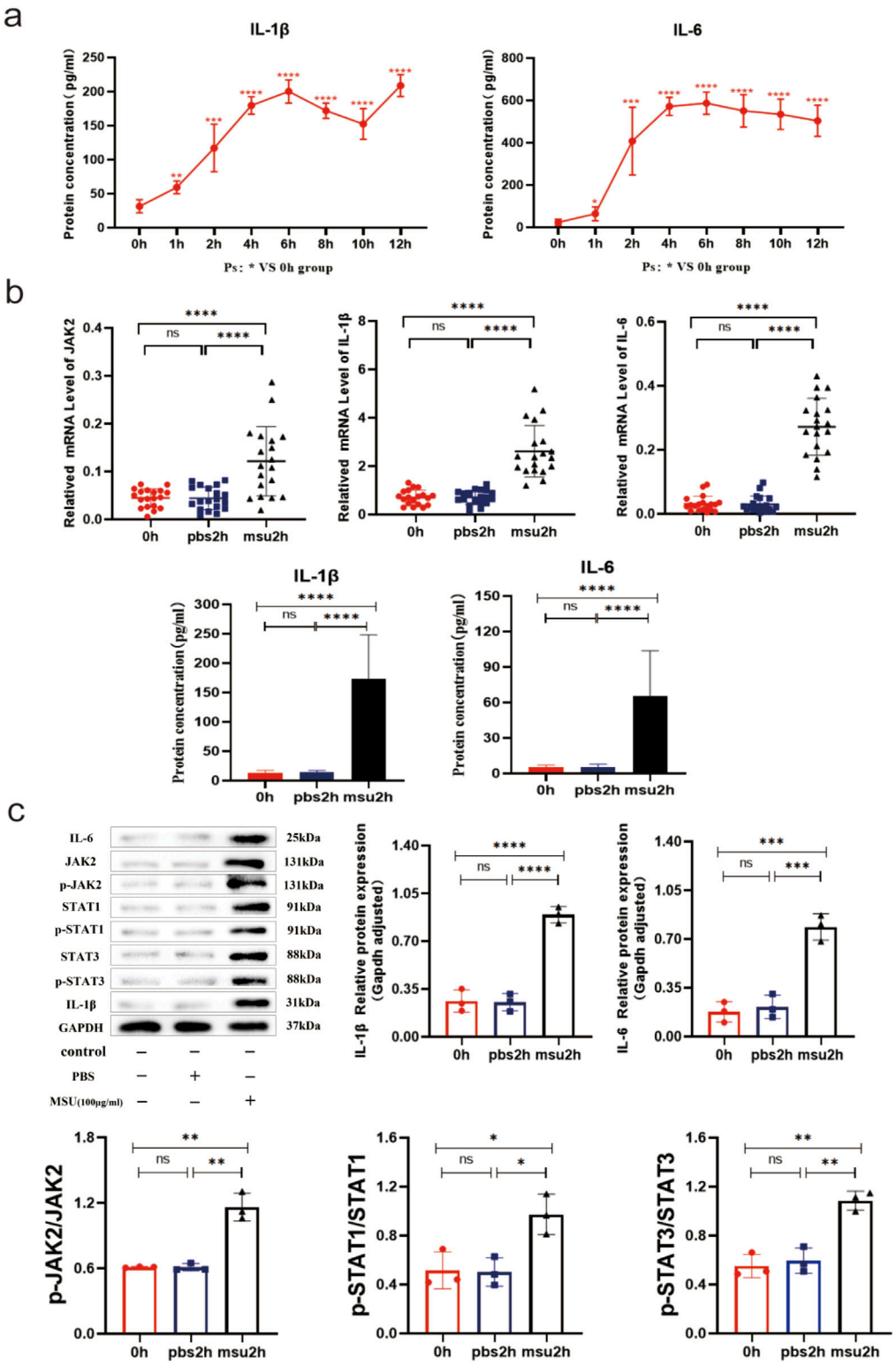

FIGURE 3
0–12h and 2 h Human Blood *In Vitro* Gout Inflammation Model. **(a)** IL-1β and IL-6 serum ELISA results in the 0–12 h human blood *in vitro* gout inflammation model. **(b)** JAK2 and STAT1/3 mRNA results, along with IL-1β and IL-6 serum ELISA results in the 2 h human blood *in vitro* gout inflammation model. **(c)** Protein bands and expression histograms for IL-6, JAK2, STAT1/3, p-JAK2, p-STAT1/3, and IL-1β in the 2 h human blood *in vitro* gout inflammation model. Data are expressed as mean ± SD from three independent experiments. *p < 0.05, **p < 0.01, ***p < 0.001, ****p < 0.0001, ns p > 0.05.

10.3389/fphar.2025.1480844

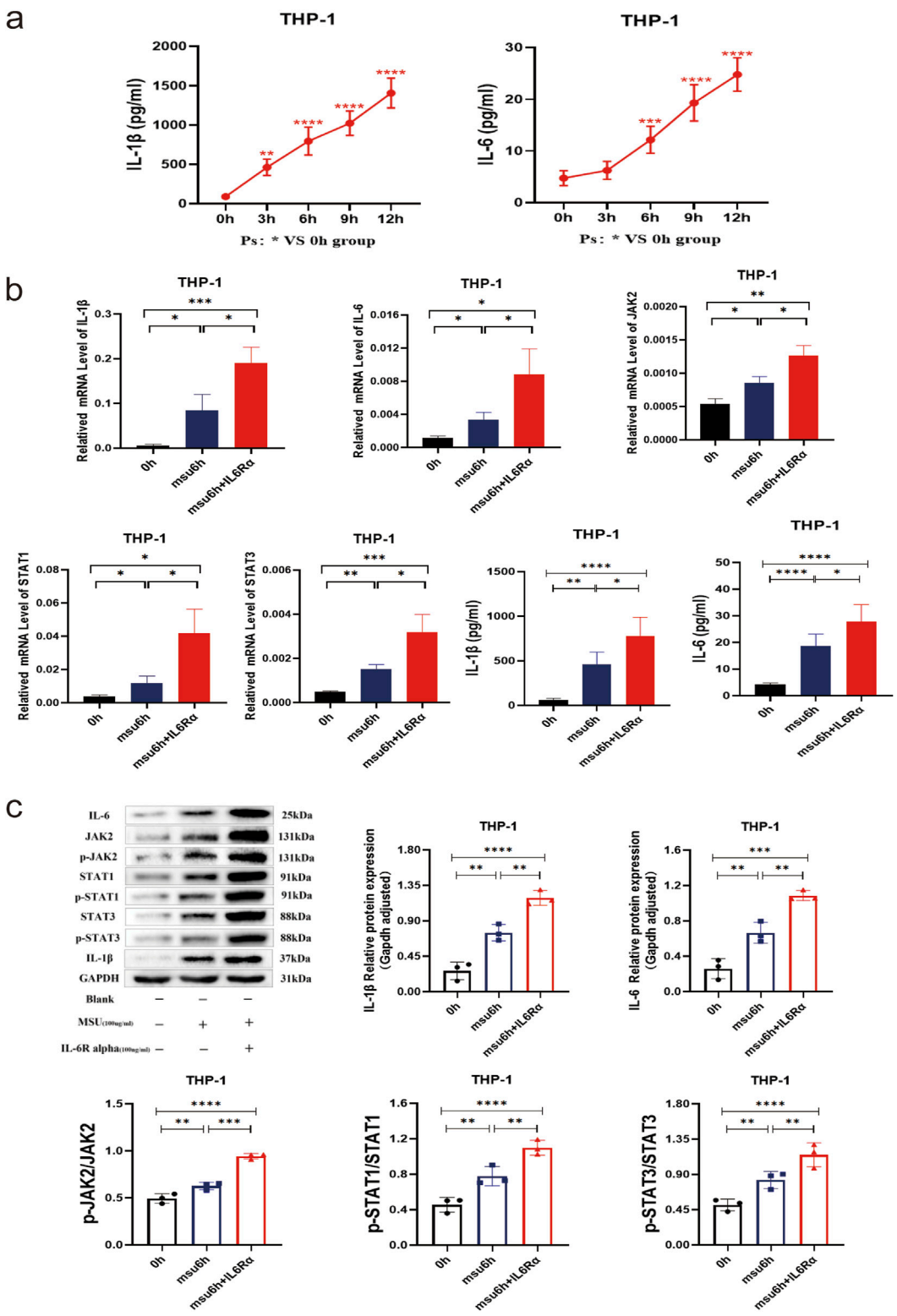

FIGURE 4
THP-1 Gout 6 h Inflammation Model with Combined IL-6 Agonist (IL-6Rα) to Observe the Potential Role and Effect on the JAK2-STAT1/3 Signaling Pathway. **(a)** ELISA results of IL-1β and IL-6 in supernatants from the 0–12 h THP-1 gout inflammation model. **(b)** IL-1β, IL-6, JAK2, and STAT1/3 mRNA results, along with IL-1β and IL-6 supernatant ELISA results in the THP-1 gout 6 h inflammation model with combined IL-6 agonists. **(c)** Protein bands and expression histograms for IL-6, JAK2, STAT1/3, p-JAK2, p-STAT1/3, and IL-1β in the THP-1 gout 6 h inflammation model with combined IL-6 agonists. Data are expressed as mean ± SD from three independent experiments. *p < 0.05, **p < 0.01, ***p < 0.001, ****p < 0.0001, ns p > 0.05.

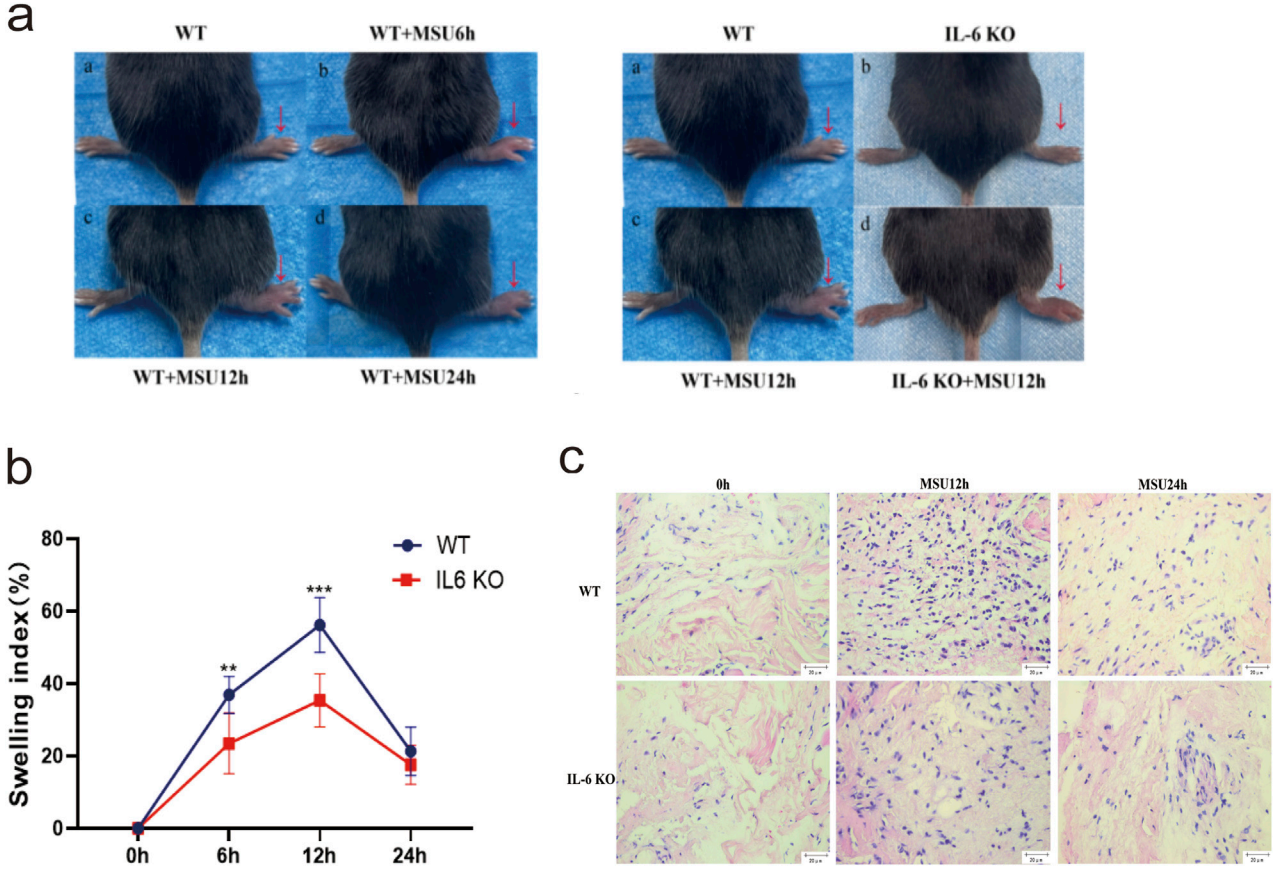

FIGURE 5
IL-6 KO Mouse and WT Mouse Gout Models. **(a)** 150 μL of MSU (80 mg/mL) was injected into the right foot pads of mice, and the thickness of the foot pads was measured at 0, 6, 12, and 24 h, with photographs taken at each time point. The WT and WT + MSU12 h panels are re-used for illustrative purposes. **(b)** Swelling index plots of the foot pads at 0, 6, 12, and 24 h. Data are expressed as mean ± SD from three independent experiments(n = 8). *p < 0.05, **p < 0.01, ***p < 0.001. **(c)** HE staining of synovial tissue in the foot pads at 0, 12, and 24 h (scale = 20 μm, magnification ×400). Blue staining indicates inflammatory cell infiltration.

In the THP-1 gout inflammation model lasting 6 hours, the addition of an IL-6 agonist enhances the inflammatory response via the JAK2-STAT1/3 signaling pathway

THP-1 macrophages were stimulated with MSU to establish an acute gout cell model, and gene expression was monitored at different time points. Compared to baseline (0 h), the expression of IL-1β and IL-6 proteins gradually increased, becoming statistically significant after 3 h (both $P < 0.05$). Analysis from the data suggests that inflammation peaks after 12 h (Figure 4a). In the 6-h cellular model of acute gout, the expression levels of IL-1β, IL-6, JAK2, STAT1/3 mRNA, and their respective proteins, including phosphorylated forms, were significantly higher in the model group compared to the blank control group (all $P < 0.05$) (Figure 4b). Additionally, when an IL-6 agonist was introduced to the model group, the expression of IL-1β, IL-6, JAK2, STAT1/3 mRNA, as well as IL-1β, IL-6, JAK2, STAT1/3, p-JAK2, and p-STAT1/3 proteins, showed significant elevation compared to the model group without agonist addition (all $P < 0.05$) (Figure 4c). These findings indicate that IL-6 agonists intensify the inflammatory response and amplify inflammation through the JAK2-STAT1/3 signaling pathway.

IL-6 knockout mice (IL-6 KO) exhibit milder arthritis compared to wild-type B6 mice (WT)

MSU crystals were injected into the footpads of IL-6 KO and WT mice to establish an acute gouty arthritis model. The left panel of Figure 5a shows that the swelling index of footpads in WT mice significantly differed from the baseline (0 h) at 6, 12, and 24 h ($P < 0.05$), confirming the successful establishment of the gout model. The right panel of Figure 5a illustrates that, at 12 h, the footpads of WT mice were more visibly swollen and exhibited a higher swelling index than those of IL-6 KO mice (Figure 5a). Specifically, at 6 and 12 h post-injection, the swelling index of footpads in IL-6 KO mice was significantly lower than that in the WT control group($P < 0.05$). The most substantial difference was observed at 12 h, prompting further experimental focus on this time point (Figure 5b). HE staining revealed more pronounced inflammatory cell infiltration in WT mice at 12 h and 24 h compared to IL-6 KO mice, with no

10.3389/fphar.2025.1480844

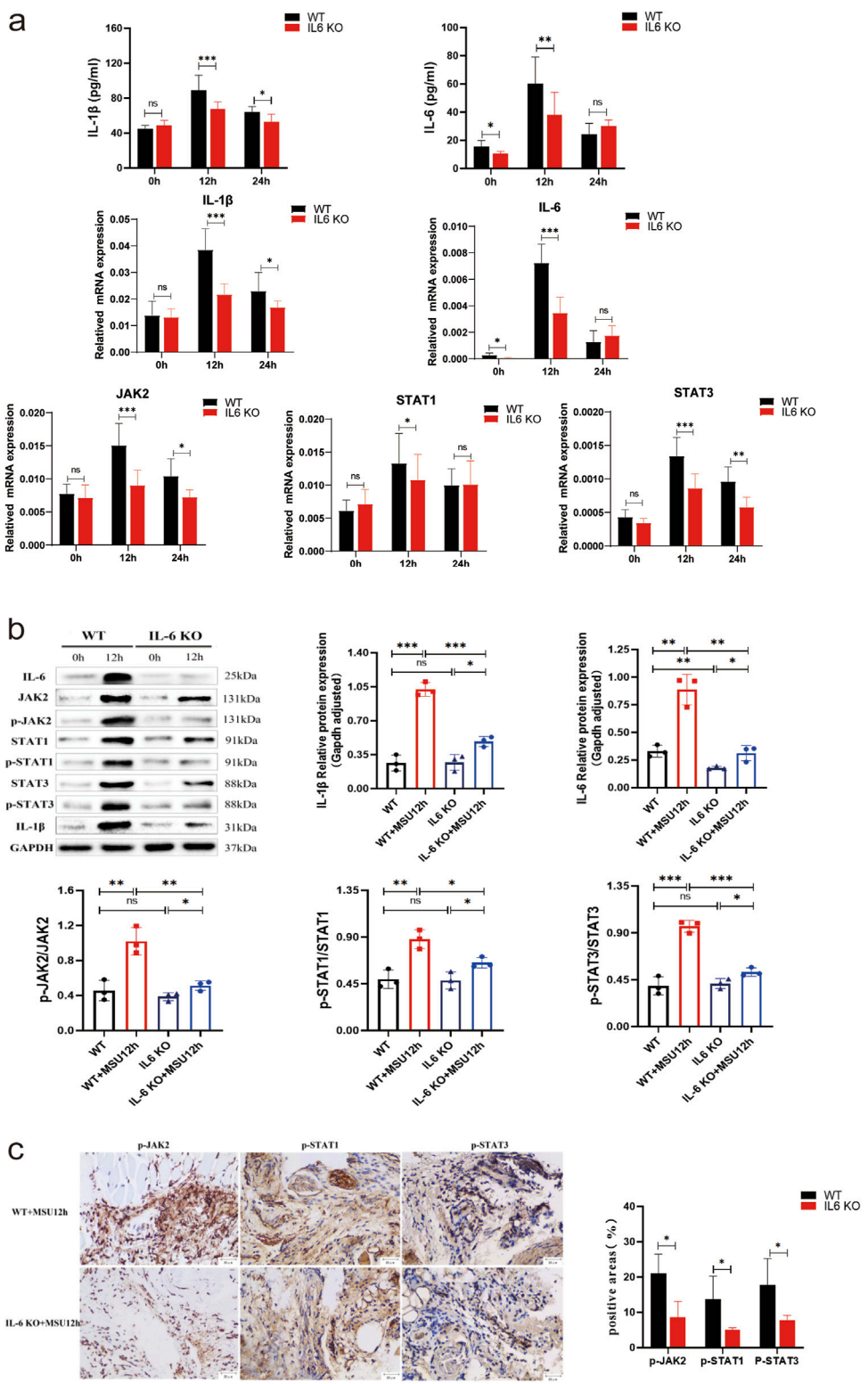

FIGURE 6
Observation of Potential Roles and Effects of IL-6 Knockout on the JAK2-STAT1/3 Signaling Pathway in a Mouse Model of Acute Gouty Arthritis. **(A)** ELISA results of IL-1β and IL-6 in tissue supernatants, and mRNA results of IL-1β, IL-6, JAK2, and STAT1/3. **(B)** Protein bands and expression histograms for IL-6, JAK2, STAT1/3, p-JAK2, p-STAT1/3, and IL-1β. **(C)** Images of IHC staining for p-JAK2 and p-STAT1/3 in the footpad synovium after 12 h of MSU stimulation, along with results of positive areas (scale = 20 μm, magnification ×400). Tan coloration indicates positive expression. Data are expressed as mean ± SD from three independent experiments. *p < 0.05, **p < 0.01, ***p < 0.001, ****p < 0.0001, ns p > 0.05.

significant difference observed at 0 h (Figure 5c). These results underscore that IL-6 knockout mitigates MSU-induced inflammation and arthritis in the experimental model.

IL-6 KO mice avoid developing more severe gouty arthritis by impairing the JAK2-STAT1/3 signalling pathway

In IL-6 KO mice, both mRNA and protein levels of IL-6 were significantly reduced compared to untreated WT mice ($P < 0.05$), while the transcription and translation of other genes remained comparable. This suggests that heterozygous IL-6 KO mice may have been utilized to generate the gout model (Figures 6a, b). In the acute gout model, the mRNA and corresponding protein(contain their phosphorylated proteins) levels of IL-1β, IL-6, JAK2, and STAT1/3 were significantly lower in IL-6 KO mice compared to WT mice at 12 h post-injection ($P < 0.05$) (Figures 6a, b); Additionally, IHC staining revealed a decrease in the positive expression of phosphorylated JAK2 and STAT1/3 in IL-6 KO mice ($P < 0.05$) (Figure 6c). At 24 h, while IL-6 mRNA and protein expression levels were similar to WT mice ($P > 0.05$), IL-1β mRNA and protein levels, as well as JAK2 and STAT3 mRNA, were significantly downregulated in IL-6 KO mice ($P < 0.05$). In contrast, STAT1 mRNA expression remained unchanged ($P > 0.05$) (Figures 6a, b). These findings suggest that IL-6 deletion not only reduces inflammation but also mitigates the severity of gouty arthritis by impairing the JAK2-STAT1/3 signaling pathway.

Discussion

GA is a clinical syndrome precipitated by a persistent increase in blood uric acid levels, resulting in the abnormal accumulation of MSU crystals in joints and tissues. This condition manifests as joint swelling, severe pain, and restricted movement, largely due to the release of inflammatory mediators, such as cytokines and chemokines, from cells within the affected joints. Consequently, managing inflammation is vital for preventing GA attacks. In our study, we noted elevated levels of IL-6, ESR, hsCRP,WBC, GR, and Mo in GA patients compared to the HC group. These markers were significantly more elevated in the AG group than in the IG group, indicating a pronounced increase in serum IL-6 and other inflammatory markers in gout patients during acute episodes (Table 3). Moreover, logistic regression analysis identified IL-6 as a significant risk factor for acute gout attacks (Table 4). The development of AGA is strongly associated with the production of IL-6 and IL-1 (Figure 7). Initially, MSU crystals trigger the MYD88-NFκB signaling pathway *via* Toll-like receptors (TLRs) on immune cell membranes, leading to the release of cytokines such as IL-6 and IL-1β. IL-6 interacts with either membrane-bound (mIL-6R) or soluble (sIL-6R) receptors, in conjunction with gp130, to activate the JAK2/STAT signaling pathway. This activation promotes the transcription and expression of downstream genes. Recent studies have shown (Kothari et al., 2021) that prolonged stimulation by IL-1 increases the phosphorylation of STAT proteins (STAT1/3/5) across various immune cells, with IL-1β-induced IL-6 leading to later activation and phosphorylation of STAT1/3. Consequently, we hypothesize that the IL-6-mediated JAK2-STAT1/3 pathway contributes to the progression of gout, possibly enhancing TLRs-mediated mechanisms. Previous research has mainly focused on downstream effects, but our study is the first to clinically validate IL-6 as a risk factor for gout. Moreover, IL-6 acts upstream of JAK2/STAT1/3, initiating an inflammatory cascade that, through positive feedback, produces more IL-6, thus exacerbating inflammation. In animal models, targeting IL-6 disrupted the IL6-JAK2/STAT1/3-IL6 feedback loop, offering a potential therapeutic approach for effectively treating gout. This strategy could lead to novel therapeutic methods or drugs that target the IL-6 signaling pathway in gout management.

To date, the TLR4 receptor is recognized as the primary sensor in gout, capable of recognizing pathogen-associated molecular patterns (PAMPs) and damage-associated molecular patterns (DAMPs) to initiate signaling. Subsequently, MyD88 mediates the translocation of NF-κB to the nucleus, enhancing the transcription of IL-6 and other pro-inflammatory cytokines, such as TNF-α and IL-1β, in monocytes (Silva et al., 2023). Furthermore, IL-6 mRNA transcription can be stimulated by signals from TNF or IL-1. Beyond monocytes and cytokines, stromal cells, certain immune cell subsets, lipid mediators, and adipokines also produce IL-6 in response to cellular stress induced by Toll-like receptor agonists (Millrine et al., 2022). IL-6 serves as a key immunomodulatory cytokine, influencing the pathogenesis of autoimmune diseases, chronic inflammatory conditions, cancers, and other disorders. It induces intracellular signaling through the JAK/STAT, Ras/MAPK, and PI3K pathways. Within the JAK/STAT pathway, dimerization of Gp130 results in the proximity of JAKs, leading to phosphorylation of tyrosine residues on the Gp130 cytoplasmic domain. Molecules containing the Src homology 2 (SH2) structural domain, STAT1/3 and protein tyrosine phosphatase 2 (SHP2) containing the SH2 structural domain are attracted to the tyrosine phosphorylation motif of gp130. This recruitment facilitates the phosphorylation of STAT1/3 by JAKs, which then translocate to the nucleus to activate transcriptional outputs and trigger the mitogen-activated protein kinase pathway *via* SHP2. Concurrently, STAT3 activation induces various IL-6 response genes, including acute phase proteins. STAT3 also induces SOCS1 and SOCS3, which bind to phosphorylated JAK and phosphorylated Gp130, respectively, forming a negative feedback loop to terminate IL-6 signal transduction (Figure 7). Multiple mechanisms regulate IL-6 expression; however, its abnormal expression plays a crucial role in the pathogenesis of various autoimmune and inflammatory diseases (Aliyu et al., 2022). This study revealed decreased mRNA levels of IL6-JAK2-STAT1/3 in the peripheral blood of gout patients compared to the HC group (Figure 1a), suggesting a potential negative feedback mechanism in humans. Additionally, the levels of IL-6 protein and JAK2 mRNA were positively correlated with certain inflammatory markers(Figure 2a), reflecting their association with gout's clinical and laboratory activities. These findings align with Nara Gualberto Cavalcanti's research (Cavalcanti et al., 2016), which also associated IL-6 with tophi presence and joint deformities in gout patients. Elevated IL-6 levels in children with hyperuricemia (Di Y et al., 2018) also correlated with disease activity, an interesting parallel. Subgroup

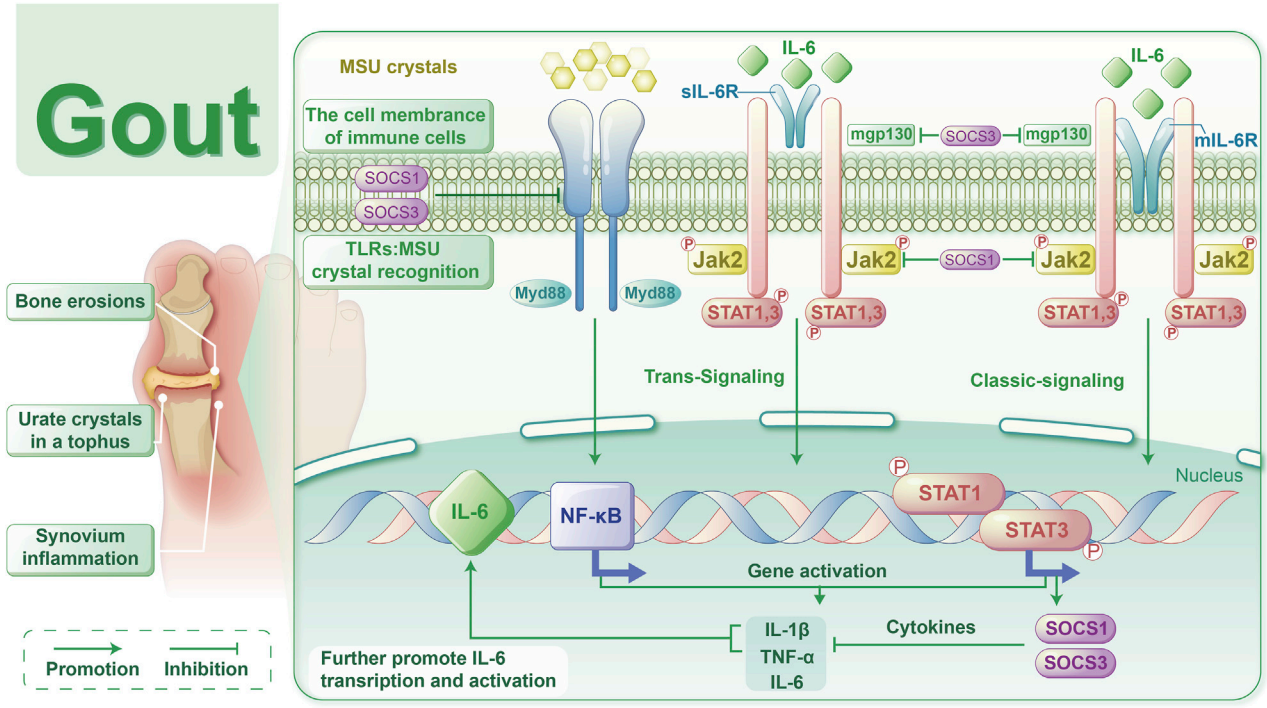

FIGURE 7
Schematic representation of the mechanism by which the IL-6-mediated JAK2-STAT1/3 signalling pathway affects gout.

analysis showed significant increases in IL-1β and IL6-JAK2-STAT1/3 proteins and their phosphorylated forms in the AGA group, while the IG group exhibited higher levels of IL-1β and total IL6-JAK2-STAT3 proteins, with decreased phosphorylated STAT1 and JAK2-STAT1/3 proteins (Figure 1b). This suggests a crucial role for phosphorylated proteins in gout's inflammatory response and indicates involvement of the IL-6 and JAK2-STAT1/3 signaling pathways in gout pathogenesis. Further subgroup analysis indicated reduced expression of JAK2-STAT1/3 proteins and their phosphorylated forms in the IG group compared to the AG group (Figure 1b). This suggests a decrease in JAK2-STAT1/3 signaling pathway activation as gout transitions to the intercritical phase. The spontaneous resolution of acute gout attacks may relate to this pathway's downregulation, paralleling findings by Jumpei Temmoku et al. (Temmoku et al., 2021). Contrarily, IL-6 protein levels in peripheral blood serum were significantly higher in the AG group than in the IG group, indicating rapid increases during acute gout attacks. This rise in IL-6 could potentially trigger JAK2 activation, thereby initiating the JAK2-STAT1/3 signaling pathway and intensifying the inflammatory response. Numerous studies have linked excessive or sustained IL-6 production with various inflammatory diseases (Narazaki and Kishimoto, 2018) supporting the hypothesis that IL-6 dysregulation plays a critical role in gout pathogenesis. Additionally, in the MSU-induced human blood *ex vivo* gout model over 0–12 h (Figure 3a), IL-1β and IL-6 protein expression levels increased at 1 h and peaked between 4 and 6 h compared to baseline. Furthermore, the 2-h human blood *ex vivo* gout inflammation model (Figures 3b, c) showed significantly elevated levels of IL-1β, IL-6, JAK2 mRNA, and their respective proteins, including phosphorylated JAK2 and STAT1/3, compared to both control groups. Collectively, these data indicate that the IL-6/JAK2/STAT1/3 signaling pathway may play a role in the activation of acute gout inflammation and its pathogenesis.

The JAK/STAT pathway is integral to signal transduction driven by extracellular cytokine-activated receptors, playing critical roles in cell proliferation, differentiation, apoptosis, organ development, and immune homeostasis (Xin et al., 2020). Biologic therapies highlight cytokines as key mediators of immune-driven diseases, with JAK inhibitors proving to be safe and effective for treating numerous autoimmune and inflammatory conditions (Schwartz et al., 2017). Research extensively shows that IL-6 regulates nuclear target genes *via* the JAK2-STAT1/3 pathway (Zeng et al., 2023; Deng et al., 2023). To determine whether IL-6 agonists exacerbate gouty arthritis *via* the JAK2-STAT1/3 signaling pathway, we conducted *in vitro* experiments. Therefore, THP-1 cells were treated with IL-6 agonists to establish an acute gouty inflammation model. In a gout model using THP-1 cells treated with MSU at different time points, varying degrees of upregulation in IL-1β and IL-6 proteins were observed over time (Figure 4a). In the 6-h acute gout cell model, expression levels of IL-1β, IL-6, JAK2, STAT1/3 mRNA, and their respective proteins—including phosphorylated JAK2 and STAT1/3—were significantly elevated in the model group compared to the blank control group. Moreover, treatment with an IL-6 agonist further increased these expression levels compared to the untreated model group, demonstrating a notable enhancement in inflammatory signaling (Figures 4b, c). These results suggest that the IL-6 agonist enhances the expression of

the JAK2-STAT1/3 pathway, intensifying the inflammatory response and indicating that it amplifies inflammation *via* this signaling route. Supporting evidence indicates that IL-6 activates the JAK2/STAT3/SOCS3 pathway, playing a critical role as an inflammatory cytokine that promotes both pro-inflammatory and anti-inflammatory responses (Wang et al., 2013). Furthermore, activation of the JAK2/STAT3 pathway has been implicated in uric acid-induced kidney damage and the overproduction of inflammatory cytokines (Lin et al., 2021). It has also been reported that purine-induced interferon-γ activates STAT1 and, in synergy with interferon regulatory factor 1, upregulates xanthine oxidoreductase expression, promoting uric acid generation and inducing inflammation (Wang et al., 2022). Moreover, studies involving LPS-induced macrophages and adjuvant-induced arthritis in rats demonstrate that the production of pro-inflammatory cytokines such as IL-6, IL-1β, and TNF-α requires activation through the NF-κB, JAK1-STAT1/3, and MAPK signaling pathways to exert inflammatory effects (Luan et al., 2022). In summary, once inflammatory mechanisms are activated, IL-6 plays a crucial role in acutely amplifying its signaling pathways. IL-6 activation of the JAK2-STAT1/3 signaling pathway stimulates acute-phase protein production and induces leukocytosis, fever, and angiogenesis during the acute phase. In later stages, IL-6 promotes the transition to chronic inflammation by sustaining monocyte chemoattractant protein-1 secretion, vascular proliferation in T cells, and anti-apoptotic functions, facilitating mononuclear cell aggregation at the injury site. Overall, these findings highlight IL-6's role and impact as a cytokine that promotes autoimmune phenomena and amplifies acute inflammation *via* the JAK2-STAT1/3 signaling pathway.

The JAK/STAT pathway is a principal signaling cascade regulated by cytokines, essential for initiating innate immunity, coordinating adaptive immune responses, and ultimately moderating inflammation. To explore whether IL-6 KO alleviates gouty arthritis through the JAK2-STAT1/3 pathway, and to confirm the role of IL-6 KO in the inflammatory response induced by MSU crystals, we conducted *in vivo* experiments in mice. MSU crystals were injected into the footpads of both WT and IL-6 KO mice to simulate human AGA. In this model, WT mice developed more severe arthritis compared to IL-6 KO mice. In this model, WT mice exhibited more severe arthritis and greater footpad swelling than IL-6 KO mice, as consistently documented (Figures 5a, b). Histological analysis with HE staining showed increased inflammatory cell infiltration in WT mice compared to IL-6 KO mice (Figure 5c). These observations suggest that genetic deletion of IL-6 mitigates MSU-induced inflammation and arthritis, highlighting the potential of targeting IL-6 as a therapeutic approach for managing MSU-induced arthritis. In IL-6 KO mice, basal transcription and translation levels of JAK2-STAT1/3 remained unaffected. However, during MSU-induced arthritis, these levels were significantly reduced (Figures 6a, b), indicating that targeting IL-6 can inhibit the activation and phosphorylation of the JAK2-STAT1/3 pathway, thereby alleviating arthritis inflammation. After establishing the acute gout mouse model with MSU (Figure 6), significant downregulation in the transcription and translation levels of IL-1β and IL-6-mediated JAK2-STAT1/3 signaling was observed in IL-6 KO mice compared to WT mice at 12 h. Moreover, at 24 h, there was a decrease in IL-1β mRNA and protein expression, along with reduced expression of JAK2 and STAT3 mRNA in IL-6 KO mice compared to WT mice. The combined trends of IL-1β and IL-6 suggest that IL-6 gene knockout attenuates the JAK2-STAT1/3 signaling pathway, inhibiting pro-inflammatory cytokine production and alleviating MSU-induced gouty arthritis. These findings corroborate that IL-6 gene knockout can downregulate inflammation through the JAK2-STAT1/3 pathway. Literature reviews, coupled with network pharmacology and bioinformatics predictions, have identified IL-6 and STAT1/3 as critical targets for anti-gout treatment (Yang et al., 2023; Liu et al., 2022). These targets modulate the IL-6/STAT1/STAT3 pathway, which has been shown to significantly prevent and treat gout and arthritis. Similar therapeutic outcomes and mechanisms have been observed with the use of extracts from Ephedra sinica (Han et al., 2016) and Simiao Wan(Shi et al., 2021) in managing gouty arthritis. Evidence suggests (Yen et al., 2015; Jaramillo et al., 2004) that targeting the JAK2 or JAK2/STAT1α pathways induced by MSU crystals in macrophages can release anti-inflammatory mediators, counteracting the formation of pro-inflammatory cytokines. Previous studies have implicated the JAK2/STAT3 signaling pathway and downstream IL-6 in uric acid-induced kidney injury, highlighting potential strategies for preventing and treating hyperuricemia-associated kidney damage. Extracts of Cortex Phellodendri (Pan et al., 2021) and berberine (Lin et al., 2021) reportedly reduce the invasion of inflammatory factors and uric acid accumulation in the kidneys by inhibiting STAT3 expression or activating the JAK2/STAT3 signaling pathway, thereby alleviating hyperuricemic nephropathy progression. Based on the above, inhibiting or reducing IL-6 expression and the IL-6-mediated JAK2-STAT1/3 signaling pathway in AGA can alleviate the severity of MSU crystal-induced arthritis and inflammation. This evidence could serve as a foundation for developing new therapeutic approaches and medications for treating gout.

Conclusion

Previous studies have largely concentrated on the JAK2/STAT3 or JAK2/STAT1α signaling pathways and their downstream mediator, IL-6. Our study enriches this field by demonstrating that IL-6 acts as an upstream regulator of the JAK2-STAT1/3 signaling pathway. For the first time, our research identifies IL-6 as a risk factor for acute gout attacks, elucidating that the IL-6-mediated JAK2-STAT1/3 signaling pathway participates in the inflammation and pathogenesis of acute gout through positive feedback mechanisms. Overall, targeting IL-6 signaling could be an effective therapeutic strategy for treating gout or managing gout attacks.

Data availability statement

The original contributions presented in the study are included in the article/Supplementary Material, further inquiries can be directed to the corresponding authors.

Ethics statement

Clinical specimens were approved by the Ethics Committee of the Affiliated Hospital of Chuanbei Medical College. The studies were conducted in accordance with the local legislation and institutional requirements. The participants provided their written informed consent to participate in this study. Mice were handled and experimental procedures were conducted in accordance with the requirements of the Institutional Animal Care and Use Committee and with permission from the Animal Ethics Committee of Chuanbei Medical College. The study was conducted in accordance with the local legislation and institutional requirements.

Author contributions

ZZ: Conceptualization, Data curation, Formal Analysis, Investigation, Methodology, Project administration, Validation, Visualization, Writing–original draft, Writing–review and editing. PW: Conceptualization, Data curation, Formal Analysis, Investigation, Validation, Visualization, Writing–review and editing. TL: Conceptualization, Data curation, Formal Analysis, Investigation, Validation, Visualization, Writing–review and editing. JG: Data curation, Formal Analysis, Validation, Visualization, Writing–review and editing. YJ: Data curation, Formal Analysis, Validation, Visualization, Writing–review and editing. YL: Data curation, Formal Analysis, Validation, Visualization, Writing–review and editing. JZ: Data curation, Formal Analysis, Validation, Visualization, Writing–review and editing, Funding acquisition. SW: Data curation, Formal Analysis, Validation, Visualization, Writing–review and editing. HX: Data curation, Formal Analysis, Validation, Visualization, Writing–review and editing, Funding acquisition. GJ: Data curation, Formal Analysis, Validation, Visualization, Writing–review and editing. QZ: Funding acquisition, Project administration, Resources, Supervision, Writing–review and editing. YQ: Funding acquisition, Project administration, Resources, Supervision, Writing–review and editing.

Funding

The author(s) declare that financial support was received for the research, authorship, and/or publication of this article. This work was supported by the Nanchong Science and Technology Project (20SXCXTD0002, 20SXQT0308), the Chuanbei Medical College Unveiling and Hanging Project (2022JB004), the Youth Project of Natural Science (CBY23-QNA30, CBY21-QA50), and the Doctoral Start-up Fund Project (CBY21-QD33).

Conflict of interest

The authors declare that the research was conducted in the absence of any commercial or financial relationships that could be construed as a potential conflict of interest.

Publisher's note

All claims expressed in this article are solely those of the authors and do not necessarily represent those of their affiliated organizations, or those of the publisher, the editors and the reviewers. Any product that may be evaluated in this article, or claim that may be made by its manufacturer, is not guaranteed or endorsed by the publisher.

Supplementary material

The Supplementary Material for this article can be found online at: https://www.frontiersin.org/articles/10.3389/fphar.2025.1480844/full#supplementary-material

References

Aliyu, M., Zohora, F. T., Anka, A. U., Ali, K., Maleknia, S., Saffarioun, M., et al. (2022). Interleukin-6 cytokine: an overview of the immune regulation, immune dysregulation, and therapeutic approach. *Int. Immunopharmacol.* 111, 109130. doi:10.1016/j.intimp.2022.109130

Cavalcanti, N. G., Marques, C. D., Lins, E. L. T., Pereira, M. C., Rego, M. J., Duarte, A. L., et al. (2016). Cytokine profile in gout: inflammation driven by IL-6 and IL-18? *Immunol. Invest.* 45 (5), 383–395. doi:10.3109/08820139.2016.1153651

Deng, J., Huang, Y., Wang, L., and Sun, X. (2023). The role of IL-6/JAK/STAT signal in female infertility caused by hydrosalpinx. *Immun. Inflamm. Dis.* 11 (6), e871. doi:10.1002/iid3.871

Di, Y., Wang, J., Chen, Y., Sun, N., Wu, L., Dai, X., et al. (2018). Elevated interleukin 1β and interleukin 6 levels in the serum of children with hyperuricemia. *JCR-J. Clin. Rheumatol.* 24 (2), 65–69. doi:10.1097/RHU.0000000000000611

Han, J. W., Shim, D. W., Shin, W. Y., Kim, M. K., Shim, E. J., Sun, X., et al. (2016). Juniperus rigida Sieb. extract inhibits inflammatory responses via attenuation of TRIF-dependent signaling and inflammasome activation. *J. Ethnopharmacol.* 190, 91–99. doi:10.1016/j.jep.2016.05.059

He, Y. X., Zhang, Q. B., Dai, F., Zheng, J. X., and Qing, Y. F. (2023). Association of microRNA-146a rs57095329 polymorphism with susceptibility to primary gout in a Chinese han population. *Curr. Rheumatol. Rev.* 19 (3), 336–344. doi:10.2174/1573397119666230214104242

Hu, X., Li, J., Fu, M., Zhao, X., and Wang, W. (2021). The JAK/STAT signaling pathway: from bench to clinic. *Signal Transduct. Target. Ther.* 6 (1), 402. doi:10.1038/s41392-021-00791-1

Jaramillo, M., Naccache, P. H., and Olivier, M. (2004). Monosodium urate crystals synergize with IFN-gamma to generate macrophage nitric oxide: involvement of extracellular signal-regulated kinase 1/2 and NF-kappa B. *J. Immunol.* 172 (9), 5734–5742. doi:10.4049/jimmunol.172.9.5734

Kaneko, Y., and Takeuchi, T. (2021). An update on the pathogenic role of IL-6 in rheumatic diseases. *Cytokine* 146, 155645. doi:10.1016/j.cyto.2021.155645

Keysser, G. (2020). Gout arthritis: pathogenesis, diagnostics and treatment. *Dtsch. Med. Wochenschr.* 145 (14), 991–1005. doi:10.1055/a-1036-8348

Kothari, H., Williams, C. M., Mcskimming, C., Drago, F., Marshall, M. A., Garmey, J., et al. (2021). Identification of human immune cell subtypes most responsive to IL-1β-induced inflammatory signaling using mass cytometry. *Sci. Signal.* 14 (673), eabc5763. doi:10.1126/scisignal.abc5763

Lin, G., Yu, Q., Xu, L., Huang, Z., Mai, L., Jiang, L., et al. (2021). Berberrubine attenuates potassium oxonate- and hypoxanthine-induced hyperuricemia by regulating urate transporters and JAK2/STAT3 signaling pathway. *Eur. J. Pharmacol.* 912, 174592. doi:10.1016/j.ejphar.2021.174592

Liu, Y., Luo, D., and Xu, B. (2022). The combination of molecular docking and network pharmacology reveals the molecular mechanism of Danggui Niantong decoction in treating gout. *Med. Baltim.* 101 (47), e31535. doi:10.1097/MD.0000000000031535

Luan, X., Cong, Z., Anastassiades, T. P., and Gao, Y. (2022). N-butyrylated hyaluronic acid achieves anti-inflammatory effects *in vitro* and in adjuvant-induced immune activation in rats. *Molecules* 27 (10), 3267. doi:10.3390/molecules27103267

Millrine, D., Jenkins, R. H., Hughes, S., and Jones, S. A. (2022). Making sense of IL-6 signalling cues in pathophysiology. *FEBS Lett.* 596 (5), 567–588. doi:10.1002/1873-3468.14201

Mokuda, S., Kanno, M., Takasugi, K., Okumura, C., Ito, Y., and Masumoto, J. (2014). Tocilizumab improved clinical symptoms of a patient with systemic tophaceous gout who had symmetric polyarthritis and fever: an alternative treatment by blockade of interleukin-6 signaling. *SAGE Open Med. Case Rep.* 2, 2050313X13519774. doi:10.1177/2050313X13519774

Narazaki, M., and Kishimoto, T. (2018). The two-faced cytokine IL-6 in host defense and diseases. *Int. J. Mol. Sci.* 19 (11), 3528. doi:10.3390/ijms19113528

Pan, J., Zhang, C., Shi, M., Guo, F., Liu, J., Li, L., et al. (2021). Ethanol extract of Liriodendron chinense (Hemsl.) Sarg barks attenuates hyperuricemic nephropathy by inhibiting renal fibrosis and inflammation in mice. *J. Ethnopharmacol.* 264, 113278. doi:10.1016/j.jep.2020.113278

Pinto, J. L., Mora, G. E., Fernandez-Avila, D. G., Gutierrez, J. M., and Diaz, M. C. (2013). Tocilizumab in a patient with tophaceous gout resistant to treatment. *Reumatol. Clin.* 9 (3), 178–180. doi:10.1016/j.reuma.2012.06.009

Pinto, L. G., Pinho-Ribeiro, F. A., and Verri, W. J. (2021). Editorial: cytokines and pain. *Front. Immunol.* 12, 788578. doi:10.3389/fimmu.2021.788578

Rose-John, S., Jenkins, B. J., Garbers, C., Moll, J. M., and Scheller, J. (2023). Targeting IL-6 trans-signalling: past, present and future prospects. *Nat. Rev. Immunol.* 23 (10), 666–681. doi:10.1038/s41577-023-00856-y

Schwartz, D. M., Kanno, Y., Villarino, A., Ward, M., Gadina, M., and O'Shea, J. J. (2017). JAK inhibition as a therapeutic strategy for immune and inflammatory diseases. *Nat. Rev. Drug Discov.* 16 (12), 843–862. doi:10.1038/nrd.2017.201

Shi, L., Yuan, Z., Liu, J., Cai, R., Hasnat, M., Yu, H., et al. (2021). Modified Simiaowan prevents articular cartilage injury in experimental gouty arthritis by negative regulation of STAT3 pathway. *J. Ethnopharmacol.* 270, 113825. doi:10.1016/j.jep.2021.113825

Silva, C. R., Saraiva, A. L., Rossato, M. F., Trevisan, G., and Oliveira, S. M. (2023). What do we know about toll-like receptors involvement in gout arthritis? Endocr. *Metab. Immune Disord.-Drug Targets.* 23 (4), 446–457. doi:10.2174/1871530322666220523145728

Temmoku, J., Fujita, Y., Matsuoka, N., Urano, T., Furuya, M. Y., Asano, T., et al. (2021). Uric acid-mediated inflammasome activation in IL-6 primed innate immune cells is regulated by baricitinib. *Mod. Rheumatol.* 31 (1), 270–275. doi:10.1080/14397595.2020.1740410

Tzeng, H. T., Chyuan, I. T., and Lai, J. H. (2021). Targeting the JAK-STAT pathway in autoimmune diseases and cancers: a focus on molecular mechanisms and therapeutic potential. *Biochem. Pharmacol.* 193, 114760. doi:10.1016/j.bcp.2021.114760

Wang, H., Xie, L., Song, X., Wang, J., Li, X., Lin, Z., et al. (2022). Purine-induced IFN-gamma promotes uric acid production by upregulating xanthine oxidoreductase expression. *Front. Immunol.* 13, 773001. doi:10.3389/fimmu.2022.773001

Wang, Y., van Boxel-Dezaire, A. H., Cheon, H., Yang, J., and Stark, G. R. (2013). STAT3 activation in response to IL-6 is prolonged by the binding of IL-6 receptor to EGF receptor. *Proc. Natl. Acad. Sci. U. S. A.* 110 (42), 16975–16980. doi:10.1073/pnas.1315862110

Xin, P., Xu, X., Deng, C., Liu, S., Wang, Y., Zhou, X., et al. (2020). The role of JAK/STAT signaling pathway and its inhibitors in diseases. *Int. Immunopharmacol.* 80, 106210. doi:10.1016/j.intimp.2020.106210

Yang, X., Wang, Y., Ding, X., Ju, S., An, X., Zhang, B., et al. (2023). Network pharmacology identification and *in vivo* validation of key pharmacological pathways of Qin Jiao for gout and arthritis. *Pharm. Biol.* 61 (1), 1525–1535. doi:10.1080/13880209.2023.2288289

Yao, X., Huang, J., Zhong, H., Shen, N., Faggioni, R., Fung, M., et al. (2014). Targeting interleukin-6 in inflammatory autoimmune diseases and cancers. *Pharmacol. Ther.* 141 (2), 125–139. doi:10.1016/j.pharmthera.2013.09.004

Yen, J. H., Lin, L. C., Chen, M. C., Sarang, Z., Leong, P. Y., Chang, I. C., et al. (2015). The metastatic tumor antigen 1-transglutaminase-2 pathway is involved in self-limitation of monosodium urate crystal-induced inflammation by upregulating TGF-β1. *Arthritis Res. Ther.* 17 (1), 65. doi:10.1186/s13075-015-0592-7

Zeng, Z., Lan, Y., Zhang, L., Chen, Y., Gong, Y., Zuo, F., et al. (2023). The m6A reader YTHDF2 alleviates the inflammatory response by inhibiting IL-6R/JAK2/STAT1 pathway-mediated high-mobility group box-1 release. *Burns Trauma* 11, tkad023. doi:10.1093/burnst/tkad023

Zhang, Q. B., Zhu, D., Dai, F., Huang, Y. Q., Zheng, J. X., Tang, Y. P., et al. (2021). MicroRNA-223 suppresses IL-1β and TNF-α production in gouty inflammation by targeting the NLRP3 inflammasome. *Front. Pharmacol.* 12, 637415. doi:10.3389/fphar.2021.637415

Zhu, B., Wang, Y., Zhou, W., Jin, S., Shen, Z., Zhang, H., et al. (2022). Trend dynamics of gout prevalence among the Chinese population, 1990-2019: a joinpoint and age-period-cohort analysis. *Front. Public Health* 10, 1008598. doi:10.3389/fpubh.2022.1008598

frontiers | Frontiers in Pharmacology

TYPE Original Research
PUBLISHED 25 April 2025
DOI 10.3389/fphar.2025.1514284

OPEN ACCESS

EDITED BY
Pietro Minuz,
University of Verona, Italy

REVIEWED BY
Sandip V. Pawar,
Panjab University, India
Sachin Bhagchandani,
Massachusetts Institute of Technology,
United States

*CORRESPONDENCE
Dongli Li,
wyuchemldl@126.com
Jingwei Jin,
wyuchemjjw@126.com

†These authors have contributed equally to this work

RECEIVED 20 October 2024
ACCEPTED 01 April 2025
PUBLISHED 25 April 2025

CITATION
Wu J, Ou Y, Yao M, Liu J, Ran H, Wu Z, Wu R, Gan L, Li D and Jin J (2025) The immunostimulatory activity of *Epimedium* flavonoids involves toll-like receptor 7/8. *Front. Pharmacol.* 16:1514284. doi: 10.3389/fphar.2025.1514284

The immunostimulatory activity of *Epimedium* flavonoids involves toll-like receptor 7/8

Jingyu Wu[1,2†], Yi Ou[1,2†], Min Yao[1,2], Jiaquan Liu[1,2], Hengxing Ran[1,2], Zhengrong Wu[1,2], Rihui Wu[1,2], Lishe Gan[1,2,3], Dongli Li[1,2*] and Jingwei Jin[1,2*]

[1]School of Pharmacy and Food Engineering, Guangdong Provincial Key Laboratory of Large Animal Models for Biomedicine, Wuyi University, Jiangmen, China, [2]International Healthcare Innovation Institute, Jiangmen, China, [3]College of Pharmaceutical Sciences, Zhejiang Chinese Medical University, Hangzhou, China

Background: The flavonoids found in *Epimedium* exhibit a wide range of pharmacological activities, with their immunostimulatory effects emerging as a significant area of research in recent years. However, the underlying mechanism of their immunostimulatory activity remains unclear.

Purpose: To investigate the immunostimulatory effects and elucidate the specific mechanisms of *Epimedium* flavonoids both *in vitro* and *in vivo*.

Methods: The immunostimulatory effects and underlying mechanisms of flavonoids from *Epimedium* were evaluated *in vitro* using a variety of techniques, including cell viability assays, flow cytometry, real-time reverse transcription-quantitative polymerase chain reaction (qRT-PCR), enzyme-linked immunosorbent assay (ELISA), molecular docking, plasmid recombination and transformation, recombinant protein expression, surface plasmon resonance (SPR), and NF-κB/SEAP assays. To investigate the immune response in animal experiments, *Epimedium* flavonoids were compared with traditional adjuvants, utilizing biochemical analysis and flow cytometry.

Results: *Epimedium* flavonoids, primarily composed of icaritin, icariin I and icariin II, were observed to significantly enhance the expression of surface co-stimulatory molecules (CD40, CD80, CD86) and major histocompatibility complex (MHC-I, MHC-II) in bone marrow-derived dendritic cells (BMDCs) and RAW 264.7 cells. Additionally, the production of chemokines and pro-inflammatory cytokines was significantly increased in RAW 264.7 cells. *In vivo*, the findings demonstrated that the vaccine adjuvant containing *Epimedium* flavonoids significantly increased the serum concentration of total OVA-specific IgG compared to the control group. SPR analysis revealed that icariin II exhibited the highest binding response to TLR7, while icariin I and icariin II showed the strongest interactions with TLR8 protein, even surpassing the positive control drug, Resiquimod. The NF-κB/SEAP assay further confirmed that icaritin, icariin I, and icariin II enhanced NF-κB activity and stimulated SEAP secretion through TLR7/8 activation.

KEYWORDS

Epimedium flavonoids, immunostimulatory activity, vaccine adjuvant, TLR7, TLR8

1 Introduction

Vaccination is one of the most effective strategies for preventing and treating infectious diseases (Goff et al., 2015). The primary objective of vaccination is to elicit a robust and targeted immune response that provides long-lasting protection against infection. Additionally, it aims to stimulate the immune system to develop adaptive immunity against pathogens (Verma et al., 2023). Early vaccine formulations were often impure and contained extraneous antigens, which compromised their effectiveness. The advent of recombinant DNA technology and synthetic chemistry has facilitated the production of highly purified antigens (Liu X. et al., 2021), allowing for a more precise and targeted immune response. However, a major drawback of vaccines composed solely of purified antigens is their reduced immunogenicity (Chilamakuri and Agarwal, 2021). As a result, these antigenic formulations often require the inclusion of adjuvants to enhance immunogenicity and elicit a protective immune response (Takahama and Yamamoto, 2020).

Adjuvants are employed to enhance and modulate the immunogenicity of vaccines without directly inducing a specific immune response (Chen H. et al., 2024). Most subunit vaccines rely on adjuvants to enhance their efficacy; however, the development of novel adjuvants has progressed relatively slowly. To date, only a limited number of adjuvants have been approved for human use (Liu T. et al., 2021). Researchers are actively exploring more effective adjuvants with reduced adverse effects, improved ease of synthesis, and lower production costs (Wei et al., 2023). In this context, scientists have recently been investigating the potential of natural adjuvants, including traditional Chinese herbs.

Traditional Chinese herbal remedies contain a diverse array of bioactive compounds, including flavonoids, glycosides, polysaccharides, acids, terpenes, polyphenols, and alkaloids (Zebeaman et al., 2023). Among these, flavonoids represent a significant class of bioactive compounds with a broad spectrum of pharmacological activities, most notably their immunomodulatory effects. In traditional Chinese medicine, flavonoids regulate the immune system by binding to various receptors on immune cells and activating distinct signaling pathways. The host immune system recognizes microorganisms, including viruses, bacteria, and fungi, primarily through the detection of conserved molecular structures known as pathogen-associated molecular patterns (PAMPs).

Epimedium is one of the most well-known Chinese medicinal herbs, first documented in the Shenlong Materia Medica between the 2nd and 3rd centuries CE (Wang, 2021). With a long history of clinical application, *Epimedium* has been traditionally used to reinforce kidney function and invigorate Yang in traditional Chinese medicine. However, the complexity of interactions among its various components has made it challenging to determine a precise safe dosage, despite previous evidence supporting its safety. This thesis primarily focuses on the screening and analysis of flavonoids present in *Epimedium*, including icariin, icaritin, icariin I, icariin II, Epimedin A, Epimedin B, Epimedin C, and other related compounds (Zhang et al., 2020).

Pattern recognition receptors (PRRs) are germline-encoded receptors that detect pathogen-associated molecular patterns (PAMPs), serving as key upstream regulators of the immune response. Upon pathogen infection, PRRs activate innate immune signaling pathways and induce immune responses, playing a critical role in the initiation of innate immunity (Kawasaki and Kawai, 2014). Based on their structural and functional characteristics, pattern recognition receptors (PRRs) are classified into six families: Toll-like receptors (TLRs), C-type lectin receptors (CLRs), NOD-like receptors (NLRs), RIG-I-like receptors (RLRs), AIM2-like receptors (ALRs), and other receptors (OLRs) (Howard et al., 2022). This paper focuses on the roles of TLR7 and TLR8, which specifically recognize distinct RNA sequences and are functionally localized within endosomes (Wang et al., 2021). Studies conducted in 2011 demonstrated the pivotal role of TLR7 and TLR8 in initiating both innate and adaptive immune responses. These highly conserved proteins interact with a variety of small molecules and nucleic acids. Activation of TLR7/8 plays a crucial role in protecting the host from invading pathogens while enhancing the overall immune response (Huang et al., 2021). However, sustained TLR7/8 signaling can result in an exaggerated immune response, potentially contributing to chronic inflammation and autoimmune disorders (Singh et al., 2014). Therefore, agonists and antagonists targeting the TLR7/8 pathway represent promising therapeutic candidates for the treatment of immune-related diseases (Sun et al., 2022).

TLR7 and TLR8 play pivotal roles in the acquired immune response, and their structural and functional similarities have attracted considerable attention. Ligand binding to TLR7 and TLR8 triggers the activation of NF-κB signaling, leading to the production of pro-inflammatory cytokines and type I interferons (IFNs). These immune mediators enhance the bactericidal activity of leukocytes and promote the maturation and function of antigen-presenting cells (APCs), thereby orchestrating the acquired immune response. A review of the literature suggests that most immunomodulatory drugs of natural origin are polysaccharides, which are characterized by their large molecular structures. While small-molecule compounds with immunomodulatory activity have garnered increasing attention, their initial recognition by pattern recognition receptors and mechanisms of action remain relatively unexplored (Deng et al., 2014). Most of these small molecules are either synthetic drugs or nanomaterials, with relatively few derived from natural products. Investigating the interactions between small-molecule compounds extracted from *Epimedium* and TLR7/8 could enhance our understanding of small-molecule immunomodulation and provide new insights into the immunoregulatory role of traditional Chinese medicine.

Abbreviations: APCs, Antigen presenting cells; CLRs, C-type lectin receptors; CFA, Complete Freund's Adjuvant; DCs, Dendritic cells; DMSO, Dimethyl sulfoxide; ELISA, Enzyme-linked immunosorbent assay; FBS, Fetal bovine serum; HE, Hematoxylin-eosin; IL, Interleukin; Ig, Immunoglobulins; LPS, Lipopolysaccharide; MCP-1, Monocyte chemotactic protein 1; MHC, Major histocompatibility complex; MIP-1α, Macrophage inflammatory protein 1α; OVA, Ovalbumin; PBS, Phosphate buffered saline; SPR, Surface Plasmon Resonance; Th, T helper cells; TLRs, Toll-like receptors; TNF-α, Tumor necrosis factor α.

2 Materials and methods

2.1 Materials and reagents

RAW 264.7 macrophages and 293T cells were purchased from Procell (Wuhan, China). Dulbecco's Modified Eagle Medium (DMEM), RPMI-1640 culture medium, phosphate-buffered saline (PBS), penicillin-streptomycin solution, and tryspin were obtained from Gibco Life Technologies (Waltham, MA, United States). Fetal bovine serum (FBS) was sourced from Cytiva (Shanghai, China). The tested compounds were purchased from Yuanye Bio-Technology Co., Ltd (Shanghai, China). Fluorophore-conjugated antibodies, including PE-CD40, PE-CD80, PE-CD86, PE-MHC-I, PE-MHC-II and PE-CD11c were acquired from Thermo Fisher Scientific (Waltham, MA, United States) and eBioscience (San Diego, CA, United States), IL-4 and IFN-γ enzyme-linked immunosorbent assay (ELISA) were obtained from Universal Biotech Co., Ltd (Shanghai, China). ELISA kits for IL-6, TNF-α, MIP-1α, and MCP-1 were purchased from NeoBioscience Technology Co., Ltd (Shanghai, China). For molecular assays, StarScript III RT kit and 2×RealStar Fast SYBR qPCR Mix were sourced from GenStar (Beijing, China). And the pNF-κB/SEAP kit was obtained from Novus Biologicals (Colorado, United States). Immunoglobulin antibodies (IgG, IgG2a, IgG2b, IgG1, IgG3 and IgE) were sourced from Abcam (Hong Kong, China).

2.2 Cell culture

RAW 264.7 and 293T-cell were cultured in DMEM medium supplemented with 10% FBS, 100 μg/mL streptomycin, and 100 units/mL penicillin at 37°C in a 5% CO_2 incubator.

2.3 Cell viability

RAW 264.7 cells were seeded in 96-well plate at a density of 1×10^5 cells/well and incubated for 24 h. After removing the old medium, 100 μL of *Epimedium* flavonoids at varying concentrations (10, 20, 30, 40 μM) was added to each well, followed by incubation for an additional 24 h. Subsequently, 10 μL of MTT solution (5 mg/mL) was added to each well and incubated for 4 h. 100 μL of DMSO was added to dissolve the formazan crystals and absorbance was measured at 550 nm using a microplate reader.

2.4 Flow cytometry

RAW 264.7 cells were seeded in a 12-well plate at a density of 2.5×10^5 cells/well and incubated for 24 h. After removing the old medium, 20 μM *Epimedium* flavonoids were added to each well and incubated for another 24 h. IFN-γ (30 ng/mL) was used as a positive control. The cells were then washed three times with PBS. Subsequently, cells were incubated with 100 μL of 0.05% BSA containing PE-CD80, PE-CD86, PE-CD40, PE-MHC-I, and PE-MHC-II for 30 min. After incubation, the cells were washed 2–3 times with PBS and analyzed by flow cytometry.

2.5 The mRNA isolation and qRT-PCR

RAW 264.7 cells were seeded in a 6-well plate at 5×10^5 cells/well and incubated at 37°C for 24 h. The cells were then treated with 20 μM icaritin, icariin I, icariin II for an additional 24 h. LPS (2 μg/mL) was used as positive control. Following Trizol lysis, total RNA was extracted and reverse transcribed into cDNA. qRT-PCR was performed to quantify the expression of inflammatory factors, with all data normalized to the control group. Relative mRNA expression was determined using the $2^{-\Delta\Delta CT}$ method.

2.6 BMDCs and flow cytometry

Bone marrow cells were isolated from the femur of 6-8-week-old C57BL/6 mice and differentiated into BMDCs using GM-CSF (20 ng/mL) and IL-4 (10 ng/mL). Immature BMDCs were harvested on day 7. BMDCs were seeded in a 12-well plate at 1×10^6cells/well and treated with 20 μM icaritin, icariin I, icariin II for 24 h. LPS (2 μg/mL) served as positive control. Cells were then incubated with PE-CD11c, PE-CD40, PE-CD80, PE-CD86, PE-MHC-I and PE-MHC-II at 4 °C in the dark, followed by flow cytometry analysis.

2.7 Animal experiments and materials

2.7.1 Animals

BALB/c mice were purchased from Zhuhai BesTest Bio-Tech (Zhuhai, China). Adult mice were housed in a controlled laboratory environment at 23°C ± 1°C with a 12 h light/dark cycle (lights on at 07:00 AM). Mice had *ad libitum* access to food and water.

2.7.2 Animal grouping and administration

A total of 48 female BALB/c mice (6–8 weeks old) were randomly assigned to one of eight experimental groups: normal saline (NS), OVA group, water-in-oil adjuvant, complete Freund's adjuvant (CFA), aluminum salt adjuvant, icaritin (20 mg/kg), icariin I (20 mg/kg), icariin II (20 mg/kg). After 7 days of acclimation, mice were immunized once, followed by two additional immunizations every 14 days, totaling three immunizations. Body weight was recorded weekly. Prior to each immunization, 200–300 μL of blood was collected from the tail tip, and 42 days after the first immunization, blood was collected via retro-orbital bleeding. The mice were then euthanized, and the heart, liver, spleen, lungs, and kidneys were harvested for further analysis.

2.7.3 Serum antibody titration test

A 100 μL OVA antigen solution (1 mg/mL) was added to the plate and incubated overnight at 4°C. The next day, diluted serum samples were added and incubated at 37°C for 1 h, followed by plate sealing. Subsequently, secondary antibodies (IgG, IgG1, IgG2a, IgG2b, IgG3, IgE) were respectively added and incubated at 37°C for 1 h. TMB substrate solution was then added and incubated in the dark at room temperature for 15–30 min. Finally, absorbance was measured at 450 nm to complete the experiment.

2.7.4 Lymphocyte proliferation and cytokines detection in mouse spleen

The mice were dissected under sterile conditions, the spleens were removed and weighed. The spleens were homogenized and centrifuged, after which the supernatant was discarded. Spleen cells were obtained by resuspending in 1,640 medium, and the cell concentration was adjusted to 5×10^6cells/mL. For the proliferation assay, 100 μL/well of the spleen cell suspension was seeded into 96-well plates, and the experimental groups were stimulated with 5 μg/mL ConA, 10 μg/mL LPS, or 40 μg/mL OVA, respectively. For cytokine analysis, 500 μL of spleen cells was inoculated into 48-well plates, with the experimental group stimulated with 40 μg/mL OVA and the control group treated with PBS. After 48 h of incubation, spleen cell proliferation and cytokine secretion were assessed using CCK-8 and ELISA.

2.7.5 Pathological tissue analysis

The hearts, livers, spleens, lungs, and kidneys of the mice were excised and fixed in 4% paraformaldehyde. Then tissues were paraffin-embedded, sectioned, and stained with hematoxylin-eosin (HE). Subsequently, the stained sections were examined under microscopes at various magnifications and photographed for documentation.

2.8 Molecular biology

2.8.1 Computer simulation of molecular docking

Molecular docking experiments were performed using MOE software, where the three molecules icaritin, icariin I, and icariin II were analyzed. TLR7 and TLR8 were selected as the receptor proteins for docking calculations.

2.8.2 Protein expression and purification

Using Snap Gene software, five pairs of primers were designed based on the vector and gene sequence (Supplementary Table S1). The synthesized gene served as a template for amplification. The TLR7 and TLR8 genes were cloned into pMAL-p5x, pMAL-c5x and pGEX-2T vectors via homologous recombination. The recombinant vectors were introduced into *Escherichia coli* to facilitate the expression of the Toll-like receptor 7/8 (TLR7/8) proteins in the supernatant. Subsequently, the TLR7/8 proteins were isolated and purified.

2.8.3 Surface plasmon resonance (SPR)

The affinity of recombinant mouse TLR7 and TLR8 proteins for 80 μM of the small molecules Resiquimod, icaritin, icariin I, and icariin II was assessed using a Biacore S200 system.

2.9 NF-κB/SEAP assay

During the logarithmic growth phase, HEK 293T cells were seeded at a density of 1×10^5 cells per well in a 12-well plate. After 24 h, the cells were transfected with pcDNA3.1-TLR7, pcDNA3.1-TLR8 and p-NF-κB/SEAP plasmids. Following an additional 24 h incubation, the cells were treated with icaritin, icariin I and icariin II. After another 24 h, the supernatant was collected, and SEAP secretion was measured to evaluate its activity.

2.10 Statistical analysis

Statistical analysis was performed using Prism 10 software (GraphPad, San Diego, CA, United States), and results were expressed as mean ± SD. Differences among experimental groups were assessed using one-way ANOVA, followed by either the least significant difference (LSD) test or Dunnett's T3 *post hoc* test. Statistical significance was set at $p < 0.05$.

3 Results

3.1 Effect of *Epimedium* flavonoids on cell viability and expression of surface co-stimulatory molecules and histocompatibility complexes in RAW 264.7 macrophages

The results indicated that none of the seven selected *Epimedium* flavonoids exhibited toxic or adverse effects on RAW 264.7 cells at a concentration of 20 μM. However, at concentrations of 30 μM and 40 μM, icariin I and icariin II induced mild cytotoxic effects on RAW 264.7 cells. Notably, icariin II caused nearly 50% cell death at 40 μM (Figure 1). To ensure the safety and consistency of subsequent experiments, the concentration of *Epimedium* flavonoids was uniformly set to 20 μM for all cell assays.

Macrophages are unique in that they function as both innate immune cells and professional antigen-presenting cells (APCs). Upon stimulation, macrophages upregulate the expression of antigen-presenting proteins on their cell surface, including major histocompatibility complex (MHC) molecules (MHC-I and MHC-II) and co-stimulatory molecules (CD40, CD80 and CD86).

Flow cytometry was used to evaluate the expression levels of co-stimulatory molecules and major histocompatibility complex (MHC) molecules on the surface of RAW 264.7 cells following drug treatment. As depicted in Figure 2, *Epimedium* flavonoids enhanced the expression of co-stimulatory molecules and MHC molecules. Specifically, icaritin, icariin I and icariin II significantly increased the expression levels of MHC-I, MHC-II, CD40, CD80 and CD86. Notably, icariin II induced MHC-I and MHC-II expression was comparable to that of the positive control, LPS. The effect of icariin I was less pronounced than expected, possibly due to its larger molecular weight, which may affect its cellular absorption. Based on these findings, icaritin, icariin I and icariin II were selected for further investigation.

3.2 The expression of costimulatory molecules in BMDCs induced by icaritin, icariin I and icariin II

Antigen-presenting capability is a key metric for evaluating the efficacy of adjuvants. CD11c serves as a molecular marker for dendritic cells (DCs), while MHC-I, MHC-II, CD80, CD86 and CD40 are crucial indicators of antigen presentation in DCs. The results demonstrated that icaritin, icariin I and icariin II enhanced the expression of CD86 and MHC-II in mouse BMDCs. However, they did not significantly increase the expression of CD40, CD80 and MHC-I (Figure 3). This may be attributed to the role

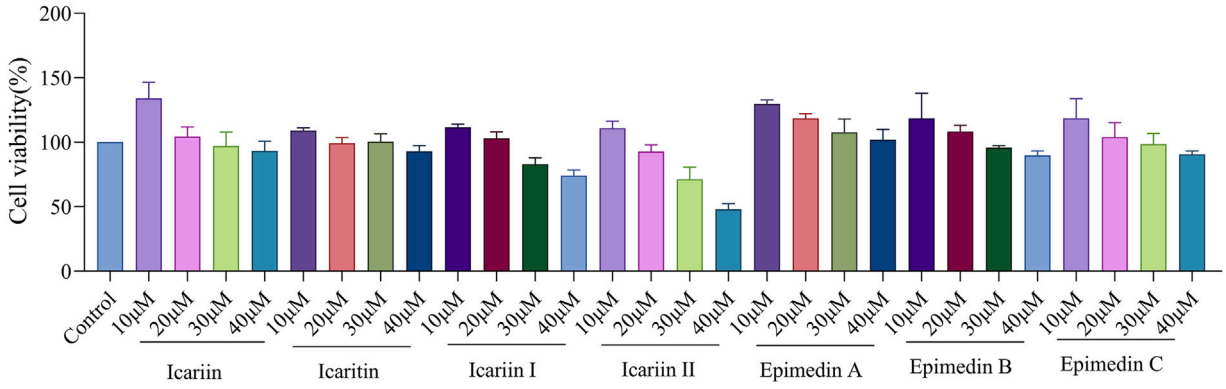

FIGURE 1
Effect of *Epimedium* flavonoids on cell viability of RAW 264.7 cells. Cell viability was assessed 24 h after compounds treatment in RAW 264.7 cells. The experiment was repeated three times for consistency. Statistical analyses were performed using one-way ANOVA, followed by Tukey's multiple comparisons test to adjust for multiple comparisons. All data are expressed as mean ± SD (n = 3). Statistical significance is indicated as follows: ****$p < 0.0001$, ***$p < 0.001$, **$p < 0.01$, *$p < 0.05$, compared with the control group.

of CD80, which is associated with the persistence and expansion of later T cell responses (Damoiseaux et al., 1998), whereas CD86 plays a critical role in the early T cells co-stimulation, often determining T cell activation (Leifeld et al., 1999; Van Gool et al., 1996). Notably, icariin II elevated CD86 expression to a level even exceeding that of the positive control, LPS. These findings suggest that *Epimedium* flavonoids can promote the maturation and activation of BMDCs. In summary, icaritin, icariin I, and icariin II promote the maturation and activation of various cell lines, enhance antigen-presenting cell activation, and exhibit immunomodulatory effects. Further studies are needed to elucidate the specific immunological mechanisms and explore their potential role in activating antigen-presenting cells (APCs) through the TLR7/8 pathway.

3.3 The expression of proinflammatory cytokines and chemokines mRNA levels in RAW 264.7 cells induced by icaritin, icariin I and icariin II

Cytokines and chemokines are essential for immune system function, playing a crucial role in the recruitment and activation of immune cells. As shown in Figure 4, icariin II significantly upregulated the mRNA levels of IL-6, IL-12, TNF-α, MIP-1α, MCP-1 and COX-2 in RAW 264.7 cells. Icariin I increased the mRNA levels of TNF-α and COX-2 in RAW 264.7 cells. In contrast, icaritin did not enhance the mRNA expression of pro-inflammatory cytokines and chemokines.

3.4 The expression levels of proinflammatory cytokines and chemokine proteins in RAW 264.7 cells induced by icaritin, icariin I and icariin II

Macrophages secrete pro-inflammatory cytokines that enhance T cell responses. To evaluate the effects of *Epimedium* flavonoids on the protein expression of pro-inflammatory cytokines and chemokines in RAW 264.7 cells, the concentrations of these factors in the cell culture supernatant were measured using ELISA kits. As illustrated in Figure 5, icariin II significantly increased the secretion levels of IL-6, TNF-α, MIP-1α and MCP-1, which aligns with the qRT-PCR results. Icariin I did not induce a high level of IL-6 protein secretion, a finding consistent with the qRT-PCR results. However, it significantly increased the secretion levels of TNF-α, MIP-1α and MCP-1. Similarly, icaritin also led to a significant increase in the secretion levels of IL-6, TNF-α, MIP-1α and MCP-1. In comparison to the qRT-PCR results, both icaritin and icariin I exhibited discrepancies in secretion patterns, suggesting potential post-transcriptional regulation or translational inefficiencies following treatment with icaritin and icariin I.

3.5 The immunoenhancing activity of icaritin, icariin I and icariin II *in vivo*

3.5.1 IgG antibody titer

To evaluate the systemic immune response, the OVA-specific immunoglobulin antibody titer (IgG) antibody titer was measured in mouse serum collected 14 days after each immunization.

As shown in Figure 6A, the water-in-oil emulsifier group exhibited a significantly stronger immune effect than the group receiving direct OVA antigen injection. Although both the CFA group and the *Epimedium* flavonoid oil emulsion adjuvant groups had higher antibody titers than the oil emulsion adjuvant group without the compound, the differences were not statistically, warranting further investigation.

Subsequently, immune response types were partially characterized. As shown in Figures 6B–E, both the CFA group and *Epimedium* flavonoid oil emulsion adjuvant group significantly increased the IgG1, IgG2a, IgG2b and IgG3 antibody titers, indicating that *Epimedium* flavonoids could induce robust Th1 (IgG2a, IgG2b and IgG3) and Th2 (IgG1) immune responses. In contrast, the aluminum salt adjuvant group only promoted IgG1 titers, suggesting an induced Th2 immune response (Howard et al., 2022).

Additionally, antigen-specific IgE antibody levels induced by each vaccine group were examined, as shown in Figure 6F. With

10.3389/fphar.2025.1514284

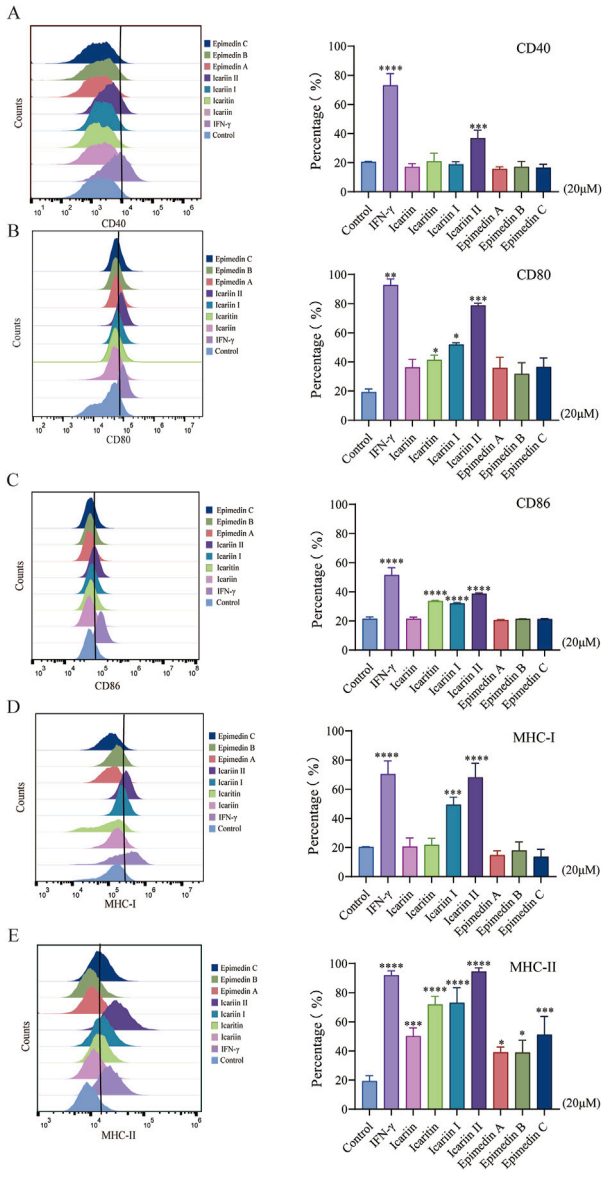

FIGURE 2
Effects of *Epimedium* flavonoids on the maturation of RAW 264.7 cells. Cell was assessed 24 h after compounds treatment in RAW 264.7 cells. The experiment was repeated three times for consistency. **(A–C)**. Effects of *Epimedium* flavonoids on the expression of CD40, CD80, and CD86, and **(D, E)** effects on MHC-I and MHC-II in RAW 264.7 cells, as detected by flow cytometry. RAW264.7 cells were gated on size and complexity using a two-dimensional FSC vs. SSC plot, then assessed for MHC-I, MHC-II, CD40, CD80 and CD86. Statistical analyses were performed using one-way ANOVA, followed by Tukey's multiple comparisons test to adjust for multiple comparisons. All data are expressed as mean ± SD (n = 3). Statistical significance is indicated as follows: ****$p < 0.0001$, ***$p < 0.001$, **$p < 0.01$, *$p < 0.05$, compared with the control group.

the exception of the CFA and aluminum adjuvant groups, no increase in IgE antibody levels was observed in the other groups. Since IgE is associated with allergic reactions, these findings suggest that icaritin, icariin I, and icariin II are unlikely to trigger allergic responses.

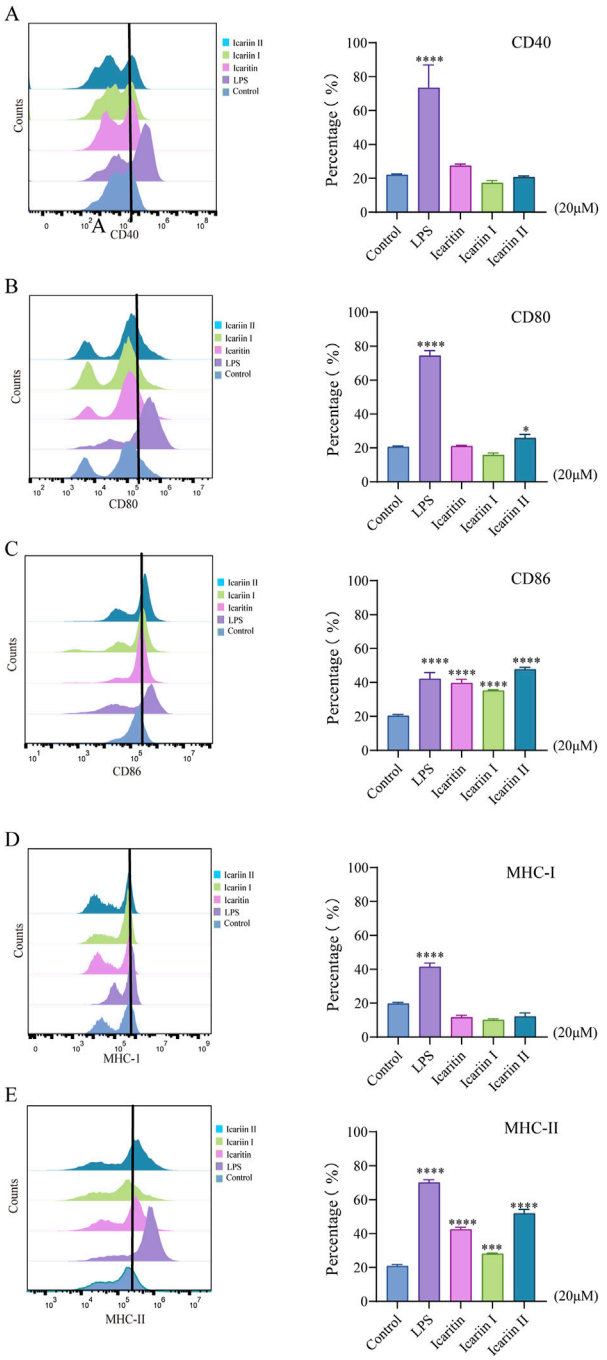

FIGURE 3
Effects of icaritin, icariin I and icariin II on the maturation of BMDCs. Cell was assessed 24 h after compounds treatment in BMDCs. The experiment was repeated three times for consistency. **(A–C)** Effects of *Epimedium* flavonoids on the expression of CD40, CD80, and CD86, and **(D, E)** effects on MHC-I and MHC-II in BMDCs, as assessed by flow cytometry. BMDCs cells were selected using a two-dimensional FSC vs. SSC plot, followed by gating on CD11c for DCs. Then assessed for MHC-I, MHC-II, CD40, CD80 and CD86. Statistical analyses were performed using one-way ANOVA, followed by Tukey's multiple comparisons test to adjust for multiple comparisons. All data are presented as mean ± SD (n = 3). Statistical significance is indicated as follows: ****$p < 0.0001$, ***$p < 0.001$, **$p < 0.01$, *$p < 0.05$, compared with the control group.

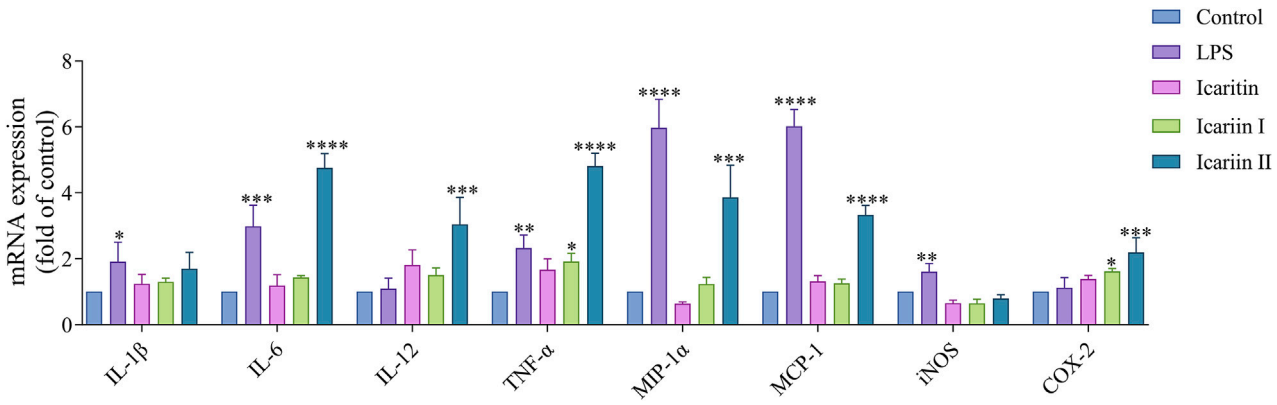

FIGURE 4
Icaritin, icariin I, icariin II induces an inflammatory response in RAW 264.7 cells. Cell was assessed 24 h after compounds treatment in RAW 264.7 cells. The experiment was repeated three times for consistency. The mRNA levels of IL-1β, IL-6, IL-12, TNF-α, MIP-1α, MCP-1, iNOS and COX-2 in RAW 264.7 cells were examined by qRT-PCR. Statistical analyses were performed using one-way ANOVA, followed by Tukey's multiple comparisons test to adjust for multiple comparisons. All data are presented as mean ± SD (n = 3). Statistical significance is indicated as follows: ****$p < 0.0001$, ***$p < 0.001$, **$p < 0.01$, *$p < 0.05$, compared with the control group.

3.5.2 Proliferation of mouse splenic lymphocytes and cytokine secretion levels

Different cytokine types serve as indicators of Th1 or Th2 biased immune responses. The immune function of T cells was evaluated by analyzing the expression of OVA-specific cytokines in splenic cells. As shown in Figure 7A, the stimulation indices of T lymphocytes, B lymphocytes and total lymphocytes in the icaritin, icariin I and icariin II vaccine group were significantly higher than those in the saline and adjuvant-free groups. Furthermore, the icaritin, icariin I and icariin II vaccine groups significantly enhanced the secretion levels of both IFN-γ and IL-4, with IFN-γ and IL-4 secretion levels in the icariin group comparable to those in the CFA group (Figure 7B). The cytokine secretion results were consistent with the IgG antibody subtype analysis, further indicating that icaritin, icariin I, and icariin II can induce robust Th1 and Th2 immune responses (Shen et al., 2022).

3.5.3 Pathological tissue analysis

During the experiment, mice in the CFA group exhibited significant swelling at the injection site after immunization, whereas no such swelling was observed in the other groups. To evaluate *in vivo* toxicity, pathological tissue analysis was performed after three immunizations. As shown in Figure 8, inflammatory cell infiltration was observed in the heart, liver, lungs and kidneys of CFA treated mice. In contrast, no significant differences were noted in these organs in the other groups compared to the saline group. These findings suggest that the effective doses of icaritin, icariin I and icariin II did not cause damage to major tissues and organs in mice.

3.6 Molecular docking simulation using computers

Computer-simulated molecular docking is a widely used technique for identifying potential targets of compounds and accelerating the screening process for specific molecules. This approach employs flexible and semi-flexible docking methods to evaluate interaction forces between receptors and ligands, thereby predicting the binding modes and affinities of receptor-ligand complexes.

As shown in Supplementary Figures S7–S12, the findings indicate that TLR7 and TLR8 exhibited the strongest interactions with icaritin, icariin I, and icariin II. These interactions were primarily mediated through hydrogen bonding.

3.7 The interaction between TLR7 and TLR8 proteins with resiquimod, icaritin, icariin I and icariin II molecules

SPR analysis demonstrated that the pattern recognition receptors (PRRs) targeted by *Epimedium* flavonoids were TLR7 and TLR8. As show in Supplementary Figure S13, icariin I (43 RU) and icariin II (50 RU) exhibited the highest response values with TLR8 protein, with icariin II displaying the strongest binding affinity to TLR8 ($KD_8 = 1.03 \times 10^{-5}$ M).

3.8 NF-κB/SEAP assay

Secreted placental alkaline phosphatase (SEAP) is a recombinant form of placental alkaline phosphatase used as a reporter for gene function analysis. It is commonly employed to study promoter activity and gene expression in cell cultures and animal sera. NF-κB, a key transcription factor, regulates genes involved in both innate and adaptive immune responses. The activation or inhibition of the NF-κB promoter can be modulated by specific ligands or inhibitors. TLR7/8 ligands activate NF-κB, leading to increased SEAP expression (Caballero et al., 2013; Bender et al., 2020), which is used to evaluate ligand binding to TLR7/8. Resiquimod (R848) exerts immunomodulatory and anti-tumor effects primarily by activating TLR7 and TLR8 on innate immune cells. Therefore, R848 (30 μM) was used as a positive control in this study.

10.3389/fphar.2025.1514284

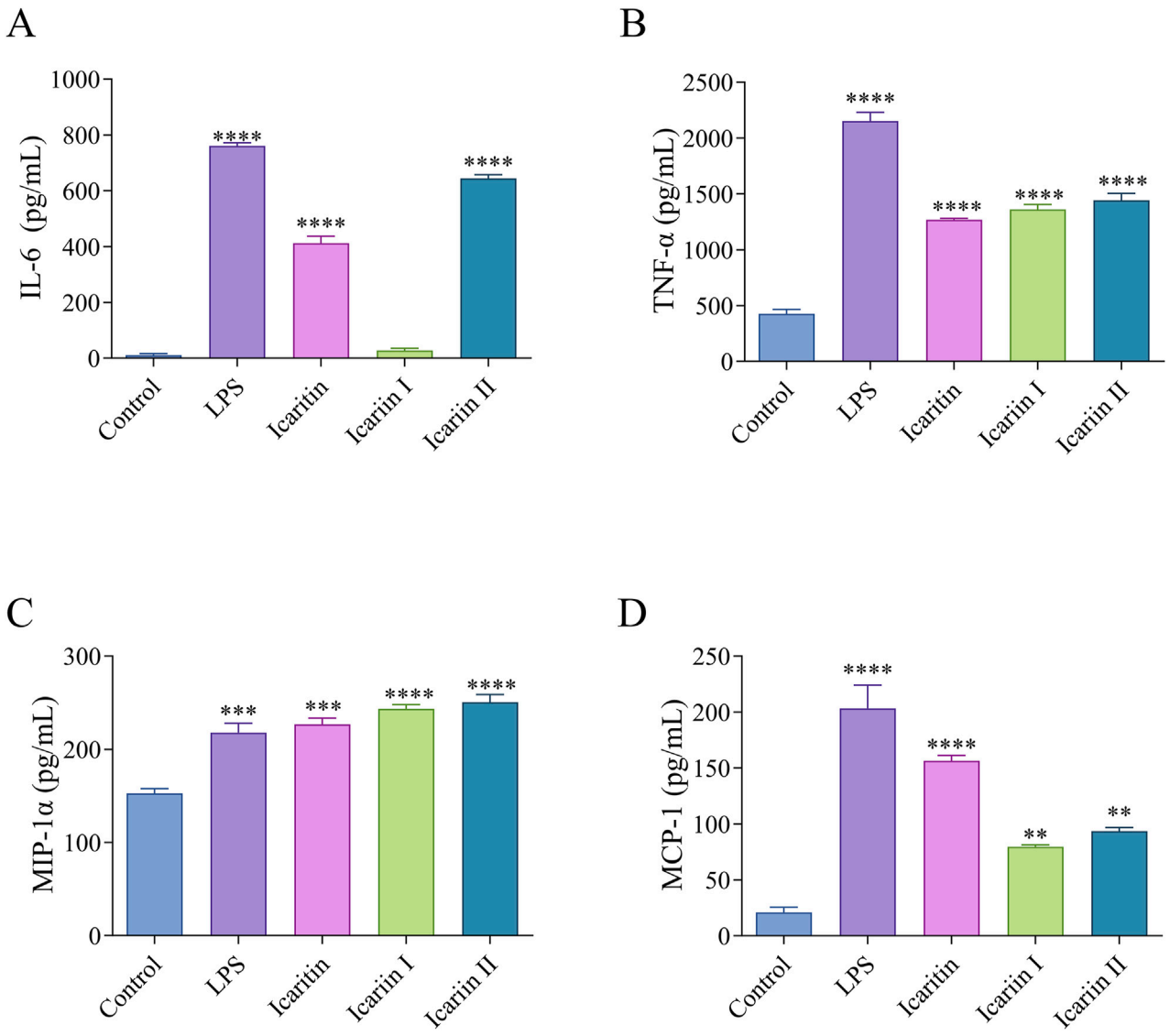

FIGURE 5
Icaritin, icariin I, icariin II induced an inflammatory response in RAW 264.7 cells. The protein expression levels of **(A)** IL-6, **(B)** TNF-α, **(C)** MIP-1α and **(D)** MCP-1 in RAW 264.7 cells were evaluated by ELISA. Statistical analyses were performed using one-way ANOVA, followed by Tukey's multiple comparisons test to adjust for multiple comparisons. Values are expressed as mean ± SD (n = 3). Statistical significance is indicated as follows: ****$p < 0.0001$, ***$p < 0.001$, **$p < 0.01$, *$p < 0.05$, compared with the control group.

As shown in Figure 9A, compared with the NF-κB/SEAP group, the NF-κB/SEAP + TLR7 group, Resiquimod group, icaritin group and icariin I group all showed significant differences, suggesting that the TLR7 and NF-κB/SEAP plasmids were successfully transfected and can be stably expressed. However, compared with the NF-κB/SEAP + TLR7 group, only the icaritin group exhibited a significant difference, while the icariin I group and icariin II did not. This indicates that icaritin can stimulate SEAP secretion by activating the signaling pathway mediated by TLR7, effectively enhancing the activity of NF-κB.

Furthermore, as shown in Figure 9B, the experimental results also demonstrated that, following the overexpression of TLR8 and NF-κB/SEAP, icariin II can remarkably enhance the expression of SEAP. This indicates that icariin II can stimulate SEAP secretion by activating the signaling pathway mediated by TLR8 and effectively enhancing the activity of NF-κB.

In conclusion, icaritin was able to specifically interact with TLR7, while icariin II specifically interacted with TLR8. Both compounds activated the downstream NF-κB signaling pathway (Piras and Selvarajoo, 2014), consequently promoting the secretion of SEAP. Therefore, icaritin, icariin I, and icariin II can activate the TLR7/8-NF-κB pathway. Combined with the molecular docking and SPR results discussed earlier, it can be concluded that icaritin, icariin I, and icariin II likely bind to TLR7/8 receptors, leading to the activation of APCs.

4 Discussion

Vaccines are among the most effective measures for preventing infectious diseases, and vaccine adjuvants play a crucial role in

10.3389/fphar.2025.1514284

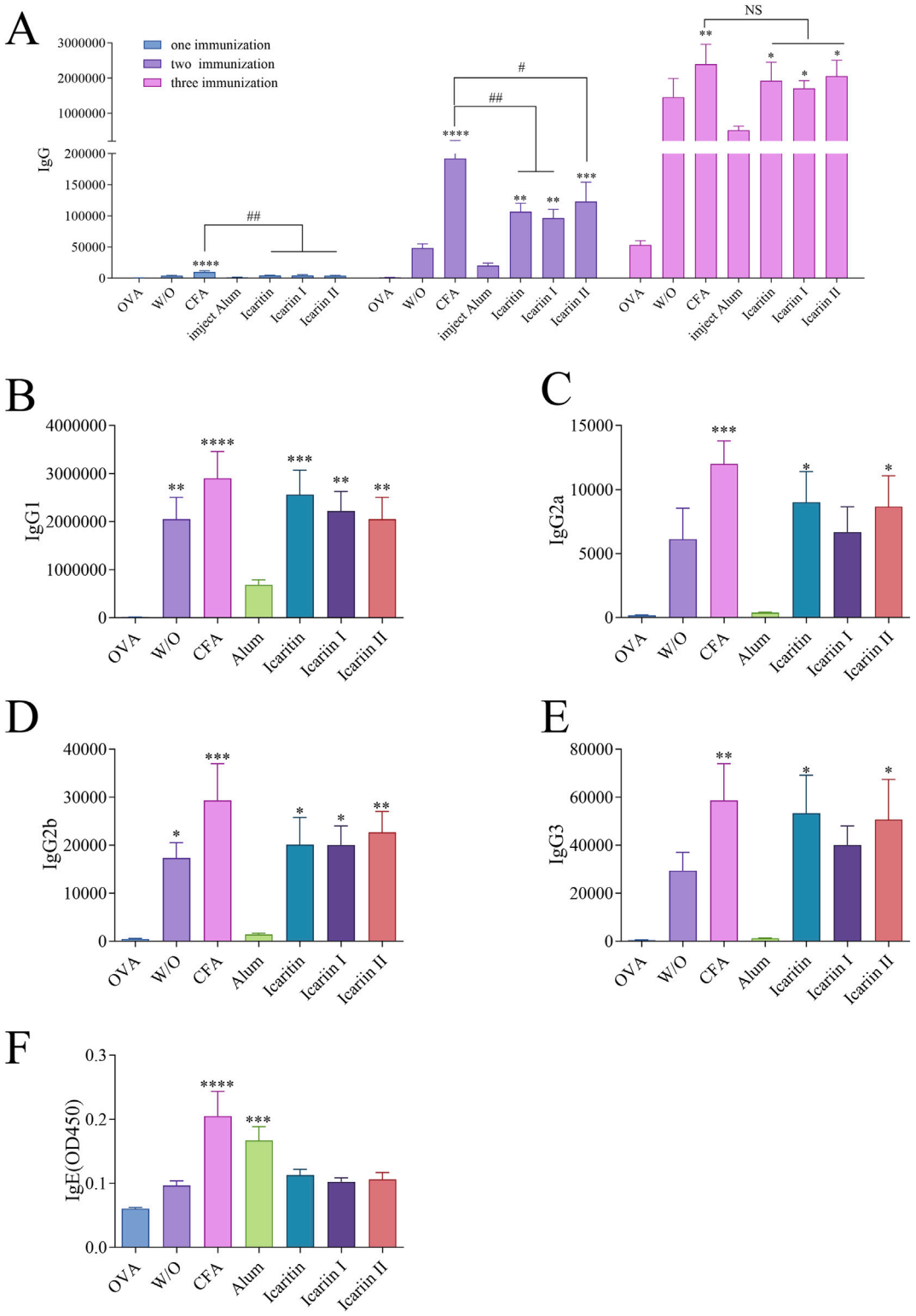

FIGURE 6
Serum levels of antigen-specific IgG isoforms in mice after immunization. **(A)** Total IgG levels after three immunizations **(B–E)** Serum levels of antigen-specific IgG subtypes (IgG2a, IgG2b, IgG1 and IgG3) after the third immunization, detected by ELISA. **(F)** Serum levels of IgE after three immunizations, measured by ELISA. Statistical analyses were performed using one-way ANOVA, followed by Tukey's multiple comparisons test to adjust for multiple comparisons. Values are expressed as mean ± SD (n = 6). Normal saline is NS. Statistical significance is indicated as follows: ****p < 0.0001, ***$p < 0.001$, **$p < 0.01$, *$p < 0.05$, compared with the OVA group. ####$p < 0.0001$, ###$p < 0.001$, ##$p < 0.01$, #$p < 0.05$, compared with the CFA group.

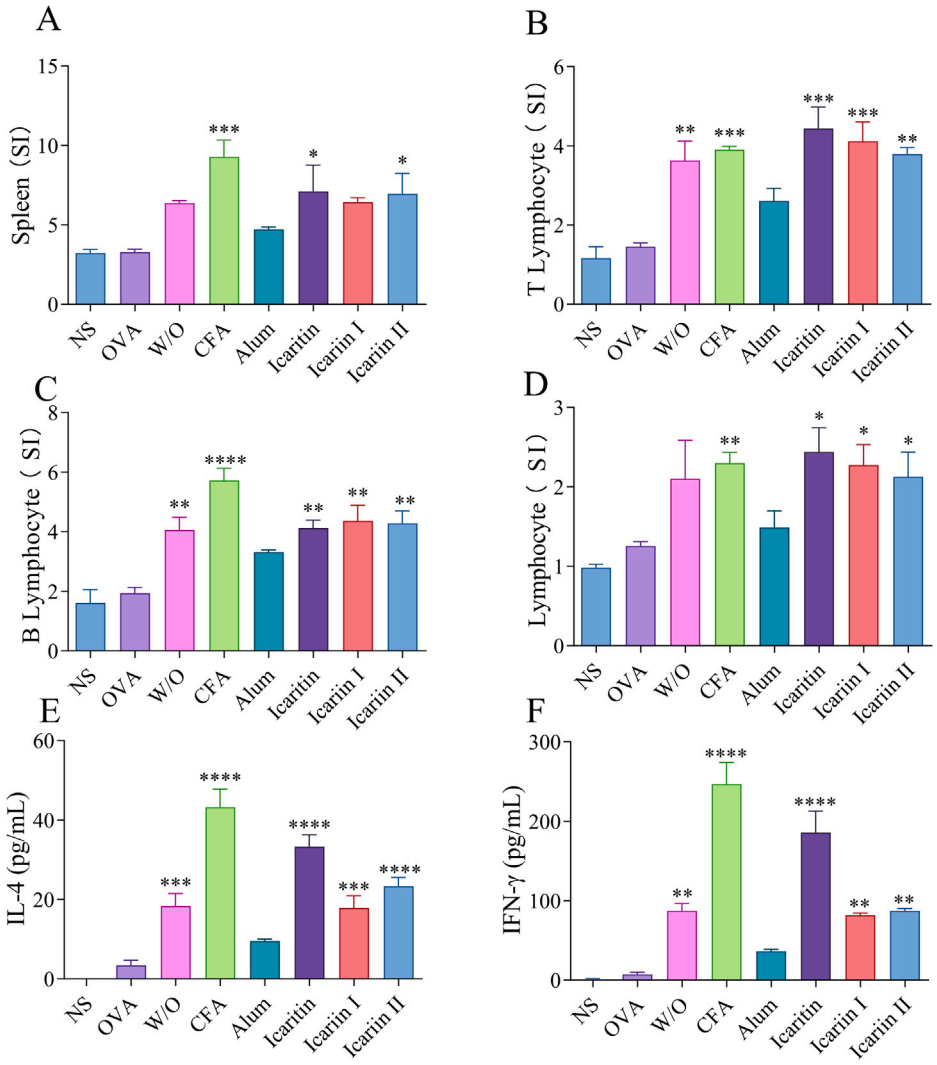

FIGURE 7
Analysis of splenocytes after the third immunization. **(A)** Spleen organ index **(B)** T-lymphocyte **(C)** B-lymphocyte and **(D)** lymphocyte. Secretion levels of **(E)** IFN-γ and **(F)** IL-4 were detected by ELISA. Statistical analyses were performed using one-way ANOVA, followed by Tukey's multiple comparisons test to adjust for multiple comparisons. Values are expressed as mean ± SD (n = 3). Statistical significance is indicated as follows: ****$p < 0.0001$ ***$p < 0.001$ **$p < 0.01$ *$p < 0.05$, compared with the OVA group.

enhancing their efficacy. Adjuvants amplify the immune response against specific antigens present in vaccines (Pulendran et al., 2021). RAW 264.7 and DCs are common APCs responsible for initiating and regulating both innate and adaptive immune responses. Upon detecting PAMPs or other danger signals, immature RAW 264.7 and DCs upregulate the expression of co-stimulatory molecules and adhesion molecules such as MHC-I, MHC-II, CD40, CD80 and CD86, facilitating their maturation. Fully mature DCs also secrete various cytokines, including IL-6 and TNF-α, further modulating the immune response.

In vitro activity studies revealed that *Epimedium* flavonoids significantly enhanced the expression of co-stimulatory molecules, MHC-I and MHC-II, while also promoting the expression and secretion of pro-inflammatory cytokines and chemokines, including IL-6, TNF-α, MIP-1α and MCP-1. *In vivo* studies demonstrated that mice immunized with *Epimedium* flavonoids exhibited high levels of total IgG antibodies in their serum, with antibody levels increasing over time and significantly elevating IgG1, IgG2a, IgG2b and IgG3 antibody titers. These findings indicate that *Epimedium* flavonoids can induce robust Th1 (IgG2a, IgG2b and IgG3) and Th2 (IgG1) immune responses. Splenocyte experiments futher confirmed the production of Th1- and Th2-related cytokines, with IFN-γ levels being significantly higher than IL-4, indicating a stronger Th1-biased response. Additionally, recombinant plasmids encoding TLR7 and TLR8 were constructed and overexpressed in 293T cells. NF-κB/SEAP asssays confirmed that *Epimedium* flavonoids exert their immunomodulatory effects through the TLR7/8 pathway. Finally, this study successfully expressed mouse TLR7 and TLR8 proteins using prokaryotic expression systems and confirmed via SPR technology that the PRRs targeted by *Epimedium* flavonoids are indeed TLR7 and TLR8.

In conclusion, icaritin, icariin I and icariin II can recognize receptors through TLR7/8 pattern and exert immunomodulatory effects both *in*

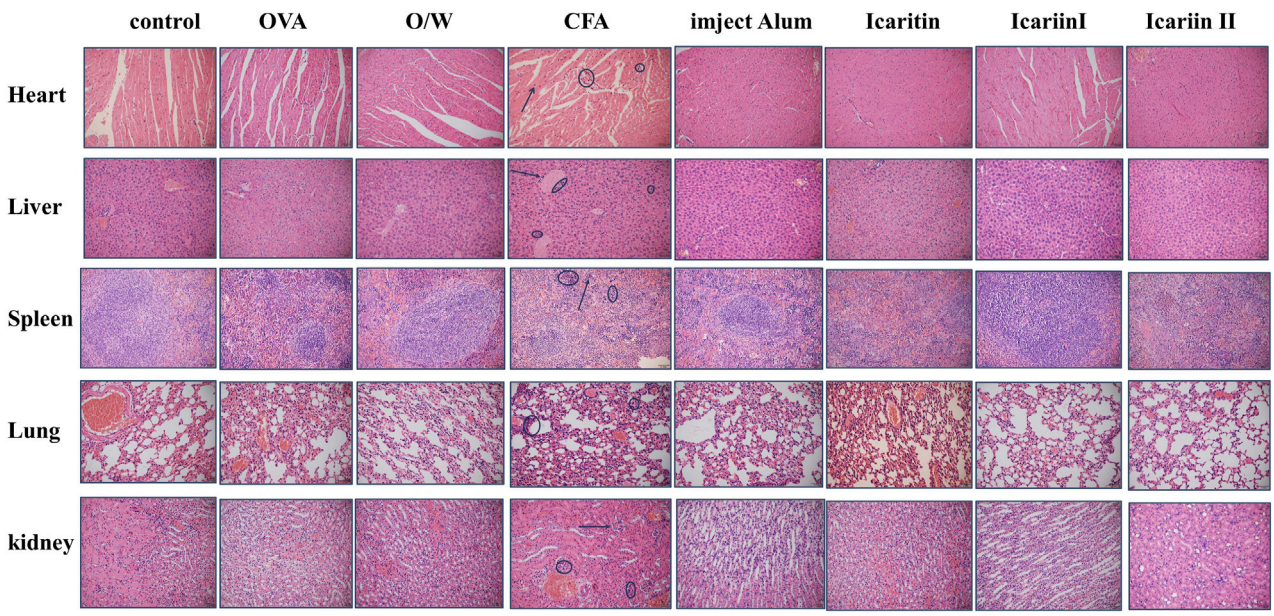

FIGURE 8
HE staining of major organs of mice after the third immunization. Scale bar = 1 mm, magnification = ×20. Arrows and circles in the figure indicate tissue damage caused by inflammatory cell infiltration (n = 4).

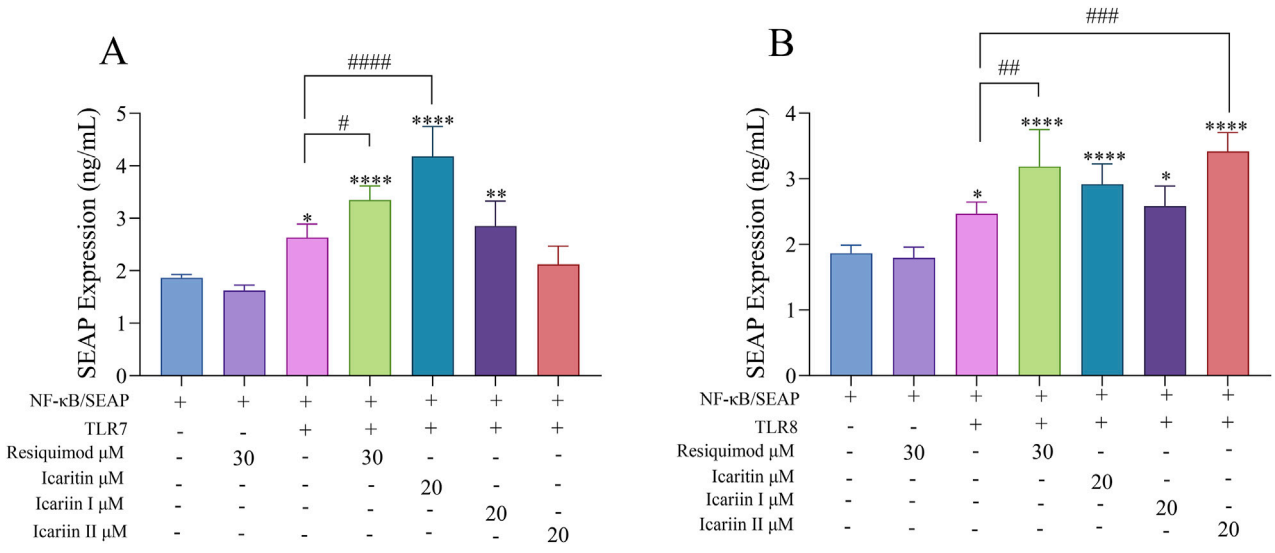

FIGURE 9
Effects of *Epimedium* flavonoids on SEAP Secretion in Cell supernatants following overexpression of TLR7 and TLR8. Cell was assessed 24 h after compounds treatment in 293T cells. The experiment was repeated three times for consistency. **(A)** TLR7 overexpression. **(B)** TLR8 overexpression. Statistical analyses were performed using one-way ANOVA, followed by Tukey's multiple comparisons test to adjust for multiple comparisons. Values are expressed as mean ± SD (n = 3). Significant differences are indicated as follows: ****$p < 0.0001$, ***$p < 0.001$, **$p < 0.01$, *$p < 0.05$, compared with the NF-κB/SEAP group; ####$p < 0.0001$, ###$p < 0.001$, ##$p < 0.01$, #$p < 0.05$, compared with the NF-κB/SEAP + TLR7 group or NF-κB/SEAP + TLR8 group.

vivo and *in vitro* models. Furthermore, they do not cause tissue damage at safe concentrations.

Icaritin, icariin I and icariin II were compared with TLR7/8 agonists imiquimod, resiquimod. Although they are among the most extensively studied TLR7/8 agonists, they exhibit certain limitations. For instance, imiquimod specifically targets TLR7 but is largely ineffective in murine models, and its immunostimulatory capacity is relatively weak. Resiquimod, while capable of activating both TLR7 and TLR8 in humans, lacks activity toward murine TLR8, making it challenging to accurately model its effects in mice.

Moreover, due to its high potency, resiquimod may induce cytotoxicity and even trigger excessive immune responses such as cytokine storms (Dockrell and Kinghorn, 2001).

In contrast, icaritin, icariin I, and icariin II, as natural compounds derived from traditional Chinese medicine, exhibit favorable biosafety profiles and broader therapeutic windows (Yong et al., 2021). When administered subcutaneously in mice, these compounds do not induce noticeable local inflammatory responses such as redness, swelling, or pain, indicating good tolerability. More importantly, they demonstrate a strong affinity for both TLR7 and TLR8, effectively activating immune signaling pathways while eliciting relatively mild immune reactions. These characteristics suggest promising potential for their application as novel, safe, and effective immunomodulatory agents.

These findings provide theoretical support for the development of *Epimedium* as an immunomodulatory agent and offer insights into vaccine adjuvant research. Additionally, this study contributes to futher investigations into *Epimedium*, a prominent traditional Chinese herbal medicine. In recent years, cancer immunotherapy has become a hot research topic, particularly in the development of TLR7/8 immunomodulators. The *Epimedium* flavonoid compounds mentioned in this study—icaritin, icariin I, and icariin II—have drawn our attention due to their potential role as TLR7/8 modulators and their anticancer activity. *Epimedium* flavonoid compounds exhibit diverse biological activities, including direct anticancer effects, such as inhibiting tumor proliferation, promoting apoptosis, and suppressing tumor cell invasion and metastasis (Chen Y. et al., 2024; Ding et al., 2024). Additionally, these compounds can modulate the tumor microenvironment (TME) by reducing M2 polarization of tumor-associated macrophages (TAMs), increasing $CD8^+$ T cell infiltration, and enhancing antitumor immune responses.

TLR7/8 immunomodulators activate dendritic cells (DCs), promoting antigen presentation and enhancing T cell responses, particularly by increasing $CD8^+$ T cell activity (Zhou et al., 2022). They exert antitumor effects via IFN-γ and IL-12-mediated mechanisms, altering the tumor microenvironment (TME), promoting M1 macrophage polarization, and suppressing M2 pro-tumor macrophages (Michaelis et al., 2019). Moreover, when combined with immune checkpoint inhibitors (ICIs), TLR7/8 agonists can improve the immune microenvironment of "cold" tumors (low T cell infiltration), making them more responsive to PD-1/PD-L1 therapies (Smits et al., 2008).

According to our study, icaritin, icariin I, and icariin II are potential TLR7/8 immunomodulators. As natural products, they may offer advantages over conventional TLR7/8 agonists like R848, potentially exhibiting lower toxicity and higher bioavailability (Singh et al., 2014). Therefore, exploring *Epimedium* flavonoids as TLR7/8 immunomodulators for anticancer applications holds great promise—not only for their direct tumor-inhibitory effects but also for their ability to modulate the tumor microenvironment, enhance antigen presentation, and activate systemic antitumor immunity.

Data availability statement

The original contributions presented in the study are included in the article/Supplementary Material, further inquiries can be directed to the corresponding authors.

Ethics statement

The animal study was approved by the Institutional Animal Care Committee of the International Healthcare Innovation Institute (Jiangmen). The study was conducted in accordance with local legislation and institutional requirements.

Author contributions

JW: Conceptualization, Data curation, Formal Analysis, Investigation, Methodology, Project administration, Software, Validation, Visualization, Writing – original draft. YO: Conceptualization, Data curation, Formal Analysis, Funding acquisition, Investigation, Methodology, Project administration, Resources, Software, Validation, Visualization, Writing – original draft. MY: Conceptualization, Data curation, Formal Analysis, Funding acquisition, Investigation, Methodology, Project administration, Resources, Software, Validation, Writing – original draft. JL: Supervision, Writing – original draft. HR: Supervision, Writing – original draft. ZW: Supervision, Writing – original draft. RW: Supervision, Writing – review and editing. LG: Supervision, Writing – review and editing. DL: Supervision, Writing – review and editing. JJ: Conceptualization, Formal Analysis, Funding acquisition, Project administration, Resources, Supervision, Writing – review and editing.

Funding

The author(s) declare that financial support was received for the research and/or publication of this article. The authors thank the support of the National Natural Science Foundation of China (Grant: 81901678), the Jiangmen Basic and Theoretical Scientific Research Science and Technology Plan project [No. Jiangke (2023) 111]. Guangdong and Macao cooperation project from Department of Science and Technology of Guangdong Province and Jiangmen Science and Technology Bureau (2022A0505020026).

Conflict of interest

The authors declare that the research was conducted in the absence of any commercial or financial relationships that could be construed as a potential conflict of interest.

Generative AI statement

The authors declare that no Generative AI was used in the creation of this manuscript.

Publisher's note

All claims expressed in this article are solely those of the authors and do not necessarily represent those of their

affiliated organizations, or those of the publisher, the editors and the reviewers. Any product that may be evaluated in this article, or claim that may be made by its manufacturer, is not guaranteed or endorsed by the publisher.

Supplementary material

The Supplementary Material for this article can be found online at: https://www.frontiersin.org/articles/10.3389/fphar.2025.1514284/full#supplementary-material

References

Bender, A. T., Tzvetkov, E., Pereira, A., Wu, Y., Kasar, S., Przetak, M. M., et al. (2020). TLR7 and TLR8 differentially activate the IRF and NF-κB pathways in specific cell types to promote inflammation. *ImmunoHorizons* 4, 93–107. doi:10.4049/immunohorizons.2000002

Caballero, I., Al Ghareeb, S., Basatvat, S., Sánchez-López, J. A., Montazeri, M., Maslehat, N., et al. (2013). Human trophoblast cells modulate endometrial cells nuclear factor κB response to flagellin *in vitro*. *PLoS ONE* 8, e39441. doi:10.1371/journal.pone.0039441

Chen, H., Wang, L., Zhao, X., Jiang, H., Wu, M., Ding, Y., et al. (2024a). A polymer-based antigen carrier activates two innate immune pathways for adjuvant-free subunit vaccines. *ACS Nano* 18, 9160–9175. doi:10.1021/acsnano.4c00925

Chen, Y., Xia, H., and Zhong, X. (2024b). *In vitro* evaluation of the anti-pancreatic cancer activity of epimedium herb. *Front. Pharmacol.* 15, 1389221. doi:10.3389/fphar.2024.1389221

Chilamakuri, R., and Agarwal, S. (2021). COVID-19: characteristics and therapeutics. *Cells* 10, 206. doi:10.3390/cells10020206

Damoiseaux, JGMC, Yagita, H., Okumura, K., and Van Breda Vriesman, P. J. C. (1998). Costimulatory molecules CD80 and CD86 in the rat; tissue distribution and expression by antigen-presenting cells. *J. Leukoc. Biol.* 64, 803–809. doi:10.1002/jlb.64.6.803

Deng, Y., Chu, J., Ren, Y., Fan, Z., Ji, X., Mundy-Bosse, B., et al. (2014). The natural product phyllanthusmin C enhances IFN-γ production by human NK cells through upregulation of TLR-mediated NF-κB signaling. *J. Immunol.* 193, 2994–3002. doi:10.4049/jimmunol.1302600

Ding, J., Li, C., Wang, G., Yang, Y., and Li, J. (2024). Cancer-related therapeutic potential of *Epimedium* and its extracts. *Nutr. Cancer* 76, 885–901. doi:10.1080/01635581.2024.2383336

Dockrell, D. H., and Kinghorn, G. R. (2001). Imiquimod and resiquimod as novel immunomodulators. *J. Antimicrob. Chemother.* 48, 751–755. doi:10.1093/jac/48.6.751

Goff, P. H., Hayashi, T., Martínez-Gil, L., Corr, M., Crain, B., Yao, S., et al. (2015). Synthetic toll-like receptor 4 (TLR4) and TLR7 ligands as influenza virus vaccine adjuvants induce rapid, sustained, and broadly protective responses. *J. Virol.* 89, 3221–3235. doi:10.1128/JVI.03337-14

Howard, F. H. N., Kwan, A., Winder, N., Mughal, A., Collado-Rojas, C., and Muthana, M. (2022). Understanding immune responses to viruses—do underlying Th1/Th2 cell biases predict outcome? *Viruses* 14, 1493. doi:10.3390/v14071493

Huang, X., Zhang, X., and Lu, M. (2021). Recent trends in the development of Toll-like receptor 7/8-targeting therapeutics. *Expert Opin. Drug Discov.* 16, 869–880. doi:10.1080/17460441.2021.1898369

Kawasaki, T., and Kawai, T. (2014). Toll-like receptor signaling pathways. *Front. Immunol.* 5, 461. doi:10.3389/fimmu.2014.00461

Leifeld, L., Trautwein, C., Dumoulin, F. L., Manns, M. P., Sauerbruch, T., and Spengler, U. (1999). Enhanced expression of CD80 (B7-1), CD86 (B7-2), and CD40 and their ligands CD28 and CD154 in fulminant hepatic failure. *Am. J. Pathology* 154, 1711–1720. doi:10.1016/S0002-9440(10)65427-2

Liu, T., Zhao, M., Zhang, Y., Qiu, Z., Zhang, Y., Zhao, C., et al. (2021b). Pharmacokinetic–pharmacodynamic modeling analysis and anti-inflammatory effect of Wangbi capsule in the treatment of adjuvant-induced arthritis. *Biomed. Chromatogr.* 35, e5101. doi:10.1002/bmc.5101

Liu, X., Zhang, Y., Zhang, C., Xu, C., Qin, W., Shen, G., et al. (2021a). The complete chloroplast genome of Epimedium platypetalum K. Mey. (Berberidaceae), a rare plant species from China. *Mitochondrial DNA Part B* 6, 3292–3294. doi:10.1080/23802359.2021.1974968

Michaelis, K. A., Norgard, M. A., Zhu, X., Levasseur, P. R., Sivagnanam, S., Liudahl, S. M., et al. (2019). The TLR7/8 agonist R848 remodels tumor and host responses to promote survival in pancreatic cancer. *Nat. Commun.* 10, 4682. doi:10.1038/s41467-019-12657-w

Piras, V., and Selvarajoo, K. (2014). Beyond MyD88 and TRIF pathways in toll-like receptor signaling. *Front. Immunol.* 5, 70. doi:10.3389/fimmu.2014.00070

Pulendran, B. S., Arunachalam, P., and O'Hagan, D. T. (2021). Emerging concepts in the science of vaccine adjuvants. *Nat. Rev. Drug Discov.* 20, 454–475. doi:10.1038/s41573-021-00163-y

Shen, P., Rother, M., Stervbo, U., Lampropoulou, V., Calderon-Gomez, E., Roch, T., et al. (2022). Toll-like receptors control the accumulation of neutrophils in lymph nodes that expand CD^{4+} T cells during experimental autoimmune encephalomyelitis. *Eur. J. Immunol.* 53. doi:10.1002/eji.202250059

Singh, M., Khong, H., Dai, Z., Huang, X.-F., Wargo, J. A., Cooper, Z. A., et al. (2014). Effective innate and adaptive antimelanoma immunity through localized TLR7/8 activation. *J. Immunol.* 193, 4722–4731. doi:10.4049/jimmunol.1401160

Smits, ELJM, Ponsaerts, P., Berneman, Z. N., and Van Tendeloo, V. F. I. (2008). The use of TLR7 and TLR8 ligands for the enhancement of cancer immunotherapy. *Oncol.* 13, 859–875. doi:10.1634/theoncologist.2008-0097

Sun, H., Li, Y., Zhang, P., Xing, H., Zhao, S., Song, Y., et al. (2022). Targeting toll-like receptor 7/8 for immunotherapy: recent advances and prospectives. *Biomark. Res.* 10, 89. doi:10.1186/s40364-022-00436-7

Takahama, S., and Yamamoto, T. (2020). Pattern recognition receptor ligands as an emerging therapeutic agent for latent HIV-1 infection. *Front. Cell Infect. Microbiol.* 10, 216. doi:10.3389/fcimb.2020.00216

Van Gool, S. W., Vandenberghe, P., Boer, M. D., and Ceuppens, J. L. (1996). CD80, CD86 and CD40 provide accessory signals in a multiple-step T-cell activation model. *Immunol. Rev.* 153, 47–83. doi:10.1111/j.1600-065X.1996.tb00920.x

Verma, S. K., Mahajan, P., Singh, N. K., Gupta, A., Aggarwal, R., Rappuoli, R., et al. (2023). New-age vaccine adjuvants, their development, and future perspective. *Front. Immunol.* 14, 1043109. doi:10.3389/fimmu.2023.1043109

Wang, H., Chen, H., Liu, S., Zhang, J., Lu, H., Somasundaram, R., et al. (2021). Costimulation of γδTCR and TLR7/8 promotes Vδ2 T-cell antitumor activity by modulating mTOR pathway and APC function. *J. Immunother. Cancer* 9, e003339. doi:10.1136/jitc-2021-003339

Wang, P. (2021). Natural and synthetic saponins as vaccine adjuvants. *Vaccines* 9, 222. doi:10.3390/vaccines9030222

Wei, Y., Qin, G., Wang, Z., Zhao, C., Ren, J., and Qu, X. (2023). Bioorthogonal activation of TLR7 agonists provokes innate immunity to reinforce aptamer-based checkpoint blockade. *ACS Nano* 17, 5808–5820. doi:10.1021/acsnano.2c12313

Yong, E.-L., Cheong, W. F., Huang, Z., Thu, W. P. P., Cazenave-Gassiot, A., Seng, K. Y., et al. (2021). Randomized, double-blind, placebo-controlled trial to examine the safety, pharmacokinetics and effects of Epimedium prenylflavonoids, on bone specific alkaline phosphatase and the osteoclast adaptor protein TRAF6 in post-menopausal women. *Phytomedicine* 91, 153680. doi:10.1016/j.phymed.2021.153680

Zebeaman, M., Tadesse, M. G., Bachheti, R. K., Bachheti, A., Gebeyhu, R., and Chaubey, K. K. (2023). Plants and plant-derived molecules as natural immunomodulators. *BioMed Res. Int.* 2023, 7711297. doi:10.1155/2023/7711297

Zhang, J.-W., Tan, L., Yuan, J.-B., Qiao, R.-F., Wang, C.-Z., Yang, F.-Q., et al. (2020). Extraction of activated epimedium glycosides *in vivo* and *in vitro* by using bifunctional-monomer chitosan magnetic molecularly imprinted polymers and identification by UPLC-Q-TOF-MS. *Talanta* 219, 121350. doi:10.1016/j.talanta.2020.121350

Zhou, J., Xu, Y., Wang, G., Mei, T., Yang, H., and Liu, Y. (2022). The TLR7/8 agonist R848 optimizes host and tumor immunity to improve therapeutic efficacy in murine lung cancer. *Int. J. Oncol.* 61, 81. doi:10.3892/ijo.2022.5371

Frontiers in Pharmacology

Explores the interactions between chemicals and living beings

The most cited journal in its field, which advances access to pharmacological discoveries to prevent and treat human disease.

Discover the latest Research Topics

See more →

Frontiers

Avenue du Tribunal-Fédéral 34
1005 Lausanne, Switzerland
frontiersin.org

Contact us

+41 (0)21 510 17 00
frontiersin.org/about/contact